IJERT

NCEASE-2015

National Conference on Emerging Advances In Science and Engineering

27 February, 2015

Organized by :

St. Anne's College of Engineering and Technology

Conference Proceedings

Published By

International Journal of Engineering Research and Technology

(www.ijert.org)

About St. Anne's College of Engineering and Technology

St. Anne's College of Engineering and Technology (St.Anne's CET) is a pioneer educational institute of The Congregation of the Sisters of St. Anne of Tiruchirapalli.The college bloomed in the year 2009 with an aim of uplifting the life style and providing opportunity for higher professional education to the rural youth in the surrounding districts. We are committed to promote and propagate quality and value based education at par with international standards. We believe that our sincerity, dedication and focus towards our goal have been instrumental in this accomplishment. Our vision is to apply the knowledge to expand the personal growth and to create the miscellany of ideas leading to the development of the society. The institution provides a healthy, democratic and interactive environment to students where they can evolve into responsible and knowledgeable engineers and manage to set new frontiers on the global form.

College offers six Under Graduate programs.

UG Courses

- Mechanical Engineering
- Electrical & Electronics Engineering
- Electronics & Communication Engineering
- Computer Science and Engineering

About NCEASE'15

National Conference on Emerging Advances in Science and Engineering - 2015 (NCEASE'15) in association with International Journal of Engineering Research and Technology (IJERT) is a premier event that address new advancements and challenges in the field of Science and Engineering. This multidisciplinary conference NCEASE'15 aim to provide confidence, deftness and motivation to achieve success in our launch. It is an opportunistic forum and vibrant platform to promote, encourage, bring together researches and industrial practitioners to share their original research work and practical development experiences on specific new challenges and emerging issues in all Science and Engineering. The conference hopes to stimulate the growth of worldwide community that places priority on developing technology for sustainable human development.

Message from Chief Patron

I am please to know that St.Anne's CET is going to organize a National Conference on Emerging Advances in Science and Engineering.Today,the technology is developing at a very fast pace. We have observed the progress of last 100 years, but if we compare it with the progress of last 10 years it is much more than last 100 years. As we all know that our country can only make progress if the scientists and technocrats can utilize their knowledge for exploring newer fields of research and development. We experience new development every day and every moment. Now it is high time that everybody from us will have to think and commit for the contribution. Moreover, there is a growing need of more and more industry-institute interaction and linkage, the young faculty members St.Anne's CET have rightly sensed this need and provided good platform for the researchers all around the globe to bring forward their thoughts and help society at large. Many congratulations to the Principal, Convener and the organizing committee members for organizing an event of national stature. Once again I convey my blessings and good wishes to all members of St.Anne's CET family involved dedicatedly for this event.

Rev.Mother Victoria, SAT
Secretary
St. Anne`s College of Engineering and Technology
Anguchettypalayam, Panruti Taluk, Tamilnadu.

Message from Patron

Conferences open up avenues for further research, as it is the cradle of ideas. Besides, candidates get an opportunity to showcase their talents in their respective fields. Development in any area requires empirical studies and research. When students are made aware of events taking place around them in the world, they too look forward to further research and inventions. Frequent conferences of this sort must be organized in all educational institutions.

I am extremely happy that the all departments of our college is organizing “National Conference on Emerging Advances in Science and Engineering - 2015 (NCEASE’15)”. I sincerely congratulate all staff members of the department, especially the organizers of the conference, and wish them all success in this endeavour.

I sincerely convey my heartily congratulation to all members, teaching as well as non-teaching, who have put the name of St.Anne’s CET on global map.

I hope that all local as well as foreign delegates will get useful deliberations during the conference. I also wish their stay at St.Anne’s CET is joyful and useful.

Dr. R. Arokiadass – ME, Ph.D
Principal,
St. Anne's College of Engineering and Technology,
Anguchettypalayam,Panruti Taluk,Tamilnadu.

Message from Convener

The mission of this conference is to provide value education and motivate young professionals in building cognitive characteristics, evoke creative expression and cultivate the budding engineers with recent trends in technology, prepare emerging engineers with concept oriented subject knowledge supplemented with practical orientation to face the challenges of modern world.

Research and academics should go hand in hand in the making of better future technocrats and engineers. The conference is honoured to have eminent professors from various fields of Engineering &Technology for imparting knowledge and experience to young aspirants. I extend my sincere thanks to all of them. On the occasion of this event, I heartily welcome all the participants and wish them to bid farewell to this campus with new ideas and cherished memories.

Mr. D. Ommurugadhasan,
Associate Professor,
Department of Mechanical Engineering
St. Anne`s College of Engineering and Technology
Anguchettypalayam, Panruti Taluk, Tamilnadu.

ADVISORY COMMITTEE

Dr. K. Mahadevan,
Professor,
Pondicherry Engineering College,
Puducherry.

Dr. M. Sudhakaran,
Professor,
Pondicherry Engineering College,
Puducherry.

Dr. N. Alagumurthi,
Professor,
Pondicherry Engineering College,
Puducherry.

Dr. N. Sreenath,
Professor,
Pondicherry Engineering College,
Puducherry.

Dr. Narasimman Sundararajan,
SRF,Nanyang Technological University, Singapore.

Dr. A. Senthil Kumar,
Principal,
University College of Engineering,
Panruti.

Prof. F. A. Naik,
BMIT, Solapur,
Maharashtra.

Dr. C. Senthil Kumar,
Assistant Professor,
Annamalai University,
Chidambaram.

Dr. I. B. Shameem Banu,
Professor & Dean,
B.S. Abdur Rahman University,
Chennai.

Dr. K. Thirumalaivasan,
Professor & Head,
Achariya College of Engg. and Tech.,
Puducherry.

Dr. K. Palani Radja @ Kichena,
Professor,
Pondicherry Engineering College,
Puducherry.

Mr. J. Jaya Samraj,
Director,
National Power Training Institute,
Neyveli.

Dr. V. Cyril Raj,
Dean (E&T)Dr. M.G.R University,
Maduravoyal, Chennai.

Dr. S. Perumal Shankar,
Professor,
Toc H Institute of Science and
Technology, Kerala.

Dr. N. Madhusudana Rao,
Professor,
VIT University, Vellore.

Mr. G. Chandramouli,
Development Engineer,CISCO,
Chennai.

Dr. T. Saravanan, Professor & Head,Bharath University, Chennai.

Mr. A. Benjamin Aravinth, Architect, Cognizant Technology Solutions, Chennai

Preface

This book reports the proceedings of the National Conference on Emerging Advances in Science and Engineering - 2015 (NCEASE'15) held at St. Anne's College of Engineering and Technology on Feb 27, 2015. The conference was organized by Department of Electronics and Communication Engineering, Computer Science and Engineering, Electrical & Electronics Engineering and Mechanical Engineering in association with IJERT. The goal of this conference is to provide intellectual forum for sharing knowledge and innovation amongst young students, researchers, academicians and professionals in order to peep and comprehend the exciting and challenging future of latest trends in the fields of Mechanical, Electrical, Electronics and Communication, Computer science and Applied Science and Mathematics for Engineering. The participants include delegates from various top most universities including Pondicherry University, Anna University, Annamalai University, etc. True to its trend, the response to the call for NCEASE'15 has been fantastic. We had received about 100 papers covering huge array of diverse topics like Digital Signal Processing, VLSI design, Embedded System, RFID applications, Wireless sensor networks ,Power Electronics, Data Communication and Networking. All papers went through, peer review process. About 80 were selected out of which 57 of these are included in these proceedings. The vision for the National Conference remains consistent with its origin. The priorities remain to keep the conference as a conversational forum, to sustain a climate for personal interaction, to feature leading professionals and top scholars, and to provide information and new ideas that are useful and meaningful to conference participants. No conference can be organized successfully without dedication and selfless hard work by an array of people to whom we remain ever obliged. These include the authors, the reviewers, the committee members and invited speakers. We gratefully acknowledge the support we have received from our management, IJERT and staff members and students of our college. We take this opportunity to thank all the members of the Advisory Committee, Technical Committee and organizing committee for the inspiration, advice and other help they have provided us in making this conference successful. We would like to thank Lord Almighty for providing us with strength and courage for completing the work in time.

Editors,
Members of Organising Committee

Direct Current Control based Bidirectional AC/DC Single Phase Converter in a Grid-Tied Micro Grid Systems

A. Annai Theresa
Department of Electrical and Electronics Engineering
St. Anne's College of Engineering and Technology
Panruti, Tamilnadu

M. Arun Noyal Doss
Department of Electrical and Electronics Engineering
SRM University
Chennai, Tamilnadu

***Abstract*— This paper presents a novel simplified direct current control strategy for the bidirectional ac/dc single phase converter in a micro grid system. Based on the simplified Pulse Width Modulation (PWM) strategy, a feasible feed forward control scheme is developed to achieve better rectifier mode and inverter mode performance compared with the conventional dual loop control scheme. The proposed simplified PWM strategy with the proposed feed forward control scheme has lower total harmonic distortion. The features of the proposed converter will be verified by the simulation using MATLAB.**

Keywords—direct current control, PWM strategy, feed forward control, Total Harmonic Distortion.

I.INTRODUCTION

THE single-phase ac/dc pulse PWM converter is widely used in many applications such as adjustable-speed drives, switch-mode power supplies, and un- interrupted power supplies. The single-phase ac/dc PWM converters [1],[2],[4] are usually employed as the utility interface in a grid-tied renewable resource system, as shown in Fig. 1. To utilize the distributed energy resources (DERs) efficiently and retain power system stability, the bidirectional ac/dc converter plays an important role in the renewable energy system. When DERs have enough power, the energy from the dc bus can be easily transferred into the ac grid through the bidirectional ac/dc converter. In contrast, when the DER power does not have enough energy to provide electricity to the load in the dc bus, the bidirectional ac/dc converters can simultaneously and quickly change the power flow direction (PFD) from ac grid to dc grid and give enough power to the dc load and energy storage sys- tem. There are many requirements for ac/dc PWM converters as utility interface in a grid-tied system; for instance, providing power factor correction functions [1], low distortion line currents [20], [21], [22], high-quality dc output voltage [1], and bidirectional power flow capability [6], [7]. Moreover, PWM converters are also suitable for modular system design and system reconfiguration. In this paper, a novel PWM control strategy with feed forward control scheme of a bidirectional single-phase ac/dc converter is presented.

In the existing PWM control strategies of a single-phase ac/dc converter, the converter switches are operated at higher frequency than the ac line frequency so that the switching harmonics can be easily removed by the filter [20], [21], [22]. The ac line current waveform can be more sinusoidal at the expense of switching losses. Until now several PWM strategies have been utilized in a single-phase ac/dc converter such as bipolar PWM (BPWM), unipolar PWM (UPWM) [8]–[10],

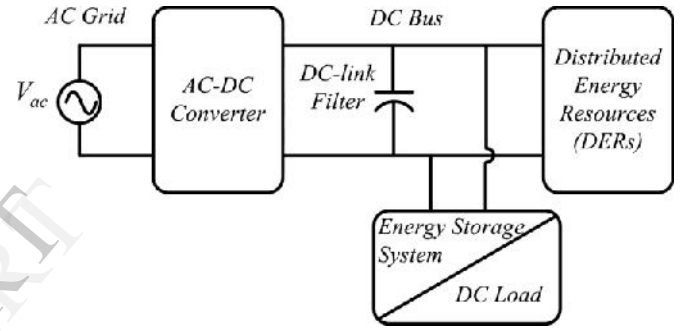

Fig. 1 Distribution Energy System.

HPWM [11]–[14], and Hysteresis switching [15],[16]-[19]. UPWM results in a smaller ripple in the dc side current and significantly lower ac side harmonic content [10] compared to the BPWM. The UPWM effectively doubles the switching frequency in the ac voltage waveform harmonic spectrum allowing the switching harmonics to be easily removed by the passive filter. The HPWM [12]–[14] utilizes two of the four switches modulated at high frequency and utilizes the other two switches commutated at the (low) output frequency to reduce the switching frequency and achieve better quality output. However, the switching loss in the HPWM is still the same as that of the UPWM [12]. The hysteresis switching method utilizes hysteresis in comparing the actual voltage and/or current to the reference Although the hysteresis switching method has the advantages of simplicity and robustness [15],[16]-[19] the converters' switching frequency depends largely on the load parameters, and consequently, the harmonic ripples are not optimal. Hysteresis control methods [15], [16]–[19] with constant switching frequency have recently been presented. Those are usually based on the voltage and/or current error zero-crossing time to achieve a constant switching frequency. However, the capacitor ripple voltage and inductor ripple current are assumed to be ignored and the implemented inductor and/or capacitor are not very practical. The switching frequency jitter [15] problem would occur during the inverter dead-time control

(i.e., dead- time effects) in the hysteresis modulation.

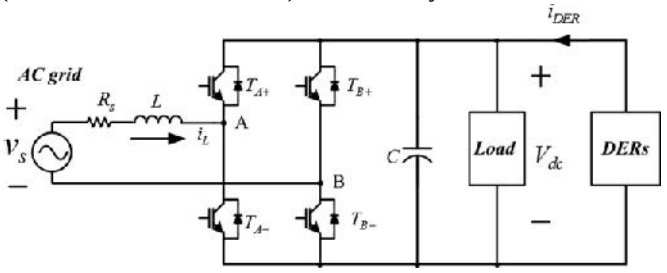

Fig. 2 Application of a bidirectional single-phase ac/dc converter in the renewable energy system.

The proposed simplified PWM reduces harmonic pollution in Distribution power systems and replaces conventional diode front end rectifier stage in order to reduce the total harmonic distortion. This proposed topology follows an active ripple energy storage method that can effectively reduce the energy storage capacitance. A novel feed forward control scheme is also developed so that both the rectifier and inverter mode can be operated in a good manner. It is worth mentioning that the proposed feedforward control scheme is also suitable for the conventional UPWM and BPWM to provide fast output voltage response as well as improve input current shaping.

II.OPERATION PRINCIPLE OF THE PROPOSED PWM STRATEGY WITH LINEAR CONTROL TECHNIQUE

A bidirectional single-phase ac/dc converter is usually utilized as the interface between DERs and the ac grid system to deliver power flows bidirectionally and maintains good ac current shaping and dc voltage regulation, as shown in Fig. 2. Good current shaping can avoid harmonic pollution in an ac grid sys- tem, and good dc voltage regulation can provide a high-quality dc load. To achieve bidirectional power flows in a renewable energy system, a PWM strategy may be applied for the single-phase full-bridge converter to accomplish current shaping at the ac side and voltage regulation at the dc side. Generally, BPWM and UPWM strategies are often utilized in a single-phase ac/dc converter. In this paper, a novel simplified PWM strategy with linear control technique is pro- posed. In this control scheme, the compensation current or voltage signal is compared with its estimated rated reference signal through the compensated error amplifier to produce the control signal. The resulting control signal is then compared with a saw tooth signal through a pulse width modulation (PWM) controller to generate the appropriate gating signals for the switching transistors. The frequency of the repetitive saw tooth signal establishes the switching frequency. This frequency is kept constant in linear control technique. As shown in Figure, the gating signal is set high when the control signal has a higher numerical value than the saw tooth signal and vice versa. With analogue PWM circuit, the response is fast and its implementation is simple. Nevertheless, due to inherent problem of analogue circuitry, the linear control technique has an unsatisfactory harmonic compensation performance. This is mainly due to the limitation of the achievable bandwidth of the compensated error amplifier.

A.PI controllers for DC-bus voltage control

A PI controller used to control the DC-bus voltage is shown in Figure. Its transfer function can be represented as Kp +K_i/S. where Kp is the proportional constant that determines the dynamic response of the DC-bus voltage control, and Ki is the integration constant that determines it's settling time. It can be noted that if Kp and Ki are large, the DC-bus voltage regulation is dominant, and the steady-state DC-bus voltage error is low. On the hand, if Kp and Ki are small, the real power unbalance gives little effect to the transient performance.

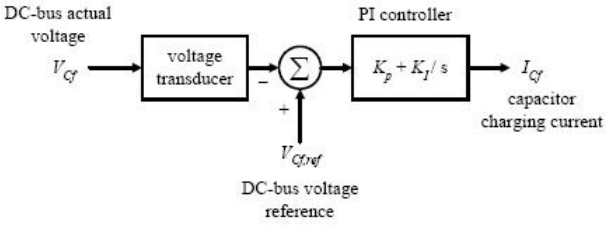

Fig.3. Design of PI Regulator

In the design of single-phase PWM rectifier control system, the general use is dual-loop control, namely, voltage and current loops. The outer voltage loop controls the voltage in DC side, while the current loop as the inner loop, it forces the input current tracking current instruction (gained from the output of the outer voltage loop), in order to achieve sinusoidal current control unity power factor. The current instruction and grid-side voltage have same frequency and opposite phase.

B. Design of Inner Current Loop

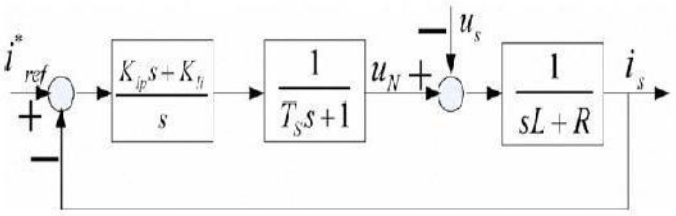

Fig.4.Block Diagram of transfer function in current loop

The control performance of input current is the key of rectifier control, because the essence of the rectifier is an energy conversion system between the AC and DC power, the grid voltage is essentially certain, so the rapid and effective control of the input current is important.

III. PROPOSED DIRECT CURRENT CONTROL SCHEME

A. Conventional Dual-Loop Control Scheme

In the conventional dual loop control scheme applied to the single-phase bidirectional ac/dc converter, the inner current loop and outer voltage loop are utilized as shown in Fig. 5, where Vdc* is the dc voltage command, Vdc is the actual dc voltage; i_L is the ac current command, and I_L is the actual

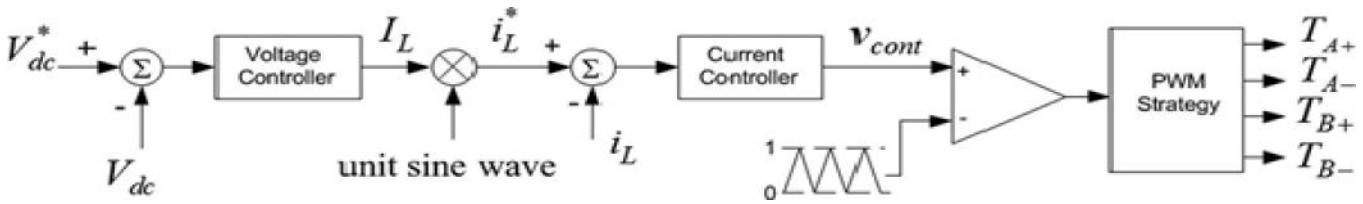

Fig. 5.Conventional dual-loop control scheme for a single phase bidirectional ac/dc converter.

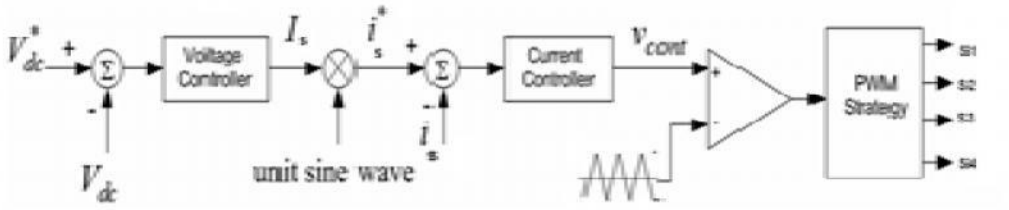

Fig.6. Proposed control scheme block diagram for a single phase bidirectional ac/dc converter.

ac current. The voltage controller calculates the voltage error and generates the current amplitude command IL multiplied by the unit sinusoidal waveform, obtained from the phase lock loop to generate the current command i*. In general, a proportional-integral controller is adopted as the voltage controller and current controller to achieve power factor correction at the ac side and voltage regulation at the dc side.

B. Proposed Direct current Control Scheme

Based on the proposed simplified PWM, a novel Direct current scheme is presented in this section. The converter is operated in the rectifier mode and inverter mode. To derive the state-space averaged equation for the proposed simplified PWM strategy, the duty ratio Don is defined as Don = ton /T , where ton is the time duration when the switch is turned ON, i.e., Son = 1, and T is the time period of triangular waveform. The duty ratio Doff is defined as Doff = 1 – Don ,which is the duty ratio when the switch is turned OFF. By introducing the state-space averaged tech- nique and volt–second balance theory, the state-space averaged equation is derived as follows:

$$Vs - (1 - Don)\,Vdc = O. \qquad (1)$$

When the converter is operated in the steady state, the dc voltage is equal to the desired command Vdc* = Vdc ; (1) can also be expressed in the following form:

$$Don = 1 - (Vs/Vdc^*)$$

By introducing the state-space averaged technique and volt–second balance theory, the state-space averaged equa- tion is derived as follows, while the ac grid voltage source is operating in the negative half-cycle vs < O:

$$vs + Don\,Vdc = O.$$

Similarly, when the converter is operated in the steady state, the output voltage is equal to the desired command Vdc = V dc∗. According to the PWM properties, the switching duty ratio can be expressed in terms of the control signal Vcont* and the peak value Vtri of the triangular waveform Don = Vcont*/Vtri

$$Vcont^* = \begin{cases} \left[\frac{1-Vs}{Vdc^*}\right] Vtri & , \text{if } Vs > O \\ \left[-\frac{Vs}{Vdc^*}\right] Vtri & , \text{if } Vs < O \end{cases}$$

While the converter is operated in the inverter mode, the control signal v can be obtained using a similar manner in the rectifier mode. Because the control signals Vcont is proportional to Don.

IV. SIMULATION RESULTS

To verify the validity of the proposed PWM strategy and the direct current control scheme, the well-known soft- ware MATLAB was adopted to carry out the simulation process.

A. Direct source current method

Consider that the converter is operated in the rectifier mode. Fig. 7 shows the measured grid voltage Vs and line current i_L when the converter is operating the dual loop control scheme in the proposed simplified PWM strategy. The measured THD of the converter ac line current is 34.23% and the power factor is O.92. In contrast, Fig. 1O shows the corresponding measured grid voltage vs and line current i_L waveforms with the proposed feed forward control scheme in the proposed simplified PWM strategy operated in the rectifier mode. In the feed forward control scheme, the measured ac line current THD of the converter is 3.34% and the power factor is O.99. Figs. 11 and 12 show the input voltage and source current which are in phase and very low THD. So from this one can find that the proposed source current control method indeed further improves the converter ac current shaping com- pared to the dual-loop control scheme in the actual distorted ac grid voltage source condition.

Fig.7. Measured grid voltage Vs and line current i_L waveforms of the converter using the dual-loop control scheme in the proposed simplified PWM strategy operated in the rectifier mode.

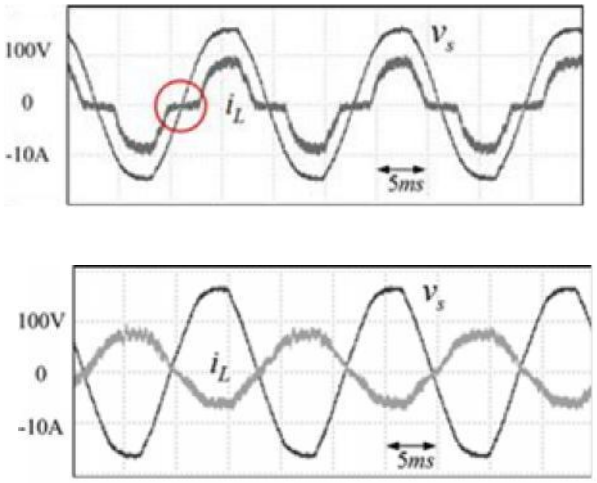

Fig.S. Measured grid voltage Vs and line current iL waveforms using the feed forward control scheme in the proposed simplified PWM strategy operated in the inverter mode.

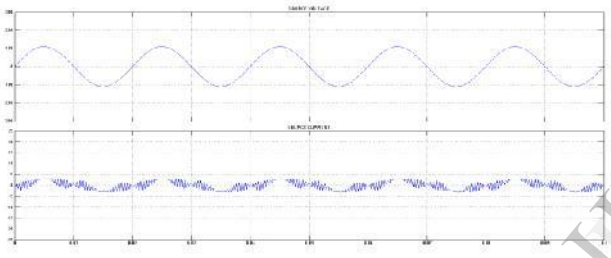

Fig.**11**.simulated source voltage and source current conventional PWM rectifier

Consider next that the converter is operated in the inverter mode. Fig. 9 shows the measured grid voltage Vs and line current i_L of the converter with the dual-loop control scheme in the proposed simplified PWM strategy. When the converter is operated in the dual-loop control scheme, one can find that zero cusp distortion exists near the zero crossing. The serious distortion may occur when the controller is not designed well. The measured THD of the converter ac line current is 6.64% and the power factor is –0.967. In contrast, Fig. 8 shows the corresponding measured grid voltage vs and line current iL waveforms with the feed forward control scheme in the pro- posed simplified PWM strategy operated in the inverter mode. In the proposed feed forward control scheme, the measured ac line current THD of the converter is 4.69% and the power fac- tor is –0.985. Comparing Fig. 9 with Fig. 10, the feed forward control scheme also improves the ac/dc converter current shaping when operated in the inverter mode compared to the conventional dual-loop. By using source current control method the THD level further current and pwm output voltage during PV supplying power to battery charging system and inverter.

Fig.9. Measured grid voltage Vs and line current iL waveforms using feed- forward control scheme in the proposed simplified PWM strategy operated in the rectifier mode.

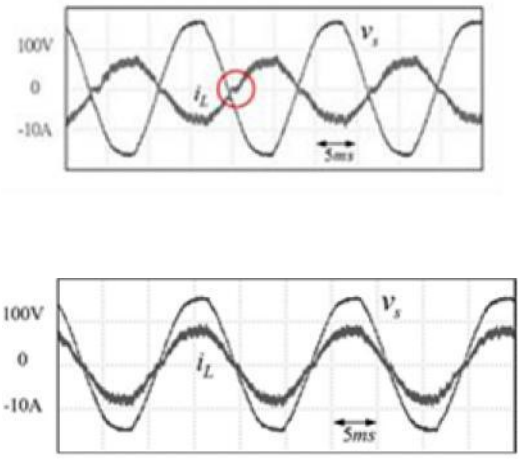

Fig.**1**0. Measured grid voltage Vs and line current iL waveforms of the converter using the dual-loop control scheme in the proposed simplified PWM strategy operated in the inverter mode.

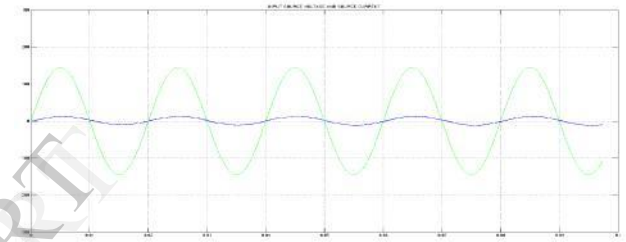

Fig.**1**2. simulation results of source voltage and source current of proposed ac-dc converter

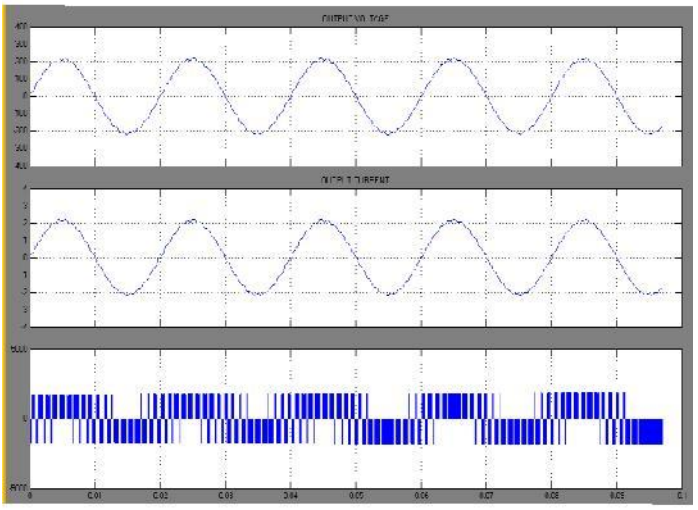

Fig.**1**3. Inverter output voltage, output current and pwm output voltage (during PV supplying power to battery charging system and inverter)

V.CONCLUSION

This paper presented a Direct current control based bidirectional AC/DC single phase converter in a Grid-Tied Micro grid Systems. The proposed simplified PWM strategy with the proposed feed forward control scheme has lower total harmonic distortion. Based on the proposed feed forward control scheme, both the ac current shaping and dc voltage regulation are achieved in both the rectifier and converter operating modes. The THD of the proposed PWM strategy is very low. The features of the proposed converter were verified by the simulation using MATLAB.

REFERENCES

(1) R. Wang, F. Wang, D. Boroyevich, R. Burgos, R. Lai, P. Ning, and K.Rajashekara, "A high power density single-phase PWM rectifier with active ripple energy storage," IEEE Trans. Power Electron., vol. 26, no. 5, pp. 1430–1443, May 2011.

(2) S.-H. Hwang, L. Liu, H. Li, and J.-M. Kim, "DC offset error compensa- tion for synchronous reference frame PLL in single-phase grid- connected converters," IEEE Trans. Power Electron., vol. 27, no. 8, pp. 3467–3471, Aug. 2012.

(3) S. Golestan, M. Monfared, F. D. Freijedo, and J. M. Guerrero, "Design and tuning of a modified power-based PLL for single-phase grid- connected power conditioning systems," IEEE Trans. Power Electron., vol. 27, no. 8, pp. 3639–3650, Aug. 2012.

(4) R. I. Bojoi, L. R. Limongi, D. Roiu, and A. Tenconi, "Enhanced power quality control strategy for single-phase inverters in distributed generation systems," IEEE Trans. Power Electron., vol. 26, no. 3, pp. 798–806, Mar.2011.

(5) S. Dasgupta, S. K. Sahoo, and S. K. Panda, "Single-phase inverter control techniques for interfacing renewable energy sources with microgrid—Part I: Parallel-connected inverter topology with active and reactive power flow control along with grid current shaping," IEEE Trans. Power Electron., vol. 26, no. 3, pp. 717–731, Mar. 2011.

(6) S. Dasgupta, S. K. Sahoo, S. K. Panda, and G. A. J. Amaratunga, "Single- phase inverter-control techniques for interfacing renewable energy sources with microgrid—Part II: Series-connected inverter topology to mitigate voltage-related problems along with active power Flow control,"IEEE Trans. Power Electron., vol. 26, no. 3, pp. 732–746, Mar. 2011.

(7) J. Salmon, L. Wang, N. Noor, and A. W. Krieger, "A carrier-based unipolar PWM current controller that minimizes the PWM-cycle average current- error using internal feedback of the PWM signals," IEEE Trans. Power Electron., vol. 22, no. 5, pp. 1708–1718, Sep. 2007.

(8) Z. Guo and F. Kurokawa, "A novel PWM modulation and hybrid con trol scheme for grid-connected unipolar inverters," in Proc. Appl. Power Electron. Conf. Expo., 2011, pp. 1634–1641.

(9) N. Mohan, T. Undeland, and W. Robbins, Power Electronics—converters Applications, and Design. New Delhi, India: Wiley, 2003.

(10) T. H. Ai, J. F. Chen, and T. J. Liang, "A random witching method for HPWM full-bridge inverter," IEEE Trans. Ind. Electron., vol. 49, no. 3, pp. 595–597, Jun. 2012.

(11) R-S. Lai and K. D. T. Ngo, "A PWM method for reduction of switching loss in a full-bridge inverter," IEEE Trans. Power Electron., vol. 10, no. 3, pp. 326– 332, May 1995.

(12) V. Blasko, "Analysis of a hybrid PWM based on modified space-vector and triangle-comparison methods," IEEE Trans. Ind. Appl., vol. 33, no.3, pp. 756–764, May/Jun. 1997.

(13) R. T. H. Li, H. S.-H. Chung, W.-H. Lau, and B. Zhou, "Use of hybrid PWM and passive resonant snubber for a grid-connected CSI," IEEE Trans. Power Electron., vol. 25, no. 2, pp. 298–309, Feb. 2010.

(14) H. Mao, X. Yang, Z. Chen, and Z. Wang, "A hysteresis current controller for single-phase three-level voltage source inverters," IEEE Trans.power Electron., vol. 27, no. 7, pp. 3330–3339, Jul. 2012.

(15) A. Shukla, A. Ghosh, and A. Joshi, "Hysteresis modulation of multilevel inverters," IEEE Trans. Power Electron., vol. 26, no. 5, pp. 1396–1409, May 2011.

(16) A. Z. Albanna and C. J. Hatziadoniu, "Harmonic modeling of hysteresis inverters in frequency domain," IEEE Trans. Power Electron., vol. 25, no.5,pp.1110-1114,May 2010.

(17) C. Yu and K. Yong, "The variable-bandwidth hysteresis-modulation sliding-mode control for the PWM–PFM converters," IEEE Trans. Power Electron., vol. 26, no. 10, pp. 2727–2734, Oct.2011.

(18) P. A. Dahono, "New hysteresis current controller for single-phase full- bridge inverters," IET Power Electron., vol. 2, no. 5, pp. 585–594, Oct 2009.

(19) W. Wu, Y. He, and F. Blaabjerg, "An LLCL power filter for single- phase grid-tied inverter," IEEE Trans. Power Electron., vol. 27, no. 2, pp. 782–789, Feb. 2012.

(20) H. Mao, X. Yang, Z. Chen, and Z. Wang, "A hysteresis current controller for single-phase three-level voltage source inverters," IEEE Trans. Power Electron., vol. 27, no. 7, pp. 3330–3339, Jul. 2012.

(21) A. Abrishamifar, A. A. Ahmad, and M. Mohamadian, "Fixed switching frequency sliding mode control for single-phase unipolar inverters," IEEE Trans.Power Electron., vol. 27, no. 5, pp. 2507–2514,May 2012. [23] Cursino Brenda Jacobina, Single-Phase to Three-Phase Drive System

(22) Using Two Parallel Single-Phase Rectifiers Senior Member, IEEE,
Euzeli Cipriano dos Santos Jr., Member, IEEE,Nady Rocha and Edgard
Luiz Lopes Fabr´ıcio VOL. 25, NO. 5, MAY 2010

(23) Dong-Choon Lee, Control of Single-Phase-to-Three-Phase AC/DC/AC PWM Converters for Induction Motor Drives Member, IEEE, and Young-Sin Kim VOL. 54, NO. 2, APRIL 2007

(24) Li Taofeng, Ouyang Hui,Kang Yong, Xiong Jian, Fan Shengfang, Zhang Kai, "The Research of Single-phase PWM Rectifier Based on Direct Current Control" IEEE2009.

Distributing Transformer Voltage Regulation by using Solid State Tap Change Mechanism

Balaji. J,
Department Of EEE Annai Velankanni
Polytechnic College, Panruti - 607110

Ramesh. J
Department Of EEE
st. Anne's College of Engg.
& Tech., Panruti-607110

***Abstract*—Distributed Generation has gained its significance after considering the environmental hazards and recent developments in the renewable energy sector. The access of Distributed Generation and varying load at the consumer side has its own demerits of maintaining the constant output voltage at the consumer side. Since voltage is one of the most significant parameter for the control of electric power system, hence it needs to be maintained at least near to its constant value. The method involve in maintaining the output voltage within the acceptable limit at the consumer side is by Tap changing mechanism associated with the distributing transformer. This project work deals with the replacement of conventional Electro-mechanical way of On-Load Tap changers with the Solid State Tap Changers for voltage regulation. With fully electronic control of tap changing the problems associated with the mechanical On-Load tap changing which includes excessive conduction losses, slow operation and arcing in the diverter switch have been properly rectified. It also explains the sequential switching of the Thyristor to regulate the voltage, based on the voltage feedback taken from the output side. Here Pulse Width Modulation (PWM) technique is adopted for sequential switching of the Thyristor, depending on the voltage feedback. By adopting Solid State tap changers in the distribution transformers fast and reliable operation is ensured and also encourages the proliferation of Distribution Generation.**

***Keywoads*—On-Load Tap Changer, Pulse Width Modulation, Silicon Controlled Rectifier (SCR), pulse transformer.**

I.INTRODUCTION

Voltage is one of the most important parameter for the control of power system. A distribution transformer is a transformer that provides the final voltage transformation in the electric power distribution system, stepping down the voltage used in the distribution lines to the level used by the customer. A voltage regulator is designed to automatically maintain a constant voltage level.

A. Distribution Trans!ormer

A distribution transformer is a transformer that provides the final voltage transformation in the electric power distribution system, stepping down the voltage used in the distribution lines to the level used by the customer. The invention of a practical efficient transformer made AC power distribution feasible.

B. Automatic Voltage Regulator

A voltage regulator is designed to automatically maintain a constant voltage level. A voltage regulator may be a simple "feed-forward" design or may include negative feedback control loops. It may use an electromechanical mechanism, or electronic components. Depending on the design, it may be used to regulate one or more AC or DC voltages.

C. Variable Shunt Reactor

Variable Shunt Reactors are used in high voltage energy transmission systems to stabilize the voltage during load variations. A traditional shunt reactor has a fixed rating and is either connected to the power line all the time or switched in and out depending on the load. The regulation speed is normally in the order seconds per step and around a minute from max to min rating. The VSR can continuously compensate reactive power as the load varies and thereby securing voltage stability.

D. Tap Changer

A tap changer is a connection point selection mechanism along a power transformer winding that allows a variable number of turns to be selected in discrete steps. A transformer with a variable turn's ratio is produced, enabling stepped voltage regulation of the output. The tap selection may be made via an automatic or manual tap changer mechanism. Generally tap changers are classified into two types.

(i) Off-circuit or de-energized tap changing (DETC) is sometimes employed in high voltage transformer designs. Since the different tap points are at different voltages, the two connections cannot be made simultaneously, as this would short-circuit a number of turns in the winding and produce excessive circulating current. Consequently, the power to the device must be interrupted during the switchover event. It is only applicable to installations in which the loss of supply can be tolerated.

(ii) On-Load Tap Changer (OLTC) is employed for many power transformer applications, where supply interruption during a tap change is unacceptable. On- load tap changers may be generally classified as either mechanical, or electronically assisted, or fully electronic.

A mechanical tap changer physically makes the new connection before releasing the old using multiple tap selector switches, but avoids creating high circulating currents by using a diverter switch to temporarily place large diverter impedance in series with the short-circuited turns. This technique overcomes the problems with open or short circuit taps. In a typical diverter switch powerful springs are tensioned by allow power motor, and then rapidly released to affect the tap changing operation. To reduce arcing at the contacts, the tap changer operates in a chamber filled with insulating transformer oil, or inside an SF6vessel.

Thyristor-assisted tap changers use thyristors to take the on-load current while the main contacts change over from one tap to the previous. This prevents arcing on the main contacts and can lead to a longer service life between maintenance activities.

Solid State Tap Changers are typically employed only on smaller power transformers. Solid state tap changers which uses thyristors both to switch the load current and to pass the load current in the steady state.

E. Distributed Generation

The development of Distributed Generation in India has been quite impressive. Over the last few years, a number of influences have been combined to lead to the increased interest in the use of small-scale generation, connected to local distribution systems, which is commonly called "Distributed GenerationD (DG).The DG on the networks will make a significant reduction of the total consumption of fossil fuelled electricity, hence allowing a substantial minimisation of Carbon-di-oxide emission.

F. Overview of penetration of distributed generation

Control of Distributed Generation (DG) systems in power distribution systems is very important task that must be considered carefully. The presence of local generation in a distribution system will affect the distribution system. Distribution networks have not been designed to cope with power injections from DG, therefore the proliferation of DG on the electric networks results in a number of adverse effects. Typically, one the most severe situation is that voltage magnitude at the proximity of DG exceeds the statutory limits during maximum power output from DG and minimum power demand from the network. In such case the DG will alter the power flow in the distribution system, and the distribution system can no longer be considered as a system with unidirectional power flow. Here the network experiences the largest reverse power flow and large voltage change; hence the network has become active distribution network. An active distribution network is defined as distribution network with system in place to control a combination of distributed energy resource comprising of both generator and storage which affects the network safety and stability.

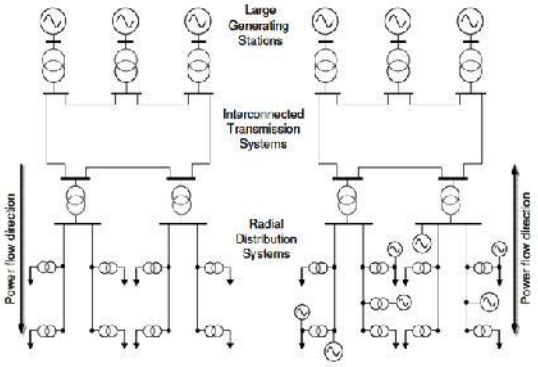

Fig. 1. Traditional electric power (left) and electric power system with distributed generations (right).

Voltage is one of the most important parameters for the control of electric power systems. Hence the voltage stability cannot be compromised. An easily implemented and cost-efficient method for grid integration of DG and regulating the voltage at consumer side is by improving the transformer control concept of MVILV-transformer, which is typically an On-Load Tap Changing transformer control. The On-Load Tap Changer (OLTC) transformers are used between these multiple voltage levels to regulate and maintain the voltage which is supplied to consumers within statutory limits. The OLTC voltage regulation is naturally operated by changing the number of turns in one winding of the transformer to physically alter the ratios of the transformers.

Voltage regulation at the sub-transmission and distribution levels strongly relies on the use of transformer tap changers, implemented now-a-days by means of sophisticated electromechanical mechanisms. The possibility of replacing such slow and prone-to-wear switches by electronic devices has been the subject of much interest in the last few years.

G. Existing model

The conventional OLTC transformer adopts the mechanical on-load tap-changer. The major parts of the mechanical tap changer are on-off selector or tap-changer, diverter switch, transition resistance. A mechanical tap changer physically makes the new connection before releasing the old using multiple tap selector switches, but avoids creating high circulating currents by using a diverter switch to temporarily place large diverter impedance in series with the short-circuited turns. In a typical diverter switch powerful springs are tensioned by a low power motor (motor drive unit (MDU)), and then rapidly released to effect the tap changing operation. To reduce arcing at the contacts, the tap changer operates in a chamber filled with insulating transformer oil, or inside an SF6vessel.To prevent contamination of the tank oil and facilitate maintenance operations, the diverter switch usually operates in a separate compartment from the main transformer tank, and often the tap selector switches will be located in the compartment as well. All of the winding taps will then be routed into the tap changer compartment through a terminal array.

H. Problems in existing model

- The mechanical regulating tap-changer of the traditional OLTC transformer produces the electric arc in the tap changing process, and the tap-changer's movement speed is slow, the regulating response time is long.
- Mechanical drive components, brushes and contractors require regular maintenance and/or replacement.
- Frequent overloads can damage brushes.
- Speed of voltage correction correct may not be fast enough for electronic loads
- It has the high failure rate, maintains difficultly and is unable to accurately control regulating time.

So this kind of mechanical on-load tap changer has not been able to completely satisfy the security of the modern electrical network and the request of economical movement

I. Proposed model

Like the conventional electro-mechanical OLTC, the solid state tap changer also needs a transformer with several tapings. The solid state tap changer is connected in series to an MV or LV feeder. In addition to a common MV/LV transformer the solid state tap changer is an alternative to an conventional OLTC in the MV/LV transforming station. The solid state tap changer operates as follows:

In order to increase the voltage during a voltage drop on the output side, the equipment extracts voltage feedback via the Transformer. Through controlling the thyristor using Pulse Width Modulation (PWM) technique, the solid state tap changer regulates the voltage by changing the tap on the primary side of the transformer with the aim of obtaining a constant operating voltage on the output side according to the reference value. If there is a voltage increase in the output side, the solid state tap changer operates correspondingly. The solid state tap changer has several advantages compared to the conventional OLTC. The solid state tap changer regulates the voltage within milliseconds, while the conventional OLTC needs at least several seconds. Furthermore, the solid state tap changer is normally used with a timing relay to reduce the number of tap settings. The solid state tap changer regulates the voltage continuously, while the voltage is set in stages by the conventional OLTC. Furthermore, the solid state tap changer is able to regulate each single phase.

II. VOLTAGE STABILITY

Voltage stability refers to the ability of a power system to maintain steady voltages at all buses in the system after being subjected to a disturbance from a given initial operating condition. It depends on the ability to maintain/restore equilibrium between load demand and load supply from the power system. Instability that may result occurs in the form of a progressive fall or rise of voltages of some buses. A possible outcome of voltage instability is loss of load in an area, or tripping of transmission lines and other elements by their protections leading to cascading outages that in turn may lead to loss of synchronism of some generators.

III. VOLTAGE CONTROL IN ELECTRIC DISTRIBUTION NETWORK

The voltage variation ΔV across the line can be approximated and represented by the following equation:

$$\Delta V = + \frac{X}{V} \qquad (1)$$

Where ΔV indicates voltage variation, P and Q represent active and reactive power output of DG, X and R are reactance and resistance of the line connecting to DG, V is nominal voltage at the terminal of DG. An on-load tap changer (OLTC) transformer, a local load, a reactive power compensator, an automatic voltage controllers (AVCs), a line drop compensator (LDC) and a energy storage device are also connected on the network.

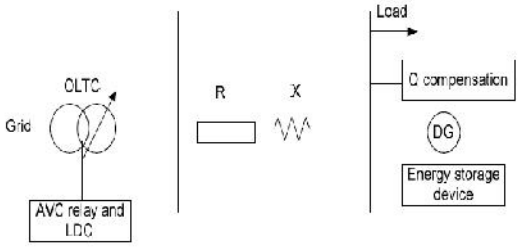

Fig. 2. Simple radial feeders with connected DG

Generally, compared with transmission line, the X/R ratio is relatively low in a distribution network. According to equation, any significant amount of power injected by DG will result in voltage rise/drop on the distribution network, especially in a weak distribution feeder with high impedance. The voltage variation would also depend on several factors including DG size and location, and method of voltage regulation.

A. Role of Olte

The most common voltage control technique on the distribution network is to use OLTCs which maintain a stable secondary voltage by selecting the appropriate tap position. It is an effective way to control the voltage by shifting phase angle and adjusting voltage magnitude. It is usually in conjunction with AVC relay and LDC. The AVC relay continuously monitors the output voltage from the transformer; a tap change command will be initiated when the voltage is above the pre-set limits. The LDC is used to compensate additional voltage drop on the line between the transformer and load location, particular, in the far end of the feeder.

- In order to cope with dramatic changes on network management system, intelligent distributed controllers will be widespread on the network to minimise.
- The voltage impacts. The control structure will move from simple control strategy to two hierarchical level operations. The fundamental level is local level and the second level is coordinated level. The local voltage control aims to maintain voltage at DG units in a fast control response. The coordinated level considers a system wide perspective for voltage control of a distribution network.

B. Coordinated voltage and Reactive power control

The voltage and reactive power control in distribution systems has for many years been based on local operation of the OLTC and shunt capacitors. However in line with the mode mutation of electricity distribution, coordinated voltage and reactive power control with short term operation planning has been adopted in to distribution systems. The OLTC is controlled by considering the dispatch schedule of all capacitors in order to reduce the number of OLTC operations.

IV. VOLTAGE CONTROL BY STATIC OLTC

A. Basic control mechanism

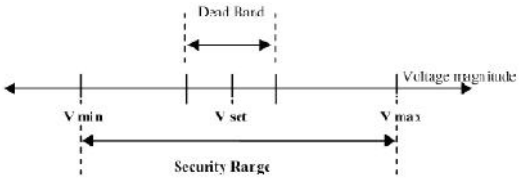

Fig. 3. Voltage Control representation

The control scheme of a conventional OLTC transformer is briefly explained in this chapter. Automatic OLTC controls within ±18% change of nominal voltage. The upper most tap represents -18% changes to nominal voltage, while lower most tap represents +18% changes. The **V**min refers to -18% and **V**max to +18%. OLTC transformer reduces the error in voltage till secondary voltage is within the dead band operating tap positions. Tap changing results step change in voltage.

The voltage in between two steps i.e., between two taps can be obtained through static/semiconductor tap changing systems with sequence control with voltage error less than ±O.1%.

The voltage at load end / secondary side of automatic OLTC transformer is measured and compared with the pre-set value. If the difference is within the dead band, no operation takes place and if the difference lies outside the dead band an appropriate lower or raise correction will start after a pre-determined delay. This process will be repeated until the secondary voltage is within the inner dead band. The main purpose of time delay is to prevent unnecessary tap operations due to temporary voltage fluctuations. Tap changing is done by switching Thyristor in respective taps. In addition to the above automatic tap control; a sequence control is introduced between taps for obtaining fine secondary voltage.

B. Sequence voltage control

An attempt is made to adjust output voltage by controlling Thyristors in between taps. The control of Thyristors is achieved through firing angle control. A typical output waveform using sequence modulation method.

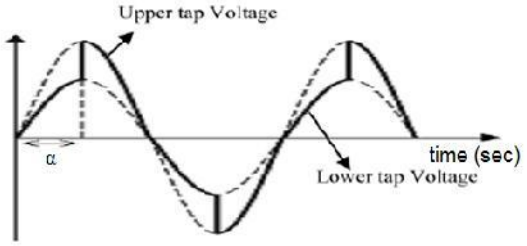

Fig. 4. Firing Angle Control of Voltage

In this method of control, output voltage can be represented as a function of a (firing angle), as given below

Vrms is f (a)

$$\frac{1}{\pi}\left[\int_{o}^{\alpha} Vlt \sin\ \omega t\ ^{2}\, d\ \omega t \;+\; \int_{\alpha}^{\pi} (Vup \sin(\omega t))^{2}\, d(\omega t)\right] \qquad (2)$$

a - firing angle, Vlt - Peak Value of Lower taps voltage

Vup - Peak Value of Upper taps voltage

Vrms – Resultant rms value

Using above stated equation by varying the firing angle, voltage control in between taps can be obtained.

Condition: 1

Vref> Present selected Tap Voltage

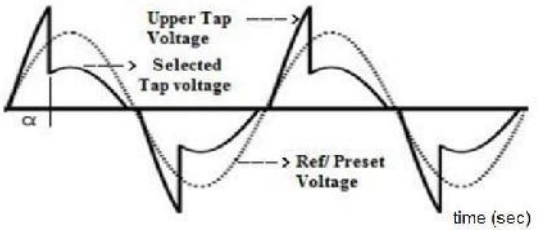

Fig. 5. Firing control between upper tap voltage & selected tap voltage

In this condition firing control is being performed between present selected tap and lower voltage tap, to reduce the voltage further to reach pre-set voltage.

Condition: 2

Vref< Present selected Tap Voltage

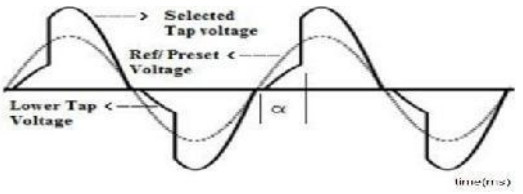

Fig. 6. Firing control between lower tap voltage & selected tap voltage

In this condition firing control is being performed between present selected tap and lower voltage tap, to reduce the voltage further to reach pre-set voltage.

V.BLOCK DIAGRAM DESCRIPTION

The proposed model consists of many blocks. Each and every block has its own features and applications

1. Full Wave Rectifier
2. LM324 (Operational Amplifier)
3. Flip flop
4. Timer
5. Counter
6. Decoder
7. Pulse Transformer
8. SCR Controlled Regulator
9. Voltage Regulator
10. SCR control board

Each of the blocks is individually and elaborately mentioned in this chapter. The proposed model consists of varying load but the output voltage is constant.

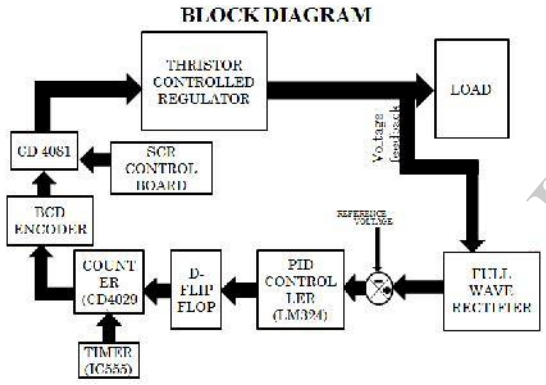

Fig. 7. Block diagram of the proposed system

A. *Pulse transformer*

Pulse transformer designers usually seek to minimize voltage droop, rise time, and pulse distortion. Droop is the decline of the output pulse voltage over the duration of one pulse. It is caused by the magnetizing current increasing during the time duration of the pulse. It is used to avoid core saturation and therefore needs to understand the voltage-time constant. Pulse Transformers are small in size and provide all the desirable qualities expected from the transformers designed to handle square pulses. The Magnetic flux in a typical AC transformer core alternates between positive and negative values. But the Magnetic flux in a pulse transformer does not. Pulse transformer operates in a unipolar mode.

B. *Voltage regulator*

Any Electrical or Electronic device that maintains the voltage of a power source within the acceptable limits and the voltage regulator is needed to keep the voltages within the prescribed range that can be tolerated by the electrical equipment using that voltage. Voltage Regulators used in Electronic equipment in which excessive variations in voltage would be determined.

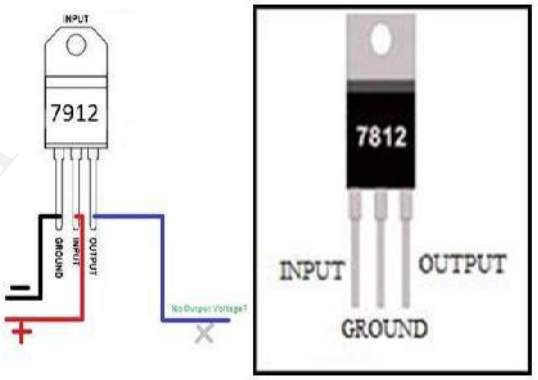

Fig. 8. Pin diagram of 7912 and 7812

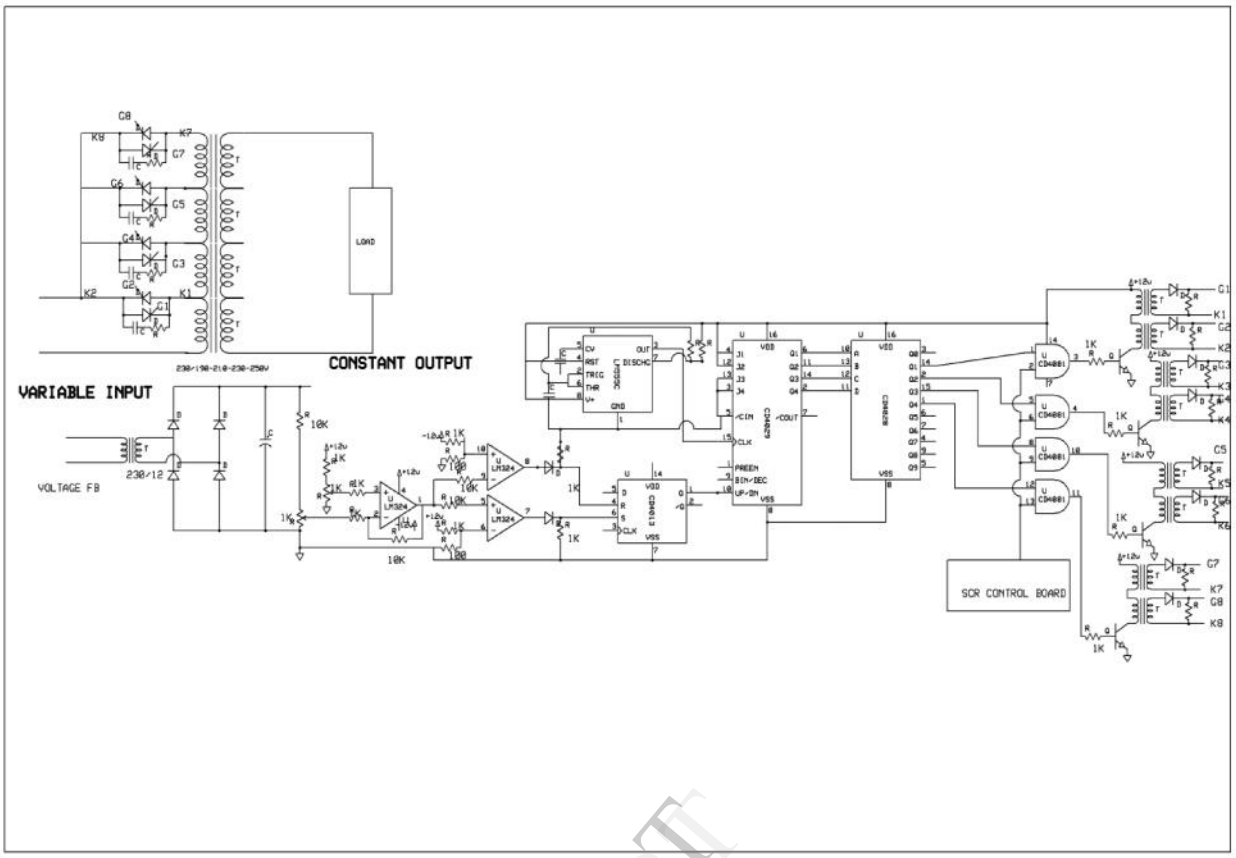

Fig. 9. Circuit Diagram of the Proposed Model.

In this project we are using 7812 as a positive regulator. The input may be 16V or even 20V, output will be 12V. Here the negative side is taken as common line, common to both input and output. 7912 is a negative regulator. You can derive -12 from -16 to -20V. The positive of the input is common to both input and output.

VI. CIRCUIT DESCRIPTION

The hardware of the proposed model consists of three taps on the winding of the transformer to regulate the voltage at the consumer side. The circuit diagram of the proposed model is briefly explained.

The power source is connected to the cathode K1 and K2 and anode G1 and G2 of the thyristor switch. Thyristor gets triggered and the voltage is fed to the load. The voltage feedback is taken from the lines feeding the load. Then voltage feedback is connected to the 230/12 V step down transformer followed by rectifier circuit with filter. Hence the output from the full wave rectifier will be smooth DC voltage. This DC voltage is compared with the reference voltage with the help of LM324 comparator. The error voltage from the comparator circuit is used to modulate the counter values. Depending upon counter value the pulse width is modulated, where the pulses are generated with the help of IC555 and the modulated pulse width output is taken from the JAM lines of the counter.

The output from the counter is binary; hence it is connected to the decoder which makes only one pin to HIGH at any time. So the corresponding AND gate connected to the output pin of the counter will be triggered. The modulated pulse signal is given to the pulse transformer to switch the thyristor to increase/decrease the tap based upon the voltage feedback to regulate the voltage on the consumer side.

VII.CIRCUIT OPERATION

The implementation of the hardware falls into two categories, it either increase the tap position or decrease the tap position depending upon the under load or overload condition. This can be briefly explained by the following two cases.

Case 1: Consider a case if the loads connected to the supply are suddenly switched off, the voltage of the lines feeding the loads will be increased; hence the voltage feedback gets increased. The feedback voltage is stepped down by 230/12 V transformer and fed to full wave rectifier. This causes the output from full wave rectifier to rise. This voltage is compared with the reference DC voltage by using a comparator LM324. The comparator produces negative error at the output of the comparator. This error is taken by the upper negative reference comparator to increase the gain of the error signal. This error signal forward biases the diode and fed to reset terminal of the flip flop. Because of the reset terminal gets triggered, output of the flip flop will be LOW. Hence the counter counts down. Clock pulses generated from the IC555 is given to the counter to count the number of clock pulses. The output of the counter will be binary output. It is then given to the input to the decoder. Only one pin of the decoder is enabled as HIGH. This high pulse waveform is

connected to the one of the input of AND gate and the other input is connected from the timer IC555. So for each clock cycle at some period of time, the two inputs will be same. At that time the pulse wave form is generated at the output of the AND gate and is given to the pulse transformer. Pulse transformer generates pulses to trigger the gate of the thyristor and then the tap gets decreased to maintain the constant output voltage.

Case 2: Consider a case if the loads connected to the supply are suddenly increased, the voltage of the lines feeding the loads will be decreased; hence the voltage feedback gets decreased. The feedback voltage is stepped down by 230/12 V transformer and fed to full wave rectifier. This causes the output from full wave rectifier to lower. This voltage is compared with the reference DC voltage by using a comparator LM324. The comparator produces positive error at the output of the comparator. This error is taken by the lower positive reference comparator to increase the gain of the error signal. This error signal forward biases the diode and fed to set terminal of the flip flop. Because of the set terminal gets triggered, output of the flip flop will be HIGH. Hence the counter counts up. Clock pulses generated from the IC555 is given to the counter to count the number of clock pulses. The output of the counter will be binary output. It is then given to the input to the decoder. Only one pin of the decoder is enabled as HIGH. This high pulse waveform is connected to the one of the input of AND gate and the other input is connected from the timer IC555. So for each clock cycle at some period of time, the two inputs will be same. At that time the pulse wave form is generated at the output of the AND gate and is given to the pulse transformer. Pulse transformer generates pulses to trigger the gate of the thyristor and then the tap gets increased to maintain the constant output voltage.

A. *Scr Controlled Regulator*

A Thyristor (silicon controlled rectifier or SCR) is a little like a transistor. It consists of four layers of silicon in a p–n–p–n structure. Its circuit symbol shows that it is basically a diode, but with an additional terminal, called the GATE. The purpose of the gate is to enable the device to be switched from a non-conducting (forward blocking) mode into a low resistance, forward conducting state. Thus a small current applied to the gate is able to switch a much larger current (at a much higher voltage) applied between anode and cathode. Once the thyristor is conducting however, the gate current may be removed and the device will remain in a conducting state.

To turn the thyristor off, the current flowing between anode and cathode must be reduced below a certain critical "holding current" value, (near to zero); alternatively the anode and cathode may be reverse biased. The thyristor is normally made to conduct by applying a gating pulse, while the main anode and cathode terminals are forward biased. When the device is reverse biased the gating pulse has no effect.

VIII. SIMULATION RESULTS

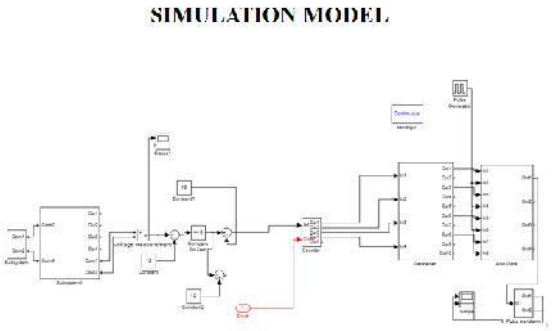

Fig. 10. Simulation Model Using MATLAB.

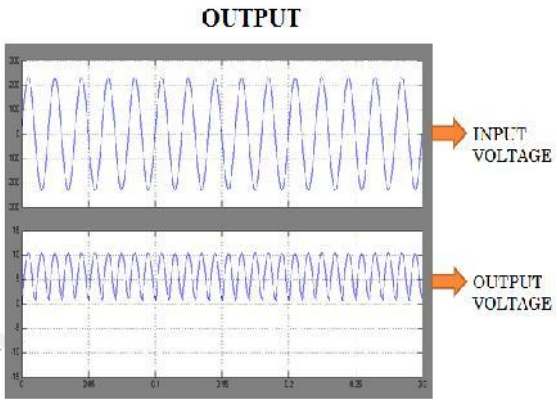

Fig. 11. Simulation Of Output Voltage.

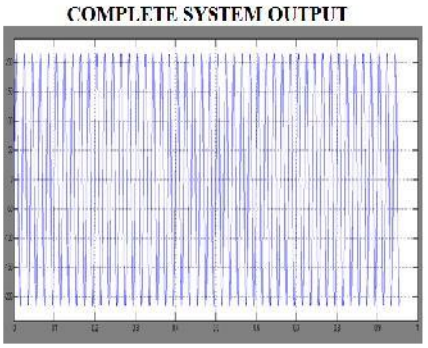

Fig. 12. Complete System Output (Output Side To Maintain the Constant Output Voltage)

IX. CONCLUSION

The way distributed networks are operated now-a-days is properly conditioned by the need to keep the voltage magnitude within the acceptable limits especially at the LV levels on penetration of the Distributed Generation. This requirement is achieved by Mechanical tap changers. Power Electronic semiconductor switches which are becoming cheaper and more reliable, hence offer better opportunities to provide added control flexibility. In this project solid state tap changer employing thyristor switch control with 3 tap positions is proposed to regulate the voltage at the consumer side depending on the voltage

feedback taken from the load side. Pulse Width Modulation (PWM) technique is adopted for sequential switching of the thyristor.

X. FUTURE ENHANCEMENT

The magnitude of output voltage which needs to be maintained constant cannot be altered in the proposed model. But it is possible by changing the reference point. Changing the reference point in the proposed model is not possible because of the technical difficulties. A fuzzy algorithm can be adopted to provide an adaptive reference of the OLTC controller which can mitigate the effect of the high penetration of the DG units. The motivations behind using the fuzzy logic are:

- It can map nonlinear relations behind its inputs and output.
- It can provide a smooth transition, which lead to a more relaxed tap operation.
- It requires less remote data measurements compared to the centralized approaches.

REFERENCES

1) J. Faiz and B. Siahkolah, "New Solid-State On load Tap-Changers Topology For Distribution Transformers", IEEE Trans. on Power Delivery, vol.18(1), pp. 136-141, January 2003.

2) Cigre, Working Group B4.35, "Thyristor controlled voltage regulators", February 2004.

3) R. Shuttleworth, A.J. Power, X. Tian, H. Jiang, and B. A. T. Al Zahawi, "A novel thyristor-assisted tap changer scheme," in *CIRED 97, IEE Con!erence Publication No. 438*, pp.1.28.1-1.28.5, June 1997.

4) Su Z G, Li J S. Developing trends of on-load tap-changer based on Power electronic technology. Power Electric,24(4): 43-45,June 2005.

Congestion Management by Particle Swarm Optimization

T.Harish kumar,
PG Scholar,
M.E(power Systems Engineering),
Joseph's college of engineering,

Mrs.V.C. Eugin Martin Raj, M.E,
Assistant professor,
Department of Electrical and Electronics, St
St Anne's College of Engg and Tech,

Abstract: **The electricity industry throughout the world, which has long been dominated by vertically integrated utilities, is undergoing enormous changes. The electricity industry is evolving into a distributed and competitive industry in which market forces drive the price of electricity and reduce the net cost through increased competition. The objective of deregulated power system is to provide a reliable power at competitive price. Congestion in the system would cause the objective failure. To overcome this effective congestion management s required. Congestion management is one of the key features of System Operator. There are many congestion management techniques available like operation of FACTS devices, outages of congested lines, Re-dispatching of generators, load curtailment, etc. whenever an raise in load at particular bus or an outage of line due to fault occurs in the system the line flow in the system hit its transfer limits thus causing the system to be in a congested state. In this work minimizing the line flows are taken as objective function and thus the generators are re-scheduled to elevate congestion in the system.**

I. INTRODUCTION

The electrical power supply industry around the world has experienced a period of rapid and irreversible change since the middle of 1980. the need for more efficiency in power production and delivery has led to a restructuring of the power sectors in several countries traditionally under control of federal and state governments. the privatization process in great britain is the best known example, followed by others such as spain, new zealand, argentina and chile. even in countries with privately own utilities, such as the u.s., there has been a strong drive towards deregulation and a more intense participation of third-party generation. other countries also considering the restructuring of their electricity power sector so as to introduce more competition among producers and to offer more choices for customers. those changes are concerned with the ownership and management of the industry. under deregulation, the former vertically integrated utility, which performed all the functions involved in power i.e. generation, transmission, distribution and retail sales, is dis-aggregated into separate companies devoted to each function. the electricity bill for end consumer now involves at least two components: one from the distribution and transmission network-operator responsible for the network and services, and the other from the company that generates the electrical energy. this for many decades, vertically integrated electric utilities (viu) monopolized the way they controlled, sold and distributed electricity to customers in their service territories. this monopoly involves three main sectors namely: generation company (genco), transmission company (transco) and distribution company (disco).

Monopolies could not provide services as efficiently as competitive firms. The electric power industry plans to improve its efficiency by providing a more reliable energy at least cost to customers. A competition is guaranteed by establishing a restructured environment in which customer could choose to buy from different
suppliers and change suppliers as they wish in order to
pay market-based rates.

II. CONGESTION

Whenever the physical or operational constraints in a transmission network become active, the system is said to be in a state of congestion. The possible limits that may be hit in case of congestion are, line thermal limits, transformer emergency ratings, us voltage limits, transient or oscillatory stability, etc. These limits constrain the amount of electric power that can be transmitted between two locations through a transmission network. Flows should not be allowed to increase to levels where a contingency would cause the network to collapse because of voltage instability.etc.

The peculiar characteristics associated with electrical power prevent its direct comparison with other marketable commodities. First, electrical energy cannot be stored in large chunks. In other words, the demand of electric power has to be satisfied on a real time basis..Due to other peculiarities, the flexibility of directly routing this commodity through a desired path is very limited. The flow of electric current obeys laws of physics rather than the wish of traders or operators. Thus, the system operator has to decide upon such a

pattern of injections and take-offs, that no constraint is violated. Congestion, as used in deregulation parlance, generally refers to a transmission line hitting its limit. The ability of interconnected transmission networks to reliably transfer electric power may be limited by the physical and electrical characteristics of the systems including any or more of the following.

- Thermal limits
- Voltage limits
- Stability limits

III. IMPORTANCE OF CONGESTI0N MANAGEMENT IN THE DEREGULATED ENVIRONMENT

If the network power carrying capacity is infinite and if there are ample resources to keep the system variables within limits, the most efficient generation dispatch will correspond to the least cost operation Kirchoff's laws combined with the magnitude and location of the generations and loads, the line impedances and the network topology determine the flows in each line. In real life, however, the power carrying capacity of a line is limited by various limits as explained earlier. These power systems, security constraints may therefore necessitate a change in the generator schedules away from the most efficient dispatch. In the traditional vertically integrated utility environment, the generation patterns are fairly stable. From a short term perspective, the system operator may have to deviate from the efficient dispatch in order to keep line flows within limits. However, the financial implication of such re-dispatch does not surface because the monopolist can easily socialize these costs amongst the various participants, which in turn, are under his direct control. From planning perspective also, a definite approach can be adopted for network augmentation.

However, in deregulated structures, with generating companies competing in an open transmission access environment, the generation/flow patterns can change drastically over small time periods with the market forces. In such situations, it becomes necessary to have a congestion management scheme in place to ensure that the system stays secure; however, being competitive environment, the re-dispatch will have direct financial implications affecting most of the market players creating a set of winners and losers. Moreover, the congestion bottlenecks would encourage some strategic players to exploit the situation.

EFFECTSS OF CONGESTION

- Market inefficiency
- Market power
- Economic efficiency

CONGESTION MANAGEMENT SCHEME MUST SATISFY THE FOLLOWING

- Non discriminative
- Be transparent

IV. OPF BASED CONGESTION MANAGEMENT

The general idea of nodal pricing is to model an electricity market with its various economical and technical specifications, such as generators' cost functions, demand elasticity, generation limits, line power flow limits and optimize the system for maximizing social welfare. This problem represents one of the commonly employed formulations of Optimal Power Flow (OPF). The name OPF does not stand for any specific optimization problem, rather a number of optimization problems falls onto the OPF category, the basic aim of an OPF analysis is to reach an optimum power transfer situation without violating the network constraints. In other words, the congestion management problem, with a set of constraints representing network constraints.

The practical OPF uses a formulation wherein ac power flow equations are added to the economic dispatch as equality constraints with inequality constraints involving the flow MW, MVA or current on a transmission line and voltages at a substation bus. A version of OPF is developed that takes into account various contingencies referred to as security constrained OPF or SCOPF. OPF problems are formulated with a number of objectives. A brief list is outlined here:

- Minimize the total cost of production
- Maximize total social welfare
- Minimize total system loss
- Minimize the re-dispatch cost
- Minimize the total adjustment

V. PARTICLE SWARM OPTIMIZATION

Particle swarm optimization (PSO) is a population based stochastic optimization technique developed by Dr. Eberhart and Dr.Kennedy in 1995, inspired by social behavior of bird flocking or fish schooling.

PSO shares many similarities with evolutionary computation techniques such as Genetic Algorithms (GA). The system is initialized with a population of random solutions and searches for optima by updating generations. However, unlike GA, PSO has no evolution operators such as crossover and mutation. In PSO, the potential solutions, called particles, fly through the problem space by following the current optimum particles. The detailed information will be given in following sections.

Compared to GA, the advantages of PSO are that PSO is easy to implement and there are few parameters to adjust. PSO has been successfully applied in many areas: function optimization artificial neural network training, fuzzy system control, and other areas where GA can be applied.

THE ALGORITHM

As stated before, PSO simulates the behaviors of bird flocking. Supposes the following scenario: a group of birds are randomly searching food in an area. There is only one piece of food in the area being searched. All the birds do not know where the food is. But they know how far the food

is in each iteration. So what'sthe best strategy to find the food? The effective one is to follow the bird which is nearest to the food.

PSO learned from the scenario and used it to solve the optimization problems. In PSO, each single solution is a "bird" in the search space; we call it "particle". All of particles have fitness values which are evaluated by the fitness function to be optimized; and gave velocities which direct the flying of the particles. The particles fly through the problem space by following the current optimum particles.

PSO is initialized with a group of random particles (solutions) and then searches for optima by updating generations. In every iteration, each particle is updated by following two "best" values. The first one is the best solution (fitness) it has achieved so far. (The fitness value is also stored.).The value is called pbest. Another "best" value that is tracked by the particle swarm optimizer is the best value, obtained so far by any particle in the population. This best value is a global best and called the gbest. When a particle takes part of the population as its topological neighbors, the best value is a local best and is called lbest.

After finding the two best values, the particle updates its velocity and positions with following equations.

v[]=v[]=c1*rand()*(pbest[]-present[]+c2*rand()*(gbest[]-present[]
present []=present]+v[]

where

v [] is the particle velocity, Present [] is the current particle (solution).

Pbest [] and gbest [] are defined as stated before.

Rand () is a random number between (0,1)

c1, c2 are learning factors. Usually c1=c2=2.

VI. SOLUTION METHODOLOGY

The mathematical formulation is given the line flows are taken as objective function. Whenever a fault or overload contingency occurs in the system then some lines hit their limits causing congestion in the system. The generators are re-dispatched such that the congestion in the system is elevated.

ASSUMPTIONS

The following assumptions are made so as to reduce the complexity of the presentation problem

- Bus voltage assumed to be constant at 1 p.u.
- PV buses are numbered from 1 to N-1 where N is the total no. of buses.
- Nth bus is taken as a reference bus where phase angle =0

PROBLEM FORMULATION

To determine:

Optimal scheduling of generators P_{gi} i=1, 2...NG

Objective function

Minimize line flow $\sum S_{ij}$ i=j=1,2,…nbs

Subject to:

Equality constraint:

Load angle mismatch

$\delta = o$

Load balance equation

$P_{gi} = P_{di}$

Inequality constraint:

Line flow constraint : $g\ \theta\ - g^{max} \leq o$

Limits: $P_{gi_{min}} \leq P_{gi} \leq P_{gi_{max}}$ i=1, 2……NG

Where

$\theta = [\theta_1, \theta_2, \ldots \ldots \ldots, \theta_{N-1}]$ Represents the voltage phase angle.

g(θ) is the vector of the active power flow carried by transmission lines.

g^{max} Is the vector of the transmission line rating.

P_{gi} Is the real power generation of ith generator.

P_{gimax}, P_{gimin} are minimum and maximum generation limits.

Nbs is the number of bus.

NG number of generators.

S_{ij} line flow.

VII. RESULTS AND DISCUSSION CONTINGENCY CONDITIONS

CASE A	OVER LOADED LINES	LINE FLOW	LINE LIMITS	VIOLATION
Load at bus 14 raised by 80% from base case loadings with line 1 – 2 out	1 – 3 3 – 4	153.077 141.094	130 130	34.171
Load at bus 19 raised by 55% from base case loadings with line 1 – 2 out	1– 3 3 – 4	153.567 141.522	130 130	35.089

RESULT AFTER SCHEDULING

CASE A	OVER LOADED LINES	LINE FLOW	LINEFLOW AFTER RESCHEDULING	VIOLATION
Load at bus 14 raised by 80% from base case loadings with line 1 – 2 out	1 – 3 3 – 4	153.077 141.094	130 130	NIL
Load at bus 19 raised by 55% from base case loadings with line 1 – 2 out	1– 3 3 – 4	153.567 141.522	129.41 120.27	NIL

CASE B	OVER LOADED LINES	LINE FLOW	LINE LIMITS	VIOLATION
load at bus 14 raised by 80% from base case loadings	1 – 3 3 – 4	146.9 135.764	130 130	22.664

CASE B	OVER LOADED LINES	LINE FLOW	LINEFLOW AFTER RESCHEDULING	VIOLATION
load at bus 14 raised by 80% from base case loadings with line 1 – 2 out	1 – 3 3 – 4	146.9 135.764	129.45 120.30	NIL

GENERATOR RESCHEDULED VALUES

CASE A(**1**)	CASE A(2)	CASE B
Overloaded lines=0	Overloaded lines=0	Overloaded lines=0
Generator reschedule G1= 61.8019 G2= 31.4515 G3= 35.2538 G4= 24.9058 G5= 17.9127 G6= 35.2879	Generator reschedule G1= 54.3771 G2= 33.6175 G3= 38.0149 G4= 20.6371 G5= 21.7172 G6= 34.456	Generator reschedule G1= 59.377 G2= 31.317 G3= 37.014 G4= 18.637 G5= 19.717 G6= 28.148

are first evaluated and the local best termed as best is updated for all particles and then the local best termed as best is updated. This process is continued until the global best is achieved. The global best gives the generator rescheduled and thus the load flow is performed and the line limit violations are identified to be within the thermal limits. Thus the generators are rescheduled for the contingency condition and the outputs are verified.

VIII. CONCLUTION

The base case load flow is performed and the line flows are identified as within the limits. A contingency condition whit overloading and outage of line is created and the load flow analysis is performed and the overloaded lines are identified and this result are shown. The data's are loaded to the optimization problem as given and the particle swarm optimization technique which uses the generators as population and

IX. REFERENCES

(1) Ettore Bompard, Member, IEEE, Pedro Correia, George Gross, Fellow, IEEE, and Mikael Amelin "Congestion-Management Schemes: A Comparative Analysis Unified Framework",IEEE transactions on power systems, vol. 18, no. 1, February 2003

(2) Tulika Bhattacharjee , Ajoy Kumar Chakraborty "Congestion Management In Deregulated power System By Rescheduling Of Sensitive Generators And Load Curtailment Using PSO", IJETAE Volume 2,Issue 3, March 2012,

(3) Naresh Acharya, N. Mithulananthan "Locating Series FACTS Devices For Congestion Management In Deregulated Electricity Markets" Electric Power System Management, Energy Field of Study, Asian Institute of Technology, 2 May 2006.

(4) Management Of Multiple Congested Conditions In Unbundled Operation Of A Power System, Hans Glavitsch swiss federal institute of technology zurich, Switzerland, Fernando Alvarado The University of Wisconsin Madison, Wisconsin, USA, IEEE Transactions on Power Systems, Vol. 13, No. 3, August 1998.

(5) Transmission Congestion Management In An Electricity Market R.S. Fang A.K. David Department Of Electrical Engineering Hong Kong Polytechnic University kowloon, Hong Kong, IEEE Transactions on Power Systems, Vol. **14,** No. 3, August 1999.

D-Statcom with PI Controller for Voltage Stability

A. Sherly
Jayaram college of engineering and technology
Electrical and Electronics Engineering Trichy

G. Susithra
Jayaram College of engineering and technology
Electrical and electronics Engineering
Trichy

Abstract— In this paper the voltage stability is achieved by the distribution static compensator. The distribution static compensator is a shunt connected device consisting of a voltage source converter, which absorb or inject the current to the system. The STATCOM is connected at the load end or distribution side is termed as D-STATCOM in order to achieve the voltage stability. The D-STATCOM is controlled by PI controller.

***Index Terms*—** D-STATCOM, voltage stability, PI Controller

I. INTRODUCTION

The generation of electricity and consumption has been increased due to the load growth. Now a days the loads are mostly drawn the reactive power [1]. Due to the enormous consumption of reactive power the power system subjected to the power quality problems. Among the power quality issues the under voltage issues are occurred due to the consumption of reactive power and it is stated as the voltage magnitude decreased between 0.9 p.u to 0.1 more than 0.5sec. The requirements of reactive power compensation are,

1. To maintain voltage stability in order to improve the active power along the transmission lines
2. To provide load compensation in order to improve the power factor and better regulation of voltage due to the large fluctuating loads
3. To provide voltage support to electronics controllers .These devices are sensitive to voltage disturbances [2].

This reactive power compensation is achieved using the shunt compensation. In conventional methods the shunt compensation is achieved by capacitors and reactors. Due to the switching of devices, the transient problems are occurred. In order to avoid these problems the FACTS devices are introduced [3]. A Flexible AC transmission system incorporates power electronics devices and controllers to enhance controllability and increase the power transfer capability [4]. FACTS devices can improve power system operations are by providing a means to control power flow, to improve stability, and to better utilize the existing transmission infrastructure [5]. Recently the Distributed Flexible AC Transmission System (D-FACTS) devices are introduced [6-8]. D-FACTS devices are power flow control devices which are small, lightweight, and made of easily purchased mass-produced parts. The static compensator is applied in a distribution system is called as D-STATCOM and it is used for reactive power compensation of industrial loads and also stability improvements for wind turbine system [9]

II. BASIC PRINCIPLE OF DSTATCOM

A Distribution Static Compensator is a three phase shunt connected device. It consists of a Voltage Source Converter (VSC) and DC link capacitor. It is connected in a shunt manner and it is have the capacity of generating and/or absorbing reactive power. The operating principles of a distribution static compensator are same as the synchronous compensator. The AC terminals of a VSC are connected to the Point of Common Coupling (PCC) through the inductance; the inductance can be a filter inductance or the leakage inductance of the coupling transformer, as shown in Fig. 1[10].

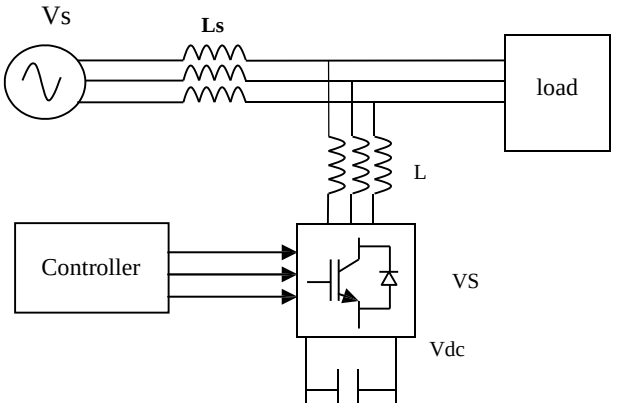

Figure 1.Basic structure of D-STATCOM

III. MODES OF OPERATION OF D-STATCOM

There are three modes of operation in the D-STATCOM with its output current is known as I, it changes according to v_i . If $v_i=v_s$, then reactive power will be 0 and also the D-STATCOM will not produce or absorb the reactive power.

Whenever vi will be greater than vs, the D-STATCOM will act as an inductive reactance over its terminal and the equipment will generate capacitive reactive-power. When Vs is larger than VI, the distribution static compensator is seen by the system as capacitive reactance. When the flow of the current is from the alternating current system to the D-STATCOM it will result in the absorption of the inductive Power [11].

a) No load mode (Vs = Vi)
b) Capacitive mode (Vi > Vs)
c) Inductive mode (Vi < Vs)

provides a faster response, flexible to control and easy to implement the controllers. The control algorithm of a DSTATCOM are mainly implemented in the following steps:

1. Measurements of system voltages, current and Signal conditioning.
2. Calculation of compensating signals.
3. Generation of firing angles of switching devices.

Different control schemes employed in a control strategies.
1. Phase Shift Control
2. Decoupled Current Control (p-q theory)
3. Hysteresis control [12].

S.NO	ALGORITHMS ↓ PARAMETE	PHASE SHIFT CONTROL	DECOUPLED CURRENT CONTRO	REGULATION OF AC/DC LINK VOLTA
1	REACTIVE POWER COMPENSA	Partial	Complete	Complete
2	PERFORMAN CE UNDER BALANCED AND NONLINEAR LOADS	Contains undesired harmonics in case of nonlinear load	Satisfactory in case of linear loads	Capable to maintain upf and below 5% harmonic level in both the
3	APPLICABLE FOR SINGLE PHASE	Yes	No	Yes
4	TOTAL HARMONIC	----	Much higher than 5%	Below 5%

Table 1. Comparison of control algorithm

V. PHASE SHIFT CONTROL

In this method the voltage regulation is achieved by D-STATCOM by the measurement of rms ac voltage at the load side and the sinusoidal Pulse width Modulation technique is used. This control is simple and gives good response. The error signal is obtained by comparing the measured voltage and the reference voltage.

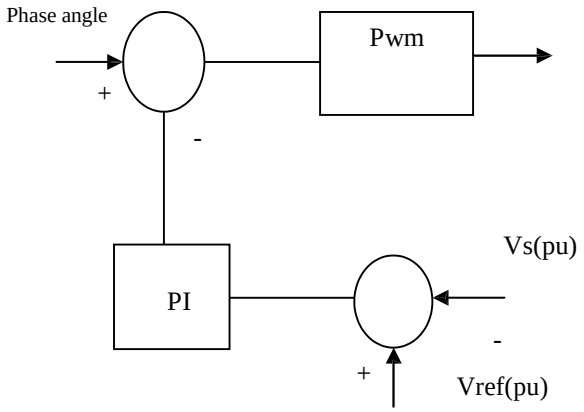

Figure 2. Block diagram of phase shift control

The error signal is fed to the PI controller which generates the necessary phase angle that decides the phase shift between the VSC output voltage and the terminal voltage.
The source current and the source voltage are in phase, inorder to correcting the power factor of the system during balanced fluctuating load.[12][13].

VI. TEST CASE

The simulation are carried out in Simulink with the data presented in the table 2 and the results are compared with and without DSTATCOM.

Three phase source	230kV, 50 HZ
DSTATCOM capacitor	750 microfarad
Load 1	250 KW 100 VAR
Load 2	10 KW, 100 VAR

Table 2. Test System Data

The source voltage maintained at 11KV and the loads are connected to the distribution system.

VII. SIMULATION RESULTS

A. Without D-Statcom

The simulation results are carried out without DSTATCOM. And the voltage magnitude valued are in maintained in 0.65pu value. Due to load the voltage value are dipped.

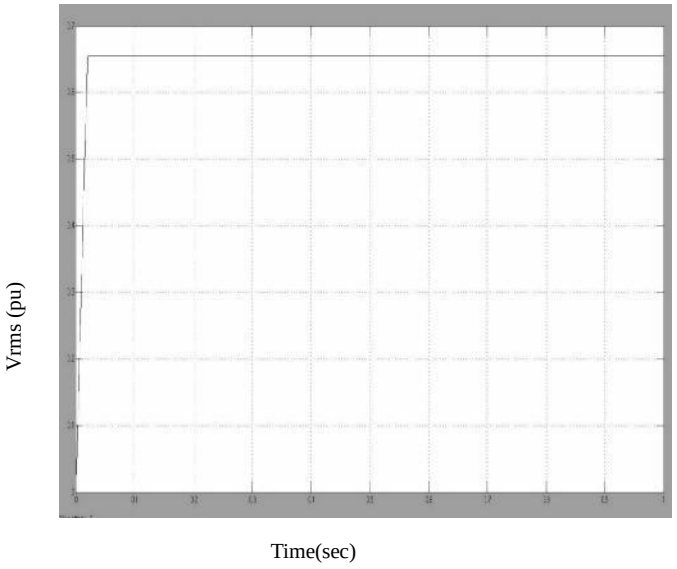

Figure 3. The Voltage Magnitude Value without D-Statcom

The graphs are plotted between the voltage magnitude in per unit value to the time

B. WITH D-STATCOM

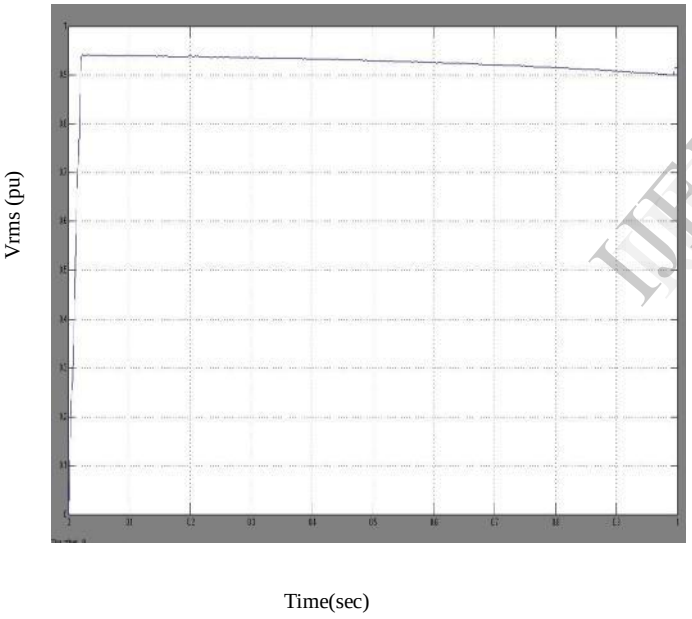

Figure 4. The voltage magnitude value with d-statcom

While adding d-statcom the voltage profile value is improved. The voltage value is improved from 0.65 to 0.95pu

VIII. CONCLUSION

The voltage stability improvement by using distribution static compensator is simulated in this paper. The simulation shows that the voltage profile improved using D-STATCOM.

IX. REFERENCES

[1] Deepak Divan "Improving power line utilization and performance with D-FACTS devices" *IEEE transaction 2005*

[2] Mr.Vinod S.Tejwani, Mr.Hites B. Kapadiya, Dr.A S Pandya, Mr.Jignesh B Bhati " Power Quality Improvement in power distribution system using D-STATCOM" *Nirma university international con!erence on engineering 2013*

[3] Abhishek Kumar, Vinay Kumar Dwivedi and Mohit Bajaj "Performance comparison of control algorithms for load compensation using D-STATCOM under abnormal source voltage" *Journal o! automation and control engineering vol. 2,No 1, march 2014*.

[4] Singh Bhim and Solanki Jitendra, 2009. "A comparison of control algorithms for DSTATCOM", *IEEE Transactions on IndustrialElectronics, vol.56, no.7, pp.2738-2745*.

[5] Noramin Ismail and Wan norainin Wan Abdullah "Enhancement of power quality in distribution system using D-STATCOM" *the 4th international power engineering and optimization con!erence june 2010*.

[6] Molavi.H, Ardehali M.M "Application od distribution static compensator (D-STATCOM) to voltage sag mitigation" *universal journal o! electrical and electronics engineering 1(2):11-15,2013.*

[7] FACTS Working Group, "Proposed Terms and Definitions for Flexible AC Transmission System (FACTS)", *IEEE Transactions on Power Delivery, Vol. 12, Issue 4, October 1997, p 1848-1853*.

[8] Alper Cetin and Muammer Ermis " VSC Based D-STATCOM with selective harmonic elimination" IEEE transaction on industry applications vol 45, No 3 May / june 2009.

[9] Katherine M.Rogers and Thomas J.Overbye "Power Flow Control With Distributed Flexible AC Transmission System (D-FACTS) Devices", IEEE transaction2010.

[10] Deepika Masand, Shailendra Jain, Gayatri Agnihotri "control algorithms for distribution static compensator" IEEE transaction 2006.

[11] Mahesh K.Mishra , Arindam Ghosh and Avinash Joshi "operation of DSTATCOM in voltage control mode" IEEE transaction 2003

[12] Padiyar K.R., 2008. FACTS Controllers in Power Transmission and Distribution, New Age International, New Delhi.

[13] Narain G. Hingorani and Laszlo Gyugyi, "Understanding FACTS:concepts and technology of flexible AC transmission systems",1 st edition,IEEE PRESS, New York, 2000.

Design of Induction Motor using Magnet Software and Analysis using Finite Element Analysis

A. Richard Pravin
Assistant Professor

B. Siva
UG Student

V. Venkata Srinivasan
UG Student

Department of Electrical and Electronics Engineering
st. Anne's College of Engineering and Technology
Panruti, Tamil nadu, India.

***Abstract*—Induction motor is one of the most commonly preferred motors used in the industry due to its long life & rugged construction. Faults occurring in an induction motor can significantly affect the performance of the motor and the drive which is running it. This paper aims to design and an induction motor .To implement analysis first the machine is modeled using MAGNET software. The motor is studied under healthy conditions. In the model of induction rotor bars are studied mostly based on magnetic field analysis of the motor under healthy conditions.**

MAGNET Soltware, Finite Element Analysis, Magnetic Field Intensity (key words)

1. INTRODUCTION

Motors convert electrical energy to mechanical energy by the interaction of magnetic fields set up by in the stator & rotor windings. All the four motors have the same operating components: stator (stationary parts), rotor (rotating parts), bearings & enclosure. The name induction motor arises from the nature of the developed torque. Torque is developed when voltage is applied to the stator and current begins to flow in the stator windings.

The stator winding currents produce a magnetic field that rotates in a counterclockwise direction. The changing magnetic field of the stator induces electromotive force in the rotor cage winding. The induced emf causes current to flow and magneto motive force in the rotor windings. In turn the rotor mmfs produce a magnetic flux pattern which also rotates in the air gap at the same speed as the stator winding field. Induction motors are the most commonly used prime movers in industrial applications. They are best suited for constant speed applications. Speed control can also be done with the help of power converter circuits. The 3-phase squirrel cage induction motor is the workforce of the industry as it is rugged & reliable.

The interaction between the primary field and secondary currents produces torque from zero rotor speed onwards. The rotor speed at which the rotor currents are zero is called ideal no-load or synchronous speed. The rotor windings may be multiphase (wound motors) or made of bars short-circuited by end rings (cage rotors). All primary and secondary windings are placed in the uniform slots stamped into thin silicon steel sheets called laminations. The induction machine has a rather uniform air gap of 0.2 to 3mm.The secondary windings may be short circuited or connected to an external impedance or to a power source of variable voltage and frequency.

Induction motors are the most commonly used prime movers in industrial applications. They are best suited for constant speed applications. Speed control can also be done with the help of power converter circuits. The 3-phase squirrel cage induction motor is the workforce of the industry as it is rugged & reliable. Electrical related faults are frequently occurring faults in three-phase induction machine which will produce more heat on both stator and rotor winding. This leads to the reduction the life time of induction machine.

Stator winding fault in Induction Motors can be detected using Unknown Input Observer (UIO) & Extended Kalman Filter methods. They are used for speed estimation and fault detection methods respectively[1].Using analysis of permeance and MMF harmonics, frequency of air gap flux density harmonics which occur due to irregularities are calculated. It helps in detecting faulty ball bearing conditions [2]. A procedure for electromagnetic design of three phase Induction Motor is discussed. This procedure is based on self-consistent equations. The electrical and magnetic properties are imposed by the user but the geometric dimensions are automatically calculated [3].The choice between Copper rotor bar s and

fabricated Aluminum rotor bars is discussed and debated. The fundamentals of rotor construction and basic information on how the Induction Motor works are discussed [10]. The new IEC standard which defines the stator winding insulation requirement when the Induction Motor operates with Adjustable frequency drives (AFDs) is discussed. The magnetic noise that may be generated if higher frequency voltage harmonics are present in the AFD is minimized.

2. DESIGNING THE THREE PHASE INDUCTION MOTOR USING MAGNET SOFTWARE

Designing the induction motor consists of designing the stator, rotor, ball bearings, end rings & shaft. The stator consists of the stator core & winding. Stator core is made up of laminated sheet steel of thickness of 0.5mm. The stator core internal diameter & length are the main dimensions of the induction motor. All the values of the diameter & length have been by measuring them from a real induction motor. Hence the respective values for diameters of different parts are:

1. Stator frame-600mm
2. Stator Bore-460mm
3. Rotor-324mm
4. Shaft-1mm
5. Ball bearings-2.2mm
6. End Rings-3mm

The length of the motor has been assumed to be 40.5mm. Air gap can be calculated from the following formulae:

Lg=0.2+2[(DL)^1/2] in mm where Lg-air gap, D=Diameter of the stator bore & L= Length of the motor.
Lg=0.2+D in mm where D is the diameter of the stator.

Rotor core is made up of laminated sheet steel of thickness 0.5mm.The Copper bars & end rings are directly casted over the rotor core. The current rating assigned=7.5Amperes & Number of conductors=100. When Copper is employed, the rotor bars are inserted on the slots from the end of the rotor & end-rings are joined to them by bracing. Cold Rolled Stainless Steel is used as design material for stator, rotor, and ball bearing. Aluminium is used for the construction of end ring. The bars used in the rotor are made up of Copper & are skewed. The conductors used are also made up of copper.

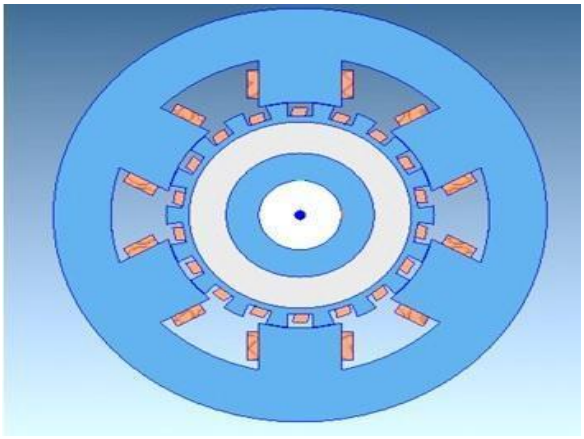

Fig 1: Designed Model of Three Phase Induction Motor Using MAGNET

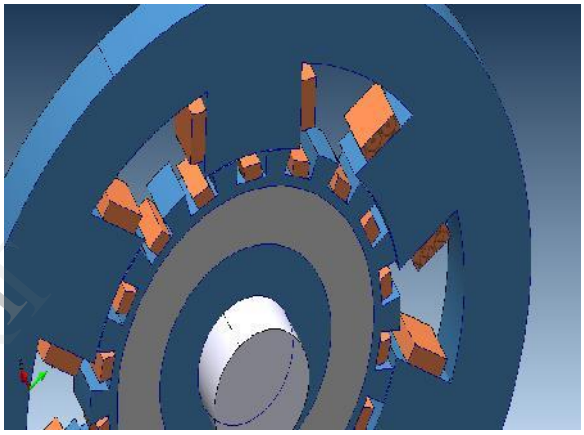

Fig.2.Close View of the Induction Motor

Fig.2. shows a close view of the induction motor modelled using MAGNET software. Shaft is denoted by the white coloured cylindrical structure protruding outside

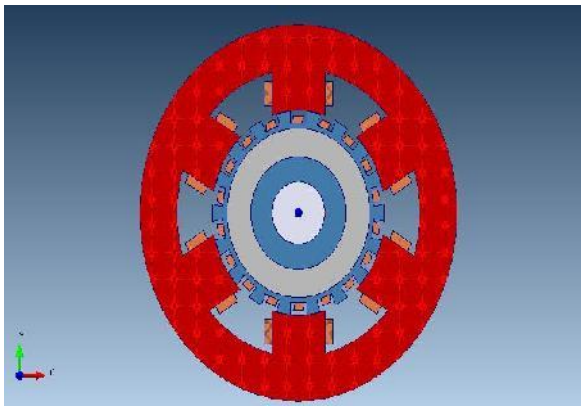

Fig. 3. Checking leakage of modelled induction motor

In MAGNET software an area depicted by the deep-red colour shown above is a proof that the component doesn't have any holes or leakage. In the above figure it means the stator component is perfectly designed and it doesn't have any leakages or air gap. Similarly the accuracy of the design of all the components was verified by implementing the features of the MAGNET software to all other parts

Fig.4. depicts the arrow plot of the magnetic field lines. The red colored lines show heavy magnetization while the blue color arrows show relatively weak magnetization. The direction of the magnetic field is in accordance with the polarity of the excitation. The left-hand side pole windings are given positive excitation & the right-hand side pole windings have been given negative polarity. Hence one can clearly see the magnetic flux lines rotating in an anticlockwise direction. The magnetic field is the strongest n ear the stator poles and then on the rotor slots. This observation is in accordance with the working principles of an induction motor

Fig.4. depicts the arrow plot of the magnetic field lines. The red colour lines show heavy magnetization while the blue colour arrows show relatively weak magnetization. The direction of the magnetic field is in accordance with the polarity of the excitation. The left-hand side pole windings are given positive excitation & the right- hand side pole windings have been given negative polarity. Hence one can clearly see the magnetic flux lines rotating in an anticlockwise direction. The magnetic field is the strongest n ear the stator poles and then on the rotor slots.

The application of the finite element method in the design of electrical machines is proficient in the determination of important design parameters, such as flux linkages, induced voltages, core losses, winding inductances and electromagnetic torque developed, with a very high accuracy.

3.FLUX PLOTS

Prediction of flux distribution is very useful for the design process. It gives the status of magnetic saturation throughout the machine as well as the ratio of leakage to useful flux in various parts of the magnetic circuit. Once the value of the vector potential has been determined at each node, the flux distribution is plotted.

4. CALCULATION OF FLUX LINKAGES

Consider one pole of the motor carrying a concentrated winding. The flux that is linked by a representative turn of a coil can be expressed in terms of the flux density B and the area enclosed by the coil. At this point, non-linear continuum problem, will be reduced to a set of non-linear algebraic equations. The most common solution method is the Newton - Raphson (N-R) algorithm and the resulting set of equations is solved by Gaussian elimination. The N-R algorithm starts from an assumed value for the reluctivity D and proceeds by means of iterations. In each iteration, D is updated with respect to the B-H characteristics of the material.

5. ANALYSIS OF THREE PHASE INDUCTION MOTOR

After the three phase motor was designed, it was simulated in 2D. The resultant magnetic field intensity plot was obtained and analyzed. The resultant field circle graph shows the magnetic field intensity at a radius of 160mm from the centre at various points around the circle. From point 0 to 0.05, H is highest as this part of the rotor comes directly under the stator and is the slot area of the rotor. Just as it reaches the edge of the rotor pole, it bec omes 0. It remains 0 from 0.05 to 0.1 as some of the part of this region falls in the air gap and most of the field lines pass through this region due to low reluctance

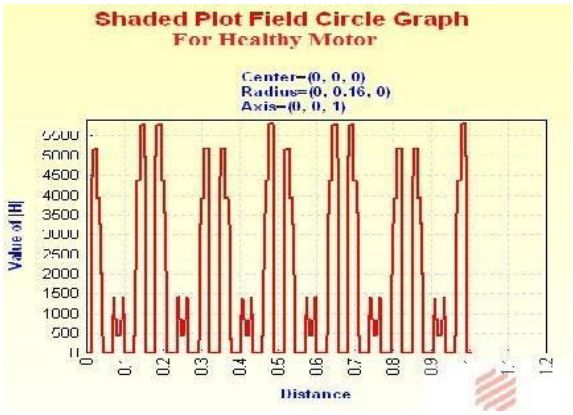

Fig. 5. Variation of Magnetic Field Intensity with Radii for Healthy Motor

The breaks in the peaks arise due to the positioning of the rotor copper bars with respect to the stator poles. When they are perfectly aligned, the field intensity is less compared to when they are just moving out of the influence of
1 stator pole & entering the influence of the second. The torque value was calculated to be
15.92 Nm under healthy conditions

6. CONCLUSION

A three phase induction motor was designed using MAGNET software. Its magnetic field intensity was analyzed near the rotor bars. Flux distribution and magnetic saturation are plotted and analysed for this three phase induction motor by using MAGNET software.

REFERENCES

[1] Knight A.M., Bertani S.P.: Mechanical Fault Detection in a Medium Sized Induction Motor Using Stator Current Monitoring, IEEE Transactions on Energy Conversion, Vol.20, No.4, December 2005.

[2] Dorrel D.G., Evans L., Staton D.A., Knight A.M.: Comparison of Permanent Magnet Drive Motor with a Cage Induction Motor Design for a Hybrid Electric Vehicle, The International Power Electronics Conference, 2010.

[3] Dorrel D.G., Combined Thermal and Electromagnetic Analysis of Permanent Magnet and Induction Machines to Aid Calculation, IEEE Transactions on Industrial Electronics, Vol 55, No.10.October 2008, pp.3566-3574.

[4] Ghazal M., Poshtan J., Robust Stator Winding Fault Detection in Induction Motors, 2nd

[5] Power Electronics, Drive Systems & Technologies Conference, 2011.

[6] Vargan L.M, Jatskevich J., Marti J.R., Load Modelling of an Induction Motor Operated with a Variable Frequency Drive, IEEE Electrical Power & Energy Conference, 2008.

[7] Arabaci H., Bilgin O., Effect of Rotor Faults in Squirrel - CagecInduction Motors on The Torque-Speed Curve, The 19th International Conference on Electrical Machines-ICEM 2010,Rome.

[8] Watson J.F., Paterson N.C., The Development of an Accurate Finite Element Model to Investigate the Factors which Influence the Fault-Indicating Components of Current in Three-Phase Induction Motors, The Ninth International Conference on Electrical Machines and Drives, Conference Publication No.468,pp. 247-252.

[9] Boglietti A., Cavagnino A., Lazzari M.,Geometrical Approach to Induction Motor Design, The 33 rd Annual Conference of the IEEE Industrial Electronics Society (IECON), Nov 5-8, Taipei, Taiean, pp.149-156.

[10] Nawrocki S., Hao L., Tang X., Modelling and Analysis of Weld Short Faults of Bar-Wound Propulsion IPM Machine, Part-2,Phase-to-Phase Short, IEEE Transactions, 2011.

[11] Hayes P.E.,Wood B.M.,Horn D.G., Mechanical Design of Induction Motors Applied on Adjustable Speed Drives, IEEE IAS PCIC Conference Record,1997.

Embedded based Maximum Power Demand Indicator and Controller for Efficient Power Management using Proteus

Ramesh J
Assistant Professor, EEE Department
St. Anne's College of Engg. & Technology
Panruti, India

Stephen Raj C
Final year B.E, EEE Department
St. Anne's College of Engg. & Technology
Panruti, India

Abstract— **The demand for energy is increasing as a result of the growth in both population and industrial development. To improve the energy efficiency, consumers need to be more aware of their energy consumption. In recent years, utilities have started developing new electric energy meters which are known as smart meters. A smart meter is a digital energy meter that measures the consumption of electrical energy and provides other additional information as compared to the traditional energy meter. The aim is to provide the consumer and supplier an easy way to monitor the energy. Smart energy meter can also store and review our consumer energy.**

Keywords*— *MDI, Power factor, Penalty, Load management

I. INTRODUCTION

Power is measured in momentary amounts, while energy is the vital of power over the long run. For instance, a 100 W light retains 100 W of power. On the off chance that worked for one hour, that light ingests 100 W - hours of energy. Greatest demand is the most extreme quick power devoured over a detailed window of time. On account of that 100 W bulb, as it is exchanged on and off, the immediate demand goes from zero to 100 W to zero, and so on. Not exceptionally intriguing. At the same time if that bulb is worked in parallel with a second 100 W light that is left on constantly, the demand will switch promptly between 100 W and 200 W, and the greatest demand of the blend will be 200 W. Presently, the way this is connected is that electric appropriation utilities frequently incorporate demand as one of the components used to focus the charge the buyer gets. Notwithstanding measuring incorporated energy utilization over the charging period (regularly a month), they additionally measure demand. Instead of measure genuinely immediate qualities, they really measure energy over a short window of time, and after that partition the energy devoured amid that interim by the length of the interim to touch base at successful peak esteem for the interim.

The best normal estimation of the power, apparent power, or current devoured by a client of an electric power system, the midpoints being assumed control progressive time periods, normally 15 or 30 minutes long and It is the best demand of burden on the power station amid a given period, i.e., the most extreme of every last one of demands that have happened amid a given period (may be a day, may be an hour, and so forth).

- Need of maximum demand in Electricity bill?

When the rate of electrical energy is charged on the basis of maximum demand of the consumer and the units consumed, it is called two-part tariff.

- In this total charge is divided into two.

1. Fixed charge depends on maximum demand of consumer.
2. Running charge depends on no. of units consumed. It is measuring by installing maximum demand meter. Charges are made on the basis of maximum demand in KVA and not in kW.

It is important to note that while maximum demand is recorded, it is not the instantaneous demand drawn, as is often misunderstood, but the time integrated demand over the predefined recording cycle.

As example, in an industry, if the drawl over a recording cycle of 30 minutes is:

2500 KVA for 4 minutes

3600 KVA for 12 minutes

4100 KVA for 6 minutes

3800 KVA for 8 minutes

The MD recorder will be computing MD as: (2500 * 4 + 3600 * 12 + 4100 * 6 + (3800 * 8)/

$$\frac{}{30} = 3606.7 \text{ KVA}$$

As can be seen from the Figure 1 below, the demand varies from time to time. The demand is measured over predetermined time interval and averaged out for that interval as shown by the horizontal dotted line.

I. MDI PENALTY

The MDI penalty can be avoided by improving the power factor and by using more efficient appliances.

The MDI penalty can be avoided by improving the power factor and by using more efficient appliances. Another option of avoiding MDI penalty is by shifting your peak load to a time of day when your load is less.

There are 2 methods of calculating MD (Maximum Demand):

Figure 1: Power and Demand Curve

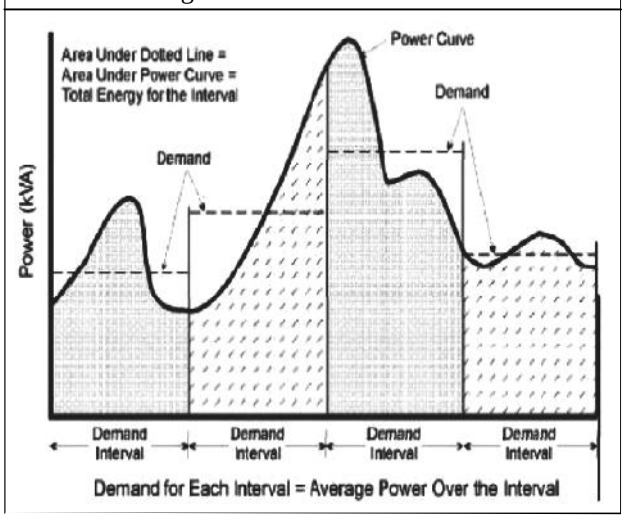

III. NORMAL OR BLOCK METHOD

Toward the end of each one fix integrating period, normal power for that period is ascertained. On the off chance that this quality is more noteworthy than officially existing esteem then this is put away as the MD.

IV. SLIDING WINDOW METHOD

Toward the end of a sub incorporating period the average power is ascertained for one coordinating period. In the event that this quality is more prominent than the officially existing esteem than this is put away as MD. The incorporating period slides by a window of the sub incorporating period (Capasso and so forth every one of the., 1994; and World Bank, 2012).

MO No.	MO No.	MO No.	MO No.
MD 1	MD 1	MD 1	MD 1
MD 2	MD 2	MD 2	MD 2

Assume a load pattern of following type:

$T = 09.00$, $T = 09.15$, $T = 09.30$, $T = 09.45$, $T = 10.00$

20 KVA, 30 KVA, 30 KVA, 20 KVA

15 mins, 15 mins, 15 mins, 15 mins

For MD 1 (Sliding window method) Demand – 09.00 to 09.30 block

$$\frac{(20 * 15 + 30 * 15)}{30} = 25\text{KVA}$$

Demand - 09.15 to 09.45 block

$$\frac{(30 * 15 + 30 * 15)}{30} = 30\ \text{KVA}$$

Demand - 09.30 to 10.00 block

$$\frac{(30 * 15 + 20 * 15)}{30} = 25\ \text{KVA}$$

MD 1 at the end of 10.00 = 30 KVA.

For MD 2 (Block method)

Demand - 09.00 to 09.30 block

$$= \frac{(20 * 15 + 30 * 15)}{30} = 25\ \text{KVA}$$

Demand - 09.30 to 10.00 block

$$= \frac{(30 * 15 + 20 * 15)}{30} = 30\text{KVA}$$

MD 2 at the end of 10.00 = 25 KVA Normally MD is reset on the first of every month, i.e., on a Monthly basis.

V. MICROCONTROLLER BASED MDI

The conventional greatest demand metering utilized conventional meters with current transformers and the meter dealt with a 15 moment normal with a pointer which showed the most extreme arrived at since the last time the pointer was reset.

It has several drawbacks, as:

The meter did not correspond precisely to the supply authority's meter values because of differences in the averaging times and differences in reset time.

This meter couldn't be monitored continuously and high greatest demand values were regularly recorded when problems happened on the factory and the administrator had neglected to recognize the excessive most extreme demand.

Figure 2: Microcontroller Based MDI

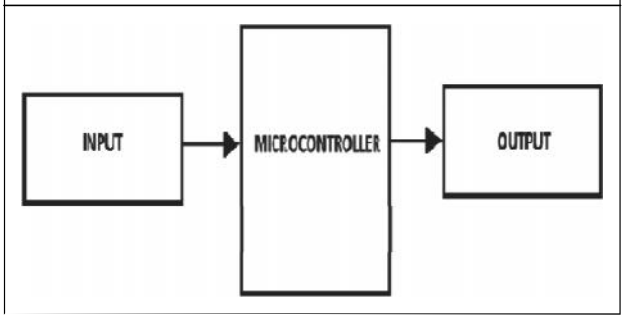

• It was very difficult to discover exactly when the maximum demand had been exceeded due to a lack of any recording.
• It was difficult to predict the effects of adding or removing load.

In addition to the measurement of the MDI this project has a capability of f detection and indication as there is a close relationship between the frequency and the power (demand/supply) which is shown in Figure 3 below.

VI. ELECTRICAL LOAD MANAGEMENT

Need for Electrical Load Management

In a macro perspective, the growth in the electricity use and diversity of end use segments in time of use has led to shortfalls in capacity to meet demand. As capacity addition is costly and only a long time prospect, better load management at user end helps to minimize peak demands on the utility infrastructure as well as better utilization of power plant capacities.

VII. MAXIMUM DEMAND CONTROL

Step By Step Approach for Maximum Demand Control:

A. Load Curve Generation

Presenting the load demand of a consumer against time of the day is known as a 'load curve'. If it is plotted for the 24 hours of a single day, it is known as an 'hourly load curve' and if daily demands plotted over a month, it is called daily load curves.

These types of curves are useful in predicting patterns of drawl, peaks and valleys and energy use trend in a section or in an industry or in a distribution network as the case may be.

B. Rescheduling of Loads

Rescheduling of large electric loads and equipment operations, in different shifts can be planned and implemented to minimize the simultaneous maximum demand. For this purpose, an operation flow chart and a process chart are prepared. Analyzing these charts and with an integrated will help to improve the load factor which in turn reduces the maximum demand approach.

C. Storage of Products/in Process Material/Process Utilities like Refrigeration

It is possible to reduce the maximum demand by building up storage capacity of products materials, water, chilled water and hot water, using electricity during off peak periods.

D. Shedding of Non-Essential Loads

When the maximum demand tends to reach preset limit, shedding some of non- essential loads temporarily can help to reduce it. Sophisticated microprocessor controlled systems are also available, which provide a wide variety of control options like:

• Accurate prediction of demand.

• Graphical display of present load, available load, demand

E. Operation of Captive Generation and Diesel Generation Sets

When diesel generation sets are used to supplement the power supplied by the electric utilities, it is advisable to connect the DG sets for durations when demand reaches the peak value. This would reduce the load demand to a considerable extent and minimize the demand charges.

F. Reactive Power Compensation

The maximum demand can also be reduced at the plant level by using capacitor banks and maintaining the optimum power factor. Capacitor banks are available with microprocessor based control systems. These systems switch on and off the capacitor banks to maintain the desired Power factor of system and optimize maximum demand thereby (Calcutta *et al.*, 1998; and Collabus, 2003).

VIII. POWER FACTOR IMPROVEMENT AND BENEFITS

A. Power Factor Basics

In all industrial electrical distribution systems, the major Loads are resistive and inductive. Resistive loads are

incandescent lighting and resistance heating. In case of pure resistive loads, the voltage (V), current (I), resistance (R) relations are linearly related,

Active power is measured in kW (Kilo Watts). Reactive power is measured in KVAR (Kilo Volt-Amperes Reactive).

The vector sum of the active power and reactive power make up the total (or apparent) power used. This is the power generated by the SEBs for the user to perform a given amount of work. Total Power is measured in KVA (KilloVolts-Amperes).

The active power (shaft power required or true power required) in kW and the reactive power required (KVAR) are 9 0° apart in a pure inductive circuit,

Figure 5: Power Triangle

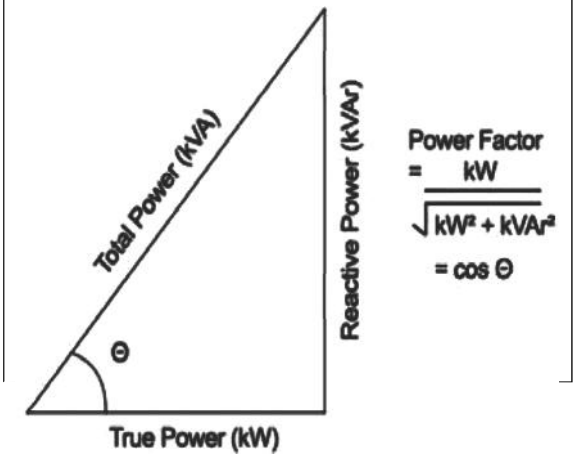

The active power (shaft power required or true power required) in kW and the reactive power required (KVAR) are 90° apart vector in a pure inductive circuit, i.e., reactive power KVAR lagging the active kW. The vector sum is called the apparent power or KVA, as illustrated above and the KVA reflects the actual electrical load on distribution system (Brown, 2008).

The ratio of kW to KVA is called the power factor, which is always less than or equal to unity. Theoretically, when electric utilities supply power, if all loads have unity power factor, maximum power can be transferred for the same distribution system capacity. However, as the loads are inductive in nature, with the power factor ranging from 0.2 to 0.9, the electrical distribution network is stressed for capacity at low power factors.

B. Improving Power Factor

The solution to improve the power factor is to add power factor correction capacitors to the plant power distribution system.

They act as reactive power generators, and provide the needed reactive power to accomplish kW of work. This reduces the amount of reactive power, and thus total power, generated by the utilities.

IX. ADVANTAGES OF PF IMPROVEMENT BY CAPACITOR ADDITION

- Reactive component of the network is reduced and so also the total current in the system from the source end.

- 12R power losses are reduced in the system because of reduction in current. Voltage level at the load end is increased.

- KVA loading on the source generators as also on the transformers and lines up to the capacitors reduces giving capacity relief. A high power factor can help in utilizing the full capacity of your electrical system (Calcutta *et al.*, 1998; and Mc Donald, 2003).

X. COST BENEFITS OF PF IMPROVEMENT

While costs of PF improvement are in terms of investment needs for capacitor addition the benefits to be quantified for feasibility analysis are:

- Reduced KVA (Maximum demand) charges in utility bill.

XI. MAXIMUM DEMAND CONTROLLER

High-Tension (HT) consumers need to pay a maximum demand charge notwithstanding the usual charge for the number of unit s expended. This charge is generally taking into account the most astounding measure of force utilized amid some period (say 30 minutes) amid the metering month. The maximum demand charge regularly speaks to an extensive extent of the total bill and may be in view of one and only segregated 30 moment episode of high power utilization.

Figure 6: Demand Controller

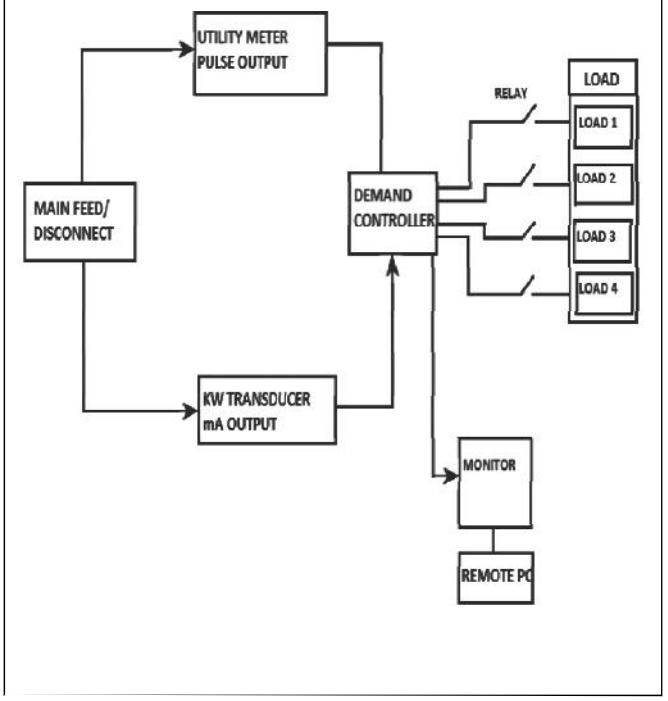

XII. CONCLUSION

A good record of the load pattern is obtained which enables accurate predictions and better load distribution. The capital outlay for maximum demand control is low. With good maximum demand indication, it is possible to create awareness of where and when power is used and consequently gets greater power utilization. The data obtained from the MDI controller may be used for the design and development of Smart Grid and helpful for prediction of estimated load in large load dispatch centre.

Proper utilization of electrical power during off peak period and the data obtained from the MDI controller is useful for the automation of Distribution system.

REFERENCES

[1] Mc Donald John D (2003), Electric Power Substation on Engineering, pp. 124-192.
[2] Cobus S (2003), Electrical Network Automation and Communication Systems, pp. 142-153.
[3] Calcutta David M, Cowan J Frederick and Parchizadeh Hassan G (1998), 8051Microcontrollers Hardware, Software and Applications, pp. 1-13.
[4] Mostafa Al Mamun, Ken Nagasaka and Salim Reza S (2004), 3rd International Conference on Electrical & Computer Engineering, ICECE 2004, December 28-30, Dhaka, Bangladesh.
[5] El-Sayed Y M (1999), "Revealing the Cost Efficiency Trends of the Design Concepts of Energy-Intensive Systems", Energy is Conversion and Management, Vol. 40, pp. 1599-1615.
[6] Capasso A, Grattieri W *et al*. (1994), "A Bottom-Up Approach to Residential Load Modeling", IEEE Transactions on Power Systems, Vol. 9, No. 2,May.
[7] Brown Richard (2008), Electrical Power Distribution Reliability, pp. 17-34.
[8] World B a n k, World DevelopmentIndicators – Last Updated March 2, 2011Energy Statistics 2012 (19th Issue), Issued by Central Statistics Office, Ministry of Statistics and Progra mmed Implementation, Govt. of India, New Delhi.
[9] Microco ntroller Ba sed Subst ation Monitoring and Control System with GSM Modem" , IOSR Journal of Electrical and Electronics Engineering (IOSRJEEE).

Dual-Input Isolated Full-Bridge Boost DC-DC Converter based on the Distributed Transformers

A. Richard Pravin
Assistant Professor

P. Muthu Kumar
UG Student

E. Karthick
UG Student

Department of Electrical and Electronics Engineering
st. Anne's College of Engineering and Technology
Panruti, Tamil nadu, India.

Abstract: **In this paper, a new two-input isolated boost dc-dc converter based on a distributed multi-transformer structure which is suitable for hybrid renewable energy systems is investigated and designed. With a novel transformer winding- connecting strategy, the two input ports can be decoupled completely, so the proposed converter can draw the power from the two different dc sources, which have low output voltage, and transfer it to the dc bus, which has high voltage, separately or simultaneously. The detailed operation principles of the proposed converter have been analyzed in the dual-input mode and the single-input mode, respectively. The main advantage of the proposed topology is that the four transformers and the secondary rectifiers are fully utilized whether the converter is connected with two input power sources or only one input. Although the four transformers are employed, the nominal powers of each transformer and rectifier are both reduced by four times. Furthermore, some special issues on converter design, such as increasing number of the input ports, the magnetic integration and the ground loop decoupling are discussed.**

Key words:- **Current-fed, DC-DC converter, isolated, multiple inputs, transformer.**

1. INTRODUCTION

Nowadays, clean and renewable energies including fuel cell, wind energy, photovoltaic, etc., have been widely applied to achieve environment friendly objectives [1] [2]. Because of the discontinuity of renewable sources, like wind energy and solar energy, generally, an auxiliary power supply is necessary to 1 smooth output power and keep output voltage stable under various load conditions. Thus, an efficient combination of different energy sources, to be a hybrid renewable power conversion system, has become an interesting topic [3]. Moreover, high power solar cells or fuel cells are often faced with a need of boosting their low output voltage to a high dc-link voltage subjected to the requirements in grid-connecting applications [4].

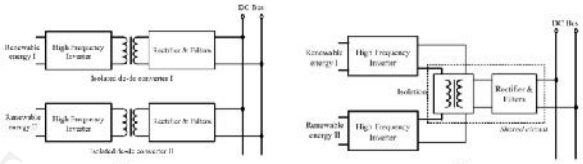

Fig. 1: Block diagram of the systems with two input power sources: (a) Structure based on two isolated individual converters, (b) structure based on the isolated multiple-port structure.

In the last decade, various hybrid system structures have been proposed. For the applications with galvanic isolations, basically, high frequency isolated converters with different input sources can be connected in parallel on a mutual dc bus and thereby each sub-converter can be designed as an individual power module. The block diagram of this system is shown in Fig. 1 (a). The main disadvantage of this system is that if one input source is connected, only one converter will be operated and the other one will be completely under the idle condition that will reduce the power density of the whole system. Due to this reason, multi-port converters have been proposed and received more and more attention in recent years. In these topologies, some parts of the dc-dc converters (such as rectifiers and filters) can be utilised by different input ports mutually, as shown in Fig. 1 (b). Although it will cause complex system control, the power density of the system can be increased in some applications. For the sustainable energy with a low output terminal voltage such as fuel cell, a boost-type converter is favorable for a high efficiency operation. A multi-input isolated boost dc-dc converter with multi-windings based on

the flux additive concept was proposed in [5], but the reverse current block diode is connected in series with the MOSFETs on the primary side, which makes the bidirectional power flow impossible, so the auxiliary circuit for rechargeable elements is needed. In [6], a high step-up isolated converter with two input sources was investigated, and the converter utilizes the current-source type applying to both of the input power sources. To avoid the switch voltage spikes caused by the leakage inductor, an active clamping circuit is added.

The aim of this paper is to investigate an innovative dual-input full-bridge isolated dc-dc converter [7] for a hybrid renewable energy system. With the novel winding connection and the interleaved PWM modulation strategy, two current- fed power sources with low input voltage can deliver the power to the high voltage dc bus or the load, individually or simultaneously. In this paper, firstly, a review on the state of the art of the multiple-input isolated converters is given to express the background and novelty of this research work. Then, based on the proposed topology, a detailed analysis of the steady-state operation principles of the converter is given and hereby the characteristics of the converter are explained in depth. In order to improve the converter performance further, some issues such as the input port extension, the magnetic integration and the common mode current deduction, which affect the hardware design in practice, are discussed, and some possible solutions are presented. The operating performance of the proposed dual- input converter is examined and is validated through some computer simulations.Using the above study procedure, the salient features of the proposed converter can be summarized: a high step-up ratio, an electric isolation between the clean energy and output voltage, multiple input power sources, and magnetic integration.

2. BASIC PRINCIPLE AND STEADY-STATE OPERATION

As shown in Fig. 2 (a), the proposed dc-dc converter consists of two boost inductors, two high frequency full-bridge inverters, four transformers and a common output-stage circuit. It is driven by two dc voltage sources, that when associated with large inductors become dc current sources. *Tr*l♦*Tr*4 are four identical transformers with same number of turns and turns ratio. According to the converter's operation, its operating principles can be analysed with two different modes: dual-input mode and single input mode.

2.1 Dual-Input Mode

The timing diagrams and the basic operating waveforms in this mode are shown in Fig. 2 (b). There is I80° phase shift between each pair of drive signals, namely *S*l, *S*4 and *S*2, *S*3. The switches *S*5 to *S*8 have the same operating principle with that of *S*l to *S*4. It is worth noting that when the switches in the diagonal position in one of the H-bridges form a simultaneous conduction switch pair to transfer power to the secondary side, it will cause every transformer winding current on the primary side to be clamped as *I*Ll or *I*L2. The appearance of the clamped current will disable the normal operation of the other dc input-stage circuit, because the current sources can not be connected in series, which means two input ports can not transfer power at same time. To solve this problem, the phase-shift PWM scheme is utilized, which gives 90° phase shift between *S*l and *S*5. With that, the two input power sources can deliver power to the secondary side simultaneously.

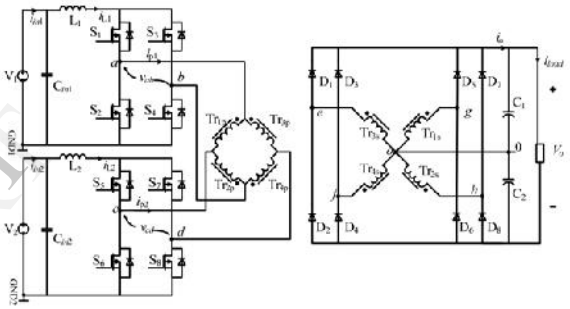

(a) The proposed converter topology

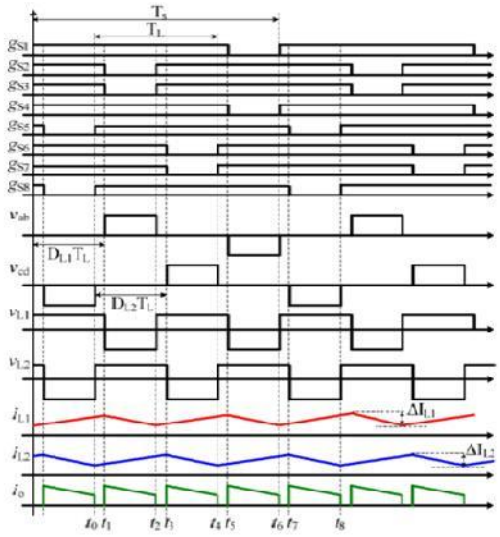

(b) Timing diagrams of the basic operating waveforms in steady state

Fig. 2: Topology and operation of the proposed dual-input isolated boost converter.

In subinterval (*t*o-*t*l), all the eight primary side switches operate in their ON states. As shown in Fig. 3 (a), the inductors *L*l and *L*2 connect across the dc input sources *V*l and *V*2, respectively. With primary and secondary coils shorted, all the diodes on the secondary side are reverse-biased. Here, two input inductors are charged by the input sources and no power is delivered to the secondary side. Thus, the load current is provided by the output capacitors *C*l and *C*2. The primary inductor currents $iL1(t)$ and $iL2(t)$ can be expressed respectively as

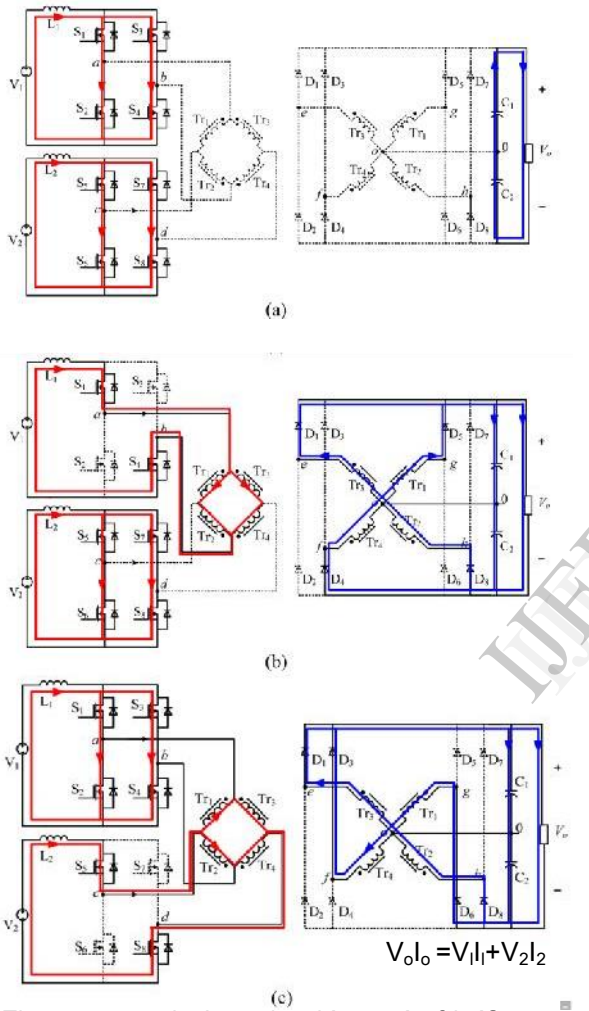

Fig. 3: The current paths in each subinterval of half period: (a) (t_o-t_l); (b) (t_l-t_2); (c) (t_3-t_4).

$$i_{L1}\ t\ = \quad 0.5\Delta\ i_{L1} \quad + \frac{V_1}{L_1}(t-t_1) \qquad \text{(l)}$$

$$i_{L2}\ t\ = \quad 0.5\Delta\ i_{L2} \quad + \frac{V_1}{L_1}(t-t_0) \qquad (2)$$

During the second subinterval (*t*l-*t*2), *S*2 and *S*3 operate in their OFF states so that the inductor *L*l is connected via the transistors *S*l and *S*4 through the paralleled paths: one is *Tr*l in series with *Tr*2 and the other one is *Tr*3 in series with *Tr*4. On the secondary side, the diodes *D*l, *D*4, *D*5, and *D*8 are forward-biased to carry the output current. Thus, *v*ab is clamped to *Voln*, and *v*cd is clamped to o, where *n* is the turn ratio of transformer. The current paths are plotted in Fig. 3 (b). $iL2(t)$ can be expressed as same as that in subinterval (*t*o-*t*l), and $iLl(t)$ is calculated by

$$i_{L1}\ t\ = I_{L1} + \ 0.5\Delta\, i_{L1} + \frac{(V_1 - \frac{V_0}{n})}{L_1}(t-t_1) \qquad (3)$$

In subinterval (*t*2-*t*3), all the switches on the primary side are turned on, so the operation principle is same to that in (*t*o-*t*l) and the equivalent current paths can also be illustrated by Fig. 3(a).

During the subinterval (*t*3-*t*4), *S*6 and *S*7 operate in their OFF states so that the inductor *L*2 is connected via the transistors *S*5 and *S*8 through the paralleled paths: one is *Tr*2 in series with *Tr*4 and the other one is *Tr*l in series with *Tr*3. On the secondary side, the current flows through the diodes *D*l, *D*3, *D*4 and *D*8 to the dc output, as shown in Fig. 3 (c). So *v*cd is clamped to *Voln* and *v*ab is clamped to o. $iLl(t)$ and $iL2(t)$ are given,

$$i_{L1}\ t\ = I_{L1} + \ 0.5\Delta\, i_{L2} + \frac{V_1}{L_1}(t-t_2) \qquad (4)$$

$$i_{L2}\ t\ = I_{L2} + \ 0.5\Delta\, i_{L2} + \frac{(V_2 - \frac{V_0}{n})}{L_2}(t-t_3) \qquad (5)$$

Having described the subintervals in a half period, the operating principle of each subinterval in the second half period is similar.

The proposed converter can be completely decoupled into two independent isolated boost converters based on the utilized winding connection and the interleaved PWM modulation strategy. Neglecting all the losses, the output power *P*o is the summation of the input power *P*l and *P*2 and can be expressed as

$$P_0 = P_1 + P_2 \qquad (6)$$

The derived large-signal, small-signal and steady-state models of the proposed converter as well as the detailed design procedure of the voltage and current closed-loop controllers can be found in [8].

2.2 Single-Input Mode

The single-input mode can be seen as a special condition of the double-input mode and its equivalent circuit is shown in Fig. 4. The operation principle in single-input mode is similar to that of the conventional isolated boost converter with H-

bridge input circuit [9]. In order to ensure the ON states of the switches overlap, the switch duty cycle Ds has to be bigger than O.5. Hence there is a continuous current path for the inductor $L1$. The conversion ratio of the converter in the continuous current mode (CCM) is

$$\frac{V_O}{V_1} = \frac{n}{1-D_L} = \frac{n}{2\ 1-D_S} (D_s \geq O.5) \qquad (7)$$

As we can see, all the four transformers can also be utilized completely in the single-input mode. Hereby, the proposed converter has the potential ability to achieve high power density, in comparison to the system consisting of two individual isolated boost converters in parallel. This is true especially for high power applications, where the main power stage is fully used both in dual-input and single-input conditions.

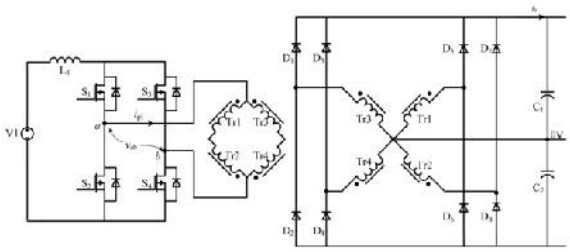

Fig. 4: The equivalent circuit in single-input mode of the converter.

3. SPECIAL ISSUES ON THE CONVERTER DESIGN

To improve the performance of the proposed dc-dc converter, some practical issues such as how to reduce the inductive elements, extending the number of inputs and common mode current deduction are discussed below.

3.1 Magnetic Integration

The complex winding connection makes an optimal layout of the primary side difficult. But by an effective magnetic integration, the number of the inductive elements can be reduced [1O]. In the dual-input mode, the voltages across every primary winding are listed in Table 1.

Table 1 Voltages across each primary winding

Subintervals	v_{Tr1a}	v_{Tr2a}	v_{Tr3a}	v_{Tr4a}
$(t_1\text{-}t_2)$	$+V_O/2n$	$-V_O/2n$	$+V_O/2n$	$-V_O/2n$
$(t_3\text{-}t_4)$	$-V_O/2n$	$-V_O/2n$	$+V_O/2n$	$+V_O/2n$
$(t_5\text{-}t_6)$	$-V_O/2n$	$+V_O/2n$	$-V_O/2n$	$+V_O/2n$
$(t_7\text{-}t_8)$	$+V_O/2n$	$+V_O/2n$	$-V_O/2n$	$-V_O/2n$

It can be seen that windings $Tr1a$ and $Tr4a$ as well as $Tr2a$ and $Tr3a$ always have opposite voltage. In order to reduce the transformer footprint area and increase the power density, the two input inductors $L1$ and $L2$, and the four individual transformers, $Tr1$, $Tr4$, and $Tr2$, $Tr3$, can be wound with two sets of E-I- E cores, shown in Fig. 5 (a). The windings of each transformer are equally divided into the outer legs of E-cores. In transformer $Tr1$, P1/2 and S1/2 represent the half of primary winding and the half of secondary winding respectively. P4/2 and S4/2 are the same properties for the transformer $Tr4$. $L1$-1 in parallel with $L1$-2 wound in the center legs of E-cores to form the boost inductor $L1$. The middle I-core provides a shared flux return path. @1 and @4 represent ac flux generated by the transformers $Tr1$ and $Tr4$ respectively.

By arranging the directions of the windings on the outer legs for each transformer, zero ac flux can be achieved in the centre legs. @1 and @4 have their own flux paths due to a low reluctance path provided by shared I-core meaning the two transformers $Tr1$ and $Tr4$ are uncoupled. Because @1 is equivalent to @4 in this work, the ac flux will partially cancel in shared I-core. The dc flux $@L1$ generated by the inductor $L1$ goes through the centre legs of E cores. Half of $@L1$ runs in the outer legs of the E-cores and no dc flux exists in the shared I-core due to complete cancellation effect. To verify the validity of the proposed design approach and theoretical analysis, a 2D simulation

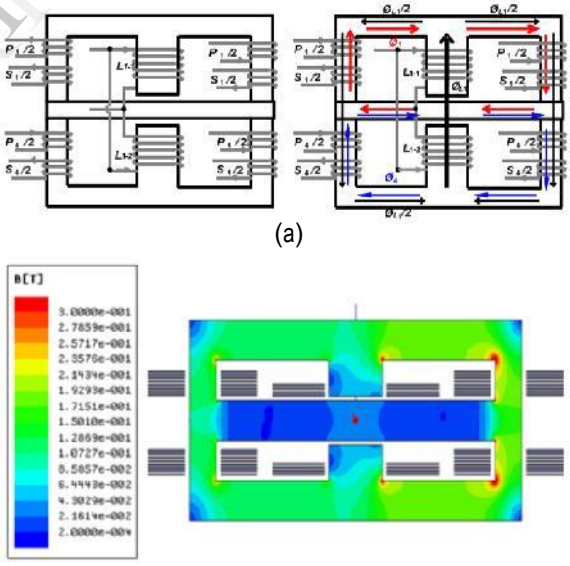

(a) (b)

Fig. 5: Two transformers and one input inductor in E-I-E integration, (a) winding arrangement; (b) 2D simulation by FEA analysis.

model linked with external circuit has been built in a finite element analysis (FEA) tool. As shown in Fig. 5 (b), the right side has higher flux density B because half of @$L1$ adds to @1 and @4 but on the left side, these fluxes subtract. In the shared I core, @1 and @4 cancels out. Hence, based on this magnetic integration idea, the four transformers and two inductors can be integrated into two sets of E-I-E cores. It reduces the number of magnetic elements as well as the core losses. More detailed design procedure can be found in [10].

3.2 Method to Increase the Number of Inputs

The primary and secondary windings of the transformers from the Fig. 2 are re-illustrated in Fig. 6(a). The voltage vector across the different terminals, from a to d on primary side, and the current vectors, from e to h on secondary side can be plotted in Fig. 6 (b), where the employed primary windings are numbered as 1–4. According to the operating sequence, the potential and current vectors will rotate clockwise like a 2-pair-pole dc motor. Based on this simplified model, the other 2-pair poles can be added symmetrically in the system with a phase shift: 45 degree electrical angle, as shown in Fig. 6 (c), and thereby the proposed dual-input converter can be extended to a converter with 4 input ports by the winding connection shown in Fig. 6 (d). Thus, the number of inputs *Ninput* and the corresponding number of transformer *NTr* can be derived as

$$N_{input} = 2^m \quad (m=1,2,\ldots)$$

$$N_{Tr} = 2\,N_{input} \qquad (8)$$

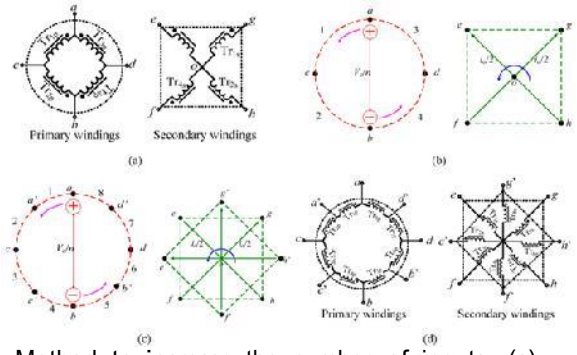

Fig. 6: Method to increase the number of inputs: (a) windings for two inputs, (b) equavilent voltage and current vectors for two inputs, (c) equavilent voltage and current vectors for four inputs, (d) windings for four inputs.

It is worth noting that: 1) the number of inputs must be exponent of 2; 2) with increasing number of input ports, the number of the transformers is increased by twice that of input ports. If the converter has multiple inputs, utilizing the high order magnetic integration method can simplify the converter circuit further, but it is out of scope of this paper and will not be discussed here.

4 Observations and simulation Results

Fig. 7 shows SimulinkiPLECS simulation results. Simulation parameters are based on the above design parameters ($V1$=$V2$=30V and Vo=400V). The simulation results in Fig. 7 agree with the theoretical analysis described in section 2.
The experimental waveforms are shown in Fig. 12. In the single input mode with 50 V input voltage, Fig. 8(a) shows the primary side voltage and current, i.e. *vab* and *ip*1, which have been annotated in Fig. 2. While Fig. 8(b) shows the plots of the primary voltages *vab* and *vcd*, and primary current *ip*1 and *ip*2 in the dual-input mode with the conditions: $V1$=50 V and $V2$=30 V, which verifies the theoretical analysis results that two input voltage sources can deliver the power together.

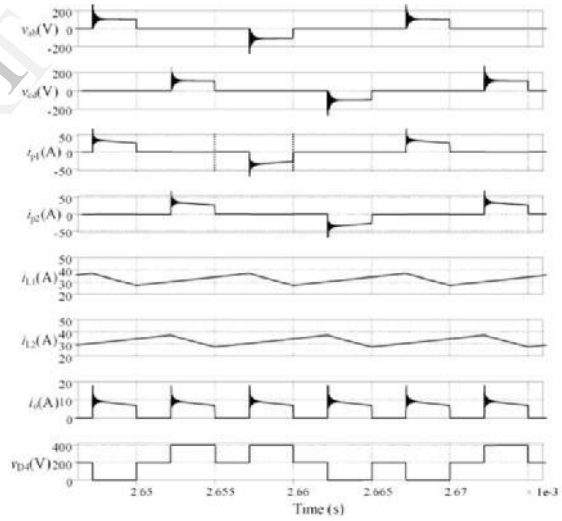

Fig. 7:Simulation results – v_{ab}, v_{cd}, i_{p1}, i_{p2}, i_{L1}, i_{L2}, i_0 and v_{D4}.

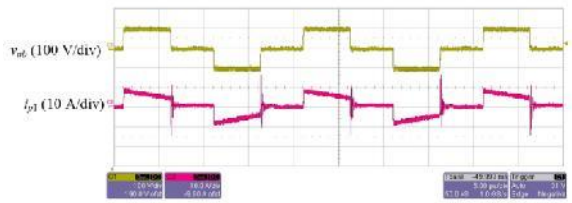

(a)Primary side voltage and current under single – input mode(time base: 5 usidiv)

The efficiencies are measured without including the gate driver losses, and presented in Fig. 13. The efficiency curves with respective to the input voltage in the single input mode are plotted in Fig. 9(a). It exhibits a maximum efficiency of 96.5% with 50 V input, and the measured efficiency is 92.1% at 1500
W with 30 V input.

The measured efficiency curve of the converter with the conditions: input voltages $V1=V2=30$ V, output voltage of 400 V, and $P1 \approx P2$, are shown in Fig. 13 (b). Comparing to the efficiency curves shown in Fig.
13(a), in dual-input mode, the measured efficiency is about 92.4% at the output power of 200 W, which is lower than that in single-input boost mode because of higher switching losses. But at high output power, the efficiency is higher in dual-input operation mode, which is around 94.0% (Po=1450 W). Fig. 13 (c) shows the measured efficiency with input voltages $V1$=50 V, $V2$=30 V, output voltage of 400 V, and input power $P1 \neq P2$. The maximum efficiency is measured as 95.7%.

5. CONCLUSION

There are some solutions to the multi-input-port voltage-fed or current-fed isolated converters which can be utilized in the applications in which hybrid sustainable energy sources involved. Comparing to the existing topologies, the converter proposed in this paper has the promising points: the lower input current ripple, two controllable independent input power ports (can be extended to multiple ports), the symmetrical circuit structure which is favourable to achieving magnetic integration and modularizing. The most prominent characteristic of the proposed converter is that the main power flow path, consisting of 4 transformers and full bridge rectifier, is shared by both of the input ports, and the nominal power of each transformer and rectifier can be reduced, so a higher power density can be achieved. There are still some negative sides such as complex transformer windings connection and no common ground, and in the future research, the dc offset of transformers caused by unbalance on the voltages or the switching times has to be investigated in depth. Overall, the proposed converter is one of the promising candidate circuits, and is suitable to the applications with hybrid renewable energies.

REFERENCES

[1] [1]F. Blaabjerg, Z. Chen, and s. B. Kjaer, "Power electronics as efficient interface in dispersed power generation systems," *IEEE Trans. Power Electron*, 2004, 19, (5), pp. 1184-1194.

[2] Z. Chen, J. Guerrero, and F. Blaabjerg, "Areview of the state of the art of power electronics for wind turbines," *IEEE Trans. Power Electron.*, 2009, 24, (8), pp. 1859–1875.

[3] M. Bragard, N. Soltau, S. Thomas and R. W. De Doncker, "The balance of renewable sources and user demands in grids: power electronics for modular battery energy storage systems," *IEEE Trans. Power Electron.*, 2010, 25, (12), pp. 3049– 3056.

[4] H. Cha, J. Choi and P. N. Enjeti, "A three- phase current-fed DC/DC converter with active clamp for low-dc renewable energy sources," *IEEE Trans. Power Electron.*, 2008, 23, (6), pp.2784–2793.

[5] Z. Qian, O. Abdel-Rahman, H. AI-Atrash, and I. Batarseh, "Modeling and control of three- port DC/DC converter Interface for satellite applications," *IEEE Trans. Power Electron.*, 2010, 25, (3), pp.637-649.

[6] Y.C.Liu and Y.M. Chen, "A systematic approach to synthesizing multi-input DC–DC converters," *IEEE Trans. Power Electron.*, 2009, 24, (1), pp. 116–127.

[7] Y. Li, X. Ruan, D. Yang, F. Liu and C. K. Tse, "synthesis of multiple-input DC/DC converters," *IEEE Trans. Power Electron.*, 2010, 25, (9), pp. 2372–2385.

[8] H. Tao, J. L. Duarte and M. A. M. Hendrix, "Three-port triple-half-bridge bidirectional converter with zero-voltage switching," *IEEE*

[9] M. Nymand, R. Tranberg, M. E. Madsen, U. K. Madawala, M. A. E. Andersen, "What is the best converter for low voltage fuel cell applications- A buck or boost," Proc. Annual Conference of the IEEE Industrial Electronics Society, 2009, pp. 959-964.

[10] Z.Zhang, O. C. Thomsen and M. A. E. Andersen, "Modeling and control of a dual-Input isolated full-bridge boost converter," Proc. Applied Power Electronics Conf. and Exposition, 2012. (in press)

[11] V.Vaisanen, T.Riipinen and P. Silventoinen, "Effects of switching asymmetry on an isolated full-bridge boost converter," IEEE Trans. Power Electron., 2010, 25, (8), pp. 2033–2044. Z. Ouyang, Z. Zhang, O. C. Thomsen, M. A. E. Andersen, "Planar integrated magnetics (PIM) module in hybrid bidirectional DC/DC converter for fuel cell application," ," IEEE Trans. On Power Electron., 2011, 26, (11), pp.3254-3264.

Zero Carbon Emission-Future
Wind Energy In The Traction [WET]

Saravanan L
Department of Electrical & Electronics Engineering
Jayaram College of Engineering & Technology
Trichy, India, e-mail: lrsnpng@gmail.com

Siva Sankari P
Department of Electrical & Electronics Engineering
Jayaram College of Engineering & Technology
Trichy, India, e-mail: tulasi.vt@gmail.com

***Abstract*— The requirements of fuel for transportations, electricity and other process are all plays major role in the development of nation. Hence not only developed countries but also developing and non-developed countries all are depends on fossil fuel to fulfill their requirements. Due to burning of fossil fuels, green house gases include carbon dioxide level in atmosphere goes to increases in huge rate. Hence global temperature rising, snow melting, ozone layer depletion etc are taken place. To control the rate of carbon emission using renewable energy sources for power generations, transportations etc is only way. This is achieving by building zero carbon emission city.**

Keywords—Fuel requirements; fossil fuel; Nation development-Renewable energy sources; Zero carbon emission cities.

I. INTR0DUCTI0N

It is necessary to reduce $C0_2$ emissions against global warming, and the activities are expanding all over the world. As the world continues its reliance on fossil fuels to meet its growing energy demand, the associated environmental and climate change challenges must be adequately addressed. The world is undergoing the largest wave of urban growth in history and this process is mainly a domain of developing countries. The growth in human population is largest in the developing world, with Africa's and Asia's urban population projected to double between 2000 and 2030. With approximately 3.4 billion people, more than 50 percent of the world population living in cities and both human activities and the use of energy also concentrated in cities, the urban areas have become the root cause of orientating societies toward mass production, mass consumption and mass dumping of waste. In the world-wide urbanization process a particular significance has mega-cities more than 600 million people will be living in about 60 mega-cities worldwide. While megacities have captured much public attention, most of the new growth will occur in smaller towns and cities, which have fewer resources to respond to the magnitude of the change. Urban areas sprawl deeply into regions surrounding cities and towns. Increased income and wealth has enabled extensive new construction of infrastructures, power demand and transportation within functional urban regions.

II. CARB0N EMISSI0N

Carbon dioxide ($C0_2$) is the primary greenhouse gas emitted through human activities. Carbon dioxide is naturally present in the atmosphere as part of the Earth's carbon cycle. Human activities are altering the carbon cycle—both by adding more $C0_2$ to the atmosphere and by influencing the ability of natural sinks, like forests to remove $C0_2$ from the atmosphere.

While $C0_2$ emissions come from a variety of natural sources, human-related emissions are responsible for the increase that has occurred in the atmosphere since the industrial revolution. The main human activity that emits $C0_2$ is the combustion of fossil fuels like coal, natural gas and oil for energy and transportation, although certain industrial processes and land-use changes also emit $C0_2$. The main sources of $C0_2$ emissions are described below.

Electricity,
Transportation,
Industry.

Power-generating stations worldwide release 12 billion tones of $C0_2$ every year as they burn coal, oil or natural gas; home and commercial heating plants release another 11 billion tons. Carbon dioxide levels varied between about 180 and 300 parts per million during the 650,000 years prior to industrialization as recorded in air bubbles trapped in ice in Antarctica. But since industrialization began in the 18th century, the concentration of carbon dioxide in the atmosphere has increased from about 280 to 390ppm a rise of about 40%.

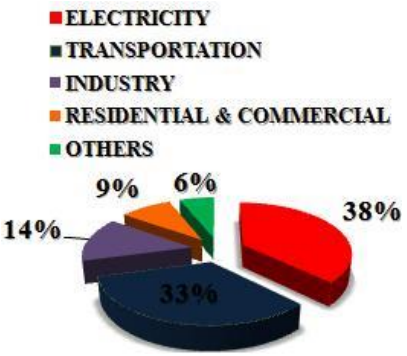

Fig-1: Various sources for $C0_2$ Emission in atmosphere

We also know that human activities, such as burning fossil fuels, producing cement and destroying rainforests, have disturbed the natural equilibrium of the carbon cycle by emitting an additional 7billion tones each year. From figure.1 it is clear. Major amount of carbon emission taken place during power generation and transportations. In earlier 18 centuries there are only few power generating stations and carbon emitting vehicles. But in middle of 19th and 20th centuries due to world war, urbanizations, nuclear weapons etc the rate of CO_2 emission increasing jet speed in atmosphere. Due to this we forced to meet serious climate changing, pollutions, global warming, ozone depletion etc.

III. CLIMATE CHANGES

Climate change is a change in the statistical distribution of weather patterns when that change lasts for an extended period of time. Climate change may refer to a change in average weather conditions, or in the time variation of weather around longer-term average conditions. Climate change is caused by factors such as biotic processes, variations in solar radiation received by Earth, plate tectonics, and volcanic eruptions. Certain human activities have also been identified as significant causes of recent climate change, often referred to as "global warming".

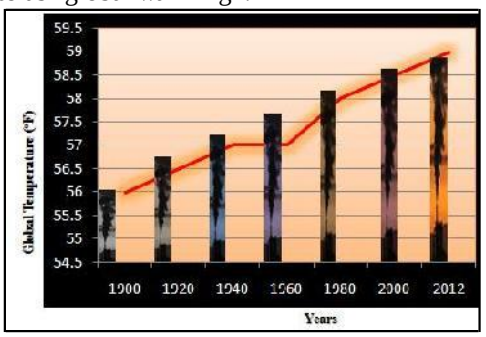

Fig-2: Global temperature changes in last 100 years.

A climate record extending deep into the Earth's past has been assembled, and continues to be built up, based on geological evidence from borehole temperature profiles, cores removed from deep accumulations of ice, floral and faunal records, glacial per glacial processes, stable-isotope and other analyses of sediment layers, and records of past sea levels.

IV. CARBON EMISSION LEVEL

Carbon dioxide is a greenhouse gas, and geological observations that we now have for the last 20 million years lend strong support to the idea that carbon dioxide is an important agent for driving climate change throughout Earth's history. By analyzing the chemistry of bubbles of ancient air trapped in Antarctic ice, we have been able to determine the composition of Earth's atmosphere going back as far as 800,000 years for good understanding of how carbon dioxide levels have varied in the atmosphere since that time. But there has been little agreement how to reconstruct carbon dioxide levels prior to 800,000 years ago. We are able, for the first time, to accurately reproduce the ice-core record for the last 800,000 years the record of atmospheric $C0_2$ based on measurements of carbon dioxide in gas bubbles in ice. When there is evidence for the growth of a large ice sheet on Antarctica or on Greenland or the growth of sea ice in the Arctic Ocean, the evidence for a dramatic change in carbon dioxide levels over the last 20 million years. A slightly shocking finding is that the only time in the last 20 million years that we find evidence for carbon dioxide levels similar to the modern level of 387 parts per million was 15 to 20 million years ago, when the planet was dramatically different. Levels of carbon dioxide have varied only between 180 and 300 parts per million over the last 800,000 years until recent decades. It has been known that modern-day levels of carbon dioxide are unprecedented over the last 800,000 years, but the finding that modern levels have not been reached in the last 15 million years is new.

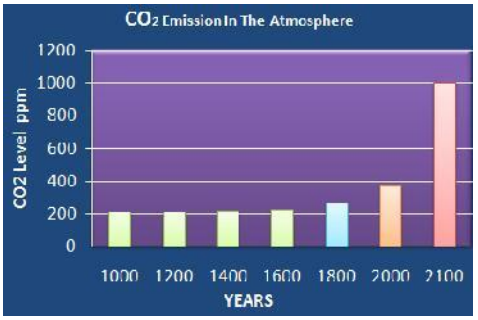

Fig-3: CO_2 level in atmosphere

Prior to the Industrial Revolution of the late 19th and early 20th centuries, the carbon dioxide level was about 280 parts per million. Globally, temperatures were 5 to 10 degrees Fahrenheit warmer. We can now have confidence in making statements about how carbon dioxide has varied throughout history. In the last 20 million years, key features of the climate record include the sudden appearance of ice on Antarctica about 14 million years ago and a rise in sea level of approximately 75 to 120 feet. But now shown that this dramatic rise in sea level is associated with an increase in carbon dioxide levels of about 100 parts per million. Today the Arctic Ocean is covered with frozen ice all year long, an ice cap that has been there for about 14 million years. Prior to that, there was no permanent sea ice cap in the Arctic. Some projections show carbon dioxide levels rising as high as 600 or even 900 parts per million in the next century if no action is taken to reduce carbon dioxide.

V. CARBON NEUTRALIZATION

Carbon neutrality, or having a net zero carbon footprint, means achieving net zero carbon emission by balancing a measured amount of carbon released with an equivalent amount sequestered or offset, or buying enough carbon credits to make up the difference. It is used in the context of carbon dioxide releasing processes associated with transportation, energy production, and industrial processes such as production of carbon neutral fuel.

COUNTRIES	CO_2 EMISSION PER YEAR
China	7,711mtonne
Usa	5,425mtonne
India	1,602mtonne
Russia	1,572mtonne
Japan	1,098mtonne

TABLE: I. Top 5 nations and its annual carbon emission ratings

The carbon neutrality concept may be extended to include other greenhouse gases (GHG) measured in terms of their carbon dioxide equivalence the impact a GHG has on the atmosphere expressed in the equivalent amount of $C0_2$. The other GHG gases are methane (CH_4), nitrous oxide (N_20), hydro fluorocarbon (HFC), per fluorocarbons (PFC), and sulphur hexafluoride (SF_6). Carbon emission is controlled by using renewable energy resources.

A. Zero Carbon Emission City

A zero-carbon city runs entirely on renewable energy; it has no carbon footprint and will not cause harm to the planet. Most cities throughout the world produce energy by burning coal, oil and gas, unintentionally emitting carbon. Almost every activity humans do involves burning one of these fossil fuels. To become a zero carbon city, an established modern city must collectively reduce emissions of greenhouse gases to zero and all practices that emit green house gases must cease. Zero-carbon city is a renewable-energy-economy city. This transition which includes decarbonising electricity and zero-emission transport is undertaken as a response to climate change. Zero-carbon cities maintain optimal living conditions while eliminating environmental impact. Instead of using established cities, many developers are starting from scratch in order to create a zero-carbon city. This way they can make sure every aspect of a city contributes to it being carbon free.

B. ZCEC is way to reduce carbon level in atmosphere

Zero carbon emission city is only way to reduce huge amount of $C0_2$ present in atmosphere. We need zero carbon dioxide emissions because of the planet carbon cycle. The various systems on Earth can remove carbon dioxide only at a very slow rate. At the same time, our fossil fuel economy is dumping $C0_2$ into the atmosphere at a very fast rate. Earth's slow systems involve converting carbon into rock which is an ocean since process and converting carbon into coal, natural gas and oil which is a land sink process. But both of these processes take thousands and millions of years. As a result, 20% of all carbon dioxide emissions remain in the atmosphere for 1,000 years. To give the planet the chance to remove some of the $C0_2$ that has been around for the past 900+ years, we need to move immediately to zero carbon emissions.

VI. WIND ENERGY IN TRACTI0N

In this WET [Wind Energy in the Traction] method the wind turbine has been placed on the sides of the traction. By this way we can eliminate the aero dynamical problems cause in traction. When train runs above the rail wind turbine starts to rotate due to kinetic energy of the wind.

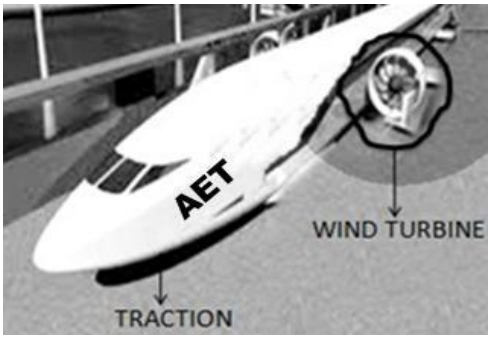

Fig -4: Wind Turbine positioned on sides of the traction

The speed of rotation of wind turbine depends on the speed of train. When train moves at high speed the wind flow also cross the turbine blades at high speed, hence it makes the large power output. But if very high speed flows of train danger to wind turbines because it damage the wind turbines. The wind turbines are covered by protection shield, the speed of wind also continuously measured by Propeller-type wind-speed sensor or Cup-type wind-speed sensor. The opposing force produced in this method is more than normal diesel engine train. It has been eliminated by made some modification in the traction design. By using a limited number of blocks for passengers, by using a light weight metals for construction. The amount of power production depends on wind turbine capacity, train speed and other some factors. Because of the method we also want to done some modification around the area near to train roots.

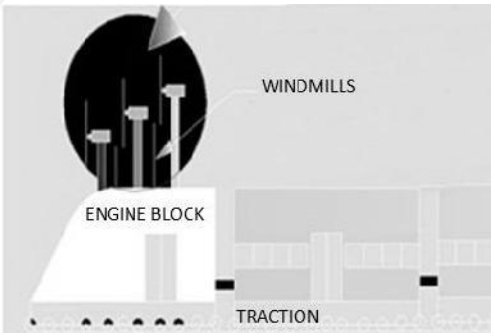

Fig -5: Wind Turbine positioned above roof of the traction

The size of system depends on how plan to use the power that is generated. Small wind turbines can range in size from 20 watts to 100 kilowatts (kw) with a 20-500 watt system being used to charge batteries 5 to 15 kw. Normally wind systems consist of a rotor or blades, a generator mounted on a frame, a tower, the necessary wiring and the balance of system components: controllers, inverters, and possibly batteries. Through the spinning Blades, the rotor trap the kinetic energy of the wind and convert it into rotary motion to drive the generator, which produces electricity. But in this method the tower has been not necessary. The diameter of the rotor and the maximum wind speed determine the amount of power that can be produced.

In above specified figure 2, the windmills are placed above the traction. This is another method of producing wind energy in traction. The small size windmills are placed above the traction. The electric train run over railroad tracks, the alternative form of wind energy produced by train is very

unique. If the wind is properly directed towards the wind turbine blades, optimum electricity may be generated.

The desired direction of wind is obtained by a means for channeling wind, in the direction of the wind turbine.

A. Aerodynamics

Aerodynamics is the science and study of the physical laws of the behavior of objects in an air flow and the forces that are produced by air flows. The shape of the aerodynamic profile is decisive for blade performance. Even minor alterations in the shape of the profile can greatly alter the power curve and noise level. Therefore a blade designer does not merely sit down and outline the shape when designing a new blade. The aerodynamic profile is formed with a rear side, is much more curved than the front side facing the wind.

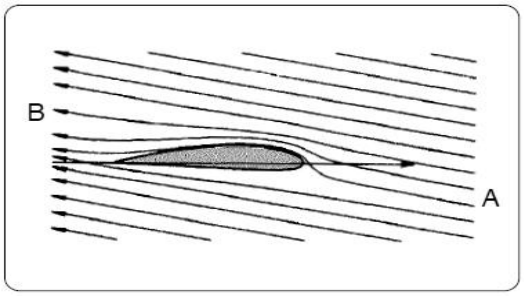

Fig -6: Wind flow across blade

Two portions of air molecules side by side in the air flow moving towards the profile at point A will separate and pass around the profile and will once again be side by side at point B after passing the profile's trailing edge. As the rear side is more curved than the front side on a wind turbine blade, this means that the air flowing over the rear side has to travel a longer distance from point A to B than the air flowing over the front side.

Therefore this air flow over the rear side must have a higher velocity if these two different portions of air shall be reunited at point B. Greater velocity produces a pressure drop on the rear side of the blade, and it is this pressure drop that produces the lift. The highest speed is obtained at the rounded front edge of the blade.

B. Power production

A train moving at 125mph would generate a wind speed equivalent to 60 feet/second. Wind blowing with such speed will let a normal wind power generator harness about 3500w of power. If a train is about 656 feet long, running at the pace of 187mph, and it moves along a 0.62 mile railway track in about 18 seconds, the power generated in this small period by the turbine laid on the tracks will be 2.6kW. The kinetic energy of the wind is the source of the driving force of a wind turbine. That kinetic energy can be depicted by the formula

$$E = f.\ mspec\ .v3$$

E = the kinetic energy
mspec =the specific mass (weight) of air
v = the velocity of the moving air (the wind)
f = a calculating factor without any physic meaning
The power in the wind is proportional to:
a) The area of windmill being swept by the wind
b) The cube of the wind speed
c) The air density - which varies with altitude.
The formula used for calculating the power in the wind is shown below:
Power = (density of air x swept area x velocity cubed)/2

$$P = ½.\ p\ (A)\ (V)^3$$

Where,
P is power in watts (W)
p is the air density in kilograms per cubic meter (kg/m3)
A is the swept rotor area in square meters (m2) & V is the wind speed in meters per second (m/s).

C. Problems to face

The major problem occurring in this system is some alternation has want to made in train design the train not able to move on the overflows or bridges, because mass of windmill producing opposing force toward the train. Similar the train subjected to meet some problems related to aerodynamically.

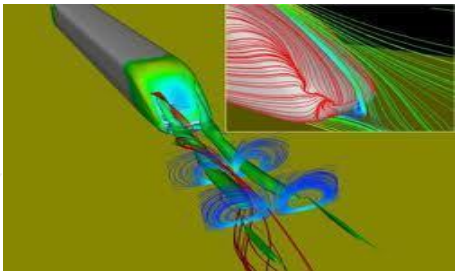

Fig -7: Traction facing aerodynamic problems

The wind turbine is position above the traction reduce the speed of train and it over come by placing it on the sides traction.

CONCLUSION

From the above topic the conclusion is we found world get polluted huge amount in last hundred years as compared with past few million years. By the process of implementing AET we are able to produce an alternate fuel, thus we are not only finding up a new way of energy but also the way to protect the natural world from fossil fuel (pollution). Thus using this new concept and project we can expect a greener and pollution free tomorrow. The whole project demands to call wind energy not only used from supplying power to consumer but also alternative fuel in transportation also. By moving toward zero carbon emission cities, we save our world for future generations. We kept pull stop for carbon emission by continuous research & development in the field of renewable energy resources. This is achieved by planting green seeds in the heart of future generations.

REFERENCE

1. Rebecca Lefton and Cathleen Kelly- Saving the arctic the urgent need to cut black carbon emission and slow climate change [August 2014].
2. Shyam Lal Verma, Ajay Bangar, Ankit Soni, Shravan

Study on Characterization and Mechanical Behavior of Ti-Sic P/M Composites

K. Patterson[a], R. Badrinath[a,] K. Rajesh Ragunath[b], J. Karthik[b], G. Murali Manoj[b]
a: Assistant Professor,
Department of Mechanical Engineering,
Christ College of Engineering and Technology, Puducherry.
b: Student, Department of Mechanical Engineering,
Christ College of Engineering and Technology, Puducherry.

Abstact **-Now a day's automobile industries were more concentrating in replacing with a light weight material for various fuel consumption of the vehicle can be reduced. Titanium is a highly density material were blended with Silicon carbide to improve the bonding nature of two metal matrix composites. However, commercial applications of titanium alloys in important structural parts are limited because of hardness properties. To meet the demands of more applications, titanium alloys with high strength and excellent room temperature property must be developed. A major issue is achieving the best potential of silicon carbide reinforced metal matrix composite is to disperse homogeneously within the matrix of Titanium by using powder metallurgy technique namely blending, compacting and sintering was conducted. The sintering temperature of the Titanium and Silicon carbide is 1200 C in vacuum sintering. Micro hardness, compression, wear tests were analyses on various parameters and their results reveals the intensive and extensive properties the metal matrix composites materials. The characterization of the sintered billets were analyzed using Scanning Electron Microscope (SEM)**

1. INTRODUCTION

Powder metallurgy is a continually and rapidly evolving technology embracing most metallic and alloy materials, and a wide variety of shapes. Powder metallurgy is a highly developed method of manufacturing reliable ferrous and non-ferrous part. Created by mixing elemental (or) alloy powders and compacting the mixture in a die, the resultant shapes are then heated or "sintered" in a controlled atmosphere furnace to bond the particles metallurgical. The high precision forming capability of powder metallurgy generates components with near net shapes intricate features and good dimensional precision pieces are often finished without the need of machining. Many metals can be obtained in the form of fine powder, by different methods. The powdered metal is then compressed in moulds under high pressure. By subsequent heating a fairly strong component is obtained. The Powder metallurgy is consist of four basic steps such as Powder manufacture, Powder blending, Powder compacting, Powder sintering. Compacting is generally performed at room temperature, and elevated temperature process of sintering is usually conducted at atmospheric pressure. The main process consists in cold pressing the metal powders followed by heating. The temperature during the heating process is kept below the melting point in case of pure metals but with alloys the melting point of one constituent is often exceeded. Bonding is obtained by cold pressing but sometimes nonmetallic materials are added to provide metallic bond. Final cohesion is caused by heating in suitable atmosphere.

A much wider range of products can be obtained from powder processes than from direct alloying of fused materials. In melting operations the "phase rule" applies to all pure and combined elements and strictly dictates the distribution of liquid and solid phases which can exist for specific compositions. In addition, whole body melting of starting materials is required for alloying, thus imposing unwelcome chemical, thermal, and containment constraints on manufacturing. Unfortunately, the handling of aluminum/iron powders poses major problems other substances that are especially reactive with atmospheric oxygen, such as titanium, are sinter able in special atmospheres or with temporary coatings.

In powder metallurgy or ceramics it is possible to fabricate components which otherwise would decompose or disintegrate. All considerations of solid-liquid phase changes can be ignored, so powder processes are more flexible than casting, extrusion, or forging techniques. Controllable characteristics of products prepared using various powder technologies include mechanical, magnetic, and other unconventional properties of such materials as porous solids, aggregates, and inter metallic compounds. Competitive characteristics of manufacturing processing (e.g., tool wear, complexity, or vendor options) also may be closely controlled.

2. EXPERIMENTAL DETAILS

2.1 Titanium

Titanium is a chemical element with symbol of Ti. It is a lustrous transition metal with a silver color, low density and high strength. It is highly resistant to corrosion in sea water, aqua regia and chlorine. Titanium can be alloyed with iron, aluminum, vanadium & molybdenum among other elements to produce strong and lightweight alloys for Aerospace. (jet engines , missiles and spacecraft).Titanium Powder metallurgy offers the possibility of creating net shape (or) near net shape parts without the material loss and cost associated with having to machine intricate components from wrought billet.

2.2. Silicon Carbide

Silicon Carbide is the only chemical compound of carbon and silicon. It was originally produced by a high

temperature electro-chemical reaction of sand and carbon. Silicon carbide is an excellent abrasive and has been produced and made into grinding wheels and other abrasive products for over one hundred years. Today the material has been developed into a high quality technical grade ceramic with very good mechanical properties. it is used in abrasives, refractories, ceramics, and numerous high-performance applications. The material can also be made an electrical conductor and has applications in resistance heating, flame igniters and electronic components. Structural and wear applications are constantly developing. Silicon carbide is composed of tetrahedral carbon and silicon atoms with strong bonds in the crystal lattice. This produces a very hard and strong material. Silicon carbide is not attacked by any acids or alkalis or molten salts up to 800°C. In air, SiC forms a protective silicon oxide coating at 1200°C and is able to be used up to 1600°C.

2.3 Material

2.3.1 Preparation of Die & Die Manufacturing:

Die is a hollow or solid metal form used in cutting aping coins or shape, drawing bars or wires, embossing (or) thread insides (or) outsides. Hollow die used in casting of forming is also called as mold. A die specialized tool used in manufacture industries to cut on shape material mostly using a press. Like in olds dies are generally customized to the item they are used to create products made with dies range from simple paper lips to complex pieces used in advanced technology.et in Chennai. The Elements used in the Preparation of die materials are D2 STEEL. The high carbon high chromium (HCHR) material is used to make elements like Upper Punch, Lower Punch, and Injector.

2.4 Powder Compacting:

Powder compacting process of compacting metal powder through the application of high pressures. Compacting or briquetting is the process of converting loose metal powder particles into a Green Compacting as it is called of accurately defined size and shape. The Briquette is considered fairly fragile, but it can be handled. The Compacting stage is carried out at room temperature in a die set up on press. The die consists of cavity, the shape of the desired part, but from two to ten times deeper, according to the material handled. Pressure is applied by the upper and lower punch and the powder gets compressed to approximately one third of its volume and the required component is produced. The bottom punch also acts as ejector for the compressed parts. The dies are commonly made up of high carbon steel and high chromium vanadium steel. Metal powder is poured in the cavity, and leveled off flush with the top of the die.

2.5 Powder Sintering:

Sintering is a process of taking metal in the form of a powder and placing it into a mold (or) die. Once compacted into the mold the material is placed under a high heat for a long period (or) time. . It may also be carried out under protective gas normally hydrogen or in a vacuum if the material tends to react with the protective gas. The heating causes the metal particles to sinter, that is a proportion of them partly melt and by so doing cement the remaining particles together in a cellular structure. From the economic point of view, the sintering time should be as short as possible, but the time must be long enough to obtain the required properties. Sintering is performed to achieve all possible final strength and hardness needed in the finished product. The three most important variables governing the sintering process are temperature, time and sintering atmosphere. The work piece dimensions change during sintering. Such changes may be either a shrinkage or growth. In general, bronze tends to expand and iron and brass to contract. After being compacted into a briquette having the shape of the finished work piece, the cold welded aggregate of metal particles is heated in a furnace to the temperature close to the melting point of the basic metal which goes into the mixture. This is carried out in controlled atmosphere furnaces billets are consolidated for Sintering in the Furnace under the temperature of the 1200^0c at the approximate 5hours in the furnace

3. TESTING

3.1 Scanning electron microscopy

A scanning electron microscope (SEM) is a type of electron microscope that produces images of a sample by scanning it with a focused beam of electrons. The electrons interact with atoms in the sample, producing various signals that can be detected and that contain information about the sample's surface topography and composition. The electron beam is generally scanned in a raster scan pattern, and the beam's position is combined with the detected signal to produce an image. SEM can achieve resolution better than 1 nanometer. Specimens can be observed in high vacuum, in low vacuum, in wet conditions (in environmental SEM), and at a wide range of cryogenic or elevated temperatures. The most common mode of detection is by secondary electrons emitted by atoms excited by the electron beam. On a flat surface, the plume of secondary electrons is mostly contained by the sample, but on a tilted surface, the plume is partially exposed and more electrons are emitted. By scanning the sample and detecting the secondary electrons, an image displaying the topography of the surface is created.

3.2 Micro Hardness test

The Metals Handbook defines hardness as "Resistance of metal to plastic deformation, usually by indentation. However, the term may also refer to stiffness or temper or to resistance to scratching, abrasion, or cutting. It is the property of a metal, which gives it the ability to resist being permanently, deformed (bent, broken, or have its shape changed), when a load is applied. The greater the hardness of the metal, the greater resistance it has to deformation. In mineralogy the property of matter commonly described as the resistance of a substance to being scratched by another substance. In metallurgy hardness is defined as the ability of a material to resist plastic deformation. The dictionary of Metallurgy defines the indentation hardness as the resistance of a material to indentation. This is the usual type of hardness test, in which a pointed or rounded indenter is pressed into a surface

3.4 Compression test

A compression test determines behavior of materials under crushing loads. The specimen is compressed and deformation at various loads is recorded. Compressive stress and strain are calculated and plotted as a stress-strain diagram which is used to determine limit,proportional, yield point, yield strength and, for some materials, compressive strength.

REFERENCES

1. Synthesis of Ti–Sn–Nb alloy by powder metallurgy Alireza Nouri a, Xiaobo Chena, Yuncang Li a, Yasuo Yamadab, Peter D. Hodgsona, Cui'e Wen
2. Fabrication of Ti–Nb–Ag alloy via powder metallurgy for biomedical applications Ming Wen, Cuie Wen, Peter Hodgson, Yuncang Li.
3. Characterisation of titanium–titanium boride composites processed by powder metallurgy techniques: M. Selva Kumar, P. Chandrasekar, P. Chandramohan, M. Mohanraj

Studies on Mechanical, Morphological Analysis of Ti – B_4c Composites

R.Badrinath[a] , K.Patterson[a], T. Rahul Raj[b], A. Sasindar[b], V. Muthukumar[b]
[a:] Assistant Professor, Department of Mechanical Engineering,
Christ College of Engineering and Technology, Puducherry.
[b:] Student, Department of Mechanical Engineering,
Christ College of Engineering and Technology, Puducherry

Abstact-**Now a day's automobile industries and medical application were more concentrating in replacing with a light weight material thereby the fuel consumption of the vehicle can be reduced. Titanium is comparatively material and its mechanical properties can be further more increased by proper alloying and reinforcement. However, commercial applications of titanium alloys in important structural parts are limited because of hardness properties. To meet the demands of more applications, titanium alloys with high strength and excellent room temperature properties must be developed. A major issue is achieving the best potential of (B_4C) Boron carbide reinforced metal matrix composite is to disperse homogeneously within the matrix of Titanium by using powder metallurgy technique namely , blending , compacting, sintering was conducted. Then it sinter into 1200^{0}C in vacuum atmosphere. Scanning electron microscopy (SEM) by using this to characterized the sintered samples. The mechanical properties of newly formed titanium composite were need to measure by micro hardness, and compressive test.**

1. INTRODUCTION

Powder metallurgy is a process of blending fine powdered materials, pressing them into a desired shape or form (compacting) and then heating the compressed material in a controlled atmosphere to bond material (sintering). The preparation and processing of powdered iron and nonferrous metals is called as Powder metallurgy. Many metals can be obtained in the form of fine powder, by different methods. Parts made in these way exhibit properties which cannot be produced in any other way. The powdered metal is then compressed in moulds under high pressure. By subsequent heating a fairly strong component is obtained. The Powder metallurgy consist of four basic steps Powder Manufacture , Powder blending, Powder compacting, Powder sintering Compacting is generally performed at room temperature, and elevated temperature process of sintering is usually conducted at atmospheric pressure. The main process consists in cold pressing the metal powders followed by heating. The temperature during the heating process is kept below the melting point in case of pure metals but with alloys the melting point of one constituent is often exceeded. Bonding is obtained by cold pressing but sometimes nonmetallic materials are added to provide metallic bond. Final cohesion is caused by heating in suitable atmosphere.

2. EXPERIMENTAL DETAILS

2.1 Titanium

Titanium is a chemical element with symbol of Ti. It is a lustrous transition metal with a silver color, low density and high strength. It is highly resistant to corrosion in sea water, aqua regia and chlorine. Titanium can be alloyed with iron, aluminum, vanadium & molybdenum among other elements to produce strong and lightweight alloys for Aerospace jet engines, missiles and spacecraft. Titanium Powder metallurgy offers the possibility of creating net shape (or) near net shape parts without the material loss and cost associated with having to machine intricate components from wrought billet.

2.2 Boron Carbide

Boron Carbide (B_4C) is crystalline compound of boron and carbon. The Another name of Boron Carbide is Carbon Tetra boride, it molecular weight is 55.25.It is an extremely hard boron-carbon ceramic material used in tank armor, bullet proof , vests engine sabotage powders, as well as numerous industrial applications. With a Mohs hardness of about 9.497,it is a one of the hardest materials known being cubic boron nitride and diamond Boron carbide it's insoluble in water. The ability of boron carbide to absorb neutrons without forming long lived radio nuclides makes it attractive as an absorbent for neutron radiation arising in nuclear power plants. Nuclear applications of boron carbide include shielding, control rod and shut down pellets. Within control rods, boron carbide is often powdered, to increase its surface area. The ability of boron carbide to absorb neutrons without forming long lived radio nuclides makes it attractive as an absorbent for neutron radiation arising in nuclear power plants. Nuclear applications of boron carbide include shielding, control rod and shut down pellets. Within control rods, boron carbide is often powdered, to increase its surface area

2.3 Preparation of Die & Die Manufacturing

Die is a hollow or solid metal form used in cutting aping coins or shape, drawing bars or wires, embossing (or) thread insides (or) outsides. Hollow die used in casting of forming is also called as mold. A die specialized tool used in manufacture industries to cut on shape material mostly using a press. Like in olds dies are generally customized to the item they are used to create products made with dies range from

simple paper lips to complex pieces used in advanced technology.et in Chennai. The Elements used in the Preparation of die materials are D_2 steel. The high carbon high chromium (HCHR) material is used to make elements like Upper Punch, Lower Punch, and Injector.

2.4 Powder Compacting

It is the process of compacting metal powder through the application of high pressures. Compacting or briquetting is the process of converting loose metal powder particles into a Green Compacting as it is called of accurately defined size and shape. The Briquette is considered fairly fragile, but it can be handled. The Compacting stage is carried out at room temperature in a die set up on press. The die consists of cavity, the shape of the desired part, but from two to ten times deeper, according to the material handled. Pressure is applied by the upper and lower punch and the powder gets compressed to approximately one third of its volume and the required component is produced. The bottom punch also acts as ejector for the compressed parts. The dies are commonly made up of high carbon steel and high chromium vanadium steel. Metal powder is poured in the cavity, and leveled off flush with the top of the die. When compacting briquettes from hard materials, most of the holding force between the powder particles results from an interlocking effect which takes place between the irregular surfaces of the powder particles. A binder is usually needed to make the compact self-supporting. The process used for compacting may be either mechanical or hydraulic or a combination of the two and the pressure used in form 100 to 1000N/m2.

2.5 Pre sintering

Pre sintering is the process of heating the green compact to a temperature below the sintering temperature. This is done to remove the lubricants and binders added during blending and to increase the strength of compact. All metals do not require pre sintering. But some metals like tungsten carbide are easily machined after pre sintering. After sintering they become so hard that they cannot be machined.

*2.6 Powder Sintering***:**

Sintering is a process of taking metal in the form of a powder and placing it into a mold (or) die. Once compacted into the mold the material is placed under a high heat for a long period (or) time. . It may also be carried out under protective gas normally hydrogen or in a vacuum if the material tends to react with the protective gas. The heating causes the metal particles to sinter, that is a proportion of them partly melt and by so doing cement the remaining particles together in a cellular structure. From the economic point of view, the sintering time should be as short as possible, but the time must be long enough to obtain the required properties.

Sintering is performed to achieve all possible final strength and hardness needed in the finished product. The three most important variables governing the sintering process are temperature, time and sintering atmosphere. The work piece dimensions change during sintering. Such changes may be either a shrinkage or growth. In general, bronze tends to expand and iron and brass to contract. After being compacted into a briquette having the shape of the finished work piece, the cold welded aggregate of metal particles is heated in a furnace to the temperature close to the melting point of the basic metal which goes into the mixture. This is carried out in controlled atmosphere furnaces billets are consolidated for Sintering in the Furnace under the temperature of the 1200^0c at the approximate 5hours in the furnace

3. TESTING

3.1 Scanning electron microscopy

A scanning electron microscope (SEM) is a type of electron microscope that produces images of a sample by scanning it with a focused beam of electrons. The electrons interact with atoms in the sample, producing various signals that can be detected and that contain information about the sample's surface topography and composition. The electron beam is generally scanned in a raster scan pattern, and the beam's position is combined with the detected signal to produce an image. SEM can achieve resolution better than 1 nanometer. Specimens can be observed in high vacuum, in low vacuum, in wet conditions (in environmental SEM), and at a wide range of cryogenic or elevated temperatures. The most common mode of detection is by secondary electrons emitted by atoms excited by the electron beam. On a flat surface, the plume of secondary electrons is mostly contained by the sample, but on a tilted surface, the plume is partially exposed and more electrons are emitted. By scanning the sample and detecting the secondary electrons, an image displaying the topography of the surface is created.

3.2 Vickers Hardness test

The Vickers test is often easier to use than other hardness tests since the required calculations are independent of the size of the indenter, and the indenter can be used for all materials irrespective of hardness. The basic principle, as with all common measures of hardness, is to observe the questioned material's ability to resist plastic deformation from a standard source. The Vickers test can be used for all metals and has one of the widest scales among hardness tests. The unit of hardness given by the test is known as the Vickers Pyramid Number (HV) or Diamond Pyramid Hardness (DPH). The hardness number can be converted into units of pascals, but should not be confused with pressure, which also has units of Pascal's. The hardness number is determined by the load over the surface area of the indentation and not the area normal to the force, and is therefore not pressure. It was decided that the indenter shape should be capable of producing geometrically similar impressions, irrespective of size; the impression should have well-defined points of measurement; and the indenter should have high resistance to self-deformation. The dictionary of Metallurgy defines the indentation hardness as the resistance of a material to indentation. This is the usual type of hardness test, in which a pointed or rounded indenter is pressed into a surface

3.4 Compression test

The compressive strength is the capacity of a material or structure to withstand loads tending to reduce size. It can be measured by plotting applied force against deformation in a testing machine. Some materials fracture at their compressive

strength limit; others deform irreversibly, so a given amount of deformation may be considered as the limit for compressive load. Compressive strength is a key value for design of structures. Compressive strength is often measured on a Universal testing machine these range from very small table- top systems to ones with over 53 MN capacity Measurements of compression test are affected by the specific test method and conditions of measurement. Compression test is measured on materials, components, and structures.

REERENCES

1. Characterization of titanium–titanium boride composites processed by powder metallurgy techniques M. Selva Kumara, P. Chandrasekarb, P. Chandramohanb, M. Mohanrajc
2. In situ reacted titanium carbide-reinforced aluminum alloys composite R.F. Shyu a, C.T. Ho
3. Powder metallurgy titanium metal matrix composites reinforced with carbon nanotubes and graphite ShufengLi,Bin Sun, Hisashi Imai a, TakanoriMimoto, KatsuyoshiKondoh
4. In situ preparation of titanium base composites reinforced by TiB single crystals using a powder metallurgy technique S. Gorsse, J. P. Chaminade and Y. Le Petitcorps
5. Microstructure and properties of titanium alloy produced in the newly developed blended elemental powder metallurgy process Takahiro Fujita a, Atsushi Ogawa, Chiaki Ouchi, Hidenori Tajima

Advanced Concrete Technology in Construction Field

Siva Priyanka. S,
II nd Year Civil Engineering.
CK COLLEGE OF ENGINEERING & TECHNOLOGY
Jayaram Nagar, Chellangkuppam,
Cuddalore – 607003.

Pre-Tensioning & Post- Tensioning:
Pre-tensioning :

Pre Stress Concrete
Technology :

The recent and emerging technology in construction field is Pre Stress Concrete. It is widely used in foreign countries, the pre stress concrete can be classified into two categories. They are

- Pre-tensioning
- Post-tensioning

Pre-Tensioning & Post- Tensioning:

Pre-tensioning :

The method in which the wires are stretched before concreting is referred to as pretensioning.

The grip of concrete on wires increases slightly when the wires are released from the stretching device due to a slight shortening and swelling of the wires.

Post-tensioning

Cast the concrete in which a sheath or other wrapping is preembeded which allows the wires to move freely during stressing.

Anchor the wires or tendons at the ends of the beam by fixing to an anchor plate, or other devices such as wedging with concrete cones**.**

POST - TENSIONING

WHAT IS POST-TENSIONING?

Post-tensioning- is a method of reinforcing (strengthening) concrete or other materials with high-strength steel strands called tendons.

Post-tensioning allows construction that would otherwise be impossible due to either site constraints or architectural requirements.

Requires specialized knowledge and expertise to fabricate, assemble and install.

After adequate curing of concrete, reinforcing tendons (placed in side the voids of the structure) are tensioned/stretched by jacks on the sides & grouts filled with appropriate mix.

Applications – a) Structural members beams, bridge-deck panels, Roof –Slabs, Concrete Silos Etc.

Types of Post-Tensioning

Bonded post-tensioned concrete: unstressed pre-stressing steel is placed with in the concrete and then tension stressed after concrete has harden to required strength

Un-bonded post-tensioned concrete:

It differs from bonded post- tensioning by providing the pre-stressing steel permanent freedom of movement relative to the concrete.

Prestressing tendons:

Prestressing tendon may be in the form of stands , wires , round bar , or threaded rods.

Classification and types

- Pretensioning v.s. Post-tensioning
- External v.s. Internal
- Linear v.s. circular
- End-anchored v.s. non end- anchored
- Bonded v.s. unbonded tendon
- Precast v.s. cast in-place v.s. composite
- Partial v.s. full prestressing

Prestressing steel Materials

- High strength steel
- Fiber-reinforced composite (glass or carbon fibers)
- RC vs. PPC vs. PC
- Common shapes of prestressing tendons.

Tendons :

Typical stress-strain curves of reinforcing and prestressing steel

Concerns With Pre-tension :

Usually uses a mold which is able to resist the forces within the tendons. Which are more expensive than regular molds.

Exception comes when the sides of the mold our anchored allowing mold to be created between the anchors without supporting stress.

Since it may only tightened once and cannot be retightened the designer must also account for Creep of concrete, elastic shortening of concrete, shrinkage of concrete, relaxation of steel, slip at the anchorage, and friction losses due to intended and unintended (wobble) curvature in the tendons in calculations for the camber of the member in order to have lasting quality of the structure.

Pretension requires for a slightly higher compression rating to cut the steel over post-tensioned .6 instead of .55 of the compressive strength of concrete at the time of initial pre-stress before accounting losses such as creep, relaxation and shrinkage, and redistribution of force effect.

Prestressing Steel

Forms

- Wires
- Strands
- Tendons
- Cables
- Bars

Source of Force

- Mechanical
- Hydraulic
- Electrical
- Chemical

Why Prestressed Concrete?

- Concrete remains un-cracked
- Reduction of steel corrosion
- Increases durability
- Good for pressure vessels
- High span to depth ratio (ex: 45:1 vs. 28:1)
- less dead load
- More economical

CONSTRUCTION Prestress losses :

Prestress force at any time is less than that during jacking.(Jacking means using a mechanical device to raise and support a heavy object)

Sources of prestress loss

Elastic shortning:

Because concrete shortens when the prestressing force is applied to it , the tendon attached to it also shortens, causing stress loss.

Anchorage set :

The wedge in the anchorage may set in slightly to lock the tendon , causing a loss of stress.

Friction :

Friction in the duct of posttensioning system causes stress at the far end to be less than that at the jacking end . Thus , the average stress is less than the jacking stress.

Shrinkage :

Concrete shrinks over time due to loss of water , leading to stress loss on attached tendons.

Creep :

Concrete shortens over time under compressive stress , leading to stress loss on attached tendons.

Steel relaxation :

Steel loses its stress with time due to constant elongation , the larger the stress , the larger the loss.

References

- www.todaysconcretetechnology.co m
- www.utexas.edu
- www.dywidag-systems.com
- www.enotes.com
- www.tech9.com

Earthquake Resistant Building and Disaster Management

Ilackiya. S,
II nd Year Civil Engineering.
Ck College Of Engineering & Technology JayaramNagar,
Chellangkuppam, Cuddalore – 607003.

EARTHQUAKE:

- Earthquake occurs when to tectonic plates move suddenly against each other.
- Earthquake is also known as temblors.
- Waves spread from the epicenter, the point on the surface above the hypo centre.
- During earthquake rock suddenly shift from their position and fracture occur on the earth surface.
- Ground shaking from earthquake can collapse buildings, bridges, phone services etc.,

TECHNIQUES TO RESIST EARTHQUAKE

- Active and passive system
- Shear walls
- Bracing
- Dampers
- Rollers
- Isolation
- Light weight material
- Bands
- Others

BASE ISOLATION

- Introduce flexibility to the structure.
- Building is rested on flexible pads (base isolators)
- When earthquake strikes the building does not moves
- It is suitable for hard soil only
- In India base isolation technique was first demonstrated after 1993 killari earthquake.

SEISMIC DAMPERS

TYPES OF SEISMIC DAMPERS

- Viscous dampers (energy is absorbed by silicone-based fluid passing between piston cylinder arrangement).

- Friction dampers (energy is absorbed by surfaces with friction between them rubbing against each other).
- Yielding dampers (energy is absorbed by metallic components that yield).
- Viscoelastic dampers (energy is absorbed by utilizing the controlled shearing of solids).
- Immediate steps must be taken to preserve our environment for our future generation.

SHEAR WALL

- Vertically oriented wide beams
- It carries seismic loads down to the bottom of foundation
- Provides large strength and stiffness to buildings.
- Thickness generally varies from 150mm to 400mm in high rise buildings.

"AVOID SOFT STOREY- CONTINUE WALLS IN GROUND STOREY"

LIGHT WEIGHT MATERIAL

- The group called paksbab is to find the solution for all problems.
- It is to protect and improve the lives of the poor, especially in seismic and temperature region.
- It is simple load bearing design.
- Made with locally fabricated compression moles and manually operated form jacks.

BANDS

- Strong column, weak beam
- Horizontal band necessary through the masonry(a building with no horizontal linet band collapse of roof and walls).
- Latur earthquake incident(a building with horizontal linet band in killari village: no damage).

KEEPING BUILDING UP-RIGHT

- When the quakes strikes the system dissipates energy in the building cores and exteriors.
- The frames are free to rock up and down within fittings fixed at their bases.
- Recently discovered technique of japan

- It has found to be survived even in extreme earthquakes.

QUALITY CONTROL

- Regular testing of construction material at qualified laboratories.
- For example, testing of bricks.
- Period training of workmen at proffosional training house.
- Onsite evaluation of the technical work.

IS-CODES

- Is 1893 (part i), 2002, indian standard criteria for earthquake resistant design of structures (5^{th} revision)
- Is 4326, 1993, indian standard code of practice for earthquake resistant design and construction of buildings (2^{nd} revision)
- Is 13827, 1993, indian standard guidelines for improving earthquake resistance of earthen buildings
- Is 13828, 1993, indian standard guidelines for improving earthquake resistance of low strength masonry buildings
- Is 13920, 1993, indian standard code of practice for ductile detailing of reinforced concrete structures subjected to seismic forces

CONCLUSION

- We civil engineers are here only to provide safety to public to lead their life happily.
- Let us work together to build a cultu

Prediction of Mechanical Properties for Aluminium- Boron Corbide and Fly Ash Hybrid Composites

R. Manivannan and N. Subramanian[2]
[1] PG Student,
Department of Mechanical Engineering,
Dr. Pauls Engineering College,
Villupuram-605109, India,

N. Subramanian[2]
Assistant Professor,
Department of Mechanical Engineering,
Dr. Pauls Engineering College,
Villupuram-605109, India

***Abstract* - Hybrid composite materials have found application in many areas of daily life for quite some time. Materials like aluminium with silicon carbide, boron carbide, fly ash, consisting of carbides and metallic binders, also belong to this group of composite materials. For many researchers the term hybrid composites is often equated with the term light metal matrix composites (mmcs). Substantial progress in the development of hybrid composites has been achieved in recent decades, so that they could be introduced into the most important applications. These innovative materials open up unlimited possibilities for modern material science and development; the characteristics of mmcs can be designed into the material, custom-made, dependent on the application. The advantages of the composite materials are only realized when there is a reasonable cost performance relationship in the component production. The reinforcement of metals can have many different objectives. The reinforcement of light metals opens up the possibility of application of these materials in areas where weight reduction has first priority.**

The development objectives for hybrid composite materials are:

- **Increase in yield strength and tensile strength at room temperature and maintaining the minimum ductility or rather toughness,**
- **Increase in creep resistance at higher temperatures,**
- **Increase in fatigue strength, especially at higher temperatures**
- **Increase in young's modulus.**

The objectives of this project are fabricate hybrid composites with the base metal as LM 25 Aluminum alloy reinforced with a different percentage of Volume of boron carbide particulates and fly ash (5% to 15%) by stir casting manufacturing method. The Specimen for prepared as per the requirements of testing. The mechanical properties like tensile strength, yield strength, material toughness and hardness will be analysed and these results will compare with the conventional materials and existing composite material. Suggest the suitable volume proportioned in hybrid composite.

INTRODUCTION

In the recent advancement of engineering design and manufacturing technology also requirement of our day today applications, the composite materials are play a vital role. The Fiber glass, developed in the late 1940s, was the first modern composite and is still the most common. It makes up about 65 per cent of all the composites produced today and is used for boat hulls, surfboards, sporting goods, swimming pool linings, building panels and car bodies. A piece of wood is a composite, with long fibers of cellulose (a very complex form of starch) held together by a much weaker substance called lignin. Cellulose is also found in cotton and linen, but it is the binding power of the lignin that makes a piece of timber much stronger than a bundle of cotton fibers. In engineering materials, composites are formed by coatings, internal adhesives and laminating. An important metal composite is clad metals. Thermostatic controls are made by roll-bonding a high expansion alloy such as copper to a low expansion alloy like steel. When the composite is heated it will deflect to open electrical contacts. Plywood is also a common composite. Since wood is weaker in its transverse direction than its long direction, the alternating grain in plywood over comes the transverse deficiency.

Humans have been using composite materials for thousands of years. The greatest advantage of composite materials is strength and stiffness combined with lightness. In Modern aviation, both military and civil would be much less efficient without composites. In fact, the demands made by that industry for materials that are both light weight and strong has been the main force driving the development of

composites. The airframes of some smaller aircraft are made entirely from composites, as are the wing, tail and body panels of large commercial aircraft. Composites can be molded into complex shapes. Another advantage of composite materials is that they provide design flexibility. Over recent decades many new composites have been developed, some with very valuable properties. There are varieties of composites that can be manufactured according to the requirements of desired properties for a particular application.

The Composites also a one type of engineering materials provides almost unlimited potential for higher strength, stiffness and corrosion resistance over pure material systems of metals, ceramics and polymers. This will probably be "the steels" of the next century.

The Composite materials are formed by combining two or more materials that have quite different properties. The different materials work together to give the composite unique properties, but within the composite the materials can be differentiated since they do not dissolve or blend into each other. Composites are made up of two materials namely matrix and reinforcement. The matrix or binder surrounds and binds together a cluster of fibers or fragments of the stronger material (reinforcement). In Metal Matrix Composites (MMCs), ceramics or metals in form of fibers, whiskers or particles used to reinforce in a metal matrix.

The objectives of this project are:

- To fabricate Metal matrix composites with the base metal as Aluminum reinforced with a different percentage of Volume of boron carbide particulates (5% to 15%) by a suitable manufacturing method.
- Specimen to be prepared for mechanical testing.
- Determining the mechanical properties like tensile strength, yield strength, material toughness and hardness will be tested.
- Compare the properties with the conventional material and existing composite material.
- Suggest the suitable volume proportioned metal matrix material and Develop the light weight metal matrix composite.

 FABICATION METHOD

- STIR CASTING

The stir casting technique was used to fabricate the composite specimen as it ensures a more uniform distribution of the reinforcing particles. This method is most economical to fabricate composites with discontinuous fibers or particulates. In this process, matrix alloy (LM25) was first superheated above its melting temperature and then temperature is lowered gradually below the liquids temperature to keep the matrix alloy in the semisolid state. At this temperature, the preheated B_4C particles and fly ash of 5-15% (by weight) and graphite particle of average size of 10 µm and 200 µm respectively were introduced into the slurry and mixed using a graphite stirrer. The composite slurry temperature was increased to fully liquid state and automatic stirring was continued to about five minutes at an average stirring speed of 300-350 rpm under protected organ gas. The B_4C particles help in distributing the graphite particles uniformly throughout the matrix alloy.

HYBRID COMPOSITES

Reference to hybrid composites most frequently relates to the kinds of fibre-reinforced materials, usually resin-based, in which two types of fibres and ceramics are incorporated into a single matrix. The concept is a simple extension of the composites principle of combining two or more materials so as to optimize their value to the engineer, permitting the exploitation of their better qualities while lessening the effects of their less desirable properties. As such, the definition is much more restrictive than the reality. Any combination of dissimilar materials could in fact be thought of as a hybrid. A classic example is the type of structural material in which a metal or paper honeycomb or

a rigid plastic foam is bonded to thin skins of some high-performance FRPs, the skins carrying the high surface tensile and compressive loads and the core providing lightweight (and cheap) structural stability. The combination of sheets of aluminium alloy with laminates of fiber-reinforced resin, as in the commercial product ARALL (aramid-reinforced aluminium, Davis, 1985) is a related variety of layered hybrid and the mixing of fibrous and particulate fillers in a single resin or metal matrix produces another species of hybrid composite. In this research, overview is given on the current state of art on aluminium matrix composites with regard to processing, microstructure, properties and applications of AMCs. This research is predominantly concerned with discontinuous fibre reinforcement metal matrix composites, in which Aluminium alloy used as a matrix material and silicon carbide, titanium oxide used as reinforcement materials. Properties of AMCs can be tailored by varying the nature of constituents and their volume fraction. The major advantages of AMCs are as follows:

- Greater strength and Hardness
- Improved stiffness
- Reduced density(weight)
- Creep resistance
- Controlled thermal expansion coefficient
- Improved abrasion and wear resistance
- Improved damping capabilities.

REFERENCES Text

[1] Walter D. pilkey 1997 “peterson's stress concentration factors”, 2nd edition. Wiley Interscience
[2] Vikram Singh and R.C Prasad, 2004 “Tensile and Fracture Behavior of 6061 $AlSic_p$ Metal Matrix Composite”, International symposium of research on materials science and engineering
[3] A.Shakesheff, 1996, "Elevated Temperature Performance of Particulate Reinforced Aluminum Alloys," Materials Science Forum, Vol. 217-222, pp. 1133-1138
[4] Vidya Sagar Avadutala, 2005, “Dynamic Analysis of Cracks in Composite Materials” Wiley Interscience
[5] P. Rohatgi, 1991, "Cast Aluminum Matrix Composites for Automotive Applications," Journal of Metals.
[6] Dr.A.V.Phan, ANSYS Tutorials -2D Fracture analysis
[7] ANSYS Documentation
[8] M.Ramachandran”Material science-Poland, Vol24,No21,2006.
[9] Introduction to Fracture Mechanics, Dr.Prashant kumar.
[10] Mechnical Metallurgy, George Dieter

Analysis of Microchannel Heat Exchanger for Electronic Equipments Cooling using SiO_2/Water Nanofluid

A.Sivakumar[1] Associate Professor,
K.Thamizhmaran[2] Assistant Professor
G.Kadiravan[3], B.Porselvan[4], G.Gunaseelan[5]
Department of Mechanical Engineering
Christ College of Engineering and Technology, Puducherry

Abstract—In this work the experimental and numerical investigation for the improved heat transfer characteristics of parallel type microchannel heat sink using SiO_2/water is done. The fluid flow characteristics is also analyzed for the parallel type microchannel. The experimental results of the heat transfer using SiO_2/water is compared with the numerical values. The results in this work suggest that the best heat transfer enhancement can be obtained in a system with water-cooled micro channel with parallel type fluid flow. The heat transfer from smaller area is achieved through microchannels.The maximum heat transfer is achieved in microchannels with minimum pressure drop across it.

Keywords—Parallel type,Microchannel Heat sink, Heat Transfer enhancement , Friction factor, Nanofluid SiO_2/Water.

INTRODUCTION

The application of micro channels in heat transfer was first proposed by Tuckerman and Pease [1] in the electronic chip which could be effectively cooled by means of water flow in microchannels fabricated on the circuit board on which the chips are mounted. The need for thermal management in high end power electronic workstations cooling,application servers and data centers [2] is an exceedingly demanding area that requires continuous research efforts to develop efficient and cost competitive cooling solutions. Some of the commonly used heat transfer fluids are the Air, ethylene glycol and engine oil for the past some decades[3].

The water was formulated by Lee et al [4]without any chemical dispersants and performed experiments to show that water have good suspension and dispersion characteristics and high thermal conductivities. The importance of micron size mechanical devices are emphasized both in commercial and scientific application [5,6]. Kandlikar et al[7].also insisted the the need of micro system in for heat transfer enhancement in micro scale devices.

Jung-Yeul et al [8] have reported that the Nusselt number increases with increasing Reynolds number in laminar in his experimental study. Microchannel heat exchangers are classified as micro, meso, compact and conventional heat exchanger based on channel diameters [9]. In this study the heat transfer characteristics of water /SiO2 flowing through Parallel MC and hydraulic diameter of 0.81mm is investigated.

EXPERIMENT STUDY

PREPERATION OF NANOFLUID

Gamma Silicon Dioxide was used for the preperation of γ SiO_2Nanofluid with water as the Base material. γSiO_2nanoparticales were dispersed in 3.5 lits of ultra pure double distilled water under sonification at different volume fraction say 0.01,0.02,0.03,0.1,0.2,0.3 and tested for the heat trasfer property of the material in the microchannel.

PROPERTIES OF WATER

The standard properties of water is

Density	=1000 kg/m^3
Thermal conductivity	=0.56 W/mK
Specific Heat Capacity	=4.217 KJ/kgK

PROPERTIES OF NANOPARTICLES

Various researchers have published the properties of nanoparticles and thermal properties of nanofluids as the basis of research on nanofluids applications. The published specific heat, thermal conductivity and density of SiO2 nanoparticles is

Density	= 2.4x103 kg/m^3
Specific Heat Capacity	= 680 j/kgK
Thermal Conductivity	= 1.3W/Mk

DIAGRAM FOR MICROCHANNEL

Upper Part — Parallel Type Microchannel

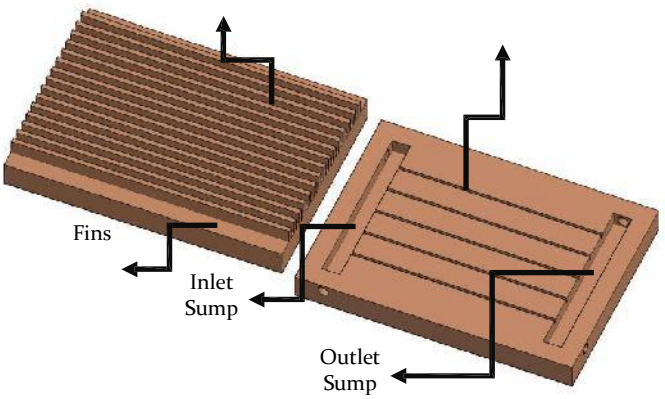

Fig.(1) Three Dimensional View

As per the given dimensions, Fig.(1) can be machining using a EDM process. With help of bed type surface grinding machine, a copper plate can be grinded and inlet, outlet sumps can be drilled using a milling process. Upper part and Lower part is brazed after the machining process respectively.

THEORITICAL DATA ANALYSIS

HYDRAULIC DIAMETER

A Hydraulic Diameter can be used for to circulate the SiO2 nanofluids with base fluid in parallel type microchannel. It can be calculated using this formula,

$$Dh = 2WH/(W+H)$$

where,

W - Width of the microchannel = 0.8mm

H - Height of the microchannel = 0.9mm

Using this formula we calculated the hydraulic diameter is 0.81mm.

THEORITICAL HEAT TRANSFER COEFFICIENT

Theoritical heat transfer can be calculated using this formula,

$$h= Nu.k/D$$

where,

Nu - Nusselt Number = 0.024Re0.7Pr0.9
k - Thermal conductivity
D - Hydraulic Diameter

REYNOLDS NUMBER

Assuming the Reynolds number between 100 to 1300,

$$Re = UD_h/Vf$$

VISCOSITY

Viscosity for nanofluids formula is

$$\mu nf = \mu bf(1+2.5)*Ø$$

From this we found the Flow velocity, U is $2.3177x10^{-4}$ m/s.

CORRELATIONS FOR NANOFLUIDS

a) Density = (1- Ø)Pbf + ØPp

b) Specific heat capacity =(1- Ø)Cbf +Ø(Cp)p
c) Thermal Conductivity
={(kp+2kbf+2(kp-kbf)(Ø))/(p+2kbf-2(kp-kbf)(Ø))}kbf

From this, the theoretical heat transfer coefficient is $7.022x10^{-6}$ W/m^2K.

EXPERIMENTAL SETUP

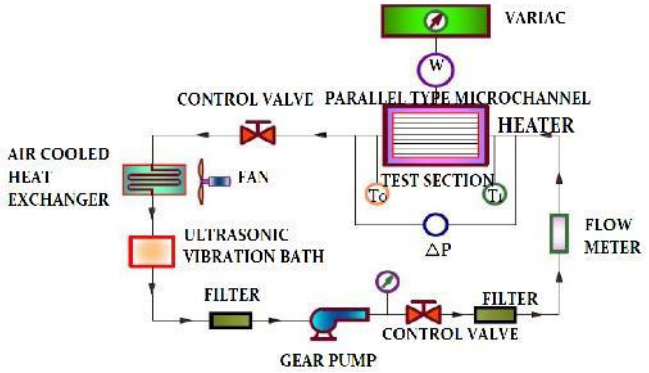

The experimental setup consists of a Ultrasonic vibration Bath, Pump, Filter, Flow meter ,Micro-channel, Heater and Air cooled heat exchanger. SiO2 nanofluids are stored in the ultrasonic vibration bath and it acts as a reservoir and sonificator. A heater is fixed on the surface of the microchannel. A pump is attached between the bath and the microchannel to circulate nanofluids through the entire circuit. The unwanted micron size particle are removed using filters. Flow meter is placed between the pump and micro channel. Fluid flow rate is controlled by the control valve and it is placed between the pump and channel.

The pressure gauges are fixed at the inlet and outlet of the micro channel and used to measure the pressure drop of the channel. When the nano fluid passes through microchannel, it absorbs some amount of heat supplied by the heater and the excess heat carried by the nano fluid is released when it passes through the air cooled heat exchanger, then the fluid moves to the bath and the cycle is repeated. The entire set-up is kept airtight in order to prevent any leakage of the fluid.

CONCLUSIONS

In this work the heat transfer characteristics of parallel type microchannel heat sink with SiO_2water is experimented. The convective heat transfer coefficient for the low volume percentage there is considerable enhanced thermal conductivity for the water. Thermal performance of water in all concentration study showed has better efficiency. Temperature distributions on the parallel type MC were very higher using pure water.

Thermal Resistance of the MC heat sink was decreased when using water.When the volume fraction is increased in the water, then the water thermal conductivity increases considerably. The experimental performance study of MC load with water proved. In this work, a parallel type microchannel heat exchanger can try to prove that the high heat transfer absorption rate, here a rectangular duct used to flow the fluids. After the design, experimental work has been fabricated and analysed.

REFERENCES

(1) D.B. Tuckerman, R.F.W.Pease, Hight-performance heat sinking for VLSI, IEEE Elecr. Dev.Lett.EDL-2(1981) 126-129.

(2) Randeepsingh ,Aliakbar,Sintered porous heat sink for cooling of high-powered microprocessors for server applications for International Journal of Heat and Mass Transfer 52 (2009) 2289-2299. 15

(3) Tu-ChiehHung , Wei-Mon Yan , Xiao-Dong Wang, Chun-Yen Chang , Heat transfer enhancement in microchannel heat sinks using nanofluidsforInternational Journal of Heat and Mass Transfer 2012.

(4). Bar-Cohen, P. Wang, E. Rahim, Thermal management of high heat flux nanoelectronic chips, Microgravity Science and Technology 19 (3) (2007) 48-52.

(5) A. Bar-Cohen, P. Wang, E. Rahim, Thermal management of high heat fluxnanoelectronic chips, Microgravity Science and Technology 19 (3) (2007)48-52.

(6) T.A. Ameel, R.O. Warrington, R.S. Wegeng, M.K. Drost, Miniaturization technologies applied to energy systems, Energy Convers. Mgmt. 38 (1997) 969–982.

(7) Kandlikar S, Garimella S, Li D, Colin S, King MR. Heat transfer and fluid flow in minichannels and microchannels. Great Britain: Elsevier Ltd.;

(8) Jung-YeulJung.,Hoo-Suk Oh, and Ho-Young Kwak, 2009. Forced convective heat transfer of nanofluids in micro- channels. Int. J. Heat Mass Transfer 52, pp: 466-472.

(9) W.Qu, I. Mudawar, A systematic method for optimal design of two-phase micro channels heat sink, ASME J.Electron, packaging 127(2005) 381 390.

A Study on the Mechanical Properties of Aluminium Reinforced With Nano Sic by Powder Metallurgy

1. Mathiazhagan.S [a], 2.Anbazhagan.S [a], 3.Arul Kumar. A [a], 4.Pradeep Devaneyan.S [b]
a: Student,
Department of Mechanical Engineering,
Christ College of Engineering and Technology, Moolakulam, Puducherry-605010.
b: Associate Professor,
Department of Mechanical Engineering,
Christ College of Engineering and Technology, Moolakulam, Puducherry-605010.

***Abstract*—Reinforcing aluminium matrix with much smaller particles, submicron or nano-sized range, is one of the key factor in producing high-performance composites, which yields improved mechanical properties. The aluminium based metal matrix composites reinforced with nano SiC using powder metallurgy process is to increase the mechanical properties like low density, high elastic modulus, wear resistance and strength. Production of a homogenous, high strength and net shape structural components made from aluminium-silicon carbide composites can be achieved using powder metallurgy (PM) technology. The composition is mixed with required ratio and is compacted in the die for obtaining the green compact. Generally the results show the tendency for both the strength and ductility to increase upon increasing the sintering temperature and almost there are very small changes above specific sintering temperature which mainly depends upon the silicon carbide content. And the final stage process consists of sintering the billet at suitable aluminium temperature range. The billets are tested for SEM, compression test, ring compression test and micro-hardness test for investigating the different micro structural and mechanical properties of a metal matrix composite.**

Keywords*— *Metal Matrix Composite, powder metallurgy, SEM, micro hardness test.

I.INTRODUCTION

The aluminium which known for its low density, high elastic modulus and wear resistance are used as main MMC. The nano SiC is used as reinforcement for aluminium and the proper bonding of nano SiC with the surrounding particles of aluminium particles depends upon the compaction and sintering process of the billet. Using powder metallurgy (PM) method to produce aluminium composites reinforced with SiC particulates produce a homogenous distribution of reinforcement in the matrix [1].

Figure:1 Pure Aluminium Powder

Aluminium alloys are preferred engineering material for automobile, aerospace and mineral processing industries for various high performing components that are being used for varieties of applications owing to their lower weight, excellent thermal conductivity properties [2]. In the Fig.1 shows the pure aluminium which has the mesh size of 300 which was for this project. Powder metallurgy is a process in which parts are produced from metallic powders and is used to manufacture the parts to near net shape. In the usual powder metallurgy production sequence, the powders are blended into the certain ratio and are compacted (pressed) into desired shape and then heated (sintered) to bond the particles into a hard and rigid product. It is an important method to produce the parts to net shape, eliminating or reducing the need for subsequent machining and the waste is very about negligible of 3%. In the powder metallurgy process there are three steps which required forming the billet namely: the mixing (blending), compacting, and sintering. Industrial applications of powder metallurgy parts are several which include: self lubricating bearings, porous metal filters and a wide range

of engineered shapes such as gears, cams, brackets, sprockets, etc. The reinforcement that are present abundantly and are highly used to strengthen the application parts nowadays are aluminium oxide, silicon carbide and tungsten carbide. Silicon carbide is comparatively high than aluminium oxides in physical properties such as stiffness, improved wear resistance and low when compared to tungsten carbide.

Figure:2 Nano Silicon Carbide

The Fig.2 shows nano silicon carbide which has the nano size of less than 100µm. When nano SiC is used as reinforcement with aluminium it further increase the mechanical application of aluminium and used in automobile and aerospace industries. Scanning Electron Microscope, X-Ray diffraction, Energy dispersive X-ray analysis, micro-hardness test, ring compression test and wear test are conducted to identify the characteristics and the study of aluminium and nano silicon carbide composites. The testing involves both micro-structural study and normal mechanical testing.

II.EXPERIMENTAL DETAILS

A) Introduction:

Powder metallurgy is a process in which parts are produced from metallic powders and is used to manufacture the parts to net shape. In principle, continuously reinforced materials offer better specific strength, and the effort involved in their development has been higher than for other composites[5]. The powder metallurgy process generally consists of four basic steps: powder manufacture, powder blending, compacting, and sintering. Compacting is generally performed at room temperature, and the elevated-temperature process of sintering is usually conducted at atmospheric pressure. In the Fig.3 shows the various stages involved in powder metallurgy to manufacturing the complete product.

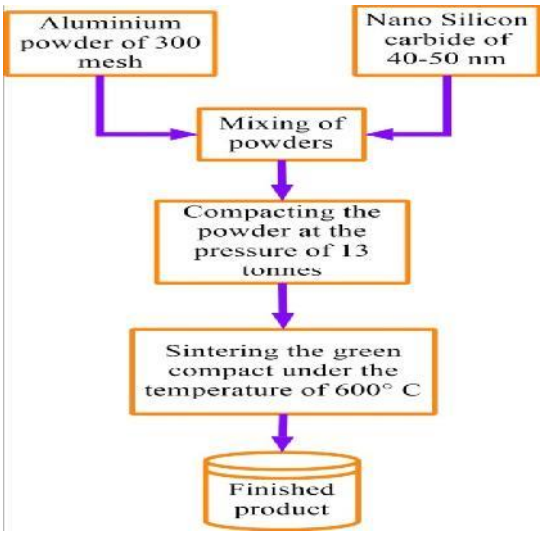

Figure:3 Flowchart of powder metallurgy process

B) Fabrication of Die:

The die is made up of D2 steel (It is an air hardening, high-carbon, high-chromium tool steel and it has high wear and abrasion resistant properties). The punch is made up of EN24 steel (It is supplied in the condition with a tensile strength of 850/1000 N/mm^2). The Fig.4 shows the parts of the die which was fabricated for the present project work. The most basic consideration is being able to remove the billet from the die after it is pressed, along with avoiding sharp corners in the design. Die consists of two punches namely the upper punch and lower punch which are positioned at Universal Testing Machine [UTM] for compaction of powder material to the required shape.

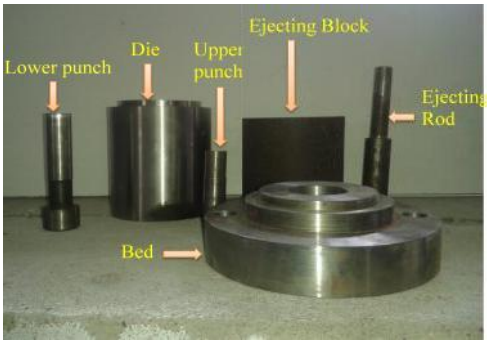

Figure 4: Photograph of fabrication die and its components

C) Compaction:

Powder compaction is the process of compacting metal powder in a die through the application of high pressure. Generally the tools are held in the vertical orientation with the punch tools forming the bottom of the cavity. Al-based metal matrix composites with high strength combined with considerable plastic deformation were maintain the temperature of 600° C and then it is synthesized using P/M methods[6]. The metal matrix composites of aluminium are reinforced with 0%, 2%, 4%, 6%, 8% and 10% of SiC particles. The powders is then compacted into a shape and ejected from the die cavity. The density of the compacted powder is directly proportional to the pressure applied. The work piece after the pressing is called a green compact. The powders are compacted according to the composition shown in Table:1

TABLE:1 COMPOSITIONS OF THE POWDERS

Sl.No	Compositions of Al	Composition of SiC
1	90%	10%
2	92%	8%
3	94%	6%
4	96%	4%
5	98%	2%
6	100%	0%

But the punch adopted here is single punch since the size of the billet which was manufactured for testing is flat billet withstands the extreme pressure without deforming or bending. Tools must be made from materials that are polished and wear-resistant. Filling a die cavity with a known volume of the powder feed-stock, delivered from a fill shoe compaction of the powder within the die with punches to form the compact. The powder is compacted at the pressure of 13 tonnes in the die and zinc state is used as the lubricant for the ejection of punch.

D) Sintering:

Sintering is the process of compacting and forming a solid mass of material by heat and without melting it to the point of liquefaction. Heat treatment process is done to bond the metallic particles, thereby increasing strength and hardness. Moreover, the melting point of aluminium is high enough to satisfy many application requirements, yet sufficiently low to render composite processing reasonably convenient[4]. Usually it is carried out between 70% and 90% of metal's melting point. However, the hardness of the sintered part increases remarkably the density of the sintered part becomes smaller than that of the green compact [7]. Once compacted into the mould the material is placed under a muffle furnace which is shown in for a period of time (six hours) and left for cooling naturally. Under heat, bonding takes place between the porous aggregate particles and once cooled the powder has bonded to form a solid component. And the green compact is kept inside the muffle furnace with the help of silica crucible.

E) Preparation of the samp ɛ:

Polishing is defined as the process of making the fine surface of the specimen performed after manufacturing of that using specimen polishing methods. It is the most important step in preparing a specimen for micro-structural analysis. Aluminium powders are also used as a material to achieve the weight reduction of the compacts[8]. It is the step which is required to completely eliminate previous damage. After the completion of sintering process the billets are polished by two methods

- Rough polishing.
- Fine polishing.

Rough polishing is the method in which the billets are rubbed in the various scales in emery sheets by rubbing the billets into horizontal and vertical direction. After completion of rough polishing the billets are rubbed in a specimen polishing machine for getting fine polishing for micro-structural analysis. The billets are dipped in the distilled water for viewing the clear surface and then the alumina paste is applied to the billet and the surface of polishing machine. And the Fig. 5 shows the billets of different compositions having fine surface for the micro-structural analysis.

Figure:5 Billets of different compositions

III.TESTING DETAILS

A)Scanning Electron Microscope (SEM) analysis:

Scanning electron microscopy (SEM) uses a focused electron probe to extract structural and chemical information point-by-point from a region of interest in the sample. The high spatial resolution of an SEM makes it a powerful tool to characterise a wide range of specimens at the nanometre to micrometre length scales. And the name of the samples for the required composition are shown in table.4

TABLE:4. SAMPLE NAME FOR REQUIRED COMPOSITION

Sl no	Sample name	Composition of aluminium	Composition of nano sic
1.	1A	90%	10%
2.	2A	92%	8%
3.	3A	94%	6%
4.	4A	96%	4%
5.	5A	98%	2%
6.	6A	100%	0%

B) Micro-hardness test:

The term Micro Hardness Testing usually refers to static indentations made by loads of 1kgf. or less. The Baby Brinell Hardness Test uses a
1mm carbide ball, while the Vickers Hardness Test employs a diamond with an apical angle of 136°, and the Knoop Hardness Test uses a narrow rhombus shaped diamond indenter. The test surface usually must be highly polished. The smaller the force applied the higher the metallographic finish
required. Microscopes with a magnification of
around 500x are required to accurately measure the indentations produced. From six to four indentations were made for each sample**.** According to the reputability of the reading and an average of these reading was calculated. The position of indentation in the sample was chosen randomly in the sample to take in consideration the effect of present of two distinct materials the matrix and the reinforcement.

D) Ring compression test:

The method of free ring compression is the most widely applied method for determining contact conditions in bulk forming processes; therefore it is treated as the standard, universal method for determining coefficient / factor of friction. In each compression step, deformation was made to half the total fracture height. The final compression test was the one, which resulted in immediate crack observation[3]. And the hole is made on the surface of the billet by the help of the
10 mm drill bit in the drilling machine. The billet is compressed with the help of the Universal Testing Machine [UTM] for the time period of 1minute.

III.CONCLUSION

This paper has highlighted mechanical parameters like hardness, strength, porosity and wear resistance of aluminium increased by reinforcement with nano SiC by powder metallurgy method. The grain factor and density factor is obtained from its microstructure study. Sintering temperature of 600° C was enough to produce a successful sintering for the aluminium with no silicon carbide content. Hence the proper bonding of nano SiC to aluminium must occur at high optimum level and in order to achieve the material that are used for industrial application or uses. The microstructure examination showed that composite has a homogenous distribution and the interaction between the constituents.

REFERENCES

[1] W. M. Khairaldien, A.A. Khalil and M. R. Bayoumi, production of aluminium-silicon carbide composites using powder metallurgy at sintering temperatures above the aluminium melting point

[2]I.Mobasherpour, A.A.Tofigh, M. Ebrahimi, Effect of nano- size Al_2O_3 reinforcement on the mechanical behaviour of synthesis 7075 aluminium alloy composites by mechanical alloying, Materials Chemistry and Physics 138 (2013) 535-541.

[3] Mohamed A. Taha, Nahed A. El-Mahallawy, Ahmed M. El-Sabbagh, Some experimental data on workability of aluminium particulate-reinforced metal matrix composites, Journal of Materials Processing Technology 2 0 2 (2 0 0 8) 380–385.

[4] C. Srinivasa Rao and G. S. Upadhyaya, 2014 and 6061 aluminium alloy-based powder metallurgy composites containing silicon carbide particles/fibres.

[5] J.M. Torralbaa,, C.E. da Costab, F. Velascoa, P/M aluminium matrix composites: an overview, Journal of Materials Processing Technology 133 (2003) 203–206.

[6] S. Scudino, G. Liu, K.G. Prashanth, B. Bartusch, K.B. Surreddi, B.S. Murty, J. Eckert, Mechanical properties of Al- based metal matrix composites reinforced with Zr-based glassy particles produced by powder metallurgy, Acta Material 57 (2009) 2029–2039.

[7] Akira Fujiki, Present state and future prospects of powder metallurgy parts for automotive applications, Materials Chemistry and Physics 67 (2001) 298–306.

[8] K. Yamaguchi, N. Takakura and S. Imatani, Compaction and Sintering Characteristics of Composite Metal Powders, Journal ofMaterials Processing Technology 63 (1997) 364-369

Mechanical Behaviour of Powder Metallurgy based Copper Reinforced with Nano Sic

1.Kathiravan.M [a], 2.Gladson Sargunam.C [a], 3.Ezhumalai.N [a], 4.Pradeep Devaneyan.S[b]

a: Student, Department of Mechanical Engineering, Christ College of Engineering and Technology, Moolakulam, Puducherry-605010.

b: Associate Professor, Department of Mechanical Engineering, Christ College of Engineering and Technology, Moolakulam, Puducherry-605010.

***Abstract*— This project comprises of manufacturing copper metal matrix composites reinforced with nano SiC using powder metallurgy process to increase the mechanical properties like hardness, porosity and wear resistance. In this powder metallurgy method, the SiC particulate -reinforced copper composites were prepared by compacting and then by conventional sintering. The copper is selected as metal matrix composites for its high hardness, high strength and good wear resistance. The mixtures of powders are compacted at 600 Mpa, and sintered at 900^0c in the furnace. The density, hardness, strength and micro structures were investigated on the metal matrix composites. The SEM studies show the uniform distribution of silicon carbide over the copper matrix and XRD analysis represents the presence of Cu and SiC in the composites. The physical and mechanical properties of the copper SiC metal matrix composites are determined using compression, ring compression method and micro-hardness test. During this investigation both ductility and brittle nature were also examined. The idea of this project is to reinforce the SiC with the copper as per proportion tabulated for producing metal matrix composite which can be most applicable metals in the industries.**

***Keywords*— Reinforcement, powder metallurgy, SEM, ring compression test.**

I.INTRODUCTION

Copper possess high strength, good wear resistance, excellent current and thermal conductivity than other metal, like iron & Al. Hence it's been widely used in today's manufacturing field for production of unique parts. The material such as silver, gold having physical properties higher than that of copper, but were not economic when compared to its cost for utilizing in manufacturing sector[1].Copper having high melting point of 1050^0c could be heated up to 950^0c which enables the criteria of blending the shape of copper to appreciated forms. The cables, wires and electric contacts which is used to pass current in between the appliance are extensively made from copper[1].Copper is also used as heat sink to remove heat from hot spots quickly[7].Elemental powders like copper are more compressible which produce compacted objects with good strength. The aerospace auto motive drive shafts, ground vehicle brake rotors and explosive engine components widely use copper [4]. As the machined product are facing so many problems during the mechanical operations. Like cracks, breakages, tool wear cause the major issue in reduction of product life. Hence of the powder metallurgy are best suited methods to enhance the wear, strength, toughness properties of material, by reinforced with most particles such as SiC, Al_2o_3, WC, SiO_2 etc.

Powder Metallurgy is the process of blending fine powdered materials, pressing them into a desired shape or form (compacting), and then heating the compressed material in a controlled atmosphere to produce thedesired product. Powder metallurgy is most advantageous since, it make use of raw materials without any wastage as scrap during the process. The economical mass production can be performed better by powder metallurgy process. In the powder metallurgy process the following three steps are followed in sequence namely the mixing (blending), compacting, and sintering. Industrial applications of powder metallurgy parts are several which include self lubricating bearings, porous metal filters and a wide range of engineered shapes such as gears, cams, brackets, sprockets, etc. By introduction of dispersoid particles in copper matrix will increase the mechanical strength dramatically which are known as reinforcement [1].The reinforcement is a main criteria that has been introduced in powder metallurgy to strengthen the manufactured parts. Silicon carbide is comparatively high than aluminium oxide in physical properties (stiffness, improved wear resistance) and low when compared to tungsten carbide, yet SiC used for its economic cost as

tungsten carbide being costlier [3].There will be a significant improvement in the mechanical properties when copper was incorporated with particulate reinforcement such as SiC [6].The application of Cu-SiC matrix are used in preparing automobile parts and also used in spacecraft. SEM, XRD, EDS, micro-hardness test and ring compression test were conducted on Cu-SiC matrix to study its micro-structural characteristics and mechanical properties. The objective of this project is to produce copper by reinforcing with nano SiC which ought to be utilized in making components of high strength and good wear resistance.

II.EXPERIMENTAL DETAILS

A) Introduction:

Powder metallurgy is the process of blending fine powdered materials by pressing them into a desired shape or form (compacting), and then heating of the compressed material in a controlled atmosphere for a proper composite material (sintering). The powder metallurgy process generally consists of four basic steps: powder manufacture, powder blending, compacting, and sintering. Compacting is generally performed at room temperature, and the elevated-temperature process of sintering is usually conducted at atmospheric pressure. The use of powder metal technology bypasses the need to manufacture the resulting products by metal removal processes, thereby reducing costs.

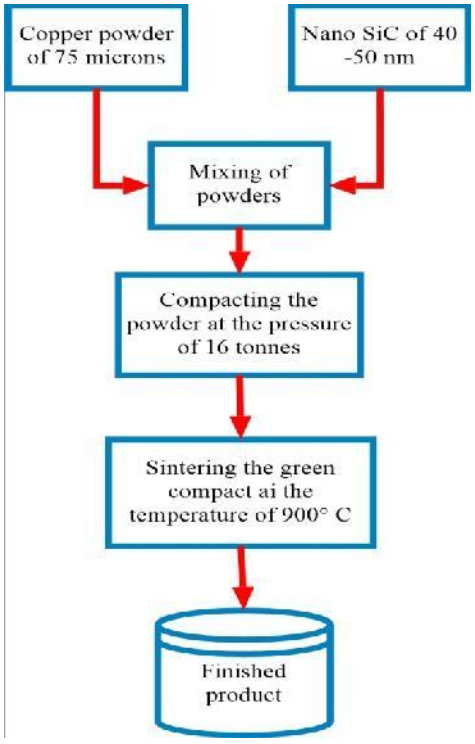

Fig .1. Flow chart of powder metallurgy process.

B) Fabrication of Die:

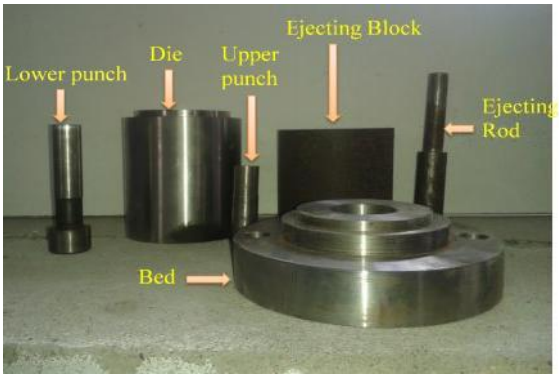

Fig .2.Photograph of the Fabrication die

Fig.2 shows that parts of the die which was fabricated for the present project work most basic consideration is being able to remove the part (billet) from the die after it is pressed, along with avoiding sharp corners in the design. Die consist of two punches namely the upper and lower punch which are positioned at compacting machine(UTM) for compaction of powder material to the required shape.

C) Compaction:

The Powder compaction is the process of compacting metal powder in a die through the application of high pressures using compacting machine. The metal matrix composite of copper is reinforced with 0%, 2%, 4%, 6%, 8% and 10% of SiC particles. The density of the compacted powder is directly proportional to the amount of pressure applied. There are four major classes of tool styles: single-action compaction, used for thin, flat components; opposed double-action with two punch motions, which accommodates thicker components; double-action with floating die and double action withdrawal die. Double action classes give much better density distribution than single action. But the punch adopted here is single punch since the size of the billet which was manufactured for testing is flat billet. Tooling must be designed so that it will withstand the extreme pressure without deforming or bending. Tools must be made from materials that are polished and wear-resistant. Filling a die cavity with a known volume of the powder feed-stock, delivered from a fill shoe followed by compaction of the powder within the die with punches to form the billet.

D) Sintering:

Sintering is the process of compacting and forming a solid mass of material by heat and without melting it to the point of liquefaction. Heat treatment process is done to bond the metallic particles, thereby increasing strength and hardness.

Usually it is carried out between 70% and 90% of metal's melting point. However, the hardness of the sintered part increases remarkably the density of the sintered part becomes smaller than that of the green compact [9]. Once compacted into the mould the materials is placed under a muffle furnace for a period of time (six hours) and maintain the temperature of 900° C and then it is left for cooling naturally. Under heat, bonding takes place between the porous aggregate particles and once cooled the powder has bonded to form a solid component. And the green compact is kept inside the muffle furnace with the help of silica crucible.

Once compacted into the mould the material is placed under a high heating furnace for a period of six hours and then it is left for cooling naturally. Under heat, bonding takes place between the porous aggregate particles and once cooled the powder has bonded to form a solid component. The hardness of copper-SiC bonding increase with increase in temperature. The critical loads were the one that causes severe wear increases with the reinforcement content at high temperature.

E) Preparation of sample

Polishing is defined as the process of making the fine surface of the specimen performed after manufacturing of that using specimen polishing methods. It is the most important step in preparing a specimen for micro-structural analysis. It is the step which is required to completely eliminate previous damage. After the completion of sintering process the billets are polished by two methods

- Rough polishing.
- Fine polishing.

Rough polishing is the method in which the billets are rubbed in the various scales in emery sheets by rubbing the billets into horizontal and vertical direction. After completion of rough polishing the billets are rubbed in a specimen polishing machine for getting fine polishing for micro-structural analysis. The billets are dipped in the distilled water for viewing the clear surface and then the alumina paste is applied to the billet and the surface of polishing machine. And the fig.3 shows the billets of different compositions having fine surface for the micro-structural analysis.

Fig .3.Sample of different composition

III.TESTING DETAILS

A) Scanning Electron Microscope (SEM) analysis:

Scanning electron microscopy (SEM) uses a focused electron probe to extract structural and chemical information point-by-point from a region of interest in the sample. The high spatial resolution of an SEM makes it a powerful tool to characterise a wide range of specimens at the nanometre to micrometre length scales.

TABLE.1. PERCENTAGE COMPOSITION OF Cu & SiC IN SIX SAMPLE

Sl no	Sample name	Composition of Cu	Composition of SiC
1.	11A	90%	10%
2.	12A	92%	8%
3.	13A	94%	6%
4.	14A	96%	4%
5.	15A	98%	2%
6.	16A	100%	0%

B)Micro-hardness test

The term Micro Hardness Testing usually refers to static indentations made by loads of 1kgf. or less. The Baby Brinell Hardness Test uses a 1mm carbide ball, while the Vickers Hardness Test employs a diamond with an apical angle of 136°, and the Knoop Hardness Test uses a narrow rhombus shaped diamond indenter. The test surface usually must be highly polished. The smaller the force applied the higher the metallographic finish required. Microscopes with a magnification of around 500x are required to accurately measure the indentations produced. From six to four indentations were made for each sample. According to the reputability of the reading and an average of these reading was calculated. The position of indentation in the sample was chosen randomly in the sample to take in consideration the effect of present of two distinct materials the matrix and the reinforcement.

C) Ring compression test

The method of free ring compression is the most widely applied method for determining contact conditions in bulk forming processes; therefore it is treated as the standard, universal

method for determining coefficient / factor of friction. And the hole is made on the surface of the billet by the help of the 10 mm drill bit in the drilling machine. The billet is compressed with the help of the Universal Testing Machine [UTM] for the time period of 1minute.

CONCLUSION

This paper as highlighted the mechanical parameters like high hardness, high strength and good ductility of the powder metallurgical produced pure copper reinforced with nano SiC .The grain and density factor are obtained from micro structural study .Hence the proper bonding of nano SiC to the copper particles at required level increases the properties of the billet to extent that are required for industrial applications. The sintering are ought to be done accordingly to the copper recommended temperature scale for avoiding dis appropriate mechanical failures.

REFERENCE

1. G.Celebi Efi,S.Zeytin,C.Bindal,The effect of SIC particle sizeon the properties of CU-SIC composites, Materials and design 36(2012) 633-639.
2. Th.Schubert,B.Trindade,T.Weibgarber,B.Keiback,Interfical design of CU-based composites prepared by powder metallurgy for heat sink application, Material science and engineering A 475(2008) 39-44.
3. S.F.Moustafa,Z.Abdel-Hamid,A.M.Abd-Elhay, Copper matrix SIC and AL_2O_3 particulate composites by powder metallurgy technique, Material letters 53 (2002) 244-249.
4. Hailong wang,Rui Zhang,Xing Hu,Chang-An Wang,Yong Huang, Characterization of a powder metallurgy SIC/Cu-Al composites, Journal of materials processing technology I 97 (2008) 43-48.
5. Y.C.Lin,H.C.Li,S.S.Liou,M.T.Shie,Mechanism of plastic deformation of powder metallurgy metal-matrix composites of CU-Sn/Sic and 6061/Sic under compressive stress ,Material science and engineering A 373 (2004) 363-369.
6. G.Celebi Efi,T.Yener,I.Altinsoy,M.Ipek,S.Zeytin,C.Bindal,The effect of sintering temperature on some properties of Cu-Sic composites, Journal of alloys and compounds 509 (2011) 6036-6042.
7. Th.Schubert,A.Brendel,K.Schmid,Th.Koeck,L.Ciupinski,W.Zielinski,T.Wiebgarber,B.Kieback,Interfacial design of Cu/Sic composites prepared by powder metallurgy for heat sink applications,Composites : parts A 38 (2007) 2398-2403.

Experimental Investigation of CuO and SiO_2 Nano Particles with Water on Solar Flat Plate Collector

A.Sivakumar[1] Associate Professor,
K.Thamizhmaran[2] Assistant Professor
N.Anandakannan[3], P.Ramesh[4], A.Velankani[5]
Department of Mechanical Engineering
Christ College of Engineering and Technology, Puducherry

***Abstract*—Renewable energy is an alternative source. Among all renewable energies, we have solar energy in abundance and solar collectors are commonly used to harvest the energy. The conventional fluids which are used as the heat transfer medium in solar collectors suffer from poor thermal and heat absorption properties. It has been found that these conventional fluids have a limited capacity to carry heat up, which in turn limits the collector performance. It has been observed that for conventional fluids, suspending the nanoparticles in a liquid (Nanofluid) can be a good substitute because of the improved thermal properties. A new type solar collector named 'Direct Solar Absorption System' (DSAS) is used as the experimental set-up. DSAS is more efficient collector then the conventional type solar collector.**

Keywords: Nanofluid. Flat-plate, Solarcollector, water-CuO, SiO_2.

I. INTRODUCTION

Sun is the main source of energy in solar system. It offers use the energy of great potential in terms of supplying the world's need. As the primary energy resources are depleting continuously, solar energy draws attention of researchers throughout the world. Solar energy is one of the alternative energies that have vast potential. It is estimated that the earth receives approximately 1000W/m^2 amount of solar irradiation in a day [1]. The solar radiation incident on the Earth's surface is comprised of two types of radiation – beam and diffuse, ranging in the wavelengths from the ultraviolet to the infrared (300 to 200 nm), which is characterized by an average solar surface temperature of approximately 6000°K[2] . The mount of this solar energy that is intercepted is 5000 times greater than the sum of all other inputs – terrestrial nuclear, geothermal and gravitational energies, and lunar gravitational energy[3]. To put this into perspective, if the energy produced by 25 acres of the surface of the sun were harvested, there would be enough energy to supply the current energy demand of the world. When solar radiation incident on a surface then some of this radiation is absorbed and in turn, increase the temperature of the surface. As the temperature of the body increases, the surface loses heat at an increasing rate to the surroundings. Steady-state is reached when the rate of the solar heat gain is balanced by the rate of heat loss to the ambient surroundings The total energy received from the sun, per unit time, on a surface of unit area kept perpendicular to the radiation, in space, just outside the earth's atmosphere is known as Solar Constant. The solar radiation that reaches the surface of the earth is known as beam (direct) radiation, and the scattered radiation that reaches the surface from the sky is known as sky diffuse radiation.

II. EXPERIMENT STUDY

A. *Material selection criteria*

- *Glass*-low iron tempered and durability
- *Absorber plate*-high thermal conductivity,absorbe maximum amount of radiation
- *Tube*-high thermal conductivity
- *Insulation and outer cover*-low thermal conductivity,resistance to heat

B. *Flat plate collector*

It basically consists of a flat surface with high absorbtivity for solar radiation, called the absorbing surface, is a schematic representation of a typical flat-plate solar collector. Typically metal plates, usually of copper, steel or aluminum material with tubing of copper in thermal contact with plates, are the mostly commonly used materials. The absorber plate is usually made from a metal sheet 0.3 to 0.5 mm thickness. For the absorber plate, corrugated galvanized sheet is a material widely available throughout the world and it is one of the simplest particle applications. The methods of bonding and clamping tubes to flat or corrugated sheet is the tube in strip or roll bond design, in which the tubes are formed in the sheet, ensuring a good thermal bond between the sheet and the tube.fig(1)

C. Selection of Materials for flat-plate collectors.

(a)Absorber Plate Materials:

- The collector absorber plate should have high thermal conductivity, adequate tensile and compressive strength, and good corrosion resistance.
- Copper is generally preferred because of its extremely high conductivity and resistance to corrosion. Collectors are also constructed of aluminium, steel and various thermoplastics.
- Absorber plates for flat-plate solar collectors were usually constructed with tubes soldered or welded onto a metal plate, which was then blackened.

(b) Cover plate

The cover plate through which the solar energy must be transmitted is also extremely important to the function of the collector. The purposes of the cover plate are:

1. To transmit as much solar energy as possible to the absorber plate
2. To minimize heat loss from the absorber plate to the environment
3. To shield the absorber plate from direct exposure to weathering and
4. To receive as much of solar energy as possible for the longest period of time each day.

- The most critical factors for the cover plate materials are strength, durability, non-degradability and solar energy transmission.
- Tempered glass is the most common on to a flat-plate collector, is highly resistance to breakage both from thermal cycling and from natural events. Glass is also effective in reducing radiated heat loss because it is opaque to the longer wavelength infra-red radiation re-emitted by the hot absorber plate.

`D. Work model

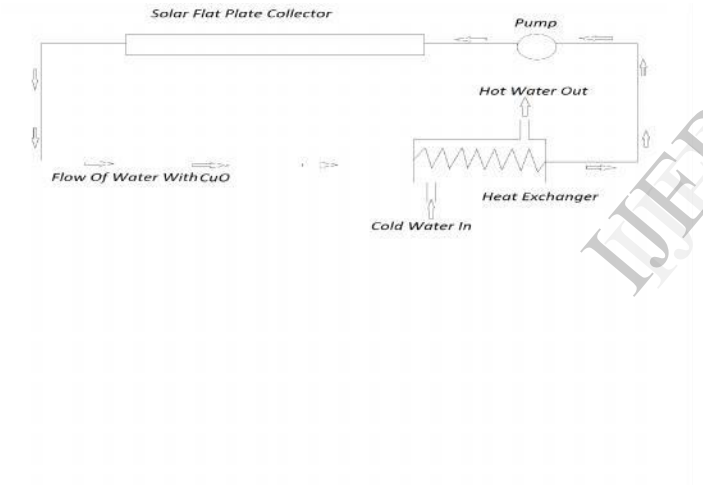

Solar flat plate collector

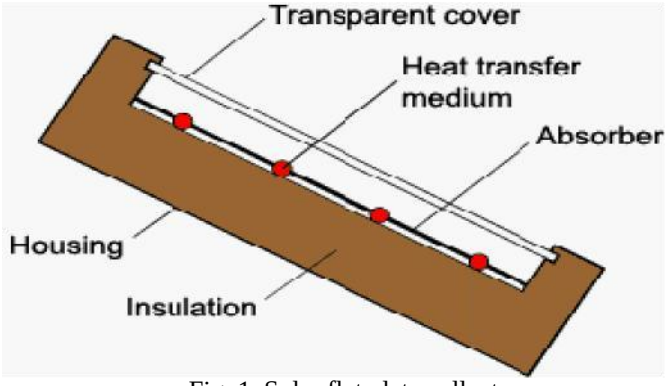

Fig..1. Solar flat plate collector

E. Pyranometer

A pyranometer is an instrument which measures total or global radiation over a hemispherical field of view. It is a sensor that is designed to measure the solar radiation flux density from a field of view of 180 degrees. The name pyranometer is originated from greek word "pyr" meaning "fire" and "ano" meaning "above sky". The pyranometer measures both beam as well as diffused radiations. To make a measurement of irradiance, the sensitive surface of pyranometer. The temperature difference between hot and cold junctions is a function of the radiation falling on the surface. A pyranometer produces voltage as a function of the incident radiation, from the thermopile detectors. The black coating on the thermopile sensor absorbs the solar radiation. This radiation is converted to heat. The heat flows through the sensor to the pyranometer housing. The thermopile sensor generates a voltage output signal that is proportional to the solar radiation

F. Properties of nano-fluids

Thepropertiesof nanoparticles and thermal properties of Nano fluidsas thebasis of research on Nano fluids application.Specific heat, thermal conductivity and density of different nanoparticles. Improvement in thermal properties of nanofluids such as thermal conductivity and convective heat transfer. However, all this special characteristics cannot be achievedunless the nanoparticles are properly dispersed and stable. Surfactants can play a major role in achieving better dispersion and stability of nanofluids.

G. Insulation

Insulation which should be provided at the back and sides to minimize the heat losses. Thermal insulation of 25 to 50mm thickness is usually placed behind the absorber plate to prevent the heat losses from rear surface. Insulation material is generally mineral wool or glass wool or a heat resistant fiber glass.

III. TESTING DETAIL

- Performance test on water with copper oxide
- Performance test on water with silicon di oxide
- Performance test on water

IV. CONCLUSION

A Direct Absorption Solar Collector was modeled numerically using a 2-dimensional heat transfer analysis. A nanofluid a mixture of water and copper oxide and silicon die oxide nanoparticle was used as the working fluid in the solar collector. The influences of various parameters, such as nanoparticle size and volume fraction, and collector geometry on the collector efficiency were studied, and finally the performance of this collector was compared with that of a conventional flat-plate type collector. The collector efficiency was found to increase with particle volume fraction, Finally the results showed about 10% higher absolute efficiencies for the nanofluid-based Direct Absorption Solar Collector in comparison with conventional flat-plate type collectors that use pure water, under similar operating conditions.

1. By using CuO nanofluid in DASC efficiency enhancement on the order of 4 – 6%, when compared to water.

2. One of the main reasons of getting higher efficiency is the very small particle size, which enhances the absorption capacity of nanofluid so, improvement in efficiency could be obtained by using various particle size distribution.

3. By overcoming the above problems the improvement of collector efficiency can be achieved up to 5– 10 %

REFERENCES

[1] R.Winston, J.C.Minano, P.Benitez, Nonimaging Optics, Elsevier Academic Press, pp. 217, (2005)

[2] Rapp, Donald, Solar Energy, Prentice-Hall, Englewood Cliffs, NJ, (1981)

[3] Goswami, Yogi.D, Kreith, Frank, and Kreider, Jan F., Principles of Solar Engineering, 2nd edition. Taylor and Francis, Philadelphia, PA, (2000)

[4] Choi SUS. Enhancing thermal conductivity of fluids with nanoparticles. ASME FED-Vol .231/MD-Vol.66 1995:99–103.

[5] Wong KV, Leon OD. Applications of nanofluids: current and future. Advances in Mechanical Engineering 2010(ID 519659):pp 11.

[6] Ho CD,Chen TC. The recycle effect on the collector efficiency improvement of double-pass

[7] Sheet-and-tube solar water heaters with external recycle. Renew Energy 2006; 31(7):953–970.

[8] Hussain AM. The performance of a cylindrical solar water heater. Renew Energy 2006; 31(11):1751–1763.

[9] Xiaowu W, Hua B. Energy analysis of domestic-scale solar water heaters. Renew Sustain Energy Rev 2005; 9(6):638–645.

Mathematical Modelling and Optimization of Electro Co-Deposition Process Parameters Using Response Surface Methodology and Genetic Algorithm

1.NaveenKumar[a],2.Vengatesh[a], 3.Nexon Brissac[a], 4.MadhanRaj[b]
[a] Student, Department of Mechanical Engineering, Christ College Of Engineering and Technology, Moolakulam, Pondicherry-605 010.
[b]Assistant Professor, Department of Mechanical Engineering, Christ College Of Engineering and Technology, Moolakulam, Pondicherry- 605 010.

Abstract: **The Process electro co-deposition is a ceramic matrix composites processing method having ability to coat non-metallic ceramic particles in the substrate along with metals. The mathematical modelling of responses of a process helps us to predict the process and further used as the objective functions for optimization.**

In this paper, Response Surface Methodology is used for making empirical relation for each response by taking Current Density, W/L of SiC Added and Voltage as a governing parameters. The responses were analysed and discussed by ANOVA and Surface Plots. The wear rate for micro DC and micro PC is optimized as 4.78580E-9 and 2.13633E-9 using Genetic Algorithm. The optimized wear rates are found to be approximate to actual value. The Actual value and the Predicted Value are compared.

1.INTRODUCTION

Electro co-deposition is a chemical process in which atoms of metallic materials will be deposited on the surface of another material along with the non-metallic (ceramic) atoms in the electrolytic bath. In this process one of the materials is taken as anode and other as cathode. And this works by the principle of faradays's law of electrolysis. This method is more advantageous than conventional electro-plating process, because by electro co-deposition method we can make non-metallic atoms to be deposited on the substrate.

RSM is a collection of mathematical and statistical techniques that are useful for the modelling and analysis of problems in which a response of interest is influenced by several variables and the objective is to optimize this response. RSM also quantifies relationships among one or more measured responses and the vital input factors. The Design Expert version7 software was used to develop the experimental plan for RSM. The same software was also used to analyse data collected.

Genetic algorithm(GA) is a non-conventional optimization method which is based on the darwin's theory of "survival of the fittest". The biological terms like genes, chromosomes were used to represent the values of the parameters. Using GA we can solve constrained and unconstrained optimization problems to find the maximum or minimum of an objective function. The solution converges or diverges by repeatedly modifies a population of individual solution. The GA is applicable to solve variety of optimization problems that are not well suited for standard optimization algorithms, including problems in which the objective function is discontinuous, non-differentiable, stochastic or highly nonlinear

2.MATHEMATICAL MODELLING

There are many methods to plan and design an experiment. Response Surface Methods are design and models for working with continuous treatments when finding optima or describing the response is the goal.

RSM is an important subject in the statistical design which is a collection of mathematical and statistical techniques used to model and analyze a problem in which

response is influenced by several input variables and the objective is to optimize this response.

The second order polynomial regression equation is to fit the non linear curve. The equation contains interaction of the variables and the square of them.

The second order equation is represented as follows:

$$Y = b_0 + \sum b_i x_i + \sum b_{ii} x_i^2 + \sum b_{ij} x_i x_j \qquad (a)$$

In this paper, mathematical model were developed and optimized the parameters to find the operating condition to get minimum wear rate. This analysis has three dependent such as %Wt of SiC incorporation in the coating, Specific Wear Rate and Wear Co-efficient are related to the three independent variables Current Density, W/L of SiC and Voltage.

$$Responses = b_0 + b_1(A) + b_2(B) + b_3(C) + b_{11}(A^2) + b_{22}(B^2) + b_{33}(C^2) + b_{12}(AB) + b_{13}(AC) + b_{23}(BC) \qquad (b)$$

The second order polynomial Equations were developed using DESIGN EXPERT - 7 software for the prediction of %Wt of SiC incorporation in the coating, Specific Wear Rate and Wear Co-efficient in terms of three independent variables.

A – Current Density

B – W/L of SiC supplied

C – Voltage

The Regressions equations are created for the two different experiments values, since the input and output parameters are same for these experiments the same Central composite design can be used.

Composite Method Design Matrix is used for all the Experiments. The Experiments are,

1. Micro SiC DC Supply
2. Micro SiC PC Supply

The parameters are almost same only differences are the Type of Current Supplied (DC or PC) and the Size of the SiC Particle Supplied in the Bath.

Table 1 Important Co-deposition process parameters

Factors	Unit	Variables	-2	-1	0	1	2
Current Density (DC/PC)	A/dm^2	A	0.5	1	1.5	2	2.5
W/L of SiC (Micro)	%W/L	B	0	5	10	15	20
Voltage	Volts	C	0.5	1	1.5	2	2.5

2.1.Micro-SiC for DC supply

The current supply to the electrolyte bath is Direct current and the experimental values are taken from the Literature [1]. The responses are obtained for varying current and amount of SiC in Electrolyte bath. The voltage also changed during experiment.

2.2.Micro-SiC for PC supply

In this experiment method every parameters are same as in the micro-SiC for DC supply except the type of current . The Pules Current is supplied during the deposition process. Other parameters like W/L added and Voltage are maintained unchanged.

Table 2 Experimental design matrix and respones

Micro DC						Micro PC					
Current Density	W/L of SiC	Voltage	%Wt of SiC incorporation in the coating	Specific Wear Rate	Wear Co-efficient	Current Density	W/L of SiC	Voltage	%Wt of SiC incorporation in the coating	Specific Wear Rate	Wear Co-efficient
1	1	-1	27.31	5.06E-09	2.86E-07	1	1	-1	30.23	3.01E-09	2.45E-07
-1	1	1	22.41	5.72E-09	3.43E-07	-1	1	1	24.78	4.34E-09	3.23E-07
-1	1	-1	24.56	5.15E-09	3.12E-07	-1	1	-1	27.01	4.12E-09	3.01E-07
0	0	0	22.38	8.58E-09	5.43E-07	0	0	0	25.12	6.55E-09	5.12 E-07
2	0	0	16.35	1.74E-08	1.45E-06	2	0	0	18.95	1.43E-08	1.99E-06
1	-1	-1	18.27	1.20E-08	8.51E-07	1	-1	-1	19.79	1.10E-08	8.23E-07
0	0	0	22.38	8.58E-09	5.43E-07	0	0	0	25.12	6.55E-09	5.12E-07

0	0	0	22.38	8.58E-09	5.43E-07	0	0	0	25.12	6.55E-09	5.12E-07
0	0	0	22.39	8.69E-09	5.92E-07	0	0	0	25.11	6.25E-09	4.98E-07
-1	-1	-1	19.21	1.14E-08	7.72E-07	-1	-1	-1	22.44	1.00E-08	7.00E-07
0	-2	0	0	2.23E-08	2.03E-06	0	-2	0	0	1.28E-08	1.12E-06
1	-1	1	19.5	1.23E-08	8.86E-07	1	-1	1	22.21	1.12E-08	8.56E-07
0	0	0	22.39	8.69E-09	5.92E-07	0	0	0	25.12	6.55E-09	5.12E-07
0	2	0	30.24	8.58E-09	2.03E-06	0	2	0	32.34	6.32E-09	4.01E-07
-2	0	0	16.3	1.54E-08	9.25E-07	-2	0	0	18.61	1.21E-08	9.01E-07
0	0	-2	21.28	1.01E-08	6.00E-07	0	0	-2	23.23	1.00E-08	5.97E-07
-1	-1	1	20.72	1.08E-08	7.10E-07	-1	-1	1	22.87	1.01E-08	7.43E-07
0	0	2	25.54	6.86E-09	2.57E-07	0	0	2	27.32	5.83E-09	2.34E-07
0	0	0	22.37	8.47E-09	5.01E-07	0	0	0	25.13	6.65E-09	5.45E-07
1	1	1	29.97	4.56E-09	2.73E-07	1	1	1	30.98	3.52E-09	2.45E-07

3. DEVELOPING EMPIRICAL RELATION

The %W/T of SiC incorporated in the substrate, Wear rate and Wear co-efficient are the responses. For this responses the second order polynomial regression equation were created in terms of Current Density(A), W/L of SiC Added in electrolyte(B) and Voltage(C) to predict. The empirical relation for coded values are shown below for micro-SiC DC and PC supply.

3.1. For Micro-SiC DC supply

%W/L of SiC incorp=+23.00+0.52*A+5.44*B+0.74*C+1.56*A*B+0.57*A*C-0.28*B*C-1.20*A^2-1.50*B^2+0.57*C^2 (c)

WearRate=+7.884E-009+2.974E-010*A-3.353E-009*B-4.174E-010*C-4.118E-010*A*B-2.122E-011*A*C+3.963E-011*B*C+1.615E-009*A^2+1.367E-009*B^2-3.719E-010*C^2(d)

Wear Coefficient=+4.547E-007+7.561E-008*A-1.254E-007*B-4.345E-008*C-4.398E-008*A*B+6.783E-009*A*C+5.628E-009*B*C+1.159E-007*A^2+3.275E-007*B^2-7.382E-008*C^2 (e)

3.2. For Micro-SiC PC supply

%W/LofSiCincorp=+25.79+0.42*A+5.65*B+0.60*C+1.59*A* B+0.62*A*C-0.54*B*C-1.25*A^2-1.90*B^2+0.38* C^2 (f)

WearRate =+6.131E-009+2.870E-010*A-2.519E-009*B-4.546E-010*C-5.035E-010*A*B+5.207E-011*A*C+5.142E-011*B*C+1.479E-009*A^2+5.705E-010*B^2+1.552E-010*C^2 (g)

WearCoefficient =+4.688E-007+1.436E-007*A-2.159E-007*B-3.926E-008*C-4.617E-008*A*B-4.034E-009*A*C-6.759E-009*B*C+2.103E-007*A^2+3.868E-008*B^2-4.818E-008*C^2 (h)

The above equations are obtained at 95% confidence level and Central composite design is used to obtain the coefficients

4. OPTIMIZATION BY GENETIC ALGORITHM

The Genetic Algorithm is a non-conventional search and optimization method based on natural selection mechanics. The genetic algorithm is ease in operation, global perspective and it can solve problems which are difficult to solve in conventional methods.

The Genetic Algorithm parameters are: Population Size = 100, Selection operator = Roulette Method, Crossover operator = Single point operator, Crossover Probability =0.9, length of chromosome = 90 and fitness parameter = Wear rate.

The objective function is the form of:

Wear Rate = f (Current Density, W/L of SiC added, Voltage)

The constraints are:

Current Density 0.5 – 2.5

W/L of SiC Added 0 – 20

Voltage 0.5 – 2.5

The optimization is carried out in the MATLAB software using GA tool. The objective function for wear rate is taken from the empirical relation developed through RSM in this previous work. The optimization is done for the wear rate of both DC supply and PC supply.

The Fitness value and generation plot is plotted while optimizing and the solution converges at around

50thGeneration. Before this many local minima are reached and the average distance of the population decrease with the increase in the generation.

5. RESULTS AND DISCUSSION

5.1. Micro-SiC for DC supply

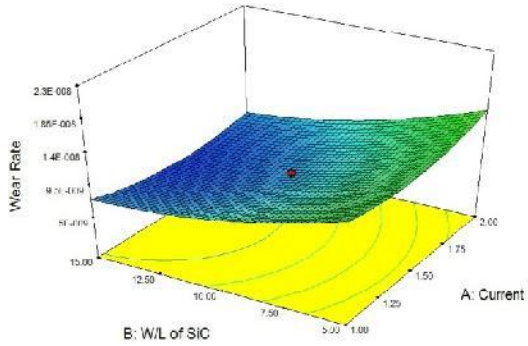

Fig. 1.Surface Plot for Wear Rate

The Surface Plot for the wear rate of micro –SiC under DC supply is shown in Fig. 1. This plot indicates that the wear rate is minimum for the maximum deposition of the SiC (15% addition) on the substrate and the respective current range is also found as around 1.50. The voltage factor is set to 1.50. It is inferred that wear rate is maximum for the minimum amount of SiCadded in the bath even though the current supply is maximum(2.0).

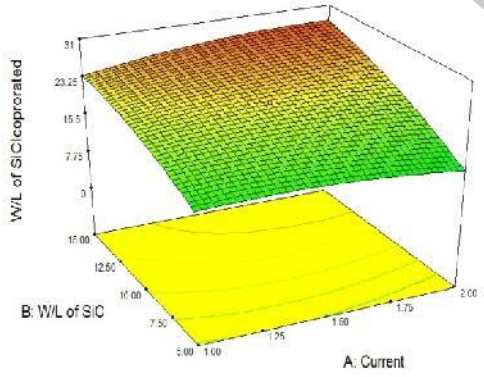

Fig. 2.Surface Plot for W/L of SiC Incorporated

The surface plot for the SiC incorporation for the micro-SiC DC supply in Fig.2.shows that the deposition of the SiC on the substrate is maximum at the 15% of SiC added and 2A/dm^2 of Current. The amount of SiC deposited is 30.24. And the minimum deposition is attained at minimum addition of SiC(5%) on the bath and the minimum current supply(1A/dm^2). The plot also shows that the deposition of the SiC on the substrate increases linearly proportional to the increase in the SiC addition in the bath and the current supply.

5.2. Micro-SiC for PC supply

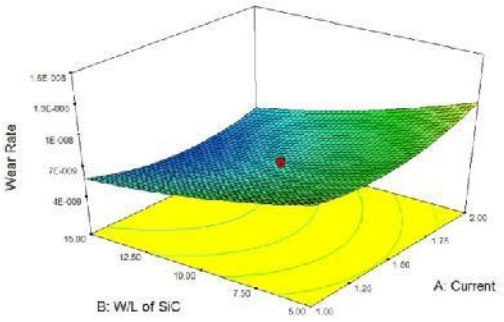

Fig. 5. Surface Plot for Wear Rate

This surface plot in Fig.5.is for the wear rate of the substrate obtained by micro-SiC for PC supply in the bath. The wear rate is minimum at 15% of SiC addition in the bath and the respective current supply is around 1.52A/dm^2. At 5% of SiC the wear rate is maximum at both 1A/dm^2 and 2A/dm^2. At the center of the surface plotthe wear rate is 1.21102E-008 where the SiC added is 10% and the current supply is 1.5A/dm^2.

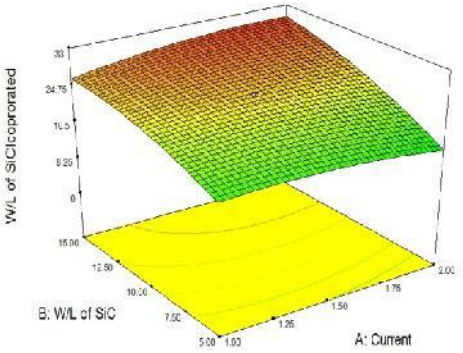

Fig. 6. Surface Plot for W/L of SiC Incorporated

The surface plot for the SiC incorporated in micro-SiC for PC supply in Fig.6. shows that the SiC deposition is maximum at 15% of SiC added in the bath and 2A/dm^2 of current supply. The SiC deposition in the substrate increases linearly as the increase in the current and SiC addition in the bath. It is also found the deposition of SiC on the substrate is minimum at 1A/dm^2 even though the SiC addition in bath is maximum(15%). So that the SiC addition and current should be mutually increased to get maximum deposition and hence to minimize the wear rate.

5.3. Genetic Algorithm optimization

The optimized input parameters range are used to calculate the respective Incorporation of SiC on the substrate by substituting the optimized Current density,, %W/L of SiC added and Voltage values in the
%W/L of SiC incorporated empirical relation developed through RSM. Both the Wear Rate and the respective incorporation of SiC obtained by mathematical method are approximate with the experimental value.

6. CONCLUSION

1) Empirical relation are developed to predict the %W/L of SiC deposited in the substrate, Wear rate and Wear coefficient for both DC and PC supply.
2) Surface Plots were developed to study the responses with respect to the governing parameter.
3) It is found that PC supply produces optimum SiC deposition and also has minimum wear than DC supply.
4) The wear rate is optimized by GA and found that PC has minimum wear rate.
5) The predicted values of the governing parameters are in good agreement with the experimental values.

REFERENCES

[1] PradeepDevaneyan S, T.Senthilvelan, An Experimental Study of the Effect of Nickel with SiCCodeposited on Aluminium 7075 under Direct Current and Pulse Current, International Journal of Composite Materials 2014,4(5)
[2] D.C.Montgomery, Design and Analysis of Experiments, 4th ed., Wiley, New York, 1997.
[3] G.MAHENDRAN, V.BALASUBRAMANIAN, T.SENTHILVELAN, Influences of diffusion bonding process parameters on bond characteristics of Mg-Cu dissimilar joints, Trans. Nonferrous Met. Soc. China 20(2010) 997-1005.
[4] M.Y.Noordin, V.C.Venkatesh, S.Sharif, S.Elting, A.Abdullah, Application of response surface methodology in describing the performance of coated carbide tools when turning AISI 1045 steel, Journal of Materials Processing Technology 145 (2004) 46-58.
[5] G.Padmanaban,V.Balasubramanian, Optimization of laser beam welding process parameters to attain maximum tensile strength in AZ31B magnesium alloy.

Improving the Corrosion Resistance of Az91d Magnesium Alloy by Electro less Plating

S. Diwakar[1]
Department of Mechanical Engineering
Dr. Pauls Engineering College
Villupuram-605109, India

N. Subramanian[2]
Department of Mechanical Engineering
Dr. Pauls Engineering College
Villupuram-605109, India

***Abstract* -This paper presents an experimental study on the influence of four different types of surfactants namely sodium trimethyl ammonium bromide (CTAB), sodium layryl sulphate (SDS), N- Dimethylmyristylammonio and polyethylene glycol hexadecyl ether on the micro hardness and wear resistance of electroless nickel phosphorus (Ni–P) coatings using electroless coating method. Corrosion performance of the electroless Ni–P coatings was evaluated by Potentiodynamic Polarization technique. The results showed that SDS anionic surfactant causes increasing of corrosion resistance.**

1 INTRODUCTION

Usage of magnesium and its alloy in industry has been gradually increasing because of their high strength to light weight ratio with a density one fourth that of iron and two third that of aluminum. Magnesium and its alloy have low corrosion resistance and wear resistance value because it's high chemical and electro chemical reactivity which resulting in formation of porous oxide carbonate film on the surface 1.

To improve the corrosion resistance and wear resistance of magnesium alloy electroless nickel plating method is used because of its good property and uniform coverage in surface 2. Direct plating on Mg is a challenge because of highly chemically active alloy. Hence Mg alloys needs special bath formulation and pretreatments process 3. Chromium-free pre-treatments for the electroless nickel phosphorous (Ni-P) deposit are always desirable, as it is environment friendly 1. The pretreatment steps included degreasing, alkaline cleaning, acidic cleaning, activation and electroless nickel plating, with a fluoride layer formed after activation between substrate and coating 3. According to electrochemical mechanism, electroless deposition was resulted from mixed anodic and cathodic reactions. By using hypophosphite as reducing agent, anodic partial process was the oxidation of reducer with water, and the electrons generated in the anodic reaction were utilized in the coupled cathodic processes for deposition of Ni and P. Meanwhile, the evolution of hydrogen gas was account for a result of the secondary reaction of hydrogen ions 2. Electroless plating deposition process is based on a redox reaction, in which the reducing agents are oxidized and Ni^{2+}ions are reduced on the substrate surface 5.

By adding surfactant in the bath improves the deposition rate and its properties. Surface active agents having both hydrophobic and hydrophilic structural units; the adsorption generally results in the modification of the surface or interfacial properties of the system. A surfactant can be classified by the presence of formally charged groups in its head. A non-ionic surfactant has no charge groups in its head and an ionic surfactant carries a net charge. If the charge is negative, the surfactant is called anionic; if the charge is positive, it is called cationic 4. Hence, this study mainly focuses on surfactants influence on the micro hardness and wear properties of the electroless Ni-P deposits on magnesium substrate. However, there was no such investigation on magnesium alloy and moreover it is complicated because of corrosive nature in the electrolyte bath. Hence, in this investigation, four types of surfactants namely sodium trimethyl ammonium bromide (CTAB), sodium layryl sulphate (SDS), N-Dimethylmyristylammonio and polyethylene glycol hexadecyl ether used in the electrolyte for electroless Ni–P deposit on magnesium alloy, which affects the surface tension forces between solid/liquid interfaces 4. By adding surfactant in the bath solution deposition rates, surface morphology, surface topography and micro hardness are investigated in this study.

2 EXPERIMENTAL DETAILS

2.1 Sample and bath preparations

Circular shaped AZ91D die cast magnesium alloy with a size of 30 mm × 7 mm used as a substrate material in the present investigation 1. Samples were mechanically polished with emery paper (400,600, 800, 1000 and 2000 size) and then surface pretreatment is to be done. Samples should be transferred as quickly between surface treatments process. The bath composition and all the operation parameters for the electroless Ni–P deposition are reported in Table 1

2.2 Steps for Surface Preparation

All the samples were subjected to the following pre-treatment procedure:

1. Ultrasonic cleaning in absolute acetone for 2 min.
2. Alkaline cleaning in sodium hydroxide and tri-sodium orthophosphate at 65 0C for 20 min.
3. Rinsing with tap water at room temperature (RT) for 2 min.
4. Acid pickling in chromic-nitrate for 10 sec.
5. Rinsing by immersion in tap water at RT for 2 min.
6. Activation in 16 vol. % HF at RT for1 min.
7. Rinsing with distilled water at RT for 2 min.
8. EN plating process
9. Rinsing by immersion in 60 0C water for 1 min.

2.3 Surfactant added

Surfactant is necessary in the chemical baths to stabilize the dispersion and improve the deposition of Ni-P coatings. In addition, anionic surface activator sodium lauryl sulphate (SDS), cationic surface activator cetyl tri-methyl ammonium bromide (CTAB), Zwitterionic surface activator N-Dimethylmyristylammonio and non-ionic surface activator polyethylene glycol hexadecyl ether were used in this study as a surface activator in the electrolyte bath and to enhance the properties of the deposits 1.

The surface and cross-section micrographs of the coatings were investigated by scanning electron microscope (SEM) and then their hardness was measured using a Vickers diamond indenter under a 200 g load for 10 s 5.

Wear tests were conducted under dry condition using a JM-IV tribometer .The coated sample was placed onto a disc which was rotated at a constant speed of 70 rev min21, and two wheels of w50612 mm hard material (HRC 62) with a load of 1 kg which rotated in opposite direction were inflicted on the coated sample. The wear tests were conducted with different cycles and the wear resistance was calculated by the weight loss measurement using electronic balance with precision of 0.01 mg 5

Electrochemical polarization measurements were performed by an electrochemical analyzer, which was controlled by a computer software system. Potentiodynamic experiments were conducted at ambient temperature. The experiments were carried out in a 3.5 wt% NaCl aqueous solution using a three-electrode cell with a platinum plate as counter electrode and a saturated calomel electrode was fitted through the rubber stopper and used as a reference electrode and scan rate of 5 mV/s was used 1.

3 RESULTS AND DISSCUSION

3.1 Corrosion properties of electroless Ni P deposits with surface activator

The corrosion properties of the electroless Ni P deposition were improved by using surfactant. Figures 1, 2, 3, 4 and 5 shows the Potentiodynamic polarization curves obtained from a coated AZ91 alloy and as-plated EN samples. In order to avoid the negative effects of the porosity in the coating that causes extra galvanic corrosion during the polarization testing, a simple porosity test was performed by immersing the as-plated samples into 3.5 % NaCl solution. Any samples failing this test were removed from subsequent polarization testing. After these tests, it was found that the anionic surfactant coatings remained bright in appearance of Ni plating. According to the potentiodynamic curves in as shown in Figure the anionic surfactant coatings exhibited much higher positive corrosion potential Ecorr and lower corrosion current density Icorr than that of other surfactant used magnesium substrate, showing that the coatings can completely protect the substrate material from corroding. In the anodic region of every curve, an activation control dominated the anodic reaction, and the corrosion current increased quickly with the increasing anodic potential.

The corrosion rate (CR) can be determined using the Faraday law

$$E_{COR} = K \quad EW$$

Where E_{CR} is given in mm/year, $K = 3.27\times10^{-3}$ mmg/Acm year, ρ the density of the substrate (g/cm3) and EW the equivalent weight of the substrate. Similar evaluation of corrosion rate has been reported in the literature. The corrosion potential (Ecorr) and corrosion current density (icorr) calculated with Tafel extrapolation method are given in Table 5.1 for plated EN and uncoated AZ91 samples. The corrosion potential (Ecorr) of the as-plated EN coatings show a significant shift to the positive direction, and the corrosion current density (icorr) decreases to a certain extent, which indicates that the EN coatings have corrosion resistance.

The corrosion potential (Ecorr) and corrosion current density (icorr) calculated with Tafel extrapolation method are given in Table 5.1 for plated EN and uncoated AZ91 samples. The corrosion potential (Ecorr) of the as-plated EN coatings show a significant shift to the positive direction, and the corrosion current density (icorr) decreases to a certain extent, which indicates that the EN coatings have corrosion resistance. Therefore, the corrosion behavior of the coatings is largely determined by the porosity in the coatings. The relatively high icorr does not reflect the nature of the coating materials. Porosity and microstructure of the coatings play important parts in their corrosion behaviors.

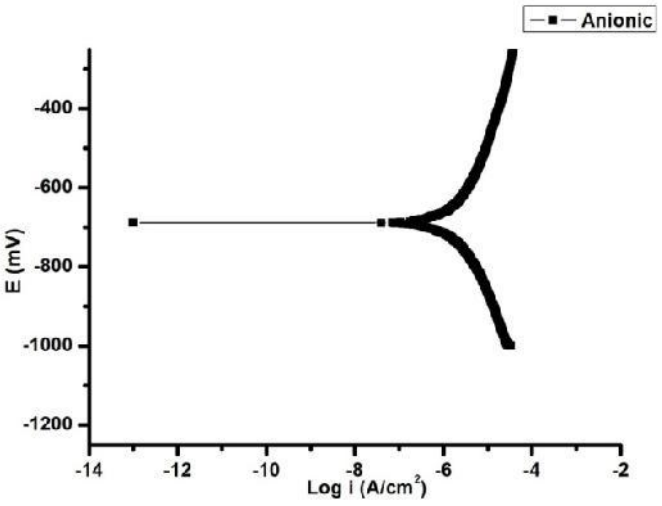

Fig. 1 Potentiodynamic polarization curves for anionic coating

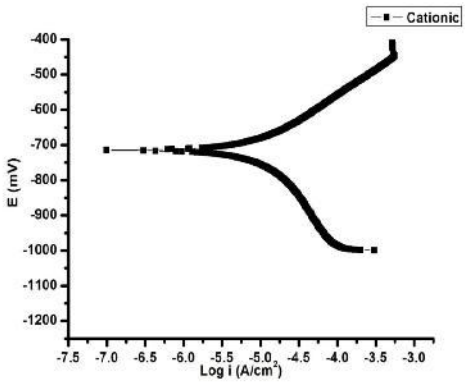

Fig. 2 Potentiodynamic polarization curves for cationic coating

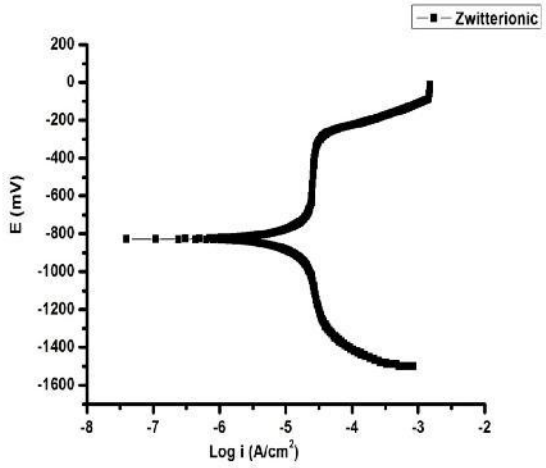

Fig. 3 Potentiodynamic polarization curves for zwitterionic coating

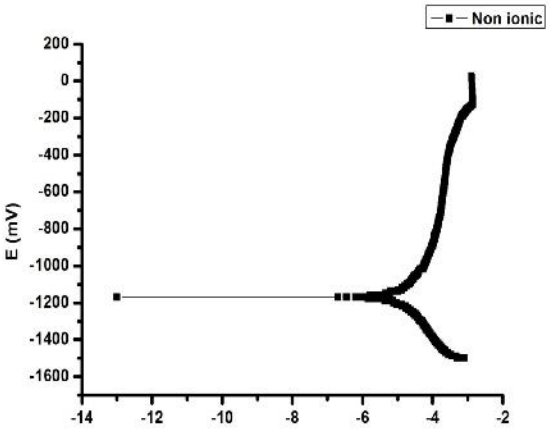

Fig. 4 Potentiodynamic polarization curves for Non ionic

4 CONCLUSIONS

The corrosion resistance was improved by electroless Ni P deposits with surfactants on magnesium alloy. The following conclusion can be drawn from the study that the addition of surfactant significantly improved the corrosion resistance of the electroless Ni P deposit on magnesium substrate (polarization test). The influence of anionic activator is more that cationic, zwitterionic and non ionic in resisting the corrosion. The surfactants increase the smoothness and increased amorphous plus nano-crystalline phases, which were the main reason for the corrosion resistance. On the whole, the study concluded that corrosion resistance was enhanced by adding a surfactant in the electroless Ni P deposits on magnesium alloy

REFRENCES

1. Sudagar, Jothi, et al. "Influence of Surfactants on the Corrosion Properties of Chromium-Free Electroless Nickel Deposit on Magnesium Alloy." *Surface Review and Letters* 19.03 (2012).
2. Xie, Zhihui, et al. "Polarization Behavior of Electroless Ni-P Plating on Magnesium Alloys." *Int. J. Electrochem. Sci* 8 (2013): 6664-6677.
3. Liu, Zhenmin, and Wei Gao. "Electroless nickel plating on AZ91 Mg alloy substrate." *Surface and coatings Technology* 200.16 (2006): 5087-5093.
4. Sudagar, J., et al. "The performance of surfactant on the surface characteristics of electroless nickel coating on magnesium alloy." *Progress in Organic Coatings* 74.4 (2012): 788-793.
5. Song, Y-W., et al. "Study on electroless Ni–P–ZrO2 composite coatings on AZ91D magnesium alloys." *Surface Engineering* 23.5 (2007): 334-338.
6. Sade, Wagner, et al. "Electroless Ni-P Coatings: Preparation and Evaluation of Fracture Toughness and Scratch Hardness." *ISRN Materials Science* 2011 (2011).

Performance and Emission Characteristics of Diesel Engines fuelledby Vegetable Oils

R. Sasikumar[1] and Dr. G. Sankaranarayanan[2]
[1] Research Scholar, Department of Mechanical Engineering,
St.Anne's College of Engineering and Technology, Panruti-607110, India,
[2]Research and Dean, Department of Mechanical Engineering,
Sree Sastha Institute Engineering College, Chennai -600123, India

ABSTRACT: Raw vegetable oils can be used successfully in short-term performance test in nearly any percentage as a replacement for diesel fuel. When tested in long-term, blends above 20% always result in engine damage or maintenance problems because, this oil has certain inherent problem like high viscosity and poor volatility. This affects the combustion in diesel engine and deteriorates the whole performance considerably. Hence, turpentine, a resinous extract of pine tree can be chosen as a thinning agent for reducing the viscosity of neat vegetable oil and made suitable for DI diesel engine. A various proportion of turpentine-vegetable oil blends are prepared and fueled into the DI diesel engine test setup for conducting performance test. The performance of kirloskar, AV1model, Single cylinder, Water cooled, Vertical, Direct injection diesel engine is evaluated using modified jatropha oil as fuel. This performance is compared for the same engine using mineral diesel as fuel. The exhaust emission parameters are also compared for these two fuels. From the obtained results, the 50TV blend performs quite similar to that of diesel baseline operation in terms of performance and pollutant emission and it has almost equal combustion characteristics with that of diesel fuel. It offers lower smoke and lower NO_x emission with slightly increased UBHC and CO emission without worsening SFC.

Key words: turpentine, bio fuel, thinning, alternate fuel, emission analysis, vegetable oil and combustion analysis.

I INTRODUCTION

Increasing industrialization and modernization of world lead to steep rise in petroleum cost. Also with the present consumption rate, deplete all petroleum resources within a decade or two. In addition, combustion of fossil fuel accumulates greenhouse gas emissions and leads to rapid rate of global warming. By spending more amount of money we import not only petroleum fuel but also much emission. Considering these disaster effects many alternative fuels were identified and tested successfully in IC engines.

Generally bio fuels are the oils obtained from the living plant sources. These oils may be obtained from resin and plant seeds. Plant oils are renewable and have low sulfur in nature. As the bio fuels are more expensive than fossil fuels, the wide spread use of bio fuel was restrained from its use in I.C engines. The use of vegetable oil in diesel engine has been identified well before. However, despite the technical feasibility, vegetable oils as fuel could not get acceptance, as they were more expensive than petroleum fuels. Also, the vegetable oils were all extremely viscous, with viscosities ranging 10–20 times greater than diesel fuel. This leads to the retardation in scientific efforts to investigate the further acceptability of vegetable oil as fuel.

This fuels take away more carbon dioxide from the atmosphere during their production than is added by combustion. Therefore, it alleviates the increasing carbon dioxide content of the atmosphere. In view of the potential properties, large number of investigations has been carried out internationally in the area of vegetable oils as fuel. Some of the vegetable oils from farm and forest origin have been identified. The most predominantly sunflower, safflower, soybean, cottonseed, winter rape, canola and peanut oil have been reported as appropriate substitute of petroleum based fuels.

Since, the production cost of vegetable oils are slightly lower than those of alcohols and plant oil esters (bio diesel), it can be suggested that direct application of crude vegetable oils would be most advantageous.

The vegetable oils are found to be promising alternative fuels because of their renewable, eco-friendly and can be produced easily in rural areas. The cost of edible oil is some what more. Use of such oil will result in food crises in feature. So that the use of non-edible oil is more significant. The Jatropha curcas grows in all over India irrespective of any climate conditions and areas.

The neat vegetable oil (Jatropha) is not suitable to use as the fuel directly in IC engines. Generally, in diesel engine, straight chain paraffin fuels are preferred for better ignition quality. But due to the large molecular mass and complex chemical structure, vegetable oils are not directly suitable for diesel engine application. This intern leads to problems related to combustion and atomization in the injector systems of a diesel engine. Due to the high viscosity, the long-term operation of the engine with vegetable oils normally introduces the development of gumming, the formation of injector deposits, ring sticking and problems related to the lubricating oils. That is the reason why the diesel oil cannot be replaced by neat vegetable oil without fuel modification and engine modifications. Therefore, the reduction of viscosity of vegetable oils is of prime importance to make it a suitable alternative fuel for diesel engines.

The problem of high viscosity of vegetable oils can be reduced in several ways, such as transesterification, micro emulsification, preheating the oils and blending with other fuels such as diesel, oxygenated organic compounds, and methanol.

Usually, Essential oils (Turpentine) are offering good fuel characteristics and this is the only fuel offering high calorific value than that of other bio fuels and its calorific value almost equal to that of diesel fuel.

As the Turpentine, resinous extract of pine tree possess good fuel value, it could be considered as a one of the possible alternative fuel for diesel engine. Oil of turpentine is a colourless, oily, odorous, flammable, water-immiscible liquid with a hot, disagreeable taste. Chemically, oil of turpentine is a mix hydrocarbon, the predominant constituent being pinene. The turpentine used in this study was distilled from resin obtained from pine trees.

The objective of the present work is to investigate the performance and emission characteristics of the C.I Engine fueled with turpentine-thinned vegetable oil. During this investigation, the C.I engine was fueled with the different TV blends in proportions varying from 30TV to 50TV (30:70, 40:60 and 50:50). The performance and emission characteristics of turpentine - vegetable oil blends are then compared to diesel fuel. The regulated emission species and particulate matters are measured and its variation in the engine exhaust has been compared with the diesel base line operation.

I. DETAILS OF EXPERIMENTAL SET-UP

A single cylinder, 4- stroke, water-cooled, diesel engine coupled with electrical dynamometer as shown in figure 1 was used as experimental set-up.

The specifications of engine & dynamometer are given in table 1 & 2. The measuring instruments used in this project is listed in table 3.

The suction side of the test engine is attached with anti-pulsating drum to measure air inflow quantity. The inlet temperature of air is measured with inlet air thermometer. The exhaust side of the engine consisting of series of devices such as Exhaust Gas Thermometer (EGT), gas analyser probe and smoke meter probe.

A combustion analyser is also attached with the test rig to study the combustion behavior of engine.

The set-up also consists of fuel flow measuring device to measure the fuel consumption of the engine. The output side of the engine consists of an electrical dynamometer and followed by a loading rheostat.

The output is measured in terms of watts using digital wattmeter mounted in the panel. An 8 bit Data Acquisition System (DAS) is also connected with the test rig to acquire the combustion pressure and crank angle,pressure – volume, MFB and HRR data for a stipulated number of cycles.

The schematic diagram and photographic view of the experimental setup are shown below:

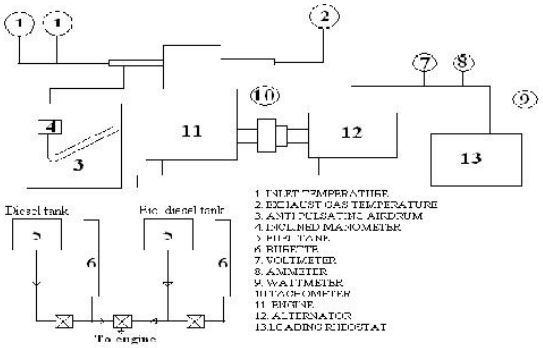

Table 1
Engine Specification

Make	Kirloskar AV 1 model
Type of Engine	Vertical, 4 – Stroke cycle, single acting, High speed, compression ignition, diesel engine
Number of Cylinder	One
Speed	1500 rpm
Maximum power output	5 Hp (= 3.7kW)
Bore	80 mm
Stroke	110mm
Cubic capacity	0.553 litres
Norminal compression ratio	16.5 : 1
Fuel timing by spill	23 Deg. BTDC
Lubrication	Forced Full pressure lubrication
Type of cooling	Water cooled
BMEP at 1500 rpm	5.42 bar

Table 2
Alternator Specification

Make	Kirloskar
Power	5 KVA
Speed	1500 rpm
Voltage	230 v
Ampere	21.7 amps
Frequency	50 Hz
Power factor	0.8

Table 3
Measuring Instruments Used

S.No.	Measuring Parameters	Instruments Used
1	HC,CO,NO_x, CO_2 and O_2	Exhaust gas Analyser
2	Smoke	Bosch Smoke meter
3	Cylinder pr, and Crank Angle	Data aquisition system
4	Exhaust gas temperature	Digital Thermometer
5	Air flow rate	Orifice & manometer

RESULTS AND DISCUSSION

Based on the objectives and methodologies mentioned in the earlier chapters, the experimental investigations were conducted and the results are presented and discussed in this chapter. From the results, the respective graphs for the parameters such as brake thermal efficiency, volumetric efficiency, exhaust gas temperature, peak cylinder pressure, ignition delay, heat release rate, rate of pressure rise and the emission parameters such as carbon monoxide, hydro carbon, NOx and smoke emission were drawn against the engine load.

The engine is tested and its performance is evaluated by using different fuels and blends. The results are found out and analysed one by one as follows.

This chapter consists of the results and discussions of the following fuels while used in engine.

1.Pure diesel(for base line test.
2.Turpentine-Diesel blend.
3.Turpentine- Neat jatropha oil blend.
4.Jatropha biodiesel.

the variation of brake thermal efficiency of various turpentine-diesel blends (TD blends) with respect to engine load. From the figure, it is observed that the brake thermal efficiency of TD blends increases with respect to increase in turpentine fraction in the blend. This is due to improved volatility, increased heat content and remarkable change in viscosity of the blend.

Basically, turpentine possess larger fraction of cyclic compound- terpens (approximately 90% by volume). It has four carbons in its molecule; hence the fuel has low viscosity and higher volatility (usually, number of carbon and chain length of molecule determines the viscosity and volatility of the substance). In addition, turpentine decomposes very easily at lower temperature and releases more volatile intermediate compounds.

It also possesses unstable molecular structure, which helps to combust the mixture faster than the neat diesel fuel. Hence, the combustion duration of higher turpentine blends shortens with respect to increase in turpentine fraction in the blend.

Higher turpentine blends react faster than lower turpentine blends. This is due to finer spray, improved air entrainment and improved oxidation ability. The release of lighter fraction from the higher turpentine blends during combustion is more rapid and abundant due to the presence of higher proportion of cyclic compounds (turpentine). The increased heat content and higher density are also other reasons for higher brake thermal efficiency.

The maximum brake thermal efficiency obtained with 40T blend is 31.5% and it is 2.5% higher than that of DBL operation. Though the blends beyond 40T (50T and 60T) contains higher heat content, these are not considered for analysis because these blends offered poor cold starting and misfires during idling. Hence, the maximum blend proportion was limited to 40T.

the variation of specific energy consumption (SEC) of TD blends with respect to engine loads. The SEC of TD blends decreases with respect to increase in turpentine fraction in the blend. Addition of turpentine in diesel oil not only changes the physical properties but also improves the combustion behavior of the blend. The higher turpentine blends are more reactive than lower turpentine blends and diesel fuel. Hence, in higher turpentine blends the combustion occurs at relatively higher temperature and pressure resulting in lower SEC. Improved spray characteristics, improved volatility, increased heat content and shorter burn duration are some of the additional reasons for lower SEC of higher turpentine blends.

it is observed that the EGT of TD blends are closer to that of diesel base line operation except at higher loads. This is mainly due to higher latent heat of turpentine. Therefore, during evaporation the higher turpentine blends reduces the cylinder temperature considerably lower than diesel operation. However, during combustion, it sufficiently raises the cylinder temperature and keeps it closer to that of DBL operation.

EMISSION ANALYSIS

the CO emission of TD blends with DBL operation at various load conditions. It shows only a small variation in CO emission up to 75% load for all TD blends. Normally, higher turpentine blends are having higher heating value, improved volatility, low cetane number and more cyclic compounds. Hence, the combustion of TD blends is occurring at comparatively higher temperature resulting in lower CO emission. This trend persists up to 75% load beyond which, there is remarkable change in CO emission. This is mainly due to more fuel admission and poor fuel utilization. one of the reasons for rapid production of intermediate volatile compounds, resulting in lower HC emission. the variation of NOx emission of various TD blends with respect to the load. From the figure it is observed that the NOx emission of all TD blends is higher than that of DBL operation. The cetane suppressing property of turpentine is the main reason for higher NOx emission. Usually, low cetane fuels offer longer ignition delay, which promotes more heat release during first stage of combustion and resulting in higher combustion temperatures. The higher combustion temperature provides a conducive ambient for reacting oxygen with nitrogen and yielding more NOx compounds. However, this can be resolved by adopting suitable NOx reduction technique. The maximum NOx emission obtained with 40T blend is 1380ppm.

The shift of peak pressure of TD blends is not much distinguishable and the occurrence of peak pressures is not far away from the DBL operation (within 5 degrees). Hence, the power loss due to longer ignition delay is insignificant.

Compares the heat release rate of 40T blend with that of DBL operation at full load. From the figure it is seen that the two phase of combustion is clearly visible and distinguishable. The height of premixed phase of combustion is increasing with respect to increasing turpentine fraction in the TD blends. This is attributed to low cetane number of turpentine. This is also one of the reasons for higher brake thermal efficiency and higher peak pressure of 40T blend.

Terpens possesses only four carbons hence the fuel has low viscosity and higher volatility. In addition, turpentine decomposes very easily at lower temperature and releases more volatile intermediate compounds. These gaseous products combust rapidly and releases heat energy in shorter duration. This is the major reason for higher brake thermal efficiency of 40T blend.

4. NOx emission of 50TJ blend is slightly lower than that of diesel base line operation.
5. The CO and UBHC emission of 50TJ blend is very closer to DBL operation.
6. Based on the net heat release rate, Pee Theta diagram and ignition delay, 50TJ blend does not deviate much more than the diesel base line operation.
7. As the combustion and emission performance of operation, it is proposed to be the best blend than that of other TJ blends and NJO. In addition the following observations were also made while running the engine under biodiesel mode.

9. Higher thermal efficiency.
10. Less EGT.
11. Lower CO and CO_2
12. Slightly increased Nox emissions.

REFERENCES

[1] Achten W.M.J, Maes W.H, Aerts R, Verchot L, TrabuccoA, Mathijs E, Singh V P and Muys B(2009) Jatropha: From global hype to local opportunity. Journal OF Arid Environments xxx(2009) 1-2.

[2] Alamu O J, Akintola Ta, Enweremadu C C and Adeleke A E (2008) Characterization of palm-kernel Figure 1 Comparison of SFC of DBL, 50TJ,NJO and oil biodiesel produced through NaOH catalyzed transesterification process. Scientific Research and Essay vol.3 (7),pp 308-311.

[3] Amba Prasad Rao G, Rama Mohan P (2004) Performance Evaluation of DI and IDI Engines with Jatropha Oil based Bio-diesel. IE(I) Journal-MC, p72-76.

[4] Anjan Kumar Prusty B, Rachna Chandra and Azeez P A, Biodiesel: Freedom from Dependence on Fossil Fuels?

[5] Bacon, D. M., F. Brear, I. D. Moncrieff, and K. L. Walker. 1981. The use of vegetable oils in straight and modified form as diesel engine fuels. Beyond the Energy Crisis -- Opportunity and Challenge Volume III. Third International Conference on Energy Use Management. Berlin (West). Eds. R. A.

[6] Fazzolare and C. R. Smith, 1525-33. Pergamon Press, Oxford.

[7] Bartholomew, D. 1981. Vegetable oil fuel. J. Am. Oil Chem.

BIODIESEL

The variation of SFC with brake power output is shown in
Figure 1.

The SFC of TJ blends varies with respect to turpentine proportions in the blend. Usually, higher turpentine blends are offering lower SFC and lower turpentine blends are offering higher SFC. From the Figure it is clear that the 50TJ blend offers lower SFC than NJO, other TJ blends and it is very closer to DBL. Hence, the 50TJ blend could be suggested as a replacement fuel for petro diesel. The reasons for lower SFC of 50TJ blend are increased calorific value, improved spray performance, better air entrainment, reduced soughter mean diameter and improved volatility. EGT

CONCLUSIONS

From the detailed test conducted with turpentine- thinned jatropha oil and biodiesel the following conclusions have been derived.

1. The 50TJ blend offers maximum brake thermal efficiency of 30.6% at full load. It is around 5% higher than that of DBL and 8.5% higher than that of NJO and 2.6% higher than biodiesel.
2. The SFC of turpentine-jatropha oil blends found decreases with respect to increase in turpentine fraction in the blend. The 50TJ blend has the SFC very closer to DBL operation. But SFC of biodiesel is lowest among the all.
3. The EGT of 50TJ blend is slightly higher than that of diesel base line operation due to higher turpentine content in the blend. At the same time EGT of biodiesel is less than the DBL mode.

Effect of Red Mud on Aluminium- Silicon Carbide Metal Matrix Composites

R. Sasikumar
Mechanical department/
Christ College of Engineering and Technology,
Pondicherry

M. R. Mahadevan
Mechanical department
Christ College of Engineering and
Technology, Pondicherry

I. Dharanidharan
Mechanical department/
Christ College of Engineering andTechnology,
Pondicherry

R. Jayavel
Mechanical department
Christ College of Engineering and
Technology, Pondicherry

Abstract— **The project is completely based on Powder Metallurgy domain where which specific powders are blended, compacted and sintered and planned to undergo performance characteristics by tests and properties verifications. The project title is "Effect of Red Mud on Aluminium-Silicon Carbide metal matrix composites" which strictly adheres powder metallurgy domain. Aluminium-Silicon Carbide Metal Matrix composites is one of the important composite material which is very extensively used for wide over applications in Aerospace, Automobile and other Industrial applications. The desired strength which it posses made every material to be fabricated and designed very successfully but some of the major problems faced during its utilization were very vast due to the loss of value of its essential properties. The main intention is to enhance the Pre-defined properties which it possessed by the utilization of a property enhancer "Red mud" during a Metal matrix composite production.**
The "Red Mud" is a slag obtained at the outlet part of an Aluminum metal extraction factory. This slag contains about 95% of Alumina content which consists of very high possessing properties of rigidity, heat withstanding capability, toughness and due to which when it is combined with an aluminum reinforced metal matrix composites using Powder Metallurgy concept, the properties of the manufactured component will be outstanding in its applicative point of view and so they can be used for various engineering applications effectively.

Keywords— Al, SiC, Red mud

I. INTRODUCTION (*Heading 1*)

1. Aluminium- The matrix (Base metal):-

Aluminum powder is a light, silvery-white to gray, odourless powder. It is a reactive flammable material. Aluminum powder is a fine granular powder made from Aluminium. In form of powders, Aluminium is used for several applications such as manufacture of slurry, explosive and detonators, thermit process used for manufacture of ferro alloys and forspecialised welding applications such as rails, pyrotechnic to manufacture crackers, sparkles and other pyrotechnic products; manufacture of aluminium paste, paints and several powder components used in automobiles.Aluminum powders are used in paints, pigments, protective coatings, printing inks, rocket fuel, explosives, abrasives and ceramics; production of inorganic and organic aluminum chemicals; and as catalysts. Pyro powder is mixed with carbon and used in the manufacture of fireworks. The coarse powder is used in aluminothermics. We selected Aluminium due to the above discussed applications which are adapted in our day to day life and mainly due to its cost effectiveness factor. So, a reinforcement is done on this base powder to increase its extensive properties in its applications which were used typically at present.

1.1 Silicon Carbide- The Reinforcement metal:-

Silicon Carbide is the only chemical compound of carbon and silicon. It was originally produced by a high temperature electro-chemical reaction of sand and carbon. Silicon carbide is an excellent abrasive and has been produced and made into grinding wheels and other abrasive products for over one hundred years. Today the material has been developed into a high quality technical grade ceramic with very good mechanical properties. It is used in abrasives, refractories, ceramics, and numerous high-performance applications. The material can also be made an electrical conductor and has applications in resistance heating, flame igniters and electronic components. Structural and wear applications are constantly developing. Some essential properties which silicon carbide possess are listed as follows,

- High strength
- Low thermal expansion
- High thermal conductivity
- High hardness
- High elastic modulus
- Excellent thermal shock resistance
- Superior chemical inertness

1.11 Red mud- The property enhancer:-

Red mud or red sludge is a toxic waste product of the Bayer process, the principal industrial means of refining bauxite in order to provide alumina as raw material for the electrolysis of aluminium by the Hall–Héroult process. A typical plant produces one to two times as much red mud as alumina. This ratio is dependent on the type of bauxite used in the refining process.

Red mud is composed of a mixture of solid and metallic oxide-bearing impurities, and presents one of the aluminium industry's most important disposal problems. The red colour is caused by the oxidised iron present, which can make up to 60% of the mass of the red mud. In addition to iron, the other dominant particles include silica, unleached residual aluminium, and titanium oxide. So, due to its highest nature of exhibiting part of alumina content in its outcome part as a slag it is planned to utilize red mud in the metal matrix composite material to improve its properties.

II. EASE OF USE

A. Aluminium

[1] The scientists who preceded Héroult and Hall had been concerned entirely with a chemical process for producing the metal. Héroult and Hall introduced a new concept. They believed that the answer to economic production lay in an electrolytic method. They had the idea that if some substance could be found which would conduct electricity and in which aluminium oxide (Al2O3), known as alumina, would dissolve, then an electriccurrent passed through the solution could deposit the aluminium as metal.

B. Silicon Carbide

[1, 2] In the past, the list of ceramics used as industrial materials consisted of alumina and other oxides. In recent years, there have been strong demands for the use of
ceramics as structural materials in place of metals and alloys and for use in harsh environments. Consequently, new ceramics such as nitrides, carbides and other covalently bonded materials have received increased attention because of their unique characteristics. The formation of SiC from the reaction between silicon
and carbon can take place at temperatures below the melting point of silicon. A eutectic point between silicon and SiC exists at 1402°C and 0.75 atom % carbon. The liquidus curve between Si and SiC is shown up to 2600°C and 27 atom
% C. A peritectic point is located at 2540°C and 27 atom % C under normal conditions. There are numerous (~200) polytypes for SiC, but only a few are common. All of the structures may be visualized as being made up of a single basic unit, a layer of tetrahedra, in which each silicon atom is tetrahedrally bonded

C. Red mud

Red mud or red sludge is a toxic waste product of the Bayer process, the principal industrial means of refining bauxite in order to provide alumina as raw material for the electrolysis of aluminium by the Hall–Héroult process. A typical plant produces one to two times as much red mud as alumina. This ratio is dependent on the type of bauxite used in the refining process.

Red mud is composed of a mixture of solid and metallic oxide-bearing impurities, and presents one of the aluminium industry's most important disposal problems. The red colour is caused by the oxidised iron present, which can make up to 60% of the mass of the red mud. In addition to iron, the other dominant particles include silica, unleached residual aluminium, and titanium oxide.

Red mud cannot be disposed of easily. In most countries where red mud is produced, it is pumped into holding ponds. [2] Red mud presents a problem as it takes up land area and can neither be built on nor farmed, even when dry. As a waste product of the Bayer process the mud is highly basic with a pH ranging from 10 to 13. Several methods are used to lower the alkaline pH to an acceptable level to decrease the impact on the environment. Research is being performed to find a suitable way to use the mud for other applications, but drying the mud requires much energy (latent heat for water evaporation) and can represent high costs if fossil fuels have to be used in the drying process.

III. EXPERIMENTAL PROCESS

Powder metallurgy is the process of blending fine powdered materials, pressing them into a desired shape or form (compacting), and then heating the compressed material in a controlled atmosphere to bond the material (sintering). The powder metallurgy process generally consists of four basic steps: powder manufacture, powder blending, compacting, and sintering. Compacting is generally performed at room temperature, and the elevated-temperature process of sintering is usually conducted at atmospheric pressure. Optional secondary processing often follows to obtain special properties or enhanced precision.

3.1.2 Powder Blending:-

The powders are blended according to the calculated individual mass obtained after calculation and it is blended properly. The powders are blended and then placed in the center cavity of the manufactured die. Initially the composition of the samples without red mud

is first analyzed and then the composition of samples with red mud is analyzed.

3.1.3 Composition of samples:-

It is subjected to have two different set of samples of Aluminium- Silicon Carbide combination and Aluminium- Silicon Carbide and Red mud composition. The main intention is to compare the prepared samples and to make the metal matrix composites and to compare them by undertaking different types of tests and to state the strength and extent of utilization of the metal matrix composites manufactured.

Composition calculation:-

Theoretical density is calculated as,

Theo density = 100/ ((% Al / density of Al + % of SiC / density of SiC)) (g/cc)

Mass of powder required for 95% achievement is calculated as,

Mass = [(3.14/4)* D^2* L* theo density* 95%] (g)

For calculating individual amount of composition of powders, say 95%

*Mass of Al = Mass for 95% * % of Al selected (g)*

Mass of SiC = Mass of 95% * % of SiC selected (g)

Mass of red mud = Mass of 95% * % of Red Mud selected (g)

Compaction process

Coming to compaction part of the sample, the powders are compacted under the compaction pressure of 240 Mpa on the blended powder. In sedimentology, compaction refers to the process by which a sediment progressively loses its porosity due to the effects of loading. This forms part of the process of lithification. When a layer of sediment is originally deposited, it contains an open framework of particles with the pore space being usually filled with water. As more sediment is deposited above the layer, the effect of the increased loading is to increase the particle-to-particle stresses resulting in porosity reduction primarily through a more efficient packing of the particles and to a lesser extent through elastic compression and pressure solution. High pressure loading is been provided to the powder which is been placed at the centre part of the die cavity. The compaction process can be made using Universal Testing Machine by providing sufficient loading on the powder part.

Sintering process

Sintering is the process of compacting and forming a solid mass of material by heat or pressure without melting it to the point of liquefaction. Sintering happens naturally in mineral deposits or as a manufacturing process used with metals, ceramics, plastics, and other materials. The atoms in the materials diffuse across the boundaries of the particles, fusing the particles together and creating one solid piece. The study of sintering in metallurgy powder-related processes is known as powder metallurgy. Sintering is effective when the process reduces the porosity and enhances properties such as strength, electrical conductivity, translucency and thermal conductivity; yet, in other cases, it may be useful to increase its strength but keep its gas absorbency constant as in filters or catalysts. During the firing process, atomic diffusion drives powder surface elimination in different stages, starting from the formation of necks between powders to final elimination of small pores at the end of the process.

IV TESTING DETAILS

It is planned to undertake three important tests to check whether our manufactured metal matrix composites are capable to withstand high strength, compressive strength and resistant to wear factor. Hence the three tests are

1. Hardness test
2. Compression test
3. Wear test

Metallurgical tests

Scanning Electron Microscopy (SEM) is used to image and investigate the properties and compositions of a broad range of sample types.

- High resolution surface inspection and backscatter analysis of samples
- Non-destructive, semi-quantitative elemental analysis of solids using energy dispersive X-ray microanalysis

Authors and Affiliations

A[1] R. Sasikumar

a) Profession: Student

b) Degree and Department: B.Tech and Mechanical engineering

c) Name of the college: Christ College of Engineering and Technology, Puducherry- 10

A[1] M. R. Mahadevan

a) Profession: Student

b) Degree and Department: B.Tech and Mechanical engineering

c) Name of the college: Christ College of Engineering and Technology, Puducherry- 10

A[1] I. Dharanidharan

a) Profession: Student

b) Degree and Department: B.Tech and Mechanical engineering

c) Name of the college: Christ College of Engineering and Technology, Puducherry- 10

A[2] Mr. R. Jayavel

a) Profession: Assistant professor

b) Degree and Department: B.Tech, M.Tech and Mechanical engineering

c) Name of the college: Christ College of Engineering and Technology, Puducherry- 10

.REFERENCES

[1] A Study on Mechanical Properties of Silicon Carbide, E-Glass and Red Mud Reinforced Aluminium (LM25) Composite by Mr. Prasanna, Mr. Devraj, Mr. Rakeshkumar, Mr. Mahadevappa, Asst Prof. Sharanabasappa R P

[2] Evaluation of the properties of Red Mud Concrete by Ramesh R. Rathod, Nagesh T.Suryawanshi, Pravin D. Memade

[3] Mechanical and physical properties of sintered aluminum powders by A.Gökçe, F. Fındık

[4] Sintering Characteristics of Red Mud Compact by Rahul Agarwal and M.Shashikanth

[5] Fabrication of Al–4.5% Cu alloy with fly ash metal matrix composites and its characterization by K.V. MAHENDRA, K. RADHAKRISHNA

Improving the Effectiveness of Automobile radiator using Copper Oxide Nanofluid as a Coolant

1.Kader[a], 2.Karthikeyan[a], 3.Navaneetha Kannan[a], 4.Arumugam[b]
[a] Student, Department of Mechanical Engineering,
Christ College Of Engineering and Technology, Moolakulam, Pondicherry- 605 010.
[b] Assistant Professor, Department of Mechanical Engineering,
Christ College Of Engineering and Technology, Moolakulam, Pondicherry- 605 010.

***Abstract*— In this project work, we are using the nanofluid copper oxide with pure water and ethylene glycol as a coolant in a automobile radiator. The nanofluid is varied with three different concentration in the range of 0.1-1% have been prepared by the addition of copper oxide nanoparticles into pure water and ethylene glycol. The effect of the radiator on heat transfer co-efficient has also been analyzed for pure water, ethylene glycol with nanofluids. Comparing the heat transfer co-efficient of the nanofluids copper oxide with pure water and ethylene glycol coolant of a automobile radiator**.

Keywords— Copper oxide
Ethylene glycol
Radiator
Heat transfer coefficient

I. INTRODUCTION

The application of ethylene glycol / copper oxide (CuO) nanofluid instead of pure water in the radiator as a coolant. It is common in the area of cold or hot weathers that some additives are added to the copper oxide in the automotive radiator which decrease freezing point of copper oxide. It keeps the radiator fluid from freezing when it is very cold and keeps the car from overheating on very hot days. The additive which is used is specially ethylene glycol. The major use of ethylene glycol is as a medium for convective heat transfer. Because copper oxide is a much better engine coolant, the mixture of copper oxide and ethylene glycol has been used. The trouble with ethylene is that it freezes or boils at extreme temperatures. Anti – freezing agents like ethylene glycol can withstand much greater temperature extremes, so by adding it to the copper oxide nanofluids.

Convectional fluids such as refrigerants, water, engine oil, ethylene glycol have poor heat transfer performance and therefore high compactness and effectiveness of heat transfer system are necessary to achieve the required heat transfer. An experimental investigation of the convective turbulent heat transfer characteristics of nanofluid (CuO – ethylene glycol) with 0.1 – 1% vol. the Nusselt number for the nanofluid increase with the increase of volume concentration and Reynolds number. The convective heat transfer of nanofluid in the region under laminar flow condition. It is based on the copper oxide nanofluid along with ethylene glycol. The laminar flow heat transfer of nanofluid (CuO – ethylene glycol) in a constant wall temperature boundary condition. An investigation of the laminar flow convective heat transfer of CuO–ethylene under constant wall temperature with 0.1 – 1% vol of nanoparticle for Reynolds number varying between 700 and 2050. 1% vol of CuO which is mixture with ethylene glycol which is used as a coolant to cool the heat transfer through the tubes in the radiator.

By this method we are improving the effectiveness of radiator by using copper oxide as a nanofluid and the effects of the operating conditions on its heat transfer performance are analyzed. The minimum freezing point is observed when the ethylene glycol percent in copper oxide is about 70%. However the boiling point for aqueous ethylene glycol increases monotonically with increasing glycol percentage. Thus the use of ethylene glycol not only declines the freezing point but also elevates the boiling point such that the operating range for the heat transfer fluid is broadened on both ends of the temperature scale. Nanofluids are formed by suspending metallic or non-metallic oxide nanoparticles. It has been proved that conventional fluids, such as copper oxide and ethylene glycol have poor convective heat transfer performance and therefore high compactness and effectiveness of heat transfer systems are necessary to achieve the required heat transfer. In car radiators, the coolant media is pumped through the flat tubes while the air is drawn over the fins by forced convection, thereby heat exchanges between the hot circulating fluid and air constant velocity and temperature of air are considered throughout the experiments in order to clearly investigate the internal heat transfer.

Radiator is used for storing cooling water which is circulated around the cylinder. The radiator is provided fins for air venting. This experiment includes a storage tank, a heating element (radiator), a pump and a pressure gauge. The test fluid flows through the five layer insulated tubes from the feed tank to the radiator by a centrifugal pump with constant flow rate of 12 l/min. water from the sump enters the heating element which is heated to absorb the heat and enters to the

radiator tube. Hot water which is enters to the radiator and goes out as cold water because of the copper oxide which is used as a nanofluid enters to the radiator tube as a coolant which is high heat resistance through it, and comes out as cold water. Inside the radiator, the tube present is copper tube.

Temperature indicator is used to indicate the range of temperature of inlet, intermediate and outlet. Also with that we are using sensor which is connected to it. Pressure gauge is used to noted the flow range of fluid which passes through the tube. The range of pressure gauge is 0-10kgf/cm^2. heating coil which is we use similar to the induction coil which shows the range of 230-240^{0}C. pump is used to circulate the fluid which passes through the tubes along with the nanoparticle which is present in it. Collecting tank is used to collect the fluid and help to pass through the tubes. On the bottom of the collecting tank there is a drain plug is present which is used to remove the fluid out when it is not necessary. The capacity of collecting tank contains 1-1.5lits of storage fluids.

Nanofluids are the new window which was opened recently and it was confirmed by several authors that these working fluid can enhance heat transfer performance. Further enhancement in heat transfer is always in demand, as the operational speed of these device depends on the cooling rate. New technology and advance fluid with greater potential to improve the heat transfer performance. The test section is made up with a typical automobile radiator and the effects of the operating condition on its heat transfer performance are analyzed.

It has been proved that conventional fluids, such as copper oxide and ethylene glycol have poor convective heat transfer performance and therefore high compactness and effectiveness of heat transfer systems are necessary to achieve the required heat transfer. In car radiators, the coolant media is pumped through the flat tubes while the air is drawn over the fins by forced convection, thereby heat exchanges between the hot circulating fluid and air constant velocity and temperature of air are considered throughout the experiments in order to clearly investigate the internal heat transfer.

COMPONENTS:

- Radiator (heat exchanger).
- Heating element.
- Temperature indicator.
- Fan.
- Pressure gauge.
- Circulating pump.

RADIATOR:

Radiator is used for storing cooling water is circulated around the cylinder. The radiator is provided fins for air venting. This experiment include storage tank, a heating element (radiator), a pump and a pressure gauge. The test fluid flows through the five layer insulated tubes from the feed tank to the radiator by a centrifugal pump with constant flow rate of 12 l/min. water from the sump enters the heating element which is heated to absorb the heat and enters to the radiator and goes out as cold water because of the copper oxide which is used as a nanofluid enters to the radiator tube as a coolant which is high heat resistance through it, and comes out as a cold water. Inside the radiator, the tube present is copper tube.

HEATING ELEMENT:

FOR HEATING THE WORKING FLUID, AN ELECTRICAL HEATER AND A CONTROLLER WERE USED TO MAINTAIN THE TEMPERATURE OF AROUND 200-250*C. (WHICH IS USED TO WITHSTAND HIGH HEAT RESISTANCE). SINCE THE HEATING ELEMENT IS A DEVICE WHICH PRODUCE A HEAT TO THE EXPERIMENTAL SETUP. THE HEAT SOURCE IS MAIN IN THIS EXPERIMENT SO THE HEATING ELEMENT WHICH IS USED MUST BE HAVING GREATER EXTENT OF HEAT. SO THAT THE HEATING ELEMENT IS MUST REQUIRED FOR THIS EXPERIMENTAL SETUP. IN THIS EXPERIMENT IS INDUCTION COIL WHICH HAS A TEMPERATURE OF AROUND 240^{0}C. HEATING ELEMENT WHICH IS AROUND IN THE COLLECTING TANK. WHEN THE WATER FROM THE COLLECTING TANK ENTERS THROUGH THE HEATING COIL IS HEATED TO THE CERTAIN TEMPERATURE OF 230^0-240^{0}C AND ENTERS THE RADIATOR

temperature indicator:

The thermostat is device used for measuring the temperatures at 3 stages of the experiment. Since three thermostats are used in this experiment, which should be placed in 3 different stages, Such as inlet, outlet and intermediate stages. The inlet thermostat is used to measure the of water flow at the inlet opening. The outlet is used to measure the temperature at the outlet of the experimental set up, the intermediate thermostat is used to measure the temperature at the intermediate. Three temperature measurement is connected to the sensor with the help of a switch which is rotated the reading of the inlet, outlet and intermediate temperature is noted. Hot water which is enters to the radiator and goes out as cold water because of the copper oxide which is used as a nanofluid enter to the radiator tube as a coolant which is high heat resistance through it comes out as cold water. Inside the tube the flow of water along with the mixture of nanofluid to measure the velocity along with the pressure regulator. Temperature indicator is used to measure the temperature range which is done by the flow of water enters to the tubes and it reaches to a certain temperature.

RADIATOR FAN:

Radiator fan is used to reduce the heat of the coolant which is passing in the tube of the radiator. Here using 1400rpm fan with 45watts and 0.35amps.

PRESSURE GAUGE:

Pressure gauge is used to measure the flow of coolant. In this experiment dial gauge is used to measure the flow of coolant of the radiator. Pressure gauge range 0-10kgf/cm^2. Two pressure gauge is used, to measure the inlet and outlet flow of coolant.

CIRCULATING PUMP:

Pump is used to circulate the coolant into the radiator tube. In this experiment centrifugal pump is used to circulate the flow rate of 10-12 l/min. it has the rate of 0.05kw. the total volume of circulating liquid is constant in this experiment.

ETHYLENE GLYCOL:

The ethylene glycol mixture is used as coolant for the radiator to increase the cooling efficiency. Since it is mixed with the nano particle as the coolant to cool the engine in the radiator. It is a solution which has high cooling efficiency when compare with all other common solutions. And it dissipate high heat when compare with the other solutions. The nano particle will easily dissolve in this solution, then the ethylene glycol has high capacity.

copper oxide nanoparticles (0.1, 0.2, 0.3, 0.4 …….., 2) have been added to different base fluids including pure water and ethylene glycol (5, 10,….20 % vol EG). There was no dispersant or stabilizer added to the nanofluid. This is due to the fact that the addition of any agent may change the fluid properties and the authors were interested to estimate the easiest actual condition encountered in the radiator. Additionally creating highly turbulent flow condition in the radiation tubes connecting pipes can improve the stabilization of the nanoparticles in copper oxide fluid. By assuming that the nano particle are well dispersed within the base fluids. the particle concentration can be considered uniformly throughout the system. The following correlations have been used to predict nanofluid density, specific heat, and thermal conductivity respectively at different temperatures and concentration.

COPPER OXIDE:

Copper oxide is a nanofluid which is used as a coolant in the radiator. This is due the fact that the addition of any agent may change the fluid properties. By assuming that nanoparticle are well dispersed within the base fluids. Copper oxide has better heat transfer performance when compare to the aluminum oxide and silicon oxide.

Ethylene glycol:

Conventional fluids such as refrigerants, water, ethylene glycol, engine oil, etc have poor heat transfer performance and therefore high compactness and effectiveness of heat transfer systems are necessary to achieve the required heat transfer. Among the efforts for enhancement of heat transfer the application of additives to liquids is more noticeable.

Copper oxide

The liquids are water based nanofluid which consists of water and small amount of copper oxide nanoparticle. There was no dispersant or stabilizer added to nanofluid. Additionally creating highly turbulent flow condition in the radiator tubes connecting pipes guarantees the stabilization of the nanoparticle in water.

TESTING:

The following testing which is based on:

I. Ethylene glycol.
II. Pure water.
III. CuO+ethylene glycol.
IV. CuO+pure water.

REFERENCES:

[1] L.D. Tijing, B.C. Pak, B.J. Baek, D.H. Lee, A study on heat transfer enhancement using straight and twisted internal fin inserts, International Communications in Heat and Mass Transfer 33 (6) (2006) 719e726.

[2] P. Naphon, Effect of coil-wire insert on heat transfer enhancement and pressure drop of the horizontal concentric tubes, International Communications in Heat and Mass Transfer 33 (6) (2006) 753e763.

[3] B. Sahin, A. Demir, Performance analysis of a heat exchanger having perforated square fins, Applied Thermal Engineering 28 (5e6) (2008) 621e632.

[4] Z. Zhnegguo, X. Tao, F. Xiaoming, Experimental study on heat transfer enhancement of a helically baffled heat exchanger combined with threedimensional finned tubes, Applied Thermal Engineering 24 (14e15) (2004) 2293e2300.

[5] M.Y. Wen, C.Y. Ho, Heat-transfer enhancement in fin- and-tube heat exchanger with improved fin design, Applied Thermal Engineering 29 (5e6) (2009) 1050e1057.

[6] S.H. Hashemabadi, S.Gh. Etemad, Effect of rounded corners on the secondary flow of viscoelastic fluids through non-circular ducts, International Journal of Heat and Mass Transfer 49 (2006) 1986e1990.

[7] S.H. Hashemabadi, S.Gh. Etemad, M.R. Golkar Naranji, J. Thibault, Laminar flow of non-Newtonian fluid in right triangular ducts, International Communications in Heat and Mass Transfer 30 (1) (2003) 53e60.

[8] S.M. Peyghambarzadeh, S.H. Hashemabadi, S.M. Hoseini, M. Seifi, Experimental study of heat transfer enhancement using water/ethylene glycol based nanofluids as a new coolant for car radiators, Int. Commun. Heat Mass Transfer 38 (2011) 1283e1290.

[9] S.M. Peyghambarzadeh, S.H. Hashemabadi, M. Seifi Jamnani, S.M. Hoseini, Improving the cooling performance of automobile radiator with Al2O3/water nanofluid, Appl. Therm. Eng. 31 (201

[10] M. Naraki, S.M. Peyghambarzadeh, S.H. Hashemabadi, Y. Vermahmoudi, Parametric study of overall heat transfer coefficient of CuO/water nanofluids in a car radiator, Int. J. Therm. Sci. 66 (2013) 82e90.

[11] S.M. Peyghambarzadeh, S.H. Hashemabadi, M. Naraki, Y. Vermahmoudi, Experimental study of overall heat transfer coefficient in the application of dilute nanofluids in the car radiator, Appl. Therm. Eng. 52 (2013) 8e16. 1) 1833e1838.

A Study on Heat Cured Fly Ash based Geo Polymer Concrete

Annie John[1] Rahul John Roy[2]
1 Assistant Professor, St Anne's College of Engineering and Technology, Panruti.
2 Student, Civil Engg Department, NIT Trichy.

Abstract:- **Continuous increase in production of cement causes large amount of carbon dioxide emission which results in green house effect. In order to overcome this problem many researchers have put in their efforts to achieve optimum strength of concrete by replacing cement with fly ash, when it combine with alkaline solution to produce Geopolymers concrete(GPC). GPC is an improved way of concreting execution made by complete elimination of ordinary Portland cement. GPC were synthesized from low calcium fly ash, activated by combination of Sodium Hydroxide and Sodium Silicate solution. This report is an attempt to find out suitable utilization of fly ash by studying the compressive strength of GPC and to observe durability characteristics of GPC. In this experimental study different concentrations of alkaline liquid are being used. Mix samples of different molarities were prepared to study the influence of alkaline solution on compressive strength of GPC. Increased alkaline solution concentration proved to have positive effect on Geopolymerization process and this is revealed by the improved compressive strength.**

1. INTRODUCTION

The global demand of cement for construction of infrastructures is continuously increasing in order to maintain the ongoing growth and accommodate the needs of the increasing population. OPC has been traditionally used as the binder in concrete. About 1 tonne of carbon dioxide is emitted into the atmosphere in the production process of 1 tonne of cement. This makes a significant contribution to the global greenhouse gas emission. Therefore, development of alternative binders utilising industrial by-products is necessary to reduce the carbon footprint of the construction industry. Geo polymer is an emerging alternative binder for concrete that uses by-product materials. A base material that is rich in Silicon (Si) and Aluminium (Al) is reacted by an alkaline solution to produce the geopolymer binder. Source materials such as fly ash, metakaolin and blast furnace slag can be used to make geo polymer.

Fly ash blended with blast furnace slag and rice husk ash has also been used as the base material for geopolymer. The product of the reaction is an inorganic polymer which binds the aggregates together to make geopolymer concrete. The coal- fired power stations worldwide generate substantial amount of fly ash as a by-product that can be efficiently used in geopolymer concrete to help reduce the carbon footprint of concrete production.

The results of recent studies have shown the potential use of heat-cured fly ash based geopolymer concrete as a construction material. As a relatively new material, it is necessary to study the various properties of GPC as compared to the traditional OPC concrete in order to determine its suitability for structural applications. The ongoing research on fly ash-based geopolymer concrete studied several short-term and long-term properties. It was shown that heat-cured geopolymer concrete possesses the properties of high compressive strength, low drying shrinkage and creep, and good

resistance to sulphate and acid. Geopolymer concrete was found to have higher bond strength with reinforcing steel and relatively higher splitting tensile strength than OPC concrete. Geopolymer concrete beams and columns were tested to failure and they showed similar or better performance as compared to OPC concrete members. Heat-cured geopolymer concrete showed higher residual strength than OPC concrete cylinders after exposure to high temperature heat of up to 800^0 C .Therefore heat-cured geopolymer concrete is considered as an ideal material for precast concrete structural members.

Development of the constitutive model for a material requires its fracture parameters. The fracture characteristics of a material are used to describe the formation and propagation of cracks in the material. The crack path through a composite material such as concrete is dependent on the mechanical interaction between the aggregates and the binder matrix. Fracture energy of a composite material depends on the deviation of the crack path from an idealized crack plane. Since the binder in geopolymer concrete is different from that in OPC concrete, the effect of the interaction between the aggregates and the geopolymer binder needs to be investigated. Thus, it is necessary to study the fracture parameters of geopolymer concrete to understand its failure behaviour. In this study, the fracture properties of heat cured fly ash based geopolymer concrete specimens were determined from three-point bending test of notched beams. Fracture energy and the critical stress intensity factor were also determined for OPC concrete specimens to compare with those of geopolymer concrete specimens of similar compressive strengths and containing the same aggregates. The fracture behaviours of both types of concrete were compared using the test results.

2. EXPERIMENTAL DETAILS.

2.1 Materials

Lignite fly ash was obtained from Neyveli Lignite Power Station, Neyveli, Tamil Nadu.The particle shape of fly ash was mainly spherical with the main chemical composition of 37% SiO_2 , 2% Fe_2 O_3 ,21% Al_2O_3, 14% CaO. A median particle size of fly ash was 50µ m. Sodium Silicate solution (Na_2SiO_3) and Sodium Hydroxide (NaOH) were used as Alkali activators. Coarse aggregate with a maximum size of 20mm diameter with a specific gravity of 2.85 was used for making Geopolymer concrete. Sand used for the experiment was passed through the 4.75mm IS Sieve with a fineness modulus of 2.46.

2.2 Mix proportion, mixing and casting.

Mix chosen in this study is 1:1.5:3 with 100% replacement of cement with fly ash. Alkaline liquid was a combination of Sodium hydroxide and Sodium Silicate solution. Sodium hydroxide and Sodium Silicate obtained as pellets were dissolved in distilled water to form the alkaline liquid. In order to study the effects of alkaline solution on the geopolymer concrete properties, three concentrations of alkaline solutions 8, 10, 12 molar were used. Mix proportions are shown in Table 1.

Table 1 Mix proportion of geo polymer concrete

	Mix Proportion(kg/m)					
Mix No	Fly ash	FA	CA	**Alkaline liquid**	Liquid	Water
S1	418	628	1256	10 M	150	50
S2	418	628	1256	10 M	100	100
S3	418	628	1256	8 M	150	50
S4	418	628	1256	8 M	100	100
S5	418	628	1256	8 M	50	150
S6	418	628	1256	12 M	150	50
S7	418	628	1256	12 M	100	100
S8	418	628	1256	12 M	150	150

The coarse aggregate and sand is saturated surface dry condition was first mixed in laboratory pan mixer with the fly ash for about three minutes. At the end of this mixing, the alkaline solutions and extra water were added to the dry materials and the mixing continued for another four minutes. Immediately after mixing, the fresh concrete was cast into moulds. All cubes were cast in two layers. Each layer was compacted into limited capacity of the laboratory mixer. The slump of every batch of fresh concrete was measured in order to observe the consistency of the mixtures. Casted cubes were kept in oven for 48 hours at the temperature of

70^0C for curing. After curing, the cubes were

removed from the chamber and left air-dry at room temperature for another 24 hours before demoulding.The test specimens were then left in the laboratory ambient conditions until the day of testing. The laboratory temperature varied between

25^0C and 35^0C during that period.

2.3 Testing Detail

2.3.1 Void Content

The void content of Geopolymer concrete was tested using the casted cubes. The void content was determined in accordance with ASTM and calculated using Eq (1).The reported void contents were the average of three samples

Table 2 Total void ratio

Mix	Void content%
S1	15.5
S2	16.6
S3	17.1
S4	17.7
S5	18.6
S6	10.5
S7	11.1
S8	12.3

$V_T = (T-D)*100/ T$----------(1)

$T = M_s / V_s$

Where V_T is the void content (%),

T is the theoretical density of Geopolymer concrete computed on an air free basis (kg/m^3).

M_s is the total mass of all the materials batched (kg),

V_S is the sum of absolute volumes of component ingredients in the batch (m^3).

2.3.2 Compressive strength

The compressive strength was tested at the age of 3^{rd} day. The crushing strength of concrete cube is determined by applying a compressive load at the rate of $2.88N/mm^2$, till the specimen fails.

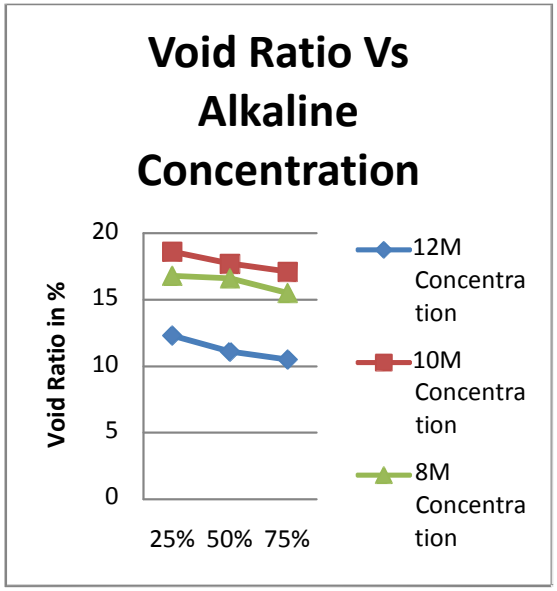

3. RESULTS AND DISCUSSION

3.1 Void Content

The results of void content are summarized in Table 2.The void content of geopolymer concrete were relatively low between 10.5% and 18.6%. Generally the void content of Portland cement concrete depends on the gradation of aggregate and the method of compaction. However in this test, the gradation of aggregate and the method of compaction were not varied. The results however indicated that voids content in this study slightly decreased with the increase in the alkaline concentration.

For instance the void content of $S_{6,}$ S7, S8 were

10.5%, 10.8% and 11.2% respectively. The adding of alkali liquid in the mixture increased the paste content and the excess paste fill the voids resulting in a dense concrete with low void content.

3.2 Compressive Strength

Compressive strength tests of all specimens were conducted using a compressive testing machine. A minimum of three specimens (150mm*150mm) cubes for each type were tested for 3-day compressive strengths after casting, which is equivalent to a typical OPC strength development after 28 days. It has been found that age does not have a significant effect on strength of Geopolymers after completion of heating curing cycle.

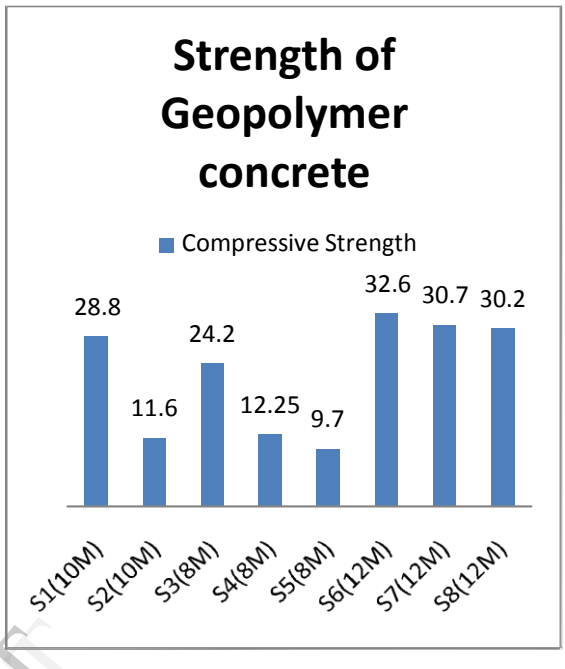

The strength of the fly ash based geopolymer concrete is significantly increased the geopolymer paste undergoes high early strength development at an accelerated rate. This behaviour is the characteristics' of the quick geopolymerization process, which contrasts with the hydration process of OPC that gains strength over longer time periods. In geopolymers, alumino-silicate gel is the major binding phase that provides interparticle bonding, which in turn enhances the macroscopic strength.

Compressive strength of Geopolymer concrete increases marginally with an increase in alkaline content. For example compressive strength of 9.70
– 24.2, 11.6 – 28.8, 30.2 – 32.6 MPa were obtained for GPC with 8 M, 10M and 12M respectively. With regard to Sodium Hydroxide concentration, the optimum concentration to produce GPC is 12M. Increasing the concentration to 12M increases the compressive strength.

3.3 Relationship of void content and compressive strength

The relationship between void content and compressive strength can be shown using the exponential curve as in figure. It can be seen that compressive strength increases as void content decreases.

CONCLUSION

In order to expand the use of fly ash Geopolymer concrete which can be prepared easily from alkali activated fly ash and coarse aggregate. The void content and compressive strength were determined. Compressive strength between 9.7 and
32.6 were obtained according to the molarity of the alkaline content. These values show that optimum alkaline content can be chosen between 10M and
12M according to the requirement. In addition the relationship of void content – alkaline content, compressive strength – alkaline content of GPC was shown in graph. It has therefore been demonstrated that fly ash geo polymer concrete could be used as replacement for ordinary Portland cement concrete with acceptable strength.

REFERENCES

[1] N P Raja mane, Head, Concrete Composites Lab, and N Lakshmana, former Director and Project Advisor, Structural Engineering Research Centre,,Chennai,Nataraja M C, S J College of Engineering, Mysore; Geo polymer Concrete-A New Eco friendly Material of Construction (2009)

[2] Davidovits, J. (1988) "Soft Mineralogy and Geo polymers." In proceeding of Geo polymer 88 International Conference, the University de Technologies, Compiegne, France.

[3] Davidovits, J. (1999) "Chemistry of geo polymer systems, terminology." In Proceedings of Geo polymer '99 International Conferences, France.1992

[4] Malhotra, V. M. (1999) "Making concrete 'greener' with fly ash." ACI Concrete International, 21, pp. 61-66.

[5] M D J Sumajouw & B V Rangan, Low Calcium fly ash based Geo-polymer concrete (2006), Faculty of Engineering, Curtin University of Technology, Perth, Australia.

[6] Davidovts.J,(1988), Soft Mineral usage and Geo polymers," In proceeds of Geo polymer 88 International Conference, The University de Technologies', Compiegne, France.

[7] V.M. Malhotra, "Introduction: Sustainable Development & Concrete Technology", ACI Concrete International, 24(7), pp. 22, 2002.

[8] J. Davidovits, "Geo polymers: inorganic polymeric new materials" Journal of Thermal Analysis, 37(8), pp. 1633–1656, 1991.

[9] Palomo A Gruzeck M W and Blanco M T,"Alkali-Activated Fly Ashes, A Cement for the future", Cement and Concrete Research, V29, no8 1999, pp 1323

[10] Warner R F, Rangan, B V Hall, A S, and Faulkies K A, Concrete structures, Melbourne: Addison Wesley Longman Australia Ltd,1998,974pp

[11] Studies on development of Geo polymeric low energy cement from fly ash for structural applications. N P Raja mane, D. Sabitha, Sajana Mary James, SERC, Chennai

[12] Concrete Technology Theory and Practice by M S Shetty, edition 2005, 66 – 115,599

[13] Wallah, S E, Sumajouw D M J, and Rangan B V., "Sulphate Resistance of Fly ash based Geo polymer concrete" Concrete in the third millennium,21st Biennial conference of the of the Concrete Institute of Australia, Brisbane, Queensland, Australia, 2003 pp.205 – 212

[14] Bal guru P N, Kurtz S, and Rudolph J (1997) Geo polymer for Repair and Rehabilitation of Reinforced Concrete Beams"; The State University of New Jersey Geo polymer Institute, Rutgers, 5

[15] Davidovits, J. (1994) "High-Alkali Cements for 21st Century Concretes. in Concrete Technology, Past, Present and Future." In proceedings of V. Mohan Malhotra Symposium. 1994. Editor: P. Kumar Mehta,ACI SP- 144. pp. 383-397.

[16] Hardjito, D., Wallah, S. E., Sumajouw, D. M. J. & Rangan, B. V. (2004c) "The Stress - Strain Behaviour of Fly Ash – Based Geo polymer Concrete." In Development in Mechanics of Structures & Materials, vol. 2, Eds. A.J. Deeks and Hong Hao, A.A. Balke

Surface Roughness Model and Parametric Optimization in End Milling using Carbide Tools: Response Surface Methodology and Taguchi Approach

R.Arokiadass[1], D.Ommurugadhasan[2], K.Saravanan[3]
Department of Mechanical Engineering
St.Anne's College of Engineering and Technology, Panruti- 607 110, Tamilnadu, India.

***Abstract*—The surface roughness prediction model for the end milling of LM25 Al/SiC_p metal matrix composite was investigated in this study. This paper highlights the features of the development of a comprehensive mathematical model for correlating the interactive and higher-order influences of various machining parameters on the Surface roughness (Ra) through response surface methodology (RSM), utilizing relevant experimental data as obtained through experimentation. Experiments were conducted through the Taguchi's Design of Experiments (DOE) in CNC milling machine using solid carbide end mill. The results indicate that the developed model is suitable for prediction of surface roughness in end milling of LM25 Al/SiC_p metal matrix composites. The effect of different parameters on surface roughness was analyzed. Optimal combination of these parameters can be used in order to achieve minimum surface roughness.**

Keywords— Taguchi method, Metal Matrix Composite, Surface roughness, Response surface methodology, optimization.

I. INTRODUCTION

Metal matrix composites (MMC) are a relatively new class of materials characterized by lighter weight, greater strength and wear resistance than those of conventional materials. Due to their superior strength and stiffness, MMCs have good potential for application in the automotive and aerospace industries [1–3]. The machining of MMCs is very difficult due to the highly abrasive and intermittent nature of the reinforcements.

Stir casting is the simplest and the most commercial technique. The development of MMCs by stir-casting technology has been one of the unique and feasible processes because of producing better matrix particle bonding, easier control of matrix structure, simplicity, higher production rate, and low cost [4]. It involves stirring the melt along with solid silicon carbide particles and then allowing the mixture to solidify. Due to the addition of reinforcing materials, which are normally harder and stiffer than matrix, machining becomes significantly more difficult than those of conventional materials [5].

LM 25 aluminum alloy reinforced with green bonded silicon carbide particles of size 25 µm with different volume fractions was used for experimentation. The machining experiments were conducted on the lathe using tungsten carbide tool inserts (K10). It was concluded that feed rate has the greater influence on surface roughness, followed by cutting speed and percent volume fraction of SiC [6].

High speed, low feed rate, and low depth of cut was recommended for achieving better surface finish during turning of Al/SiC-MMC using tungsten carbide insert [7]. Surface roughness increased due to increasing feed rate values. It was found that increase in particle ratio affects roughness negatively [8].

In this investigation, effects of process parameters on surface roughness in end milling of LM25 Al/SiC_p metal matrix composites by carbide tools are evaluated. A second order quadratic model is developed for predicting the surface roughness in end milling of LM25 Al/SiC_p metal matrix composites by response surface methodology approach. The predicted and measured values are fairly close to each other. Their proximity to each other indicates that the developed model can be effectively used to predict the surface roughness in end milling of LM25 Al/SiC_p metal matrix composites.

II. RESPONSE SURFACE METHODOLOGY

Response surface methodology is a collection of mathematical and statistical techniques useful for analyzing problems in which several independent variables influence a dependent variable or response and the goal is to optimize the response [9].

In many experimental conditions, it is possible to represent independent factors in quantitative form as given in equation (1). Then these factors can be regarded as having a functional relationship or response as follows

$$Y = f(x_1, x_2 \ldots\ldots x_n) \pm \varepsilon \quad (1)$$

Between the response Y and $x_1, x_2 \ldots\ldots x_n$ of n quantitative factors, the function f is called the response surface or response function. The residual ε measures the experimental errors. In applying the RSM, the independent variable was viewed as a surface to which a mathematical model is fitted. Representing the surface roughness (R_a), the response is a

function of spindle speed (*N*), feed rate (*f*), depth of cut (*d*) and %wt. of silicon carbide (*S*); it can be expressed as

$R_a = f\{N, f, d, S\}$ (2)

The second-order polynomial (regression) equation used to represent the response surface Y is given by

$R_a = b_0 + \Sigma b_i X_i + \Sigma b_{ii} X_i^2 + \Sigma b_{ij} X_i X_j$ (3) and for four factors, the selected polynomial could be expressed as:

$R_a = b_0 + b_1 N + b_2 f + b_3 d + b_4 S + b_{12} Nf + b_{13} Nd + b_{14} NS + b_{23} fd + b_{24} fS + b_{34} dS + b_{11} N^2 + b_{22} f^2 + b_{33} d^2 + b_{44} S^2$ (4)

where b_0 is the average of the responses, and b_1, b_2, b_3……b_{44} are regression coefficients [10] that depend on the respective linear, interaction, and squared terms of factors.

III. EXPERIMENTAL DETAILS

The experiments were planned using Taguchi's orthogonal array in the design of experiments (DoE), which helps in reducing the number of experiments. The four process parameters selected in the present investigation were spindle speed, feed rate, and depth of cut and various % wt. of silicon carbide (S). This needs 25 runs and has 24 degrees of freedom (DOFs). In the present experimental study, the material to be machined is LM25 Al alloy reinforced with SiC_p particles, at a composition of 5%wt., 10%wt., 15%wt., 20%wt. and 25%wt.

and of 25 mm particle size. The dimensions of the specimens were of 100 mm × 50 mm × 40 mm. The composition of the LM25 Al alloy specimen is Si 7%; Mg 0.33%; Mn 0.3%; Fe 0.5%; Cu 0.1%; Ni 0.1% and Ti 0.2%.

Table.1 Experimental parameters and their levels

No	Factor	Levels				
		(-2)	(-1)	0	(+1)	(+2)
1	*N, RPM*	2000	2500	3000	3500	4000
2	*F, mm/rev*	0.02	0.03	0.04	0.05	0.06
3	*d, mm*	0.5	1	1.5	2	2.5
4	*S, %wt.*	5	10	15	20	25

The machining is done on HASS CNC milling machine. The tool used was carbide having diameter 12 mm and number of flutes: 4. The parameters and their levels were selected is given in the Table.1. The surface roughness (Ra) of the machined test specimens were measured using a Talysurf tester with a sampling length of 10mm.

IV. RESULTS AND DISCUSSION

Surface roughness plays a predominant role in determining the machining accuracy. The study of surface roughness characteristics of LM25 Al/SiC_p MMC is more influenced by the process parameters. The influence of different process parameters in end milling of LM25 Al/SiC_p MMC can be studied by using response graph is shown in figure 1 and response table is shown in Table 2.

The observed surface roughness decreases at high spindle speed as compared to the low spindle speed. But surface roughness increases at high feed rate when compared to the low feed rate. The effect of depth of cut on end milling of LM25 Al/SiC_p MMC is less on surface roughness. Also it indicates that low surface roughness is observed for low %wt. of silicon carbide as compared to high %wt. of silicon carbide.

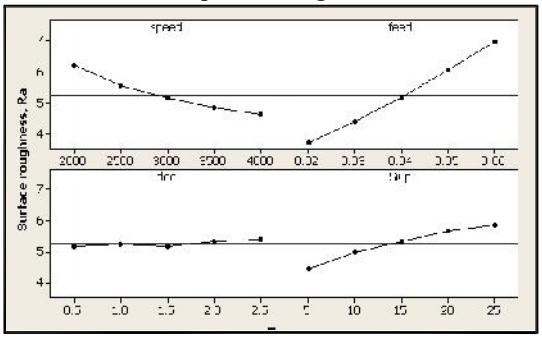

FIGURE 1: Effect plot for surface roughness

The response table for surface roughness shows the effect of different process parameters, which is shown in Table. 2. From the table, it can be found that the feed rate is the main parameters which affect the surface roughness followed by spindle speed, %wt. of silicon carbide and depth of cut.

Table.2 Response table for surface roughness

Level	Spindle speed N (RPM)	Feed rate f (mm/rev)	Depth of cut d (mm)	%wt. of SiC_p S (%wt.)
1	6.240	3.673	5.154	4.473
2	5.541	4.362	5.254	5.002
3	5.190	5.242	5.257	5.372
4	4.833	6.132	5.382	5.713
5	4.633	7.027	5.390	5.877
Delta	1.607	3.354	0.236	1.404
Rank	**2**	**1**	**4**	**3**

The experimental values are analyzed using response surface analysis and the following relation has been established for surface roughness (Ra) in un coded units as:

$Ra = 4.970 - 0.002N + 57.236f + 0.344d + 0.131S + 353.895f^2 - 0.043d^2 - 0.002S^2 - 0.003N \times f + 0.399f \times S$ (5)

A result of ANOVA for the response function surface roughness is presented in Table 3. This analysis is carried out for a level of significance of 5% i.e., for a level of confidence of 95%. From the table, it is apparent that, the F calculated value is greater than the F-table value ($F_{0.05}$, 12, 12= 2.69) and hence the second order response function developed is quite adequate.

Table 3: ANOVA for the response function of the R_a

Source of variation	DF	Sum of squares	Mean sum of squares	*F* value	p value
Regression	12	50.6778	4.223146	687.70	0.000
Residual	12	0.0737	0.006141		

Error		
Total	24	50.7514

The plot of normal probability of the residual, the plots of the residuals versus the fitted values for surface roughness is shown in figure. 2 and 3 respectively. From figure 2, it is evident that the data are spread roughly along the straight line. Hence it is concluded that the data are normally distributed [11]. In addition, Fig. 3 revealed that there is no noticeable pattern or unusual structure present in the data. Hence, the RSM model developed is significant & adequate.

$R^2 = 99.85\%$

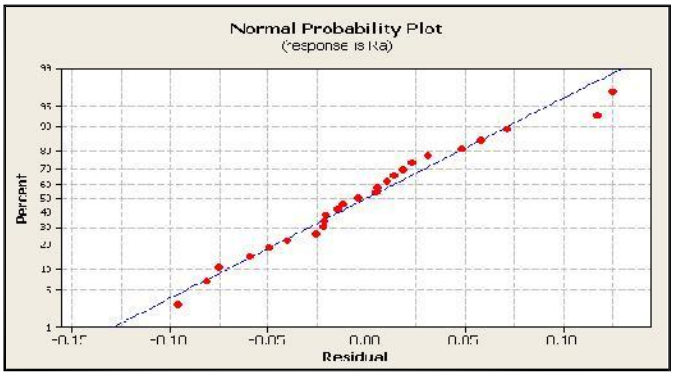

FIGURE 2: Normal Probability plot for surface roughness, Ra

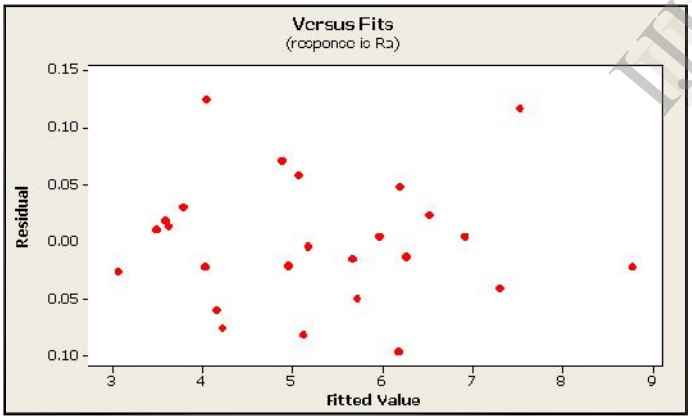

FIGURE 3:Residual Vs fitted values for surface roughness, Ra

Figure 5 shows the experimental values and their corresponding predicted values through Eq. (5). From the analysis of figure, it can be observed that the predicted values were very close to the experimental results.

V. ANALYSIS FOR OPTIMIZATION OF THE RESPONSES

The After building the regression model, a numerical optimization technique using desirability functions can be used to optimize the response. The objective of optimization is to find the best settings that minimize a particular response [12]. A desirability value, where $0 \leq d \leq 1$. The value of d increases as the "desirability" of the corresponding response increases. The factor settings with maximum desirability are considered to be the optimal parameter conditions. Most of the standard statistical software packages (Minitab, Design, Expert, etc.) employ this popular technique for response optimization. In the present case, Minitab was used to optimize the response parameters. The optimization plot for surface roughness has been shown in figure. 4. It is revealed that highest desirability could be obtained at high spindle speed, low feed rate and low depth of cut and low percentage weight of silicon carbide. The goal was to minimize the surface roughness.

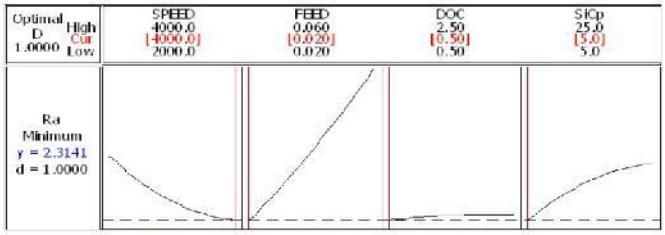

FIGURE: 4 Optimum results for minimum Ra

The upper value and target has been fixed at 8.748 and 3.040 µm, respectively. The parameter setting for achieving a surface roughness as low as of 2.3141 µm has been predicted as spindle speed (N) 4000 rpm, feed rate (f) 0.020 mm/rev, depth of cut (d) 0.50 mm, and weight of silicon carbide (S) 5%. The desirability of optimization has been calculated as 1.0000, i.e., all the parameters are within their working range.

VI. CONCLUSIONS

The surface roughness in the end milling process has been measured for machining of LM25 Al/SiC_p under different cutting conditions with a carbide tools using Taguchi's orthogonal array. Based on the experimental and analytical results the following conclusions are drawn.

1. The developed second-order response surface model can be used to calculate the surface roughness of the machined surfaces at different cutting conditions with the chosen range with 95% confidence intervals. Using such model, one can obtain remarkable savings in time and cost.
2. From the results, it can be asserted that moderate spindle speed, low feed rate, less %wt. of silicon carbide and moderate depth of cut are preferred for machining of LM25 Al/SiC_p MMC.
3. The feed is the dominant parameter which affects the surface roughness of LM25 Al/SiC_p MMC followed by spindle speed, %wt. of silicon carbide. Depth of cut shows a minimal effect on surface roughness compared to other process parameters.
4. From the developed mathematical model, the optimal machining parametric combination, i.e., spindle speed (N) 4000 rpm, feed rate (f) 0.020 mm/rev, depth of cut (d) 0.50

mm, and weight of silicon carbide (S) 5% was found out to achieve the minimum Ra as 2.3141 μm.

REFERENCES

[1] F.E. Kennedy, A.C. Balbahadur and D.S. Lashmore, "The friction and wear of Cu-based silicon carbide particulate metal matrix composites for brake applications", *Wear*, vol. 203/204, pp. 715–721, 1997.

[2] A.Ravikiran and M.K,Surappa, "Effect of sliding speed on wear behavior of A356 Al 30 wt % SiCp MMC", *Wear*, vol.206, pp. 33–38, 1997.

[3] J.E.Allision and G.S.Gole, "Metal-matrix composites in the automotive industry: opportunities and challenges", *J Min Met Mater Sci*, vol.45 (1), pp.

[4] Y.Sahin and G.Sur, "The effect Al2 O3,TiN and Ti(C,N) based CVD coatings on tool wear in machining metal matrix composite", *Surface Coating Technology*, vol.179, pp. 349–355, 2004.

[5] N.Tomac and K.Tonnessen, "Machinability of particulate aluminium matrix composites", *Annals CRIP*, vol.42(1), pp. 55–58, 1992.

[6] K.Palanikumar and R.Karthikeyan "Assessment of factors influencing surface roughness on the machining of Al/SiC particulate composites", *Mater Des*, vol.28, pp. 1584–1591, 2007.

[7] A.Manna and B.Bhattacharayya "Influence of machining parameters on the machinability of particulate reinforced Al/SiC- MMC", *Int J Adv Manuf Technol*, vol.25, pp. 850–856, 2005.

[8] T.Ozben, E.Kilickap, and O.Cakir, "Investigation of mechanical and machinability properties of SiC particle reinforced Al-MMC", *J Mater Process Technol*, vol.198, pp. 220–225, 2008.

[9] T.Ozel and A.Nadgir, "Prediction of flank wear by using back propagation neural network modeling when cutting hardened H-13 steel with chamfered and honed CBN tools," J *Machine Tools & Manufacture*, vol. 42, pp. 287–

[10] K.G. Murti and S.Sunderesan, "Structure and properties of friction welds between high-speed steel and medium carbon steel for bimetal tools", *J Mater Sci Technol*., vol. 2, pp. 865–870, 1986.

[11] S.Kumar, P.Kumar, and H.S.Shan, "Effect of evaporative pattern casting process parameters on the surface roughness of Al–7% Si alloy castings", *J Mater Processing Technol*, vol.182, 615–623, 2007.

[12] R.H.Myers and D.C.Montgomery, "Response surface methodology: process and product optimization using designed experiments", NY:John Wiley & Sons Inc., 2002.

Combustion Characteristics of Macro and Micro Algae Biodiesel

A.Ganesh[1] , K. Gokula Kannan[1]
Student,
Department Mechanical Engineering, Sathiyabhama University,
Chennai, India

Abstract: The interest on biodiesel research in India is mainly due to fluctuating crude prices, limited oil reserves and the strict emission standards. Here the experimental work has been carried out on a single cylinder, direct injection Diesel engine using Macro and Micro biodiesel blends under constant speed by varying the injection timings. The results show increased specific fuel consumption. The Brake thermal efficiency values of biodiesel are closer to Diesel. Compared to Diesel both the biodiesel blends give lesser un burnt hydrocarbons, Carbon monoxide and smoke emissions. Slight higher NOx emissions were found in Bio Diesel blends. While advancing the injection timing the performance and emission characteristics were good, compared to retarding it.

INTRODUCTION

At present, India is producing only 30% of the total petroleum fuels required. The remaining 70% is being imported. Biodiesel, an alternate of diesel, is defined as fatty acid methyl or ethyl esters from vegetable oils or animal fats. It is a renewable, biodegradable and oxygenated fuel .There are four methods normally used to convert oil and fats into bio diesel, they are direct use and blending, thermal cracking, transesterification, micro emulsion, out of which transesterification is the most popular method for making bio diesel from vegetable oil. Transesterification process is called as the chemical conversion of the oil to its fatty ester . In the Transesterification process, a catalyst (sodium hydroxide or potassium hydroxide) is used to split the oil molecules. An alcohol (methanol or ethanol) is used to combine with the separated esters. The byproduct from the reaction is glycerin. The viscosity of the end product is considerably reduced after the reaction. An alga has several advantages like being a potentially greener fuel feedstock and also it can be grown on nonarable areas. But still it struggles to find a place in the list of known biofuel crops. An alga is the preferred source because of its higher yield. The biomass can be doubled within 24hrs; the doubling time estimated was approximately 3.5hrs .The recent studies show that from the cultivation point of view, the algae are easy to cultivate, need very little or no attention, less nutrients and the water which is unsuitable for human consumption can be used. Even though many reports explained the techniques about the conversion of algae oil in to biodiesel there are no or less reports gives the algae esters properties in comparison with diesel and almost no significant amount of work to explain the performance of it in a diesel engine. Many reports indicate Gracileria, Gelidium, kappaphycus etc are being cultivated in large scale in India for food and pharmaceutical applications. But only few of them have concentrated on biofuel from algae. There is lack of information regarding performance on a diesel engine using alga biodiesel. Therefore the main aim of this work is to extract the oil from an alga and to present the physical and chemical properties. The Performance, combustion, and emission characteristics of Esters of Algal oil are to be carefully investigated in a CI engine.

OIL EXTRACTION PROCESS

The Macro and Micro algae around 20 Kgs were collected from Central Marine Fisheries Research Institute, Chennai. The algae were shade dried for two days. The dried algae (5.5kg) powder was crushed in mortar and pestle with hexane and isoproponal solvent mixture (3/2 volume ratio). The extract was filtered and was allowed to stand in a separating funnel for a day; the top layer was taken and evaporated to remove the solvent. The resulting oil (1300 ml) was subjected to transesterification process. Transesterification of Algal Oil into Biodiesel.

Fig-1: Macro Algae

Fig 2: Micro Algae

Characte ristics Test	Micro	Macro	Prot ocol
Density	0.792	0.795	AST M D 1298
Viscosity @40℃	3.51cS T	4.84	AST M D
			445
Calorific Value	40362K J/Kg	33290K J/Kg	AST M D 240
Flash Point	92℃	132℃	AST M D 93
Fire Point	124℃	142℃	AST M D 93
Cetane Number	57	48	AST M D 613
Sulphur Content	Nil	18	AST M D 524
Carbon Residue	Nil	Nil	AST M D 524
Pour Point	-18.3℃	-2℃	AST M D 2500

Table 1

TRANSESTERIFICATION OF ALGAL OIL INTO BIODIESEL

In this work sodium hydroxide is used as the catalyst, methanol is used as alcohol. The reaction is held between algal oil (the triglyceride), methanol and sodium hydroxide pellets at 65°C for 3hrs duration and the solution is stirred to ensure proper mixing. The reaction produces biodiesel and glycerol. The top layer is the required methyl esters and it is separated after filtering the glycerol, the methyl ester is then washed with water and the top layer is separated (850ml) and is then dried for property testing. The Properties of the biodiesel sample was tested by adapting ASTM testing protocols and are presented in Table 1.

Engine test

The test was conducted at constant speed, four stroke, vertical, and air cooled Diesel engine. Two blends of algae biodiesel B10 and B20 were tested and the performance, combustion and emission parameters were taken. The loading is by means of an eddy current dynamometer.

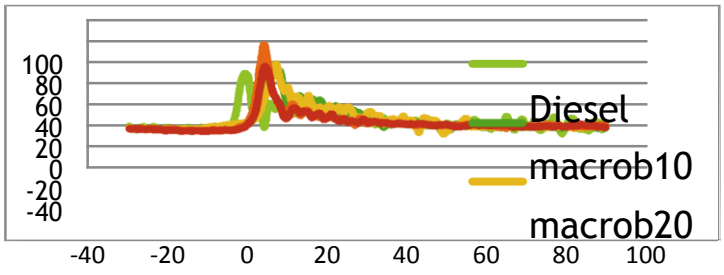

CA vs HR (0% Load)

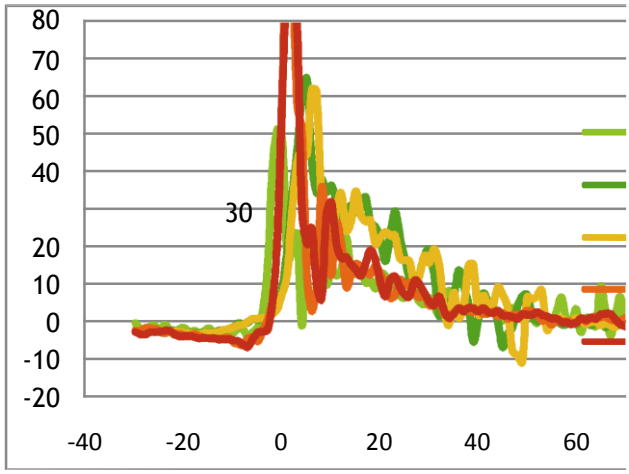

CA vs HR (25% Load)

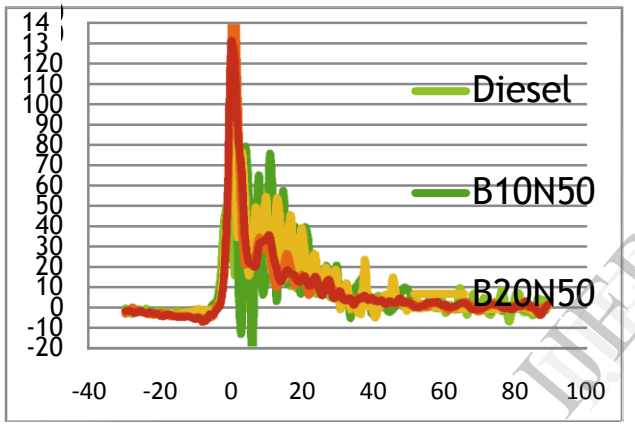

CA vs HR (50% Load)

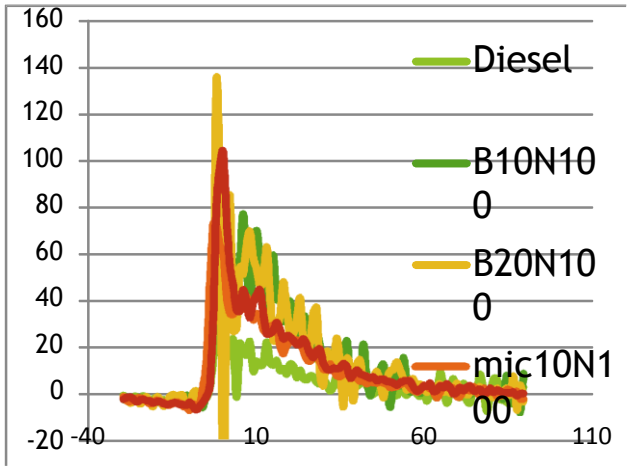

CA vs HR (100% Load)

Conclusion

The performance and emission analysis of both the biodiesel fuel types shows that, they are better alternative to Diesel. Except NOX emission the other emission values are less compared to Diesel. Biodiesel blends consume more fuel and the volumetric efficiency values for them are slightly lesser than Diesel. The advancement in the injection timing brought better results than other two injection timings. From the results we can conclude that the Rice bran oil and algae oil biodiesel blends (B20) can be a used modifying the Engine.

REFERENCES

1) Murugesan, A. Umarani, C. Subramanian, R. Nedunchezhian, N. (2009). "Bio-diesel as an alternative fuel for diesel engines—A review", Renewable and Sustainable Energy Reviews 13,653–662.
2) Jinlin Xue, Tony E. Grift, Alan C. Hansena (2011). "Biodiesel Effect of biodiesel on engine performances and emissions", Renewable and Sustainable Energy Reviews 15 1098–1116.
3) Meher LC, Sagar DV, Naik S N (2006). Technical aspects of biodiesel production by Transesterification – a review. Renew Sustain Energy Rev; 10:248–68.
4) Oette K, Doss M. (1968) Mikromethode zur schnellen umesterung von lipoiden aufdünnschichtplatten mit natriummethylat für die gas-chromatographische analyse der fettsäuremethylester. J Chromatogr A; 32:439–50.
5) Ma F, Hanna MA. Biodiesel production: a review. Biores Technol (1999); 70:1–15.
6) Dmytryshyn SL, Dalai AK, Chaudhari ST, Mishra HK, Reaney MJ. Synthesis and characterization of vegetable oil derived esters: evaluation for their diesel additive properties. Bioresour Technol 2004; 92:55–64.
7) Bala BK. (2005) Studies on biodiesels from transformation of vegetable oils for Diesel engines. Energy Edu Sci Techno; 15:1–43.
8) Demirbas A. (2003) Biodiesel fuels from vegetable oils via catalytic and noncatalytic supercritical alcohol transesterification and other methods: a survey. Energy Convers Manage 44:2093–109.

Design of Mixed Mode Solar Dryer

1. Vigneshwaran.T [a], 2.Aravindh.A [a], 3.Jayaraj.R [a], 4.Balachandar.B [a], 5.Arumugam.P [b]
a: Student, Department of Mechanical Engineering, Christ College of Engineering and Technology, Moolakulam, Puducherry-605010.
b: Assistant Professor, Department of Mechanical Engineering, Christ College of Engineering and Technology, Moolakulam, Puducherry-605010.

Abstract-- Mixed mode solar dryer composed of solar collector and a solar drying chamber. The flat plate collector is the most widely used solar collector for domestical and industrial purpose because it is simple and portable design and required less maintenance. The drying process uses only a solar energy. The air allowed in through air inlet is heated up in the solar collector channeled through the drying chamber where it is utilized in drying and (removing the moisture content from the agriculture product). This paper presents a design of mixed mode solar dryer for drying agriculture product which is fully based on geographical location in puducherry and metrological data were obtained from proper design specification.

Key words—solar collector; solar dryer; agriculture product;

I. INTRODUCTION

Solar energy is a very large, inexhaustible source of energy. The power from the sun intercepted by the earth is approximately 1.8×10^{11}MW which is many thousands of times larger than the present consumption rate on the earth of all commercial energy sources. Presently there are several applications which use the solar energy as a source such as water heater, space heating, and distillation, drying, cooking, power generation.

One of the traditional uses of solar energy has been for drying agriculture product. The drying process removes moisture and helps in the preservation of the product. Traditionally, drying is done on open ground. The disadvantages associated with this system are that the process is slow and that insect and dust get mixed with the product. The use of solar dryers helps to eliminate this factor. Drying can be done faster and a better quality product is obtained. In addition to this operating cost is reduced as compared to electrical dryer. With drying, most agriculture product can be preserved and this can be achieved more efficiently through the use of solar dryer.

Solar dryer are a very useful device for:

- Agricultural crop drying.
- Food processing industries for dehydration of fruits and vegetables.
- Fish and meat drying
- Dairy industries for production of milk powder.
- Seasoning of wood and timber.

Several type of solar drying system are available, they are cabinet solar dryer, indirect solar dryer and mixed mode solar dryer. In this paper mixed mode solar dryer is used. This dryer has an advantages of reducing the drying time of product which is due to the solar radiation falling on both solar collector and drying chamber. As a result there is an easy removal of moisture from the product. This is possible by passing preheated air from the solar collector and also direct drying will take place in the drying chamber.

II. MATERIAL AND METHOD

General description

The most commonly seen design type of mixed mode solar dryer has solar collector which is coupled with drying chamber. Both are made up of wooden boxes with glass cover. There is an air inlet to the solar collector where air entering and is heated up by the solar radiation, the hot air rises through the drying chamber passing through the tray and around the food, removing the moisture content and exists through the air outlet near the top of glass cover.

The hot air acts as the drying medium; it extracts and conveys the moisture from the product to the atmosphere under forced convection, thus the system is active solar system and mechanical device (i.e. blower or fan) is required to control the intake of air into the dryer.

MATERIAL USED

The following materials were used for the construction of the mixed mode solar dryer:

- Wood (plywood) - as the casing of the entire system. In addition with glass wool is used to minimize the conduction and convection losses to the atmosphere.
- Glass (low iron tempered glass) – as the solar collector cover and the cover for drying chamber. It permits the solar radiation into the system.
- Aluminium plate of 1mm thickness with smoke black coating for absorption of solar radiation.
- Aluminium tray for placing drying material.

III. Design consideration

1. Temperature – the minimum temperature for drying product is 30°C and the maximum temperature is 70°C, therefore 50°C and above is considered average and normal for drying agriculture product.
2. The design was made for optimum temperature for the dryer. T_o of 70°C and the air inlet temperature T_i of 30°C (approximately outdoor temperature).
3. Air gap – a gap of 50mm should be created as air inlet and air passage.
4. Mass flow rate – assuming the maximum flow rate is 0.015Kg/s and minimum flow rate is 0.013Kg/s.
5. Dimension – assuming the width of solar collector is 640mm and absorber plate is 600mm. The average dimension of dryer was 400×330×300mm. the dryer was roofed with glass tilted at the same angle with that of solar collector. The air inlet of the collector is 120×40mm and the outlet is same as the inlet.
6. Dryer tray – aluminium was selected as dryer tray to aid air circulation within the drying chamber. The tray dimension is 350×280mm with wooden stick used as a frame.

Plywood is used to make a drying chamber and glass cover at the top of dryer for direct drying of product from the direct solar radiation.

IV. DESIGN CALCULATION

Peak radiation is obtained when the declination angle is maximum of 23°26' on June 21.

The values A, B and C are constant which is predicting solar radiation on clear days.

For June 21:

Beam radiation (I_b) and = 886W/m^2

Diffuse radiation (I_d) = 124W/m^2

Global radiation (I_g) = 1010W/m2

Latitude of puducherry (φ) = 11°55'

1. Angle of tilt(β) of solar collector

   It states that the angle of tilt of the solar collector should be

   $\beta = 10° + \text{latitude } (\varphi)$

   Hence the value of β used for the collector

   $\beta = 10° + 11°55' = 21°55'$

2. Declination angle(δ)

   $\delta = 23.45\sin [(360/365)\times(284+n)]$

   n - Number of days = 172

   $\delta = 23° 26'$

3. Angle of incident(θ_z)

   It states that the angle of incident of solar radiation on horizontal surface should be

   $\cos \theta_z = \sin\varphi \sin\delta + \cos\varphi \cos\delta \cos\omega$

   At 12 noon $\omega = 0$

   $\cos \theta_z = 0.98$

   The angle of incident of solar radiation on tilted surface should be

   $\text{Cos}\theta = \sin(\varphi-\beta) \sin\delta + \cos(\varphi-\beta) \cos\delta \cos\omega$

   $\text{Cos}\theta = 0.835$

4. Incident solar flux absorbed in the absorber plate(S)
   A research obtained the value of absorbed solar flux for puducherre on tilted surface as
   S = 678W/m^2
5. Determination of collector area and dimension.
   The maximum mass flow rate of air = 0.015Kg/s

The width of solar collector (B) assumed to be 640mm and absorber to be 600mm.

Heat gain $Q = m \times Cp \times \Delta T$

Therefore $Q = S \times Ap$

$Ap = (m \times Cp \times \Delta T) / S$

$Ap = (0.015 \times 1005 \times 40) / 678 = 0.889 m^2$

The length of absorber (La) was taken as;

La = Aa / Ba = 0.889 / 0.6 = 1.4816m Thus, the length of the absorber was taken approximately as 1.5m.

Therefore, absorber plate area was taken as $(0.6 \times 1.5) = 0.90 m^2$

Length of solar collector was taken as (1.5+0.04) = 1.54m

6. Determination of heat losses from the solar collector

Total energy transmitted and absorbed is given by

$Q = (S \times Ap) - Q_L$

$m \times Cp \times \Delta T = (S \times Ap) - (U_L \times Ap \times \Delta T)$

$U_L = ((0.9 \times 678) - (0.013 \times 0.90 \times 40)) / 0.9 \times 40$

$U_L = 2.433 W/m^2\text{-}K$

Therefore,

$Q_L = 2.433 \times 0.9 \times 40$

$Q_L = 87.59W$

V. CONCLUSION

From the above design, it has been concluded that solar radiation can be effectively and efficiently utilized by the mixed mode solar dryer for drying the agriculture products. From the result which has been obtained, the area of the collector is small as portable. Hence the whole setup can be carried anywhere easily. By the use of this design data construction of flat plate collector is to be done in order to validate the calculated result.

REFERENCES

[1] Lyes Bennamoun *, Azeddine Belhamri ; Design and simulation of a solar dryer for agriculture products; Journal of Food Engineering 59 (2003) 259–266 .

[2] Radivoj M. Topić1, Nenad Lj. Ćuprić2, Milan R. Božović3; "Muechas"–design andconstruction of an active solar dryer for biological materials; International Journal of Mechanical Engineering and Applications 2013; 1(2): 49-58

[3] Serm Janjai; A greenhouse type solar dryer for small- scale dried food Industries; INTERNATIONAL JOURNAL OF ENERGY AND ENVIRONMENT; Volume 3, Issue 3, 2012 pp.383-398

[4] Shobhana Singh and Subodh Kumar; Comparative Thermal Performance Study of Indirect and Mixed-mode Solar Dryers; International Journal of Sustainable Energy Development (IJSED), Volume 1, Issues 1/2/3/4, March/June/September/December 2012.

[5] Chandrakumar B Pardhi1* and Jiwanlal L Bhagoria2; Development and performance evaluation of mixed-mode solar dryer with forced convection; Pardhi and Bhagoria; International Journal of Energy and Environmental Engineering 2013, 4:23.

[6] A.K. Kamble1*, I.L.Pardeshi2, P.L. Singh3 and G.S. Ade4 ; Drying of chilli using solar cabinet dryer coupled with gravel bed heat storage system ; journal of food research and technology

[7] Oguntola J. ALAMU1,a, *Collins N. NWAOKOCHA2,b and Olayinka ADUNOLA1; Design and Construction of a Domestic Passive Solar Food Dryer; . Leonardo Journal of Sciences Issue 16, January-June 2010.

[7] Sukhatme S.P., Solar-Energy-Principles of Thermal Collection and Storage, Tata McGraw Hill Publishing Company Limited, 1996

[8] C.P. Kothandaraman, S.Subramanyan; Heat and Mass Transfer Data Book, New Age

Kinetic Energy Storage and Recovery System using Torsion Spring

1. Krishna Kumar.R[a] , 2.Sabarinathan.J [a], 3.Mathew G Tharakan[a], 4.Madhan Raj.S[b]
a: Student, Department of Mechanical Engineering,
Christ College of Engineering and Technology, Moolakulam, Puducherry-605010.
b: Assistant Professor,
Department of Mechanical Engineering,
Christ College of Engineering and Technology, Moolakulam,
Puducherry-605010.

***Abstract*--Energy consumption of a nation is usually considered as an index of its development. Energy is vital for social and economic development. In fact, modern civilization is very much dependent on energy availability, and the whole infrastructure rests upon it. The fossil fuels like coal, oil and natural gas which is at present are supplying 95% of the commercial energy of the world resources and are not going to last for many more years. Our life style is changing very fast and from a simple way of life we are shifting to a luxurious life style. If we just look at the number of electric gadgets, private cars and scooters in our locality we will realize that they have multiplied many folds and all of them consume energy. To meet the increasing energy demands, efforts are being made to improve existing technologies and to develop new approaches for optimising the energy consumption. In this paper kinetic energy storage and recovery system using torsion spring is analysed, the mechanism required to transmit the energy from and to the spring is designed, then its efficiency is tested and amount of fuel saved when this system is adapted to any vehicle for every time the brake is applied is calculated.**

Keywords—KERS, Torsion spring, Energy, Planetary Gear System, Flywheel, Efficiency, Fuel consumption.

I.INTRODUCTION

The transportation sector includes all modes of transportation from personal vehicles (cars,light trucks) to public transportation (buses,trains) to airplanes, One might think that airplanes, trains and buses would consumes most of the energy used in this sector but, in fact, their percentage are relatively small about 9% for aircraft and about 3% for trains and buses. Personal vehicles, on the other hand, consume more than 60% of the energy used for transportation. Our personal vehicles consume more energy than public transportations.

Only about 15 percentage of the energy from the fuel we put in our tank gets used to move our vehicle down the road or run useful accessories, such as air conditioning. The rest of the energy is lost to engine and driveline inefficiencies and idling. Engine losses-62.4%, Idling losses-17.2%, Accessories-2.2%, Driveline losses-5.6%,Aerodynamic drag-2.6%, Rolling resistance-4.2%, Overcoming inertia and Braking losses-5.8%. Therefore, the potential to improve fuel efficiency with advanced technologies is enormous.

Regenerative brake is an energy recovery mechanism which slows down a vehicle or object by converting its kinetic energy into another form, which can be either used immediately or stored until needed. This contrasts with conventional braking systems, where the excess kinetic energy is converted to heat by friction in the brake linings and therefore wasted.

There are several types of regenerative braking systems which differs each other in several ways one of them is energy storing element. Basically there are two types of energy storing elements, electrical energy storing elements and mechanical energy storing elements. In mechanical there are two types of energy storing elements flywheels and springs.

II.SPRING

Spring is a mechanical energy storing element which stores the energy in the form of Strain energy or Elastic Potential Energy. Elastic potential energy is Potential energy stored as a result of deformation of an elastic object, such as the stretching of a spring. It is equal to the work done to stretch the spring. Since the energy which

is stored in the spring as Elastic potential energy, this energy is stored only the material deforms with its elastic limits. When the material deforms the stress is induced inside the material. When this induced stress in increased above the certain value the spring's deformation doesn't regain its original position. So the deformation of the spring is limited by its maximum allowable stress. When the stress induced in the material increased higher than its yield stress then permanent deformation occurs. So the maximum energy storing capacity as strain energy of a material and also it is called as proof resilience is depend up on the yield stress (σy) and Young's Modulus (E).

$$U=(\sigma y^2/2E)\times V$$

From the above equation it is observed that the maximum energy storing capacity of the material in terms of strain is depend only up on the Yield strength ,Young's Modulus and volume of the material. When the yield strength of the material is increased the energy storing capacity of the material is increased square the times. So the good spring should be made up of the material which has higher Yield strength and lower Young's modulus. There are different types of spring available such as Compression Spring (Open Coil Helical Spring), Expansion spring (Closed Coil Helical Spring), Torsion spring, Spiral springs etc. In torsion spring and spiral spring, the opposing force is in terms of torque. The below discussed KERS system makes use of torsion spring which is easy to fabricate and commercially easily available and gives the output effort in terms of torque. The energy storing capacity of the torsion spring is differs from the material's proof resilience value due to its geometrical shape.

For Torsion spring,

$$U = (Mb^2\times\pi\times D\times N) / (2EI)$$

Where,

Mb = Bending Moment, D = Outer Diameter,
N= Number of turns, E= Young's Modulus,
I= Moment of Inertia

III.OPTIMIZING THE ENERGY TO WEIGHT RATIO OF TORSION SPRING

In order to do the optimization of torsion spring, the energy densities of spring with 5 different dimensions are found and graph is plotted.

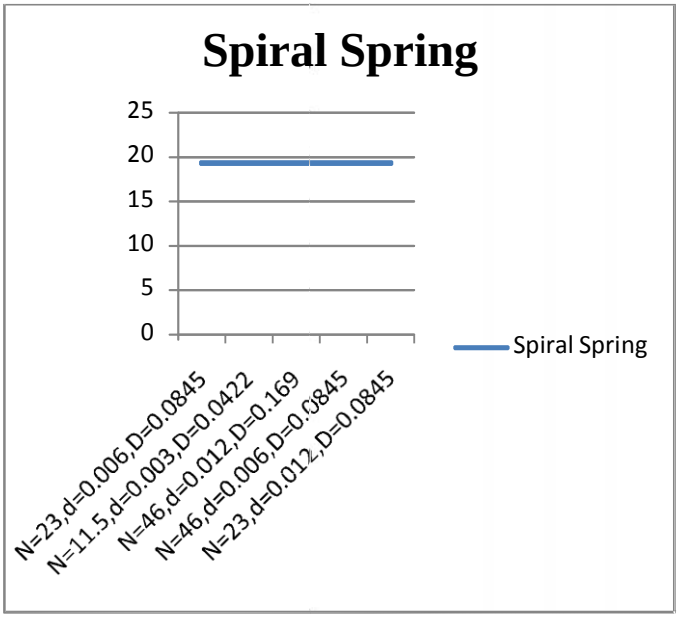

Graph 1: Comparing the energy density of the torsion springs of different geometry.

Material	N=23, d=0.006 m, D = 0.0845 m	N=11.5, d=0.003 m, D = 0.0422 m	N=46, d=0.012 m, D=0.169 m	N=46, d= 0.006 m, D = 0.0845 m	N = 23, d = 0.012 m, D = 0.0845 m	Average (J/kg)
Carbon Steel Wire	19.34 J/kg	19.34 J/kg	19.34 J/kg	19.34 J/kg	19.34 J/kg	19.34

Table 1: Comparing the energy density of the torsion springs of different geometry.

IV.CONSTRUCTIONAL DETAILS OF EXPERIMENTAL MODAL

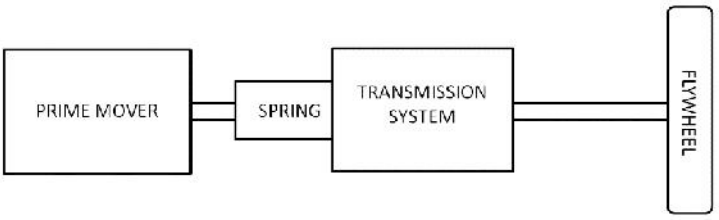

SIRAL SPRING:

Commercially available torsion spring of below specifications,

Material = Carbon Steel

Young's Modulus (E) = $207*10^9$ N/m^2

Maximum allowable stress (σ_b) = $552*10^6$ N/m^2

Inner Diameter = 70 mm

Outer Diameter =82 mm

Thickness = 6 mm

Number of turns =23

PLANETARY GEAR SYSTEM**:**

Planetary gear system consists of,

1. Ring gear.
2. Sun gear.
3. Planet gear.
4. One way bearing (one way clutch).
5. Break disk.

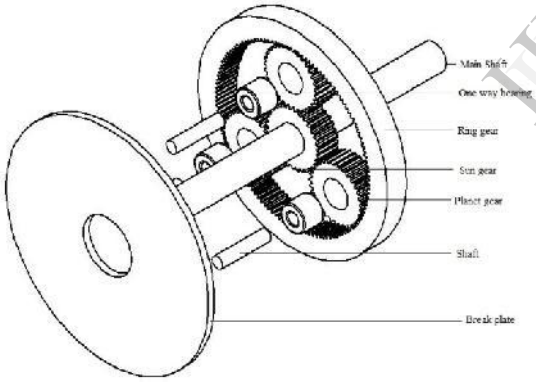

FLYWHEEL:

Flywheel is fixed at the end of the shaft to provide the inertia**.**

Material = Cast iron

Weight = 5.5 Kg

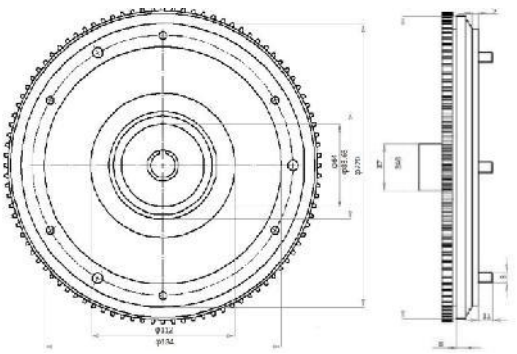

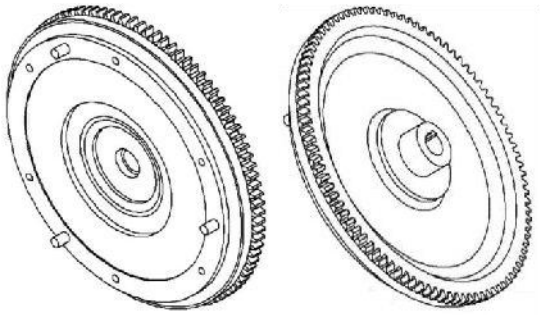

CONCLUSION:

It is observed that the energy density or energy storage capacity of the spring per unit mass remain same for various parameters such as number of turns (N), Nominal diameter (D) and wire diameter (d). The energy storing capacity is independent of geometrical features of the spring. So it is understood that to maximize the energy storing capacity of the spring, it is not necessary to find the optimal dimensions of the torsion spring. So, it is decided to select the standard available spring in the market for the KERS system. With that selected spring, the experiments are to be conducted to find the fuel economy of the IC engine if the KERS system is adopted.

REFERENCES

[1] Cibulka, J, "Kinetic Energy Recovery System By Means Of Flywheel Energy Storage." 3(2009)1, ISSN 1846-5900.

[2] Siddharth K. Patil, "Regenerative Braking System in Automobiles." IJRMET Vol. 2, Issue 2, May - Oct 2012..

[3] Sidharth Dave, Aneesh Bhardwaj, " Kinetic Energy Regeneration System For Fuel Efficiency And Performance Enhancement" International Journal of Scientific & Engineering Research, Volume 4, Issue 4, April-2013 1189 ISSN 2229-5518.

[4] R.J. Hayes, J.P. Kajs, R.C. Thompson, J.H. Beno," Design And Testing Of A Flywheel Battery For A Transit Bus" Center for Electromechanics The University of Texas at Austin, 1999-01-1159.

[5] R.S, Khurmi "Design of Spring" in "Machine Design and Elements," in 1st edition, S. Chand Publication, 2012, pp.864-866.

[6] Dr. Rajendra Karwa "Spring Helical and Leaf," in "Machine Design," second edition, ISBN 81-7008-833-X, pp.313-319.

[7] R.S, Khurmi "Design of Gear" in "Machine Design and Elements," in 1st edition, S. Chand Publication, 2012, pp.1021-1065.

[8] R.S, Khurmi "Shafts" in "Machine Design and Elements," in 1st edition, S. Chand Publication, 2012, pp.509-557.

Laser Ignition in Internal Combustion Engines a Contribution to a Sustainable Environment

A. Abdul Vadood
II YEAR MECHANICAL

Abstract **- Sustainability with regard to internal combustion engines is strongly linked to the fuels burnt and the overall efficiency. Laser ignition can enhance the combustion process and minimize pollutant formation. This paper is on laser ignition of sustainable fuels for future internal combustion engines. Ignition is the process of starting radical reactions until a self- sustaining flame has developed. In technical appliances such as internal combustion engines, reliable ignition is necessary for adequate system performance. Ignition strongly affects the formation of pollutants and the extent of fuel conversion. This paper presents experimental results on laser-induced ignition for technical applications. Laser ignition tests were performed with the fuels hydrogen and biogas in a static combustion cell and with gasoline in a spray-guided internal combustion engine. A Nd:YAG laser with 6 ns pulse duration, 1064 nm wavelength and 1-50 mJ pulse energy was used to ignite the fuel/air mixtures at initial pressures of 1-3 MPa. Schlieren photography was used for optical diagnostics of flame kernel development and shock wave propagation. Compared to a conventional spark plug, a laser ignition system should be a favorable ignition source in terms of lean burn characteristics and system flexibility. Yet several problems remain unsolved, e.g. cost issues and the stability of the optical window. The literature does not reveal much information on this crucial system part. Different window configurations in engine test runs are compared and discussed.**

Keywords -Laser ignition, spray-guided combustion, homogeneous combustion, high pressure, hydrogen, biogas, gasoline.

1 INTRODUCTION

Internal combustion engines play a dominant role in transportation and energy production. Even a slight improvement will translate into considerable eductions in pollutant emissions and impact on the environment. The two major types of internal combustion engines are the Otto and the Diesel engine. The former relies on an ignition source to start combustion, the latter works in autoignition mode. Ignition **[1]** is a complex phenomonon known to strongly affect the subsequent combustion. It is especially the early stages that have strong implications on pollutant formation, flame propagation and quenching. The spark ignited Otto engine has a widespread use and has been subject to continuous, sophisticated improvements. The ignition source, however, changed little in the last 100 years. An electrical spark plug essentially consists of two electrodes with a gap in between where, upon application of a high voltage, an electrical breakthrough occurs.A laser based ignition source, i.e. replacing the spark plug by the focused beam of a pulsed laser, has been envisaged for some time **[2]**. Also, it was tried to control autoignition by a laser light source **[3].** The time scale of a laser-induced spark is by several orders of magnitude smaller than the time scales of turbulence and chemical kinetics. In **[4]**, the importance of the spark time scale on the flame kernel size and NOx production is identified. As it will be outlined in this paper, a laser ignition source has the potential of improving engine combustion with respect to conventional spark plugs.

1.1 Alternative ignition systems

The protection of the resources and the reduction of the CO2 emissions with the aim to limit the greenhouse effect require a lowering of the fuel consumption of motor vehicles. Great importance for the reduction lies upon the driving source. Equally important are the optimization of the vehicle by the means of a reduction of the running resistance as well as a low-consumption arrangement of the entire powertrain system. The most important contribution for lower fuel consumption lies in the spark ignition (SI) engine sector, due to the outstanding thermodynamic potential which the direct fuel injection provides. Wall- and air-guided combustion processes already found their way into standard-production application and serial development, whereas quite some fundamental engineering work is still needed for combustion processes of the second generation. Problems occur primarily due to

the fact that with conventional spark ignition the place of ignition cannot be specifically chosen, due to several reasons. By the means of laser induced ignition these difficulties can be reduced significantly. The combination of technologies (spray-guided combustion process and laser induced ignition) seems to become of particular interest, since the ignition in the fuel spray is direct and thus the combustion initiation is secure and non- wearing. The engine tests in this paper are on laser ignited, spray- guided combustion. Another approach is laser ignition of a homogeneous mixture. Within the scope of this paper, laser ignition in homogeneous fuel/air mixtures was investigated in a combustion bomb without turbulence. In **[4]**, other alternative ignition systems than laser ignition are reviewed. Laser ignition, microwave ignition, high frequency ignition are among the concepts widely investigated. In this article the basics of applied laser ignition, will be illustrated and it potential compared to a conventional ignition system.

1.2 Laser ignition

Laser ignition, or laser-induced ignition, is the process of starting combustion by the stimulus of a laser light source. Basically, energetic interactions of a laser with a gas may be classified into one of the following four schemes as described in **[5]**:

• thermal breakdown
• non-resonant breakdown
• resonant breakdown
• photochemical mechanisms

In the case of thermal interaction, ignition occurs without the generation of an electrical breakdown in the combustible medium. The ignition energy is absorbed by the gas mixture through vibrational or rotational modes of the molecules; therefore no well-localized ignition source exists. Instead, energy deposition occurs along the whole beam path in the gas. According to the characteristic transport times therein, it is not necessary to deposit the needed ignition energy in a very short time (pulse). So, this ignition process can also be achieved using quasi continuous wave (cw) lasers. Another type, resonant breakdown, involves non-resonant multi-photon dissociation of a molecule followed by resonant photo ionization of an atom. As well as photochemical ignition, it requires highly energetic photons (UV to deep UV region). Therefore, these two types of interaction do not appear to be relevant for this study and practical applications.

In these experiments, the laser spark was created by a non-resonant breakdown. By focusing a pulsed laser to a sufficiently small spot size, the laser beam creates a high intensity and high electric fields in the focal region. This results in a well localised plasma with temperatures in the order of 106 K and pressures in the order of 102 MPa as mentioned in **[6,7].**

The most dominant plasma producing process is the electron cascade process: Initial electrons absorb photons out of the laser beam via the inverse bremsstrahlung process. If the electrons gain sufficient energy, they can ionise other gas molecules on impact, leading to an electron cascade and breakdown of the gas in the focal region. It is important to note that this processrequires initial seed electrons. These electrons are produced from impurities in the gas mixture (dust, aerosols and soot particles) which are always present**.** These impurities absorb the laser radiation and lead to high local temperature and in consequence to free electronsstarting the avalanche process. In contrast to multiphoton ionisation (MPI), no wavelength dependence is expected for this initiation path. It is very unlikely that the first free electrons are produced by multiphoton ionisation because the intensities in the focus (1010 W/mm2) are too low to ionise gas molecules via this process, which requires intensities of more than 1012 W/mm2 **[7,9].**

An overview of the processes involved in laser-induced ignition covering several orders of magnitude in time is shown in Fig. 1.

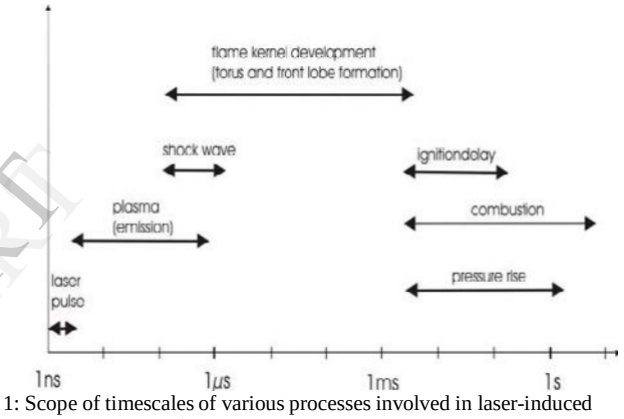

Fig 1: Scope of timescales of various processes involved in laser-induced ignition: The lengths of the double arrowed lines indicate the duration ranges of the indicated rocesses.

Laser ignition encompasses the nanosecond domain of the laser pulse itself to the duration of the entire combustion lasting several hundreds of milliseconds. The laser energy is deposited in a few nanoseconds which leads to a shock wave generation. In the first milliseconds an ignition delay can be observed which has a duration between 5 – 100 ms depending on the mixture. Combustion can last between 100 ms up to several seconds again depending on the gas mixture, initial pressure, pulse energy, plasma size, position of the plasma in the combustion bomb and initial temperature.

Below the main advantages of laser ignition are given: • a choice of arbitrary positioning of the ignition plasma in the combustion cylinder • absence of quenching effects by the spark plug electrodes • ignition of leaner mixtures than with the spark plug **[10]**
=> lower combustion
temperatures => less NOx emissions **[10,11]**
• no erosion effects as in the case of the spark plugs => lifetime of a laser ignition system expected to be significantly longer than that of a spark plug
• high load/ignition pressures possible => increase in efficiency precise ignition timing possible

• exact regulation of the ignition energy deposited in the ignition plasma
• easier possibility of multipoint ignition **[12-14]**
• shorter ignition delay time and shorter combustion time **[10, 15-17]**
• fuel-lean ignition possible
The disadvantages of laser ignition are:
• high system costs
• concept proven, but no commercial system available yet.

2 EXPERIMENTAL

This section describes the experimental setup. Laser ignition experiments were carried out in a constant volume vessel (0.9 l) and an internal combustion engine. The constant volume vessel, also termed the combustion bomb, was used to conduct basic studies of laser ignition in homogeneous fuel/air mixtures. The sustainable fuels hydrogen and biogas were used. The biogas was obtained from a municipal water purification plant. It was composed of 50.5% CH4, 31.7% CO2 and 80 ppm H2S. Schlieren photography was used for accompanying optical diagnostics.
The engine, a one-cylinder research engine, was deployed for the investigation of sprayguided combustion initiated by a laser. Gasoline was used as a fuel here. The focus of sustainability is on laser ignition for enhanced combustion and efficiency.

2.1 Laser ignition and concurrent Schlieren photography in a combustion bomb

The laser ignition experiments in the constant volume vessel were carried out with hydrogen and biogas. The xperimental setup and tests with methane are outlined in **[2].**
A pulsed Nd:YAG laser with pulse energies from 1 to 50 mJ was used for the ignition tests.
Table 1 lists the specifications of the laser. Schlieren photography was conducted in the plane of the focal spot of the igniting laser.
Perpendicularly to the igniting laser beam, a collimated light beam from a flash lamp (1 µs pulse duration) was shone through the combustion vessel. As the diffraction index of light depends on the type and mass density of a gas, areas with different temperatures or different pressures have different diffraction indices. So a parallel beam of light is diffracted at differences of temperature and pressure and the diffraction angle is proportional to the first derivate of these parameters **[18].** The experimental setup for the Schlieren experiments is outlined in **[19].**

2.2 Laser ignition in an internal combustion engine

A one-cylinder research engine was used as a test engine. The research engine was equipped with a four-valve DOHC cylinder head with a spray-guided combustion system of AVL List GmbH **[20]**. In a double-overhead-camshaft (DOHC) layout, one camshaft actuates the intake valves, and one camshaft operates the exhaust valves. Gasoline was used as a fuel. The same laser as in the combustion bomb tests in 2.1 was used (see Table 1).

One-cylinder research engine	
Four-valve cylinder head	
Spray-guided combustion process	
Multihole injector	
Stroke	85 mm
Bore	88 mm
Displacement volume	517 cm^3
Compression ratio ε	11.6

Table 1: Technical data of the laser. A solid-state laser was used here.

In Table 2 the key technical data of the test engine are listed.

Flash lamp pulsed Nd:YAG laser	
Manufacturer	Quantel S.A.
Type	Brilliant
Wavelength	1064 nm or 532 nm
Pulse energy	1-50 mJ
Pulse duration	6 ns
Max. beam performance	10 W
Power consumption	1 kW
Beam diameter	6 mm

Table 2: Technical key data of the test engine. A spray- guided research engine running on gasoline was used.

Engine test runs were carried out with two different approaches.
First, a plane window was inserted into the cylinder head of the engine. A focusing lens was
placed in front of that window in order to focus the laser beam down into the combustion
bomb ("separated optics").
Second, a more sophisticated window was deployed. A lens-like curvature was engraved
directly into the window. By using such a special window, no further lens was required
("combined optics").
This is depicted schematically in Fig. 2.

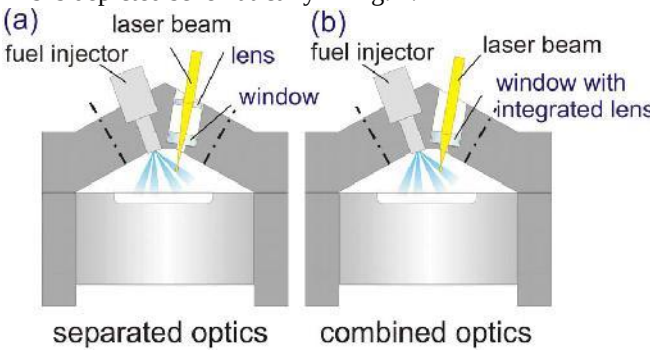

Fig. 2: Schematic cross section of the engine for laser ignition test runs. Two window/lens configurations were tested:
Fig. 2(a) shows the separated optics, Fig. 2(b) the combined optics.

3 RESULTS AND DISCUSSION

3.1.1. Laser ignition of hydrogen/air mixtures

Fig. 3 depicts a pressure history of combustions for different mixtures (λ) at an initial chamber temperature of 473 K and an initial pressure of 1 MPa. Comparable pressure histories could be seen for higher initial pressures. λ is the so called air/fuel equivalence ratio: λ < 1 signifies a fuel-rich mixture, whereas λ > 1 describes a fuel-lean mixture.

Between λ = 2.5 and 3.6 (14.4% and 10.4% H2) an oscillating pressure history could be observed having a frequency in the lower kHz region which is the resonant frequency of the combustion bomb **[11].** The oscillating combustion process is called knocking, which meansthat the combustion propagates not only by a spherical flame front, starting from the plasma but also that the mixture explodes at different locations in the end-gas (unburned gas) as an effect of self ignition conditions **[11].** With "rich" hydrogen- air mixtures (λ < 3.6) the flame propagates at a specific instant during the combustion time with sonic velocity through the gas and produces high pressure and temperature values in the end-gas region leading to auto ignition **[11]**. This auto ignition process produces shock waves which are reflected from the chamber walls and end in oscillations which can be observed in Fig. 3 for a λ between 2 and

3.6. Knocking is very disadvantageous for engine applications.

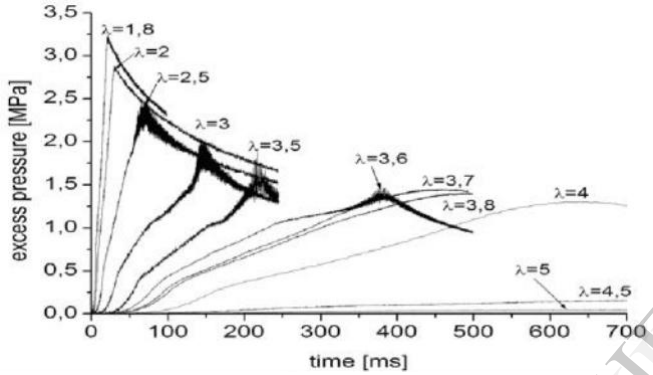

Fig. 3: Pressure history in the combustion bomb after ignition applying minimum pulse energy for ignition (MPE); λ = 1.8 - 5; initial temperature = 473 K, initial pressure = 1 MPa; If the air/fuel equivalence ratio (λ) is increasing (leaner mixtures), the peak pressure is decreasing but the total combustion time is increasing.

Pressure histories for a constant gas mixture (λ = 3.5) and constant initial temperature (T = 473 K) but different initial filling pressures are plotted in Fig. 4. The main result of this diagram is that with higher initial pressures the minimum pulse energy for ignition (MPE) is decreasing like it was observed for methane-air mixtures in **[2,6,9,10].** Further on, it can be seen that with higher initial pressures, which means higher energy contents in the combustion bomb , the peak pressures increases. Gas mixtures with λ = 3.5 represent the leaner boundary where knocking starts, as depicted in Fig. 4.

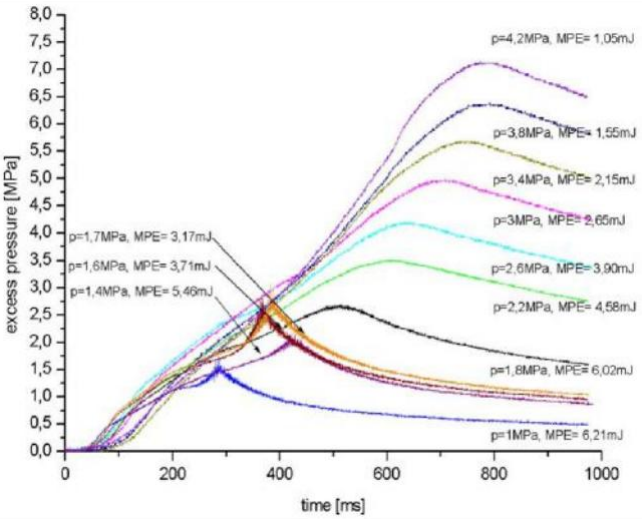

Fig. 4: Pressure history in the combustion bomb after ignition applying minimum pulse energy for ignition (MPE); λ = 3.5, initial temperature = 473 K, initial pressure = 1 – 4.2 MPa; For higher initial pressures the peak pressure, ignition delay and total combustion time is increasing but the minimum pulse energy for ignition (MPE) is decreasing.

Especially at this boundary knocking occurred only at lower filling pressures. With higher initial filling pressures no knocking could be observed. Richer gas mixtures only have a knocking combustion with no dependency on the filling pressure.

3.1.2. Laser ignition of biogas/air mixtures

Biogas is CO2-neutral and can act as a promising alternative fuel having a high availability. The two most common sources of biogas are digester gas and landfill gas. Bacteria form biogas during anaerobic fermentation of organic matters. The degradation is a very complex process and requires certain environmental conditions. Biogas is primarily composed of CH4 (50-70%) and CO2 (25-50%). Digester gas is produced at sewage plants during treatment of municipal and industrial sewage. Landfill gas is obtained during decomposition of organic waste in sanitary landfills. When using biogas as fuel one must also pay attention to several harmful ingredients such as H2S polluting e.g. the catalytic converter of the engine or blocking the window of the laser (see later for issues related to the window). With respect to laser ignition, biogas was compared to methane. The investigated methane/air and biogas/air mixtures contained similar methane concentrations but in the case of biogas additionally CO2 was present. Fuel-lean biogas/air mixtures exhibit a slower combustion process resulting in lower peak pressure and flame emission compared to methane-air mixtures of similar air to fuel equivalence ratio. The reason for these results could be due to the presence of CO2 in the biogas which reduces the burning velocity due to obstructing the flame propagation during combustion. SO2 may also be responsible for the decreased burning rate of the biogas/air mixtures reducing mainly the O-radical concentration to equilibrium state due to the recombination of the O-radicals

[21]. In Fig. 5, images of the developing flame kernel in laser ignited biogas/air mixtures are depicted (see below).

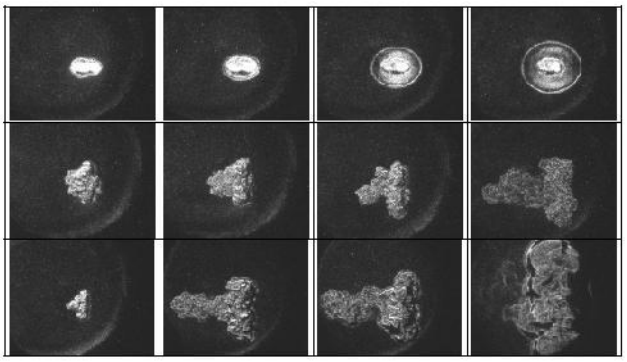

Fig. 5: Schlieren photographs of laser ignition, laser entering from the left side. The images are 11.6 mm long and 9.15 mm high.Top row: Laser-induced spark and shock wave in 25 bar air; From left to right: 500 ns, 1000 ns, 2000 ns, 3000 ns. Middle row: Laser-ignition of H2/air mixtures at 25 bar, lambda 6.0; From left to right: 100 µs, 200 µs, 300 µs, 1000 µs. Bottom row: Laser-ignition of biogas/air mixtures at 25 bar, lambda 1.8; From left to right: 100 µs, 900 µs, 1800 µs, 15000 µs.

More details on laser ignition of biogas/air mixtures can be found in **[21]**.

3.1.3. Shockwave and flame kernel development by Schlieren photography

Schlieren photography was used to obtain visual information on the shock wave formation and flame kernel development. Schlieren photography is an experimentally uncomplicated technique that has been applied successfully to the investigation of laser ignition, too. However, the literature contains very scarce information on pressures higher than ambient. In this study, high pressure tests were done. Fig. 5 shows Schlieren photographs of laser ignition test runs. In all images, the laser enters from the left side. The images are 11.6 mm long and 9.15 mm high. In the top row, images of the laser-induced spark and shock wave in pure air at 25 bar can be seen.

In the middle row, consecutives images of laser-ignition of H2/air mixtures at 25 bar and lambda 6.0 are shown.

The bottom row shows Schlieren images of laser-ignition of biogas/air mixtures at 25 bar and lambda 1.8. The shock wave carries two major implications on laser ignition: First, it transports energy away from the ignition spot. Second, it causes a significant temperature rise. When the shock wave has detached from the hot core air, both phenomena can be studied independently. The shock wave initially has an ellipsoidal shape caused by the asymmetric energy deposition of the laser.

Results and trends from the literature, predominantly existing in the ambient pressure regime, could be verified using Schlieren photography. More information on Schlieren photography of laser ignition can be found in **[19].**

3.2 Engine tests

Engine tests were conducted to investigate the optical window with respect to

- Durability of the optics (vibrations)
- Minimum ignition energy
- Wear and fouling properties of the inner window surface

The engine tests were conducted with gasoline. Whereas the focus of the previous tests and ongoing work in a static combustion bomb was on the understanding of the ignition process, the aim of the engine tests was to investigate the durability of the optical window.

3.2.1 Optics deposits and self-cleaning effect

As stated above, laser ignition is based on the principle of optical breakdown and thus it is essential to provide the necessary intensity which is approximately 1011 W/cm2 in the focus.

The energy emitted from the laser is attenuated by reflections on the surface of the window and the lens and by absorption in the lens, in the combustion-chamber window and in the deposits on the windows. The transmission of typical windows in the infrared is approximately 90%; the reflections on the surfaces further reduce the energy. Adding it up, when the laser beam passes through a window or a lens, the losses amount to approximately 15%. The laser self-cleaning effect was studied with deposits from the "true" combustion process (3.2.2), and also with artificially applied deposits (3.2.3).

3.2.2 Laser self-cleaning with deposits caused by the combustion process

Fig. 6 shows the cold start performance of the engine with a soiled window. Here, the deposits stemmed from a real combustion process inside the engine (see **[22]** for details).

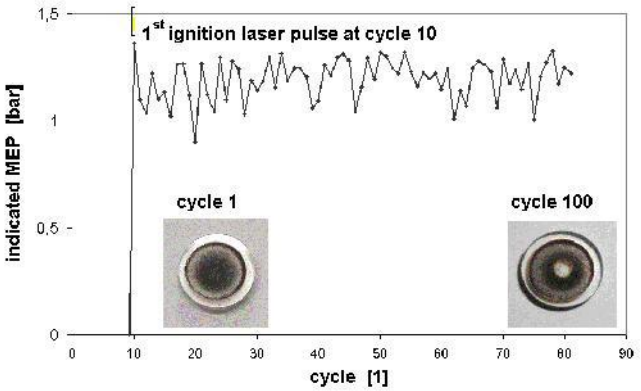

Fig. 6: Cold start performance with soiled combustion bomb window – deposits because of engine-related combustion process

These deposits, which were caused by the combustion process, were built up during the tests with a conventional spark plug. Thereby the combustion- chamber window was installed in different load points, the engine running mode being homogeneous, for about 20 hours. As it can be seen in Fig. 6, the window was soiled with a dark and opaque layer of combustion deposits after these 20 hours.

In the simulated cold-start test with a stratified engine running mode with 1000 rpm (rotations per minute) and pMEP = 1 bar, the pMEP course was recorded for each cycle, as shown in Fig. 6 (MEP = mean effective pressure). The first ignition and injection impulse occurred at cycle 10. The first laser impulse already ignites the mixture. The following ignition impulses resulted in a running without misfire. After the test (100 cycles) the window was disassembled and, as visible in Fig. 6, all deposits were removed in the beam passage area.

3.2.3 Laser self-cleaning with "worst case" deposits

In order to study the effect of the laser on a heavily soiled window, it was chosen to artificially apply a layer of dirt onto the window. This artificially applied soiling on the combustion-chamber side of the window represents a kind of "worst case scenario".

For doing so, a mixture of Diesel soot and waste oil at a ratio of 1:5 was produced and, with a thickness of 1 mm, applied to the combustion-chamber window and afterwards dried.

Fig. 7 shows the clear influence of the laser energy on the self-cleaning effect of the optics.

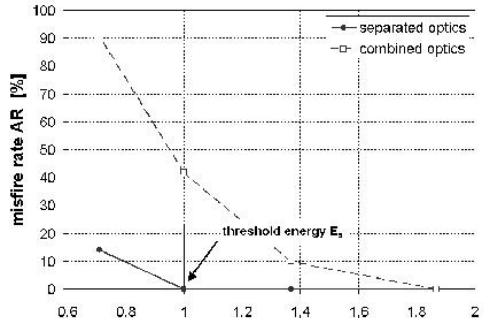

Fig. 7: Misfire rate dependent on the relative laser energy in a simulated cold start test, comparison of the optics, worst case deposits

Up to a build-up energy of the threshold energy ES, an engine operation without misfire is possible with a separated optics configuration, presupposed that a corresponding pulse number for the burning-off of the window is shot. This build-up energy ES is significantly higher in combined optics when aiming to reach a misfire rate of 0%. The relative laser energy was replaced by the actually occurring relative energy intensity I on the combustionchamber side of the window in Fig. 8.

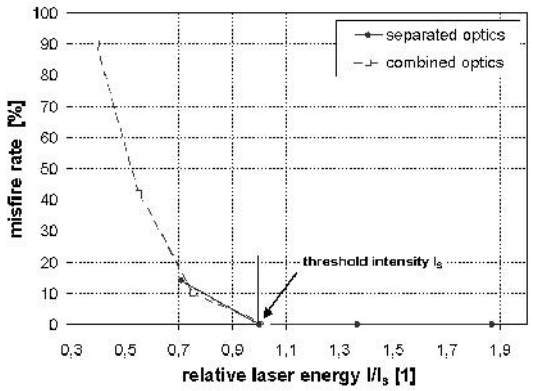

Fig. 8: Influence of the energy intensity I at the combustion bomb window on the burn off performance and the misfire rate, worst case deposits

An engine operation without misfire with both optics configurations, i.e. separated and combined optics (see Fig. 2), is possible as of a build-up intensity of IS. In separated opticsthis build-up intensity IS corresponds to the build-up energy of ES.However, the minimum intensity for keeping the combustions-chamber window clean duringthe engine running is IS/2.The minimum ignition energy when the engine running is stationary is determined by theintensity level of self-cleaning at the optics, and not by the engine-related working process. Inthe whole engine operating map a secure ignition and self- cleaning of the optics can beguaranteed with the laser energy ES.For cold start applications, the laser energy should thus be raised momentarily in order to burnoff possible deposits at the optics.

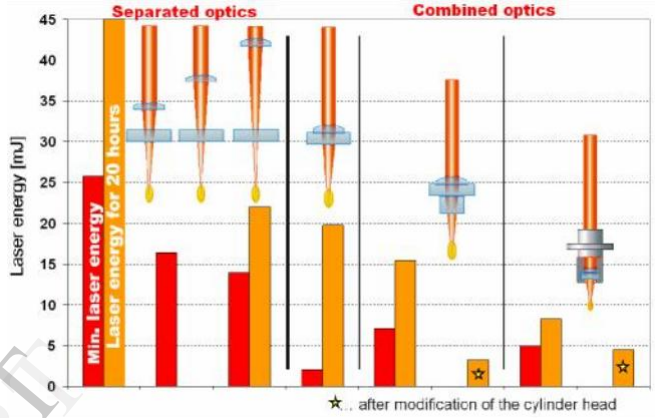

Fig. 9: Laser energy for ignition as a function of different window configurations. The separated optics, i.e. a focusing lens before a window, is less favorable than a combined optics, i.e. a window with integrated lens curvature, with respect to the minimum ignition energy.

Fig. 9 shows the laser energy for the different window configurations (compare Fig. 2). Both the minimum ignition energy (left bar) and the laser energy for a 20 hour test run (right bar) are shown.

As it can be clearly seen, the combined optics are more favorable than the separated optics with respect to required laser energy.The energy density at the window is a major criterion for the ablation of combustion bomb deposits.

During cold start, heating up and in the case of existing deposits only a high laser energy density can ensure the ablation effect at the location of the laser. The energy density is therefore an important determinant on the reliability of a future laser ignition system.

Fig. 10: Energy density at the window. It is higher for the separated optics. The higher the energy density, the better ablation works. The separated optics scheme should therefore be more reliable than the combined optics.

As it can be seen from Fig. 10, the energy density is by an order of magnitude higher for the separated optics than for the combined optics for the chosen configuration. The separated optics scheme leads to a higher energy density at the window. Especially in the case of cold start or unexpected deposits, this setup should be more reliable than the combined optics.

As can be seen from Fig.9 and Fig. 10, there is a trade-off between low laser energy requirements (combined optics) and system reliability (separated optics).

From an engine manufacturer's point of view, system reliability comes first, which translates into higher required laser energies and hence higher system costs.

3.2.4 Properties of the optical window

Potential window materials evidently have to be transparent for the laser radiation. The laser used in these tests was a Nd:YAG laser at 1064 nm. The near infrared spectral region is a common wavelength region for laser suitable for laser ignition test runs. So infrared transparent windows are good candidates for a future laser ignition system. The second, no less important prerequisite is that the window withstand the high energy density of the laser. The shorter the focal length of the lens, the higher generally the laser light intensity of the passing laser beam becomes at the window surface. Third, the window must show a weak inclination to deposits and aid laser self-cleaning. Combustion bomb deposits can either be organic (up to 300°C) or inorganic in nature. When they form on the window, they increasingly block the incoming laser light up to a point where no breakdown can be produced any more. In **[16]**, for instance, laser ignition tests of methane/air mixtures in an engine had to be aborted after 1.25 hours because of excessive combustion product build-up. ZnSe was used in that study. The formation of deposits on the window depends on the temperature, the fuel and the engine oil.The laser light also interacts with deposits. By a process called laser cleaning or ablation **[23],** deposits are removed by the laser light. The contrary can also happen, i.e. that the laser fosters the formation of deposits at the location where it enters the combustion chamber. Generally, ablation overweighs so that a kind of self- cleaning effect as shown above is achieved by the laser. Sapphire, quartz and ZnSe are among potential window materials in a future laser ignited engine. **[24]** reviews the major infrared transparent substrates suitable for window fabrication.

4 CONCLUSION

In this work, laser-induced ignition of hydrogen/air and biogas/air mixtures was investigated experimentally in a static combustion bomb. An enhanced ignition source can make a strong contribution to sustainability in internal combustion engines. Schlieren photography was applied to gain information on the shock wave propagation and early flame kernel development.

Results and trends from the literature, predominantly existing in the ambient pressure regime, could be verified.

It was found for the laser ignition tests with hydrogen that with higher initial pressures the minimum pulse energy for ignition (MPE) decreases. That behaviour was also found for methane.

Fuel-lean biogas/air mixtures exhibit a slower combustion process resulting in lower peak pressure and flame emission compared to methane-air mixtures of similar air to fuel equivalence ratio. The applicability of the laser induced ignition as a future ignition system for combustion engines with spray-guided combustion process could be proved with the basic research. The lowest required ignition energy in a stationary engine running mode is defined by the intensity level of the self-cleaning effect at the optics and not by the engine-related working cycle. In order to prevent deposits on the optics by the combustion process, a certain build-up intensity IS has to be available on the combustion bomb side of the window in order to ensure an engine operation without misfire. The energy intensity necessary to keep the burnt off optics clean during the normal engine operation is, however, lower. Half the build-up intensity IS has proven to be sufficient in order to prevent deposits. From the point of view of components development, the main goal is the creation of a laser system which meets the engine-specific requirements. Basically, it is possible to ignite mixtures with different laser systems. The concept with the greatest development potential regarding efficiency and miniaturization is the diode pumped solid-state laser.

5 ACKNOWLEDGEMENTS

This work was supported by the Austrian Industrial Research Promotion Fund (FFF) under Grant FFF 803050 and by the A3 project number 806238/7782.

The authors want to thank Heinrich Kofler for his contribution with work related to the optical window. They also want to thank Kurt Iskra for his contribution to the Schlieren photography.

6 REFERENCES

[1] Lackner, M., Winter, F., What is ignition? Combustion File 256, IFRF Online Combustion Handbook, ISSN 1607-9116, International Flame Research Foundation, Ijmuiden, The Netherlands, (2004).

[2] H. Kopecek, M. Lackner, F. Winter, E. Wintner, Laser ignition of methane air mixtures at pressures up to 4 MPa, Journal of Laser Physics 13 (11), 1365 (2003).

[3] Kopecek, H., Lackner, M., Wintner, E., Winter, F., Laser-Stimulated Ignition in a Homogeneous Charge Compression Ignition Engine, SAE 2004 World Congress, paper No 2004-01-0937, Detroit, MI, USA (2004).

[4] J. D. Dale, M. D. Checkel, P. R. Smy, Application of High Energy Ignition Systems to Engines, Prog. Energy Combust. Sci. 23, 379-398 (1997). [5] Ronney P.D., Laser versus conventional ignition of flames, Optical Engineering 33(2), 510 (1994).

[6] Phuoc T.X., White F.P., Laser-induced spark ignition of CH4/air mixtures, Combustion and Flame 119, 203-216 (1999).

[7] Radziemski L.J., Cremers D.A., Laser-induced plasmas and applications, New York- Basel: Marcel Dekker Inc., (1989).

[8] Yablonovich E., Self phase modulation and short pulse generation from laser breakdown plasmas, Phys. Rev. A10, 1888-1895 (1975).

[9] Phuoc T., Laser spark ignition: experimental determination of laser-induced breakdown thresholds of combustion gases, Optics Communication 175, 419-423 (2000).

[10] Kopecek H., Charareh S., Lackner M., Forsich C., Winter F., Klausner J., Herdin G., Wintner E., Laser Ignition of Methane-Air Mixtures at High Pressures and Diagnostics, Salzburg, Austria: Proceedings of ICES03, Spring Technical Conference of ASME Internal Combustion Engine Division (2003).

[11]Heywood J.B., Internal combustion engine fundamentals, McGraw-Hill international editions (1988).

[12] Phuoc T.X., Single-point versus multi-point laser ignition: Experimental measurements of combustion times and pressures, Combustion and Flame 122, 508-510 (2000).

[13] Morsy M.H., Ko Y.S., Chung S.H., Cho P., Laser-induced two point ignition of premixture with a single-shot laser, Combustion and Flame 125, 724-727 (2001).

[14] Morsy M.H., Chung S.H., Laser induced multi-point ignition with a single-shot laser using two conical cavities for hydrogen/air mixtures, Experimental Thermal and Fluid Science 27, 491-497 (2003).

[15] Weinrotter M., Kopecek H., Wintner E., Lackner M., Winter F., Laser ignition of hydrogen-air mixtures at high pressures, Orleans, France: Proceedings of the European Combustion Meeting, European Combustion Institute (2003).

[16] Ma J.X., Alexander D.R., Poulain D.E., Laser spark ignition and combustion characteristics of methane-air mixtures, Combustion and Flame 112, 492-506 (1998).

[17] Ma J.X., Ryan III T.W., Buckingham J.P., Nd:YAG Laser ignition of natural gas, ASME Spring Technical Conference, Paper No. 98-ICE-114 (1998).

[18] Gary S. Settles, Schlieren and shadowgraph techniques, Springer (2001).

[19] M. Lackner, S. Charareh, F. Winter, K. F. Iskra, D. Rüdisser, T. Neger, H. Kopecek, E. Wintner, Diagnostic tools for laser-induced ignition of gaseous mixtures: Schlieren photography and laser-induced fluorescence spectroscopy (LIF), to be submitted to Optics Express (2004).

[20] Josef Graf, Untersuchungen zur laserinduzierten Zündung an einem Otto-DI Brennverfahren der zweiten Generation (Investigation of laser-induced ignition of an Otto direct injection engine of the 2nd generation), Master Thesis, Vienna University of Technology, Vienna, Austria (2002).

[21] Christian Forsich, Maximilian Lackner, Franz Winter, Herbert Kopecek, Ernst Wintner, Characterization of Laser-Induced Ignition of Biogas/air Mixtures, accepted for publication, Biomass & Bioenergy (2004).

[22] Bernhard Geringer, Dominikus Klawatsch, Josef Graf, Peter Lenz, Dieter Schuöcker, Gerhard Liedl, Walter F. Piock, Markus Jetzinger, Paul Kapus, Laserzuendung, MTZ 65(3), 214-219 (2004).

[23] Boris Luk'yanchuk, Laser Cleaning, Optical Physics, Applied Physics and Materials Science, World Scientific Publishing, Singapore (2002). [24] Daniel C. Harris, Durable 3-5 μm transmitting infrared window materials, Infrared Physics and Technology 39, 185-201 (

Fabrication and Simulation of Composite Sandwich Leaf Spring for Light Commercial Vehicle

Kirubakaran.M[a], 2. Vimal Prabu.P[a], 3. Manimaran.P[b]
[a]Student, Department of Mechanical Engineering,
Christ College of Engineering and Technology, Moolakulam, Puducherry-605010.
[b]Assistant Professor, Department of Mechanical Engineering, Christ College of Engineering and Technology, Moolakulam, Puducherry-605010.

***Abstract*—In today's automobile world weight reduction is one of the major role to increase the vehicle efficiency. Which can be achieved by use Glass-fibre reinforced composite (GFRC) instead of steel. Moreover, the composite materials have more elastic strain energy storage capacity and high strength to weight ratio compared to steel. Due to increased trend in using composite materials in manufacturing. In this research work an attempt has been made to predict the structural behaviour of composite coated steel leaf spring and we too have adopted our own model of sandwiching a steel leaf spring(55Si2Mn90) with composite materials(E-Glass epoxy composite) as it would possess increase in strength and life cycle of that particular model of leaf spring. Surface pre-treatment of steel leaf spring in conducted to achieve maximum adhesion strength between steel and composite materials. Fabrication is carried by hand lay-up technique and tested. The simulated and analytical results comparison of both mono steel leaf spring and mono composite coated steel leaf spring are to be carried. The testing was performed experimentally with the help of Universal Testing Machine (UTM) and by Finite Element Analysis (FEA) using ANSYS.**

***Keywords*—composite, sandwiched, leaf spring, Eglass-epoxy, ANSYS.**

INTRODUCTION:

Composite materials consist of two or more physically dissimilar and instinctively separable components called reinforcement and matrix. These two components can be mixed in a restricted way to achieve optimum properties, which are superior to the properties of each individual component.

Composite materials have been widely used in automobile industry because of its high strength and modulus to weight ratio, low cost and flexibility in material and structure design. The suspension leaf spring is one of the potential items for weight reduction in automobile as it accounts for ten to twenty percent of the unsprung weight. This helps in achieving the vehicle with improved riding qualities.

Since the strain energy in the spring is inversely proportional to density and young's modulus of the material, it is always suggested that the material for leaf spring must have low density and modulus of elasticity. Many research have been carried out in the direction to replace conventional steel leaf spring by composites.

Material constitute nearly 60-70% of the vehicle cost and contribute to quality and the performance of the vehicle. Even a small amount in weight reduction of the vehicle, may have a wider economic impact. Composite materials are proved as suitable substitutes for steel in connection with weight reduction of the vehicle.

Design and consideration

In this research work TATA ACE mono composite leaf spring with constant width and constant thickness with constant cross section is considered. In the design point of view weight reduction is the key point to make the vehicle overall efficient and without affecting load carrying capacity. In our project TATA-ACE steel leaf spring is selected for composite coating and testing. Weight of master leaf spring is 2.95kg.

By coating the master steel leaf by composite material, we neglect the graduated leaf and the weight is almost reduced by 60%. The composite coated leaf spring has increased fatigue due to the steel core.

Surface pre-treatment:

To obtain the optimum performance from an adhesive joint, pre-treatment is required. The suitable surface pre-treatment gives

- Enhanced mechanical performance of joint
- Improved joint durability in aggressive environments
- Increased service-life of component
- Ability to bond difficult adherends.

There is wide range of surface treatments available, based on the ISO4588 for metal, leaf spring surface are pre-treated for strong adhesion. Following pre-treatment process are carried out.

- Cleaning/degreasing to remove the loose solids can be accomplished with a clean brush. Organic solvent are used remove materials such as grease, oil and wax from adherend surfaces.
- Surface roughening are done by abrasive materials using medium grit(120-200 mesh) are employed to remove unwanted layers and generate a roughened surface texture and following thus chemical treatment are carried out to remove oxidized layer.

Leaf spring specification of TATA-ACE

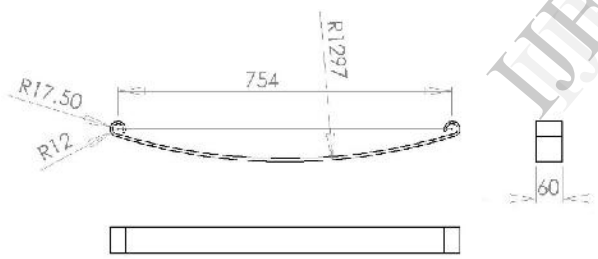

Figure 1 2D drawing of TATA-ACE master leaf spring

Table 1 Leaf spring specification of TATA-ACE

Total Length (L)	930mm
Length of leaf spring from Eye to Eye	754mm
Thickness (t)	8mm
Width (b)	60mm

Table 2 Material properties of 55Si2Mn90 steel

Ultimate tensile strength Su (Mpa)	1962
Yield tensile strength Su (Mpa)	1470
Modulus of elasticity E (Gpa)	210
Poisson ratio	0.3

Considered three specimens

1. Steel leaf spring p
2. Composite coated steel leaf spring(4 layu above and 6 layup at bottom) yup
3. Composite coated steel leaf spring(3 la above and 4 layup at bottom)

Specific design data

Gross vehicle weight: 1550Kgs
Kerb weight:840 Kgs
Payload: 710 Kgs
Acceleration due to gravity(g)=9.813m/s^2

Total weight acting downwards (i.e at full load)
= Gross Vehicle Weight × gravity
= 1550 x 9.81
= 15205.5 N

There are four suspensions two at the front and two at the back. So, Load on one suspension
= 15205.5/4
= 3801.4 N or 3800 N approx.

But 2F=3800
F=1900N
Span length, 2L=754mm
L 377mm

Bending stress, $\sigma = 6FL/bh^2$
b= 1119.21N/mm^2

Total deflection,
$\delta = 4FL^3/Ebh^3$
δ =63.12mm

where,
F Force (N)
L span length
b=bending stress (N/mm^2)
b= breadth of leaf spring (mm)
h = thickness of leaf spring (mm)
E = modulus of elasticity

Material selection for composite coating

Uni-directional e-glass fibre is selected as reinforcement and fabricated.

Fibre: E-glass fibre (uni-directional)
Resin: Epoxy

Fabrication of composite coated steel leaf spring

Fabrication of composite coating is carried by hand lay-up technique. The surface pre-treated steel leaf spring is placed on the table then mixed epoxy and hardener is layered over the steel surface and glass fibre is placed over it. This process is repeated until desired thickness is achieved.

Composite layer is lay-up on both sides of steel spring i.e (top and bottom of leaf spring). And allowing to cure for 24hours.

Testing

Composite coated steel leaf spring is to be tested in UTM (Universal Testing Machine). Front eye end of the leaf spring usually attached to the vehicle chassis and rear eye end are fixed to the chassis through the rigid link called shackle. From this front eye is translational constrained and free rotation about eye axis. The rear eye are translated horizontally as well as vertically and free rotation about eye. Flexural test conducted to obtain the deflection value until it brakes. Deflection values are to be noted for every interval of 50kg. Corresponding stiffness value should be calculated.

CONCLUSION

Due to increasing competition in automobile industry the weight of the vehicle are reduced for the increase in overall efficiency of some particular vehicle. Composite materials which has set a footmark and has been employed in manufacturing the light weight parts for the commercial vehicles.

As the leaf spring which thus constitute more amount of total vehicle weight which needs to be strong and weight bearable such that a conservative study is conducted between conventional normal leaf spring and sandwiched composite leaf spring which is fabricated. And weight and strength of these leaf springs are compared.

And even simulated result in ansys are also to be compared with actual results.

REFERENCES

[1] B. Raghu Kumar, R. Vijaya Prakash and N. Ramesh, "Static analysis of mono leaf spring with different composite materials", Journal of Mechanical Engineering Research Vol. 5(2), ISSN 2141-2383, February 2013, pp. 32- 37

[2] M. M. Patunkar, D. R. Dolas, "Modelling and Analysis of Composite Leaf Spring under the Static Load Condition by using FEA", International Journal of Mechanical & Industrial Engineering, Volume 1, Issue 1-2011

[3] B.Vijaya Lakshmi, I. Satyanarayana, "Static And Dynamic Analysis On Composite Leaf Spring In Heavy Vehicle", International Journal of Advanced Engineering Research and Studies, E- ISSN2249–8974, Vol. II/ Issue I/Oct.-Dec.,2012,

[4] J.A.M. Ferreira a, J.D.M. Costa, P.N.B. Reis, M.O.W. Richardson, "Analysis of fatigue and damage in glass-fibre-reinforced polypropylene composite materials" Composites Science and Technology 59 (1999),1461-1467

Discrete Time Geo/Geo/1 Retrial G – Queue with Server Break Down and Repair

A.Azhagappan, St.Anne's college of Engg. & Tech.

A.Sridevi, Theivanai Ammal College for Wemen
T. Deepa, Theivanai Ammal College for Wemen

***Abstract*—This paper deals with discrete-time Geo/Geo/1 retrial queue with negative customers where the server is subject to breakdown and repair due to the negative arrivals. If the server is idle, negative customer break the server down, if the server is busy, it kill a customer in service and break the server down and if the server is under repair, it has no effect. If the server is breakdown, it is sent to repair immediately and after repair it is as good as new. We analyze the Markov chain underlying the queueing system and obtain its ergodicity condition.**

Keywords—retrial queue; negative customer; break down and repair.

1. INTRODUCTION

G-networks were first introduced by Gelenbe in 1989 (see [1]) with a view to modelling neural networks and they are characterized by the following feature: in contrast with the normal positive customers, negative customers arriving to a non-empty queue remove an amount of work from the queue. The *G*-networks systems have a rich and wide range of real applications in areas such as computers, communications and manufacturing.

In the retrial queueing literature, Artalejo and G´omez-Corral[2−7] have investigated single server queues operating under the simultaneous presence of negative arrivals and repeated attempts. However, these works focus on the continuous cases. It is well known that in the field of telecommunications modern systems are more digital than analogue, hence the studies of the modern communication systems are based more on discrete-time analysis. But, as far as we know, there are no results for the discrete retrial *G*-queueing systems although the analysis of discrete-time retrial queueing models has received considerable attention in the literature.

The present paper studies a discrete-time single-server retrial queue with both positive and negative customers. An example of a queueing system with both positive and negative flows of arrivals is computer networks with virus infection. When there are no viruses, computer networks have been modeled and analyzed using conventional queueing networks with or without retrials. The customers represent the execution of algorithmic and logic operations, and the nodes represent CPUs, I/O devices, etc. When a virus enters a node, one or more files may be infected, and the system manager may have to go through a number of backups to recover the infected files. In some cases, they may not be recoverable. A virus may originate from outside the network, e.g., through a floppy disk, or may come from another node in the network, e.g., by an electronic mail. The recovery time of the infected files can be regarded as repair time of the server (node) due to an arrival of negative customer (virus).

2. MODEL DESCRIPTION

The time axis is divided into a sequence of equal subintervals (called slot or epoch) and the ends of the subinterval be marked by 0, 1,…, m. It is assumed that all queueing activities (arrivals, departures, retrials, breakdowns and repairs) occur at the slot boundaries. Different from continuous-time queues, the probability of an arrival and a departure and other queueing activities occurring concurrently may be not zero in discrete-time queues anymore. So it is necessary to specify the order in which the arrivals and departures take place in case of simultaneity. For mathematical clarity, we assume that the departures and the end of the repairs occur in the interval $(m-,m)$, and the arrivals, the retrials and the beginning of the repairs occur in the interval $(m,m+)$; that is, the arrivals, the retrials and the beginning of the repairs occur at the moment immediately after the slot boundaries and the departures and the end of the repairs occurs at the moment immediately before the slot boundaries. In the literature it is called "early arrival system" (EAS).

New customers arrive from outside the system according to a geometric arrival process with rate p. The arriving customers have two types: positive customers (with probability $q+$) and negative customer (with probability $q-$).

Positive customer (external or repeated) receives the service immediately when the server is found free. If the server is found busy or down, the customer must join the orbit and return after random amount of time (in slots). Each customer in the orbit generates independently a Bernoulli stream with rate $r = 1 - r$, where r is the probability that a repeated customer does not make a retrial in a slot.

The arrival of a negative customer causes one positive customer to be killed if any is present, and simultaneously breaks the server down. The failed server is sent to repair immediately and after repair it is assumed as good as new. The negative customer also causes the server breakdown if the server is found idle, but has no effect on the system if the server is under repair.

The repair times are independent and geometrically distributed with parameter $\alpha = 1-\alpha$, where α is the probability that the repair process does not complete in a slot. The service times are independent and geometrically distributed with probability $s = 1-s$, where s is the probability that a customer does not conclude his service in a slot. After service completion, the customer leaves the system immediately forever. Finally, various stochastic processes involved in the system are assumed to be independent of each other. To avoid trivial cases, we suppose $0 < p < 1$, $0 \le r < 1$, $0 \le q+ \le 1$ and $0 < s \le 1$.

3. *The Markov Chain*

At time $m+$, the system can be described by the process $Y_m = (C_m , N_m)$, where C_m denotes the state of the server (0, 1 or 2 according to whether the server is free, busy or down) and N_m, the number of repeated customers in the retrial orbit. It can be shown that $\{Y_m , m \in \mathrm{N}\}$ is the Markov chain of our queueing system, whose state space is $\Omega = \{(i, k) : i = 0, 1, 2; k \ge 0\}$. Let

$$\pi_{0,k} = \lim_{m\to\infty} P[C_m = 0, N_m = k], \quad k\ge 0,$$
$$\pi_{1,k} = \lim_{m\to\infty} P[C_m = 1, N_m = k], \quad k\ge 0,$$
$$\pi_{2,k} = \lim_{m\to\infty} P[C_m = 2, N_m = k], \quad k\ge 0,$$

be the stationary distributions of the Markov chain $\{Y_m, m \in \mathrm{N}\}$. Our object is to find the stationary distributions.

By routine method, the Kolmogorov equations for the stationary distribution of our system

$$\pi_{0,k} = (1-p)r^k\pi_{0,k} + (1-p)(1-s)r^k\pi_{1,k} + (1-p)(1-\alpha)r^k\pi_{2,k} \quad (3.1)$$

$$\pi_{1,k} = pq^+\pi_{0,k} + ((1-p)s + pq^+(1-s))\pi_{1,k} + pq^+(1-\alpha)\pi_{2,k} + (1-p)(1 - r^{k+1})\pi_{0,k+1} + (1-p)(1-s)(1 - r^{k+1})\pi_{1,k+1} + (1- p)(1-\alpha)(1 - r^{k+1})\pi_{2,k+1} + (1 - \delta_{0,k})pq^+s\pi_{1,k-1}, \quad (3.2)$$

$$\pi_{2,k} = pq^-\pi_{0,k} + pq^-\pi_{1,k} + ((1-p)\alpha + pq^-)\pi_{2,k} + (1 - \delta_{0,k})pq^+\alpha\pi_{2,k-1}, \quad (3.3)$$

where $\delta_{i,j}$ denotes Kronecker's delta. The normalization condition is given by

$$\sum_{k=0}^{\infty}\pi_{0,k} + \sum_{k=0}^{\infty}\pi_{1,k} + \sum_{k=0}^{\infty}\pi_{2,k} = 1$$

In order to solve Eqs.(3.1)–(3.3), we introduce the following generating functions:

$$\phi_0(z) = \sum_{k=0}^{\infty}\pi_{0,k}z^k , \ \phi_1(z) = \sum_{k=0}^{\infty}\pi_{1,k}z^k , \ \phi_2(z) = \sum_{k=0}^{\infty}\pi_{2,k}z^k$$

Multiplying Eqs.(3.1)–(3.3) by z^k and summing over k, we get

$$\phi_0(z) = (1-p)\phi_0(rz) + (1-p)(1-s)\phi_1(rz) + (1-p)(1-\alpha)\phi_2(rz), \quad (3.4)$$

$$\phi_1(z) = pq^+\phi_0(z) + ((1-p)s + pq^+(1-s))\phi_1(z) + pq^+(1-\alpha)\phi_2(z) + (1-p)/z\ \phi_0(z) - (1-p)/z\ \phi_0(rz) + (1-p)(1-s)/z\ \phi_1(z) - (1-p)(1-s)/z\ \phi_1(rz) + (1-p)(1-\alpha)/z\ \phi_2(z) - (1-p)(1-\alpha)/z\ \phi_2(rz) + pq^+sz\phi_1(z), \quad (3.5)$$

$$\phi_2(z) = pq^-\phi_0(z) + pq^-\phi_1(z) + ((1-p)\alpha + pq^-)\phi_2(z) + pq^+\alpha z\phi_2(z). \quad (3.6)$$

By substituting (3.4) into (3.5) we obtain

$$\phi_1(z) = (pq^+ + (1- p)/z)\phi_0(z) + ((1-p)s + pq^+(1-s) + (1- p)(1-s)/z + pq^+sz)\phi_1(z) + (pq^+(1-\alpha) + (1-p)(1-\alpha)/z)\phi_2(z) - 1/z\ \phi_0(z) \quad (3.7)$$

Solving the system (3.6) and (3.7), and after simplifying the expressions we find the following generating function:

$$\phi_1(z) = \{[(1 - z)pq^+(-pq^+\alpha z + (1-p)(1-\alpha) + p)]\phi_0(z)\}/\Theta(z) \quad (3.8)$$

$$\phi_2(z) = \{[(1 - z)pq^-(-pq^+sz + (1-p)(1-s) + p)]\phi_0(z)\}/\Theta(z) \quad (3.9)$$

where

$$\Theta(z) \equiv pq^-(pq^+(1-\alpha)z + (1-p)(1-\alpha) - ((1-p)sz + pq^+(1-s)z + pq^+sz^2 + (1- p)(1-s) - z)((1-p)\alpha + pq^- + pq^+\alpha z - 1).$$

Lemma 1.

(1) The inequality $\Theta(z) > 0$ holds for $0 \le z < 1$ if and only if

$$pq^+/[(1-s) + spq^-] < 1 - pq^-/[(1-\alpha) + \alpha pq^-];$$

(2) Under the above condition there exists

$$\lim_{z\to 1} (1 - z)/\Theta(z) = 1/[(pq^- + (1-p)(1-s) - pq^+s)((1-p)(1-\alpha) + pq^+(1-\alpha)) - pq^+pq^-].$$

Using the previous lemma, the auxiliary generating functions $\phi_1(z)$, $\phi_2(z)$ are defined for $0 \le z < 1$, and in $z = 1$ are extended by continuity if and only if

$$pq^+/[(1-s) + spq^-] < 1 - pq^-/[(1-\alpha) + \alpha pq^-]$$

From equation (3.8) and (3.9), we can get

$$\phi_1(1) = [pq^+((1-\alpha) + \alpha pq^-)\ \phi_0(1)]/[(pq^- + (1-p)(1-s) - pq^+s)((1-p)(1-\alpha) + pq^+(1-\alpha)) - pq^+pq^-]$$

,

$$\phi_2(1) = [pq^-((1-s) + spq^-)\ \phi_0(1)]/[(pq^- + (1-p)(1-s) - pq^+s)((1-p)(1-\alpha) + pq^+(1-\alpha)) - pq^+pq^-]$$

The normalization condition $\phi_0(1) + \phi_1(1) + \phi_2(1) = 1$ gives

$$\phi_0(1) = 1 - pq^+/[(1-s) + spq^-] - pq^-/[(1-\alpha) + \alpha pq^-],$$
$$\phi_1(1) = pq^+/[(1-s) + spq^-],$$
$$\phi_2(1) = pq^-/[(1-\alpha) + \alpha pq^-]$$

Substituting eqns. (3.8) and (3.9) into (3.4) leads to

$$\phi_0(z) = G(rz)\,\phi_0(rz), \qquad (3.10)$$

where

$$G(z) = (1-p)(1-z)/\Theta(z) \times [pq^{+}spq^{+}\alpha z^2 + pq^{+}\alpha(-(1-p)(1-s) - pq^{-} - pq^{+}(1-s))z + pq^{+}s(-(1-p)(1-\alpha) - pq^{+} - pq^{+}(1-\alpha))z + (pq^{-}(1-p)(1-\alpha) + (1-p)(1-s)(1-p)(1-\alpha) + (1-p)(1-s)pq^{+} + 2(1-p)(1-s)(1-\alpha) + (1-s)p + (1-p)s)]$$

$$\phi_0(z) = \phi_0(0)\prod_{n=1}^{\infty} G(r^n z) \qquad (3.11)$$

Lemma 2. If $pq^{+}/[(1-s) + spq^{-}] < 1 - pq^{-}/[(1-\alpha) + \alpha pq^{-}]$, then the infinite product $\prod_{n=1}^{\infty} G(r^n z)$ is convergent.

Theorem 3. If $pq^{+}/[(1-s) + spq^{-}] < 1 - pq^{-}/[(1-\alpha) + \alpha pq^{-}]$ holds, then the stationary distribution of the Markov chain $Y_m = (C_m, N_m)$ has the following generation functions:

(1) The marginal generating function of the number in the orbit when the server is idle is

$$\phi_0(z) = \{1 - pq^{+}/[(1-s) + spq^{-}] - pq^{-}/[(1-\alpha) + \alpha pq^{-}]\} \prod_{n=1}^{\infty} G(r^n z) / \prod_{n=1}^{\infty} G(r^n)$$

.

(2) The marginal generating function of the number in the orbit when the server is busy is

$$\phi_1(z) = \{(1-z)pq^{+}(-pq^{+}\alpha z - (1-\alpha)(1-p) + p)\phi_0(z)\}/\Theta(z)$$

(3) The marginal generating function of the number in the orbit when the server is down is

$$\phi_2(z) = \{(1-z)pq^{-}(-pq^{+}sz + (1-p)(1-s) + p)\phi_0(z)\}/\Theta(z)$$

(4) The probability generation function of the number of customers, N, in the orbit is

$$\psi(z) = \phi_0(z) + \phi_1(z) + \phi_2(z) = 1/\Theta(z) \times \{pq^{+}spq^{+}\alpha z^2 + pq^{+}\alpha(-(1-p)(1-s) - p)z + pq^{+}s(-(1-p)(1-\alpha) - p)z + (pp + p(1-p)(1-\alpha) + p(1-p)(1-s) + (1-p)(1-s)(1-p)(1-\alpha))].$$

(5) The probability generation function of the number of customers, L, in the system is

$$\varphi(z) = \phi_0(z) + z\,\phi_1(z) + \phi_2(z) = 1/\Theta(z) \times \{pq^{+}s(pq^{+}\alpha - pq^{-})z^2 + pq^{+}\alpha(-(1-p)(1-s) - p)z + pq^{+}s(-(1-p)(1-\alpha) - pq^{+})z + pq^{-}((1-p)(1-s) + p)z + (pq^{-}(1-p)(1-\alpha) + (1-p)(1-s)(1-p)(1-\alpha) + (1-p)(1-s)pq^{+})\}.$$

REFERENCES

[1] Gelenbe, E. Random neural networks with negative and positive signals and product form solution. Neural Comput., 1: 502–510 (1989)

[2] Artalejo, J.R., G´omez-Corral, A. Stochastic analysis of the departure and quasi-input processes in a versatile Single server queue. Journal of Applied Mathematics and Stochastic Analysis, 9: 171–183 (1996)

[3] Artalejo, J.R., G´omez-Corral, A. Generalized birth and death processes with applications to queues with repeated attempts and negative arrivals. OR Spektrum, 20: 5–14 (1998)

[4] Artalejo, J.R., G´omez-Corral, A. Analysis of a stochastic clearing system with repeated attempts. Stochastic Models, 14: 623–645 (1998)

[5] Artalejo, J.R., G´omez-Corral, A. On a singal server queue with negative arrivals and request repated. Journal of Applied Probability, 36(3): 907–918 (1999)

[6] Artalejo, J.R., G´omez-Corral, A. Performance analysis of a single-server queue with repeated attempts. Mathematical and Computer Modelling, 30: 79–88 (1999)

[7] Artalejo, J.R., G´omez-Corral, A. Computation of the limiting distribution in queueing systems with repeated attempts and disasters. RAIRO Operations Research, 33: 371–382 (1999)

On Domination and Energy of Zero Divisor Graphs

K. Ananthi
Department of Mathematics
VSA Group of Institutions
Salem, India – 636 010.

Dr. J. Ravi Sankar
School of Advanced Sciences
VIT University Vellore, India – 632 014.

Dr. N. Selvi
Department of Mathematics
ADM College for Women, Nagapattinam, India-611001

***Abstract*— The energy E (G) of a graph G is the sum of the absolute values of the eigenvalues of G. In this paper, we study the characterization of eigenvalues and energy of adjacency matrix corresponding to zero-divisor graphs of finite commutative ring. Also, we study the eigenvalue and energy of $\Gamma(Z_n)$ where n=2p, 3p, 5p, pq, p^2, 4p where p, q are distinct prime numbers. Finally, we give the relationship between the domination number, energy, rank and eigenvalues of complete zero-divisor graphs.**

Keywords — Commutative ring, Zero-divisor graph, Energy graph.

I. INTRODUCTION

The energy E(G), of a graph G is defined to be the sum of the absolute values of its eigenvalues. Hence, if A(G) is the adjacency matrix of G, and $\{\lambda_1,\lambda_2,\lambda_3...\lambda_n\}$ are the eigenvalues of A(G), then $E(G)=\sum_{i=1}^{n}|\lambda_i|$. The set $\{\lambda_1,\lambda_2,...,\lambda_n\}$ is the spectrum of G and denoted by Spec G. The totally disconnected graph K_n^c has zero energy while the complete graph K_n with the maximum possible number of edges (among graphs on n vertices) has energy 2(n-1).Graphs for which the energy is greater than 2(n-1) are called hyperenergetic graphs. If E(G) 2(n-1), then G is called non-hyperenergetic.

The energy of G was first defined by I. Gutman in 1978 as the sum of the absolute values of the eigenvalues of A(G) in [2]. Energy of graph originated from theoretical chemistry. Huckel molecular orbital theory is a field of theoretical chemistry where graph eigen values occur. The carbon atoms of a hydrocarbon system correspond to vertices of a graph associated with the molecule. From Huckel theory, the energy of a molecular graph is equal to the total - electron energy of a conjugated hydrocarbon [3].

The concept of energy has been generalized in two different directions. Let A be an m×n matrix and A^* denote its adjoint(conjugate transpose of A).The singular values $s_1(A)\geq s_2(A)\geq\ldots\geq s_m(A)$ of a matrix A are the square roots of the eigenvalues of AA^*.Note that if A is an n×nHermitian matrix(i.e , $A = A^*$) , then the singular values of A are the absolute values of the eigenvalues of A.For any $A\in M_{m,n}$define the energy of A , $E(A) = \sum_{i=1}^{m} s_i(A)$ .From the above, we note that the usual energy of a graphG , E(G) = E(A(G)).

Another generalization of energy is defined as follows:Let Mbe a matrix associated with G. Suppose $\mu_1, \mu_2,\ldots\mu_n$ are the eigenvalues of M and $\overline{\mu}$ is the average of $\mu_1, \mu_2,\ldots\mu_n$.The M – energy of G is then defined as the absolute deviation $E_{M(G)}= \sum_{i=1}^{n}|\mu_i-\overline{\mu}|$.If M is the adjacency matrix A(G), then $\overline{\mu}$ =0.Hence, the usual energy E(G) = E_A(G).For notation and zero-divisor graph terminology, we in general follow [4,5,6,7].

Let R be a commutative ring and let Z(R) be its set of zero-divisors. The zero-divisor graph of a ring is the graph (simple) whose vertex set is the set of non-zero zero-divisors, and an edge is drawn between two distinct vertices if their product is zero. Throughout this paperff, we consider the commutative ring by R and zero-divisor graph $\Gamma(R)$by $\Gamma(Z_n)$. The idea of a zero-divisor graph of a commutative ring was introduced by I.Beck in [1], where he was mainly interested in colourings. The zero-divisor graph is very useful to find the algebraic structures and properties of rings.

Claude Berge introduced the theory of Domination in 1958. The inspiration for this concept was drawn from the classical problem of covering chessboard with minimum number of chess pieces.

The most common definition given of a dominating set is that it is a set of vertices $D \subset V$ in a graph G = (V, E) having the property that every vertex v V-D is adjacent to atleast one vertex in D . The domination number (G) is the cardinality of a smallest dominating set of G.

Throughout this paper G will denote a simple (no loops or multiple edges), undirected graph with n vertices and m edges. If $\{v_1, v_2, \ldots v_n\}$ is the set of vertices of G , then the adjacency matrix of G, A(G) = A = $[a_{ij}]$ is an n × n matrix, where a_{ij}= 1 if v_i and v_j are adjacent and a_{ij}= 0 otherwise. Thus, A is a symmetric (0, 1) – matrix with real eigenvalues and zeros on the diagonal. If $\lambda_1, \lambda_2, \ldots \lambda_n$ are the eigenvalues of A, then we have $\lambda_1 \geq \lambda_2 \geq \ldots \geq \lambda_n$ *and* $\lambda_1 + \lambda_2 + \ldots \lambda_n = 0$.

II EIGENVALUES & ENERGY OF ZERO DIVISOR GRAPHS

In this paper, we evaluate the eigenvalues of zero-divisor graph and find the energy of some generalized zero divisor graphs.

Theorem1: For any graph $\Gamma(Z_{2p})$, where p is any prime number, then the eigenvalues are $\sqrt{p-1}$, $-\sqrt{p-1}$ and $E(\Gamma(Z_{2p})) = 2\sqrt{p-1}$.

Proof: The vertex set of $\Gamma(Z_{2p})$ is {2, 4, 6… 2(p-1), p}. Let u=4 and v=p then 2p must divides uv. That is 2p divides 4p. Clearly, u and v are adjacent vertices. Similarly, any vertices u in $V(\Gamma(Z_{2p}))$ and v=p then 2p must divides uv. It seems that p is adjacent to all the vertices in $V(\Gamma(Z_{2p}))$.Let u=4≠p and w=6≠p in $V(\Gamma(Z_{2p}))$ such that uw ≠0. It means that 2p does not divide uv=24. Clearly, no two vertices in $\Gamma(Z_{2p})$ are adjacent, except p.

Case(i): Let p=3.The eigenvalues of $\Gamma(Z_6)$ are $\sqrt{2}$,- $\sqrt{2}$. Then the energy of $\Gamma(Z_6)$=Sum of the absolute values of the eigenvalues= $\left|\sqrt{2}\right| + \left|-\sqrt{2}\right| = 2\sqrt{2}.$

Case(ii): Let p=5.The eigenvalues of $\Gamma(Z_{10})$ are $\sqrt{4}$,- $\sqrt{4}$. Then the energy of $\Gamma(Z_{10})$ =Sum of the absolute values of the eigenvalues= $\left|\sqrt{4}\right| + \left|-\sqrt{4}\right| = 2\sqrt{4}.$

Case (iii): Let p>5, is a prime number.

In general, the eigenvalues of $\Gamma(Z_{2p})$ are $\sqrt{p-1}, -\sqrt{p-1}$. Then the energy of $\Gamma(Z_{2p})$=Sum of the absolute values of the eigenvalues= $\left|\sqrt{p-1}\right| + \left|-\sqrt{p-1}\right| = 2\sqrt{p-1}$.

Theorem 2: For any graph $\Gamma(Z_{3p})$, where p is any prime number, then the Eigenvalues are $\sqrt{2(p-1)}, -\sqrt{2(p-1)}$ and $E(\Gamma(Z_{3p})) = 2\sqrt{2(p-1)}$.

Proof: The vertex set of $\Gamma(Z_{3p})$ is {3,6,9,…3(p-1),p,2p}. Let u and v be two vertices in $\Gamma(Z_{3p})$ with maximum degree. Let u=p and v=2p then there exist any other vertex w≠p≠2p in $\Gamma(Z_{3p})$ such that,is adjacent to both u and v. That is, uw =vw= 0. But uv=$2p^2$ which is not divided by 3p. Therefore u and v are non-adjacent vertices. Then the vertex set V can be partitioned into two parts V1 and V2 such that V_1={u,v}={p,2p} and V_2={3,6,9,…,3(p-1)}. Clearly $|V_1|$=2 and $|V_2|$=p-1, then
|V|=$|V_1|$+$|V_2|$=p+1.

Case(i): Let p=5.The eigenvalues of $\Gamma(Z_{15})$ are $\sqrt{8}$, $-\sqrt{8}$ .Then the energy of $\Gamma(Z_{15})$= Sum of the absolute values of the eigenvalues= $\left|\sqrt{8}\right| + \left|-\sqrt{8}\right| = 2\sqrt{8}$.

Case (ii): Let p=7.The Eigenvalues of $\Gamma(Z_{21})$ are $\sqrt{12}, -\sqrt{12}.$ Then the energy of $\Gamma(Z_{21})$= Sum of the absolute values of the Eigenvalues= $\left|\sqrt{12}\right| + \left|-\sqrt{12}\right| = 2\sqrt{12}$.

Case(iii):Let p>7, is a prime number.

In general, the eigenvalues of $\Gamma(Z_{3p})$ are $\sqrt{2(p-1)}, -\sqrt{2(p-1)}.$ Then the energy of $\Gamma(Z_{3p})$= Sum of the absolute values of the eigenvalues= $\left|\sqrt{2(p-1)}\right| + \left|-\sqrt{2(p-1)}\right| = 2\sqrt{2(p-1)}.$

Theorem 3: For any graph $\Gamma(Z_{5p})$,where p is any prime number, then the eigenvalues are $\sqrt{4(p-1)}, -\sqrt{4(p-1)}$ and $E(\Gamma(Z_{5p})) = 2\sqrt{4(p-1)}$.

Proof: The vertex set of $\Gamma(Z_{5p})$ is {5,10, . . .5(p-1), p, 2p,3p,4p}. Clearly $|V(\Gamma(Z_{5p}))| = p+3$ .Let u and v be any two vertices in $\Gamma(Z_{5p})$ with maximum and minimum degree, respectively. Let u = p and v=10 then 5p must divide uv which implies that u and v are adjacent.

Let u=p and v=2p then 5p does not divide uv=$2p^2$, which implies that u and v are non adjacent vertices. Then the vertex set V can be partitioned into two parts V_1 and V_2, where V_1={p,2p,3p,4p} and V_2= {5,10,…,5(p-1)}.Clearly any vertices u and v in $V_1$are non-adjacent as same as in V_2. Let u=p in V_1 and v=10 are in V_2 then 5p divides uv=10p. Finally, we note that, every vertex in V_1 is adjacent to all the vertices in V_2.Moreover $V(\Gamma(Z_{5p})) = V_1 \cup V_2$ and $V_1 \cap V_2 = \phi$.

Case(i):Let p=7.The eigenvalues of $\Gamma(Z_{35})$ are $\sqrt{24},-\sqrt{24}$ .Then the energy of $\Gamma(Z_{35})$ = Sum of the absolute values of the eigenvalues= $\left|\sqrt{24}\right|+\left|-\sqrt{24}\right|=2\sqrt{24}$.

Case(ii):Let p=11.The eigenvalues of $\Gamma(Z_{55})$ are $\sqrt{40},-\sqrt{40}$ .Then the energy of $\Gamma(Z_{55})$ = Sum of the absolute values of the eigenvalues= $\left|\sqrt{40}\right|+\left|-\sqrt{40}\right|=2\sqrt{40}$.

Case (iii): Let p>11 , is a prime number.In general, the eigenvalues of $\Gamma(Z_{5p})$ are $\sqrt{4(p-1)},-\sqrt{4(p-1)}$. Then the energy of $\Gamma(Z_{5p})$=Sum of the absolute values of the Eigenvalues= $\left|\sqrt{4(p-1)}\right|+\left|-\sqrt{4(p-1)}\right|=2\sqrt{4(p-1)}$.

Theorem 4: For any graph $\Gamma(Z_{p^2})$, where p>2 is any prime number, then the eigenvalues are $\underbrace{-1,-1,\ldots-1}_{(p-2)times},(p-2)$ and $E\left(\Gamma\left(Z_{p^2}\right)\right)=2(p-2)$.

Proof: If p is any prime, then $V(\Gamma(Z_{p^2}))$={p,2p,3p,4p,…,(p-1)p}. Clearly p is adjacent to all the vertices in $\Gamma(Z_{p^2})$. Also note that, any two vertices in $\Gamma(Z_{p^2})$is adjacent and hence $\Gamma(Z_{p^2})$is a complete graph, namely K_{p-1}.

Case(i): Let p=3.The eigenvalues of $\Gamma(Z_{3^2})$are -1,1. Then the energy of $\Gamma(Z_{3^2})$=Sum of the absolute values of the eigenvalues=2.

Case(ii): Let p=5.The eigenvalues of $\Gamma(Z_{5^2})$are -1,-1,-1,3. Then the energy of $\Gamma(Z_{5^2})$=Sum of the absolute values of the eigenvalues=6.

Case(iii): Let p=7.The eigenvalues of $\Gamma(Z_{7^2})$are -1,-1,-1,-1-1,5. Then the energy of $\Gamma(Z_{7^2})$=Sum of the absolute values of the eigenvalues=10.

Case(iv): Let p>7, is a prime number.The eigenvalues of $\Gamma(Z_{p^2})$are $\underbrace{-1,-1,\ldots,-1}_{(p-2)times},(p-2)$.

Then the energy of $\Gamma(Z_{p^2})$= Sum of the absolute values of the eigenvalues= $\left|(-1,\ldots-1)(p-2)\text{times}\right|+\left|p-2\right|=2(p-2)$.

Theorem5: In $\Gamma(Z_{pq})$, if p and q are distinct prime numbers with p<q, then the eigenvalues are $\sqrt{(p-1)(q-1)},-\sqrt{(p-1)(q-1)}$ and $E\left(\Gamma\left(Z_{pq}\right)\right)=2\sqrt{(p-1)(q-1)}$.

Proof: The proof is by the method of induction on p and q. The vertex set of $\Gamma(Z_{pq})$ is {p,2p,3p,…,p(q-1),q,2q,3q,…,(p-1)q}.

Case(i): Let p=2,q is any prime>2,Using theorem (2.1), for any graph $\Gamma(Z_{2q})$, where q>2 is any prime number, then the eigenvalues are $\sqrt{q-1},-\sqrt{q-1}$ .Without loss of generality, the eigenvalues can be written as $\sqrt{(p-1)(q-1)}$, $-\sqrt{(p-1)(q-1)}$, where p=2. Then, $E\left(\Gamma\left(Z_{2q}\right)\right)=2\sqrt{(q-1)}=2\sqrt{(2-1)(q-1)}=2\sqrt{(p-1)(q-1)}$, where p=2.

Case(ii): Let p=3,q is any prime>3,Using theorem (2.2), for any graph $\Gamma(Z_{3q})$, where q>3 is any prime number, then the eigenvalues are $\sqrt{2(q-1)},-\sqrt{2(q-1)}$. Without loss of generality, the eigenvalues can be written as $\sqrt{(p-1)(q-1)}$, $-\sqrt{(p-1)(q-1)}$,where p=3. Then, $E\left(\Gamma\left(Z_{3q}\right)\right)=2\sqrt{2(q-1)}=2\sqrt{(3-1)(q-1)}=2\sqrt{(p-1)(q-1)}$, where p=3.

Case(iii):Let p =5,q is any prime>5,Using theorem (2.3), for any graph $\Gamma(Z_{5q})$, where q>5 is any prime number, then the eigenvalues are $\sqrt{4(q-1)},-\sqrt{4(q-1)}$. Without loss of generality, the eigenvalues can be written as $\sqrt{(p-1)(q-1)},-\sqrt{(p-1)(q-1)}$,where p=4. Then, $E\left(\Gamma\left(Z_{5q}\right)\right)=2\sqrt{4(q-1)}=2\sqrt{(5-1)(q-1)}=2\sqrt{(p-1)(q-1)}$, where p=5.

Case(iv): Let p<q,The vertex set of $\Gamma(Z_{pq})$, is {p,2p,3p,…,p(q-1),q,2q,3q,…,(p-1)q}.Using theabove cases, the eigenvalues of $\Gamma(Z_{pq})$are $\sqrt{(p-1)(q-1)},-\sqrt{(p-1)(q-1)}$ where p and q are distinct primes with p<q. Then the energy of $\Gamma(Z_{pq})$is $E\left(\Gamma\left(Z_{pq}\right)\right)=\left|\sqrt{(p-1)(q-1)}\right|+\left|-\sqrt{(p-1)(q-1)}\right|=2\sqrt{(p-1)(q-1)}$.

Theorem6:If p > 4 is any prime, thenthe eigenvalues are in the form of $\pm$ x, $\pm$ 2.4142x,where x and 2.4142x are less than p and $E(\Gamma(z_{4p}))=2(x+2.4142x)$.

Proof: The vertex of $\Gamma(Z_{4p})$ is {2,4, …, 2(2p-1),p,2p,3p} with $\left|V(\Gamma(Z_{4P}))\right|=2p+1$.Let v = 2p be a vertex and let w be any vertex except p and 3p such that 4p divides vw.

Clearly, v is adjacent to all the vertices in $V(\Gamma(Z_{4P}))$ expect p and 3p. Let P, S,N(S) be the pendant set, minimum degree set, neighborhood of S, respectively. Since v has maximum degree then v ∈ N(S).

Case(i): Let p = 5.The vertex set of $\Gamma(Z_{20})$ is {2,4,…2(10-1),5,10,15} with $|V(\Gamma(Z_{20}))|=11$. Let v =2p = 10 be a vertex and letw be any vertex except 5 and 15 such that 20 divides vw. Clearly, v = 10 is adjacent to all the vertices in $V(\Gamma(Z_{20}))$ except 5 and 15 then 10 ∈ N(S).Let x = 2 and y = 14 then 28 is not divisible by 20 which implies x and y are non adjacent vertices. But xv = yv = 0.

The eigenvalues of $\Gamma(Z_{20})$ are -3.6955, -1.5307, 0, 1.5307, 3.6955. Then the energy of $\Gamma(Z_{20})$ = Sum of the absolute values of the eigenvalues = 2(1.5307+3.6955) = 2(1.5307+2.4142(1.5307)) = 10.4524.

Case(ii): Let p = 7.The vertex set of $\Gamma(Z_{28})$ is {2,4,…2(14-1), 7,14,21} with $|V(\Gamma(Z_{28}))|=2p+1=15.$ Let v = 2p =14 be a vertex and let w be any vertex except 7 and 21 such that 28 divides vw. Clearly v =14 is adjacent to all the vertices in $V(\Gamma(Z_{28}))$ except 7 and 21 then 14 ∈ N(S). The eigenvalues of $V(\Gamma(Z_{28}))$ are -4.5261, -1.8748, 0, 1.8748, 4.5261. Then the energy of $V(\Gamma(Z_{28}))$ = Sum of the absolute values of the eigenvalues = 2(1.8748+4.5261) = 2(1.8748+2.4142(1.8748)) = 12.8018

Case(iii): Let p>7is a prime numberThe vertex set of $V(\Gamma(Z_{4p}))$ is{2,4,…2(2p-1),p,2p,3p}with $|V(\Gamma(Z_{4p}))|=2p+1$.Let v =2p be a vertex and let w be any other vertex except p and 3p such that 4p divides vw. Clearly , v is adjacent to all the vertices $V(\Gamma(Z_{4P}))$ except p and 3p and v = 2p ∈ N(S).

The eigenvalues of $V(\Gamma(Z_{4P}))$ are -x, -2.4142x, 0, 2.4142x, x. Then the energy of $V(\Gamma(Z_{28}))$ = Sum of the absolute values of the eigenvalues =2(x+2.4142x)=6.8284x.

III Relationship between domination, energy, rank and eigenvalues of $\Gamma(Z_n)$ In this section, we find the bounds which relate the domination number of $\Gamma(Z_n)$, energy of $\Gamma(Z_n)$, rank of $\Gamma(Z_n)$ and eigenvalues of $\Gamma(Z_n)$,for n = p^2, where p >2 is any prime number.

G	$\gamma(\Gamma(Z_n))$	$E(\Gamma(Z_n))$	$\rho(\Gamma(Z_n))$	Eigenvalues
$\Gamma(Z_6)$	1	2	2	-1,1
$\Gamma(Z_{25})$	1	6	4	-1,-1,-1,3
$\Gamma(Z_{49})$	1	10	6	-1,-1,-1,-1,-1,5
$\Gamma(Z_{121})$	1	18	10	-1,-1,-1,-1,-1-1,-1,-1,-1,9,
…	…	…	…	…
…	…	…	..	…
$\Gamma(Z_{P^2})$	1	2p -4	p-1	$\underbrace{-1,-1,\ldots-1}_{(p-2)-times},(P-2)$

III CONCLUSION

In this paper, we study the eigenvalues and energy of zero divisor graph over finite commutative rings. Graphs are the most ubiquitous models of both natural and human made structures. In computer science, zero divisor graphs are used to represent networks of communication, network flow, clique problems. For any graph $\Gamma(Z_{4P})$, where p > 3 is any prime number and 4 <x< 4+x, then the eigenvalues are x , 2.4142x, approximately, where x is a position of consecutive prime number from 5 to so on.

If an Eigen value of a zero divisor graph is a rational number, then it is an integer. Also we note that the energy of a zero divisor graph cannot be an odd integer. The energy of a zero divisor graph cannot be the square root of an oddinteger.The energy of a zero divisor graph cannot be the square root of the double of an odd integer.

REFERENCES

[1] I.Beck, Colouring of Commutative Rings, J. Algebra, 116,(1988),208-226

[2] I.Gutman,The Energy of a Graph,Ber.Math – Statist.Sekt.Forschungsz.Graz,103,(1978), 1-22.

[3] I.Gutman,O.Polanski, Mathematical Concepts in Organic Chemistry, Springer, Berlin(1986).[4]J. Ravi Sankar and S.Meena, Changing and Unchanging the Domination Number of a Commutative ring, International Journal of Algebra,6 ,(2012), No -27,1343 – 1352.

[4] J.Ravi Sankar and S.Meena, Connected Domination number of a commutative ring, International Journal of Mathematical Research,5,(2012), No -1, 5-11.

[5] J. Ravi Sankar,S.Sangeetha, R.Vasanthakumari and S.Meena, Crossing Number of a Zero Divisor Graph, International Journal of Algebra,6 ,(2012), No -32,1499 – 1505.

[6] J.RaviSankar and S.Meena,On Weak Domination in a Zero Divisor Graph, International Journal of Applied Mathematics, 26,(2013),No – 1, 83 – 91.

The Bounds of Crossing Number in Complete Bipartite Graphs

M. Malathi
Department of Mathematics
Saradha Gangadharan College
Pondicherry, India – 605 004.

Dr. N. Selvi
Department of Mathematics
ADM College for Women, Nagapattinam,
India-611001

Dr. J. Ravi Sankar
School of Advanced Sciences
VIT University
Vellore, India – 632 014.

***Abstract*—We compare the lower bound of crossing number of bipartite and complete bipartite graph with Zarankiewicz conjecture and we illustrate the possible upper bound by a modified Zarankiewicz conjecture.**

Keywords—complete bipartite graphs, crossing numbers

I. INTRODUCTION

Let G = (V,E) be a simple connected graph with vertex set V(G) and edge set E(G).

The crossing number of a graph G, denoted by Cr(G), is the minimum number of crossings in a drawing of G in the plane[2,3,4].

The crossing number of the complete bipartite graph [7] was first introduced by Paul Turan, by his brick factory problem.

In 1954, Zarankiewicz conjectured [8] that,

$$Z(m,n) = \left\lfloor \frac{m}{2} \right\rfloor \left\lfloor \frac{m-1}{2} \right\rfloor \left\lfloor \frac{n}{2} \right\rfloor \left\lfloor \frac{n-1}{2} \right\rfloor$$

Where m and n are vertices.

Later, Richard Guy shown that the conjecture doesnot holds for all m,n. Then in 1970 D.J.Kleitman proved that Zarankiewicz conjecture holds for Min(m,n) ≤ 6.

A good drawing of a graph G is a drawing where the edges are non-self-intersecting in which any two edges have atmost one point in common other than end vertex. That is, a crossing is a point of intersection of two edges and no three edges intersect at a common point. So a good drawing is a crossing free drawing by arriving at a planar graph.

The crossing number is an important measure of the non-planarity of a graph. Therefore this application can be widely applied in all real time problems.

II A MODIFIED ZARANKIEWICZ CONJECTURE:

For any complete bipartite graphs with 'n' vertices,

$$Z(n,n) = \frac{1}{2}\left\lfloor \frac{n}{2} \right\rfloor^2 \left[\left\lfloor \frac{n}{2} \right\rfloor \left(\left\lfloor \frac{n}{2} \right\rfloor + 1 \right) + \left\lfloor \frac{n}{2} \right\rfloor \left(\left\lfloor \frac{n}{2} \right\rfloor - 1 \right) \right]$$

By using this conjecture, we can get all the possible number of crossings between every vertices for a given 'n', without any good drawing D. This reverse way of finding the crossings facilitates for large 'n' by without drawing the graph, we can get all possible crossings between every edges.

The best known lower bound on general case for all m,n $\in$ N which was proved by D.J.Kleitman [1] in the following theorem. That is,

Theorem1[6]:

$$cr(K_{5,n}) \geq 4 \left\lfloor \frac{n}{2} \right\rfloor \left\lfloor \frac{n-1}{2} \right\rfloor$$

$$cr(K_{6,n}) \geq 6 \left\lfloor \frac{n}{2} \right\rfloor \left\lfloor \frac{n-1}{2} \right\rfloor$$

From this he deduced that

$$cr(K_{m,n}) \geq \frac{1}{5} m(m-1) \left\lfloor \frac{n}{2} \right\rfloor \left\lfloor \frac{n-1}{2} \right\rfloor$$

Theorem2:

For m > n, $cr\left(Z(m,n)\right) \geq cr\left(K_{m,n}\right) \leq cr\left(K_{n,m}\right)$.

Proof:

From theorem 1,

$$cr(K_{m,n}) \geq \frac{1}{5} m(m-1) \left\lfloor \frac{n}{2} \right\rfloor \left\lfloor \frac{n-1}{2} \right\rfloor$$

By definition,

$$Z(m,n) = \left\lfloor \frac{m}{2} \right\rfloor \left\lfloor \frac{m-1}{2} \right\rfloor \left\lfloor \frac{n}{2} \right\rfloor \left\lfloor \frac{n-1}{2} \right\rfloor$$

We can prove the theorem byinduction. Since in $cr\left(K_{m,n}\right)$, there are ${}^{m}c_5 K_{5,n}$ subgraphs of $K_{m,n}$ with the partite with 'n' vertices in $K_{5,n}$. So we shall obtain the lower bound of $cr\left(K_{m,n}\right)$ for m ≥ 5 and n ≥ 3.

Case(i): Let n=3.

Subcase(i): m=5,

$$cr\left(Z(5,3)\right) = 2.2.1.1 = 4$$

$$cr\left(K_{5,3}\right) = \frac{1}{5}.5.4.1.1 = 4$$

$$cr\left(K_{3,5}\right) = \frac{1}{5}.3.2.2.2 = \frac{24}{5} = 4.8$$

$$\therefore cr\left(Z(5,3)\right) \geq cr\left(K_{5,3}\right) \leq cr\left(K_{3,5}\right)$$

Subcase(ii): m=6,

$$cr\left(Z(6,3)\right) = 3.2.1.1 = 6$$

$$cr\left(K_{6,3}\right) = \frac{1}{5}.6.5.1.1 = 6$$

$$cr\left(K_{3,6}\right) = \frac{1}{5}.3.2.3.2 = \frac{36}{5} = 7.2$$

$$\therefore cr\left(Z(6,3)\right) \geq cr\left(K_{6,3}\right) \leq cr\left(K_{3,6}\right)$$

Subcase(ii): m=7,

$$cr\left(Z(7,3)\right) = 3.3.1.1 = 9$$

$$cr\left(K_{7,3}\right) = \frac{1}{5}.7.6.1.1 = \frac{42}{5} = 8.4$$

$$cr\left(K_{3,7}\right) = \frac{1}{5}.3.2.3.3 = \frac{54}{5} = 10.8$$

$$\therefore cr\left(Z(7,3)\right) \geq cr\left(K_{7,3}\right) \leq cr\left(K_{3,7}\right)$$

$$\Rightarrow cr\left(Z(m,3)\right) \geq cr\left(K_{m,3}\right) \leq cr\left(K_{3,m}\right)$$

Case(ii): Let n=4.

Subcase(i): m=5,

$$cr\left(Z(5,4)\right) = 2.2.2.1 = 8$$

$$cr\left(K_{5,4}\right) = \frac{1}{5}.5.4.2.1 = 8$$

$$cr\left(K_{4,5}\right) = \frac{1}{5}.4.3.2.2 = \frac{48}{5} = 9.8$$

$$\therefore cr\left(Z(5,4)\right) \geq cr\left(K_{5,4}\right) \leq cr\left(K_{4,5}\right)$$

Subcase(ii): m=6,

$$cr\left(Z(6,4)\right) = 3.2.2.1 = 12$$

$$cr\left(K_{6,4}\right) = \frac{1}{5}.6.5.2.1 = 12$$

$$cr\left(K_{4,6}\right) = \frac{1}{5}.4.3.3.2 = \frac{72}{5} = 14.4$$

$$\therefore cr\left(Z(6,4)\right) \geq cr\left(K_{6,4}\right) \leq cr\left(K_{4,6}\right)$$

Subcase(ii): m=7,

$$cr\left(Z(7,4)\right) = 3.3.2.1 = 18$$

$$cr\left(K_{7,4}\right) = \frac{1}{5}.7.6.2.1 = \frac{84}{5} = 16.8$$

$$cr\left(K_{4,7}\right) = \frac{1}{5}.4.3.3.3 = \frac{108}{5} = 21.6$$

$$\therefore cr\left(Z(7,4)\right) \geq cr\left(K_{7,4}\right) \leq cr\left(K_{4,7}\right)$$

$$\Rightarrow cr\left(Z(m,4)\right) \geq cr\left(K_{m,4}\right) \leq cr\left(K_{4,m}\right)$$

In general,

$cr\left(Z(m,n)\right) \geq cr\left(K_{m,n}\right) \leq cr\left(K_{n,m}\right)$.

We also observe that the following inequality ,

$$2cr\left(Z(m,n+1)\right) \geq 2cr\left(K_{m,n+1}\right) \leq 2cr\left(K_{n+1,m}\right)$$

Also holds good for the above cases.

Hence the proof.

Theorem 2:

For m = n, $cr\left(Z(m,n)\right) \geq cr\left(K_{m,n}\right)$.That is,

$$\frac{1}{2}\left\lfloor \frac{n}{2} \right\rfloor^2 \left[\left\lfloor \frac{n}{2} \right\rfloor \left(\left\lfloor \frac{n}{2} \right\rfloor + 1 \right) + \left\lfloor \frac{n}{2} \right\rfloor \left(\left\lfloor \frac{n}{2} \right\rfloor - 1 \right) \right] =$$

$$\left\lfloor \frac{n}{2} \right\rfloor^4 \geq \frac{1}{5} n(n-1) \left\lfloor \frac{n}{2} \right\rfloor \left\lfloor \frac{n-1}{2} \right\rfloor$$

Proof:

When m = n, $Z(n,n)$ is a complete bipartite graph.

By theorem 1,

$$cr\left(K_{m,n}\right) \geq \frac{1}{5} n(n-1) \left\lfloor \frac{n}{2} \right\rfloor \left\lfloor \frac{n-1}{2} \right\rfloor$$

We shall prove the theorem for large sufficiently larger 'n' and hence deducing the result for subsequent small 'n'.

Case(i):

$$cr\left(K_{11,11}\right)=625$$

$$=\frac{1}{2}\begin{bmatrix}5(5)^2+4(5)^2+4(5)^2+4(5)^2+4(5)^2+4(5)^2\\+5(5)^2+5(5)^2+5(5)^2+5(5)^2+5(5)^2\end{bmatrix}$$

$$=\frac{1}{2}(5)^2\left[6.5+5.4\right]$$

$$=\frac{1}{2}\left\lfloor\frac{n}{2}\right\rfloor^2\left[\left\lfloor\frac{n}{2}\right\rfloor\left(\left\lfloor\frac{n}{2}\right\rfloor+1\right)+\left\lfloor\frac{n}{2}\right\rfloor\left(\left\lfloor\frac{n}{2}\right\rfloor-1\right)\right]$$

$$=\frac{1}{2}\left\lfloor\frac{n}{2}\right\rfloor^3\left[2\left\lfloor\frac{n}{2}\right\rfloor\right]$$

$$=\left\lfloor\frac{n}{2}\right\rfloor^4$$

$$cr\left(Z(11,11)\right)=550=\frac{1}{5}.11.10.5.5$$

$$=\frac{1}{5}.11(11-1)\left\lfloor\frac{11}{2}\right\rfloor\left\lfloor\frac{11-1}{2}\right\rfloor$$

$$=\frac{1}{5}.n(n-1)\left\lfloor\frac{n}{2}\right\rfloor\left\lfloor\frac{n-1}{2}\right\rfloor$$

$$\Rightarrow cr\left(Z(11,11)\right)\geq cr\left(K_{11,11}\right)$$

Case(ii):

$$cr\left(Z(9,9)\right)=256=\frac{1}{5}.9.8.4.4$$

$$=\frac{1}{5}.9(9-1)\left\lfloor\frac{9}{2}\right\rfloor\left\lfloor\frac{9-1}{2}\right\rfloor$$

$$=\frac{1}{5}.n(n-1)\left\lfloor\frac{n}{2}\right\rfloor\left\lfloor\frac{n-1}{2}\right\rfloor$$

$$cr\left(K_{9,9}\right)=256$$

$$=\frac{1}{2}\begin{bmatrix}4(4)^2+3(4)^2+3(4)^2+3(4)^2+3(4)^2+\\4(4)^2+4(4)^2+4(4)^2+4(4)^2\end{bmatrix}$$

$$=\frac{1}{2}(4)^2\left[5.4+4.3\right]$$

$$=\frac{1}{2}\left\lfloor\frac{n}{2}\right\rfloor^2\left[\left\lfloor\frac{n}{2}\right\rfloor\left(\left\lfloor\frac{n}{2}\right\rfloor+1\right)+\left\lfloor\frac{n}{2}\right\rfloor\left(\left\lfloor\frac{n}{2}\right\rfloor-1\right)\right]$$

$$=\frac{1}{2}\left\lfloor\frac{n}{2}\right\rfloor^3\left[2\left\lfloor\frac{n}{2}\right\rfloor\right]$$

$$=\left\lfloor\frac{n}{2}\right\rfloor^4$$

$$\Rightarrow cr\left(Z(9,9)\right)\geq cr\left(K_{9,9}\right)$$

In general,

$$cr\left(Z(m,n)\right)\geq cr\left(K_{m,n}\right)$$

Hence the proof.

III CONCLUSION

We have given an alternate way of finding crossings in complete bipartite graphs. We also proved in bipartite graphs, the best lower bound of $cr\left(K_{m,n}\right)$ will always be a lower bound until 'm' and 'n' are altered.

REFERENCES

[1] Daniel J. Kleitman, The crossing number of K5,n, J. Combinatorial Theory 9(1970),315–323.

[2] D.R. Woodall, Cyclic-order graph and Zarankiewicz's crossing number conjecture, J.Graph Theory. 17 (1994), 657-671.

[3] P. Erdos, R.P. Guy, Crossing number problem, American Mathematical Monthly 80 (1973), 52-58.

[4] R.K. Guy, The decline and fall of Zarankiewicz's theorem, Proof techniques in Graph Theory, F. Harary, ed. Academic Press, New York(1969),63-69.

[5] R.K. Guy and T. Jenkins, The toroidal crossing number of Km;n, J. CombinatorialTheory.6(1969),235-250.

[6] N.H. Nahas, On the crossing number of Km;n. Electron. J. Combin, 10:N8,(2003).

[7] R. Bruce Richter, Carsten Thomassen, Relations between crossing numbers of com-plete and complete bipartite graphs,The American Mathematical Monthly104 (1997),131–137.

[8] K. Zarankiewicz, On a problem of P. Turan concerning graphs, Fund. Math. 41 (1954),137-145.

English - A Global Language

Mrs.S.Bharathi AP/English
St.Annes college of Engineering and Technology
Panruti

Abstract: **This article writes on the factors which make a language become 'global language' and discusses about how English achieves that status. The impacts of Engish as a global language on Vietnamese learners, science, business, technology, education are analysed. With the development of technology, media, science, education etc. English will help students broaden knowledge, change the way of thinking and brighten career prospect.**

1. INTRODUCTION*

Today, English is becoming more and more popular all over the world. It is not only considered as the mother tongue of about 60 million speakers in many countries but also used widely in the world as an international language. English is the language of the United Nations, international summit meetings, science, technology, business, tourism, medicine etc. As the mean of communication, English brings people on Earth together and helps them understand each other and exchange material, cultural and spiritual values of their own countries.Needless to say, English is now an indispensable part of our lives; the term "global language" is now used for English with wide acceptance. In my writing, firstly, I will discuss about the term "global language" and how a language becomes a global language. Some theories, ideas and comments will be mentioned; the main features will be discussed. Secondly, why English dominates as a "global language" will be analyzed. Thirdly, the implications for students are presented. In this part, the advantages and difficulties are provided. The final part presents the summary of the study.

2. THE TERM "GLOBAL LANGUAGE" AND HOW A LANGUAGE BECOMES A "GLOBAL LANGUAGE"?

- The term "global language":

From Crystal's [1] point of view, a language can achieve its role as a "global language" when it reaches a special role which is accepted in every country. Crystal [1] also claims that there are two main ways to make it possible to make a language "global language". The first way is official way, that is, a language can be chosen to be used as "first language" or "second language" in a country. Therefore, the chosen language will be used in all kinds of communication, in academic fields as technology, science, media and in government. A language can also have "official" role, "semi-official" status or stands as foreign language. As Crystal [1] puts it "... being used only in certain domains, or taking second place to other languages while still performing certain official roles". As a result, to survive in these societies the need to master the language is very important if not essential. The second way to achieve the status is by receiving education priority. Although a language is not an "official language", it is taught in school as a compulsory subject for children or even for adults who need it. Take Russian for example, that language received education priority not only in the countries of former Soviet Union but also the countries under its sponsors as Vietnam, Mongolia. However, education privilege for a language is not always fixed, one language can replace the other in the process. Vietnam is a clear illustration of the replacement process, since Vietnam War, Russian was used as the main language and it was taught as compulsory subject in schools and universities. Since 90s, English has replaced Russian as the main language almost every where: schools, universities, magazines, books etc. In short, a language is called a "global language" when it achieves the official status and education priority in almost every nation, as a result, that language "will eventually come to be used by more people than any other language" How a language becomes a "global language" There exit several explanations about how a language achieves a "global status". Some believe that easy grammar structures, familiarity in vocabulary, and the rich in culture. etc. make a "global language" and language can exit independently. However, the said reasons above only cannot make a language "global", many languages are easy to study in terms of grammar and vocabulary but they are not "global". Here, I agree with Crystal in respect of his point that a language cannot exist independently without a strong power-base (economic, military, politic). As he puts it "language exits only in the brains and mouths and ears and hands and eyes of its users. When they succeed, on the international stage, their language succeeds. When they fail, their language fails". The essential reason to make a language "global" or "international" is the power of its people. Crystal assumes the power here includes the power of military, politic and economic. Look back at the history of Greek and Latin language which were used as international language in Middle East and Europe, we can find out that they became so popular not because of their scholars or scientists but because of their military power [1].

To achieve the "global" role, military power is needed, however, to keep and develop the status, political and economical power are essential. In other words, to maintain the status, a language needs a strong base and force to popularize itself. Hardly anyone wants to learn a language of week and poor nation with no international

political status. Needless to say, military power, political power and economic power are the three indispensable factors to make a language "global" and to keep its status.

3. WHY ENGLISH DOMINATES AS A "GLOBAL LANGUAGE"?

English is used as an official or semiofficial language in over 60 countries, and has a prominent place in a further 20. It is either dominant or well established in all six continents. It is the main language of books, newspapers, airports and air-traffic control, international business and academic conferences, science, technology, medicine, diplomacy, sports, international competitions, pop music, and advertising. Over two-thirds of the world's scientists write in English. Three-quarters of the world's mail is written in English. Of all the information in the world's electronic retrieval systems, 80% is stored in English. English radio programmes are received by over 150 million in 120 countries. Over 50 million children study English as an additional language at primary level; over 80 million study it at secondary level (these figures exclude China). In any one year, the British Council helps a quarter of a million foreigner students to learn English, in various parts of the world. In the USA alone, 337,000 foreign students were registered in 1983 Crystal [1]. "English is used as the main discourse in fields such as science, economics, politics and technology and this has cemented its place as the language of global communication". From the information above, it is hard to deny that English has achieved both official status and education priority in many countries. 400 years ago, the number of English users was around seven million people but the number now increases dramatically Philipson [3]. According to Crystal [1], in the late 1990s, around 1,2 and 1,5 billion people use English. Why English can achieve its "global status" can be explained in terms of its military might, economic and politic power. British military might in 19th century together with its world's leading industrial and trading role and its political imperialism had "sent English around the globe" and "a language on which the sun never sets" .Moreover, with the development of technology, science, media, share market, medicine… the need to have a common language is required. The reason why English is chosen may lie in the fact that the internet language or business language, airport language and also the language behind the US dollar is English . Furthermore, education systems in English speaking countries are developed, each year hundreds of thousands students apply for education training there. One of the main languages used in United Nations conferences is English, also, the language in world summits or conferences or seminars is English.

Culpepper (1997), cited in Russell claims that today English is used as the chief language in every single way of life such as commerce, diplomacy, pop music, publishing and so on. English is not only the "international language" in business, airport, tourism but also the main language used in education or academic communication as science, medicine etc, therefore, to master English, in a way, will affect the future of a person. Philipson [3] also shows that as books used in university's programs are written in English, in order to achieve higher education qualifications, students must successfully overcome the pre-requirement: English. After all, with the power in military, politic to achieve the "global status" and super power in economic to maintain and expand, English now strongly confirms its undeniable dominance as a "global language" in both academic communication and every day fields.

4. THE IMPLICATIONS FOR STUDENTS WHO USE ENGLISH AS A FOREIGN LANGUAGE

In this writing, firstly, I will look back at the languages, which once were the official language in Vietnam. Secondly, I will discuss the implications of English to students in Vietnam who use English as a foreign language. In this part, advantages and disadvantages will be presented. Since the early 90s, the open door policy has brought good opportunities for foreigners to invest into Vietnam, for tourists to visit the country. As a result, English is not only an interest but also a practical and a great demand for many people. Especially in some recent years, English has become a compulsory subject in curriculum at many secondary schools as well as universities in Vietnam, and its study has been considered as an academic pursuit. Books, magazines and internet language are written in English. Furthermore, most of university programs are strongly connected to English language. Therefore, the need to learn and master that language is essential to students who want to gain success in future. However, the need to get the competence level of English is not special if we look back at the history of languages, which once dominated as the official language in Vietnam. A language can achieve the official status in one country if its people have great influence (economic, military, politic) on that country. For a long time, Vietnam was under the conquer of China, Chinese was the official language in Vietnam, the way of thinking and the academic style in every fields as writing, laws, media are dominated by Chinese way. Thinking styles, lifestyles of Vietnamese people were nearly educated in Chinese way. To learn a language is to access and absorb its culture, as a result, Vietnam in a way became a "small part" in great Chinese family. From 1854, being one of French's colonies, Vietnam accepted French as official language, writing systems, medicine, and science. etc. changed according to French way. However, Vietnamese ways of thinking were deeply influenced by Confucian way, the power of French language as well as power of France was not strong enough to make a dramatic change in people's mind at that time. After that period, Russian was once considered as official language during Vietnam War and several following decades. Books, magazines, literature works, information, science were brought in by Russian experts. At that time (1980s) the main business partners of Vietnam came from Russia or countries of former Soviet Union, as a result, students as well as adults studied Russian because it was the only way to access to technology and science and to

master that language was the insurance for their future education or career. Russian was taught in schools, universities, hardly could we find a person who could not produce some Russian words. Since "doi moi" with "open door" policy, Vietnamese people have more chances to access to new world with various information, books, high technology and science (which are in English). Furthermore, Vietnam has more chance to do business with other countries, tourism develops, more foreigners visit Vietnam and the language often used is English; as a consequence, the need to understand and use the "global language" is essential. What's more, with the wide spread of internet and super power of English speaking countries in economic,politic (the USA, the UK, Canada…); it is natural for English to replace Russian and becomes official language in Vietnam. The implications of English can be seen clearly in every fields in Vietnam as science, business, media, and technology, education. These days, people use English as an important tool to access information and to gain knowledge for their needs. For students, English also has important implications to their study as well as their future career. The first and the most significant implication of English to students is to broaden their knowledge. Through internet, books, magazines, media, students have good chance to access to various information, lifestyles and knowledge around the world.

Today, about 80% of new and update information can be loaded down from internet, thus, students can throw themselves in the world of information, analyze, use the knowledge they acquire for their own purposes. With that knowledge, students can have their own, independent way to approach then deal the issues they have. Critical, independent and open thinking, therefore, are built up and developed. Thanks to their broaden knowledge, students will then evaluate their ways of thinking and change or develop it in a suitable and better way. The change in students' thinking can be seen in their study. Students become more open and straightforward; they can express their opinions, make their voices heard by showing their attitude to issues or even argue with teacher, which would be considered rude and illiterate according to traditional way of thinking. Vietnamese people for a long time follow the Confucian way of thinking which always ask for obedience and 'teacher- center' of students. Students had no chance to express their ideas, they had to use the indirect way to talk about a matter or issue, furthermore, what teacher said was considered "perfectly right" and the "power distance" was so strong in Vietnamese culture Pham Ha [5]. For the deep influence of Confucian, students "might be seen as passivity, insincerity and stupidity" by western people Ellis [6]. Therefore, when talking about the positive change in Vietnamese students' thinking and behavior in recent years we can't not mention the important role of English in that "wind of change". The second and no less important implication can be realized in students' ambition, that is a good position in future career. As English plays a vital role in every field (business, tourism, politic, economic etc.), success or failure in English may be decisive in their future career prospect. If a student masters or has the competence level in English, s/he will surely have more chance to have a better job or a chance to receive good training in other countries or even power over some matters than other who does not. If a student wants to receive scholarship or apply to school, university in other country, besides the study grade, one of the most important requirements is competence level in English. Moreover, English helps students built up their confidence and activeness. Armed with knowledge and the global language they can make themselves understood almost everywhere, students surely have confidence to deal with the issue or people they meet and ready to absorb new things. Surrounded by western lifestyle, Vietnamese students absorb the practical and active way of dealing and approaching new things. With English students can get more information, knowledge in the field they are interested in. Together with confidence, activeness, thus, the door of new world, good job will open wider for them. In short, with the widely spread in Vietnam, English has helped students broaden knowledge, change the ways of thinking and build up confidence and activeness, brighten career prospect for each student. Although English has made positive contributions to Vietnamese students' learning and thinking, it also goes with disadvantages. English is one of the main factors, which cause the turbulence in Vietnamese traditional culture. As mentioned above, Vietnamese ideology was strongly influenced by Chinese's philosophical traditions. The ideas of obedience, politeness and knowledge were built up under Confucian systems. Students should always place themselves in a lower position to the teacher, they should not argue or contradict their teacher publicly they should follow their teacher findings or follow wisely the already-known "proper moral norm" . Therefore, the change in students' thinking today has made a terrible shock to people, who for a long time are Confucian's followers, when students can argue with teacher and fight for their opinions. New and sometimes too direct ways of approaching and dealing an issue of students can cause the insulting feeling to the "old generation". Armed with update knowledge, new thinking way, over-open lifestyle, and practical mind, young people are obsessed by an idea of destroying the old to build the new one. Morality, family relations, and human relations can be ignored to fit with the lifestyle they learnt from western films, books etc. Many young people become more aggressive, they are too far practical to deal things with heart, sorrow and humanity, which was incredible in the past. The relationship between people is no longer in close contact as they are busy preparing plans for their future. They ignore the true fact that the so-call "old culture" or 'backward' traditions must have positive and strong base to survive through out nearly a thousand year. The change in young people' thinking and behavior has led to the sad fact that they are day by day losing their identity. The concept of morality, traditional behavior, culture is seriously damaged. Besides, English also causes unfair competitions. When English is badly in need in Vietnam, people are not examined with their real ability but degrees and English. People who do not have chance to learn English can not get the suitable job or position while other without ability but

fluent in English get all the chances. More and more people enroll in English class to get the certificate in order to have promotion in job or to keep their seats in company. Consequently, the trend to have English certificate becomes popular, and people seem to care about quantity not quality. A large number of people have degree of competence level or advanced level; however, they can hardly produce correct and meaningful English sentences or utterances. To sum up, together with advantages English also causes unsolved problems as tradition turbulence such as moral degradation, wreck in human relationships and inequality in certain form of economic and education. With the wide spread and its usefulness in many fields of life, English has helped people closer in "global village" with interconnected interests in business, politic, benefit, science, technology, military… and its role as "global language" is undeniable. Thanks to the dominance and wide use of the language in media, books etc, people have more chance to get to know about other countries, cultures, literature works etc, thus, broaden their knowledge with the help of common and popular language. Furthermore, English with the development of technology, science, media, will help opening the door to a new, better and dynamic world.

5. CONCLUSION

In this writing, I have discussed about the term "global language" and two ways to make a language "global", they are official status and education priority. I also have given examples and cite ideas of [1] explanation to the way a language achieve the status. To explain how a language becomes "global", I follow Crystal's assumption about three factors that play vital role, they are military, politic and economic power. In this part, I have presented some examples to make the assumption clear. To pursue the issue why English dominates as a "global language" I use the factors that are proved in the first part to compare to English role. By comparing and analyzing the role of English, it is shown that English has met all the requirements of "global language" with the military, politic power to achieve the status and economic super power to maintain and expand it. To illustrate the roles of English, I present the implications of English to Vietnamese students. I have analyzed and confirmed the advantages in terms of knowledge, thinking way and career prospect to student, on the other side, disadvantages of that implication such as tradition chaos and inequality in competition are also looked into.

REFERENCES

[1] D. Crystal, English as a global language Cambridge, Cambridge University Press, 1997.
[2] A. Pennycook, The Cultural Politics of English as in International Language, Longman Publishing, New York, 1994.
[3] R. Phillipson, Linguistics imperialism, Oxford University Press, HongKong, 1992.
[4] B. Russell, How can real intercultural communication be achieve?, Un published Manuscript.
[5] Pham Ha, How do Culturally situated notions of "polite" forms influence the way Vietnamese post graduate students write in English, Australian Journal of Education 3 (2001) 296.
[6] G. Ellis, The Appropriateness of the Communicative Approach in Vietnam: An Interview Study in Intercultural Communication,
Master Thesis, Latrobe University, 1992.

Learning English in Rural India- Difficulties and Remedies

Mrs. L. M. Sowmiya
Assistant Professor, Department of English,
St. Anne's College of Engineering and Technology,
Anguchettypalayam, Panruti-607110

***Abstract* :In the current scenario English is lauded as a Global Language. English Language has spread its fire wing all around the world and earned the privilege as the most successful language. English symbolizes higher intellect, better education, and better future. Getting the work done in effective manner has become more important than having the most knowledge. A number of studies have shown that an advanced proficiency and knowledge of English leads one to higher paying jobs, strong mobility, and a great deal of social success. It is quite evident that irrespective of the career whether it is engineering, medicine, management or history, command of the English will lead to great success. The growing importance placed on oral communication skills has been echoed in these two three decades. A success in this competitive environment depends not just on acquiring knowledge and hard skills, but also on developing effective communication skills. So it is essential that purposeful learning and goal oriented teaching have gained tremendous importance. On one hand the language has gained this status and Indians have proved their worth all over the world, with the help of English language. On the other hand, the rural India- the major population of India- finds it very difficult to cope up with it.**

Through this paper I'd like to discuss the difficulties of rural Indian students and some remedies for it.

I. INTRODUCTION

Now that English language has gained "official language" status, people belonging to different parts of the world, widely use English. English is a link language which links the whole world. Indians flourish all around the world because of their mastery over this language. Though Hindi is the National language, most of the people don't speak or understand Hindi, however they understand English. Education has multiplied the role of English language, because universities worldwide often use English as the common mode of learning and communication. English is an international language. English is firmly rooted in the soil of India. Different people can communicate with one another with the help of English. English is a confidence builder language. It will get you anywhere. If you are good speaker in English means good in all.

II. FAMILY BACKGROUND

Rural students from the poor families of labors, Farmers, household worker find no atmosphere of education. English language seems to be an alien to them. Since most of the students are first generation learners, how can a student get acquainted with the foreign language with regard to English without any guidance from their parents and others? Even though students are studying English, they are not able to produce even a single sentence without any grammatical error in English. Uneducated parents and neighbors get satisfied with the thought that primary education is more than enough, and a question for a good communication is never raised.

III. EDUCATIONAL SYSTEM

In their primary education students are promoted to upper classes without subject knowledge. This badly affects learning process making students inactive and lethargic. Our examination system is such that it makes students' rote memorization rather than testing their analytical and creative skills. In this process, they memorize lessons, reproduce them in exam halls and forget them in the same day itself. Students learn basic grammar at school level for the purpose of passing only in the tests and in the examinations and not to face any real life situations. Application-oriented advanced grammar is not taught in schools. Furthermore, adequate practice is not given to students to learn a language. Exposure too is far less to them. To such students it becomes difficult to cope up with the syllabus of English at graduation level. Students full of new dreams and aspirations enter the college but to face this language problem.

Most of the students fail to stand the testing period of learning through English, often develop a complex and discontinue their studies.

IV. LANGUAGE REDUCED AS SUBJECT

English language is taught and learnt as one of subject for examination. The examination process of universities is related with writing skill. Students' basic concern is to get marks only to clear the examination and most of the students have only this much of attitude which reduces the interest of in learning English. Interest is lost automatically Beauty of the language is also lost.

V. MEDIUM OF TEACHING

In rural India English is taught in their mother tongue (Tamil), which leads to unwanted confusion of comparing the languages. English teacher is in a state to adopt bilingual method. ELT specialists view this as a wrong methodology. In schools, students are being taught that English is an international language. To learn this language

requires constant practice and patience. The kind of feeling that prevails among students is that it is not possible to achieve fluency or mastery over English language. This kind of tendency prevents students from learning new languages like English. Learning second language means acquiring a system of rules, but just as a very little is known about these rules, even less is known about how such rule systems are acquired. Students find it very difficult to earn a competence in those rules and in fact they have no idea of proper sentence structure. They do not even know proper pronunciation, spellings and grammatical rules. Inwardly, they dislike the English Language and hence the sole objective of the teacher and the learner remain to clear the exams. Hence, the students never realize the importance of learning English as a language. Teacher also translates everything in mother tongue.

VI. FEAR, HESITATION, AND SHYNESS

If at all a student is capable of overcoming all this obstacles, there comes fear, hesitation and shyness to block his developing interest. Students might come to know about the importance of the English language but where is the platform to develop his interest or guidance to use the little known language. Society tends to laugh at the faults of others. When a student tries to use the language his mistakes are being highlighted. His love for learning the language is nipped in the bud.

VII. AT GRADUATE LEVEL

The system followed in colleges is different from that of schools. Moreover, students have their own whims and fancies about college life because of the tremendous influence of mass-medias like theatres and satellite channels on them. These Medias project a false perception about colleges and students. On seeing such things in movies, students take it for granted. As a result of this, they have formed an image for a college and want to act upon those images. The general thinking about college among student community is that college is very liberal in dealing with the students. No one cares for anything. They do not have responsibilities at all. Whatever they think they can implement them. Attending class is not compulsory. Keeping these views in mind they find it difficult in sitting in classrooms and listening to the lessons being taught to them. All their views about a college are shattered into pieces the moment when a teacher enters in a classroom and begins to teach and impose certain restrictions on them. At this juncture, severe problems start with the slow-learners. These students too passed in the higher secondary examinations. For them, sitting and listening a language class is something an uphill task, while others listen the class with rapt attention.

The student was never given a chance to show off his little knowledge; he is often pointed out for his ignorance. Moreover teachers, even in the graduate level, fail to make the students feel at home with the language. The teachers blame the primary educational system and they don't find time to train the students from the very basic level.

VIII. REMEDIES

Awareness about the importance of communicative English should be created. Students from rural background should be encouraged to use their little known English. We need to build a systematic approach which should later be followed seriously. The teachers should be trained on modern skill. Teachers should find some way of helping pupils to enjoy their language activities by spending sometime inside the language laboratories thereby building their confidence. The English teacher should have both wide-ranging enthusiasm and Imagination. Further, for tackling the lack of vocabulary in the students, Productive and receptive use of words should be kept in mind. The students should be made to learn simple words and their usage. This will help in inculcating a habit of learning new words in them. Their newly learnt words will become a part of their own vocabulary and they will be in a position to use those words very purposefully. This enhancement of vocabulary will result into better expression.

An English teacher has to encourage the students to talk in English only. This act makes them confident. By taking extra care, the English teacher will impart the nuances spoken aspects of a language once/twice in a week as a remedial measure. When such type of spoken English classes begins, student-friendly or learner-centric environment will certainly prevail, as more and more students will participate in the session. Teachers should motivate students for participative learning. This will solve all the stumbling blocks in students. Teaching learning is not a one-way process. It is a multi-way process. As soon as the teaching is over, students should raise their doubts, clarification, etc. By doing so, students' communication skills in English will grow. To develop this, sufficient practice must be given to students in their preliminary stage. While maintaining classroom management concurrently learner-friendly atmosphere should also prevail there. This ensures students to learn more and participate more. Above all, a teacher is not only a teacher but also a friend, guide and a philosopher to students. He/she guides students not only to pass in the exam but also to face challenges and take right decisions during the time of crisis in life. This is, of course, a real and tough task ahead of a good teacher.

Inner Urge to learn the language should be developed. Need to Enrich Vocabulary and Sentence Construction. Language consists of words and sentence structures. Each day they must learn at least five new words and try to use them in their own sentences. The old method of displaying charts of difficult words, phrases and their applications on the walls and daily observance of them will help a lot.

Students must develop a habit of careful listening of English news, lectures, and explanations during tutorials, practical sessions, seminars, technical presentations, academic discussions, and academic interactions and so on. The modern Language Labs cater all their needs. They must make most of it. One cannot be an effective communicator unless one becomes an effective listener.

Speaking skills are very important for a person's professional survival and growth. It gives practice of articulating words and boosts confidence in speaking. The students of rural area must be encouraged to ask questions in order to remove their fear, as they hesitate to ask questions considering that they may commit error or go wrong. Opportunities must be given to them to voice their opinions, agreements, disagreements, and suggestions, the credits should be given for participating discussions, making presentations of project, product, graphs, tables, charts plans, maps. They must be ensured that speaking skills are the single most important criteria in hiring professionals.

Like listening and speaking, reading is crucial to effective communication. Students need to read technical and business documents: reports, proposals, magazine articles, letters, and instruction manuals. It is hard to imagine any academic professional or business work that does not require efficient reading skills.

It is said that "Reading maketh a complete man, speaking maketh a ready man and writing maketh a perfect man". Writing is very important for students and professionals in all fields. They should practice writing projects reports lab reports, summary, synopsis, abstracts, and subject notes. As they go higher on the ladder of their career they will have to handle the correspondence independently. They will require writing business letters memos, email messages, proposals, minutes, notes reports, professional summaries and so on. Both professional and students need excellent writing skills to survive and excel in their pursuits as there is hardly any academic or professional activity that does not require writing skills.

IX. CONCLUSION

Students must try hard to reach the goal. They must analyze their pros and cons and improve themselves. Teachers should always be a moral support to them. They may come across the hindrances in their path but they are not to discourage them but to improve their quality of excellence. The excellence is never a chance but it is a result of hard and sincere efforts. In this modern era the advance technology is at their disposal. They must make the best use of it and grow as a shining star.

Recent Trends Supporting to Teach Language

A. Anne Evangelin, A. Anisha Christy
Department of Mechanical Engineering
St.Anne's College of Engineering and Technology,
Panruti- 607 110, Tamilnadu, India.

***Abstract* - The English language is used very extensively as a second or foreign language in many countries throughout the world. It has been widely taught with many approaches, methods, techniques and trends. The most recent and highly developed trend is technology. Teachers have been warming up to using computers in the language classrooms. The use of new technology allows students to engage in the online communication which will be leading for success in their academic and professional pursuits.**

Keywords: Language, Learning, Teaching, Technological Resources.

1. INTRODUCTION

In recent years, teachers have incorporated various forms of technology to support their teaching and engage students in the learning process. The teachers of today cut away from the conventional trends, followed in teaching English the most recent and advanced trend of using new technology. From task design to assessment, technology has become a helpful tool in supporting the pedagogical goals. Today's language teachers must reflect on how to best integrate technology within their methodologies to enhance the effectiveness of their teaching and learning in their classrooms.

There are three technological platforms that offer tools to enhance language teaching and learning: the Web, Network-based Communication (e-mail, chat programs, wikis, blogs, etc.) and CD-ROM or Hyper Media applications. The Web offers endless sources of materials for content-based lessons and provides plentiful opportunities for interaction with the authentic cultural material. Teachers quickly discover a wealth of on line activity for their students in the form of web quests and on-line communication. By expanding the opportunities for interaction, the teacher observed their communicative potential moving from learners to communicators who actively conversed for meaningful purposes. With the introduction of networked multimedia computing and the internet, language teachers have been warming up to using computers in the language classroom. The Internet is so vast and complex that learning how to incorporate it effectively into the language classroom can be quite challenging. This paper seeks to explore how the recent technology can be used to both assist and enhance the effectiveness of teaching in English language classrooms.

2. RECENT TECHNOLOGY IN LANGUAGE CLASSROOMS:

Teachers must consider how to use new technology so that it supports effective learning. The five guidelines may be applied differently in language learning contexts and are important components in any language classroom.

1. Teachers should use technology to support the pedagogical goals of the class and curriculum. The use of technology must be subordinated to the learning goals.

2. Teachers should make the technology accessible to all learners. The technology should be used to address the learners' own needs and be useful for a variety of instructional purposes. For example, some students prefer visual activities and others prefer verbal ones.

3. Computers are often said to play at least three roles in the classroom: tutor, teacher and tool. But the most useful way to look at technology is as a tool that supports learning in a wide variety of ways.

4. Students should learn language by making effective use of technology. By using a grammar software package in the computer lab, each student can obtain instant and appropriate feedback. In this case, the grammar software might provide more effective grammar practice than the teacher could in the classroom.

5. With less time and work, efficient use of technology accomplishes learning goals for teachers and learners. For example, a listening programme on a computer can instantly replay a passage, while an older technology, such as the audio tape, may waste the students' time because it requires rewinding many times.

Use of Multimedia technology: Technological developments like multimedia computers and the Internet helps the teacher to teach language. Multimedia technology exemplified today by the CD-ROM allows a variety of media (text, graphics, sound, animation, and video) to be accessed.

Use of Internet: The Internet is a powerful tool for supporting a socio cognitive approach to language teaching, and it largely accounts for the new-found enthusiasm for using computers in the language classroom. The internet is a vast interactive medium which can be used in a myriad of ways.

3. COMPUTER MEDIATED COMMUNICATION IN A CLASSROOM:

There are a number of different approaches for using the Internet to facilitate interaction within and across discourse communities. One way is to use the online activities to foster increased opportunities for interaction within a single class. This takes place both through the computer assisted classroom discussion and through outside of class discussion. The computer-assisted classroom discussion makes use of synchronized (real-time) writing program. The class meets in a networked computer lab and students communicate through writing rather than talking.

Computer mediated communication and the Internet can facilitate an integrative approach to using technology. For example, students of English don't just study general examples and write homework for the teacher; instead they use the Internet to actually become good writers. First, the students search the Web to find articles in their exact area of specialty and then carefully read and study those specific articles. They then write their own drafts online; the teacher critiques the drafts online and creates electronic links to his own comments and to pages of appropriate linguistic and technical explanation, so that students can find additional background help at the click of a mouse. Next, using this assistance, the students prepare and publish their own articles on the Web.

4. CONCLUSION

Recent technologies in the language classroom can only be interpreted in the light of the changing goals of language education and the changing conditions in society. Language teachers now, seek not only to teach students the rules of grammar, but rather to help them gain apprenticeship into new discourse communities. This accomplished through creating opportunities for authentic and meaningful interaction both within and outside the classroom, and providing students the tools for their own social, cultural and linguistic exploration. The computer is a powerful tool for this process as it allows students access to online environments of international communication.

The successful use of technology in language teaching lies not in hardware or software but in teachers and our human capacity as teachers is to plan, design and implement effective educational activity. By using new technologies in the language classroom, teachers can better prepare students for the kind of international cross-cultural interactions which are increasingly required for success in academic, vocational or personal life.

REFERENCES

[1] Hoopingarner, Dannie "Best Practices in Technology and Language Teaching" Language and Linguistics, 2009.

[2] N.Krishnaswamy, and Lalita Krishnaswamy "Teaching English: Approaches, Methods and Technique" Chennai: Macmillan, 2005.

[3] J.H.Sandholtz, C.Ring staff & D.C.Dwyer, "Teaching with technology: Creating student-centered classrooms" New York: Teachers College Press, 1997.

[4] Warschauer Mark and Carla, Me skill. "Technology and Second Language Teaching and Learning", ed. Judith W. Rosenthal, Handbook of Undergraduate Second Language Education, Mahwah: Lawrence Erlbaum, 2000.

[5] Dr. Pralhad Pawar, "Technological resources – a new access to the language teaching," Research Journal of English Language and Literature (RJELAL), 2014.

Metal Oxide Nanocrystals - Review

L.Vijay
I Year- MECH
St.Anne's College of Engineering and Technology
Panruti

A. John Peter
Asst.professor
Department of Physics
St.Anne's College Of Engineering and Technology
Panruti

S. Masilla Moses Kennedy
Asst.professor,
Department of Physics
SSN College of Engineering Old Mahabalipuram Road
SSN Nagar, Kalavakkam

Abstract **- Size effects constitute a fascinating aspect of nanomaterials. As the size of a crystal decreases to the nanometer regime, the associated properties are increasingly governed by considerations such as the surface-area-to-volume ratio and energy quantization. Quantum confinement is a widely used terminology in the study of nanocrystals. Size quantization refers to changes in the energy-level structures of materials as the building unit size drops below a certain size. This size, which can be identified with the Bohr diameter of the material, can vary from almost 100 nm to a single nanometer or even less. The electronic structure is altered from the continuous electronic bands to discrete or quantized electronic levels leading to the size-dependent properties. Further since the properties of nanocrystals follow from the confinement of the electrons to the physical dimensions of the nanocrystals, it would be interesting to vary the shape of the nanocrystals, study on the effect of confinement of electrons in such artificial shapes, and follow by optimizing the physiochemical properties.**

Keywords: Nano crystals, luminescence, quantum confinement and phosphors.

1. INTRODUCTION

Within the broad family of functional materials, metal oxides play a very important role in many scientific and technological areas. For decades they have been extensively investigated for their physiochemical properties and useful applications by solid-state chemists. Oxides including the transition metals and rare earths, display a very wide variety of complex structures and interesting properties. These metal elements are able to form a large diversity of oxide compounds, giving the inspiration for designing new materials. The crystal structures are often fabricated by the formation of the metal-oxygen bonds to produce simple rock salt or complex oxide with varying nearly ionic to covalent or metallic. The oxidic materials exhibit fascinating electronic and magnetic properties associating with the changes in electronic structure and bonding. Additionally, metal oxides having multivalent oxidation states have attracted much attention among specialists because they often exhibit superior catalytic reaction performance.

2 TYPES OF METAL OXIDE NANOCRYSTALS

2.1. Transition metal oxides

Transition metal oxides generally show ordered defect complexes or extended defects instead of isolated point defects (Rawls 1981). They also occur as shear structures or infinitely adaptive structures. Some structure types such as rock salt, spinel, rutile, cuprite, fluorite, and corundum type structures, play an important role in the identification of their complex structures (Corpuz and Richards 2010). A variety of transition metal oxides exhibits transformations from one crystal structure to another as the temperature or pressure is varied. The phase transformations of their crystal structure often undergo the changes of the atomic, electronic or spin configuration. Transition metal oxides include both localized and itinerant *d*-electron behavior (Thiel 1998). Typical examples of transition metal monoxides are MnO, CoO, and NiO, processing the rock salt structure. The cation *d* orbitals in the rock salt structure would be splitted into t_2g and e_g sets by the octahedral crystal field of the anions. While in transition metal monoxide, TiO and NiO ($3d^2$ and $3d^8$), the *d* levels would be partially filled; hence the simple band theory predicts them to be metallic. The prediction is true in the case of TiO and to some extent in the case of VO. Stoichiometric MnO, CoO, NiO are, however, all good insulators showing

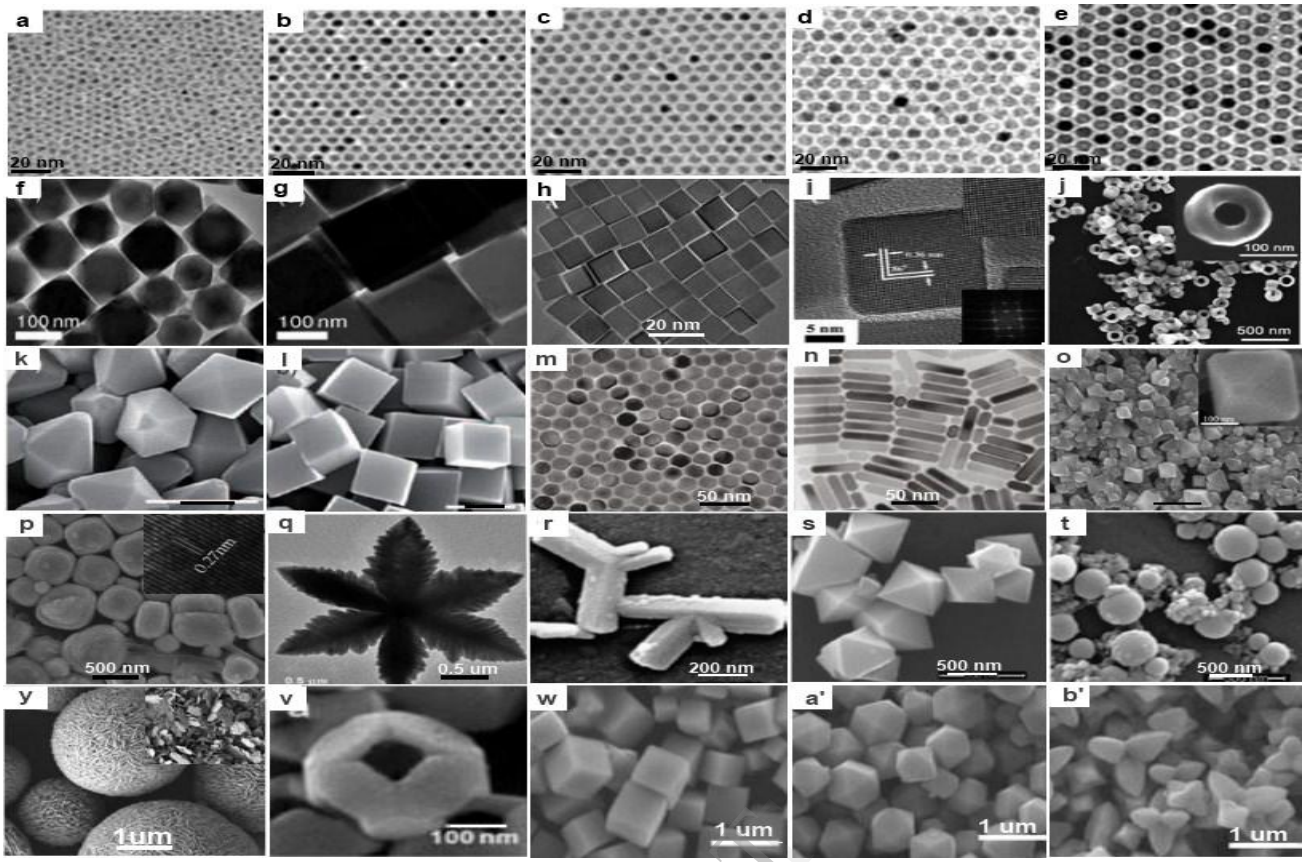

Figure 2.1. Gallery of representative TEM/HRTEM/SEM images of synthesized transition-metal oxide nanocrystals. Monodisperse iron oxide nanospheres with controlled particle sizes of (a) 6 nm, (b) 8 nm, (c) 10 nm, (d) 11 nm, (e) 13 nm(Park et al. 2005); (f) mixture of truncated cubic and truncated octahedral nanocrystals and (g) truncated nanocubes of Fe_3O_4 species (Park et al. 2005); (h,i) pseudocubic iron oxide nanocrystals, inset FFT pattern (Wang and Gao 2009); (j) single-crystalline alpha-Fe_2O_3 nanorings (Jia et al. 2008); single-crystalline iron oxide nanocrystals with (k) tetrakaidecahedron and (l) oblique parallelepiped shapes (Wang et al. 2010a); Mn_3O_4 nanocrystals with (m) spherical and (n) rod shapes and (o) $LiMn_2O_4$ nanocrystals (Wang et al. 2010c); (p) nest-like SnO nanostructures (Ning et al. 2009); (q) alpha-Fe_2O_3 nanosnowflakes, (r) Mn_2O_3 triangular nanorods, (s) CoO octahedral nanostructures, and (t) Cr_2O_3 nanospheres (Polshettiwar, Baruwati and Varma 2009); (y) hollow Cu_2O microspheres (Zhang et al. 2007a); (v) Cu_2O.

antiferromagnetism. The insulating nature of FeO can be understood by assuming that the t_{2g} subband is completely filled for the $3d^6$ configuration, but the insulating nature of MnO, CoO, NiO cannot be understood in terms of simple band theory (Baerends Evert, Gritsenko Oleg and van Leeuwen 1996).

Transition metal oxide nanocrystals are particularly useful in various applications in magnetic field (Mahmoudi et al. 2010). The synthesis of well-defined magnetic nanocrystals is an important issue, because magnetic properties change drastically with particle size. Representative TEM/HRTEM//SEM examples of a variety of transition metal oxide nanocrystals are shown in Figure 2-1. The hot injection and heat-up processes are generally carried out in hot surfactant solutions and have been widely used to synthesize uniform nanocrystals. Iron carbonyl, acetate, acetylacetonate, carboxylate, and chloride are some of the commonly used precursors for making monodisperse iron oxide nanocrystals. For example, the thermal decomposition of $Fe(CO)_5$ in octyl ether in the presence of oleic acid or lauric acid resulted in the formation of essentially amorphous iron particles (Hyeon et al. 2001). Spherical alpha-Fe_2O_3 nanocrystals could also be directly generated with size ranging from 4 to 16 nm by introducing an oxidation agent, trimethylamine *N*-oxide or $(CH_3)_3NO$, into the reaction solution. Hyeon et al.(Park et al. 2005) revealed that monodisperse iron nanoparticles with different sizes of 4, 8, 11 nm were prepared by changing the molar $Fe(CO)_5$:oleic acid ratio from 1:1 to 1:2 and 1:3. In a next step, these seed nanocrystals were reacted with iron oleate solutions of defined concentrations, resulting in monodisperse iron nanocrystals that transform into iron oxide nanoparticles of 6, 7, 8, 9, 10, 11, 12, 13 nm on exposure to air (Figure 2-5a-e). Cheon et al.(Cheon et al. 2004) had achieved the thermal decomposition of $Fe(CO)_5$ in *o*-dichlorobenzene/dodecylamine to yield alpha-Fe_2O_3 nanocrystals with controlled different shapes, including diamonds (40%), triangle plates (30%), and spheres (30%). Zeng et al.(Sun and Zeng 2002) reported the synthesis of

monodisperse magnetite nanoparticles from iron(III) acetylacetonate, $Fe(acac)_3$, using a high-temperature reaction. In this approach, 4 nm magnetite nanoparticles were formed by refluxing a reaction mixture composed of $Fe(acac)_3$, diphenyl ether, 1,2-hexadecanediol, oleic acid, and oleylamine. A seeded growth process was also demonstrated for generating large nanoparticles. By controlling the ratio of seed relative to the precursor, nanoparticles up to 16 nm in diameter were obtained. Using different precursors, including $Fe(acac)_3$, iron acetate, O'Brien et al.(Redl et al. 2004) had explored the thermal decomposition of iron pentacarbonyl in trioctylamine or octyl ether in the presence of oxidants such as pyridine *N*-oxide and trimethyl *N*-oxide hydrate to wüstite Fe*x*O ($0.84 < x < 0.95$) nanocrystals. Some recent progresses for the controlled synthesis of high-quality transition metal oxide nanocrystals were achieved. The representative examples of iron oxide nanocrystals are illustrated. Gao et al. (Wang and Gao 2009) reported the morphology-controlled synthesis and magnetic property of pseudocubic iron oxide nanoparticles using the mixture of iron(III) chloride/sodium oleate/oleic acid/ethanol. Lu et al.(Wang et al. 2010a) synthesized the single-crystalline iron oxide nanocrystals with tetrakaidecahedron and oblique parallelepiped shapes and high-index facets exposed in high yields through the solvothermal reaction of a mixture of $K_3[Fe(CN)_6]$, N_2H_4, sodium carboxymethyl cellulose at 160 ^oC for 6 h. Magnetic properties of these two kinds of nanocrystals displayed shape-dependent magnetic behaviors. Raabe et al.(Jia et al. 2008) presented a novel approach for synthesizing single-crystalline alpha-Fe_2O_3 nanorings with outer diameters of 150-170 nm, inner diameters of 70-100 nm, and heights of 80-120 nm, employing a double anion-assisted hydrothermal treatment of the aqueous solution of $FeCl_3$, $NH_4H_2PO_4$, Na_2SO_4 at 220 °C for 48 h. Gao et al.(Wang and Gao 2009) have prepared alpha-Fe_2O_3 nanoparticles enclosed by six (Burda et al.) of planes, in which the uniformity of morphology should be further improved. Yan et al.(Jia et al. 2005a) reported on the synthesis of single-crystalline alpha-Fe_2O_3 nanotubes through a coordination assisted dissolution process involving the selective adsorption of phosphate ions on hematite. Zeng et al.(Xu and Zeng 2004) synthesized Co_3O_4 nanocubes smaller than 10 nm and their superstructures by adding capping agent Tween-85 into their reaction system.

Considerable effort has been devoted to the development of alternative energy storage/conversion devices with high power and energy densities because of the up-coming depletion of fossil fuels. Recent progress has been devoted to synthesis and electrochemical applications for oxide nanomaterials. For example, the solvothermal reaction of $Mn(NO_3)_2$/oleylamine/dodecanol recently flourished by Li et al.(Wang et al. 2010c) was a successful way for shape control of highly monodisperse Mn_3O_4 nanocrystals with dot, rod wire shapes. Moreover, the as-prepared hydrophobic spherical or elongated nanoparticles were used as building blocks to be rationally assembled into three-dimensional (3D) Mn_3O_4 colloidal spheres with a facile ultrasonication route. The as-prepared colloidal spheres were chemically converted to $LiMn_2O_4$ nanomaterials in a simple solid-state reaction. Such materials showed distinct electrochemical performance, mainly depending on their crystallinity and particle size. Dai et al.(Wang et al. 2010d) reported a two-step solution-phase method for growing Mn_3O_4 nanoparticles on graphene oxide to form a Mn_3O_4-reduced graphene oxide hybrid material. The grown of Mn_3O_4 nanoparticles on graphene oxide sheets includes two steps: (i) hydrolysis of $Mn(CH_3COO)_2$ in a graphene oxide suspension with a 10:1 *N*,*N*-dimethylformamide (DMF)/H_2O mixed solvent at 80 °C, (ii) distribution of well-crystallized Mn_3O_4 nanoparticles on graphene oxide sheets by transferring the above reaction solution to deionized water and treated in hydrothermal conditions at 180 °C for 10 h. The gas-liquid interfacial route was used to synthesize water-soluble Fe_3O_4 nanoparticles in iron nitrate, ethylene glycol (EG) and ammonia solution. The Fe_3O_4 nanoparticles could be incorporated into a carbon matrix under the hydrothermal method and such materials exhibited excellent anode materials for high-performance Li^+-ion batteries (Cui et al. 2009b). The vanadium pentoxide (V_2O_5) has been attracting much attention in low-cost energy battery because it can serve as the anode in Li ion battery design or as the cathode material in rechargeable Li ion batteries.

2.2 Rare earth oxides

The chemically similar fourteen elements in the bottom of periodic table ranging in atomic number from 57 to 71 are known as the lanthanoids that have in common an open 4*f* shell. The lanthanides are sometimes referred to as the "rare earths" which originates from the isolation of these elements early in their discovery (Greinacher 1981). The lanthanide ions are trivalent and their physiochemical properties principally originate from the trivalent ions which are important rather than those of the neutral atoms. A series of lanthanide thus possesses many similar chemical and physical properties to the other members of the lanthanoid group. It is noted that lanthanum should be considered a member of the lanthanide family as it lacks *f*-electrons (Le roy and Holmberg 1963). The Group III transition metals Sc and Y are also frequently included in discussions about the lanthanides due to having many similar properties to the lanthanide family of elements. The electron configuration of the lanthanides range from [Xe] $6s^25d^1$ for lanthanum (La) to [Xe] $6s^24f^{14}5d^1$ for lutetium (Lu). The 4f orbitals lie well inside the electronic shell and are well protected from external influences by the filled 6*s* and 5*p* orbitals. Although the trend is observed from the atomic radii, it is best shown by the radii of the trivalent cations. A consequence of the lanthanide contraction is that holmium (Ho^{3+}) is the same size as the much lighter Y^{3+} with corresponding similar properties. The majority of the optical properties of the lanthanide ions can also be attributed to the shielded nature of the 4*f* orbitals (Moeller 1967).

Recently, high-quality rare-earth nanocrystals have drawn great attention because of their unique physical and chemical properties and potential applications in the fields

of catalysis, luminescence devices, optical transmission, biochemical probes, medical diagnostics, and so forth (Shen, Sun and Yan 2008, Zhang et al. 2010a). The different synthetic routes have been developed to a number of size- and shape-controlled dispersible rare earth oxide nanocrystals. Representative TEM//HRTEM/SEM examples of a variety of rare earth oxide nanocrystals are shown in Figure 2-5. Yan et al.(Si et al. 2005) synthesized the single-crystalline and monodisperse cubic rare-earth (RE = La to Lu, Y) oxide nanocrystals with plate and disk shapes via a nonhydrolytic approach in oleic acid/oleylamine/1-octadecene using various rare-earth complexes, including acetylacetonate, benzoylacetonate, and acetate, as the precursors. The selective adsorption of coordinating oleic acid ligands onto specific crystal planes of cubic RE_2O_3 nanocrystals made them adopt a plate shape with the confined growth of facets and/or a disk shape with the confined growth of facets. The as-prepared high-quality luminescent Y_2O_3:Eu ultrathin nanodisks displayed strong surface-dependent, highly pure red emissions that were due to selective incorporation of Eu^{3+} ions in the surface of the nanodisks (Si et al. 2006). The hydrolysis of metal nitrates in octadecylamine to generate the rare earth (Ce) and transition (Ni, Zn, Co) oxide nanocrystals was achieved by Li et al.(Wang et al. 2008a). Subsequently, calcination was carried out to remove the surfactants to produce mesoporous metal oxides by surfactant-assisted self-assembly process, which showed large pores thermally stable pore mesostructures, and potential applications in catalysis and lithium-ion batteries. By thermolysis of rare-earth benzoylacetonate complexes in oleic acid/oleylamine, Xu et al.(Zhang et al. 2007d) synthesized the Y_2O_3:Tb nanorods were obtained by self-assembly of long-chain alkyl amine-capped nanocrystals prepared from thermolysis of yttrium-oleate complexes.

Gao et al.(Yang and Gao 2006) reported the shape- and size-controlled synthesis of uniform CeO_2 nanocubes by reaction of cerium nitrate aqueous solution and *tert*-butylamine in toluene/oleic acid at 180 °C via a solvo-hydrothermal two-phase process. Adschiri et al.(Zhang et al. 2007b) modified this reaction system for the synthesis of CeO_2 nanocubes using cerium hydroxide precursors under supercritical water conditions. The product shape could be controlled by tuning the interaction of organic molecules with various crystallographic planes of fluorite cubic ceria. The morphology and displayed crystallite plane of CeO_2 nanocrystals could be controlled by the length of dicarboxylic acids (Taguchi et al. 2009). The ceria nanocrystals with spherical, wire, and tadpole shapes were controllably fabricated via a nonhydrolytic sol-gel process using oleic acid and oleylamine as cosurfactant (Yu et al. 2005b).

Very recently, Si et al.(Du et al. 2007b) synthesized ceria nanocrystals via an alcohothermal process at 180 °C in ethanol, using alkylamine as the base and polyvinylpyrrolidone as the stabilizer, and furthermore, the ceria nanocrystals were self-organized into chainlike and dendritic nanostructures by oriented attachment. Xia el al.(Yu et al. 2010) recently synthesized the CeO_2 nanosheets with lateral dimensions up to 4 μm and thickness of ~2.2 nm by the heating of the aqueous cerium nitrate solution in the presence of 6-aminohexanoic acid ligand. Yan et al.(Zhou et al. 2008) reported a rapid thermolysis of $(NH_4)_2Ce(NO_3)_6$ in oleic acid/oleylamine to generate the CeO_2 nanoflowers from the aggregation of tiny particle by a unique 3D oriented-attachment mechanism due to a well-maintained balance of the nucleation and growth stages. The CO catalytic performance of CeO_2 nanocatalysts with different shapes were illustrated. For CO conversion to CO_2 from 200 to 400 ^oC, the activity of the catalysts followed the trend of nanoflowers > nanopolyhedra > nanocubes, in good agreement with the order of the specific surface areas. This result indicated that the flower-shaped catalyst with higher specific surface area could provide more active sites for CO conversion.

Pure ZrO_2 can exist in three polymorphs at atmospheric pressure, e.g., monoclinic (*m*, between room temperature and 1170 °C), tetragonal (*t*, between 1170 and 2370 °C), and cubic (*c*, between 2370 and 2706 °C) phases (Srinivasan et al. 1993, Rashad and Baioumy 2008). Tang et al.(Tang et al. 2008) reported one-step controllable synthesis for ultrafine ZrO_2 nanocrystals via a two-phase interface hydrolysis reaction under hydrothermal conditions. The coexisting *m*- and *t*-ZrO_2 nanocrystals can be found under this condition.

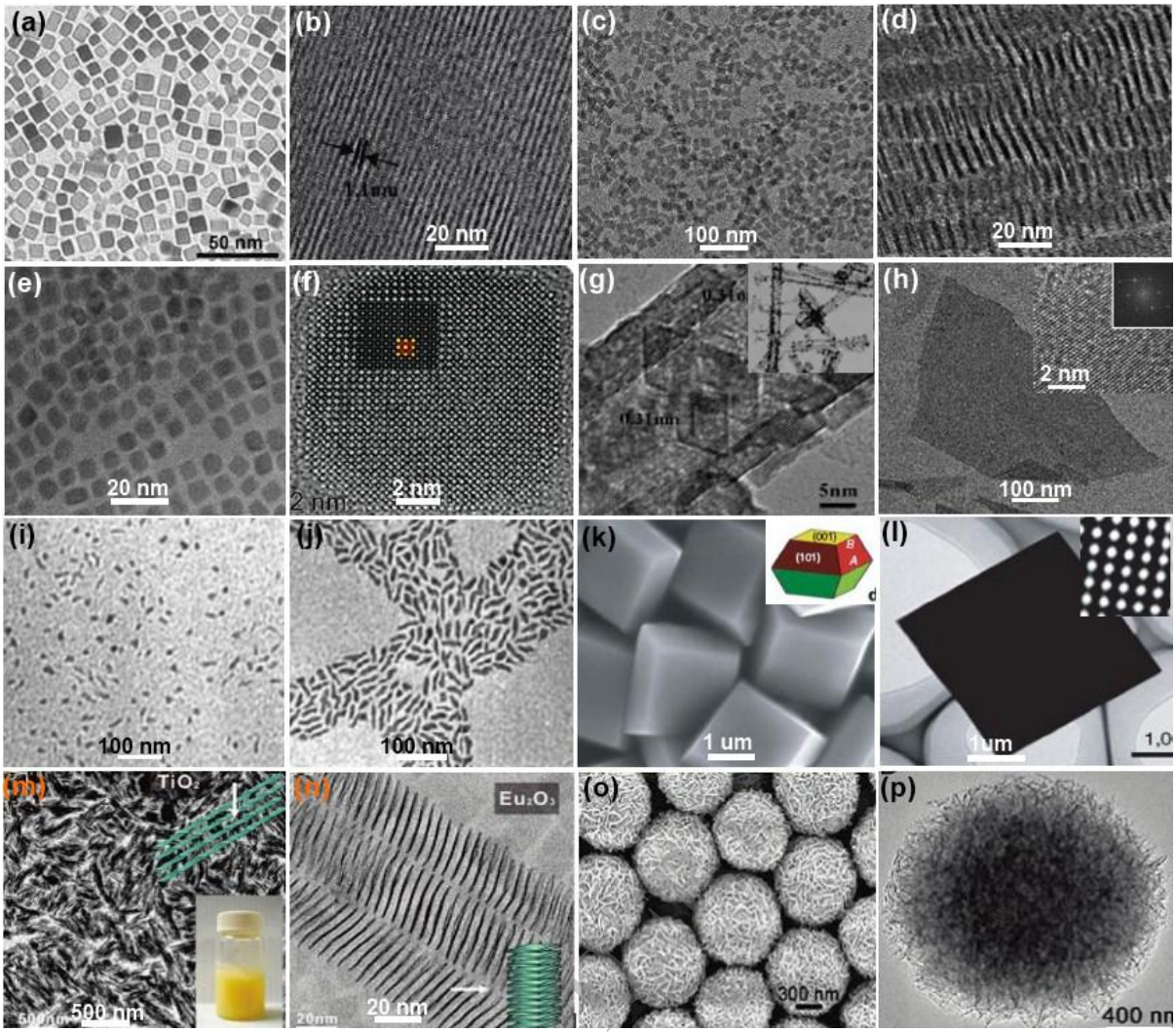

Figure 2.2. Gallery of representative TEM/HRTEM/SEM images of transition-metal oxide nanocrystals: (a) CeO_2 nanocubes (Wang et al. 2008a); Sm_2O_3 with (b) wire, (c) square, (d) plate shapes (Yu et al. 2006); (e,f) CeO_2 nanocubes (Yang and Gao 2006); (g) CeO_2 nanotubes (Zhou, Yang and Yang 2007); (h) CeO_2 nanosheets (Yu, Lim and Xia 2010); (i,j) ZrO_2 nanorices (Zhao et al. 2006); (k,l) single-crystalline truncated TiO_2 nanocrystals (Yang et al. 2008); (m) TiO_2 rod-shaped superstructures, inset of an image of the as-prepared gel-like product; (n) Eu_2O_3 nanodisks (Huo et al. 2009); (o,p) TiO_2 microspheres (Chen et al. 2010a).

Zhao et al.(Zhao et al. 2006) reported the mixed *m*- and *t*-ZrO_2 nanocrystals synthesized via a two-phase approach. Lin et al.(Lin, Zhang and Lin 2007) reported the mixed *m*- and *t*-ZrO_2 nanocrystals synthesized via the pechini-type sol-gel process. Becker et al.(Becker et al. 2008, Zheng et al. 2009) reported mixed *m*- and *t*-ZrO_2 nanocrystals synthesized in near- and supercritical water and supercritical isopropyl alcohol. The phase stability of nanocrystalline ZrO_2 depends upon the size, e.g., the critical size is 10 nm. The tetragonal ZrO2 and monoclinic ZrO_2 can coexist between 11 and 30 nm, while pure monoclinic ZrO_2 is stable with the size above approximately 30 nm. Becker et al. (Bremholm, Becker-Christensen and Iversen 2009) regarded that the critical particle size stems from the difference in the surface energy of the two ZrO_2 polymorphs, with *t*-ZrO_2 being lowest. The structure of nanomaterials surfaces contributes significantly to the energetic character of nanomaterials. The nonhydrolytic sol-gel reaction between zirconium(IV) isopropoxide and zirconium(IV) chloride at 340 °C to generate large quantities of highly monodisperse tetragonal zirconia nanocrystals (~4 nm) were performed by Hyeon et al.(Joo et al. 2003).

CONCLUSION:

Nanostructured metal oxide materials have been the focus of intense research by chemists and materials scientists in various fields due to both their unique properties and technological applications (Seshadri 2005, Burda et al. 2005, Mao et al. 2007, Yin and Alivisatos 2005). Metal oxides including the transition metals and rare earths, display a wide variety of complex structures and interesting electronic and magnetic properties associated with the changes in electronic structure and bonding and in the presence of ordered defect complexes or extended defects.

Furthermore, the size- and shape-dependent properties of nanomaterials raising expectations for a better performance generally are a consequence of quantum confinement within the particle (Alivisatos 1996).

REFERENCES

[1] Abbet, S. & U. Heiz. 2005. Nanocatalysis. Wiley-VCH Verlag GmbH & Co. KGaA.
[2] Alivisatos, A. P. (1996) Semiconductor Clusters, Nanocrystals, and Quantum Dots. Science, 271, 933-937.
[3] Bigioni, T. P., X.-M. Lin, T. T. Nguyen, E. I. Corwin, T. A. Witten & H. M. Jaeger (2006) Kinetically driven self assembly of highly ordered nanoparticle monolayers. Nat Mater, 5, 265-270.
[4] Burda, C., X. Chen, R. Narayanan & M. A. El-Sayed (2005) Chemistry and Properties of Nanocrystals of Different Shapes. Chemical Reviews, 105, 1025-1102.
[5] Cushing, B. L., V. L. Kolesnichenko & C. J. O'Connor (2004) Recent Advances in the Liquid-Phase Syntheses of Inorganic Nanoparticles. Chemical Reviews, 104, 3893-3946.
[6] Jun, Y.-w., J.-s. Choi & J. Cheon (2006) Shape Control of Semiconductor and Metal Oxide Nanocrystals through Nonhydrolytic Colloidal Routes. Angewandte Chemie International Edition, 45, 3414-3439.
[7] Kamat, P. V., K. Tvrdy, D. R. Baker & J. G. Radich (2010) Beyond Photovoltaics: Semiconductor Nanoarchitectures for Liquid-Junction Solar Cells. Chemical Reviews, 110, 6664-6688.
[8] Kinge, S., M. Crego-Calama & D. N. Reinhoudt (2008) Self-Assembling Nanoparticles at Surfaces and Interfaces. ChemPhysChem, 9, 20-42.
[9] Kroes, G.-J., A. Gross, E.-J. Baerends, M. Scheffler & D. A. McCormack (2002) Quantum Theory of Dissociative Chemisorption on Metal Surfaces. Accounts of Chemical Research, 35, 193-200.
[10] MalenfantPatrick, R. L., J. Wan, S. T. Taylor & M. Manoharan (2007) Self-assembly of an organic-inorganic block copolymer for nano-ordered ceramics. Nat Nano, 2, 43-46.
[11] Mao, Y., T.-J. Park, F. Zhang, H. Zhou & S. S. Wong (2007) Environmentally Friendly Methodologies of Nanostructure Synthesis. Small, 3, 1122-1139.
[12] Moores, A. & F. Goettmann (2006) The plasmon band in noble metal nanoparticles: an introduction to theory and applications. New Journal of Chemistry, 30, 1121-1132.
[13] Na, H. B., I. C. Song & T. Hyeon (2009) Inorganic Nanoparticles for MRI Contrast Agents. Advanced Materials, 21, 2133-2148.
[14] Nagarajan, R. 2008. Nanoparticles: Building Blocks for Nanotechnology. In Nanoparticles: Synthesis, Stabilization, Passivation, and Functionalization, 2-14. American Chemical Society.
[15] Park, J., J. Joo, S. G. Kwon, Y. Jang & T. Hyeon (2007) Synthesis of Monodisperse Spherical Nanocrystals. Angewandte Chemie International Edition, 46, 4630-4660.
[16] Rao, C. N. R., A. Müller & A. K. Cheetham. 2005. Nanomaterials – An Introduction. Wiley-VCH Verlag GmbH & Co. KGaA.
[17] Redl, F. X., K. S. Cho, C. B. Murray & S. O'Brien (2003) Three-dimensional binary superlattices of magnetic nanocrystals and semiconductor quantum dots. Nature, 423, 968-971.
[18] Schmid, G. 2005. General Introduction. Wiley-VCH Verlag GmbH & Co. KGaA.
[19] Sellinger, A., P. M. Weiss, A. Nguyen, Y. Lu, R. A. Assink, W. Gong & C. J. Brinker (1998) Continuous self-assembly of
[20] Organic-inorganic nanocomposite coatings that mimic nacre. Nature, 394, 256-260.
[21] Seshadri, R. 2005. Oxide Nanoparticles. Wiley-VCH Verlag GmbH & Co. KGaA.
[22] Shopsowitz, K. E., H. Qi, W. Y. Hamad & M. J. MacLachlan (2010) Free-standing mesoporous silica films with tunable chiral nematic structures. Nature, 468, 422-425.
[23] Sorensen, C. M. 2009. Particles as Molecules. John Wiley & Sons, Inc.
[24] Yin, Y. & A. P. Alivisatos (2005) Colloidal nanocrystal synthesis and the organic-inorganic interface. Nature, 437, 664-670.
[25] Ying, J. Y. (2000) Nanostructural tailoring: Opportunities for molecular engineering in catalysis. AIChE Journal, 46, 1902-1906.
[26] Zhang, H., E. W. Edwards, D. Wang & H. Mohwald (2006) Directing the self-assembly of nanocrystals beyond colloidal crystallization. Physical Chemistry Chemical Physics, 8, 3288-3299.

High Resolution Optical Satellite Remote Sensing Images in Road Tracking System using UPF

J. Subashini, S. Sudha and D. Arulmozhi
Department Of Electronics & Communication Engineering
St.Anne's College Of Engineering And Technology Anguchettypalayam,
Panruti – 607 110

***Abstract* - A typical way to update map is to compare recent satellite images with existing map data, detect new roads and add them as cartographic entities to the road layer. At present image processing and pattern recognition are not robust enough to automate the image interpretation system feasible. For this reason we have to develop image interpretation systems that rely on human guidance. More importantly road maps require final checking by a human due to the legal implementations of error. Our proposed technique is applied to Indian Remote Sensing and IKONOS satellite images using Unscented Particle Filter. Unscented particle filter is used for tracing the median axis of the single road segment. The Extended Kalman Filter is probably the most widely used estimation algorithm for road tracking. However, more than 35 years of experience in the estimation community has shown that is difficult to implement and is difficult to tune. To overcome this limitation, unscented particle filter is introduced in road tracking which is more accurate, easier to implement, and uses the same order of calculations as linearization. The principles and algorithm of unscented kalman filter and unscented particle filter were also discussed. The core of our system is based on profile matching. Unscented Particle filter traces the road beyond obstacles and tries to find the continuation of the road finding all road branches initializing at the road junction. The completeness and correctness of road tracking from the Indian Remote Sensing and IKONOS images were also compared**.

I. INTRODUCTION

Network of roads is an essential mode of transportation, and provides the backbone for human civilization. Hence, it is vital to maintain and restore roads to keep our transportation network being connected. Roads usually appear as dark lines while viewing from satellite images which are mostly true in rural as well as sub-urban areas. Ongoing research has led to a gamut of methods that automate the digitization process. Digitization methods for road extraction are either automatic or semi-automatic in nature. In the literature, an automatic method implies a fully automatic process. Theoretically, a fully automatic approach requires no human intervention, but this is not practical. Consider a method of automatic method; no human intervention is needed for road feature extraction at the initial or post-processing stage. Some of the automatic initialization system has been proposed based on Geographical Information System(GIS) or geographical database This paper proposes a method based on UKF. The UKF component is responsible for tracing axis coordinates of a road beyond obstacle or an intersection, tracing road branches on the other side of a road junction. There are also other improvements in our works in comparison with previous methods. The most common way of applying the KF to a nonlinear system is in the form of the extended kalman filter(EKF).In the EKF, the probability distribution function(pdf) is propagated through a linear approximation of the system around the operating point at each time instant. In doing so, the EKF needs the Jacobian matrices which may be difficult to obtain for higher order systems. Further the linear approximation of the system at a given time instant may introduce errors in the state which may lead the state to diverge over time.In order to overcome the drawbacks of the EKF,other nonlinear estimators have been developed such as the unscented kalman filter(UKF),the ensembled Kalman filter(EnKF).The overall impression is that the performance of the UKF is better than the EKF in terms of robustness and speed of convergence. The computational load in applying the UKF is comparable to the EKF. The principels and algorithm of EKF and UKF. The results of the road tracking and junction detection using UKF To compare recent satellite images with existing map data. To detect new roads and add them as cartographic entities to the road layer. At present image processing and pattern recognition are not robust enough For this reason we have to develop image interpretation systems that rely on human guidance. More importantly road maps require final checking by a human due to the legal implementations of error. So it is difficult to implement and is difficult to tune. To find the continuation of the road finding all road branches initializing at the road junction we use UPF filter

II. SYSTEM OVERVIEW

The road tracking process starts with an initial human input of a road segment, which indicates the road centerline. From this input, the computer learns relevant road information, such as starting location, direction, width, reference profile, and step size. This information is then used to set the initial state model and the related parameters

A. Prototype of the road tracking system

In most of the road tracking methods the following assumptions are made regarding road characteristics as mentioned in

- Roads are elongated,
- Road surfaces are usually homogeneous,
- There is adequate contrast between road and adjacent areas.

However these assumptions are not always true. In curved areas or ramps, the road may not be elongated. The road surface may be built of various materials that appear quite difference in the image. Background objects such as trees, houses, vehicles and shadows may occlude the road

surface and may strongly influence the road appearance. Road surfaces may not have adequate areas because of road texture, lighting, and weather conditions. Preprocessing stage includes the reference profile extraction and seed point selection. Monochromatic imagery is utilized in this technique. The tracking module is composed of the UKF module. The starting point includes the co-ordinates of the road center, road direction and a course estimate of the road width at that point. Starting from the initial point ,UKF module can sequentially proceed to the next point on the road by using some artificially defined time step .The distance along the road is considered to be as the time steps .In each step the process uses noisy measurement to obtain the best estimate of the state of the road at that point, with reference with the updated profile. Since road profile is usually different at the intersection (ie) it is usually wider, hence the result of the profile matching is not reliable for obtaining measurement. The UKF will stop after S number of steps. The value of S must be large enough to let the PF module to pass over regularsized obstacles and junctions. If UKF module cannot find any valid road branches after S steps, it will announce that the road is a dead-end road.

Figure.1 A sample of a high resolution IKONOS image

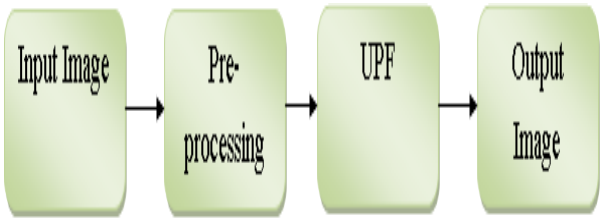

III. PREROCESSING

The preprocessing module consists of two components namely reference profile extraction and estimation of road width.

A. Reference profile extraction

An initial reference profile is extracted as a vector of grey levels from the road segment entered by the human operator. Later, new profiles are extracted from new human inputs and placed into a profile list for further use. To improve robustness of the system, we use two dimensional road features, i.e. in addition to searching along a line perpendicular to the road direction; we also search a line along the road direction. The method uses the least square error profile matching to measure the similarities between any two profiles and also to estimate the optimum shift that exist between them. Profile are extracted in both directions and combined.

The parallel profile is useful since grey level values vary little along the road direction, whereas this is not the case in off-road areas. Thus the risk of of-road tracking is reduced and, in turn, tracking errors are reduced. From each human input, we obtain a profile sequence that contains the road surface texture information which may include occluding objects we also search a line along the road direction. whereas this is not the case in off-road areas. Thus the risk of of-road tracking is reduced and, in turn, tracking errors are reduced. From each human input, we obtain a profile sequence that contains the road surface texture information which may include occluding objects

B. *Extraction of road width*

Road width determines whether road profile can be correctly extracted or not. In our approach the road width is the road width is estimated at the beginning of the tracking. A road segment is entered by the human operator with two consecutive mouse clicks with the axis joining the points defining the road center line. We assume that the roadsides are straight parallel lines on both sides of the road axis. Road width can be estimated by calculating the distance between the roadsides.Road edges, in turn can be calculated by means of sobel gradient mask.The gradient of the profile along the profile direction is calculated and one point is selected at both sides of the axis point where the largest gradient is found.

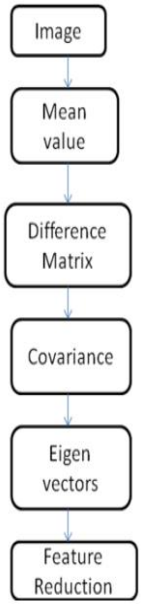

Fig1. Flow of band reduction process

IV. PRINCIPLES AND ALGORITHM OF EKF AND UPF

The state vector contain the variable of interest It describes the state of the dynamic system and represents its degree of freedom. The variable in the state vector cannot be measured directly but they can be inferred from values that measurable. In case of road tracking from an image ,it includes where rk and ck are the coordinates of road axis points, θk is the direction of the road, t θ & and is the change in road direction. The distance along the road is considered to be as time variable.

A. EKF

To illustrate the principle behind the EKF, consider the following example. Let W be a random vector and

$$y = g(x) \quad (1)$$

be a nonlinear function, g : Rn → Rm. The question is how to compute the pdf of y given the pdf of xi For example, in the case of being Gaussian, how to calculate the mean (y) and covariance (Σy) of y> If g is a linear function and the pdf of x is a Gaussian distribution, then Kalman filter (KF) is optimal in propagating the pdf. The state vector contain the variable of interest. It describes the state of the dynamic system and represents its degree of freedom. The variable in the state vector cannot be measured directly but they can be inferred from values that measurable. In case of road tracking from an image, it includes where rk and ck are the coordinates of road axis points, θk is the direction of the road, t θ & and is the change in road direction. The distance along the road is considered to be as time variable.

PARTICLE FILTERING

Multiple dynamics models are used to account for the motion uncertainty due to target We assume the motion mode state According to the idea of variable-structure multiple-model approach, whereas the stopped mode is active only when there is no detection. The stopped mode is added to the active mode set when the target is no longer detected and removed after the target is detected again. The target dynamics models for different target modes have the same linear Gaussian structure large process noise along the road is used, which is of the order of the magnitude of the maximum acceleration. Much smaller process noise is used. In the stopped model, the process noise is set to zero. The target velocity in the stopped target model is also set to zero

ALGORITHM

A number of semi-automated RNE approaches require a human operator to specify the seed points before a higher level operation can continue with the extraction process, Automating the seeding process reduces the total extraction time of such a system significantly. According to Harvey the performance of automatic road tracking algorithm depends to a large extend on the quality of starting points. Apart from automating process the quality of the seed points is consequently also imperative.

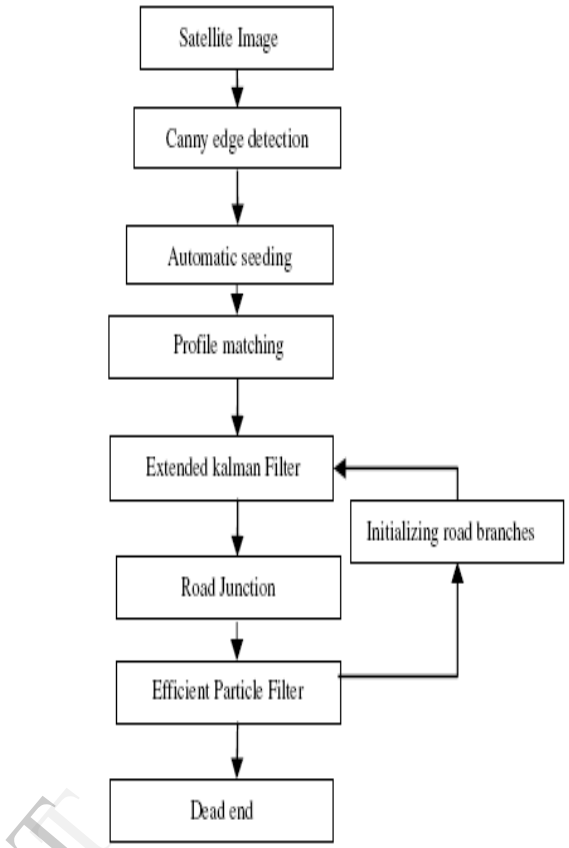

Automatic seeding

The workflow of the road extraction method is as shown in Fig 3. In the content of road extraction, seeding is the process whereby a marker is placed at certain points of interest within a road network. These points of interest can include markers along the centre of the road, point of high curvature, or intersections. The seeds are typically single points but can also be centreline segments or road regions. Seeding is not an extraction technique itself, but the marker are used as initialization points for extraction technique, such as road tracker and snakes

3.2 Canny edge detection

The Canny method finds edges by looking for local maxima of the gradient of the image. The gradient is calculated using the derivative of a Gaussian filter. The Canny method applies two thresholds to the gradient: a high threshold for low edge sensitivity and a low threshold for high edge sensitivity. Edge starts with the low sensitivity result and then grows it to include connected edge pixels from the high sensitivity result. This helps fill in gaps in the detected edges. Thus canny edge detection is considered to be the best edge detection when compared to other technique.

Profile matching

A gray-level profile, extracted perpendicular to the road direction, is a very characteristic property on a road. It often shows a good contrast between the road surface and its vicinity. Thus, like in, we also utilized the method of gray-level profile matching to acquire observations needed in the tracking algorithm. The method in uses the least square error profile matching to measure the similarities between any two profiles and also to estimate the optimum shift that exists between them. In our approach, the correlation coefficient and the difference between the profile means are used to calculate the error or difference between any two profiles.

Extended Kalman Filtering

The state vector contain the variable of interest. It describes the state of the dynamic system and represents its degree of freedom. The variable in the state vector cannot be measured directly but they can be inferred from values that measurable. In case of road tracking from an image, it the direction of the road,& and is the change in road direction.

Particle Filtering

Multiple dynamics models are used to account for the motion uncertainty due to target We assume the motion mode state According to the idea of variable-structure multiple-model approach, whereas the stopped mode is active only when there is no detection. The stopped mode is added to the active mode set when the target is no longer detected and removed after the target is detected again. The target dynamics models for different target modes have the same linear Gaussian structure large process noise along the road is used, which is of the order of the magnitude of the maximum acceleration. Much smaller process noise is used. In the stopped model, the process noise is set to zero. The target velocity in the stopped target model is also set to zero

EFFICIENT PARTICLE FILTERING

The efficient particle filter for road-constrained target tracking is designed based on the optimal particle filtering theory for jump Markov linear Gaussian systems. Analytic approximation is made for the target state distribution; approximation is needed mainly because the observation model is nonlinear, though the target dynamics is modeled as linear system with Gaussian noise.

V.RESULTS AND DISCUSSION FOR EXPEECTED OUTPUT

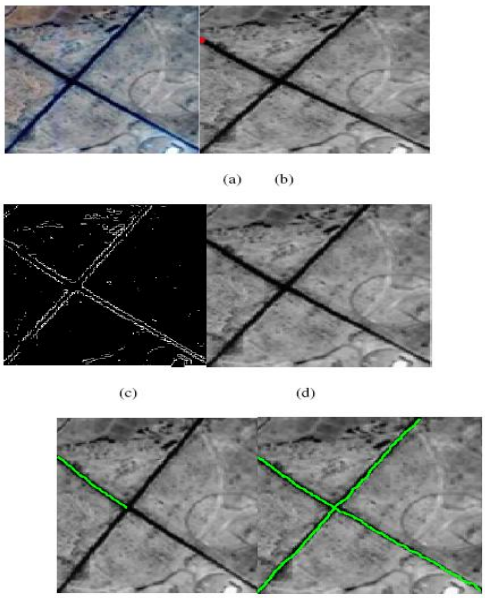

Automatic road tracking results from an IRS image using Efficient particle filtering (a) Satellite image (b) Monochromatic imagery (c) Automatic seeding (d) Edge detection using Canny edge detection (e) Road tracking by EKF (f) Road tracking by Efficient particle filtering and EKF.

VI. CONCLUSION

The method of extraction developed in this research, and the proposals for future work aimed at automating the initial step of the identification and selection of road segment points, may only work on high-resolution images. As, these processes need edge information for extraction, and geometric (width)and radiometric radiometric/intensity variation) characteristic information across the road along the direction of road, to identify and select road segment points. This information may exist only in high-resolution images, where roads exist as long continuous features with uniform width; in the case of low-resolution images, roads exist as long bright lines that may disappear or exist as very thin features after the pre-processing step. A deficiency of the algorithm is the slow operation of the PF module. Hence, to overcome this drawback a set of training data sequence can be used to automatically optimize the parameters of a particle filter. Furthermore ,performance of the algorithm on more complex uran areas is yet to be evaluated, which might necessitate some Advantage of High performance accuracy, Accurate Detection & Edge preservation is high for recognition and. Applications is Computer Vision &Pattern Recognition

REFERENCES

[1] J.Zhou,W.F.Bischof and T.Caelli,"Road tracking in aerial images based on human computer interaction and Bayesian filtering,"ISPRS J.Photogram.Remote sens.,vol.61,no.2,pp.108-124,2006
[2] J.Mena, "State of the art on automatic road extraction for GIS update: A novel classification," Pattern Recognit. Lett., vol. 24, no. 16,pp. 3037– 3058, Dec. 2003.
[3] Mckeown,D.Denlinger,J.L.,"Cooperative methods for road tracking in aerial imagery",In:Workshop Comput.Vision Pattern Recognition,pp.662- 673,1988
[4] G. Vosselman and J. D. Knecht, "Road tracing by profile matching and Kalman filtering," in Proc. Workshop Autom. Extraction Man-Made Objects Aerial Space Images, Birkhaeuser, Germany
[5] M. Bicego, S. Dalfini, G. Vernazza, and V. Murino, "Automatic roadextraction from aerial images by probabilistic contour tracking," in Proc.ICIP, 2003, pp. 585–588.

Performance Enhancements using Query Specific Semantic Signatures on Web Image Re-Ranking

S. Rosemary(M.E),
Lecturer/Dept.of CSE,
Annai Velankani Polytechnic College,
Panruti, India.

J. R. Thresphine (M.Tech),
Assistant Professor/Dept of CSE,
Prist University,
Puducherry, India.

***Abstract*--- Re-ranking of images has provided an efficient solution for the user to get the intended image. Nowadays, several search engines like Bing, Google, Ask are available to provide a pool of images. Then, the user selects a needed image, and then the remaining images are re-ranked. The proposed work introduces Query-Specific Semantic Signatures, which has offline and online part, in offline it learn semantic space of all textual information and in online images are re-ranked based on the semantic signatures.**

***Keywords*—**

I. INTRODUCTION

Image processing is a method to convert an image into digital form and perform some operations on it, in order to get an enhanced image or to extract some useful information from it. It is a type of signal dispensation in which input is image, like video frame or photograph and output may be image or characteristics associated with that image. Usually Image Processing system includes treating images as two dimensional signals while applying already set signal processing methods to them. It is among rapidly growing technologies today, with its applications in various aspects of a business. Image Processing forms core research area within engineering and computer science discipline too.

Image processing basically includes the following three steps: Importing the image with optical scanner or by digital photography.Analyzing and manipulating the image which includes data compression and image enhancement and spotting patterns that are not to human eyes like satellite photographs.Output is the last stage in which result can be altered image or report that is based on image analysis. The purpose of image processing is divided into 5 groups. They are:

- Visualization - Observe the objects that are not visible.
- Image sharpening and restoration - To create a better image
- Image retrieval - Seek for the image of interest.
- Measurement of pattern – Measures various objects in an image.
- Image Recognition – Distinguish the objects in an image.

The two types of methods used for Image Processing are Analog and Digital Image Processing. Analog or visual techniques of image processing can be used for the hard copies like printouts and photographs. Image analysts use various fundamentals of interpretation while using these visual techniques. The image processing is not just confined to area that has to be studied but on knowledge of analyst to display the images.

Association is another important tool in image processing through visual techniques. So analysts apply a combination of personal knowledge and collateral data to image processing. Digital Processing techniques help in manipulation of the digital images by using computers. As raw data from imaging sensors from satellite platform contains deficiencies. The three general phases that all types of data have to undergo while using digital technique are Pre- processing, enhancement and display, information extraction.

The Characteristics of Image Processing includes, Before going to processing an image, it is converted into a digital form. Digitization includes sampling of image and quantization of sampled values. After converting the image into bit information, processing is performed. This processing technique may be Image enhancement, Image restoration, and Image compression.

A. Image enhancement

It refers to accentuation, or sharpening, of image features such as boundaries, or contrast to make a graphic display more useful for display & analysis. This process does not increase the inherent information content in data. It includes gray level & contrast manipulation, noise reduction, edge crispening and sharpening, filtering, interpolation and magnification, pseudo coloring, and so on.

B. Image restoration

It is concerned with filtering the observed image to minimize the effect of degradations. Effectiveness of image restoration depends on the extent and accuracy of the knowledge of degradation process as well as on filter design. Image restoration differs from image enhancement in that the latter is concerned with more extraction or accentuation of image features.

C. Image compression

It is concerned with minimizing the number of bits required to represent an image. Application of compression are in broadcast TV, remote sensing via satellite, military communication via aircraft, radar, teleconferencing, facsimile transmission, for educational & business documents, medical images that arise in computer tomography, magnetic resonance imaging and digital radiology, motion, pictures, satellite images, weather maps, geological surveys and so on.

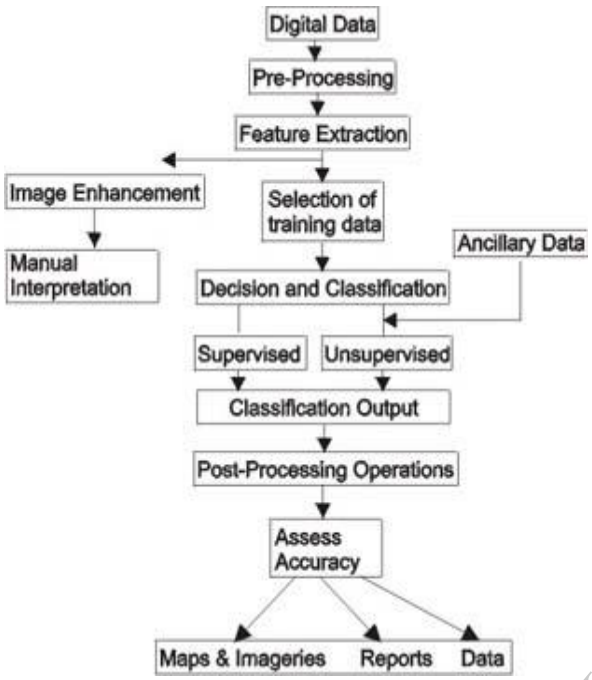

Fig. 1.Working Diagram of Image Processing

II. RELATED WORK

We have witnessed great interest and a wealth of promise in content-based image retrieval as an emerging technology. In this article, we survey almost 300 key theoretical and empirical contributions in the current decade related to image retrieval and automatic image annotation, and in the process discuss the spawning of related subfields. We also discuss significant challenges involved in the adaptation of existing image retrieval techniques to build systems that can be useful in the real world. In retrospect of what has been achieved so far, we also conjecture what the future may hold for image retrieval research.

Traditional methods of image retrieval require that meta-data is associated with the image, commonly known as keywords. These methods power many World Wide Web search engines and accomplish reasonable amounts of search accuracy. Though some content based image retrieval (CBIR) systems use both semantic and primitive attributes to match search criteria, history has proven that it is difficult to extract linguistic information from a 2D image. In this research, activity theory is used as a base to demonstrate how semantic information can be retrieved from objects identified in an image. Using an image segmentation technique by The Berkeley Digital Library Project (Blob world), and combining it with object-to-community relationships, a high-level understanding of the image can be demonstrated.

Relevance feedback schemes based on support vector machines (SVM) have been widely used in content-based image retrieval (CBIR). However, the performance of SVM-based relevance feedback is often poor when the number of labeled positive feedback samples is small. This is mainly due to three reasons: 1) an SVM classifier is unstable on a small-sized training set, 2) SVM's optimal hyper plane may be biased when the positive feedback samples are much less than the negative feedback samples, and 3) over fitting happens because the number of feature dimensions is much higher than the size of the training set. In this paper, we develop a mechanism to overcome these problems. To address the first two problems, we propose an asymmetric bagging-based SVM (AB-SVM). For the third problem, we combine the random subspace method and SVM for relevance feedback, which is named random subspace SVM (RS-SVM). Finally, by integrating AB-SVM and RS-SVM, an asymmetric bagging and random subspace SVM (ABRS-SVM) is built to solve these three problems and further improve the relevance feedback performance.

Web image search using text queries has received considerable attention. However, current state-of-the-art approaches require training models for every new query, and are therefore unsuitable for real-world web search applications. The key contribution of this paper is to introduce generic classifiers that are based on query-relative features which can be used for new queries without additional training. They combine textual features, based on the occurrence of query terms in web pages and image meta-data, and visual histogram representations of images. The second contribution of the paper is a new database for the evaluation of web image search algorithms. It includes 71478 images returned by a web search engine for 353 different search queries, along with their meta-data and ground-truth annotations. Using this data set, we compared the image ranking performance of our model with that of the search engine, and with an approach that learns a separate classifier for each query. Our generic models that use query-relative features improve significantly over the raw search engine ranking, and also outperform the query-specific models.

III. EXPERIMENTAL ARCHITECTURE

WEB-SCALE image search engines mostly use keywords as queries and rely on surrounding text to search images. They suffer from the ambiguity of query keywords, because it is hard for users to accurately describe the visual content of target images only using keywords. For example, using "apple" as a query keyword, the retrieved images belong to different categories (also called concepts in this paper), such as "red apple," "apple logo," and "apple laptop."

This is the most common form of text search on the Web. Most search engines do their text query and retrieval using keywords. The keywords based searches theyusually provide results from blogs or other discussion boards. The user cannot have a satisfaction with these results due to lack of trusts on

blogs etc.low precision and highrecall rate. In early search engine that offered disambiguation to search terms. User intention identification plays an important role in the intelligent semantic search engine.

In this paper, a novel framework is proposed for web image re-ranking is shown in the figure 2. Instead of manually defining a universal concept dictionary, it learns different semantic spaces for different query keywords individually and automatically. The semantic space related to the images to be re-ranked can be significantly narrowed down by the query keyword provided by the user. For example, if the query keyword is "apple," the concepts of "mountain" and "Paris" are irrelevant and should be excluded. Instead, the concepts of "computer" and "fruit" will be used as dimensions to learn the semantic space related to "apple." The query-specific semantic spaces can more accurately model the images to be re-ranked, since they have excluded other potentially unlimited number of irrelevant concepts, which serve only as noise and deteriorate the re-ranking performance on both accuracy and computational cost. The visual and textual features of images are then projected into their related semantic spaces to get semantic signatures. At the online stage, images are re-ranked by comparing their semantic signatures obtained from the semantic space of the query keyword. The semantic correlation between concepts is explored and incorporated when computing the similarity of semantic signatures.

We propose the semantic web based search engine which is also called as Intelligent Semantic Web Search Engines. We use the power of xml meta-tags deployed on the web page to search the queried information. We use the power of xml meta-tags deployed on the web page to search the queried information. The metadata information of the pages is extracted from this xml into rdf. our practical results showing that proposed approach taking very less time to answer the queries while providing more accurate information.

The visual features of images are projected into their related semantic spaces automatically learned through keyword expansions offline.

Our experiments show that the semantic space of a query keyword can be described by just 20-30 concepts (also referred as "reference classes").

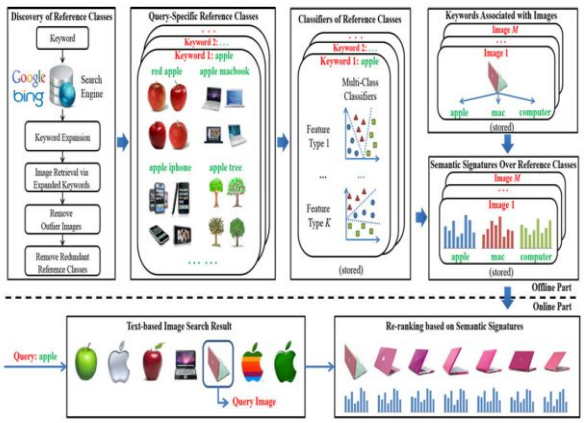

Fig. 2. System architecture

Therefore the semantic signatures are very short and online image re-ranking becomes extremely efficient. Because of the large number of keywords and the dynamic variations of the web, the semantic spaces of query keywords are automatically learned through keyword expansion.

Query-specific semantic signatures effectively reduce the gap between low-level visual features and semantic. Query-specific semantic signatures are also effective on image re-ranking without query images being selected. Collecting information from users to obtain the specified semantic space.

Localizing the visual characteristics of the user's intention in this specific semantic space is achieved.

1) Re-Ranking accuracy

The labelers were unaware of what reference classes have been discovered by our system. The number of image categories is also different than the number of reference classes. Each image was labeled by at least three labellers and its label was decided by voting.

2) Re-Ranking Images outside Reference Class

If the category of a query image corresponds to a reference class, we deliberately delete this reference class and use the remaining reference classes to train classifiers and to compute semantic signatures when comparing this query image with other images.

3) Incorporating Semantic Correlations

The re-ranking precisions for all types of semantic signatures on the three data sets. Notably, QSVSS SingleCorr achieves around 10 percent relative improvement com-pared with QSVSS Single, reaching the performance of QSVSS multiple despite its signature is six times shorter.

4) Re-Ranking with Semantic Based

It assumes that images returned by initial text-only search have a dominant topic and images belonging to that topic should have higher ranks. Our query-specific semantic signature is effective in this application since it can improve the similarity measurement of images. In this experiment QSVSS Multiple is used to compute similarities. Thus, the above Graph shows that the, after re-ranking Apple-fruit has high voting than the apple iphone, apple logo.

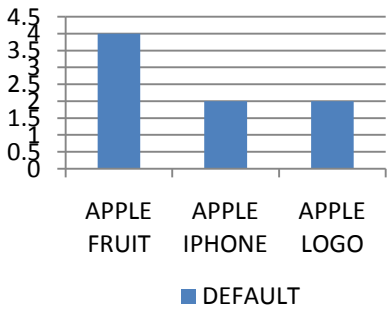

Fig. 3 Graph Analysis

IV. CONCLUSION

We propose a novel framework, which learns query-specific semantic spaces to significantly improve the effectiveness and efficiency of online image re-ranking. The visual features of images are projected into their related semantic spaces automatically learned through keyword expansions offline. The extracted semantic signatures can be 70 times shorter than the original visual features, while achieve 25-40 percent relative improvement on re-ranking precisions over state-of-the-art methods. In the future work, our framework can be improved along several directions. Finding the keyword expansions used to define reference classes can incorporate other metadata and log data besides the textual and visual features. For example, the co-occurrence information of keywords in user queries is useful and can be obtained in log data. In order to update the reference classes over time in an efficient way, how to adopt incremental learning under our framework needs to be further investigated. Although the semantic signatures are already small, it is possible to make them more compact and to further enhance their matching efficiency using other technologies such as hashing.

As a future enhancement we propose the problem of solving the ambiguity. This solution is the future enhancement where the contribution of providing more accuracy to the proposed system by enhancing using ambiguity resolving problem. Ambiguity is, Middle vision is the stage in visual processing that combines all the basic features in the scene into distinct, recognizable object groups.

As a future enhancement we propose the problem of solving the ambiguity. This solution is the future enhancement where the contribution of providing more accuracy to the proposed system by enhancing using ambiguity resolving problem. Ambiguity is, Middle vision is the stage in visual processing that combines all the basic features in the scene into distinct, recognizable object groups.

REFERENCES

[1] R. Datta, D. Joshi, and J.Z. Wang, "Image Retrieval: Ideas, Influences, and Trends of the New Age," ACM Computing Surveys, vol. 40, article 5, 2007.

[2] A.W.M. Smeulders, M. Worring, S. Santini, A. Gupta, and R. Jain, "Content-Based Image Retrieval," IEEE Trans. Pattern Analysis and Machine Intelligence, vol. 22, no. 12, pp. 1349-1380, Dec. 2000.

[3] Y. Rui, T.S. Huang, M. Ortega, and S. Mehrotra, "Relevance Feedback: A Power Tool for Interactive Content-Based Image Retrieval," IEEE Trans. Circuits and Systems for Video Technology, vol. 8, no. 5, pp. 644-655, Sept. 1998.

[4] X.S. Zhou and T.S. Huang, "Relevance Feedback in Image Retrieval: A Comprehensive Review," Multimedia Systems, vol. 8, pp. 536-544, 2003.

[5] D. Tao, X. Tang, X. Li, and X. Wu, "Asymmetric Bagging and Random Subspace for Support Vector Machines-Based Relevance Feedback in Image Retrieval," IEEE Trans. Pattern Analysis and Machine Intelligence, vol. 28, no. 7, pp. 1088-1099, July 2006.

[6] J. Cui, F. Wen, and X. Tang, "Real Time Google and Live Image Search Re-Ranking," Proc. 16th ACM Int'l Conf. Multimedia, 2008.

[7] J. Cui, F. Wen, and X. Tang, "Intent Search: Interactive on-Line Image Search Re-Ranking," Proc. 16th ACM Int'l Conf. Multimedia, 2008.

[8] X. Tang, K. Liu, J. Cui, F. Wen, and X. Wang, "Intent Search: Capturing User Intention for One-Click Internet Image Search," IEEE Trans. Pattern Analysis and Machine Intelligence, vol. 34, no. 7, pp. 1342-1353, July 2012.

[9] N. Rasiwasia, P.J. Moreno, and N. Vasconcelos, "Bridging the Gap: Query by Semantic Example," IEEE Trans. Multimedia, vol. 9, no. 5, pp. 923-938, Aug. 2007.

[10] C. Lampert, H. Nickisch, and S. Harmeling, "Learning to Detect Unseen Object Classes by Between-Class Attribute Transfer," Proc. IEEE Conf. Computer Vision and Pattern Recognition (CVPR), 2009.

Automatic Vehicle accident detection & Localization of Automobile using GPS/GSM.

L.Vincent Antony Raj[1] , Be(Cse),Student,
E.Venkatraman[2], Be(Cse),Student,
St.Anne's College Of Engineering And Technology,Panruti

Abstract: **The Rapid growth of technology and infrastructure has made our lives easier. The advantage of technology has also increased the traffic hazards and the road accident take place frequently which causes huge loss of life and property because of the poor emergency facilities. Our project will provide an optimum solution to this draw back. An integrated Cell phone GPS-GSM system is proposed to track vehicles using Google Earth application develop in android application for mobile system. The remote module has a Bluetooth mounted on the moving vehicle with attached accident detecting sensor to identify if accidents happens. Here Bluetooth will be the medium of communication with the user mobile for activating the GPS position of the cell phone. In this case cell phone will get activated its application and track the current position of the vehicle and send it to the remote located predefined phone for tracking the real time position of the situation. After data processing, Google Earth application can be used to view the current location and status of each vehicle. (To detect the real time localization of the vehicle using Bluetooth technology with GPS locator in cell phone using android application.)**

Keywords: Bluetooth system, cell phone GPS-GSM technology, android application, accident place locator

I. INTRODUCTION

The ability to accurately detect a vehicle‟s location and its status is the main goal of automobile trajectory monitoring systems.& also The high demand of automobiles has also increased the traffic hazards and the road accidents. This is because of the lack of best emergency facilities available in our country This design is a system which can detect accidents in significantly less time and sends the basic information to first aid center within a few seconds covering geographical coordinates, the time and angle in which a vehicle accident had occurred. This alert message is sent to the rescue team in a short time, which will help in saving the valuable lives. These systems are implemented using several hybrid techniques that include: wireless communication, geographical positioning and embedded applications. project will establish a communication between the control station and the unit installed in vehicles. Vehicles will have GPS/GSM enabled tracking modules and will be tracked in real time using cellular networks. The software embedded in the microcontroller will control the various operations of the device by monitoring waveform from the vibration sensor. In case of accident the device will send an alert message along with location data from GPS module to control station using GSM network. It is a comprehensive and effective solution to the poor rescue response in case of accident. The accident reporting can automatically find a traffic accident, search for the spot and then send the basic information to the rescue agency covering geographical coordinates and the time and circumstances in which a traffic accident took place. At the server end, a control function will extract relevant data

1.1 *Automatic Accident Detection and Reporting System using GSM and GPS:*

From prototypes will be polled in real time. Our system Traffic has become an important event in the national combines advanced hardware design and sophisticated interest now-a-days. We see that a lot of life spoils in control technology into a compact, reliable package. every accident because of typically long response time to access the appropriate care that may be available if The vehicle tracking systems are designed to assist informed in-time. Application of our project can corporations with large number of automobiles and several significantly shorten the response time of accident. This is usage purposes. A Fleet management system can minimize a platform for emergency rescue which will operate the cost and effort of employees to finish road assignments optimally in order to reduce the golden time of arrival of within a minimal time. Besides, assignments can be rescuers in case of road accidents, when every micro- scheduled in advanced based on current automobiles second counts. Our project aims to present a technology location. Therefore, central fleet management is essential automatically detecting the accident and a hardware to large enterprises to meet the varying requirements of tracking device based on GSM/GPS technology informing customers and to improve the productivity [1]. So taking at the occurrence of accident with sufficient details like in action all these things we are going to design and exact location and time at which accident happened. This develop a machine, which will track the real time location

of the vehicle using blue tooth technology with the help of an android base mobile phones. The ability to accurately detect a vehicle‟s location and its status is the main goal of automobile trajectory monitoring systems. These systems are implemented using several hybrid techniques that include: wireless communication, geographical positioning and embedded applications. The vehicle tracking systems are designed to assist corporations with large number of automobiles and several usage purposes. This system can minimize the cost and effort of employees to finish road assignments within a minimal time. So taking in action all these things we are going to design and develop a machine, which will track the real time location of the vehicle using blue tooth technology with the help of an android base mobile phones.

The main goals of this project is to design and develop an economical model, which requires less power with less complex in structure, easy to implement. An additional setting could be implemented to interface the system to the car‟s alarm to alert the owner on his cell phone if the alarm is set off. The automobile‟s airbag system can also be wired to this system to report severe accidents to immediately alert the police and ambulance service with the location of the accident

II. LITERATURE REVIEW

Traditionally, navigation systems have been large, expensive, and used only in aviaion or military applications. However, the presence of the GPS and the recent proliferation of small low-cost motion sensors have made possible navigation systems that are small and inexpensive enough to be used in consumer products. Commercial consumer-grade navigation systems are, in fact, readily found today in Japan, Europe, and the United States, with one application being automobile navigation systems.

The concept of in-vehicle navigation systems is not new, but implementations of such systems are relatively recent. Programs investigating the possibility of establishing an infrastructure to support widespread navigation for motor vehicles began in the U.S. as early as the late 1960‟s. However, results from these studies deemed that the supporting infrastructure for such a system would be too expensive, and further study in the United States was dropped until the 1980‟s. In the late 1980‟s, the U.S. government, recognizing that parts of the country‟s road system were taxed nearly to capacity, launched a campaign to promote the application of high-tech solutions to enhance roadway efficiency. Outlined in the National Program Plan for Intelligent Transportation Systems (NPP), this campaign includes a strategy for improving the efficiency of the U.S. highway system over a 20-year period. The NPP‟s goals include reducing highway congestion and fuel consumption and the number of traffic accidents by providing drivers with real-time traffic information, route guidance, electronic toll collection, knowledge of a vehicle‟s location lies at the heart of many services described in the NPP (e.g., route guidance and emergency response). In Japan, research efforts in real-time automobile route guidance were begun in the 1970‟s with the goal of reducing traffic congestion. Throughout the 1970‟s and 1980‟s, the Japanese government, in cooperation with industry, was continuously involved in launching initiatives which helped to mature vehicle navigation technology. Today, most Japanese car manufacturers offer factory-installed navigation systems in at least some of their models. Estimates indicate that, by the year 2000, per annum sales of vehicles with factory-installed navigation systems will be reach 2.5 million.

Many researchers have proposed the use of cutting edge technologies to served the target of vehicle tracking. These technology include Communication remote Control, GPS, GIS server systems and others.

III. ARCHITECTURE OF GPS TRACKING AND GSM MODULES

In this paper, we describe the design of a proposed tracking system in this paper is designed to track and monitor automobiles‟ status that are used by certain party for particular purposes, this system is an integration of several modern embedded and communication technologies. To provide location and time information anywhere on earth, Global Positioning System (GPS) is commonly used as a space-based global navigation satellite system. The location information provided by us GPS systems can be visualized using Google Earth technology. In wireless data transporting, Global System of Mobile (GSM) and Short Message Service (SMS) technology is a common feature with all mobile network service providers. Utilization of SMS technology has become popular because it is an inexpensive, convenient and accessible way of transferring and receiving data with high reliability. As shown in figure (1), the proposed system consists of: in-vehicle GPS receiver, GSM modems (stationary and in-vehicle), and embedded controller. The users of this application can monitor the location graphically on Google Earth; they also can view other relevant information of each automobile in the fleet.

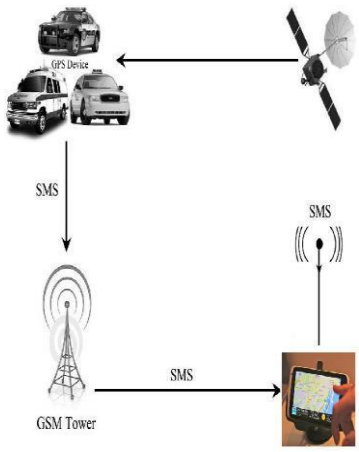

advanced vehicle collision avoidance systems, and automatic notification to authorities in the event of a traffic

The implemented tracking system can be used to monitor

various parameters related to safety, emergency services and engine stall. The paper shows an implementation of several modern technologies to achieve a desirable goal of fleet monitoring and management.

The system has two main modules, as shown in figure (2). The first module is the tracking device which is attached to the moving automobile. This module composes of a GPS receiver, Microcontroller and GSM Modem The GPS Receiver receives the location information from satellites in the form of latitude and longitude real time reading. The Microcontroller has three main tasks to read certain engine parameters from automobile data port (OBD-II), to processes the GPS information to extract desired values and to transmit this data to the server using GSM modem by SMS. The chosen engine parameters are Revaluation per minute, engine coolant temperature, vehicle speed.

The second module consists of a recipient GSM modem and workstation PC. The modem receive the SMS that includes GPS coordinates and engine parameters. This text is processed using a Visual Basic program to obtain the numeric parameters, which to be saved as a Microsoft Office Excel file The received reading of the GPS is further corrected by Kalman filter technology. To transfer this information to Google Earth, the Excel file is converted to KML, Keyhole Markup Language format.

Google Earth interprets KML file and shows automobile‟s location and engine parameters on the map. The system‟s efficiency is depend on the sufficiency of the used communication network.

An additional setting could be implemented to interface the system to the car‟s alarm to alert the owner on his cell phone if the alarm had set off. The automobile airbag system can also be wired to this system to report severe accidents to immediately alert the police and ambulance service with the location of the accident.

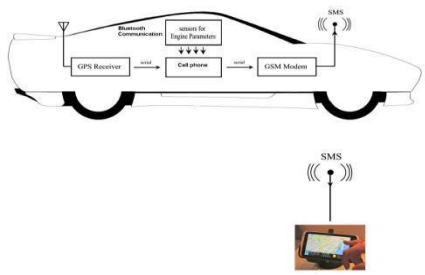

Figure 2: The system architecture: GPS tracking and GSM modules.

The second stationary module is a receiving module to collect

and process the transmitted information to a compatible format with Google Earth to remotely monitor the automobile location and status online. The transmit location of the vehicle has been filtered using Kalman filter to achieve accurate tracking. The *2DRMS* accuracy of estimated vehicle coordinates has been enhanced. The accuracy of filtered coordinates was less than 15 meters compared to about 43 meters for transmitted co-ordinates received by in vehicle GPS module.

CONCLUSION

In this paper, a real-time automobile tracking system via Google Earth is presented. The system included two main components: a transmitting embedded module to interface in-vehicle GPS and GSM devices in order determine and send automobile location and status information via SMS.

REFERENCES

[1] T. Krishna Kishore, T.Sasi Vardhan, N.Lakshmi Narayana, „Automobile Tracking Using a Reliable Embedded Data Acquisition Sysytem With GPS and GSM‟, International Journal of Computer Science and Network Security, VOL.10 No.2, 286-291, 2010.

[2] M. A. Al-Taee, O. B. Khader, and N. A. Al-Saber,“ Remote monitoring of Automobile diagnostics and location using a smart box with Global Positioning System and General Radio Service,” in Proc. IEEE/ACS AICCSA, May 13–16, 2007, pp. 385–388

[3] Tamil, E.M., D.B. Saleh, and M.Y.I. Idris, “A Mobile Automobile Tracking System with GPS/GSM Technology”, Proceedings of the 5th Student Conference on Research and Development (SCORED), Permala Bangi, Malaysia, May 2007.

[4] Fan, X., W. Xu, H. Chen, and L. Liu, “CCSMOMS:A Composite Communication Scheme for Mobile Object Management System”, 20th International Conference on Advanced Information Networking and Applications, Volume 2, Issue 18-20, April 2006, pp. 235–239.

[5] Hsiao, W.C.M., and S.K.J. Chang, “The Optimal Location Update Strategy of Cellular Network Based Traffic Information System”, Intelligent Transportation Systems Conference, 2006.

[6] Ioan Lita, Ion Bogdan Cioc and Daniel Alexandru Visan, “A New Approach of Automobile Localization System Using GPS and GSM/GPRS Transmission,” Proc. ISSE ' 06, pp. 115-119, 2006.

[7] Wen Leng and Chuntao Shi, “The GPRS-based location system for the long-distance freight”, ChinaCom '06, pp1-5, Oct.2006.

[8] Hapsari, A.T., E.Y. Syamsudin, and I. Pramana, “Design of Automobile Position Tracking System Using Short Message Services And Its Implementation on FPGA”, Proceedings of the Conference on Asia South Pacific Design Automation, Shanghai, China, 2005.

[9] C. E. Lin, C. C. Li, S. H. Yang, S. H. Lin; C. Y. Lin, “Development of On-Line Diagnostics and Real Time Early Warning System for Automobiles,” in Proc. IEEE Sensors for Industry Conference, Houston, 2005, pp. 45-51.

[10] C. E. Lin, C.-W. Hsu, Y.-S. Lee, and C.C.Li, “Verification of unmanned air Automobile flight control and surveillance using mobile communication,”J. Aerosp. Comput. Inf. Commun., vol. 1, no. 4, pp. 189–197, Apr. 2004

[11] J. E.Marca, C. R. Rindt,M.Mcnally, and S. T. Doherty, “A GPS enhanced in-Automobile extensible data collection unit,” Inst. Transp. Studies, Univ.California, Irvine, CA, Uci-Its- As-Wp-00-9, 2000.

[12] Mohammad A. Al-Khedher “Hybrid GPS-GSM Localization of Automobile Tracking system”International ournal of Computer Science & Information Technology (IJCSIT) Vol 3, No 6, Dec 2011

Reducing Mismatch Between Average and Current Queue Size using SSQRED in RED Gateways

Varadharajan D, Jeyasekar A
Dept. Of CSE, St.Annes's College Of Engineering and Technology, Panruti, India.
Dept. Of CSE, SRM University, Chennai, India.

***Abstract*-- This paper presents Single Server Queue in Random Early Detection (SSQRED) for reducing mismatch between the average queue size and current queue size. In Random Early Detection (RED), the value of average queue length increases slightly with a small weighted queue (w_q) parameter. This increases the mismatch between average and current queue length. SSQRED is applied to find the average queue length. SSQRED simulated against RED by measuring throughput, link utilization, packet loss and average delay. The results suggest SSQRED overcome the mismatch problem with the improvement in network performance.**

Keywords*: *AQM, RED, Actual queue length, Average queue length, Queuing Theory.

I. INTRODUCTION

AQM algorithm must have a more efficient congestion indicator and control function. The congestion indicator indicates whenever congestion occurs and the control function is used to avoid or control congestion [**1**]. The first developed AQM scheme to be deployed in TCP/IP networks was RED[**2**]. RED which is designed heuristically is a queue based AQM with non per-flow state [**3**]. The parameters of RED are EWMA weight (w_q), the minimum threshold (min_{th}), maximum threshold (max_{th}) and the maximum non-congestion probability of dropping (p_{max}) at the maximum threshold. Parameter-tuning is difficult in RED.

The average queue length is referred as the macroscopic behavior because it focuses on the overall and long-term behavior of a queue. The actual queue length is referred as the microscopic behavior as it focuses on the short-term behavior of the queue[QSRED algorithm]. The Red gateway calculates the average queue length using the low pass filter with an exponential weighted moving average (EWMA) [**2**]. The actual queue length is the maximum number of packets that can be enqueued.

The actual queue length will increase rapidly, when many bursts of data arrive at a RED router and eventually overflow the buffer. Since small weight (w_q) is assigned to the actual queue length, the average queue length will vary slightly. This leads to the large mismatch between the average and actual queue length. The mismatch is highly reduced, when single server queue of queuing theory is applied to find the actual queue size and average queue size for the
wired network. The paper is organized as follows. Section II deals with the related work.. Section III provides RED. Section IV examines the proposed queue management. In Section V required experimental setup is discussed Section VI examines the network performance measurement parameters. Section VII concludes the paper and the future work is discussed in Section VIII.

II. RELATED WORK

An effective mechanism for avoidance of congestion is the Random Early Detection gateways. When the average queue size exceeds the maximum threshold, RED gateways drops packets. Then the calculated average queue size is controlled. This provides Upper bound on the average delay at the gateway. A particular connection chosen by the RED gateway is proportional to the connection's share of bandwidth at the gateway. This avoids bursty traffic at the gateway**[2]**.

Studies suggest variant dynamics between average and actual queue size **[4-6].** The actual queue size increases rapidly, when the burst traffic arrives at the RED gateway. This results in the overflow of buffer. Despite congestion the average queue size increases slowly when the weight queue parameter is very small. The packet sending rate will be reduced after a congestion signal is received by the source due to the packet drop at the gateway. The actual queue size is reduced after congestion but the average queue size will remain high due to peaks in previous actual queue size. This makes Red to continue drop packets which unfairly penalizes the new packets**[7]**.

RED has difficulties detecting the mismatch between average queue size and actual queue size. This can result in RED continuing to drop packets even after the congestion is reduced. QSRED divides the buffer into six equal sectors. These sectors represent new dropping levels added to the original Red implementation. It used the actual and average queue size parameters to help RED absorb short lived bursty traffic and control congestion in a effective manner[QSRED]

Queuing theory is basically a mathematical approach applied to the analysis of waiting lines. Queuing theory uses models to represent the various types of queuing systems. Formula for each model indicates how the related queue system should perform, under a variety of conditions. Single server queuing system is the simplest queuing system to analyze. The arrivals follow poisson distribution with the mean arrival rate of λ and the service time has exponential distribution with the average service rate of μ. Utilization factor, expected number of customers in the system, average queue length, actual queue length and expected waiting time of customers in the queue and the system formulas and the corresponding notations are specified[Application of Queueing Theory for the improvement of bank service,].

The parameters used to measure network performance in wired communication are throughput, link utilization,

packet loss and average delay. For a wired network to have high performance, it should have more throughput and link utilization whereas packet loss and average delay should be less.

III. RED

The average queue length is calculated using the Exponential Weighted Moving Average (EWMA) in RED. The average queue size for non empty queue is

$$Lq \leftarrow (1 - wq)Lq + wqL \quad (1)$$

Lq represents the average queue size.
wq denotes the weighted queue parameter, $0 \leq wq \leq 1$.
L represents the current queue size.
Since the value of wq is very less i.e. it ranges from 0 to 1, the average queue size variation will be very less. Thus the difference in values between current queue size and average queue size will be high. This is illustrated in the Fig. 1.

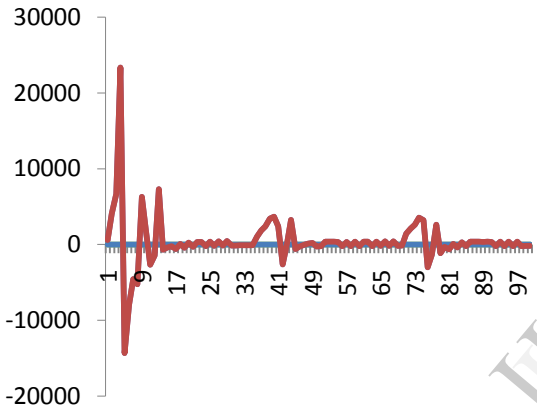

Fig. 1: Difference in Estimated and Current Queue Mismatch in RED and SSQRED

IV. PROPOSED QUEUE MANAGEMENT

The mismatch between the average queue length and the actual queue length is reduced in the proposed system. A formula is derived to find the average queue length (L_q) by applying the single server queue in queuing theory. The actual queue length, utilization factor, length of the queue in the system, arrival rate and service rate are denoted by L, ρ, L_s, $\boldsymbol{\mu}$ and λ.

$$L = \mu/\mu - \lambda \quad (2)$$

$$Ls = \rho/1 - \rho \quad (3)$$

$$Substitute\ \rho = \lambda/\mu\ in\ eqn\ 2. Then\ eqn2\ becomes$$

$$Ls = \lambda/\mu - \lambda \quad (4)$$

$$Subtracting\ eqn3\ from\ eqn1\ we\ get$$

$$L - Ls = \mu/(\mu - \lambda) - \lambda/(\mu - \lambda)$$

$$L - Ls = \mu - \lambda/\mu - \lambda$$

$$L - Ls = 1 \quad (5)$$

$$The\ average\ queue\ length\ is\ given\ by\ the\ following\ eqn$$

$$Lq = \lambda^2/\mu(\mu - \lambda) \quad (6)$$

$$Subtracting\ Lq\ from\ Ls, we\ get$$

$$Lq - Ls = \lambda^2/\mu(\mu - \lambda) - \lambda/(\mu - \lambda)$$

$$Lq - Ls = -\lambda(\mu - \lambda)/\mu(\mu - \lambda)$$

$$Lq - Ls = -\rho\ (or) Ls - Lq = \rho \quad \textbf{(7)}$$

$$from\ eqn\ 4\ Substitute\ Ls = L - 1\ in\ eqn\ 6$$

$$L - 1 - Lq = \rho$$

$$Lq = L - 1 - \rho \quad \textbf{(8)}$$

The average queue length is calculated in SSQRED. The average queue size for non empty queue is obtained using the formula

$$Lq = L - 1 - \rho$$

V. EXPERIMENTAL SETUP

The proposed queue management consists of two links. One link connects the node to the gateway and the other link connects the gateway to the sink. Drop Tail is applied between node and the gateway with a link bandwidth of 100 Mbps and a propagation delay of 100ms.

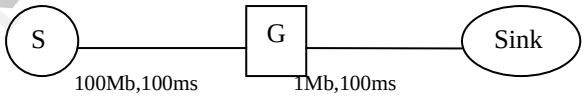

SSQRED is employed to indicate whenever there arise a congestion in the link between gateway and sink in the network with a link bandwidth of 1 Mbps and propagation delay of 100 ms. S1 denotes the source node and G denotes the gateway node. The simulation is performed for 1000 sec in ns2, estimated queue length and current queue length are measured.

VI. NETWORK PERFORMANCE

The performance of network is measured with the network performance metrics for wired networks. The four network performance measurement parameters are network throughput, packet loss, link utilization and average delay. Fig.3 to 6 depict throughput, packet loss, link utilization and average delay respectively.

In Fig.2 network throughput obtained in RED and SSQRED is plotted. In the initial stage of simulation the network throughput obtained using RED in the bottleneck link (between gateway and sink) is higher than SSQRED. In the first 46 seconds of the total simulation time i.e. 1000 sec the throughput of RED is higher than SSQRED. The throughput for RED is 139 kbps and for SSQRED is 138 kbps when the simulation time reaches 46 sec. After that as the simulation time increases the value of throughput obtained for SSQRED increases than RED. In

half way stage of simulation i.e. 500 sec the throughput for SSQRED increases over 28 kbps than RED. At the end of simulation network throughput of SSQRED increases by **15%** than RED.

In Fig.3 packet loss occurred in Red and SSQRED is plotted. The packet loss for RED is higher throughout the simulation than SSQRED. The packet loss during few seconds after the beginning of simulation say at 4 sec in Red is 116 bps and for SSQRED is only 8 bps. As the simulation progresses the packet loss in RED increases than in SSQRED. The increase in packet loss in RED over SSQRED after 500 sec is 112 bps. The increase in packet loss in RED at the end of simulation over SSQRED is **67.5%.**

In Fig.4 link utilization for RED and SSQRED is plotted. The link utilization is calculated for the bottleneck link (between gateway and sink) with a link capacity of 1 Mbps and the propagation delay of 10 ms. There is a slight difference in the link utilization between RED and SSQRED during the first quarter of the total simulation time. The difference improves during the second and third quarter of simulation. The difference in link utilization between RED and SSQRED at the end of the simulation is 12 kbps. The increase in link utilization of SSQRED over RED is **14%.**

In Fig.5 shows the average delay in RED and SSQRED. The average delay in RED is more than in SSQRED. The difference in average delay between RED and SSQRED is high during the initial stage of the simulation. The difference reduces as the simulation proceeds with RED possessing higher delay than SSQRED till the end.

From the graphs obtained it is inferred that the SSQRED has more throughput and link utilization than RED. The packet loss and average delay is less in SSQRED than RED.

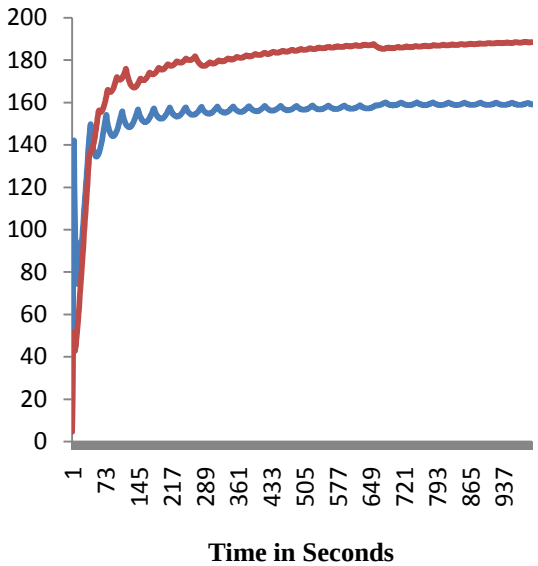

Fig. 2: Network throughput for RED and SSQRED

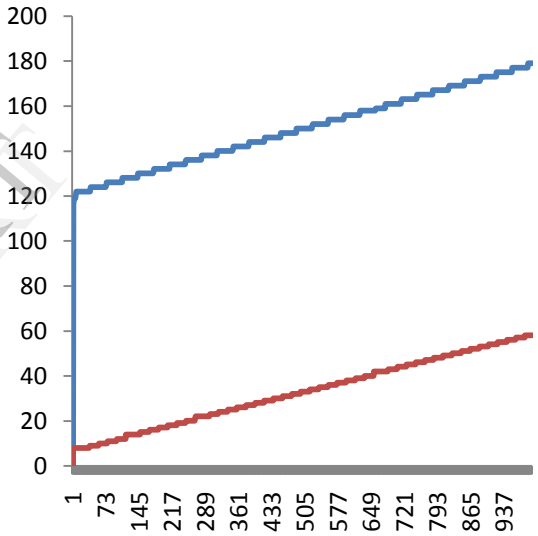

Fig. 3: Packet Loss for RED and SSQRED

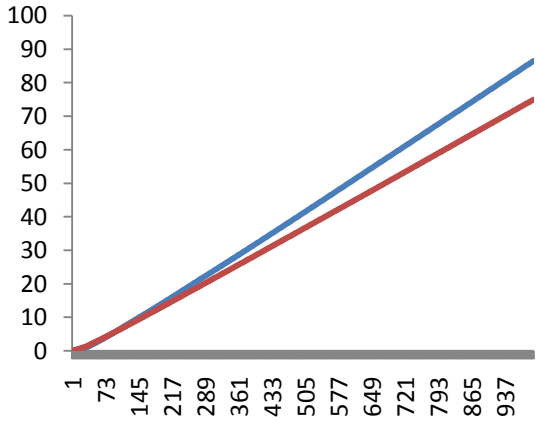

Fig. 4: Link Utilization in RED and SSQRED

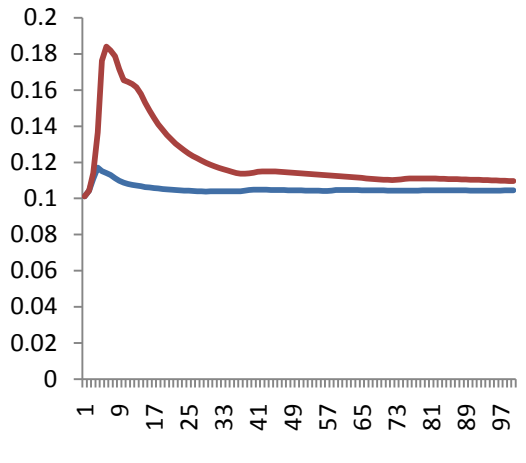

Fig. 5: Average Delay in RED and SSQRED

Thus SSQRED has high network performance when compared to RED.

VII. CONCLUSION

This paper reduces the mismatch between average queue size and current queue size of wired network using SSQRED. The mismatch increase between average and current queue size in RED is due to the low variation in the average queue size. This variation is caused by the small value of weighted queue parameter. The average queue length determined in SSQRED will not vary very much with that of the current queue length leads to the reduction in mismatch between them. The network performance is high in SSQRED than RED which is evident from the performance parameters such as throughput, packet loss, link utilization and average delay obtained.

REFERENCES

[1] Seungwan Ryu, Christopher Rump and Chunming Qiao. Advances in Active Queue Management (AQM) Based TCP Congestion Control. Telecommunication systems 25:3,4, 317-351, 2004.

[2] Sally Floyd and Van Jacobson. Random Early Detection gateways for Congestion Avoidance. IEEE/ACM Transactions on Networking. Vol. 1. No. 4. August 1993.

[3] Dong Lin and Robert Morris. Dynamics of Random Early Detection. Proc. SIGCOMM'97 Conference.

[4] christiansen, M et al.: tunning RED for Web Traffic, IEEE/ACM Trans. Net., vol. 9, no.3,pp.249 – 64, June(2001).

[5] Firoiu, V. and Borden, M.: A study of Active Queue Management for Congestion Congestion Control, Proc. INFOCOM 2000, pp. 1435-44. (2000).

[6] May, M. et al.: Influence of Active Queue Parameters on Aggregate Traffic Performance, Technical Report no. 3995, INRIA, Sophia antipolis, France, http://www.inria.fr/RRRT/RR-3995.html

[7] Nabhan Hamadneh, David Nurray, Michael Dixon and Peter Cole. Dynamic Weight Parameter for the Random Early Detection (RED) in TCP Networks. IJNCAA 2(2):342-352, The society of digital information and wireless commn. 2012.

[8] Nabhan Hamadneh, David Nurray, Michael Dixon and Peter Cole. QSRED, An Algorithm to Solve the Mismatch Between the Microscopic and Macroscopic Behavior of Red Gateways. IJCSNS, Vol.10 No.11, Nov.2010

[9] Toshiba sheikh, Sanjay kumar singh and Anil kumar kashyap. Application of Queueing Theory for the improvement of bank service. International journal of advanced computational engineering and networking, vol.1 issue-4 june-2013, issn:2320-2106

An Efficient Deduplication Storage of Virtual Machine with Bloom Filter

R. Amala,
M.E Computer Science and Engineering,
Mookambigai College of Engineering,
Pudukkotai, Tamil Nadu.

Mrs. B. Jayanthi,
Assistant Professor,CSE,
Mookambigai College of Engineering,
Pudukkotai, TamilNadu

***Abstract*—In cloud computing a virtual machine has been serving as a significant component. The virtual machine is comprised of a set of specification and configuration files and is backed by the physical resources of a host. Virtualization is run multiple operating system and applications on a single component. Existing system have reduced virtual machine files and images storage consumption. The storage area network cluster has made efforts to reduce storage consumption by use of deduplication. However, an storage area networks are very high priced, and it is difficult to satisfy increasing demand of large scale virtual machine. In this paper, we propose an exact deduplication approach that especially designed for high demand on virtual machine deployment. The design provides low storage consumption by using deduplication approach and peer to peer data transfer of instant virtual machine deployment.**

Keyword Terms—Cloud computing, virtual machine, file system, virtualization, bloom filters.

1 INTRODUCTION

Cloud Computing is the delivery of computing as a service rather than a product, are provided to computers and other devices as utility over a network. It s broad consider as possibility the next most important technology in our software industry.

Security refers to confidentiality, integrity and availability, which pose major issues for cloud computing. The Primary service model being deployed are commonly known as Software as a service, Platform as a service, Infrastructure as a service. Development models in cloud computing is Public cloud, Private cloud, Community cloud, Hybrid cloud. A virtual machine is a software computer that, like physical computers, runs an operating system and applications. The virtual machine is comprised of a set of specification and configuration files and is backed by the physical resources of a host.

Private cloud is cloud infrastructure operated solely for a single organization, whether managed internally or by a third-party, and hosted either internally or externally. Undertaking a private cloud project requires a significant level and degree of engagement to virtualized the business environment, and requires the organization to reevaluate decisions about existing resources.

When done right, it can improve business, but every step in the project raises security issues that must be addressed to prevent serious vulnerabilities. Self-run data centers are generally capital intensive. They have a significant physical footprint, requiring allocations of space, hardware, and environmental controls. These assets have to be refreshed periodically, resulting in additional capital expenditures.

The virtual machine presents a great opportunity for parallel, cluster, grid, cloud and distributed computing. Virtualization technology benefits the computers and IT industries by enabling user to share expensive hardware resource by multiplexing virtual machine on the same set of hardware hosts. Run multiple operating system and applications on a single computer. This virtualization layer is known as hypervisor or virtual machine monitor (VMM).

This leads to plain practice of storing and sharing virtual machine images and files such as storage area network and network attached storage, direct attached storage is only used for lasting for short time only storage. Cost of network storage systems are several times more than direct attached storage.

The storage consumption flow out obtain by a large number of virtual machine images and files could be identified by deduplication techniques. Existing systems have endeavour to address this flow out on a storage area network by deduplication techniques.

This is operated in assign considerable powers from the centre to its branches fashion, the deduplication is completed at virtual machines there is no equal data blocks are stored in storage area network. Nevertheless, storage area networks are high priced, and have not reduced storage consumption by using deduplication technology, and doesn't solve the bottleneck problem of metadata server.

In this paper, we have proposed, efficient deduplication storage with bloom filter using distributed file system. It is specific design for done at the same time address the above problems. The client side machine separate a whole data blocks into small data blocks, refers them by their fingerprints, and the deduplication uses to avoid storing same content data. The groups of fingerprints are saved to a meta data server and the deduplicated data blocks are saved to data server.

The client side downloads its group of fingerprints from hot backup meta data server, fetches original data blocks from data servers. The clients are peer to peer fashion, it is reduces requests directly send out to data servers.

Fast virtual machine deployment features such as instant cloning and on-demand data blocks fetching.

2 BACKGROUND

2.1 Basic Structure of Virtual Machine

Two type of basic structural of virtual machine images. First type is raw image format is only a byte by byte coping of physical disk's content into a regular file or group of regular files. Advantages of raw image format are that they have good input output performance because their byte by byte mapping is straight forward.

Nevertheless, they contain all information in the disk because this type is commonly very large in size. Another type is spare image format. It is not like byte by byte copy, the spare image format make a difficult mapping between blocks in physical disks and blocks of data in virtual machine. It is worst input and output performance compared with raw image format, this is disadvantage of spare image format.

2.2 Deduplication Techniques

Data deduplication eliminates redundant data. It only eliminates extra copies of data none of the original data is lost. It goals at improving storage utilization. The deduplication process is unique data blocks are usually identified by an examined fingerprint from their original content.

Whenever fingerprint is calculated, it will surly compared with a stored fingerprints data blocks to check for a match or not. If similar fingerprints are found, the data blocks will declared as a redundant data blocks. The redundant data blocks are removed from stored data blocks, in the place of storing the same content in multiple times.

Deduplication has two methods. There are fixed size chunking and variable size chunking. The fixed size chunking method is to break the original file into blocks of same size and except the lost block one. The simplicity is the advantage of fixed size chunking, because of data blocks are stored in same size and mapping from file system offset, file ID to data blocks. It cloud be done with very simple calculation.

Variable size chunking is more and more difficult to calculate the fingerprint of data blocks, compared with variable size chunking method, the fixed size chunking method will have better read and write performance. The fixed size chunking is good measurement of deduplication.

3 DESIGN AND IMPLEMENTATION

3.1 System Architecture

Three component more than one data servers, multiple clients and a single meta server with shadow of meta server.

The calculation of deduplication process is first virtual machine files or images are broken into fixed size data block. Each and every data block having unique fingerprint. The sequence of fingerprint is called as data blocks.

The meta server contains all file system information. This has file system offset, index extend file ID, namespace, data block's fingerprint. The fingerprints are mapping to data server. Each and every data blocks having reference count.

The data servers are controlled by the meta server. The meta server is assigned the fingerprint space to each data server. The meta server checks the data server's health periodically.

The client is a significant component because it is capable for giving reduplication on virtual machine files and images, peer-to-peer sharing of data blocks, and instant cloning. Whenever starting a new virtual machine, it creates a new virtual machine ID, name, size and data block count. Successfully create a new virtual machine. If virtual machine status is activate, then will proceed the process, otherwise if deactivated, it won't working.

The client side of file system fetches virtual machine images and files meta data information and data blocks from the meta server , data server and peer to peer clients and its provides images or files content. When shutdown of virtual machine, the client side browse the files and images and upload data into meta server, and new data blocks pushes into data server.

Peer to peer data bock sharing scheme is one advantage of an exact deduplication approach for virtual machine with bloom filter.

If meta server smashed the mirroring meta server will take over all control of the whole system. An exact copy of data blocks is stored in data server, if any crashing some data server will not damage the whole system.

The architecture of deduplication approach of virtual machine with bloom filter.

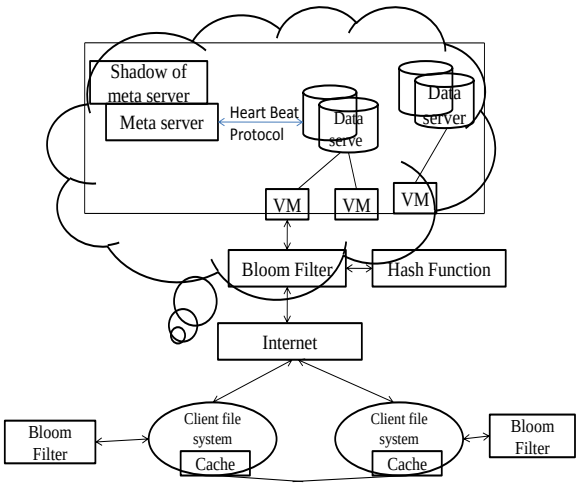

peer to peer data sharing

3.2 Fingerprint calculation

The deduplication techniques usually compare the data blocks of fingerprints to check similar data blocks. The fingerprint is smash-resistant. It is hash value calculated from data block content. Two cryptographies are MD5 and SHA-1. This hash functions are continuously used for this calculation.

The expensive of fingerprint calculation is extremely high. It is a difficult to hinder for real time deduplication. To avoid such high cost calculation of fingerprint a virtual

machine files or images are being modified, delays the calculation of fingerprint for recently modified date blocks runs deduplication techniques lazily only when it is necessary.

3.3 Caching techniques

The client side of file system contains two types of cache. There are shared cache and private cache. The shared cache maintains very recently accessed data blocks. The data blocks are read-only and currently opened in shared among all virtual machine images.

When client requested for a necessary data block, first of all it going to look it up in shared cache. Shared Cache provides distributed replicated cache to minimize the load factor. It consists the usage of two or more servers in a farm. It's replicated all data within the cluster. The big plus is simple, you have all your cache nodes on all different servers. In case one of your servers get restarted, it will receive all nodes automatically from its parent. If requested data blocks are not in shared cache, it will be waiting for data block are loaded into the shared cache. Now shared cache is filled up requested data blocks are replaced using the least recently used method. This mechanism improves the reading performance .

Private to specify that the response is cacheable only on the client and not by shared (proxy server) caches. Private cache have modified data blocks and delay calculation of fingerprint on them, after data blocks are modified in shared cache, it will be ejected from it and added to the private cache. Until data blocks are send out from the private cache, the modified data block will referred to by the private fingerprint.

No crashes will occur the private fingerprint differs from normal fingerprint. This mechanism improves the writing performance. It avoids repeated not valid calculation of fingerprint.

3.4 Data block storage

As individual files are stored directly into a local file system. According to their fingerprints split data blocks are form groups. Each group is created three files.

An extent file, an index file and a bitmap file. An extent files maintaining all the information about the data block's. An index file mapping a fingerprint of data block's offset and reference count. And a bitmap file to point out extent file is valid.

4 COMMUNICATON AMONG COMPONENTS

4.1 Heartbeat message

The meta server is take control of managing of all data servers. It checks the regular heart beat information or messages from each data server. Keep an up to date message of their health status.

In a round-robin fashion the meta server checks heartbeat messages with data servers. There are many data serves so slow to detect failed data servers. To speedup failure detection, a data server's connection problem with another data server, it will send an error message to the meta server. Immediately meta server will send the daemon thread to error according data server and it checks the heartbeat whether, it is alive or not. This is effective approach of detected failed data serves.

4.2 Peer-to-Peer Fashion

Peer to peer data bock sharing scheme is one advantage of an exact deduplication approach for virtual machine with bloom filter. All client nods are peer-to-peer fashion, unlike the client/server model, in which the client makes a service request and the server fulfills the request, the peer-to-peer model allows each node in a peer-to-peer network to function as both a client and a server.

Two computers are considered peers if they are communication with each other and playing similar roles. It allowing shared access to files and peripherals without the need for a central server.

A Bloom filter is a space-efficient probabilistic data structure, conceived by Burton Howard. That is used to test whether an element is a member of a set. False positive matches are possible, but false negatives are not, thus a bloom filter has a hundred percent recall rate.

The basic bloom filter supports two operations. There are test and add. The test is used to check whether a given element is in the set or not. If it returns, the first one is false then the element is definitely not in the set and the second one is true then the element is probably in the set. The false positive rate is a function of the bloom filter's size and the number and independence of the hash function used.

The add simply adds an element to the set. Removal is impossible without introducing false negatives, but extensions to the bloom filter are possible that allow removal for example counting filters.

The notations are S is a set of n elements. A Bloom filter is an array of m bits representing a set S = { x1, x2, … , xn} of n elements. Array set to 0 initially. k independent hash functions h1, … , hk with range{1, 2, …, m}. Assume that each hash function maps each item in the universe to a random number uniformly over the range {1, 2, …, m}. For each element x in S, the bit hi(x) in the array is set to 1, for 1 ≤ i ≤ k, A bit in the array may be set to 1 multiple times for different elements

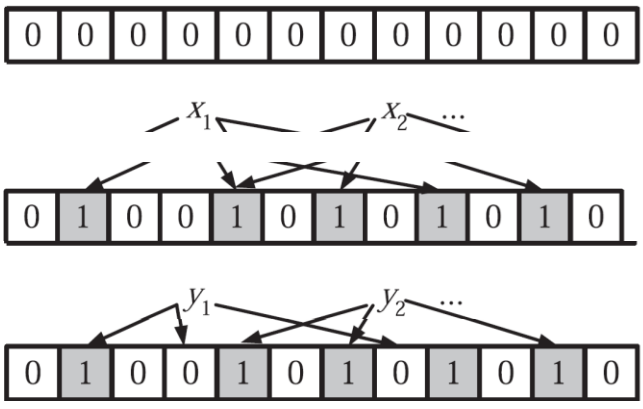

A false positive on a query of element x occurs when all of the
hash functions h1…hk applied to x return a filter position that
has a 1. Assume hash functions to be independent. Thus the probability of a false positive is

$$f = \left(1 - \left(1 - \frac{1}{m}\right) kn\right) k \cong (1 - e\frac{kn}{m})k$$

Bloom filters have random order, if bloom filter contain necessary fingerprint, it tries to bring the data blocks from a peer client. If data blocks are not in peer, the client will go and search the data blocks from the data servers. It is low cost because its simplicity.

4.3 Copy-on-read Technique

The copy-on-read techniques to carry data blocks from data server and peer clients to local cache on demand. Read-Copy Update is one such mutual exclusion method where readers threads trying to access, but not modify the data can access the shared data without acquiring any conventional lock.

4.4 On-Demand Fetching

When booting a virtual machine, even if the data blocks in the virtual machine files or images have not been all fetched into local cache, this is crucial speedup for virtual machine boot up process. Here, only accessed a part of data blocks are fetched bandwidth consumption of network is low rate.

This way is more efficient then fetching all date blocks into local cache and then booting the virtual machine. It is low read performance.

4.5 Instant cloning for virtual machine

Many virtual machine files and images are very large, and their size is several giga bytes or tera bytes. Copying those files are images byte-by-byte would be taken long time. Instant cloning is efficient solution to this problem.

Instant cloning technique provides a very simple, effective, reliable, and versatile tool for molecular cloning, chimera construction.

Copying the meta data file or images and updating data block storage, achieve cloning of a virtual machine. Modification on the cloned virtual machine files and image will not affect the original files or images, it is like copy-on-write product virtual machine could be cloned in few milliseconds in the view of user.

5. CONCLUSION AND FUTURE ENHANCEMENT

We have presented an exact deduplication file system with good input output and read write performance wide set of features. It provides good input and output performance while doing deduplication operation, and this technique avoid storing redundant data blocks. Caching techniques repeatedly accessed data blocks in memory, and only run deduplication work using has function, when it is required.

Support instant cloning virtual machine files and images by copy on read technique and to supply all information on demand fetching through network to which make something possible very fast virtual machine spread out. Peer to peer technique is highly scalable. Peer to peer data block sharing scheme is one advantage of exact deduplication approach for with bloom filter.

Virtual machine deduplication is highly effective. Caching will avoid running cost deduplication algorithms repeatedly, thus increase input and output performance.

In feature to develop a Multi Dimensional Vector in Bloom Filtering algorithm, this technique is improve the data storage and deduplication in large file system efficiently. Mainly these techniques to adapt for any bit operating system with scheduling on large scale file system on MapReduce Knowledge.

REFERENCES

[1] Data Deduplication, Sept. 2013. [Online]. Available: http://en.wikipedia.org/wiki/Data_deduplication

[2] A.V. Aho, P.J. Denning, and J.D. Ullman, ‘‘Principles of Optimal Page Replacement,’’ J. ACM, vol. 18, no. 1, pp. 80-93, Jan. 1971.

[3] A.T. Clements, I. Ahmad, M. Vilayannur, and J. Li, ‘‘Decentralized Deduplication in San Cluster File Systems,’’ in Proc. Conf. USENIX Annu. Techn. Conf., 2009, p. 8, USENIX Association.

[4] R. Coker, Bonnie++, 2001. [Online]. Available: http://www.coker.com.au/bonnie++/

[5] D. Eastlake, 3rd, Us Secure Hash Algorithm 1 (sha1), Sept. 2001.[Online]. Available: http://tools.ietf.org/html/rfc3174

[6] G.DeCandia, D.Hastorun,M. Jampani, G.Kakulapati, A. Lakshman,A. Pilchin, S. Sivasubramanian, P.Vosshall, andW.Vogels, ‘‘Dynamo:Amazon’s Highly Available Key-Value Store,’’ in Proc. 21st ACM SIGOPS SOSP, New York, NY, USA, 2007, vol. 41, pp. 205-220.

Hop-byHop Message Authentication and Source privacy in Wireless Sensor Networks

G.Lalithambal
PG scholar, Department of CSE
Moogambigai College of Engineering

M.Flora Mary
Associate Professor, Department of CSE
Moogambigai College of Engineering

***Abstract*— Message authentication is one of the most effective ways to thwart unauthorized and corrupted messages from being forwarded in wireless sensor networks (WSNs). For this reason, many message authentication schemes have been developed, based on either symmetric-key cryptosystems or public-key cryptosystems. Most of them, however, have the limitations of high computational and communication overhead in addition to lack of scalability and resilience to node compromise attacks. To address these issues, a polynomial-based scheme was recently introduced. However, this scheme and its extensions all have the weakness of a built-in threshold determined by the degree of the polynomial: when the number of messages transmitted is larger than this threshold, the adversary can fully recover the polynomial. In this paper, we propose a scalable authentication scheme based on elliptic curve cryptography (ECC). While enabling intermediate nodes authentication, our proposed scheme allows any node to transmit an unlimited number of messages without suffering the threshold problem. In addition, our scheme can also provide message source privacy. Both theoretical analysis and simulation results demonstrate that our proposed scheme is more efficient than the polynomial-based approach in terms of computational and communication overhead under *comparable* security levels while providing message source privacy.**

Keywords—Wireless Sensor Networks(WSN),Elliptic curve cryptography(ECC)Source Anonymous Message Authentication(SAMA)

I. INTRODUCTION

MESSAGE authentication plays a key role in thwarting unauthorized and corrupted messages from being forwarded in networks to save the precious sensor energy. For this reason, many authentication schemes have been proposed in literature to provide message authenticity and integrity verification for wireless sensor networks (WSNs) .These schemes can largely be divided into two categories: public-key based approaches and symmetric-key based approaches.The symmetric-key based approach requires complex key management, lacks of scalability, and is not resilient to large numbers of node compromise attacks since the message sender and the receiver have to share a secret key. The shared key is used by the sender to generate a message authentication code (MAC) for each transmitted message. However, for this method, the authenticity and integrity of the message can only be verified by the node with the shared secret key, which is generally shared by a group of sensor nodes. An intruder can compromise the key by capturing a single sensor node. In addition, this method does not work in multicast networks. To solve the scalability problem, a secret polynomial based message authentication scheme was introduced in. The idea of this scheme is similar to a threshold secret sharing, where the threshold is determined by the degree of the polynomial. This approach offers information-theoretic security of the shared secret key when the number of messages transmitted is less than the threshold. The intermediate nodes verify the authenticity of the message through a polynomial evaluation. However, when the number of messages transmitted is larger than the threshold, the polynomial can be fully recovered and the system is completely broken. An alternative solution was proposed to thwart the intruder from recovering the polynomial by computing the coefficients of the polynomial. The idea is to add a random noise, also called a perturbation factor, to the polynomial so that the coefficients of the polynomial cannot be easily solved. However, a recent study shows that the random noise can be completely removed from the polynomial using error-correcting code techniques. For the public-key based approach, each message is transmitted along with the digital signature of the message generated using the sender's private key. Every intermediate forwarder and the final receiver can authenticate the message using the sender's public key .One of the limitations of the public-key based scheme is the high computational overhead. The recent progress on elliptic curve cryptography (ECC) shows that the public key schemes can be more advantageous in terms of computational complexity, memory usage, and security resilience, since public-key based approaches have a simple and clean key management. In this paper, we propose an unconditionally secure and efficient source anonymous message authentication
(SAMA) scheme based on the optimal modified ElGamal signature (MES) scheme on elliptic curves. This MES scheme is secure against adaptive chosen-message attacks in the random oracle model. Our scheme enables the intermediate nodes to authenticate the message so that all corrupted message can be detected and dropped to conserve the sensor power. While achieving compromise resiliency, flexible-time authentication and source identity protection, our scheme does not have the threshold problem. Both theoretical analysis and simulation results demonstrate that our proposed scheme is more efficient than the polynomial-based algorithms under comparable security levels.

II. PROBLEM DEFINITION

Cloud could possess each user's private key, it can easily finish the re-signing task for existing users without asking them to download and re-sign blocks. However, since the cloud is not in the same trusted domain with each user in the group, outsourcing every user's private key to the cloud would introduce significant security issues. we need to consider is that the re-computation of any signature during user revocation should not affect the most attractive property of

public auditing data integrity publicly without retrieving the entire data. Therefore, how to efficiently reduce the significant burden to existing users introduced by user revocation, and still allow a public verifier to check the integrity of shared data without downloading the entire data from the cloud, is a challenging task.

III. SYSTEM ANALYSIS

In existing system, the symmetric-key based approach requires complex key management, lacks of scalability, and is not resilient to large numbers of node compromise attacks since the message sender and the receiver have to share a secret key. The shared key is used by the sender to generate a message. For the public-key based approach, each message is transmitted along with the digital signature of the message generated using the sender's private key. Every intermediate forwarder and the final receiver can authenticate the message using the sender's public key. One of the limitations of the public key based scheme is the high computational overhead.

A secret polynomial based message authentication scheme was introduced in. The idea of this scheme is similar to a threshold secret sharing, where the threshold is determined by the degree of the polynomial. The intermediate nodes verify the authenticity of the message through a polynomial evaluation. However, when the number of messages transmitted is larger than the threshold, the polynomial can be fully recovered and the system is completely broken. Demerits of this approach are lack of scalability, Node compromise attacks, High computational overhead and threshold problem.

IV. SYSTEM DESIGN

Fig 1.Shows the system Architecture and its functionalities and Fig 2 shows the data flow diagram .This model proposes an unconditionally secure and efficient source anonymous message authentication (SAMA) scheme based on the optimal modified ElGamal signature (MES) scheme on elliptic curves. This MES scheme is secure against adaptive chosen-message attacks in the random oracle model. Our scheme enables the intermediate nodes to authenticate the message so that all corrupted message can be detected and dropped to conserve the sensor power. While achieving compromise-resiliency, flexible-time authentication and source identity protection, our scheme does not have the threshold problem. This system provides more merits such as compromise-resiliency, flexible-time authentication, source identity protection and this scheme does not have the threshold problem.

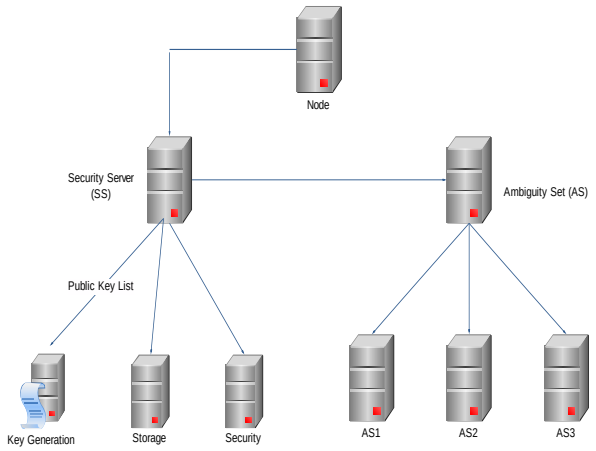

Fig .1. Software Archietecture

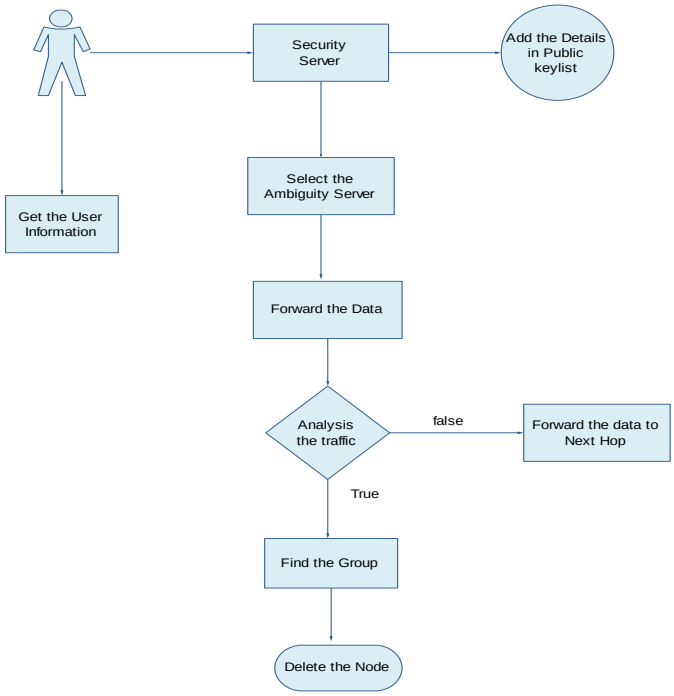

Fig. 2. Dataflow diagram

IV. PROPOSED MODEL

This system consists of following modules 1.Network Construction 2. Security server Process 3. Secure Packet Forwarding4. Analysis Message Authentication 5. Compromised Node Detection.

A.Node Creation

Fig 3 shows the node creation, construct a Node Creation. Node is constructed by getting the names of the nodes and the connections among the nodes as input from the user. While getting each of the nodes, their associated port and ip address is also obtained. For successive nodes, the node to which it should be connected is also accepted from the user.

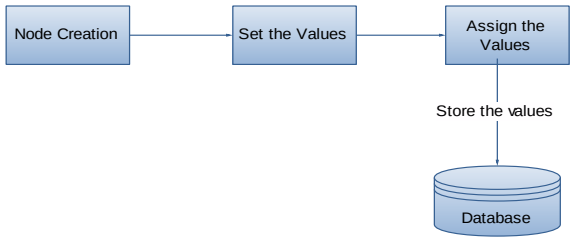

Fig .3. Node creation

B. Security Server Process

Fig 4 shows the security server process, in this process it is assumed that each sensor node knows its relative location in the sensor domain and is capable of communicating with its neighboring nodes directly using geographic routing. The whole network is fully connected through multi-hop communications. We assume there is a security server (SS) that is responsible for generation, storage and distribution of the security parameters among the network. This server will never be compromised.

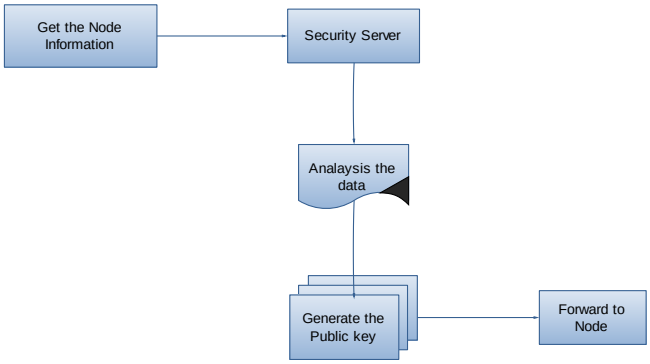

Fig .4. Security server process

C.Secure Packet Forwarding

Fig 5 shows the server packer forwarding, every forwarder on the routing path should be able to verify the authenticity and integrity of the messages upon reception.

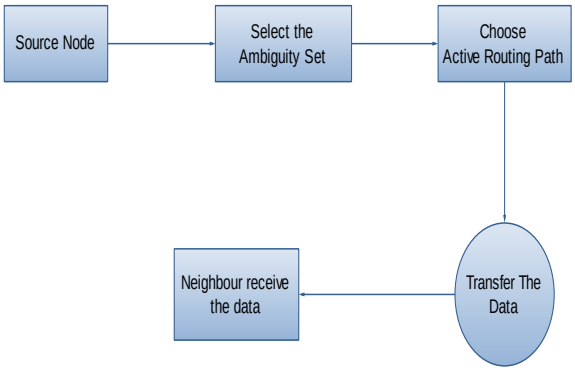

Fig .5.Secure packet forwarding

D.Analysis Message Authentication

Fig 6 shows Analysis Message Authentication, The message receiver should be able to verify whether a received message is sent by the node that is claimed, or by a node in a particular group. In other words, the adversaries cannot pretend to be an innocent node and inject fake messages into the network without being detected.

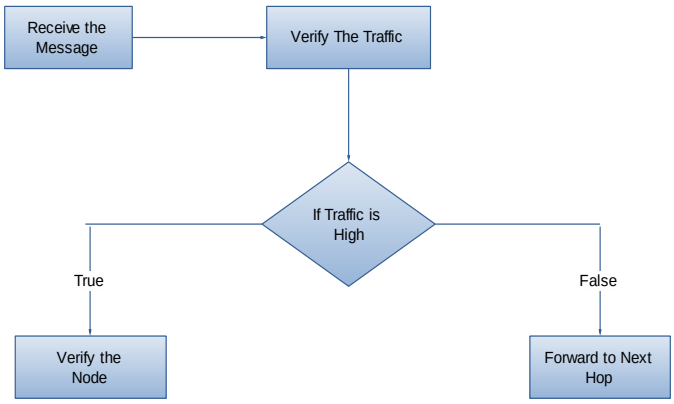

Fig. 6. Analysis Message Authentication

E.Compromised Node Detection

Fig 7 shows the Compromised node detection, When a node has been identified as compromised, the SS can remove its public key from its public key list. It can also broadcast the node's short identity to the entire sensor domain so that any sensor node that uses the stored public key for anAS selection can update its key list. Once the public key of a node has been removed from the public key list, and/or broadcasted, any message with the AS containing the compromised node should be dropped without any processing order to save the precious sensor power.

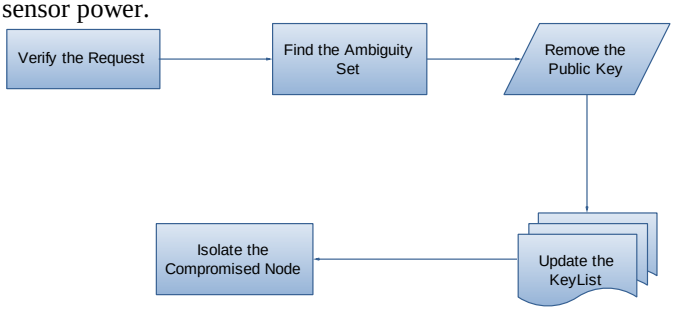

Fig. 7. Compromised Node Detection

V CONCLUSION

The proposed novel and efficient source anonymous message authentication based on elliptic curve cryptography ensures message sender privacy, SAMA can be applied to any message to provide message content authenticity. To provide hop-by-hop message authentication without the weakness of the built in threshold of the polynomial-based scheme, we then propose a hop-by-hop message authentication scheme based on the SAMA. When applied to WSNs with fixed sink nodes, it is also discussed various possible techniques for compromised node identification.

REFERENCES

1 .F. Ye, H. Lou, S. Lu, and L. Zhang, "Statistical en-route filtering of injected false data in sensor networks," in *IEEE INFOCOM*, March 2004.

2. S. Zhu, S. Setia, S. Jajodia, and P. Ning, "An interleaved hop-by-hop authentication scheme for filtering false data in sensor networks," in *IEEESymposium on Security and Privacy*, 2004.

3. C. Blundo, A. De Santis, A. Herzberg, S. Kutten, U. Vaccaro, and M. Yung, "Perfectly-secure key distribution for dynamic conferences," in *Advances in Cryptology - Crypto'92*, ser. Lecture Notes in Computer Science Volume 740, 1992, pp. 471–486.

4. W. Zhang, N. Subramanian, and G. Wang, "Lightweight and compromiseresilient message authentication in sensor networks," in *IEEE INFOCOM*, Phoenix, AZ., April 15-17 2008.

5. A. Perrig, R. Canetti, J. Tygar, and D. Song, "Efficient authentication and signing of multicast streams over lossy channels," in *IEEE Symposium on Security and Privacy*, May 2000.

6. M. Albrecht, C. Gentry, S. Halevi, and J. Katz, "Attacking cryptographic schemes based on "perturbation polynomials"," Cryptology ePrint Archive, Report 2009/098, 2009, http://eprint.iacr.org/.

Enhancement of Hidden Objects Due to Shadow of Obstacles in Urban Areas

[1.] S. Ilakkiya, [2.]D. Santhanalakshmi, [3.]D. Sarala
St.Anne's College Of Engg And Tech

Abstract **-In accordance with the characteristics of urban high-resolution color remote sensing images, we put forward an object-oriented shadow detection and removal method. In this method, shadow features are taken into consideration during image segmentation, and then, according to the statistical features of the images, suspected shadows are extracted. Furthermore, some dark objects which could be mistaken for shadows are ruled out according to object properties and spatial relationship between objects. For shadow removal, inner–outer outline profile line (IOOPL) matching is used. First, the IOOPLs are obtained with respect to the boundary lines of shadows. Shadow removal is then performed according to the homogeneous sections attained through IOOPL similarity matching. Experiments show that the new method can accurately detect shadows from urban high-resolution remote sensing images and can effectively restore shadows with a rate of over 85%.**

INTRODUCTION

IN the last ten or more years, with the availability of high-spatial-resolution satellites such as IKONOS, Quick Bird, Gooey, and Resource 3 for the observation of Earth and the rapid development of some aerial platforms such as airships and unmanned aerial vehicles, there has been an increasing need to analyze high-resolution images for different applications. In urban areas, surface features are quite complex, with a great variety of objects and shadows formed by elevated objects such as high buildings, bridges, and trees. Although shadows themselves can be regarded as a type of useful information in 3-D reconstruction, building position recognition, and height estimation .they can also interfere with the process- ing and application of high-resolution remote sensing images. gray scale, brightness, saturation, and texture. An improved algorithm exists that combines the two methods. First, the shadow areas are estimated according to the space coordinates of buildings calculated from digital surface models and the altitude and azimuth of the sun. Then, to accurately identify a shadow, the threshold value is obtained from the estimated grayscale value of the shadow areas. However, information such Scheme was proposed to detect shadows . To avoid the false shadows of dark objects such as vegetation and moist soil, normalized difference vegetation index the normalized saturation–value difference index, and the size and shape of the shadow area are considered the method used by Makarau scheme was proposed to detect shadows . To avoid the false shadows of dark objects such as vegetation and moist soil, the normalized difference vegetation index the normalized saturation–value..

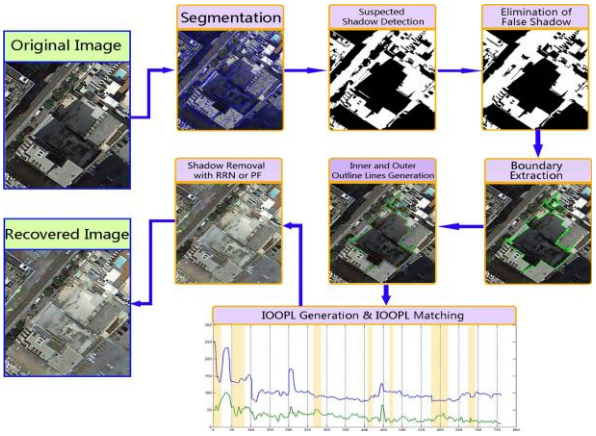

II. SHADOW DETECTION

Shadows are created because the light source has been blocked by something. There are two types of shadows: the

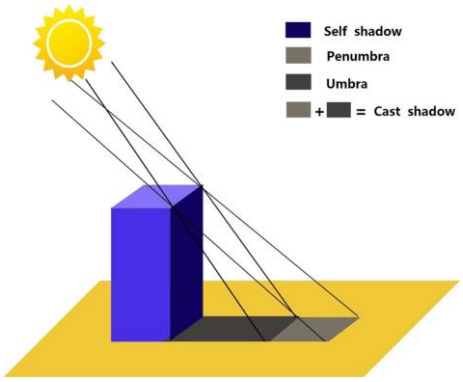

self-shadow and the cast shadow. A self-shadow is the shadow on a subject on the side that is not directly facing the light source. A cast shadow is the shadow of a subject falling on the surface of another subject because the former subject has blocked the light source. A cast shadow consists of two parts: the umbra and the penumbra. The umbra is created because the direct light has been completely blocked, while the penumbra is created by something partly blocking the direct light.

A. Image Segmentation Considering Shadow Features

Images with higher resolution contain richer spatial information. The spectral differences of neighboring pixels within an object increase gradually. Pixel-based methods may pay too much attention to the details of an object when processing high-resolution images, making it difficult to obtain overall structural information about the object. In order to use spatial information to detect shadows, image segmentation is needed. We adopt convexity model (CM) constraints for segmentation [27], [28].

Traditional image segmentation methods are likely to result in insufficient segmentation, which makes it difficult to separate shadows from dark objects. The CM constraints can improve the situation to a certain degree. To make a further distinction between shadows and dark objects, color factor and shape factor have been added to the segmentation criteria. The parameters of each object have been recorded, including grayscale average, variance, area, and perimeter. The segmentation scale could be set empirically for better and less time-consuming results, or it could be adaptively estimated according to data such as resolution.

B. Detection of Suspected SHADOW AREAS.

For shadow detection, a properly set threshold can separate shadow from nonshadow without too many pixels being misclassified [3]. Researchers have used several different methods to find the threshold to accurately separate shadow and nonshadow areas. Bimodal histogram splitting provides a feasible way to find the threshold for shadow detection, and the mean of the two peaks is adopted as the threshold [3]. In our work, we attain the threshold according to the histogram of the original image and then find the suspected shadow objects by comparing the threshold and grayscale average of each object obtained in segmentation. We chose the grayscale value with the minimum frequency in the neighborhood of the mean of the two peaks as the threshold, as shown in

$$G_q = \frac{1}{2}(G_m + G_s) \quad (1)$$

$$h(T) = \text{Min}\{h(G_q - \varepsilon), h(G_q + \varepsilon)\}. \quad (2)$$

In the equations, G_m is the average grayscale value of an image; G_s stands for the left peak of the shadow in the histogram; T is the threshold; ε represents the neighborhood of T, where $T \in [G_q - \varepsilon, G_q + \varepsilon]$; and $h(I)$ is the frequency of I, where $I = 0, 1, \ldots, 255$.

By conducting a large number of experiments, we have found that the average of the grayscale values can be used to replace the right peak. To simplify the operation, when the left peak is not obvious, G_s can be replaced by half of the grayscale average. Meanwhile, to avoid the influence of abnormal information, 2% of the pixels on the left and right sides of the histogram are not included. In addition, atmospheric molecules scatter the blue wavelength most among the visible rays (Rayleigh scattering). So for the same object, when in shadow and nonshadow, its grayscale difference at the red and green wavebands is more noticeable than at the blue waveband. Thus, we retrieve a suspected shadow with the threshold method at the red and green wavebands. Specifically, an object is determined to be a suspected shadow if its grayscale average is less than the thresholds in both red and green wavebands.

C. Elimination of false shadow

Dark objects may be included in the suspected shadows, so more accurate shadow detection results are needed to eliminate these dark objects. Rayleigh scattering results in a smaller grayscale difference between a shadow area and a nonshadow area in the blue (B) waveband than in the red (R) and green (G) wavebands. After the elimination of false shadows from vegetation, spatial information of objects, i.e., geometrical characteristics and the spatial relationship between objects, is used to rule out other dark objects from the suspected shadows. Lakes, ponds, and rivers all have specific areas, shapes, and other geometrical characteristics. Most bodies of water can be ruled out due to the area and shape of the suspected shadows of the object that they produce. However, the aforementioned method still cannot separate shadows from some other dark objects. Spatial relationship features are used to rule out dark objects in the suspected shadows. Dark objects are substantive objects, while shadows are created by taller objects which block the light sources and may be linked together with the objects that result in the shadows. An obscured area (i.e., a shadow) forms a darker area in an image. The object blocking the light forms a lighter area in an image. At the same time, the sun has a definite altitude angle, and a shadow boundary reflects the boundary of a building and the position of a light source. Buildings, trees, and telegraph poles are the main objects creating shadows in urban remote sensing images. Their shadow boundaries usually have a certain direction. To retrieve shadows using spatial rela- tionships, the linear boundaries of suspected shadows are first analyzed to predict the probable trend of a shadow, according to which the approximate position of a large object is predicted. To determine whether it is a shadow, the proximity of a dark object to a light object within this azimuth is measured. An average spectral difference can be used to decide whether there are light objects linked around a shadow.

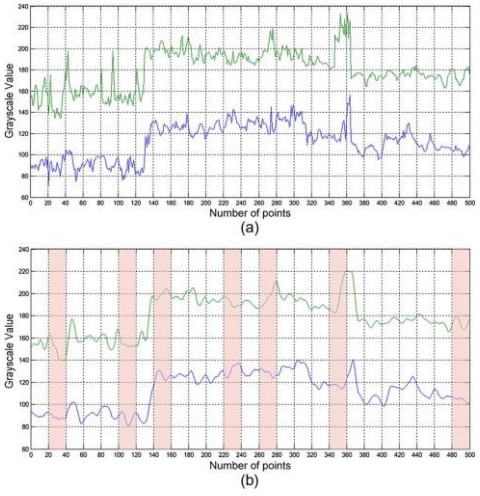

4. Diagram of IOOPL and IOOPL matching. (a) IOOPL at the red waveband. (b) Matching result after Gaussian smoothing for IOOPL, where the red background shows the parts that do not match.

II. Shadow Removal

To recover the shadow areas in an image, we use a shadow removal method based on IOOPL matching. There is a large probability that both shadow and nonshadow areas in close range on both sides of the shadow boundary belong to the same type of object. The inner and outer outlines can be obtained by contracting the shadow boundary inward and expanding it

outward, respectively. Then, the inner and outer outline profile lines are generated along the inner and outer outline lines to determine the radiation features of the same type of object on both sides. As shown in Fig. 3, R is the vector line of the shadow boundary obtained from shadow detection, R_1 is the outer outline in the nonshadow area after expanding R outward, and R_2 is the inner outline in the shadow area after contracting R inward. There is a one-to-one correspondence between nodes on R_1 and R_2. When the correlation between R_1 and R_2 is close enough, there is a large probability that this location belongs to the same type of object. The grayscale value of the corresponding nodes along R_1 and R_2 at each waveband is collected to obtain the IOOPL. The outer profile lines (OPLs) in the shadow area are marked as inner OPLs; OPLs in the nonshadow area are marked as outer OPLs (Fig. 3).

The objects on both sides of the shadow boundary linked with a building forming a shadow are usually not homogeneous, and the corresponding inner and outer outline profile line sections are not reliable. In addition, the abnormal sections on the inner and outer outlines that cannot represent homogeneous objects need to be ruled out. Consequently, similarity matching needs to be applied to the IOOPL section by section to rule out the two kinds of nonhomogeneous sections mentioned previously. The parameters for shadow removal are obtained by analyzing the grayscale distribution characteristics of the inner and outer homogeneous IOOPL sections.

IV. Experimental Analysis

A. Comparative Analysis of Shadow Detection

To validate that our method works, the following experiment was performed. The datum used in this experiment is a QuickBird image of Kunming, China. Each step of this method is described herein, and the steps and corresponding results of each step are given [from Fig. 6(a)–(e)]. Moreover, to compare with our method, we determined the pixel-level threshold shadow detection result with manually selected proper threshold according to the image grayscale scale histogramIt can be seen from the segmentation result [Fig. 6(b)] that segmentation that considers shadow features can effectively segment shadows and dark objects such as vegetation and bodies of water into different subjects This means that, in the following process, the problem of shadow and dark objects being segmented as a whole subject can be avoided. The results, shown in Fig. 6(c), show the retrieval of a rough shadow with the threshold, which indicates that vegetation, rivers, dark moist soil, and true shadows can be detected. Comparing images (c)and (f) in Fig. 6, one can see that the shadow area detected with morphological characteristics of objects, the rivers in image (d). , an object-level shadow detection method based on spectral features and spatial features can accurately and effectively detect shadows in an urban high-resolution remote sensing images with true shadow. therefore using spatial relative.

A.*IOOPL *Matching

IOOPL matching is a process of obtaining homogeneous sections by conducting similarity matching to the IOOPL section by section. During the process, Gaussian smoothing is performed to simplify the view of IOOPLTo rule out the nonhomogeneous sections, the IOOPL is divided into average sections with the same standard, and then, the similarity of each line pair is calculated section by section with (4). If the correlation coefficient is large, it means that the shade and light fluctuation features of the IOOPL line pair at this section are consistent. If consistent, then this line pair belongs to the same type of object, with different illumina- tions, and thus is considered to be matching. If the correlation coefficient is small, then some abnormal parts representing some different types of objects exist in this section; therefore, these parts should be ruled out.The sections that have failed the matching are indicated in red. If more accurate matching is needed, the two sections adjacent to the section with the smallest correlation coefficient can be detected.

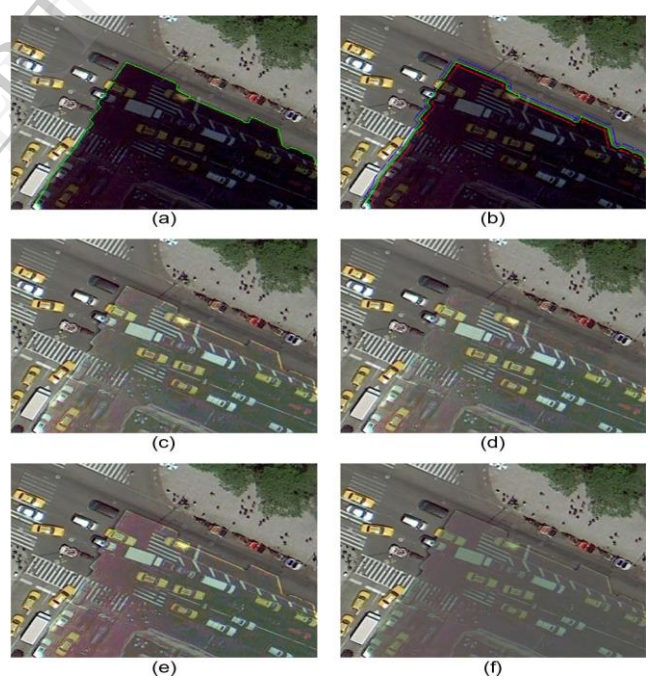

Fig. 9. Examples of shadow removal. (a) Remote sensing image in which a shadow has been detected. (b) Inner and outer outline lines generated by a shadow boundary; the red line is the inner outline line, and the blue line is the outer outline line. (c) Result of RRN after IOOPL matching. (d) Result of boundary treatment for (c). (e) Result of RRN skipping IOOPL matching.

B. Analysis of Shadow Removal Experiments

To verify our shadow removal method, the following experiment was performed. The results of each step of the method are shown in Fig. 9(a)–(d). Furthermore, to illustrate the necessity of IOOPL matching, we present a shadow removal result .

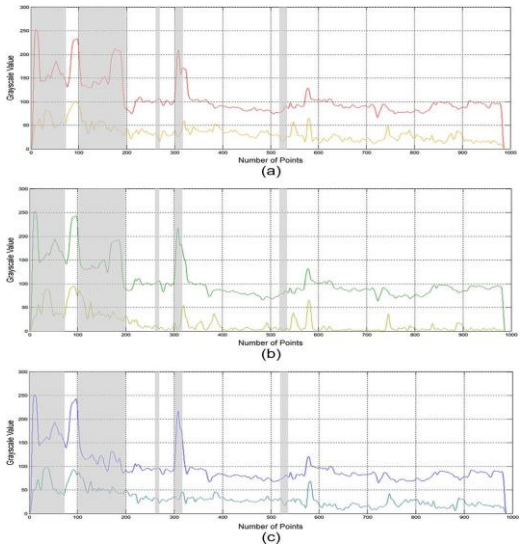

Fig. 10. Comparison charts of IOOPL after Gaussian smoothing of the following wavebands: (a) red, (b) green, and (c) blue (the light gray parts represent fail matching).

IOOPL matching did not fully solve color cast as there is still a little red in the bottom left part in Fig. 9(c). According to the contrast between Fig. 9(d) and (f), we conclude that the Plus method could restore the background radiation characteristic with poor contrast between the object and the background while our approach could restore both the background color and the contrast. Furthermore, we choose the samples with same scene in the nonshadow area, shadow area, and shadow-removed area to analyze, as shown in Fig. 11. Table I shows the sample information, which verifies the effectiveness of our approach numerically. In Table I, there is a tremendous difference between the nonshadow and shadow regions of the same scenes in spectral consistency according to the average value and standard deviation. After applying our approach, the average value and standard deviation of the shadow-removed region are close to that of the nonshadow region. Therefore, we could obtain the deshaded data which meet the needs of both vision and spectral consistency through the presented approach. As shown in Fig. 12, both relative radiometric normalization (RRN) and PF based on IOOPL matching could effectively remove the shadow. Similar to the former experiment, the Plus method can only restore the entire radiant luminance of the shadow but barely identify the objects in shadow. By comparing Fig. 12(c) and (d), we see that the results of RRN are clearer than the PF results. The PF result is better than the RRN result Of the defective shadow detection most shadow have been effectively removed.refering to the statistics of the supervised classification results the propotion of the shadow has been significantly reduced from 45.1% to 6.05%by the RRN method and form 45.1% to2.88%.the shadow removal rate could reach 86.2% by the RRN and 93.63% by the PF method in this proc.

at the whole radiant brightness in subjective sensation, although it is a little bluish.

Both RRN and PF could restore the shadow area in a visual sense, as shown in Fig. 12. To better analyze and compare the RRN and PF techniques, we classified the original image and shadow removal results with the same training samples. Comparing Fig. 13(a) with Fig. 12(a), the shadow area marked in red was correctly classified with the exception of some cars in dull color. In the classification results [Fig. 13(b) and (c)], although some trees and shadows from cars still exist because

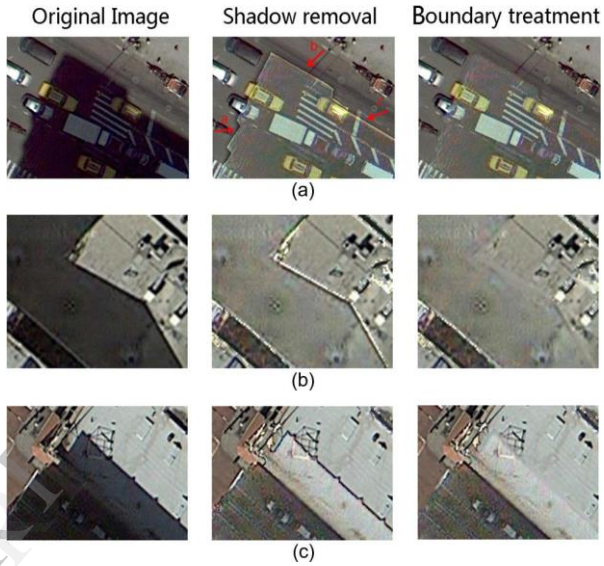

Fig. 14. Examples of shadow boundary after shadow removal.

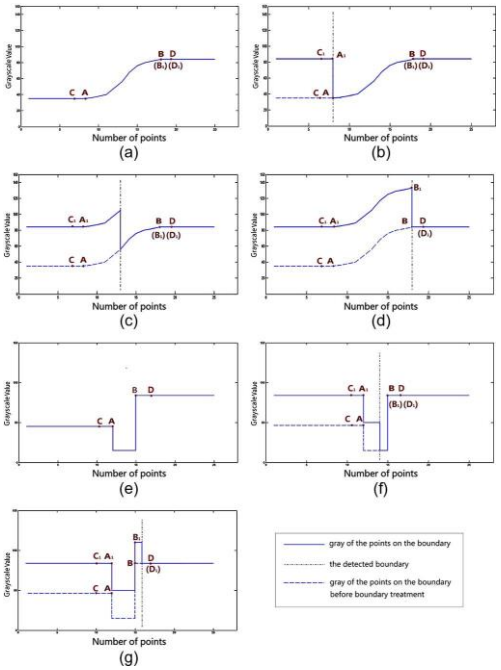

V. Boundary Processing After Shadow Removal

In the aforementioned experiment, there are several instances of the shadow boundary, shown in Fig. 14.

Because of penumbra and diffuse reflection, an exact boundary does not exist in the shadow area, so the boundary may be presented in two cases: a gradually changing boundary and a boundary with a darker color compared to the shadow area. Fig. 15(a) and (e) shows the grayscale cross section of these two cases. In Fig. 15, points A and B are the starting point and ending point of the shadow boundary, respectively. Point C is next to point A, which belongs to the shadow region, while point D is next to point B, which belongs to the nonshadow region. After boundary treatment, points $A1$, $B1$, $C1$, and $D1$ correspond to points A, B, C, and D, obtained with the segmentation method may be near point A or B.

Shadow boundaries after shadow removal may appear in different cases, as explained previously. However, we can see from Fig. 15 that the points C_1 and D_1 remain the correct gray scale after boundary treatment. Therefore, we first get the shadow boundaries according to the shadow detection result and then obtain points C and D. Finally, the points between points C and D are filled with incremental gray scale according to the grayscale values of C and D. To find points C and D, we obtain the points at a certain distance from the boundaries on both sides, and the distance will range from 3 pixels to 5 pixels based on image resolution.

VI. Conclusion

We have put forward a systematic and effective method for shadow detection and removal in a single urban high-resolution remote sensing image. In order to get a shadow detection result, image segmentation considering shadows is applied first. Then, suspected shadows are selected through spectral features and spatial information of objects, and false shadows are ruled out. The subsequent shadow detection experiments compared traditional image segmentation and the segmentation considering shadows, as well as results from traditional pixel-level threshold detection and object-oriented detection. Meanwhile, they also show the effects of different steps with the proposed method. For shadow removal, after the homogeneous sections have been obtained by IOOPL matching, we put forward two strategies: relative radiation correction for the objects one at a time, and removal of all shadows directly after PF is applied to all the homogeneous sections and correction parameters are obtained. Both strategies were implemented in high-resolution images, and their performances were compared in experiments. The experimental results revealed the following.

1) The shadow detection method proposed in this paper can stably and accurately identify shadows. Threshold selection and false shadow removal can be conducted in simple but effective ways to ensure shadow detection accuracy.
2) Compared with pixel-level detection, the object-oriented shadow detection method proposed in this paper can make full use of the spatial information of an image and can effectively rule out speckles and false shadows in the detection result. However, it is difficult to segment the small size shadows into an independent object, which will cause errors.
3) The shadow removal method based on IOOPL matching can effectively restore the information in a shadow area. The homogeneous sections obtained by IOOPL matching can show the radiation gray scale of the same object in a shadow area and a nonshadow area. The parameters calculated by using the radiation difference between inner and outer homogeneous sections can retrieve a shadow very effectively.
4) The two shadow removal strategies (RRN and PF) are both suitable for high-resolution urban remote sensing images. Moreover, there are advantages to each strategy: RRN can restore the texture details well while PF has a more stable background radiance.

Further improvements are needed in the following ways.

1) Although image segmentation considering shadows can have better segmentation results, insufficient segmentation still exists. For example, a black car and its shadow cannot be separated. Also, parts of the shadow from low trees cannot be separated from the leaves.
2) Because of the filming environment or some other reasons, obvious color cast can be seen in some parts of a shadow area. IOOPL matching could relieve this case to a certain extent but not completely resolve the problem.

Acknowledgment

The authors would like to thank the anonymous reviewers for their comments. Their insightful suggestions have significantly improved this paper.

References

[1] T. Kim, T. Javzandulam, and T.-Y. Lee, "Semiautomatic reconstruction of building height and footprints .
[2] S. Ji and X. Yuan, "A method for shadow detection and change detection of man-made objects," *J. Remote Sens.*
[3] P. M. Dare, "Shadow analysis in high-resolution satellite imagery of urban areas,"
[4] Y. Li, P. Gong, and T. Sacagawea, "Integrated shadow removal based on photogrammetric and image analysis,"
[5] W. Zhou, G. Huang, A. Troy, and M. L. Cadenzas', Object-based land cover classification of shaded areas in high spatial resolution imagery of urban areas:
[6] J. Yoon, C. Koch, and T. J. Ellis, "Shadow Flash: An approach for shadow
removal in an active illumination environment," .
[7] R. B. Irvin and D. M. McKeon, Jr, "Methods for exploiting the relation- ship between buildings …

Monitoring and Control of LDmicro PLC based Motion Control Systems Via Device-Net

K.Durgadevi
Ece Final Year
A.Suganya
Ece Final Year
V.Deepika
Ece Final Year
St.Anne's College of Engineering and Technology

Abstract— **With the rapid changes on industries and information technologies in recent years, some traditional bulk electronic appliances have to be monitored for a long time. All of their control devices such as communication interfaces gradually enter the Internet information era. Control of all equipments has been performed through the use of computers. Most equipment uses PLC (Programmable logic controller) to connect with computer to monitor consuming devices. PLC's are widely used in industrial fields because they are easy to install and very flexible in applications. A PLC interacts with the external world through its inputs and outputs. Since technology for motion control of circuit drives became available, the use of PLC with power electronics in electric machine applications has been introduced in the manufacturing automation. This study defines the real time monitoring control of a two degree of freedom motion control system with PLC based SCADA system through Device-Net web communication.**

Keywords; ***SCADA, PLC, Device-Net, Motion Control***

I. INTRODUCTION

Electric motors and their drivers have become crucial parts of the manufacturing process. They are needed in many manufacturing applications such as automotive and textile industry. Because of their effect on product quality, the observation and control of those motors and drivers are necessary. An intelligent system, PLC, which is an outcome of the development of microelectronics and telecommunication systems, is used in order to carry out the observation and control of motors and drivers. Besides that, servomotors and their drivers are often used in accurate control applications of manufacturing processes. Servomotors are widely used in industrial applications because, they can produce high torques although they have low rotor inertia. A gear box integrated to the servomotor shaft provides high torque even in low revolutions. Servomotors are used in position and velocity control because of their high power, high torque and ability to generate quick feedback. Due to their use in applications that need accurate operations, servomotors ought to be quick in open-close operations and keep their stability in instantaneous load changes .

SCADA (Supervisory Control and Data Acquisition) is a data acquisition and observation system .The operation values that belong to motor and drivers can easily be controlled and observed via SCADA in motion control systems.

This study defines the real time monitoring control of a two degree of freedom motion control system with PLC based SCADA system through Device-Net web communication. Firstly, the system architecture, secondly, the system components and thirdly the results are described. Lastly, a general evaluation is carried out.

II. SYSTEM ARCHITECTURE

Servo system drivers take the necessary signals (rotation direction, velocity, position etc.) for controlling from the microprocessor, microcontroller or the CPU. On the other hand, the feedback signal is obtained by various sensors, the encoder or the position potentiometers. The controller takes the gathered data as the real position information and calculates the parameters based on those data in order to generate the signals that the driver requires [7].

In order to make the system work in real time, the speed of the communication between the PLC (which is used as the controller) and the SCADA (which is used for user control) becomes an important factor. There are serial or parallel communication technologies for such systems. The communication speed also depends on the properties of the selected hardware. In this study, the Device-Net protocol, which is suitable for PLC and can give successful results through short distances, is used. Device-Net is an open domain web that can be used in communication of different controlling devices such as PLCs, CPUs, sensors and actuators. Additionally, it also reduces the cost of maintenance because; less amount of cable is used in the set-up of Device-Net. Moreover, it proposes a suitable structure for the systems from different manufacturers such that there are many devices that are compatible with Device-Net. Therefore, the most economical system can be established with Device-Net [8]. The functional flow diagram can be seen in Fig 1.

The generated system consists of five primary elements such as;

- SCADA software
- AC servomotor and Driver System Setup
- Development of a PLC ladder diagram
- Establishment of the feedback system
- Development of web

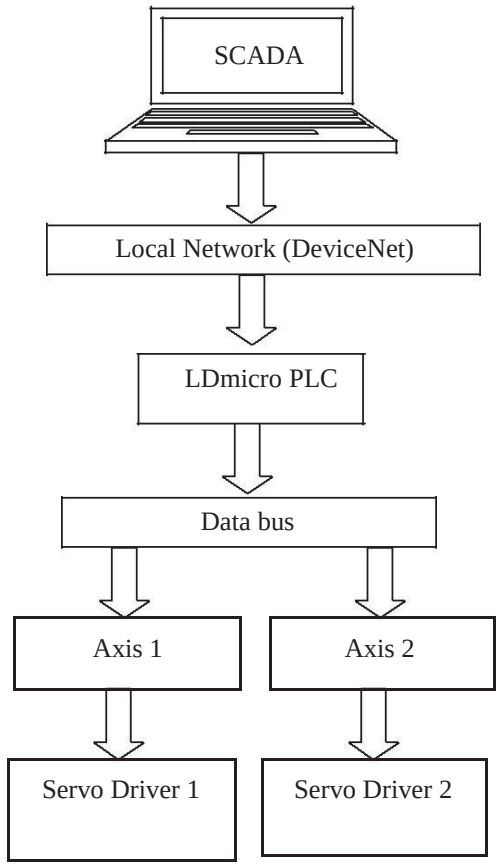

Figure 1. Axial monitoring and control system flow diagram

III. SYSTEM COMPONENTS

A. *Programmable Logic Controller (PLC)*

Programmable logic controller (PLC) is a significant controlling unit that presents a communication interface proper I/O (Input/Output) units to the hardware in order to remote and control the industrial system and carries out the software program according to the user demand [9-10]. It is an industrial CPU that is used as the maintenance unit instead of remote control systems working with relays. Those devices are widely used in industrial automation circuits with the development of new technology. Nowadays, PLCs consist of commands for special mathematical operations besides the logic based operations. More complicated remote and control operations are carried out as the command set extends [11]. An Omron CX-Programmer is used for the PLC ladder diagram. Omron PLC consists of 16 digital input and 32 digital outputs.

B. *Servomotor and Servo Driver*

The servomotor used in this study is Omron PLC and the servo driver is used. The technical details that belong to servomotor and servo driver are given in Table 1 and Table 2 respectively.

TABLE I. ldmicro SERVO DRIVER TECHNICAL SPECIFICATIONS

Servo Driver			
Continuous output current (rms)			2.6 A
Input power supply	Main circuit	Power supply capacity	0.9 KVA
		Power supply voltage	50/60 Hz
		Rated current	4.1/2.4 A *1
		Heat value *2	33/24 W *1
	Control Circuit	Power supply voltage	240VAC
		Heat value *2	4 W
Maximum applicable motor capacity			400 W

TABLE II. ldmicro SERVOMOTOR TECHNICAL SPECIFICATIONS

Servo Motor		
Rated output	W	400
Rated torque	Nm	1.3
Rated rotation speed	r/min	3000
Momentary Maximum rotation speed	r/min	6000
Momentary maximum torque	Nm	3.8
Rated current	A (rms)	2.4

The connection between the drivers of servomotors and PLC is presented in Fig 2.

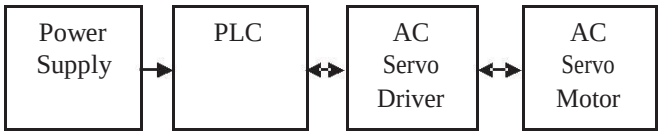

Figure 2. Schematic of the connection between the servomotor driver and PLC

C. *Device-Net Web Configuration*

The communication and data acquisition is provided by USB connection. Device-Net Ethernet protocol is used to connect the PLC and the CPU that has the SCADA software.

D. Servomotor Control Scheme

The position and velocity values demanded by the user during the control process are monitored on the screen. The block diagram that belongs to this control system is given in Fig 3.

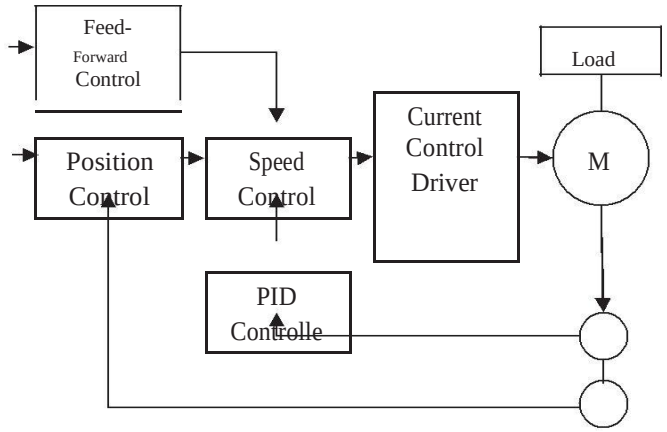

Figure 3. The block diagram of AC servomotor control

The control block diagram generates the signal in order to achieve the desired position and velocity values. The signal stops when the parameters reach the desired values.

E. SCADA

An LDmicro CX-Supervisor SCADA software program is used. The developed SCADA software provides a user interface and monitoring on the screen. The user can control the system by entering the desired position and velocity values to the software program. Besides that, the instantaneous parameters can be monitored on the screen at the same time. The software program also provides the capability of recording the actions of the user on the system. The position control form of the developed SCADA software can be seen in Fig 4.

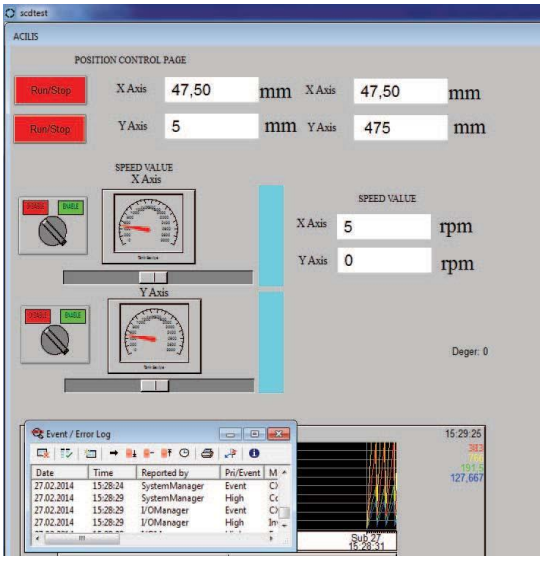

Figure 4. The position control form of SCADA software

The position values for the two degree of freedom system can be entered to the specified area and the real time position values are also monitored on the form. The system gives an alert to the user when the desired position values are satisfied. Additionally, a basic simulation of the moving system can be seen on the form.

IV. Results

Two different applications (i) velocity control, (ii) position control) are carried out on the two degree of freedom control system. The settling, rise time and overshoot values are monitored for the dynamic responses of servomotors having a revolution of 300 rpm and without loading. The ladder responses according to the PID parameters integrated to the system are shown in Fig 5.

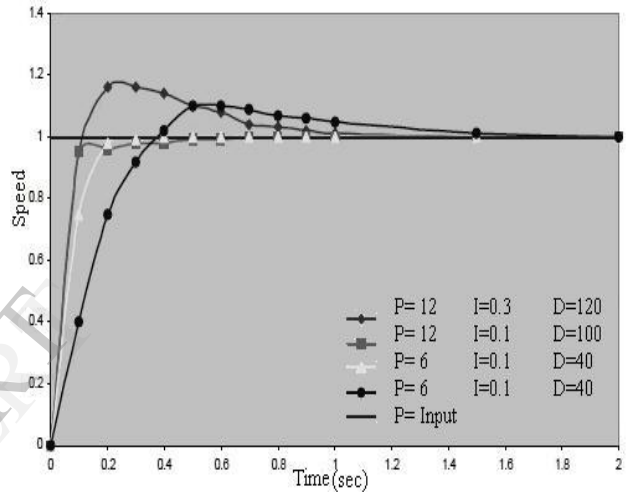

Figure 5. PID Control Step Responses

Another application is the monitoring and control of the working performance of the system based on the position change. It is seen that the position values entered to the SCADA system and the real values are convenient (Fig 6).

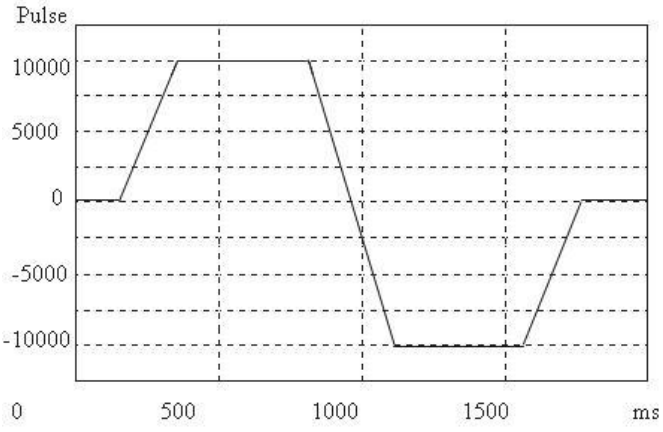

Figure 6. The position response of the system to a ramp input

The technical details that belong to DeviceNet, Ethernet and ControlNet are given in Table III [12].

TABLE III. OMRON SERVOMOTOR TECHNICAL SPECIFICATIONS

	DeviceNet	Ethernet	ControlNet
Data Rate (Mbps)	0.5	10	5
Max. Data Size (Byte)	8	1500	504
Max.Lenght (m)	100	2500	1000
Bit Time (ȝs)	2	0.1	0.2
Max.number of Nodes	64	>500	99

V. CONCLUSION

In this study, the control of position and velocity of a two degree of freedom servo system generated by PLC is carried out through SCADA and a prototype is produced. The PLC program algorithm and a CX-Programmer ladder diagram are formed. The generated ladder diagram is loaded to the PLC program via USB port. SCADA software consisting of position and velocity controlling pages is developed in order to enter the desired position and velocity values. Additional spaces are integrated to the software in order to monitor and compare the desired and real parameters. A feedback system is provided through the Encoder by making the connections of servomotors and drivers. The performance of the system, which is produced as a prototype after the experimental works, is evaluated according to the velocity and position values. As an example, servomotors are asked to move X-axis 11 mm and Y-axis 8 mm and the values are monitored on the SCADA screen. Besides that the velocity control is applied on the SCADA screen and the real parameters are monitored. The collected data verify that the developed SCADA system and the generated Device-Net web structure works properly with PLC.

REFERENCES

[1] Maria G. Ioannides, "Design and implementation of PLC-based monitoring control system for induction motor", IEEE Trans. Energy Conversion, vol. 19, no. 3, pp. 469-476, Sep. 2004.

[2] Sreejeth, M. Kumar, P. ; Singh, M.Power Electronics, Drives and Energy Systems (PEDES) & 2010 Power India, 2010 Joint International Conference on 20-23 Dec. 2010 1 - 4

[3] Khongkoom N., Kanchanathep A.,Nopnakeepong S., Tanuthong S., Tunyasrirut S., Kagawa R., "Control of the position DC servo motor by fuzzy logic," TENCON 2000. Proceedings , Volume: 3 , 24-27 Sept. 2000 Pages:354 - 357 vol.3.

[4] Özkan, A., "PLC ve SCADA Destekli Pozisyon kontrolü", Erciyes Üniversitesi Fen Bilimleri Enstitüsü, Yüksek Lisans Tezi Kayseri (1999)

[5] Akar, M., "The ComparÕng Of Servo Motor Conventioanal And Fuzzy Logic Control Method", Marmara Üniversitesi Fen Bilimleri Enstitüsü, Yüksek Lisans Tezi, østanbul,2005.

[6] Jiajun Liu ; Lixiao Yao ; Xiaoyong Liu ; Yuan An ; Ya Guo ;Zhenfeng Liang
Power and Energy Engineering Conference (APPEEC), 2010 Asia-Pacific
Digital Object Identifier: 10.1109/APPEEC.2010.5448621 Publication Year: 2010 , Page(s): 1 – 4

[7] Coúkun, ø., IúÕk M. F., (2004) "Servo Motorun Mikrodenetleyici ile Konum ve HÕz Denetimi" Gazi Üniversitesi Fen Bilimleri Enstitüsü Dergisi, Cilt 17 SayÕ 3, Sayfa: 115-125.

[8] Omron DeviceNet Operation Manual Cat. No. W267-E1-11 Revised April 2008

[9] Maria G. Ioannides, "Design and implementation of PLC-based monitoring control system for induction motor", *IEEE Trans. Energy Conversion*, vol.19, no.3, pp. 469-478, 2004.

Intelligent Navigation System for Blind People with Real Time Tracking

K. Rajan [1], E. Kalaiselvan [2]

***Abstract*—Most of the blind people in the world use white canes to go from one place to another. Due to their blindness they are not able to perceive their surroundings. So the mobility of the visually impaired people is limited. Therefore the purpose of this project is to build a navigation system that will be able to guide a visually impaired person safely and with ease, in an indoor and outdoor environment. This goal has been realized through the use of an ultrasonic sensor to determine the range of obstacles and also a microcontroller to act accordingly. The system includes a warning system through voice rendering and through the generation of vibration.**

Keywords- Ultrasonic Sensor; Blind Navigation; Obstacle Detection; Vibration; Voice feedback.

I. INTRODUCTION

India is now home to the world's largest number of blind people. Of the 37 million people across the globe who are blind, over 15 million are from India [1], [2]. Most of these people are from families with very poor economic condition and they rely on other people to help them or use white canes, to roam around. The project proposes a navigation system that includes a white cane capable of detecting obstacles and providing feedback. Since blind people are more efficient in hearing and possesses strong perception than normal people, therefore the system focused on alerting the user through vibration and voice feedback. This novel navigation system is designed for helping the blind people to navigate around safely. User does not need to move the white cane around to detect obstacle like they do with the normal cane. Therefore user can easily walk with the white cane and continuously get information about obstacles around with the help of sonar sensor. Many researches are being conducted on building a navigation system for the visually impaired people. Several researchers [3], [4], [5], [6], [7], [8] address this challenge in indoor and outdoor environment. However most of these approaches have limitations, since this challenge involve many issues (e.g., accuracy, coverage, usability and Interoperability) which are not easy to address with the current technology. Dhruv Jain *et al.* developed a system Roshni [9] that can be used for indoor navigation system for blind person. This system consists of the following functional components: assistance for determining the user's position in a building, a detailed interior map of the building and a mobile application. By pressing keys on the mobile unit, directions concerning position, orientation and navigation can be obtained from the portable system via acoustic messages. A RFID based navigation system proposed by Punit Dharani *et al.* [10]. The system provides a technological solution for the visually impaired to travel through public locations easily using RFID. Parth Mehta *et al.* proposed a novel indoor navigation system for visually impaired people [11] and the paper illustrates a structure which uses the IR sensor and magnetic compass on the VI-Navi handheld device to determine the location and orientation of the user in a fast and a robust manner using a voice enabled GPS inside a closed environment . Tarik Kapi´*etc. al.* [12] proposed a system with a special emphasis on the survey among visually impaired people that resulted in effective information on their perception of their surroundings. Koley *et al.* [13] developed a voice operated outdoor system for visually impaired person. The navigation system makes use of GPS, voice and ultrasonic sensor for obstacle detection. It can notify the users their current location and provide verbal directions for travelling to a remote destination [13]. Though this system provides verbal direction but does not have an obstacle detection and warning feedback. The proposed navigation system in this paper mainly focuses on two components: (i).Sensing of the immediate surrounding environment against obstacles for the visually impaired person and (ii).Warning about the obstacles by means of vibration and voice feedback system. This navigation aid can be an efficient and cutting edge tool for indoor and outdoor environment for visually impaired people. Therefore, the project mission is to carry out the following functions: Detection of obstacles using ultrasonic sensors, Implementation of vibrational alert and voice feedback system using vibrator motor and APR9600 ChipCorder respectively. The system contains three ultrasonic sensors HC-SR04, which will detect the barriers in the path. The control system is developed using ATMEGA16 microcontroller. With the response from the ultrasonic sensors, the distance between the person and the obstacle is measured. Delicate motor circuitry is used to create vibrational alert and APR9600 chip is interfaced to produce a speech output, so that the person can know the direction of the obstacle and sense its distance. So the overall system goal is to construct a portable, simple, less costly device that will help visually impaired people to move in unfamiliar environment.

1. K.Rajan is with the Electronics and Communication Engineering Department, RVS College of Engineering and Technology, Karaikal, Puducherry, India. (e-mail:kj.rajan28@gmail.com)

2. E.Kalaiselvan is with the Electronics and Communication Engineering Department, RVS College of Engineering and Technology, Karaikal. He completed his M.Tech Degree in Pondicherry Engineering College and currently working as Assistant Professor. (e-mail: kalai5selva@gmail.com).

II. System Architechture

This project is realized with the generation of vibration and through the voice module. The Fig. 1 shows the block diagram of stick unit which is handled by the blind people. It performs the obstacle detection and alerts the blind people. It consists of three ultrasonic sensors [14] HC-SR04, which continuously sends and receives the ultrasonic waves, the timing of the echo signal has been observed by the ATMEGA16 controller. The distance between the person and obstacle is observed by the ATMEGA16 controller using the ultrasonic sensor.

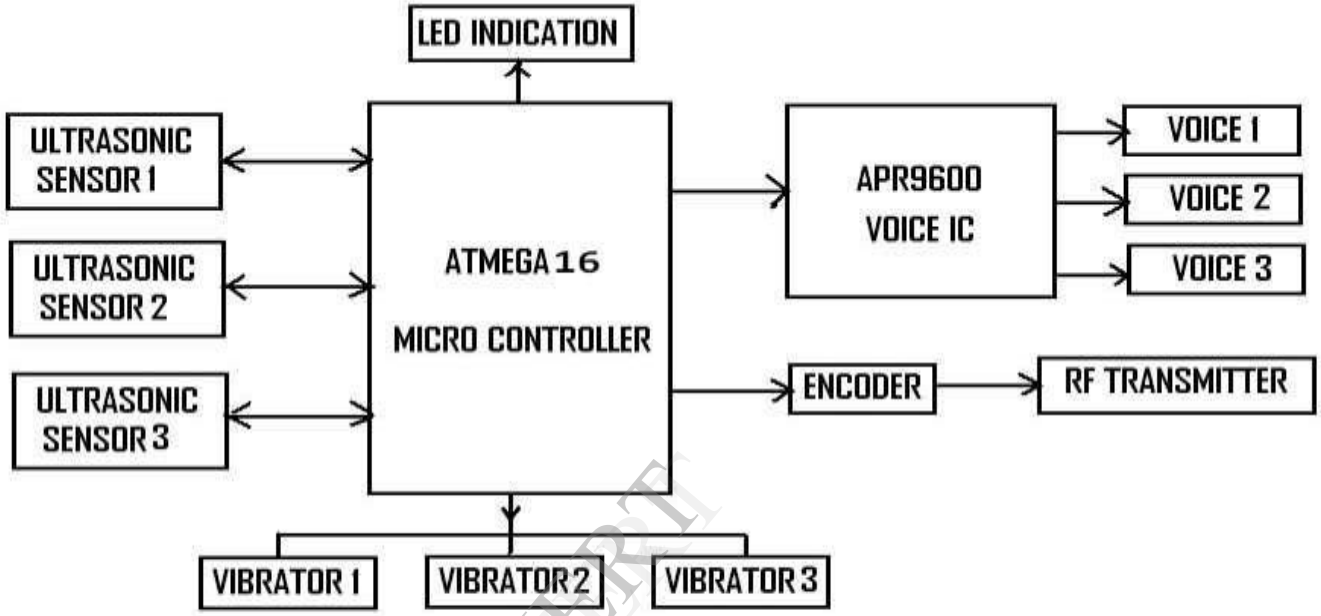

Fig. 1 Block Diagram of Stick unit

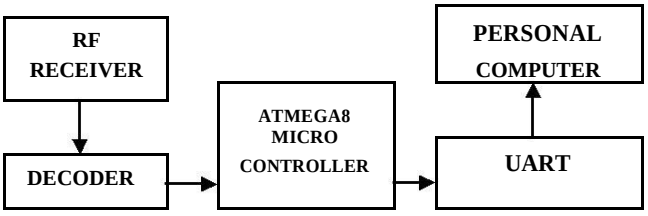

Fig. 2 Block Diagram of Monitoring Unit

The embedded controller controls the vibration motor circuit to warn the people. Correspondingly the controller interfaces the APR9600 voice ChipCorder to alert the people through the recorded voice. So the people know the direction of the obstacles. The various directions can be obtained by three sensors. An algorithm has been developed that allows the microcontroller to work in different conditions required for the navigation system. The System uses a switch for turning on or off the system.

III. Design Flow of The System

When the system is turned ON, It continuously checks for obstacles in three directions by sending ultra sound. If there are no obstacles, the system continues its search but if there is, the vibrator motor of the respective side will turn on and speech output will notify the user by speech notification.

Fig.3 shows the diagram that outlines the navigation aid's workflow.

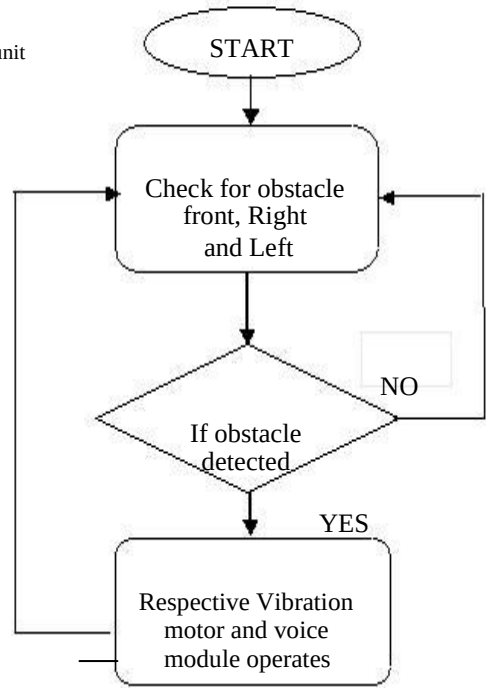

Fig.3 Flow Chart of the Navigation system

IV. PROPOSED SYSTEM

A. *Distance Measurement*:

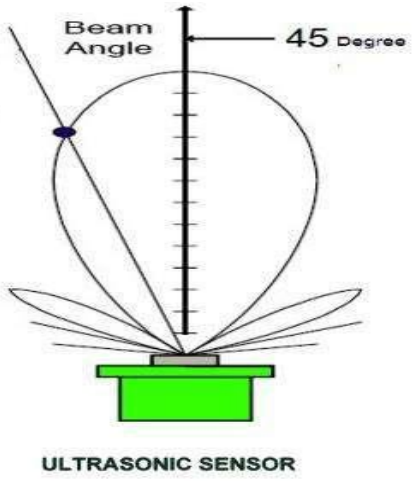

Fig. 4 Angle measurement

Distance measurement is done by a circuit using the ultrasonic sensor, microcontroller ATMEGA16 and an LED display. When there is an object the sensor will send back the signal to the microcontroller. It was found that the smallest time required for the ultrasonic sensor to detect the emitted pulse reflected off the obstacle is 200us. If there is no object the signal descends to low value. The distance calculated by the microcontroller is displayed LED display. The value obtained contained inaccuracies with respect to the actual distance measured. However, the inaccuracies are found to be consistent in every measurement and it was possible to determine the offset. Therefore a correction algorithm is introduced in order to obtain accurate distance between the sensor and the obstacles which can be viewed in the LED display. The experimental range is found to be 10cm~290cm and the signal covers an angle of 45^0 as shown in Fig.4.

B. *Interfacing*

Subsequent to the measurement of the range of the obstacle, the motors were used to generate the vibration. However, the signal generated by the ATMEGA16 does not carry enough power to run vibration motor. Therefore a transistor is introduced to generate the higher flow of current which is required for the vibration motor to run. The transistor is controlled using the ATMEGA16 microcontroller in order to provide the sufficient power to run the vibration motor. The algorithm is developed in a way so that it allows generation of vibration of different motors corresponding to the distance measured. Therefore, the navigation system allows the blind person to assess different distances of the obstacles from vibration of different directions. From the Table-1, for instance, it can be seen that at distance of 30cm the motor will vibrate at various directions belongs to ultrasonic output.

.

C. *Voice Feedback*

ASP 9600 IC as shown in Fig.1 has been incorporated in the navigation system to provide speech assistance to the blind person. It is a single chip that allows multiple messages. This chip allows the system to record 60 seconds voice and play it back with very high quality. The ultrasonic sensors are set up to detect the obstacles in the left, right, front, left -right, and right-front and left-front directions. Three sensors are set to detect obstacles in three different directions. The connections of the sonar are adjusted in such a way according to user convenience to detect obstacles of the following left, right and front direction as shown in Fig.5. Upon detection of the signal from the sensors it triggers the recorded messages stored in the different addressing memories of the ASP 9600 to be played. The voice alert is enabled when obstacles are detected. As outlined in Table-2, for obstacles in different directions, different recorded messages are played, such as, "Obstacle upfront", "Obstacle to the left" and so on.

D. *Figures and Table*

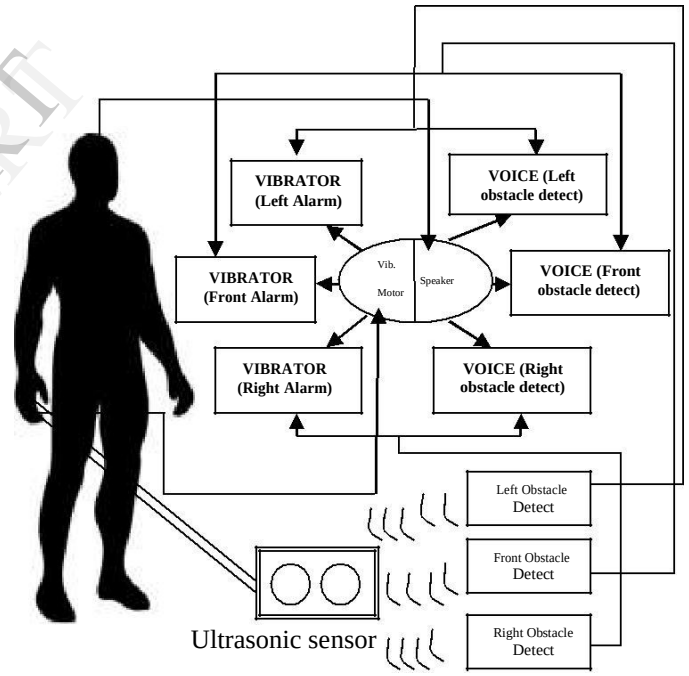

Fig. 5 Navigation aid system processing

In Fig.5 shows that the navigation aid system uses the sonar sensors for detecting waves that bounce off a surface of any object. The strength of the reflected waves activates the vibrator and the voice-alarm accordingly, to inform the users about the obstacles in their surroundings.

Table I. Alarm System Process

Distance between the obstacle and the white Cane	***Response of Vibration motor***
Distance is less then 30cm in front	Front motor vibrates
Distance is less then 30cm in Right	Right motor vibrates
Distance is less then 30cm in Left	Left motor vibrates

Table II. Voice Feedback Process

Direction of obstacle respective to the white cane	***Announcement in the speaker/Headphone***
Front	Obstacle Upfront
Left	Obstacle to the Left
Right	Obstacle to the Right
Front and Right	Obstacle Upfront and to the Right
Left and Right	Obstacle to the Left and Right
Front and Left	Obstacle Upfront and to the Left

V. RESULT

A prototype of the implemented system is shown in Fig 6. A white can is equipped with ultrasonic sensors at the bottom and control circuitry at the top for the feedback.

Fig.7 demonstrates that the ultrasonic sensor position at the front detects strong reflection of waves coming only from the front, meaning that there is an obstacle. The vibrator wrapped around the wrist band vibrate continuously and the recorded voice keep playing "Obstacle on the front" until the user moves away from the obstacle either walking towards left or towards right Similarly if the sonar receives strong ultrasonic waves from the left or right, the system will provide vibration and voice feedback accordingly. Again if the sonar do not receive any reflected wave, then the vibrator and the voice feedback will be inactive, which means the user can walk in any directions (right, left and front) unhindered

Fig. 6 A Prototype of the proposed system

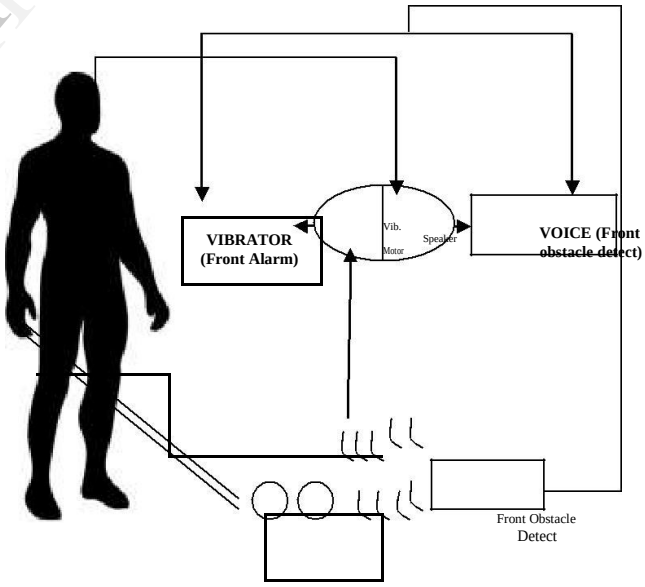

Fig. 7 An obstacle to the front side is detected and the vibrator vibrates

within 70cm range. If the white cane is tilted 45 degree with horizontal axis, then the accuracy of the system will be 95%, with 70 cm as its range. Though the ultrasonic sensor has a 10-200cm range, yet for maximum accuracy, 70 cm range was used. As long as the cane is angled at 45 degree, no matter which way the cane

moves, (i.e. left, right or straight) the accuracy will be maximum. Any shift in the angle (30^0-60^0) will reduce accuracy to 70-80%.

CONCLUSION

A novel navigation system is designed and implemented which helps blind people to navigate safely. ATMEGA16 microcontroller was used to develop the smart obstacle detection system which allows the blind person to avoid obstacles using the feedback through vibration and voice. The primary objective of this design was to make the system cost effective and easier to handle for a visually impaired person. In order to make it easier for the person to use, the navigation aid have mounted the sonars for detecting obstacles in particular directions. Therefore the person does not require moving the cane around to detect barriers like they do with the normal cane. They can easily walk with the cane and the sonars will simply detect the obstacles and help the person to maneuver around it. The system has a built in vibration and voice feedback which alerts the user if any obstacle is around and within 70cm. The sonars are adjusted in a way to ensure user convenience in detecting obstacles in three directions. The voice alert and vibration continuously inform user about the obstacle until the user moves away from the obstacle within the range of 70cm. This paper suggested that this aid will be an effective, low-cost and user friendly solution for navigation problems of visually impaired person.

REFERENCES

[1] Kounteya sinha “India has largest blind population”, The Times of India | New Delhi,October 2007..

[2] A. Alech “Bangladesh fights to end blindness”, Guardian Weekly, Tuesday 28 September 2010

[3] L. Ran, S. Helal and S. Moore, (2004, March). Drishti: an integrated indoor/outdoor blind navigation system and service. In Pervasive Computing and Communications, 2004. PerCom 2004. Proceedings of the Second IEEE Annual Conference on (pp. 23-30). IEEE.

[4] J.M.Loomis, G.G.Reginald, and R.L.Klatzky. "Navigation system for the blind: Auditory display modes and guidance." Presence: Teleoperators and Virtual Environments 7.2 (1998): 193-203.

[5] B.S.Rao, K.Deepa, H.Prasanth, S.Vivek, SN.Kumar, A.Rajendhiran, J.Saravana. “Indoor navigation system for visually impaired person using GPS” International Journal of Advanced Engineering Technology E-ISSN 0976-3945

[6] “Blind Audio Guidance System”, project by B.Danels, O.Ogunmakin, G.Agollah, E.Worley.

[7] J.Sakhardande, P.Pattanayak, M.Bhowmick, “Smart Cane Assisted Mobility for the Visually Impaired”. World Academy of Science, Engineering and Technology 70, 2012.

[8] M.H.V.Le, “Indoor Navigation System for Handheld Devices”, Worcester, Massachusetts, USA, 2012.

[9] Roshni: Indoor Navigation System for Visually Impaired by D.Jain and M.Balakrishnan, P.V.M.Rao.

[10] P.Dharani, B.Lipson and D.Thomas, “RFID Navigation System for the Visually Impaired”, Worcester Polytechnic Institute, 2012.

[11] P.Shah, P.Mehta, P.Kant and A.K.Roy, "VI-Navi: A Novel Indoor Navigation System for Visually Impaired People".

[12] T.Kapic, “Indoor navigation for visually impaired”, a project realized in collaboration with NCCR-MICS (2003).

[13] S.Koley and R.Mishra, “Voice operated outdoor navigation system for visually impaired persons”, International Journal of Engineering Trends and Technologyvol. 3, issue2- 2012.

[14] M.Bousbia-Salah, A.Redjati, M.Fezari and M.Bettayeb, “An ultrasonic navigation system for blind people”. In Signal Processing and Communications, 2007. ICSPC 2007. IEEE International Conference on (pp. 1003-1006). IEEE.

[15] “Pathfinder: A handheld device for detecting obstructions in the path of the blind and visually impaired”, project by K. Boyace, A. Patten and K. Mayall.

To Design and Analyse the Performance of Microstrip Ring Slot Antenna for 2.4GHz

Thamizhazhagi R[1], Abirami D[2], Sivasanthiya N[3]
[1]Assistant professor, [234]Students (Bachelor of Technology),
[1234]Department of Electronics and Communication Engineering
Dr. S.J.S. Paul Memorial College of Engineering and Technology,
Puducherry - 605 502, India

***Abstract* - A microstrip fed ring slot antenna is designed for 2.4GHz frequency range. To suppress the harmonics in the ring slot antenna inverted U-shaped slot is integrated into CRSA. By this, harmonic suppression over a wide bandwidth is achieved. This DGS can also be applied for the stacked annular ring microstrip-fed ring slot antennas**.

Keywords: Circular ring slot antenna (CRSA), Defected ground structure (DGS).

1 INTRODUCTION

THE ADVANCED wireless communication systems require a compact and low-cost transmitter front end without sacrificing system performance. Crucial factors for wireless transmitters include efficiency, size, and bandwidth. Ways of achieving this are typically through high system integration and improved performance. However, this may cause increased electromagnetic interference (EMI) between transmitter subsystems. This paper presents new design techniques which specifically address these factors. These goals are accomplished through increased integration between the amplifier and antenna. In a conventional system, the antenna is typically designed separately and connected to the amplifier by an interconnect.

Additionally, when multiple systems operating at neighboring frequencies exist in close physical proximity, there is an increasing EMI problem. To remedy this, a filter is often placed between the amplifier and antenna to reduce unwanted radiation. Traditionally, these components are designed with 50- input and output impedance and connected together. This conventional method works well at low frequencies and when system design requirements are not tight. However, at high frequencies, interconnects become lossy and may possibly radiate or couple with other elements. . Many planar antennas such as the microstrip patch or slot antenna can be designed for low input impedance and good radiation characteristics when operated near resonance. Therefore, the antenna and amplifier can be combined together with minimal matching circuitry in between. Perhaps the most crucial factor in power-amplifier design is increasing efficiency. Typically, most of the system power is consumed in the output power-amplifier stage. Since higher dc power adds to both system cost and weight, power-added efficiency (PAE) of the amplifier has to be maximized. Traditionally, this is done by using harmonic tuning, which reflects harmonic power back to the device [2]. Recently, biasing schemes have been reported for increasing PAE [3]. This technique optimized the power-supply voltage in accordance with the input signal level to reach maximum PAE. There are several techniques in harmonic tuning. Typically, higher order harmonics contain only a small amount of power. For this reason, practical designs usually terminate only second and third harmonics. Traditionally, tuning of the second harmonic is done by adding a quarter-wavelength (at the fundamental frequency) short-circuited stub at the output [4], [5]. Typically, this is most often placed at the drain bias line. At lower frequencies, this stub may use considerable circuit space. However, chip capacitors can also be used for rejection of the second harmonic if they have a self-resonance at the second harmonic [6]. Similar methods are used for tuning of the third harmonic. In this paper, we present several alternative methods for harmonic tuning. If designed properly, these methods offer a compact design. The first of these approaches is the active antenna approach. If the antenna input impedance is purely reactive (or zero)

at harmonic frequencies, it can be used to tune harmonics.

This has been demonstrated in [7]. In this case, tuning of the second harmonic with an integrated antenna was shown to increase the PAE by 7%. There are additional benefits to this approach. In addition to increased PAE or output power of the amplifier, a reduction of unwanted harmonic radiation that causes EMI and ultimately degrades system performance can be observed. The previously mentioned harmonic-tuning techniques are typically narrow-band. Some high-performance communication systems, for example those using multicarrier broadband code-division multiple-access communication (CDMA), require high-efficiency broad-band power amplifiers. Broadband harmonic tuning can be achieved using a microstrip filter based on the photonic bandgap (PBG) concept [8]. PBG is a periodic structure which prohibits wave propagation in certain frequency bands. Original PBG research was done in the optical region [9], but PBG properties are scalable and applicable to a wide range of frequencies. In the microwave region, PBG structures have been used in design of antennas [10], cavities [11], frequency-selective surfaces, and many other structures. In this paper, two-dimensional (2-D) structure based on etching a periodic 2-D pattern in the microstrip ground plane is used [12]. This structure has a stopband that is generally wider than can be achieved by using a single or double stub. This periodic structure is added between the antenna and amplifier. This configuration has an additional component, but can be used for broad-band operation. The analysis of active antenna amplifiers is quite challenging. Traditionally, nonlinear analysis such as harmonic balance is used to analyze power amplifiers. This kind of simulation cannot analyze antennas or PBG structures, in which a three-dimensional (3-D) full-wave solution of Maxwell's equations is usually required. In this paper, the finite-difference time-domain (FDTD) technique is used because it can simulate arbitrary 3-D structures and provide broad-band frequency response with one simulation. FDTD results can then be incorporated into nonlinear circuit design to analyze the whole structure. The amplifier design examples consist of class-AB, class-B, and class-F amplifiers, which are prevalent at microwave frequencies. However, with increasing device technology, other potentially higher efficiency types of amplifiers have been reported at microwave frequencies. Recently, a class-E amplifier has been realized at 1 GHz with 73% PAE and output power of 0.94 W [13]. In this case, approximate class-E operation is achieved by open circuiting the second harmonic only. More recently, a four-element integrated-antenna array with class-E performance was demonstrated at 5 GHz [14]. *Output power greater than* 33 *dBm was* demonstrated with a PAE of 65%. These classes of amplifiers are also expected to benefit from the above techniques.

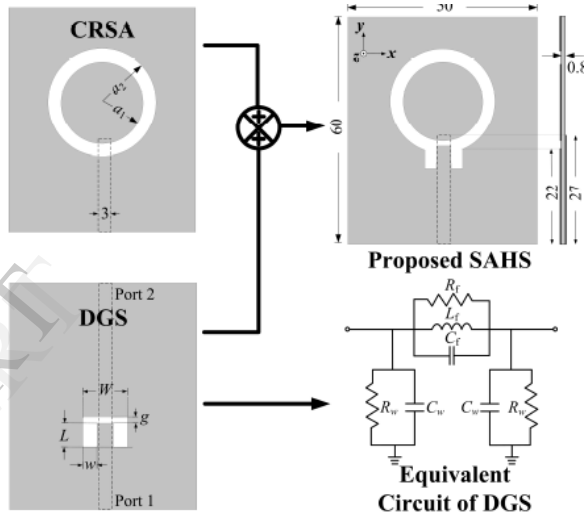

2. ANTENNA DESIGN

The antenna can be printed on an(60mm x 50mm x 0.8mm) FR4 substrate with a relative permittivity of 4.4 and loss tangent of 0.02 is depicted in fig. 1,and the corresponding photograph(both sides) is presented in Fig. 2. The proposed antenna is a combination of two simple structures, namely the microstrip-fed ring slot antenna. The main objective of this CRSA to induce a fundamental mode at approximately 2.4GHz band. Therefore, annular ring slot of inner radius

a1=10mm and outer radius a2=13.5mm were calculated according to the following.

$$f_o \approx \frac{c}{\pi(a_1+a_2)} \times \sqrt{\frac{\epsilon_r+1}{2\epsilon_r}}$$

Where c is the speed of the light in free space, and $\pi(a_1 + a_2)$ is the mean circumference of the ring slot antenna. However, the effects tuning various parameters such g and L will be discussed later.

Simulation based on high-frequency structure simulator(HFSS) was performed on CRSA. The CRSA can induce a fundamental mode(Mode 1)at exactly 2.45GHz,and other four modes were at approximately3.42GHz(Mode2),5.15GHz(Mode3),7.07 GHz

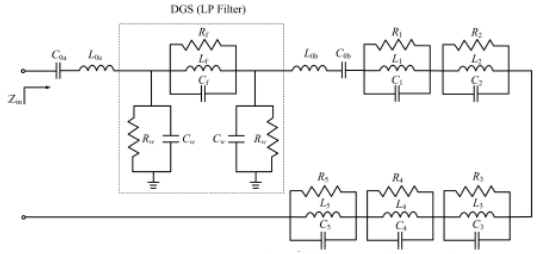

TABLE I
RLC VALUES OF ALL FIVE MODES

	MODE 1	MODE 2	MODE 3	MODE 4	MODE 5
R (Ω)	51	17	26	94	26
L (nH)	0.32	0.234	0.21	0.15	0.11
C (pF)	12.73	4.451	4.48	3.186	3.411

.

III MEASURED RESULTS AND DISCUSSION

the simulated and measured return loss is of both CRSA and two results validated well with each other in both cases. Here the measured 10-dB impedance bandwidth of 2.4GHz.

S-Parameter

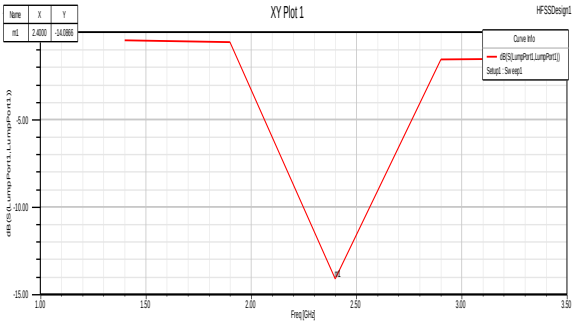

VSWR

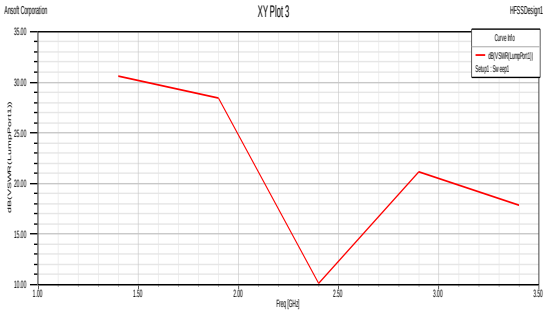

Radiation pattern

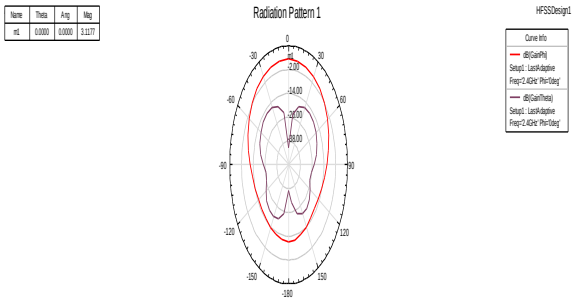

The measured radiation pattern in two principle planes namely the x-y and y-z planes, for both the antenna. The pattern measurement technique used a single axis rotational pattern that involves antenna under test(AUT) placed on a rotational positional.

During the process of measuring the antenna patterns the gain and efficiency were measured via the anechoic chamber. Here the antenna efficiency is defined as the ratio of total power radiated by an antenna to the net power accepted by the antenna from the connected transmitted which is expressed in this work. The efficiency of the proposed antenna is 79%.

IV STACKED ANNULAR RING

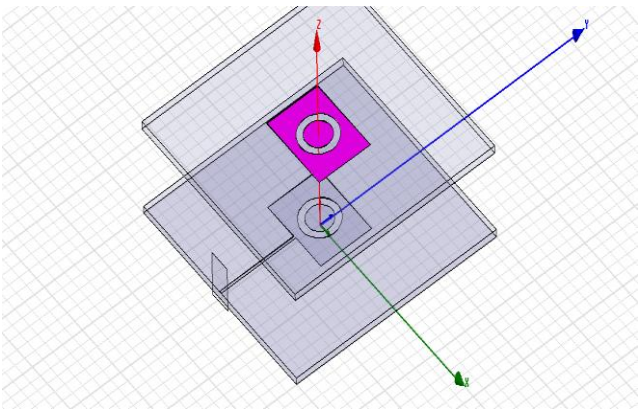

S-Parameter

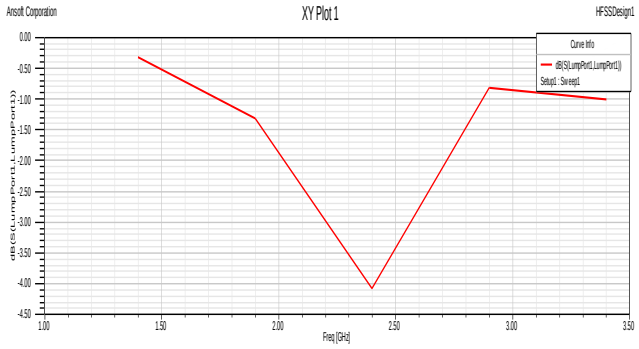

VSWR

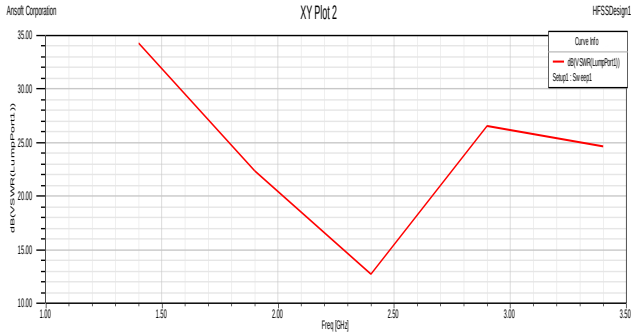

Radiation pattern

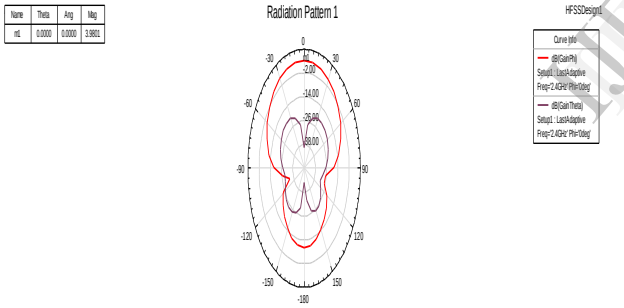

V CONCLUSION

By stacking the annular ring we improve radiation pattern and return loss. This can be used in Bluetooth and Wi-Max application

REFERENCES

[1] K. Chang, R. York, P. Hall, and T. Itoh, "Active integrated antennas,"*IEEE Trans. Microw. Theory and Tech.*, vol. 50, no. 3, pp. 937−944, Mar.2002.

[2] D. Segovia-Vargas, D. Castro-Galán, L. E. García-Muñoz, and V.González-Posadas "Broadband Active Receiving Patch With Resistive Equalization," *IEEE Trans. Microw. Theory and Tech.*, vol. 56, no. 1, pp. 56−64, Jan. 2008.

[3] V. Radisic, Y. Qian, and T. Itoh, "Novel architectures for high- efficiency amplifiers for wireless applications," *IEEE Trans.Microw. Theory and Tech.*, vol. 46, no. 11, pp. 1901-1909, Nov. 1998.

[4] F. R. Hsiao, T. W. Chiou, and K. L. Wong, "Harmonic control of a square microstrip antenna operated at the 1.8 GHz band," *Microw. conf. proceedings Asia-pacific*., pp 1052 -1055, Aug. 2001.

[5] V. Radisic, S. T. Chew, Y. Qian, and T. Itoh, "High efficiency power amplifier integrated with antenna," *IEEE Microw. Guided Wave Lett.*, vol.7, no. 2, pp. 39-41, Feb. 1997.

[6] Y. Horii and M. Tsutsumi, "Harmonic control by photonic bandgap on microstrip patch antenna," *IEEE Microw. Guided Wave Lett.*, vol. 9, no. 1, pp.13-48, Jan. 1999.

[7] X. C. Lin and L. T. Wang, "A broadband CPW-Fed loop slot antenna with harmonic control," *IEEE Antennas Wireless Propag. Lett.*, vol. 2, no. 1, pp. 323-325, 2003.

[8] A.S. Andrenko, Y. Ikeda, and O. Ishida, "Application of PBG microstrip circuits for enhancing the performance of high-density substrate patch antennas," *Microw. Opt. Technol. Lett.*, vol. 32, no. 5, pp. 340-344, Mar. 2002.

[9] Y. J. Sung, M. Kim, and Y. S. Kim, "Harmonics reduction with defected ground structure for a microstrip patch antenna," *IEEE Antennas Wireless Propag. Lett.*, vol. 2, pp. 111-113, 2003.

[10] S. Biswas, D. Guha, and C. Kumar, "Control of higher harmonics andtheir radiation in microstrip antennas using compact defected ground structures," *IEEE Trans. Antennas Propag.*, vol. 61, no. 6, pp. 3349-3353, Jun. 2013.

[11] N. A. Nguyen, R. Ahmad, Y. T. Im, Y. S. Shin, and S. O. Park, "A T-shaped wide-slot harmonic suppression antenna," *IEEE Antennas Wireless Propag. Lett.*, vol. 6, pp. 647-650, 2007

[12] D. H. Choi, Y. J. Cho, and S. O. Park, "A broadband slot antenna with harmonic suppression," *Microw. Opt. Technol. Lett.*, vol. 48, no. 10, pp.1984-1987, Oct. 2006.

[13] N. Boisbouvier, F. Le Bolzer, A. Louzir, A. C. Tarot, and K. Mahdjoubi, "Harmonic-less annular slot antenna (ASA) using a novel PBG structure for slot-line printed devices," *IEEE Antennas Propag. Soc. Int. Symp.*, vol. 2, pp. 553-556, Jun. 2003.

[14] D. J. Woo, T. K. Lee, J. W. Lee, C. S. Pyo, and W. K. Choi, "Novel U-Slot and V-slot DGSs for bandstop filter with improved *Q* factor," *IEEE Trans. Microw. Theory Tech.*, vol. 54, no. 6, pp. 2840-2847, Jun. 2006.

[15] K. L. Wong, C. C. Huang, and W. S. Chen, "Printed ring slot antenna for circular polarization," *IEEE Trans. Antennas Propag.*, vol. 50, no. 1, pp. 75-77, Jan. 2002.

[16] J. S. Park, J. H. Kim, J. H. Lee, S. H. Kim, and S. H. Myung, "A novel equivalent circuit modeling method for defected ground structure and its application to optimization of a DGS lowpass filter," *Microw. Symp. Digest, 2002 IEEE MTT-S Int.*, vol. 1, pp. 417-420, 2002.

Independent Living of Elderly Senior using Power Efficient and Interrupt- Driven Algorithm

[1.] S. Bharathi, [2.] B. Vinothini, [3.] V. Lavanya
St.Anne`S College Of Engineering And Technology
Department Of Electronics And Communication Engineering

Abstract: **This project presents the real-time activity recognition and fall detection system. It is tuned for robustness and real-time performance by combining human-understandable rules and classifiers trained with machine learning algorithms. The system consists of two wearable sensors. an accelerometer and a gyroscope, placed on the abdomen and the right thigh. The recognition of the user's activities and detection of falls is performed on a laptop using the raw sensors' data acquired through Bluetooth. The offline evaluation of the system's performance was conducted**

I. INTRODUCTION

FALLS pose major health problems for people aged 65 years and over. Falls occur in 30–60% of older adults each year, and 10–20% of these result in injury, hospitalization and/or death [1]. Without immediate help, seniors may suffer pain, emotional distress or even develop other complications including pneumonia, dehydration, hypothermia [2]. There-fore, immediate help after fall is of critical importance as it could lower the risk of complications and death, and greatly increase the likelihood of returning to independent living. In recent years, MEMS (microelectromechani cal systems) inertial sensors have sparked an intense interest in studying falls.The world's population is aging rapidly, threatening to overwhelm the society's capacity to take care of its elderly members.The percentage of persons aged 65 or over in developed countries is projected to rise from 7.5% in 2009 to 16% in 2050Fall detection is an important component of many ambient assisted living systems because approximately half of the hospitalizations of the elderly are caused by falls. The architecture of the system combines rules to recognize postures (static activities), which ensure the behavior of the system is predictable and robust, and classifiers trained with machine learning (ML) algorithms, to recognize dynamic activities, for which the rules are not sufficiently accurate.For the Fall detection, rules are used that take into account high accelerations associated with falls and the recognized horizontal orientation (e.g., falling is often followed by lying).

II.BLOCK DIAGRAM

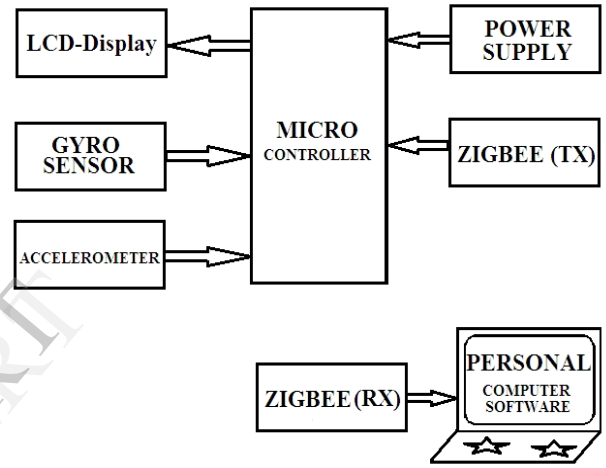

A single integrated circuit containing a processor core, memory, and microcontroller is a small computer on a programmable input/output peripherals. It act as brain of the system.

- A gyroscope is a device for measuring or maintaining orientation, based on the principles of angular momentum.
- An accelerometer is a device that measures acceleration relative to a free-fall
- A liquid-crystal display (LCD) is electronic visual display that uses the light modulating properties of liquid crystals. Liquid crystals do not emit light directly.
- A regulated power supply is an circuit that converts unregulated AC into a constant DC. This DC is used to power the circuits.
- Zigbee is a wireless device that is used for communication between UART supported devices

III.ACCELEROMETERS

.A. Hardware and Software Platform

The hardware platform for the proposed algorithms is shown in Fig. 1. It is designed to be a wrist-worn wearable device (WD) and consists of a CC2430 chip, a LED, a buzzer and an ADXL345 accelerometer. CC2430 is an enhanced 8051 MCU with a built-in ZigBee Transceiver from Texas Instruments.

IV. FALL DETECTION ALGORITHM

The proposed fall detection algorithm is derived from an algorithm [26] proposed in an application note by Ana-log Devices. The original algorithm characterizes a fall

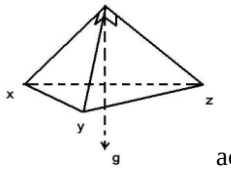

accelerometer reading by all axes converging towards zero. This pattern can be exactly captured by using FREE_FALL interrupt.

proposed 0.75 g and 30 ms for THRESH_FF and TIME_FF which are threshold and time windows of FREE_FALL interrupt respectively. There is a serious flaw with this threshold. ADXL345 asserts FREE_FALL when all axes are smaller than THRESH_FF for a time longer than TIME_FF. This assertion is not based on the vector sum of all

axes which is $sv = x^2 + y^2 + z^2$. There is a possibility that the accelerometer is positioned such that all axes have equal angles with the gravity vector.

B. Algorithm Description

The proposed algorithm is modeled as a finite-state machine. A flow chart shown in Fig. 3 is used to illustrate the algorithm. It essentially consists of six states, from F0 to F5. The details of this algorithm are described as below.

(F0) F0 is the initial state as well as reset state. ADXL345 is initialized as follows:

Data rate: 25 Hz. ACTIVITY, INACTIVITY are enabled and mapped to INT1. ACTIVITY threshold is 2.25 g. INACTIVITY threshold is 0.5 g and its detection time window is 1 second.

Link mode is enabled. By enabling link mode in the state F0, INACTIVITY will not be asserted repeatedly if seniors are not moving (e.g. sleeping).

FREE_FALL is enabled and mapped to INT2. FREE_FALL threshold is 0.5625 g and its detec-tion window is 20 ms. FIFO is initialized to TRIGGER mode and is triggered by FREE_FALL. When triggered, FIFO will hold the latest 16 samples before the trigger, discard earlier ones, continue to collect until full. When returning from other states, CC2430 timer ticks (started in F1) will be stopped and the system

Experimental Studies

Trial Study: A trial study has been carried out to evaluate fall detection accuracies in real world scenarios at Jurong Central Daycare Centre, which is a typical eldercare It is observed that during continuous walking, falls were never be falsely detected as INACTIVITY interrupt did not have a chance to assert. While sitting down, wrists occa-sionally hit the desk with high impact, a false positive fall will be accidentally triggered. It can also be observed that young subjects easily created false positives (3/20). In contrast, seniors in their real daily lives only creates 1.153 times per day as evaluated in Section IV-C.1. A very probable reason is that young stronger subjects create large impacts in their ADLs which were easily confused with a fall in the fall detection algorithm, The total current consumption of a WD is measured by connecting a 7.5_ resistor in series with it. The WD polls message from its parent range extender every 5 seconds. Fig. 5a shows a measurement of power consumption of the WD for a duration of 10 seconds when statically placed. Two current peaks spaced by 5 seconds can be easily identified. Each peak corresponds to CC2430 waking up from sleep mode for polling. The magnitude of the current peak is aapproximately $4.4 \times 50\ mV / 7.5\_ = 29.33\ m\ A$. The sleep current is too small to be readable. Instead, it was measured by a multimeter to be 69 $\mu\ A$. Within the 69 $\mu\ A$ sleeping current, 40 $\mu\ A$ is attributed to the current consumption of ADXL345 at an ODR (output data rate) of 25 Hz. The remaining 29 $\mu\ A$ is consumed by CC2430 in sleep mode and its peripherals.

TABLE I

SIMULATED FALL RESULTS

Activity type	With a fall	Falls detected
(1)	yes	19/20
(1)	no	0/20
(2)	yes	19/20
(2)	no	0/20
(3)	yes	17/20
(3)	no	0/20
(4)	no	3/20

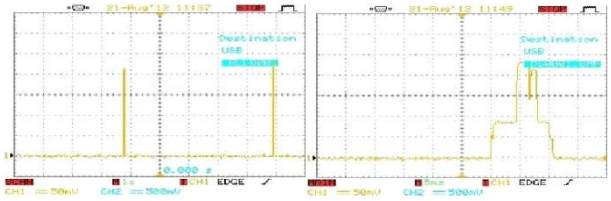

(a) (b)

activity five times for two minutes each time. Then activities (1), (2), (3) were performed again for five times, but each with a fall in the middle. Test results are shown in Table It is observed that during continuous walking, falls were never be falsely detected as INACTIVITY interrupt did not have a chance to assert. While sitting down, wrists occa-sionally hit the desk with high impact, a false positive fall will be accidentally triggered. It can also be observed that young subjects easily created false positives (3/20). In contrast, seniors in their real daily lives only creates 1.153 times per day as evaluated in Section IV-C.1. A very probable reason is that young stronger subjects create large impacts in their ADLs which were easily confused with a fall in the fall detection algorithm, as discussed in Section .

D. Battery Life Analysis

The total current consumption of a WD is measured by connecting a 7.5_ resistor in series with it. The WD polls message from its parent range extender every 5 seconds. Fig. 5a shows a measurement of power consumption of the WD for a duration of 10 seconds when statically placed. Two current peaks spaced by 5 seconds can be easily identified. Each peak corresponds to CC2430 waking up from sleep mode for polling. The magnitude of the current peak is aapproximately $4.4 \times 50\ mV/7.5\_ = 29.33\ m\ A$. The sleep current is too small to be readable. Instead, it was measured by a multimeter to be 69 $\mu\ A$. Within the 69 $\mu\ A$ sleeping current, 40 $\mu\ A$ is attributed to the current consumption of ADXL345 at an ODR (output data rate) of 25 Hz. The remaining 29 $\mu\ A$ is consumed by CC2430 in sleep mode and its peripherals.

V. CLASSIFICATION OF ACTIVITIES OF DAILY LIVING

In the proposed fall detection algorithm, depending on the wrist's movement, the algorithm flows dynamically among the six states. The time it spends in each state gives a lot of information about activities of a wearer.

Traditionally, studies of ADLs such as Wockets aim to identify a number of activities including walking, climbing stairs, sitting, sleeping, bathing, cooking, using multiple sen-sors. In this paper, since only one accelerometer is used, only a few simple activities can be inferred from accelerometer data. The identifiable activities are "Walk", "Random" (random wrist movements), and "Quiet" (no movement at all). These activities are purely inferred from accelerometer information. However, it is possible to categorize these activities into more specific activities or even abnormalities by using accelerometer data along with additional contextual information such as time and location. For instance, "Quiet" at mid night most likely means sleeping. Too many "Random" incidences during night might indicate poor sleeping quality. "Quiet" in bath rooms longer than certain time (e.g., 30 minutes) is abnormal and an alert can be raised.

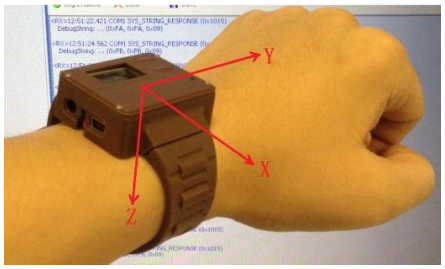

Fig. 6. Alignment of accelerometer axes when worn by a human subject.

obtained by experiments. Both interrupts need to operate in AC mode and link mode is still enabled. By setting both thresholds to the same small value, when a wrist moves a small amount, ACTIVITY will be asserted, and when the wrist is relatively static, INACTIVITY will be asserted in 1 second. This setting only lives within state F0. Whenever the fall detection algorithm transits to state F1, both thresholds will be immediately configured to 2.25 g and 0.5 g for ACTIVITY and INACTIVITY respectively.

With above hardware settings, four types of events can be identified from the fall detection algorithm and they are named with the following conventions:

*E*0 : generated whenever an INACTIVITY interrupt asserted in state F0
*E*1 : generated whenever an ACTIVITY interrupt asserted in state F1
*E*2 : generated whenever the fall detection algorithm transits from state F0 to state F1
*E*3 : generated whenever the fall detection algorithm transits from state F1 to state F2

There are underlining physical meanings associated with these four events. *E*0 is generated whenever a wrist

changes from active movements to motionless. $E1$ is generated when the wrist slightly moves or changes orientation. This cor-responds to casual movements human makes during ADLs. $E2$ corresponds to weightlessness at the wrist, which is generated when the wrist is lowered from a higher level. This happens when the subject falls, walks (swings arms) and sits down. During ADLs, accelerometer values will typically fluctuate around the gravity value. Capturing only the weight-less part is good enough to estimate the activity level. $E3$ is typically generated during drastic movements such as a fall, suddenly sitting down and putting down arms onto desks.

Along with above events, directions of Y-axis during the occurrence of these events are also taken as a feature. Fig. 6 shows the alignment of axes of the accelerometer when worn by a human subject on his left wrist. Y-axis is always aligned with the subject's lower arm. Y-axis information is critically important for estimating ADL as Y-axis is typically pointing approximately downwards when the human subject is standing or walking. During sleeping, Y-axis is usually approximately horizontal.

B. Preprocessing

Fig. 7 shows raw data collected from a WD worn by a human subject who performed two actions including "Walk" and "Random" ("Quiet" is not shown as it basically contain
no events). Each action lasted exactly a minute. Below is a list of intuitions based on the raw data.
During "Random", only $E0$ and $E1$ are generated in alternating manners (as the accelerometer's link mode is enabled).During "Walk", as the arm swings, FREE_FALL interrupt will be generated and the fall detection algorithm moves from state F0 to state F1. As there is no impact following FREE_FALL during walking, the fall detection algorithm returns to state F0 shortly. This pattern repeats and generates a lot of $E2$ as well as $E0$ and $E1$ along the way. Also observe that Y-axis values are always positive as Y-axis typically points downwards during walking. During "Quiet", no events will be generated. Leaves more energy at the present time than an event which occurred a long time ago. The host MCU could tell if an event has just occurred recently by evaluating current energy level of this event.

The proposed ADL classifier takes the second approach. The first approach requires uncertain amount of memory space to keep track of all events in the past 10 seconds, which should be avoided in an 8-bit MCU. In addition, it will compute the same event multiple times as the 10-second time-window shifts by one each time. The second approach can be easily implemented and requires less computational resources. For each of the four events ($E0$, $E1$, $E2$ and $E3$), an energy function is proposed to keep track of the activeness of this event in the recent past.

The contribution of an event to its energy function decays with time. An exponential decay function is proposed in Equation 2.

$$\eta(t) = e^{-t/\tau}. \quad (2)$$

where t is the elapsed time and τ = 10 seconds which means that an event's energy decays to $e^{-1} \approx 0.37$ of its original value after 10 seconds.

Upon the occurrence of an event, energy of all events in the past are reduced by a factor η ($0 < \eta \leq$ which is related to the elapsed time of the previous event. The energy of the occurred event will be incremented correspondingly. The exponential function for computing the decay factor can be efficiently approximated by using a look-up table and interpolation in host MCUs.

The proposed ADL classifier is completely event-driven as it only computes upon occurrence of an event. This leads to a problem when a WD is "Quiet". Consider a human subject is walking initially and suddenly keeps still. An event $E0$ will be generated one second after he keeps still. At point, the classification of his action over the past 10 second could be "Walk". As no event will be generated after this $E0$, the algorithm will not compute at all thereafter and the classification result remains as "Walk" which does not reflect the fact. To resolve this issue caused due to no events ever being generated during "Quiet", an artificial event is created and named as E_{-1} to signify its special purpose. Upon occurrence of an E_0 event, after which might follow a long "Quiet" period, a dummy check event is scheduled to be set in 5 seconds using a timer. Any other event which occurs before this timer expires will cancel this timer. If no other event cancels, the algorithm, upon seeing this dummy event, will reset energy functions of all events to zero.

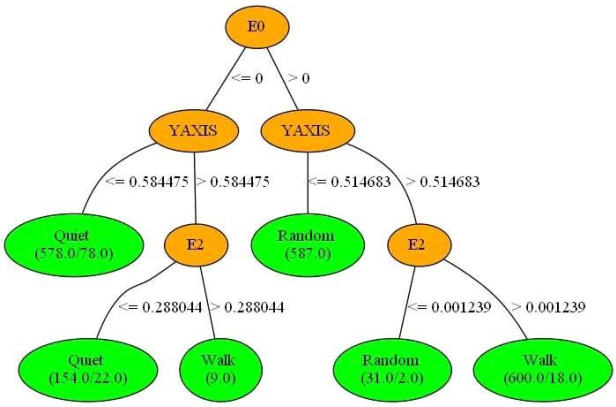

Classification Outcome

Decision tree learning has been extensively used in statistics, data mining and machine learning. C4.5, developed by

Ross Quinlan, is a well-known learning algorithm for gener-ating decision trees. As it accepts numerical attributes, data obtained from the Algorithm 1 can be conveniently fed into a C4.5 training algorithm. This paper uses a C4.5 implementa-tion in Weka (Waikato Environment for Knowledge Analysis), a data mining suite developed at the University of Waikato.

D. Classification Algorithm

Six groups of ADL data have been collected from six young human subjects. Each subject performed 4 minutes of "Walk", 4 minutes of "Quiet" and 5 minutes of "Random". Four out of the six groups of ADL data are used training data and the other two are used as testing data.

Details of the classification results for one of the testing subjects along the time line. Activity of the first 240 seconds is "Walk", followed by another 240 seconds of "Quiet" and ended by 300 seconds of "Random". It can be seen that the classifier performs fairly well. In fact, it is robust enough that in the "Random" period, the subject pauses a few seconds in between. Thus, the labels for that interval is actually incorrect. Nevertheless, the classifierrobust

VI. CONCLUSION

In this paper, a fall detection algorithm and an ADL classifi-cation algorithm for a wrist-worn device have been proposed.They are interrupt-driven and can be efficiently implemented in battery-powered MCUs with limited clock speed and RAM. Both algorithms are hardware-dependent as they are based on a modern digital MEMS accelerometer which supports various interrupts and FIFO. The advantage is that they are more power-efficient than conventional algorithms which must examine and process each sample of accelerometer data. By processing accelerometer data completely locally, a WD does not have to stream massive sensor data out wirelessly thus saving both power and bandwidth. In the context of *e-Guardian*, less bandwidth consumption results in better scalability thus allowing a single system to accommodate more WDs.

REFERENCES

- L. Z. Rubenstein, "Falls in older people: Epidemiology, risk factors and strategies for prevention," Age Ageing, vol. 35, no. 2, pp. 37–41, Sep. 2006.
- Lifeline With Autoalert Option. [Online]. Available: http:// www.lifelinesys.com/content/lifeline-products/auto-alert,accessed Jul. 14, 2013.
- F. Sposaro and G. Tyson, "iFall: An Android application for fall monitoring and response," in Proc. Annu. Int. Conf. IEEE Eng. Med. Biol. Soc. (EMBC), Sep. 2009, pp. 6119–6122.

Design and Implemntation of Vga on FRC – FPGA using VHDL

Yuvaraj .S
M.E. Applied Electronic,
Ck College Of Engineering,
Cuddalore,

***Abstract*: In proposed system, introduce real time Full VGA display @ 60HZ Frame rate conversion implemented on FPGA technology. By using the Frame rate conversion a programming design and implement VGA Controller on FPGA, VHDL is used to describe and program the gates and counters in FPGA blocks in order to construct an internal logic circuit in FPGA. The main purpose of this project is to design and implement VGA Controller on FPGA at real time based frame rate conversion. The realized function of the movement and rotation of blocks, randomly generating next blocks. The successful transplant provides a template for the development of other visual control systems in the FPGA. It introduce real time Full VGA display @ 60HZ Frame rate conversion implemented on FPGA .**

Keywords : VGA ,FRC ,FPGA,VHDL

I.INTRODUCTION

VGA interface, as a standard interface has already been applications widely.VGA have to be working in a certain display mode anytime, and there are two kinds of these modes: character display mode and graphics display mode. A high-resolution and refreshing rate, we take the standard VGA graphics display mode .Field-Programmable Gate Arrays are digital integrated circuits that contain configurable blocks of logic along with configurable interconnects between these blocks. Specifically, an FPGA contains programmable logic components called logic elements and a hierarchy of reconfigurable interconnect that allows the less to be physically connected. The combinational functions, or merely simple logic gates like AND, XOR. In most FPGAS, the logic blocks also include memory elements, which may be simple flip-flops or more complete blocks of memory VGA is a video display standard. It provides a simple method to connect a system with a monitor for showing information or images[4]. As a standard display interface, VGA has been widely used. There is more and more need in displaying the result of the process in real time as the fast development of embedded system, especially the development of high speed image processing. Apart from that, display will be replacing paper for future.

Words of wisdom; seeing is believing and picture telling thousand words, display can give correct information about something. Display is used when people present something. Pictures or texts at display catch more attention than verbal voice when people are doing presentation. When people do that kind of presentation, there must be some device involved in control the display[2]. Verilog Hardware Description Language is a popular and standard hardware description language which is now extensively used by engineers and scientists on digital hardware designs. VHDL offers many useful features for digital hardware design, that is, VHDL is a general-purpose hardware description language that is easy to learn and easy to use. It is similar in syntax to the C programming language. VHDL allows different levels of abstraction to mix in the same model .Thus, a hardware model can be defined in terms of switches, gates, RTL, or behavioural code. Also, most popular logic synthesis tools support VHDL. This makes it the language of choice for designers' .The purpose of this project to design a VGA Controller using VHDL and implement it on FPGA. FRAME RATE UP CONVERSION refers the technique that produces higher frame video from the one with a lower frame rate through the process of generating new frames and inserting them into original video .FRC is essential for reducing the motion blur and film judder and it is very challenging work to implement the complete FRC system on FPGA with real –time .In this paper we describe a real time FPGA implementation of VGA @60 HZ FRC system [7].

II. FIELD-PROGRAMMABLE GATE ARRAYS

FPGAs are a semiconductor device containing programmable logic components called "logic blocks", and programmable interconnects. Logic blocks can be programmed to perform the function of basic logic gates such as AND, and XOR, or more complex combinational functions such as decoders or simple mathematical functions. FPGAs are also known as reconfigurable devices. These reconfigurable FPGAs are generally favored in prototype building because the device does not need to be thrown away every time a change is made. This allows one piece of hardware to perform several different functions. Of course, those functions cannot be performed at the same time. Besides that, FPGAs are standard parts, they are not designed for any particular function but are programmed by the customer for a particular purpose. FPGAs have compensating advantages, largely due to the fact that they are standard parts. There is no wait from completing the design to obtaining a working chip. The design can be programmed into the FPGA and tested immediately. Apart from that, FPGAs are excellent prototyping vehicles. When the FPGA is used in the final design, the jump from prototype to product is much smaller

and easier to negotiate. Also, the same FPGA can be used in several different designs, reducing inventory costs.

III. VGA CONTROLLER

Video Graphics Array is mostly used for computer monitors, with a high-definition resolution video standard. It has the ability the ability to transmit a sharp detailed image. VGA uses separate wires to transmit the three color component signals, vertical and horizontal synchronization signals. Red, green and blue are three signals that send color information to VGA monitor. There are four main components in VGA controller which are VGA interface signals, VGA interface definition, VGA control signal, VGA timing Control and VGA monitor.

IV.VERY HIGH SPEED INTEGRATED CIRCUIT HARDWARE HESCRIPTION LANGUAGE

VHSIC was a 1980s U.S. government program to develop Very-High-Speed Integrated Circuits. The United States Department of Defense launched the VHSIC project in 1980 as a joint tri-service (Army/Navy/Air Force) project. The project led to advances in integrated circuit materials, lithography, packaging, testing, and algorithms, and created numerous computer-aided design tools. A well-known part of the project's contribution is the VHDL hardware-design language. The program also redirected the military's interest in GaAs ICs back toward the commercial mainstream of CMOS circuits. VHDL is commonly used as a design-entry language for field-programmable gate arrays and application-specific integrated circuits in electronic design automation of digital circuits

V. FRAME RATE CONVERSION

Many surveillance and monitoring videos are captured using static cameras with relatively low frame rate .the low frame rate of the videos is economics both in term of the monitoring equipment and storage requirement .other factor may influence the necessity of keeping a low frame rate ,such as limited transmission bandwidth for a remote surveillance solution .storage space may be an issue for remote surveillance solution storage space may be an issue for high definition resolution video capture however this poses a challenge in terms for the manual inspection of such video feeds ,since low frame rate videos frequently consist of non smooth motion are facts .This can lead to increased strain for the viewer. Therefore a key challenge toward improving the user experience lies in successfully obtaining a smoother video by increasing the frame rate viewer. Therefore a key challenge toward improving the user experience lies in successfully obtaining a smoother video by increasing the frame rate.

VI. METHODOLOGY

In this project the most required things will be VGA, FRC, FPGA.VGA stands for “Video Graphics Array”. It is the standard monitor or display interface used in most PCs. Therefore, if a monitor is VGA-compatible, it should work with most new computers. The VGA standard was originally developed by IBM in 1987 and allowed for a display resolution of 640x480 pixels. The VGA supports both All Points Addressable graphics modes, and alphanumeric text modes. There are two kinds of VGA interface signals to display. One is data signal, and the other one is control signal. There are three data signals red, green and blue and two control signals horizontal synchronization and vertical synchronization signals. There are different frequencies the horizontal synchronization signal and vertical synchronization signal for the changeable output resolution .Thus, if someone wants to implement any application on any higher graphics arrays, the try could be given on the VGA first. So, we did the same thing by implementing the application on the VGA. Now, if we talk of FPGA then we us FPGA of SpartanE3 family. For this we used Xilinx software in which you can specify your design by three ways i.e. schematic entry, very high speed integrated circuit hardware description language .In our case we have used the, to specify the design. It is possible to make use of even both the HDL languages together. Also, it is possible to implement the required application by just using the HDL languages but then this will make your code very lengthy and will also increase the complexity. Due to which it will reduce the easiness to understand the code and it will also put burden of the memory associated with the FPGA. Now, we know that the memories associated with the FPGA will have sufficient memory space for small information’s like limited number of characters and some image requiring very small memory to be displayed on screen, but would be insufficient to display an animated characters or images. For this kind of situation we will require some additional processor that can reduce the length of code and other information while developing some real-time applications.

VII.RESULTS AND CONCLUSION

A. VGA TIMING COMPONENT

After implementing the VGA Timing Component to the FPGA, the designed output, the puzzles, was seen on the screen as following Fig 1

At first, there are 640 pixels in one line. The result on the screen cannot fill the entire screen. It is normal that every screen requires different number of pixels to be displayed in one line. So the design should be modified as required. After changing the code, the system manages to output 648 pixels in one line and the result seems good enough for this part. The VGA Timing Component is the basis of this project. It can be used to do a lot of things. It can help provide the timing for all the 8 color pictures on the VGA screen. Normally, this component does not need to change to meet the requirement of other component in the project because it talks to the screen directly.

B.THE FINAL SYSTEM RESULT

The final system is run on the ISIM simulator by using Xilinx ISE tool. I designed a VIDEO GAME in VGA monitor by using SPARTAN 3E FPGA kit . The Simulation output of the corresponding design is completed successfully

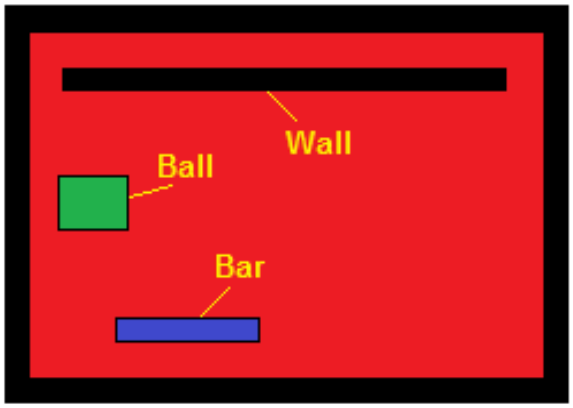

Fig 1 Output Image

C. CONCLUSION

Field programmable gate array is great invention to be used in developing in a VGA controller by using VHDL on FPGA. In this paper , the proposed system is to designed for the video game in FPGA on chip memory by the help of predefined image and to write a VGA controller program in VHDL and implement it on SPARTAN 3E FPGA KIT.

REFERENCES

[1]. Claus Nico Cordes Gerard De Haan "Key Requirements For High Quality Picture-Rate Conversion"- Sid Symposium Paper -2009
[2]. Guohui Wang Yong Guan "Designing Of Vga Character String Display Module Base On Fpga"-International Symposium On Intelligent Ubiquitous Computing And Education -2009
[3]. Saeid Moslehpour "Implementing A Soft-Core Nios Ii Processor For Vga Applications-University Of Hartford 2009
[4]. P. K. Gaikwad "Development of Fpga Based Ps/2 Mouse and Vga Monitor Interface Technique-Ijreat International Journal of Research in Engineering -2013
[5]. Mbharathi A Yogananth "Design Of Vga Monitor Control Using Altera Fpga Based System"-International Journal Of Vlsi And Embedded System 2014
[6]. Yang Yongjin Zhou Xinmei Xiang Zhongfan"Research Of Image Pre-Processing Algorithm Based On Fpga" International Journal On Smart Sensing And Intelligent Systems Vol. 6, No. 4, September 2013
[7] D.Kim Y.S Cho J.H Lee H.N Byan And C.G Kim Ana Pass Real Time Fpga Implementation Of Full Hd @120hz Frame Rate Conversion System –Ieee International Conference 2014
[8]. Dipanjan Sengupta "Low-Power Fpga-Based Display Processing Module For Head-Mounted Displays" Canada Laboratory, University Of Engineering And Technology, 2014
[9]. Van-Huan Tran, Xuan-Tu Tran "An Efficient Architecture Design For Vga Monitor Controller "Sis Laboratory, University Of Engineering And Technology-2014

Automatic Measurement and Monitoring of RF Field Strength Characteristics from GSM Systems

S. Mugilan,
Assistance Professor
CK college of Engineering and technology

Mrs. D. SENGANI M. E. ,(Ph.D.).,
Dept. of ECE

Abstract: **- Mobile communication was well known from the period of 1980's. For the past three decades, it attains more growth and getrid of the burden of wired communication. Nowadays, it is one of the essential devices for our day to day life activities to deliver the voice and data from one point to other point in fast way. Generally, the mobile communication uses two types of communications namely, GSM and CDMA. Each type has different spectrum allocation and all are microwave waves. Due to more demand in mobile communication, spectrum sharing and mode of communication also increased. Hence measurement and monitoring of the electromagnetic fields for GSM and CDMA systems are imperative. The main objective of this paper is to introduce a virtual instrumentation system and real time system for automated characterization of the electromagnetic fields generated by GSM and CDMA systems. This system consists of calibrated antennas, and controlled spectrum analyzer with USB connectivity and Lab VIEW software for monitoring and data transfer, processing and analysis. At first, RF fields are define for GSM and CDMA base stations, it can be used for examining the RF exposure from other communication technologies.**

Keywords: VIS, GSM, UMTS,CDMA,Spectrum analyzer.

1. INTRODUCTION:

During the past decade, the increased use of mobile phones has led to the installation of an extremely large number of mobile phone base stations, especially in densely populated areas. As a consequence, public concern about possible adverse health effects of the exposure to RF electromagnetic fields generated by GSM systems has often emerged. Therefore, there is a need not only for computing the RF fields from base station antennas [2]-[4], but also for performing systematic measurements of the RF exposure levels in their vicinity [4], to ensure that these levels are within the reference limits specified in applicable guidelines. Because, in most cases, the assessment of RF exposure from GSM systems require carrying out and processing a large volume of measurements, our efforts have been directed towards the development of an automated solution for RF field strength characterization. By adopting a virtual instrumentation approach focused on Lab*VIEW* graphical programming, it was possible to combine traditional equipment with "measurement"algorithms into a more flexible PC-based system, which can compute, analyze and monitor various parameters, such as electric field strength (E), magnetic field strength (H), power density (S), mean and standard deviation of these quantities, etc. The main aspects regarding the system operation andsoftware functionality, as well as a few short-term monitoring results, are presented in the subsequent sections

2. LITERATURE SURVEY

For this work existing measuring and monitoring techniques in base station extensive study on different measuring software available now. We use NI Lab*view*. For this proposed work, the various ideas are collected from the various literatures.The literature survey is done by 10papers; they are characterized by different topics as shown below.

A: VIRTUAL INSTRUMENTATION SYSTEM

the virtual instrumentationapproaches have potential to enhance the content of a widerange of courses, complementing the theoretical lessonsand promoting the experimental learning. Representativeapplication fields include, but are not limited to: sensorsand instrumentation [1, 2], electrical machines [3, 4],electric circuit analysis [3, 5], digital circuits [6, 7], digitalsignal processing [8–10], power electronics [3, 11] andautomatic control systems [12]. Additionally, this paperdemonstrates that, using a virtual instrumentationapproach, it is also possible to enhance theElectromagnetic Compatibility education through thedevelopment of new teaching resources. Working withLab*VIEW* for many years and looking for new ways tomake the EMC course in our faculty more engaging andenjoyable, we have introduced a set of computer-basedinstructional modules (VIs) concerning EMC concepts

The virtual instrumentation system (VIS) is built on a PC program and an R&S FS300 programmable spectrum analyzer, which operates in the frequency range from 9 kHz to 3 GHz. With 16 digitally implemented resolution bandwidths from 200 Hz to 1 MHz, the R&S FS300 can be optimally configured to perform narrowband measurements of the RF-fields generated by both GSM 900 and GSM 1800 base station antennas. Unfortunately, this instrument has no RMS detector (it has only positive peak detector), which is usually preferred when assessing the RF exposure originating on UMTS systems [1]Because the R&S FS300

has low power requirements andprovides full remote control via USB, the VIS can be used for performing both indoor and outdoor measurements. In the last case, a notebook computer and a common uninterruptible power supply (UPS) for home or office could provide a simple solution for ensuring portability. Such a setup is shown in Fig. 1, where the R&S FS300 is operated in conjunction with an AT4002A, 800 MHz – 5 GHz horn antenna (Amplifier Research) for measuring E-field emissions in the vicinity of a multi-system base station from n urban environment.

B: Network used

GSM900

The term GSM900 is used for a GSM system which operates in any 900MHz. The 900 MHz band defined in the ETSI standard includes the primary GSM band (GSM-P), the extension (see E-GSM) and the part of the 900 MHz band that is reserved for railways (R-GSM). The total GSM900 band defined in the standard ranges from 876 - 915 MHz paired with 921 - 960MHz. Mobiles transmit in the lower band and base stations transmit in the upper band. In daily life, the term GSM900 band is used for the parts of the band that are used by the GSM operators to offer public services, which excludes the R-GSM band. This part of the band that remains ranges from 880 - 915 MHz paired with 925 - 960 MHz band.

System	P-GSM 900	E-GSM 900	GSM 1800
Frequencies: • Uplink • Downlink	 890-915 MHz 935-960 MHz	 880-915 MHz 925-960 MHz	 1710-1785 MHz 1805-1880 MHz
Wavelength	~ 33 cm	~ 33 cm	~ 17 cm
Bandwidth	25 MHz	35 MHz	75 MHz
Duplex Distance	45 MHz	45 MHz	95 MHz
Carrier Separation	200 kHz	200 kHz	200 kHz
Radio Channels[1]	125	175	375
Transmission Rate	270 kbits/s	270 kbits/s	270 kbits/s

GSM1800

GSM1800 is the term used to denote GSM Operating in the 1800 MHz band. The 1800 MHz band ranges from 1710 - 1785 MHz and from 1805 - 1880MHz. Mobiles transmit in the lower band and base stations transmit in the upper band. GSM1800 is also known under the old name *Digital Communications System* 1800 (DCS1800).

UMTS

UMTS uses a multiple access technique, where several users as well as the signalization is separated by different spreading codes (WCDMA - Wideband Code Division Multiple Access). By multiplication with the spreading code, the data signal is spread in the spectrum. Spectrum of a UMTS signal Fig. 3 shows a real measured UMTS signal in frequency domain. The 10 dB bandwidth is about 4.3MHz, in the literature 4.6 MHz is often stated. In time domain UMTS signals are also noise like with typical crest factors in the region of 8 to10 db. In contrast to DVB-T and DAB, the crest factor at UMTS is not constant in time, but varies with the traffic of the station. The downlink frequency range for UMTS is 2110-2170 MHz Due to the power control of UMTS, the radiated power of a station is dependent on the transmitted data volume and the connection quality to the UMTS terminal.in accordance to the measured signal.

CDMA

CDMA for this method as it can be implemented very easily and effectively. According to the latest report by researcher Gartner India's mobile subscriber base should grow to 993 million by 2014, which expects the world's fastest-growing mobile market to close 2010 with more than 660 million subscribers. India is the second-largest wireless market in the world after China with its 618 million mobile subscribers at end-May, according to data from the country's telecoms regulator. Mobile connections were at 525 million at end of 2009. Latest data by the Cellular Operators Association of India (COAI) showed GSM operators had added 6.68 million in November 2012 and the GSM subscriber base was at 632.08 million. GSM operators added 7.55 million new subscribers inDecember, taking the total GSM user base to 639.64 million in the country, according to the COAI's data released. In this scenario the utilization of existing GSM network for metering in India will be a cost effective method for all class of people.

C:HORN ANTENNA

Pyramidal microwave horn antenna, with a bandwidth of 0.8 to 18 GHz. A coaxial cable feed line attaches to the connector visible at top. This type is called a ridged horn; the curving fins visible inside the mouth of the horn increase the antenna's bandwidth.Pyramidal horn antennas for a variety of frequencies. They have flanges at the top to attach to standard waveguides.

A horn antenna or microwave horn is an antenna that consists of a flaring metal waveguide shaped like a horn to direct radio waves in a beam. Horns are widely used as antennas at UHF and MICROWAVE frequencies, above

300MHz.They are used as feeders (called feed horn) for larger antenna structures such as paraboliantennas, as standard calibration antennas to measure the gain of other antennas, and as directive antennas for such devices as radar guns, automatic door openers, and microwave radiometers. Their advantages are moderate directivity (gain), low standing wave ratio (SWR), broad bandwidth, and simple construction and adjustment.[3]

One of the first horn antennas was constructed in 1897 by Indian radio researcher Jag dish Chandra Bose in his pioneering experiments with microwaves. In the 1930s the first experimental research (South worth and Barrow, 1936) and theoretical analysis (Barrow and Chu, 1939) of horns as antennas was done The development of radar in World War 2 stimulated horn research to design feed horns for radar antennas. The corrugated horn invented by Kay in 1962 has become widely used as a feed horn for microwave antennas such as satellite dishes and radio telescopes.

An advantage of horn antennas is that since they have no resonant elements, they can operate over a wide range of frequencies, a wide bandwidth. The usable bandwidth of horn antennas is typically of the order of 10:1, and can be up to 20:1 (for example allowing it to operate from 1 GHz to 20 GHz).The input impedance is slowly varying over this wide frequency range, allowing low voltage standing wave ratio (VSWR) over the bandwidth.[1] The gain of horn antennas ranges up to 25 dBs, with 10 - 20dBs being typical.

D: spectrum analyzer

The main PCB from a 20 GHzspectrum analyzer. Showing the strapline PCB filters, and modular block construction. A **spectrum analyzer** measures the magnitude of an input signal versus frequency within the full frequency range of the instrument. The primary use is to measure the power of the spectrum of known and unknown signals. The input signal that a spectrum analyzer measures is electrical, however, spectral compositions of other signals, such as acoustic pressure waves and optical light waves, can

be considered through the use of an appropriate transducer. Optical spectrum analyzers also exist, which use direct optical techniques such as a monochromatic to make measurements.By analyzing the spectra of electrical signals, dominant frequency, power, distortion, harmonics, bandwidth, and other spectral components of a signal can be observed that are not easily detectable in time domainwaveforms. These parameters are useful in the characterization of electronic devices, such as wireless transmitters.The display of a spectrum analyzer has frequency on the horizontal axis and the amplitude displayed on the vertical axis. To the casual observer, a spectrum analyzer looks like an oscilloscope and, in fact, some lab instruments can function either as an oscilloscope or a spectrum analyzer.

III. SOFTWARE

The associated software is designed to work under Windows XP and – as already stated – has been created as a Lab*VIEW* virtual instrument (VI). Therefore, it takes advantage of numerous benefits provided by this environment, including interactive graphical user interfaces, advanced data visualization, intuitive operation and possibility of further expansion. When running the software,the operation of the spectrum analyzer through its front panel is disabled and only a "blue screen" will be displayed by the instrument. Among others, the program – called RF-Field*VIEW* – is responsible for configuring the main parameters of the spectrum analyzer, retrieving the power data from the instrument, computing and displaying the field strength, time-averaged exposure and a number of statistic parameters,as well as recording data for subsequent analysis. The stored data can be analyzed by using another Lab*VIEW* program, which also allows for computing the resultant RMS field bytaking into account readings recorded on three orthogonal directions for a sufficiently long measurement time, as suggested in A. Algorithm Summary Basically, the RF-FieldVIEW software is based on the Lab*VIEW* instrument driver library for the FS300, provided by Rohde & Schwarz on its website. All these functions have been critically studied and a part of them have been incorporated as subVIs in the main program for ensuring proper control of the spectrum analyzer and receiving the trace data from the instrument, as presented in Fig. 2. Starting from the "live" trace data, further *LabVIEW* processing is devoted to compute relevant field quantities and statisticparameters. In order to provide simple system reconfiguration, the RF-FieldVIEW uses a modular approach. For instance, a number of subroutines (subVIs) are specifically designed for adding the antenna factors to the measurement results and compensating for the transmission line losses over the frequency range explored by the spectrum analyzer. If a particular antenna or transmission line must be used, the correspondent subVI will be called by the main program when it starts and no code modifications have to be made.

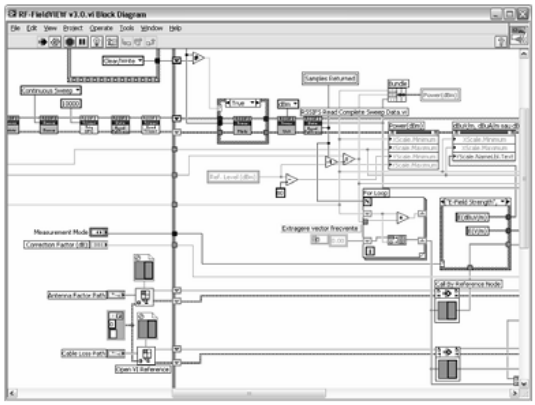

Fig. 2. Part of the block diagram.

The program runs continuously until the user aborts its execution, a specified execution time has elapsed or a communication error has been detected. In this case, an error message will be displayed for the user.

3. MONITORING RESULTS

According to the ICNIRP guidelines the reference levels for general public exposure from mobile
Communications are: 4.5 W/m2for GSM networks operating in the 900 MHz frequency band, 9 W/m2 for GSM networks operating at 1800 MHz and 10 W/m2for 3G/UMTS. In order to get an idea of the actual RF exposure levels associated with these technologies, a short-term monitoring has been conducted in a typical indoor environment. First of all, to investigate the short-term evolution of the background electromagnetic field, wideband measurements from 800 MHz to 2.6 GHz have been taken at each 0.5 minutes during 24hours.Then narrowband measurements covering the downlink frequency bands.

The power density in the frequency range from 2110 MHz to 2170 MHz, which corresponds to the UMTS downlink, is shown in Fig. 8. This plot consists of 2030 readings taken over 17 hours, in the average mode, and has a maximum of 0.0391mW/m2at the frequency of 2161.4MHz. All measurements have been automatically corrected by a factor that accounts for the limited resolution bandwidth of the spectrum analyzer with respect to the UMTS signal bandwidth.

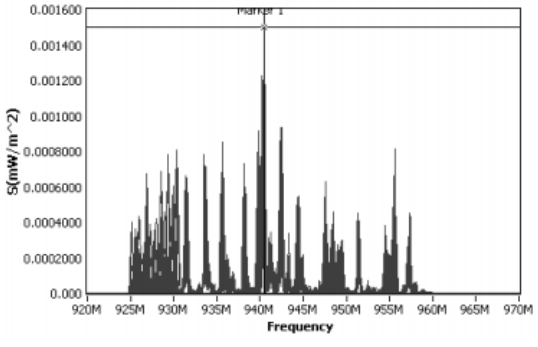

Emission of GSM 900

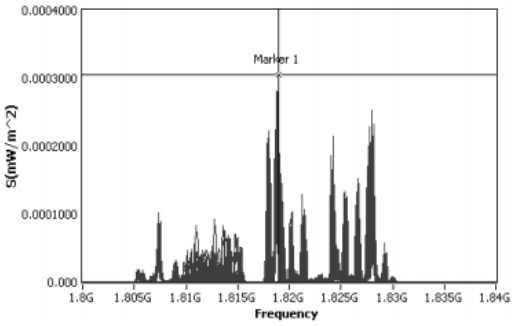

Emission of GSM 1800

4. CONCLUSION

According to the literature survey in this work is proposed to develop the full monitoring and measuringto analysis all above networks .which one is less EMF emitting that network will less human diseases affected. The associated software provides user-friendly operation and accommodates various features for fast field characterization, including spectrum view for all quantities, markers, zoom, limits, simultaneous display of a very large number of saved traces, etc.

5. REFERENCES

[1] Eduard Lunca, Member, APCBEES, Alexandru Salceanu, and Silviu Ursache"Automated measurement and Monitoring of the Electromagnetic Fields from GSM Systems"Journal of Clean Energy Technologies, Vol. 1, No. 3, July 2013

[2] B. Kamo, R. Miho, V. Kolici, S. Cela, and A. Lala, "Estimation of peak power density in the vicinity of cellular base stations, FM, UHF and WiMAX antennas," International Journal of Engineering & Technology, vol. 11, no. 2,pp. 65-71, 2011.

[3] D. Wojcik, "Evaluation of near field of the GSM base station antennas in urban environment," in Proc. 14th International Conference on Microwaves, Radar and Wireless Communications, Gdansk, 2002, pp.191-194.

[4] S. Miclaus and P. Bechet, "Estimated and measured values of the radiofrequency radiation power density around cellular base stations," Romanian Journal of Physics, vol. 52, no. 3-4,pp. 429-440, 2007.

[5] P. Baltrėnas and R. Buckus, "Indoor easurements of the power density close to mobile station antenna", in Proc. 8th International Conference "Environmental Engineering", Vilnius, 2011, pp. 16-21.

[6] D.A. Shalangwa, "Measurement of exposure of radio frequency field (RF) radiation from global system for mobile communication (GSM) masts," Journal of Electrical and Electronics Engineering Research, vol. 2, no. 3, pp. 75-84, 2010.

[7] G. Neubauer, K. Lamedschwandner, S. Cecil, and G. Schmid, "Exposure assessment methods for emerging new technologies," in Proc. XXIX URSI General Assembly, Chicago, 2008, pp. 1-4.

[8] C. Bornkessel and M. Wuschek. (2006). Exposure measurements of modern digital broadband radio services. in Proc. GeMiC 2006 - German Microwave Conference. Karlsruhe. pp. 1-4.

[9] E. Lunca and A. Salceanu, "Virtual instrumentation approach for teaching EMC concepts," Electronics and Electrical Engineering, vol.117, no. 1, pp. 75-80, 2012.

[10] ICNIRP. (1998). Guidelines for limiting exposure to time-varying electric, magnetic and electromagnetic fields (up to 300 GHz). Health Physics. vol. 71. no. 4. pp. 494-522. [Online]. Available: http://www.icnirp.de/documents/emfgdl.pdf.

Implementation and Realtime Analysis of OFDMA Networks using Hybrid Model

M. Tamizhanangu,
Student
ECE, C.K. College of Engineering and Technology,
Cuddalore, India

Mr. K. Sureshkumar M.E
Assistant Prof
ECE, C.K. College of Engineering and Technology,
Cuddalore, India

***Abstract*- To evaluate performance of any cellular network, throughput evaluation is the fundamental parameter. Orthogonal frequency division multiplexing (OFDM) has become one of the most promising radio interface technologies for future generation wireless networks. In proposed system a hybrid model consist of both analysis and simulation. The benefit of the model is that the throughput of any possible call state in system can evaluated. The probability of possible call distribution is first obtained by analysis which is used as input to event-driven based simulator to calculate throughput efficiency of a call state. By increasing the Net bit rate(R) data throughput can be increased and by introducing fading effect same efficiency can be achieved using Hybrid model. The simulation is being done by using MATLAB simulation.**

I. INTRODUCTION

In an orthogonal frequency division multiple access (OFDMA) network, .transmission is achieved by transmitting data via multiple orthogonal channels. One of the most important aspects of any commercial mobile network deployment is its information carrying capacity, and data throughput is one fundamental parameter in the capacity planning for cellular system deployment. The goal of LTE is to improve the spectral efficiency and hence increase the network capacity, improve services, lower costs. In an orthogonal frequency division multiple access (OFDMA) network, transmission is achieved by transmitting data via multiple orthogonal channels. Due to the use of multiple orthogonal channels, OFDM also performs equalization and is consequently robust to inter-symbol interference and frequency-selective fading [2], [3]. Reference [7] has evaluated the performance of the OFDMA network based on analytic and simulation approach separately has considered a hybrid simulation/analysis approach, where a detailed rate distribution obtained via simulation is used as input to a generalized processor sharing queue model, but does not consider the user-level. Simulation approach do not provide the throughput of any intermediate call state because it is not possible to obtain this data, whereas the analytical approach provide average performance. We present a hybrid model of analysis/simulation for determining the average data throughput of a system from the user point of view. Model has the benefit of evaluating the performance of any specific call state from the user perspective. OFDMA networks must not only be able to provide reliable and high quality broadband services but also be implemented cost effectively and be operated efficiently.

II. LITERATURE REVIEW

A. OFDMA BASICS

OFDMA is a multiple-access scheme that has characteristics of OFDM and frequency-division multiple accesses. OFDM transmits data from one user within a time slot, whereas OFDMA simultaneously transmits data for MUs. Inherited from OFDM, OFDMA is also immune against multipath and has other favorable characteristics. OFDMA was proposed for several broadband wireless systems such as the LTE downlink of cellular systems IEEE802.16 standard for wireless metropolitan area network, and digital video broad casting return channel terrestrial. In OFDMA systems, the multiple user signals are separated in the time and/or frequency domains. Typically, a burst in an OFDMA system will consists of several OFDM symbols. The subcarriers and the OFDM symbol period are the finest allocation units in the frequency and time domain, respectively. Hence, multiple users are allocated different slots in the time and frequency domain (i.e., different groups of subcarriers and/or OFDM symbols are used for transmitting the signals to/from multiple users).

OFDM Transmitter and receiver

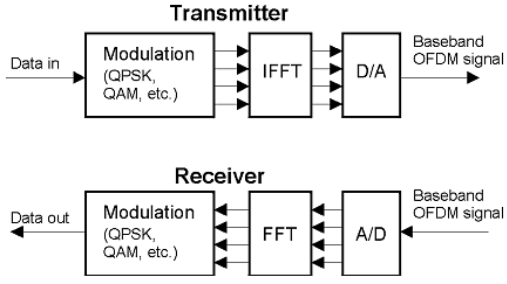

The OFDM concept is based on spreading the data to be transmitted over a large number of carriers, each being modulated at a low rate. The carriers are made orthogonal to each other by appropriately choosing the frequency spacing between them. In contrast to conventional Frequency Division Multiplexing, the spectral overlapping among sub-carriers are allowed in OFDM since orthogonality will ensure the subcarrier separation at the receiver, providing better spectral efficiency and the use of steep band pass filter was eliminated.

B.SUBCHANNELS IN OFDMA

There are three types of OFDMA subcarriers:
1. Data subcarriers for data transmission.
2. Pilot subcarriers for various estimation and Synchronization purposes.
3. Null subcarriers for no transmission at all, used for guard bands and DC carriers.

Active subcarriers are divided into subsets of subcarriers called sub channels. The subcarriers forming one sub channel may be, but need not be,

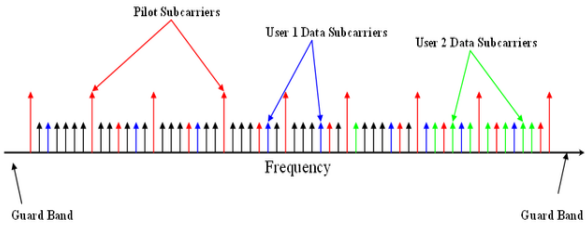

adjacent. Bandwidth and MAP allocations are done in sub channels. The sub channel is a subset of carriers out of the total set of available carriers. In order to mitigate the frequency selective fading, the carriers of one sub channel are spread along the channel spectrum [1]. The formation of these sub-channels from carriers is an important concept in OFDMA systems. The formation can be classified into 2 types; one is the mapping of a contiguous group of subcarriers into a sub-channel called *Adjacent Subcarrier Method (ASM)* and the other is the diversity/permutation based grouping called *Diversity Subcarrier Method (DSM).* In the ASM method, a sub-channel typically contains a group of contiguous subcarriers and it's expected that the channel frequency responses on the subcarriers in a sub-channel will be strongly correlated. This is based on the fact that subcarriers which fall within the coherence bandwidth have similar responses. In the DSM, subcarriers from seemingly random position in the frequency domain are grouped into a sub-channel. Thus, a channel has potential frequency diversity which can be leveraged when the data to be sent on this sub-channel is suitably coded and interleaved. The division in sub channels is a form of frequency-division multiple access (FDMA), where the subscriber transmits $1/NE = 1/32$ of the available channel bandwidth for the 2048-carrier OFDMA. Regarding interference, the sub channels constitute a form of frequency hopping spread spectrum The capacity can be optimized by managing the whole range of modulation and coding schemes specified in the standard. To maximize capacity we want to assign as many subscribers as possible to the schemes with highest throughput.

C.EFFECTIVE THROUGHPUTT

The special properties of the throughput maximization, we introduced a scheduling algorithm that yields the optimal transmission schedule. To maximize the system throughput while ensuring the full filament of each user's QoS requirements including the data rate and the bit-error-rate (BER). Hear they use iterative algorithm to maximize algorithm. The notion of effective throughput to characterize the performance of OFDM/SDMA systems by taking into account PER, number of data subcarriers in an OFDM symbol, modulation and coding scheme. Effective throughput for a user can be viewed as the average number of successfully received data bits in an OFDM symbol after excluding erroneously received packets.

Definition —User Effective Throughput:

Let Pe be the PER, N_d the number of data subcarriers in an OFDM symbol, MI the modulation index on data subcarriers, and r_c the coding rate.

Effective throughput is determined by PER, the number of data subcarriers (or the number of pilot subcarriers), modulation and coding scheme. The effective throughput can be easily translated to the average delay for transmitting a user packet when retransmission is employed.

To generate OFDM successfully the relationship between all the carriers must be carefully controlled to maintain the orthogonality of the carriers. For this reason, OFDM is generated by first choosing the spectrum required, based on the input data, and modulation scheme used. Each carrier to be produced is assigned some data to transmit.

III. PROPOSED BLOCK DIAGRAM

BLOCK DIAGRAM

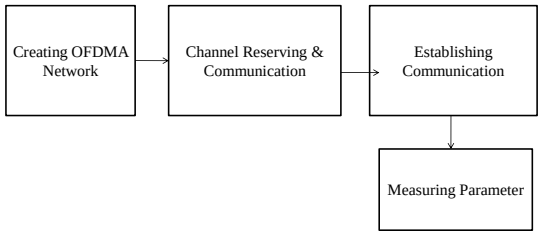

Creating OFDMA Network

IV. SYSTEM DESCRIPTION

For OFDMA-based networks, user data is divided and modulated onto a large number of narrow band subcarriers in the frequency domain, and each of them is modulated by

low rat data [9]. The subcarriers are orthogonal to each other, meaning that cross-talk between the sub-carriers is eliminated and inter-carrier guard bands are not required. The orthogonality among the subcarriers prevents inter-subcarrier interference because the subcarrier's spectrum has nulls located at the centre frequencies of adjacent subcarriers [9]. A group of consecutive subcarriers is known as a sub channel. Moreover, the time domain is split into consecutive frames that are in turn divided into time slots called OFDM symbols. As a multiple access technique, OFDMA offers the possibility of enhancing the spectral efficiency of networks by assigning distinct OFDM symbols or sub channels to distinct users, thus taking advantage of their diverse time and frequency channel conditions a compared to TDMA and FDMA techniques. For LTE, downlink transmission is based on OFDMA. The radio resources can be considered as a frequency-time resource grid as illustrated in Fig. 1. In the frequency domain, the radio spectrum is divided into a number of narrow subcarriers of 15 kHza spacing. In the time domain, a frame of 10 ms duration is divided into 10 sub frames of 1 ms each. Each sub frame is further divided into 2 time slots of 0.5 ms each. Each time slot then consists of 6 or 7 OFDM symbols depending on the length of cyclic prefix (normal or extended cyclic prefix) [9]. A grid of 1 subcarrier (15 kHz) in the frequency domain and 1 OFDM symbol (0.5 ms) in the time domain is known as 1 resource element, while a grid of 12 adjacent subcarriers (12_15 = 180 kHz) and 1 OFDM symbol (0.5 ms) is known as 1 RB. Hence, a RB is a rectangular block of resource elements, which spans 12 adjacent subcarriers in the frequency domain and 7 OFDM symbols in the time domain (180 kHz _ 0.5 ms). In LTE, a RB is also known as a sub channel, and from now on we refer to a RB as a sub channel. Depending on the transmission bandwidth, a downlink carrier comprises a variable number of sub channels in the frequency domain. The minimum bandwidth of 1.4 MHz corresponds to 6 RBs, while the maximum one of 20 MHz corresponds to 110 RB. The assignment of sub channels to users is carried out by the medium access control (MAC) scheduler, and it is performed on a sub frame-by-sub frame basis, i.e., each 1ms. The scheduler decides which users are allowed to transmit on which sub channel. It should be noted that the minimum resource scheduling unit that the scheduler can assign to a user is comprised of 2consecutive RBs and thus spans an entire sub frame.

A. *Blocking Probability*

According to the guard channel scheme, a new call in a cell j gains a subchannel if it finds that there are less than Rj-rg calls in the cell and that there is at least one subchannel available, otherwise, the new call is blocked in cell j and will be cleared from the system. On the other hand, a handoff call into a cell j gains a subchannel if it finds at least one subchannel available, otherwise, it is blocked.

B. *Channel Modelling*

The medium between the transmitting and the receiving antennas is known as the channel. The characteristics of radio signal changes as it travels from the transmitter antenna to the receiver antenna. The characteristics depend upon the parameters such as distance between these two antennas, propagation scenario (e.g., outdoor-to-outdoor, outdoor-to-indoor, indoor-to-indoor, etc.) and the surrounding environment (e.g., buildings, trees, etc.). The received signal can be estimated if we have a suitable model of the medium. This model of the medium is called the channel model. The radio channel propagation is typically modeled as the combination of three main effects: the mean path loss, the shadowing generally characterized as log-normal [11], [9] and the fading typically modeled as Rayleigh [10]. In OFDMA system, the data is multiplexed over a large number of narrow-band subcarriers that are spaced apart at separate frequencies, the subchannel consists of parallel, flat and non-frequency selective fading. The received signal is then only impacted by slow fading.

1) *Path loss model:*

Path loss is the distance dependent mean attenuation of signal as it propagates through space. A suitable model of path loss depends on the parameters such as type of the environment (e.g., macrocell, microcell, indoor, etc.), the propagation medium (e.g., outdoor-to-outdoor, outdoor-to-indoor, indoor-to-indoor, etc.), the carrier frequency and the distance.

2) *Auto-correlation shadow fading model:*

In reality, clutters from objects such as buildings, trees, terrain conditions etc. along the path of signal propagation differs for every path, and consequently signal attenuation varies from path to path. Shadow fading is used to model variations in the path loss due to such obstacles between the mobile and the base station. Shadow fading is also known as slow fading.

C. *RADIO ACCESS BEARER EFFICIENCY*

The Radio Access Bearer (RAB) is the entity responsible for transporting radio frames of an application over the radio access of the network. From the estimated SINR, a suitable modulation and coding scheme (MCS) is selected for each user provided that the SINR satisfies the threshold for the selected MCS. The higher the SINR, the higher order MCS is used satisfying the SINR threshold value.

D. *Hybrid Model*

This model combines the analytic and simulation approach, which, unlike traditional simulation approaches, enables us to estimate throughput of any intermediate call state. The probability of call distribution being in a particular state in the system is obtained from analytic expressions and is used as input to the simulation to calculate the throughput of a cell.

Statistical parameters	Value
call distribution	Uniform
call generation process	Poisson
Call mean arrival rate	0.1, 0.2, 0.3, 0.4, 0.5, 0.6, 0.7, 0.8, 0.9, 1.0
call mean holding time	0.5, 1, 1.5, 2.0, 2.5, 3.0, 3.5, 4.0, 4.5, 5.0,6.0,7
call inter arrival/ holding time dist	Exponential
LTE System PARAMETERS	
site layout	1hexagonal site with 3 cell
Carrier frequency	2GHz
Subcarrier spacing	15khz
resource block spacing	180khz
Number of sub channels	2,3,4,5,6,7
Data symbol per time slot	11 OFDMA data symbols
Frame duration	-174 dBm/Hz
Thermal noise density	-121.4 dBm
Thermal noise power	1 RB/call

SIMULATION PARAMETERS

Random bit generation:

From Transmitter by PING process BEACON signal is transmitting to check the receiver side alive. Then Random Bit Generation is passed from transmitter side and it received in Receiver side.

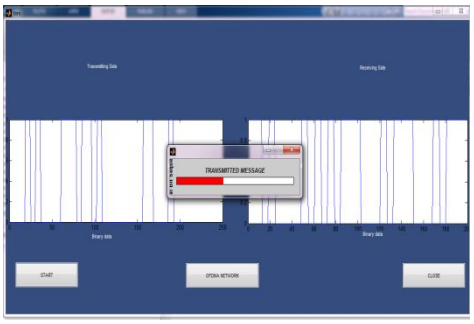

SIMULATION RESULT FOR CALL DISTRIBUTION PROBABILITY:

The performance of the system was evaluated for different call arrival rates for different numbers of subchannels to account for the variation of inter-arrival traffic while the mean holding time remained fixed.

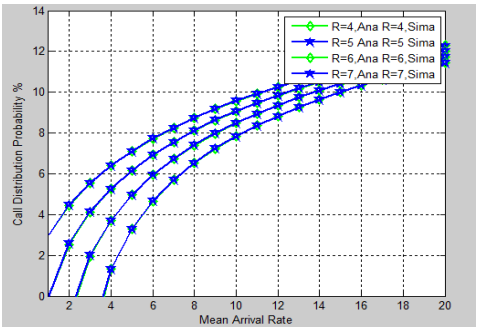

SIMULATION RESULT FOR CALL BLOCKING PROBABILITY:

The performance of the system was evaluated for different mean holding times for different numbers of subchannels to account for the variation of service-time, while the mean arrival rate remained fixed.

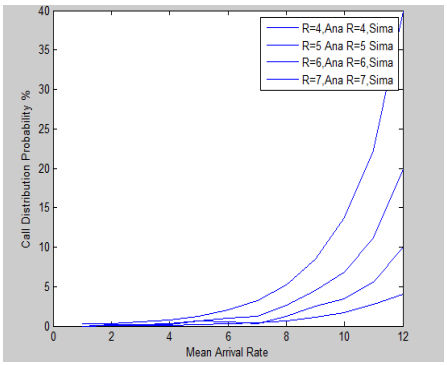

SIMULATION RESULT FOR 'THROUGHPUT' PERFORMANCE:

When the throughput increses, servicing rate will get increased and network will give efficient services. If the throughput is in 5 and 6 the servicing rate is not efficient but in 7 the servicing rate is efficient.

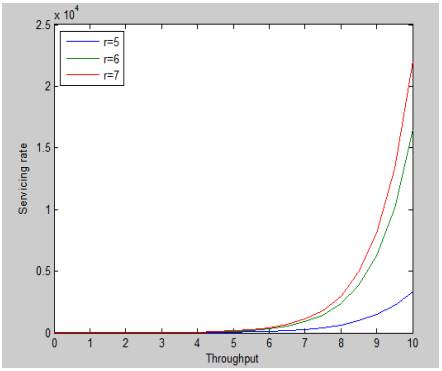

The OFDM transmission scheme has the following key advantages:

• Makes efficient use of the spectrum by allowing overlap.

• By dividing the channel into narrowband flat fading sub-channels, OFDM is more resistant to frequency selective fading than single carrier systems are.

• Eliminates Inter Symbol Interference (ISI) through use of a cyclic prefix.

• Using adequate channel coding and interleaving one can recover symbols lost due to the frequency selectivity of the channel.

• Channel equalization becomes simpler than by using adaptive equalization techniques with single carrier systems.

• It is possible to use maximum likelihood decoding with reasonable complexity, OFDM is computationally efficient by using FFT techniques to implement the modulation and demodulation functions.

• In conjunction with differential modulation there is no need to implement a channel estimate.

• Provides good protection against co-channel interference and impulsive parasitic noise.

Claimed OFDMA Advantages

- Flexibility of deployment across various frequency bands with little needed modification to the air interface.
- Averaging interferences from neighboring cells, by using different basic carrier permutations between users in different cells.
- Interferences within the cell are averaged by using allocation with cyclic permutations.
- Enables Single Frequency Network coverage, where coverage problem exists and gives excellent coverage.

CONCULUSION:

By using Hybrid model, data throughput can be increased by increasing the Net bit rate (R). And using event- driven based simulation, range of call arrival rates and mean holding time is found minimum. By introducing Fading effect the same efficiency can be achieved using Hybrid model. In Full duplex communication OFDMA network is created.

REFERENCES:

[1] Shyam Babu Mahato, Tien Van Do, Ben Allen, Enjie Liu, Jie Zhang *"A Hybrid Model for Throughput Evaluation of OFDMA Networks"* JOURNAL OF IET ENGINEERING, VOL., ISS., DECEMBER 19, 2013

[2] 3GPP TR 36.814, "*Evolved Universal Terrestrial Radio Access (EUTRA); Further Advancements for E-UTRA Physical Layer Aspects (Release 9),"* 3GPP TSG RAN, Tech. Rep. v.9.0.0, Mar. 2010.

[3] I. Koffman and V. Roman, "*Broadband Wireless Access Solutions Based on OFDM Access in IEEE 802.16,"* IEEE Communications Magazine, vol. 40, no. 4, pp. 96–103, Apr. 2002.

[4] S. Coleri, M. Ergen, A. Puri, and A. Bahai, *"Channel Estimation Techniques Based on Pilot Arrangement in OFDM Systems,"* IEEE Transactions on Broadcast, vol. 48, no. 3, pp. 223–229, Sep. 2002.

[5] M. H. Ismail and M. M. Matalgah, "*Simulation* Results *for the Impact of Users Locations and Distribution Characteristics on the Performance of Downlink WCDMA/TDD in Fading Channels*," in IEEE Radio and Wireless Conference, Sep. 2004, pp. 495–498.

[6] J. -E. Kelif and E. Alman, "*Downlink Fluid Model of CDMA Networks*," in IEEE Vehicular Technology Conference (VTC2005-Spring, IEEE 61st), vol. 4, 30 May-1 Jun. 2005, pp. 2264–2268.

[7] T. A. Kostas and C. C. Lee, "*A Performance Model for Data Throughput with Adapative Modulation*," IEEE Transactions on Wireless Communications, vol. 6, no. 1, pp. 79–89, Jan. 2007.

[8] S. Ahn and H. Wang, "*Throughput-Delay Tradeoff of Proportional Fair Scheduling in OFDMA Systems,"* IEEE Transactions on Vehicular Technology, vol. 60, no. 9, pp. 4620–4626, Nov. 2011.

[9] W. Wu and T. Sakurai, *"Flow-Level Capacity of Fractionally Loaded OFDMA Networks with Proportional Fair Scheduling,"* in IEEE Vehicular Technology Conference (VTC2012-Fall, IEEE 76th), Sep.2010,pp.1-5.

[10] Y. S. Yeh and S. C. Schwartz, "*Outage Probability in Mobile Telephony Due to Multiple Log-Normal Interferers*," IEEE Transactions on Communications,vol. 32, no. 4, pp. 380–388,Apr.1984.

[11] K. W. Sowerby and A. G. Williamson, "*Outage Probability Calculations for a Mobile Radio System `Having Multiple Rayleigh Interferers,"* Electronics Letters, vol. 23, no. 11, pp. 600–601, May 1987.

[12] R. C. French, "*The Effect of Fading and Shadowing on Channel Reuse in Mobile Radio,"* IEEE Transactions on Vehicular Technology, vol. 28, no.3, pp.171–181, Aug.1979.

Mobi Robot Control using Internet of Thing (IOT)

P. Balamurugan, K. Harikrishnan, K. Kumaraguru
(Final Year Ece)
St.Anne's College Of Engineering And Technology
Panruti

***Abstract*—Cloud robotics is an emerging field that is centered on the benefits of converged infrastructure and shared services of a cloud computing environment. In this paper, a system is designed with an autonomous robot to sense environmental data such as temperature, humidity, and air quality, along with GPS coordinates and store them on the cloud. The mobile robot is controlled using an Arduino microcontroller and communicates with the cloud via a Raspberry Pi. A private cloud is set up using OpenStack that provides Infrastructure as a Service. The collected data are stored in a cloud server which could be viewed through a web browser and can be used to create awareness about the environmental changes of the location under study. A proof-of-concept prototype has been developed to illustrate the effectiveness of the proposed system.**

***Index Terms*—Cloud Robotics, Open source software, Raspberry Pi, Mobile Robot, GPS.**

I. INTRODUCTION

Cloud robotics is an emerging field that merges the concepts of cloud technologies and service robots. It is a disruptive technology based on the advantages of rapid fall in costs of servers, data centers, and broadband access, inexpensive cloud storage, and distributed computing. Internet is used to complement the capabilities of the robots by relieving them from on -board computation-intensive tasks and enable them to provide effective services on demand. Robotics is a technology that deals with the design, construction, operation, and application of robots, as well as computer systems for their control, sensory feedback, and information processing. The human operator may manipulate the robot from a distance by sending commands and receiving information via communication network. Robotic systems have brought significant economic and social impacts to human lives over the past few decades. Recently, robotic systems are utilized as data-gathering tools by scientists for a greater understanding of environmental processes. Robots are also being designed to explore deep oceans, to track harmful algal blooms, monitor climatic condition ns, and to study about remote volcanoes .

Cloud is a service provider that provides services such as infrastructure, software or resources. Infrastructure as a Service (IaaS) models an organization that outsources the resources required for its operations, including storage and networking components. While the cloud computing paradigm was originally developed in the cyber world and applied software as a service (SaaS), in the last few years it has been extended to the cyber-physical world, including vehicles like cars and people with smartphones, and robots like ground vehicles and unmanned aerial vehicles .

Recently, researchers have started to merge cloud computing concepts with mobile robotics, e.g.. This approach has been particularly useful in the context of computation-intensive applications like image processing and cognition needed by mobile robots as these tasks take up space, power, and incur high costs. The cost and complexity of performing the basic functionalities such as sensing, actuation, and control in a single robot increases exponentially. Therefore, the cloud robot system efficiently provides different types of support. An interesting related technological development is the emergence of Robots as a Service (RAAS), analogous to system oriented architecture .

In spite of the significant potential of cloud robot systems, much of the research in literature has focused mainly on cloud-based operation of robot manipulators or arms. For example, Kehoe, et al have applied the cloud computing concept to a manipulator mounted on a mobile robot system. Their technique performs object recognition, pose estimation and grasping of common household objects with the aid of Google Goggles Image Recognition System and stores the results on a cloud server. Kamei, et al have proposed the use of cloud networked robots for providing multi-location daily activity using on-board manipulators to support elderly and disabled people. Use of vision-based servo control of manipulators with distributed computing has been proposed in .

More recently, robotics researchers have turned to the applications of cloud computing in individual and wirelessly networked mobile robot systems. Real-time path planning for mobile robots using computation-intensive evolutionary algorithms on the cloud has been studied in . Use of cloud-based multi-core graphic processing units for analysis of 3D perceptual changes in robot texture images for purposes of navigation has been made in .

A number of mobile robotic systems have been developed in recent years for monitoring climate variables both terrestrial and underwater, harmful algal blooms and volcanoes. Mobile robots with on-board environmental sensors offer several advantages - low cost, ease of automation, wide operational range, and flexibility - in the monitoring of wide geographical areas. Indoor and outdoor environmental monitoring using mobile robots has been considered by several researchers, e.g., . Small mobile robots called Boebots have been built to capture image that will be processed by a cloud setup using Microsoft windows Azure

.However, these robots are very small in size, and so not well suited for either indoor or outdoor real-world environments. consumes very less power when compared to laptop. The system developed in this project is completely based on open source hardware Arduino and Raspberry Pi and open source software OpenStack for setting up the cloud.

A standalone low cost device for transmitting data with touch screen display had been built using Raspberry Pi and Bluetooth. A robot to recognize voice had been developed using Google voice API and Raspberry Pi . Raihan et. al. had developed an economical automated toll system that work by processing images using Raspberry Pi. The system was developed as an alternative to the more costly system using RFID.

In this paper, a robot is designed to move autonomously in the open space and to monitor the environmental conditions. The sensor data collected by the robot are stored in a cloud server that could be also be displayed in a webpage as well. Since very large amounts of spatio-temporal environmental data are collected in the process, a cloud server is used for economical storage, analysis, and retrieval of the data. The cloud environment is set up using OpenStack in Ubuntu Linux. The Raspberry Pi microcontroller is used in the robot for communicating with the cloud server, while an Arduino microcontroller is used for control of the robot.

II. REVIEW OF ENVIRONMENTAL MONITORING SYSTEMS

Air quality and pollution monitoring technologies have so far been quite expensive, and beyond the reach of countries like India. Such monitoring systems have been adhoc or needed stationary constructions, with manual fetching of the data, storage, and retrieval. Even with wireless transmission of round-the-clock data to the server, the measurements are mainly applicable to the immediate vicinity of the station. For example, a recent report in the New York Times reported that for a city of 20 million population New Delhi have only six state of-art monitoring stations.

Researchers at the University of California in Berkeley in USA have developed an urban sensor network to provide real-time, neighborhood-by-neighborhood measurements of carbon dioxide. The prototype network employs 40 sensors spread over a 27 square-mile grid. Though the system uses off-the-shelf environment sensors to lower the cost from $250,000 (~ Rs. 1.5 crores) for a traditional monitoring station to $12,500 (~ Rs. 7.5 lakhs) it is still prohibitively expensive to use in India.

Previously, we have developed a low-cost mobile urban air quality monitoring system for Madurai city. The developed system was fitted in school buses to monitor pollution in the city. More recently, the authors have developed a network of three robots (one master and two slave robots) wirelessly connected to monitor the environment .The robots moved around autonomously on a flat surface and submitted the collected data to a cloud server. A laptop computer was fixed in the master robot to communicate with the cloud server.

In the present work, we have replaced the laptop which is used for communication with Raspberry Pi, a microcontroller of low cost. The advantage of this proposed system is that the microcontroller is of low power and light weight, and

III. ARCHITECTURE OF SMART CLOUD ROBOT

The architecture of the proposed smart cloud robot system is shown in Fig. 1. The mobile robot is of wheeled type that is easy to navigate indoors, but can also be used for navigation on smooth outdoor surfaces. The robot may be scaled up in the future with more powerful motors and rubber wheels for operating in uneven outdoor terrains. The robot is made to move in a fixed path using Arduino and GPS. The robot communicates the sensor readings to the cloud server using Raspberry Pi. In this experiment, temperature and humidity sensors were used to observe the changes in the environmental conditions. A LAMP server is setup in an instance of Ubuntu Linux

IV. IMPLEMENTATION DETAILS

The schematic diagram of the mobile robot architecture is shown in Fig. 2.The mobile robot is operated with a gel acid battery powering the 12 V DC servomotors, through an H-bridge motor driver under PWM outputs from the Arduino. A GPS shield is mounted on the Arduino to tag the latitude and longitude coordinates of the robot's position in addition to readings from a temperature/humidity sensor. The Raspberry Pi connected with the Arduino communicates the reading of the sensors to the cloud server through Wi-Fi. The robot is equipped with an ultrasonic sensor to measure the distance between the robot and an obstacle. On detecting an obstacle the robots takes action such as move reverse direction or rotate and then move. Arduino is based on an Atmel AVR processor, with on-board support for analog inputs, analog or pulse width modulation (PWM) outputs, and digital input/output.The microcontroller may be interfaced to a personal computer or a Raspberry Pi for programming and data acquisition through a USB port.

The Arduino board is programmed in a C-like integrated development environment, with built-in example code known as *sketches*. Extensive built-in libraries are available with custom code for various applications. Arduino can be used for creating interactive objects or environments. The microcontroller boards can be either built by hand with the help of hardware reference designs (CAD files) or purchased preassembled. A number of Arduino boards such as Arduino Uno, Arduino Due, and Arduino Mega are available.

Temperature sensor and humidity sensors are connected to the board to observe the variables in the environment. The Global Positioning System (GPS) is a satellite based navigation system that sends and receives radio signals. GPS receivers acquire these signals and provide Information. Using GPS technology we can determine location, velocity round the clock in any weather conditions anywhere in the world. We need to interface Arduino Uno with GPS. The location of

the robot is tracked in Google maps with Trimble Studio as depicted in Fig. 3.

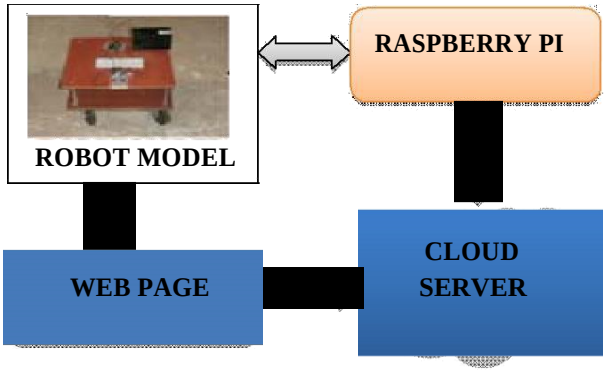

Fig. 1. Schematic of Proposed System

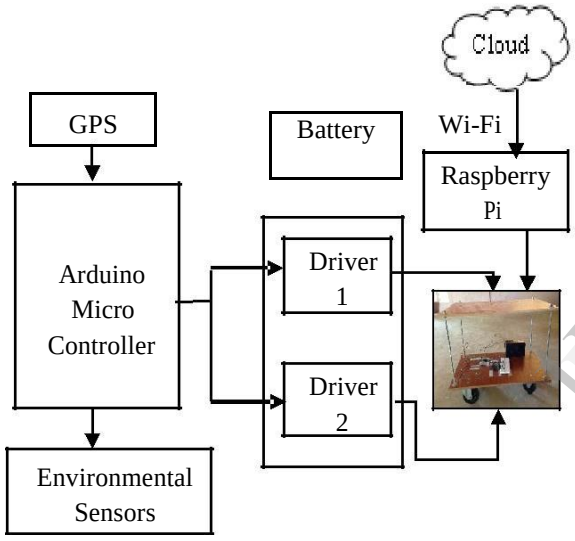

Fig.2. Mobile Robot Control Architecture

Ultrasonic sensors work on the principle of radar evaluates attributes of a target by interpreting the echoes from radio or sound waves respective .In this project, ultrasonic sensor is used for obstacle detection. The object sensor is placed in the front side of the robot model to navigate and automatically detect if any obstacle is present. The maximum coverage range of sensor is 2 to 250 centimeters. It has a Broadcom system on a chip (SoC), Which includes a 700 MHz processor, Video Core IV GPU, and a RAM of size 256 MB or 512 MB. It uses an SD card for booting and persistent storage. The Raspberry Pi is a credit-card-sized single-board computer which is used to communicate with the cloud operating system, OpenStack. Raspberry Pi is based on the Linux platform which supports the functionality of cloud environment. The sensor readings are stored in the cloud server once every minute via wireless communication using a Wi-Fi dongle device and Raspberry Pi board.

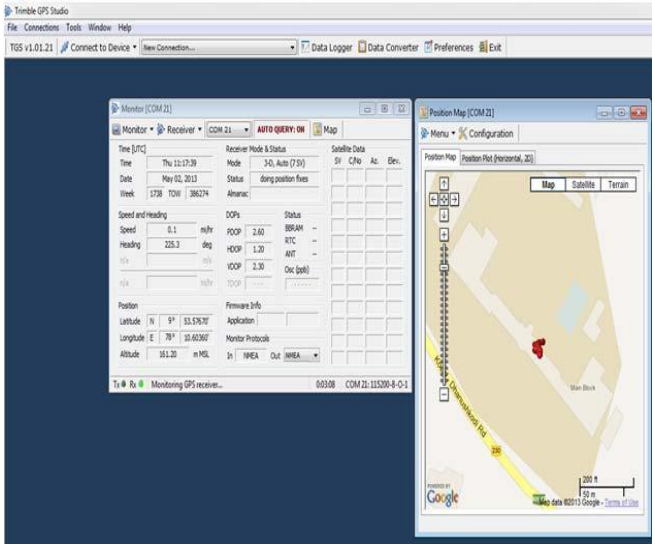

Fig. 3. Location of GPS Receiver as Viewed in Trimble Studio

V. SETTING UP THE CLOUD

A private cloud was setup to provide Infrastructure as a Service (IaaS) using OpenStack. OpenStack is a cloud operating system that manages a network of virtual machines and offers computing resources on demand. Flexibility is an important advantage of OpenStack, and it is possible to design the cloud as per the user specifications and resource availability. A web interface is provided to manage the computing resources throughout the datacenter. A cloud was setup on a single machine in the laboratory with Ubuntu operating system to conduct experiments.

Figure 4 shows the conceptual architecture of an OpenStack cloud. The Cloud Dashboard is a user interface for the administrators and clients (robots) to access and automate the resources in the cloud. Typing the host ip address in the browser opens the dashboard of the cloud. The OpenStack dashboard is a graphical interface for administrators and users to access, control and allocate the resources in the cloud .The dashboard is just one way to interact with OpenStack resources. It provides an overall view of the size and state of the cloud. Dashboard can be used to create users, projects, and assign users to the project to set limits on the resources. Keystone provides identity service by maintaining a central directory of users mapped to access the OpenStack services and authorizes the users. Neutron is an OpenStack networking system used for managing networks and IP addresses and it ensures that the network will not be a bottleneck in a cloud deployment. The jobs submitted to the cloud platform are processed by Nova, which is the main part of the IaaS. Swift is a scalable redundant storage system. Files are written to multiple disks present throughout the datacenter. The resource usage overview in the dashboard of a cloud setup using a single machine is illustrated in Fig. 5. The number of instances running, usage of virtual CPUs, and RAM are displayed in the dashboard. A Linux instance was setup in the cloud and a LAMP server was made ready. A webpage was created for

displaying the environmental data. Only authorized users can login into the webpage. LAMP is a stack comprising Linux, Apache webserver, MySQL relational database, and PHP. These are industrial-strength, open-source software that collectively can be used to develop, deploy and run web applications. After logging in, the user may view the sensor readings shown in Fig. 5.server-side programming platform).A graphical user interface (GUI) is developed for storage and retrieval of the environmental data. For ease of understanding, the values can be shown graphically for periodic intervals such as weeks, months, etc., and comparative summaries provided as column/bar charts or in tabular form.

VI. Results And Discussions

The robot was run and tested in the campus; the readings taken by the robot were submitted to the cloud server and displayed using a webpage. The robot could run smoothly on flat concrete surface and the robot had troubles in moving on an uneven surface due to lack of powerful driving motors. Raspberry Pi was mounted on a small robot for collecting as well as performs basic processing of data. Fig. 6 shows the pictorial representation of environmental data collected over a period of four months. Robots of the type proposed here can work effectively in remote places to collect data, alone or in teams. Further on-board cameras may also be mounted on the robots and used to perform surveillance. Statistical analysis of the data variation over space and time can be performed, along with data mining and analytics of the environmental data. As shown in Table 1, the cost of the proposed mobile robot for environmental monitoring is around Rs. 10000. The proposed system is quite cost effective when compared to other existing methods that require more number of hardware accessories.

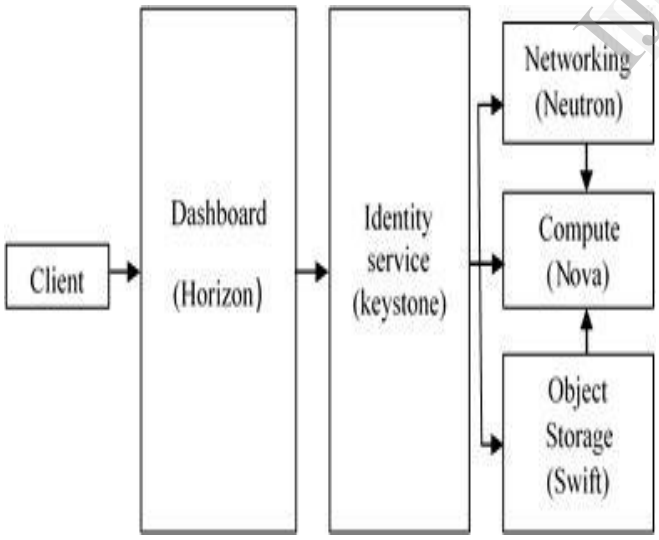

Fig. 4. Conceptual Architecture of Open Stack Cloud

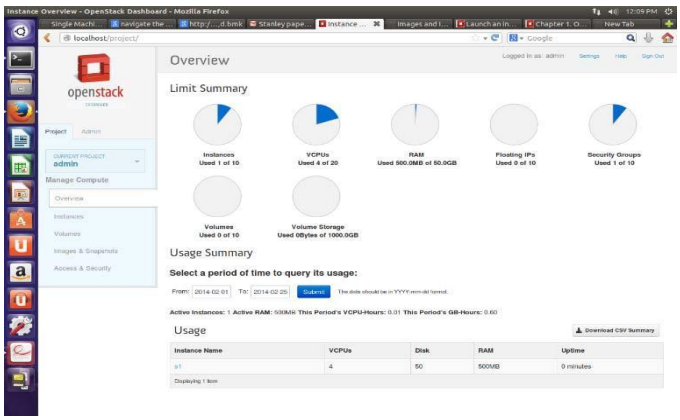

Fig.5. Dashboard depicting Utilization of Resources in Cloud

TABLE. 1. COST OF PROPOSED SYSTEM

Component	Approximate Cost in Indian Rupee
12V Battery	1000
Arduino Uno	1850
Raspberry Pi	4100
Temperature/humidity sensor	200
Other sensors	500
2 DC Motors	800
Electromechanical Components	2000

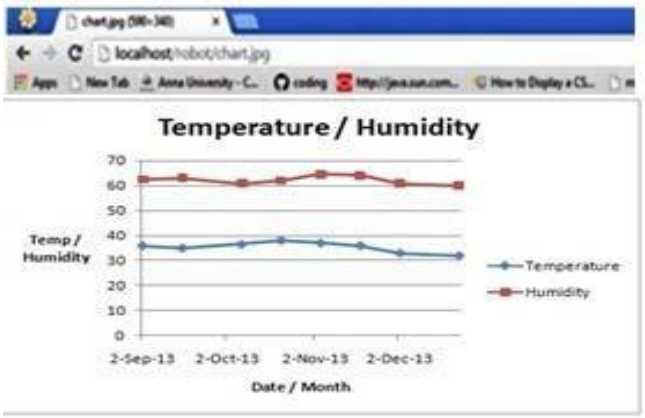

Fig. 6. Display of Temperature/Humidity on Cloud Server

VII. CONCLUSION

In this paper, we have proposed a design of a smart cloud robot to monitor the environmental condition of a remote place. A prototype has been developed and tested in our campus to illustrate the effectiveness of the proposed

methodology. The system submits the collected data to the cloud as well as displays it on the web for further investigation. Storage is one of the challenges of the mobile robot, which is being addressed in this contribution.

installed on the robot to capture images which could be submitted to the cloud for real-time processing. The image processing software available in the cloud, such as Google Object Recognition Engine could be used to identify the objects and report to officials if any intruder is found.

REFERENCES

[1] M. Trincavelli, S. Reggente, S. Coradeschi, A. Loutfi, H. Ishida and A.J. Lilienthal, 2008, "Towards Environmental Monitoring with Mobile Robots",*Proc. IEEE/RSJ Int. Conf.on Intelligent Robots and Systems*, pp. 22-26 .

[2] M. Dunbabin and L. Marques, 2012, "Robotics for Environmental Monitoring", *IEEE Robotics and Automation Magazine*, **19**, pp. 24-39.

[3] C. Kirsch, E. Pereira, R. Sengupta, H. Chen, R. Hansen, J. Huang, F. Landolt, M. Lippautz, A. Rottmann, R. Swick, R. Trummer, and D. Vizzini, 2012, "Cyber-Physical Cloud Computing: The Binding and Migration Problem", *Design, Automation & Test in Europe Conference & Exhibition (DATE)*,Dresden, Germany, pp. 1425-1428.

[4] G. Hu, W. P. Tay, and Y. Wen, 2012, "Cloud Robotics: Architecture, Challenges and Applications", *IEEE Network*, **26**, pp. 21-28.

VIII. FUTURE WORK

In further work, the environmental monitoring robot may be extended for intrusion detection. On-board camera may be

Dynamic Fuzzy-Controlled Voltage Scaling with In-Situ Detectors in Commercial FPGAs

S. Philominal, G. Kavitha, R. Sowmiya
St.Anne's College Of Engineering And Technology
Anguchettypalayam, Panruti.

***Abstract* -Energy proportional computing (EPC) enables the allocation of energy to tasks depending on computational demands. Computing at full speed and then dynamically turning off modules when they are not required for a period of time can be used to obtain EPC and it is an alternative to voltage scaling techniques in which the computation is slowed down. This project investigates the viability of physical power gating FPGA devices that incorporate a hardened processor in a different power domain. The run-time power gating approach is applied to FPGA devices that incorporate a hardened multi-processor. power down followed by a full reconfiguration can be controlled by the embedded processor autonomously is shown. The time that the FPGA must remain in power-on state is feed and remaining power is saved when the required voltage is lowered below critical level. These modules take into account the overheads of controlling the programmable voltage regulators interfaced to the FPGA and the overhead of the reconfiguration needed when the device must be returned to the active state.**

INTRODUCTION

ENERGY and power efficiency in field programmable gate arrays (FPGAs) has been estimated to be up to one order of magnitude worse than in ASICs and this limits their applicability in energy constraint applications. Since FPGAs are fabricated using CMOS transistors power can be divided into two main categories, dynamic power and static power. As a result, voltage scaling is often combined with frequency scaling in order to compensate for the variation of circuit delay. Essentially, voltage and frequency scaling attempts to exploit performance margins so that tasks complete just in time obtaining power and energy savings. An example of this is dynamic voltage and frequencyscaling (DVFS) which is a technique that uses a number of pre-evaluated voltage operational points to scale power, energy and performance. With DVFS, for worst case since it operates in an open-loop configuration. For this reason, in adaptive voltage scaling (AVS) with in-situ detectors run-time monitoring of performance variability in the silicon is used together with system characterization to influence the voltage closed-loop configuration. Addressing these issues the contributions of this work can be summarised as follows:

1.We present a power adaptive architecture based on in-situ detectors and adaptive voltage scaling suit-able for commercially available FPGAs.

2.We present fuzzy algorithm in control unit for control the power

3.We demonstrate the power and energy savings possible.

RELATED WORK

In order to identify ways of reducing the power consumption in FPGAs, some research has focused on developing new FPGA architectures implementing multi threshold voltage techniques, multi-Vdd techniques and power gating techniques.Other strategies have proposed modifying the map and place&route algorithms to provide power aware implementation. This related work is targeted towards FPGA manufacturers and tool designers to adopt in new platforms and design environments. On the other hand, a user level approach is proposed in. A dynamic voltage scaling strategy for commercial FPGAs that aims to minimise power consumption for a giving task is presented in their work. In this methodology, the voltage of the FPGA is controlled by a power supply that can vary the internal voltage of the FPGAs.

A dynamic voltage scaling strategy is proposed to minimise energy consumption of an FPGA based processing ele-ment, by adjusting first the voltage, then searching for a suitable frequency at which to operate. Significant savings in power and energy are measured as voltage is scaled from its nominal value of 1.2 V down to its limit of 0.9 V. In this paper we present the application of in-situ detectors to commercial FPGAs that deploy arbitrary user designs.. During testing, devices that can maintain nomi-nal performance at 0.9 V are programmed with the voltage identification bit set to 1. A board capable of using this feature can read the voltage identification bit and if active can lower the supply to 0.9 V reducing power by around 30 percent.

BLOCK DIAGRAM

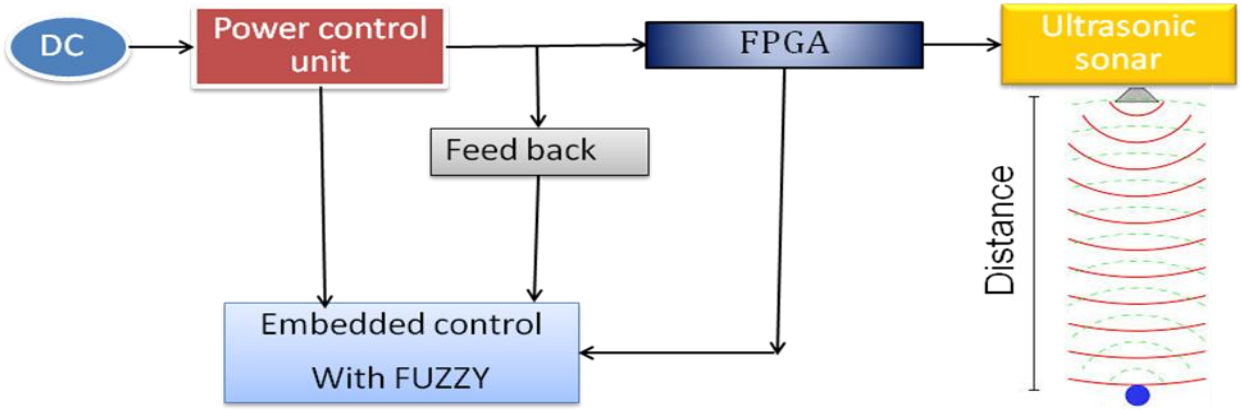

DC can be used to give the input voltage and the FPGA is used to allocate the required voltage for the correspondent process.This FPGA says the required voltage to embedded processor.Using of fuzzy is an closed loop logic and it allocates the power and it gives to the power control unit. Power control unit is to reduce the voltage and gave the voltage to FPGA. FUZZY can check the allocating voltage by feedback signal. In this the selection process is ultrasonic sonar here piezo crystal is used to produce the ultra sonic waves to the object and it reflect to the sonar and reflection distance is detect by sensor.

FUZZY LOGIC

Fuzzy logic is a superset of conventional (Boolean) logic that has been extended to handle the concept of partial truth – truth values between"completely true" and "completely false". In fuzzy logic the truth of any statement becomes a matter of degree.fuzzy logic is adopted because of its easily modeling and calculating.

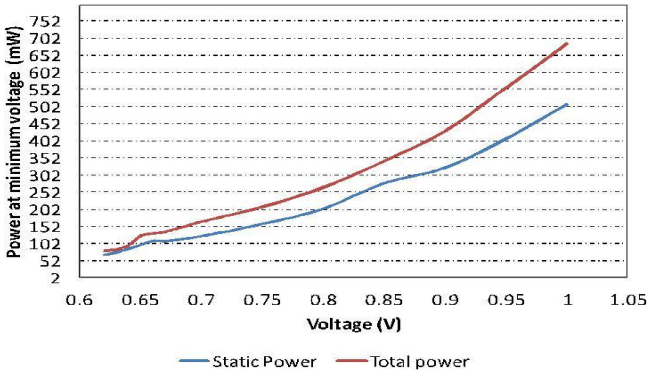

Notice that we need to consider this division between T_{active} and T_{total} because if we simply consider that energy is the multiplication of total time by power we will be assuming that a system using a faster clock will use zero power once the computation completes and static power or leakage is reduced to zero. For example a working frequency of 91 MHz requires 0.8 volts and T_{active} is 10.9 ms at which point only static power remains until the total time of 26.3 ms is reached.

IN-SITU DETECTION LOGIC

In-situ detector is used to produce new adaptive netlist.

ENERGY ANALYSIS

The paper has shown the important reduction of power that can be achieved with the power adaptive flow. An important consideration is how this relates to energy savings. Energy reductions will not be achieved if power reduction implies an equivalent increase in computational time. It is energy that limits battery run time or increases the running costs of a high performance computing centre so energy analysis is required to validate the potential of the proposed techniques. For this experiment we have assumed a task that needs 10^6 cycles to complete and which at the minimum valid frequency of 38 MHz will need 26.3 ms to complete. As the frequency and voltage increases the active computation time defined by T_{active} decreases.

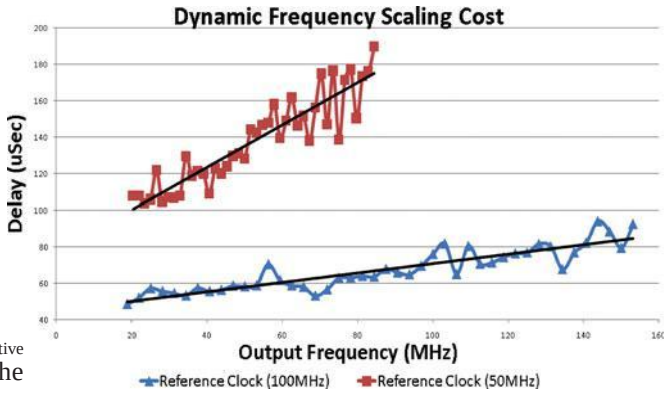

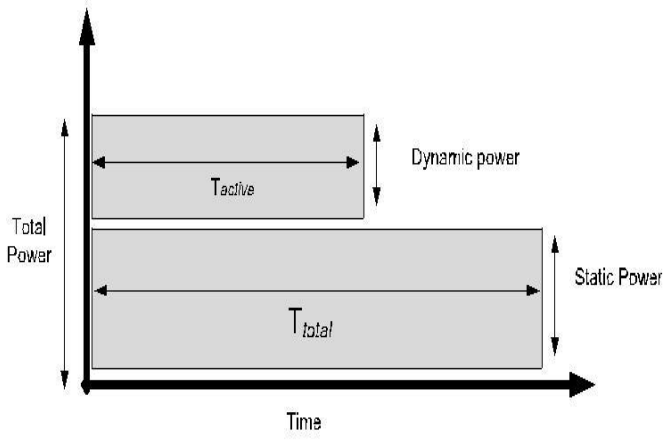

Power distribution for energy analysis.

Freq	Original Energy	Elongate Energy	Description
40 MHz	15.05 mJ	2.24 mJ	Highest energy efficient point
80 MHz	14.92 mJ	4.85 mJ	Nominal performance point
145 MHz	N/A	14.63 mJ	Highest performance

CONCLUSION

This paper has presented a closed-loop variation-aware adaptive voltage scaling in commercial FPGAs. The integration of in-situ detectors coupled to the critical paths of the design creates a robust architecture. Although the FPGA devices employed have not been validated by the manufacturer at below nominal voltage operational points, the investigation shows that savings approaching one order of magnitude are possible by exploiting the margins and overheads available in the devices. The savings in energy are comparable to those observed in power with above 85 percent less energy at the highest energy efficient point This should generate a new design in the form of adaptive voltage scaling (AVS) that can help address the energy and power challenges that current and future chips face.

REFERENCES

- A Sub-Threshold FPGA With Low-Swing Dual- VDD Interconnect In 90nm CMOS
- Heterogeneous Routing Architecture For Low-Power FPGA Fabric
- Measuring The Gap Between FPGAs And ASICs
- E. Kusse and J. Rabaey, “Low-energy embedded FPGA structures,” in ISLPED, 1998
- F. Li, Y. Lin, L. He, and J. Cong, “FPGA power reduction using configurable dual-Vdd,” Tech. Rep.
- UCLA Eng. 03-224, Electrical Engineering Department, UCLA, 2003.
- J. T. Kao and A. P. Chandrakasan, “Dual-Threshold Voltage Techniques for Low-Power Digital Circuits,” in *IEEE Journal of Solid-state circuits*, 2000.
- F. Li, D. Chen, L. He, and J. Cong, “Architecture evaluation for power-efficient FPGAs,” in *ISFPGA*, 2003.

Detection of Melanoma Skin Cancer using Segmentation and Classification Algorithm

Mrs. P. Jegadeeshwari
Assistant professor/ECE
CK College of Engineering &Technology

Mrs. K. Lakshmi
B. Nanthini Devi
I year M.E.,(Applied Electronics)
CK College of Engineering &Technology

***Abstract* - *M*elanoma is the most dangerous skin cancer. It should be diagnosed early because of its aggressiveness. To diagnose melanoma earlier, skin lesion should be segmented accurately. To reduce the cost for specialists to screen every patient, there is a need of automated melanoma prescreening system to diagnose melanoma using images acquired in digital cameras. In this frame work, an automated melanoma prescreening system is proposed to diagnose melanoma skin cancer using modified tdls algorithm and svm classifier. Representative texture distributions are obtained from texture vectors. The segmentation accuracy is improved by modification in tdls algorithm. Td metric is calculated with lesion texture distributions only. The entire system is tested using matlab software.**

Keywords: Melanoma, skin lesion, TDLS, SVM, Dermatoscope

1. INTRODUCTION

Generally there are three types of skin cancer: Basal cell carcinoma, Squamous cell carcinoma and Melanoma. Melanoma is a malignant tumour of melanocytes, it is composed of melanin cells which gives color to the skin. Melanoma skin lesions are having unique symptoms like asymmetric structure i.e., one half is not equal to other half, irregular border, different colors like pink, red and brown where normal skin lesions have black color lesions and diameter is more than 6mm[1]. UV radiations and tanning beds are causes of melanoma skin cancer. It cannot be curable if it is not detected early. Non-Hispanic white people in the United States in 2013 are mostly affected due to this skin cancer. If it is detected earlier, then life time can be increased. Otherwise it decreases the life span [1]. In earlier dermatologists used dermatoscope to acquire skin lesion images. It is a special device which is used by dermatologists to acquire skin lesion images; it acts as a magnifier and filter. The images acquired through dermatoscope are referred as dermoscopy images. These images may have low noise and good background illumination. Due to insufficient training to use the device standard digital camera is used in this framework. The dermatologists have risk to screen every patient. The existing system uses an automated prescreening algorithm for detecting melanoma skin cancer. In this frame work, the standard digital camera is used to acquire skin lesion images. It reduces the cost of screening melanoma skin cancer. Due to this non-specialists and practitioners can also analyze the skin lesion images.

.

To classify the lesion as benign or malignant, features of lesion are extracted. Before that, it is important that to find the location of lesion border, this is achieved using a segmentation algorithm. The main aim of image segmentation process is to partition the image into many regions, to locate the objects into the image for particular applications like image processing and pattern recognition. Skin lesions are abnormal growth of the skin. Benign skin lesions can be easily diagnosed; they are not harmful to patients. Malignant skin lesions like nevi are very harmful to patients, they cannot be easily diagnosed. To extract the features, it is important to estimate the accurate lesion border which is used for classification.

There is a common set of features used for classification of skin lesion called ABCD scale: Asymmetry, Border irregularity, Color variation and Diameter [1].The border irregularity depends on the accurate estimate of the lesion border. Due to this feature, it is very important to locate the skin lesion accurately in digital images.Fig.1 shows the example of melanoma skin lesion image.

.

Fig. 1. Melanoma skin lesion image

There are many segmentation algorithms to segment the skin lesions from digital images automatically. Most of the existing algorithms are suitable only for dermoscopy images. It is hard to segment the skin lesion from digital photograph due to illumination variation. Segmentation algorithms can misunderstand the shadows as skin lesions if preprocessing is not done. Illumination correction is very important for complex texture pattern skin[2]. Skin lesion and normal skin areas have different textures. Texture represents spatial arrangement of pixel intensities or color, smoothness and hardness. Segmentation algorithms for skin lesion images are based on color and texture.

This paper describes an efficient melanoma prescreening system for standard digital camera images and texture based segmentation algorithm to improve segmentation accuracy which uses textural distinctiveness metric, which allows non-specialists can also analyze such images.

The rest of this paper is organized as follows. Section2 discusses about the related work of this paper.Section3 describes about the proposed work which includes preprocessing (MSIM algorithm), skin lesion segmentation, feature extraction and skin lesion classification. Section 4 shows the experimental and Section5 describes about the conclusion and future work of this proposed work.

2. RELATED WORK

Segmentation algorithms for dermoscopy images or skin lesion photographs use texture information. Existing segmentation algorithm (Otsu-RGB) for standard digital camera images proposed by Cavalcanti [6] used three channels for thresholding. Shadings are removed using morphological operations .To segment the skin lesion local textural variability information, principal component analysis are used. The results of [6] have been proven that Otsu-RGB algorithm has reduced segmentation errors, but this algorithm has low segmentation accuracy.

Texture based segmentation algorithms have been proposed for dermoscopy images which uses first order-region statistics [7].In this paper thresholding, region based and edge based segmentation algorithms have been implemented and compared. It have been proven that these algorithms provide good segmentation results, but these algorithms are not suitable for skin lesion photographs due to illumination variation.

In texture based segmentation texture distinctiveness map is calculated to find salient region detection [4]. In this paper texture distinctiveness algorithm has been implemented, it describes the salient region detection which is based on pixel intensity variation, color and texture. Texture representation is based on rotational-invariant neighborhood pixels. Pixels are clustered using k-means algorithm. The results of [4] reveals that TD algorithm provide better salient region detection, but does not use statistical information.
In k-means clustering algorithm pixels are grouped based on their pixel intensity similarity. This algorithm is easy to implement [5]. Texture distributions are obtained for each pixel. Representative texture distributions are calculated. To improve segmentation accuracy TD metric is calculated which finds dissimilarity between two texture distributions [1].

In existing texture based segmentation algorithms there is a problem to segment the lesion accurately, some of them suitable for dermoscopy images only .So the main contribution of this frame work is to improve segmentation accuracy than existing algorithms and adapt the segmentation algorithm to skin lesion photographs

3. PROPOSED WORK

The Fig.2 shows the proposed work of this paper which is explained in the following sections.

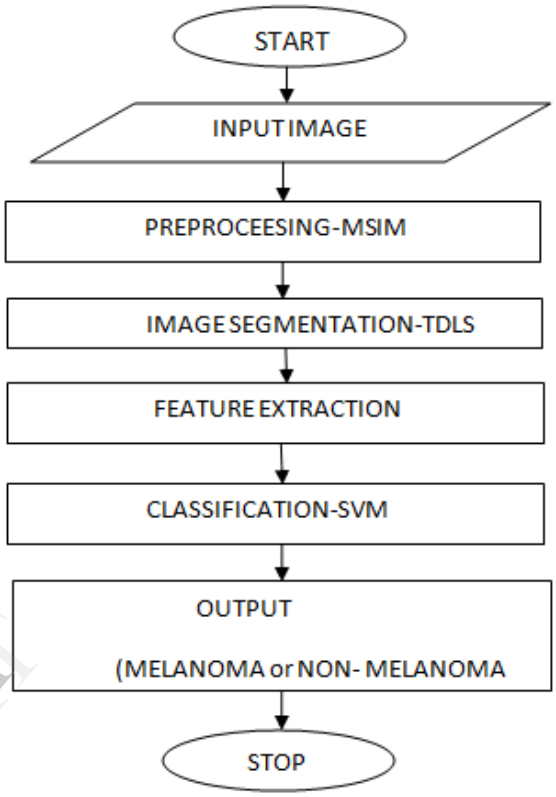

Fig.2. Work flow of proposed system

3.1. Preprocessing

Preprocessing is very important step in segmentation of skin lesions from digital images. In this proposed work standard digital camera is used to capture skin lesion images. Illumination variation occurs due to shadows, this feature allows misclassification of the shadows as skin lesion . In this paper Multistage Illumination Modeling algorithm (MSIM) [3] is implemented to remove illumination variation.

3.1.1. MSIM algorithm

The main advantage of MSIM algorithm is: It has the following special features than existing algorithms..

- It can be used for complex texture images
- It maintains consistent skin lesion color after removing shadows i.e. skin lesion color does not vary.
- It provides good illumination correction.
- It avoids misclassification of skin lesion.

MSIM algorithm involves three steps:

1. Segmentation map

2. Illumination map
3. Reflectance map

3.1.1.1 Segmentation map

To classify the pixels as normal or lesion statistical region merging algorithm (SRM) is implemented.

3.1.1.1. A. Statistical Region Merging Algorithm

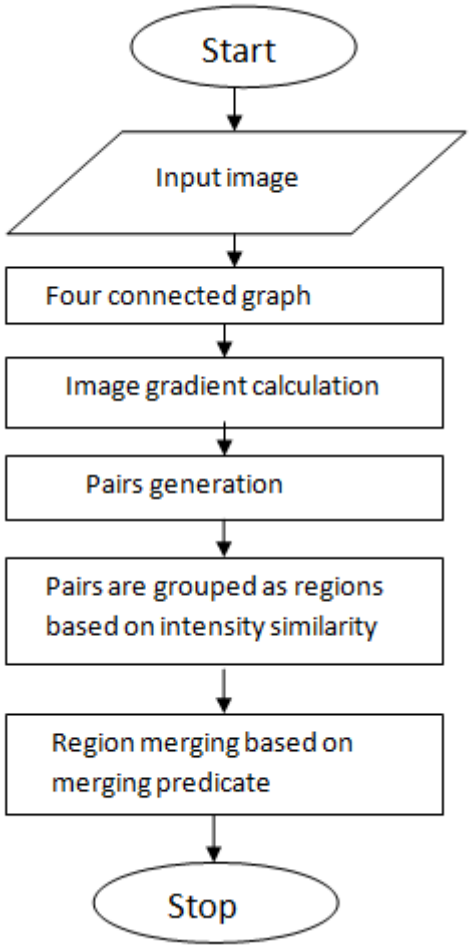

Fig.3 Work flow of SRM algorithm

Fig.3 shows the work flow of Statistical Region Merging algorithm which is explained in the following section.

3.1.1.1. (B). Algorithm steps

Step1: Start the process.

Step2: Get the input skin lesion image.

Step3: Construct four connected graph using horizontal and vertical pixels.

Step4: Calculate image gradient to find edge pixels. Image gradient provides the information about pixel intensity variation in horizontal and vertical direction.

Step5: Generate pairs using four connectivity graphs.

Step6: Group the pairs as regions based on pixel intensity similarity.

Step7: Combine regions based on merging predicate using the equation (1),(2)&(3).

$$P(R, R') = \overline{|R'_a - R_a|} \le \sqrt{b^2(R) + b^2(R')} \quad -- (1)$$

$$b(R, R') = \sqrt{b^2(R) + b^2(R')} \quad -- (2)$$

$$b(R) = g\sqrt{1/2Q\,|R|\,ln|K_{|R|}|/\delta} \quad --(3)$$

Where R'_a and R_a are observed average pixel intensities in the regions R' and R respectively , b (R,R′) is merging threshold, P(R,R′) is merging predicate which combines two regions(R,R′) of the image, g is maximum pixel intensity, Q is defined as segmentation parameter which decides the number of regions to be segmented in the image I. If K is set of regions with l pixels,δ is defined as $1/6||I|^2$.

Step8: Stop the process.

3.1.1.2. Illumination map

After classifying the pixels as skin lesion or normal skin the original RGB image is converted into HSV colour space to get illumination map. Skin lesion photograph is illuminated through white light. Due to this only V channel is downscaled. Hue and saturation channels are not used.

3.1.1.3. Reflectance map

To get final illumination corrected image reflectance map should be estimated, it is obtained from V channel pixel intensity and illumination map. Finally hue and saturation channels are added to value channel to corrected image.

$$v(s) = i(s).r(s)$$

Where s is pixel location, v(s) is V channel pixel intensity, i(s) is illumination component, r(s) is reflectance component.

3.2. Segmentation

In this paper Modified Texture Distinctiveness lesion segmentation algorithm (M-TDLS) is proposed to segment the skin lesion. M-TDLS algorithm involves two steps.

1. TD metric Calculation
2. Region Classification

3.2.1. TD Metric Calculation

Original RGB image is converted to XYZ colour space, which gives efficient skin lesion detection. Texture vectors are extracted for each pixel to find representative texture distributions [4], probability of distinctiveness between two texture distributions is calculated.

TD metric is calculated to find dissimilarity between two texture distributions. Skin lesion distributions have high TD metric due to having high pixel intensity variation,

where normal skin distributions are same.TD metric is based on only lesion texture distributions.

3.2.2. Region Classification

The second step is to oversegment the input image to classify the regions as normal or lesion. Otsu threshold value is used to divide the set of texture distributions into two classes, which classifies texture distributions belongs to normal or lesion. Region Distinctiveness metric is used for region classification which is based on TD metric. After classification morphological dilation operator is used to refine the lesion border which provides accurate estimate of lesion border.

3.3. Feature extraction

After segmenting the skin lesion, to classify it as melanoma or non-melanoma some unique feature is

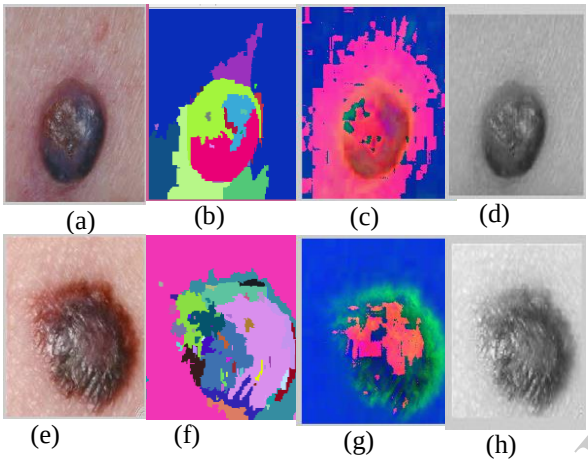

Fig.4.Segmentation and Illumination map

extracted, these features are given as input to the classifier. Unique features of melanoma are asymmetry, border irregularity, colour variation and diameter.

To find asymmetry of lesion solidity, equivalent diameter features are calculated, for Border irregularity mean and variance are calculated. To determine colour variation maximum and minimum pixel intensities of RGB channels are calculated.

3.4. Classification

There are many classification algorithms to classify segmented lesion image like ANN classifier, hybrid classifier, SVM classifier, In this paper Support Vector Machine (SVM) classifier algorithm is used to classify the segmented lesion as melanoma or non-melanoma. SVM classifier [2] provides good classification results in image processing. SVM constructs hyper planes to classify a set of data.

4. RESULTS AND DISCUSSIONS

In this paper Statistical Region Merging algorithm have been tested for different input skin lesion images. The pixels in the image are classified as lesion or normal skin [8].

In Fig.4.(a)and(e) reveal the original images of skin lesions , (b)and(f) show segmentation maps which is used to classify the pixels as belongs to normal skin or lesion ,(c)and(g) show HSV images of input images to get V channel,(d)and(h) shows down sampled images to get illumination map.

From the results in fig.4 it is observed that segmentation map and illumination map are obtained which can be used to get reflectance map to remove illumination variation. Here, original RGB image is converted to HSV colour space because the skin lesion in the photograph is illuminated through white light only. So V channel is used to remove illumination variation.

Based on the segmentation parameter Q, the regions of image can be segmented. As the Q factor increases, the number of regions can also be increased and vice versa. In this frame work Q is set as 256, which increases number of small regions. Gaussian filters are used to smooth the image to remove noise. Sobel filter mask [1 2 1] is used to find image gradients between neighbour pixels .To generate pair pixel intensity difference can also be calculated as given in (4).

$$f(p,p')=|p-p'| \qquad ---(4)$$

where p and p′ are pixels of region R and R′ respectively. Here pixels are sorted in ascending order, this motivates to generate pairs(p,p′). Images are segmented using SRM algorithm without any pre-processing. This feature is the main advantage of this algorithm. In four connectivity graph, the neighbourhood pixels are considered in horizontal vertical directions. Therefore image gradients for both directions to find edge pixel $(\partial x, \partial y)$ are needed. The pixels which are having high image gradient value are identified as edge pixels.

4. CONCLUSION & FUTUREWORK

In this paper as a part of the frame work SRM algorithm is implemented to classify the pixels as normal or lesion to get segmentation map. Q parameter controls the regions to be segmented. To correct illumination variation MSIM algorithm is used. V channel in the HSV color space is downscaled to get illumination map. In future illumination variation would be corrected and using Modified TDLS algorithm the skin lesion would be segmented, unique features of skin lesion will be extracted and will be classified as melanoma or non-melanoma using SVM classifier.

REFERENCES

[1] Jeffrey Glaister and David A. Clausi, Senior Member, "Segmentation of Skin Lesions From Digital Images Using Joint Statistical Texture Distinctiveness" IEEE Transactions on Biomedical Engineering,Vol.,61,No.4,pp.1220-230,April.2014.

[2] Pedram Ghamisi,Micael S.Couceiro,Fernando M.L.Martins,JonAtli Benediktsson" Multilevel Image Segmentation Based on Fractional-Order Darwinian Particle Swarm Optimization",IEEE Transactions on Geoscience and Remote sensing,vol,52,no. 5,pp.2382-2394,May 2014.

[3] J. Glaister, R.Amelard, A. Wong, and D. A.Clausi, "MSIM: Multi-stage illumination modeling of dermatological photographs for illumination corrected skin lesion analysis," IEEE Transactions on Biomedical Engineering, vol. 60, no. 7,pp.1873-1883, Jul. 2013.

[4] C. Scharfenberger, A. Wong, K. Fergani, J. S. Zelek, and D. A. Clausi,"Statistical textural distinctiveness for salient region detection in natural images," In IEEE Conference on Computer Vision and Pattern Recognition. Jun. 2013, pp. 979–986.

[5] M. Celebi, H. Kingravi, and P. A. Vela, "A comparative study of efficient initialization methods for the k-means clustering algorithm," Expert Systems with Applications, vol.40, no.1, pp.200–210, Sep. 2012.

[6] P. G. Cavalcanti and J. Scharcanski, "Automated prescreening of pigmented skin lesions using standard cameras" ,Elsevier, Computerized Medical Imaging Graphics , vol. 35, no. 6, pp. 481–491, Sep. 2011.

[7]. M. Silveira, J. Nascimento, J. Marques, A. R. S. Marcal, T. Mendonca, S. Yamauchi, J. Maeda, and J. Rozeira, "Comparison of segmentation methods for melanoma diagnosis in dermoscopy images," IEEE Journals of Selected Topics in Signal Processing. vol. 3, no. 1, pp. 35–45, 2009.

[8] R. Nock and F. Nielsen, "Statistical region merging," IEEE Transactions on Pattern Analysis and Machine Intelligence , vol. 26, no. 11, pp. 1452–1458, Nov 2004.

Fuzzy based PID Controller for Active Queue Management in TCP Networks

Mr. K. Vijayakumar,
ME-II year(Applied Electronics)
C.K.College of engineering and technology
Cuddalore,india

Mrs. D. Sengeni M. E.,(Ph. D).,
Assistant professor/dept of ECE,
C.K.College of engineering and technology
Cuddalore,india

Abstract: **-A robust Active Queue Management (AQM) scheme based on fuzzy PID controller is introduced. In the TCP network ,AQM is important to regulate the queue length by passing or dropping the packets at the intermediate routers under dynamically changing network situations. The hybrid controller are used to reduce packet loss and improve network utilization in TCP/IP networks. Simulation and real time implementations will be carried out to demonstrate the effectiveness of the proposed method than the existing methods.**

Keywords: AQM, Fuzzy controller, Fuzzy PID controllers, PID controllers, adaptive hybrid controllers

1. INTRODUCTION

The increased demand to use the Internet necessitates the design and utilization of effective congestion control algorithms. Recently, many active queue management (AQM) schemes have been proposed to provide high network utilization with low loss and delay by regulating queues at the bottleneck links in TCP/IP best-effort networks, including random early detection (RED) [1], adaptive RED (A-RED) [2], proportional-integral (PI) controller [3], and random exponential marking (REM) [4].

As PID is regarded as the standard control structures of the classical control theory, and fuzzy controllers have positioned themselves as a counterpart of classical PID controllers on the same dominant role at the knowledge rich spectrum [5].PID controllers are designed for linear systems and they provide a preferable cost/benefit ratio. However, the presences of nonlinear effects limit their performances. Fuzzy controllers are successful applied to non-linear system because of their knowledge based nonlinear structural characteristics. Hybridization of these two controller structures comes to ones mind immediately to exploit the beneficial sides of both categories. Naturally various hybrid controller structures have been arisen in literature [6, 7, 8, 9, 10, 11]. In some applications, these two control structures are combined by a switch [12, 13, 14, 15]. In [16] a fuzzy switching method between fuzzy controller and conventional PID controllers is used to achieve smooth control during switching.

Based on linearized fluid TCP/AQM model, a proportional-integral (PI) controller was developed [17] to regulate the queue length, round trip time and packet loss. The virtual rate control (VRC) algorithm for AQM in TCP networks has been proposed in [18]. Additionally, a saturated nonlinearity of the control input usually exists in such a control problem due to the property of packet-dropping probability. Therefore, the effect of a saturated actuator should also be considered; otherwise it may cause serious degradation and instability of the network especially in large-scale, complex ones.

In this paper, a PID controller for a time-delayed TCP/IP network with input saturation is developed to achieve a stable and desired queue length, low packet loss and high link utilization. Numerical simulations show that the proposed scheme is of good stability and is robust with respect to variations in number of TCP sessions.

2. AQM MECHANISMS

AQM mechanisms aim to provide high link utilization with low loss rate and queuing delay, while responding quickly to load changes. Several schemes have been proposed to provide congestion control in TCP/IP networks. RED [1], which was the first AQM algorithm proposed, simply sets some minimum and maximum marking thresholds in the router queues. In case the average queue size exceeds the minimum threshold, RED starts randomly marking packets based on a probability depending on the average queue length, whereas if it exceeds the maximum threshold every packet is dropped.

The properties of RED have been extensively studied in the past few years. Issues of concern include: problems with performance of RED under different scenarios of operation and loading conditions [19]; the correct tuning of RED parameters implies a “global” parameterization that is very difficult, if not impossible to achieve as it is shown in [21]; some researchers have advocated against using RED, in part because of this tuning difficulty [20]; linearity of the dropping function has been questioned by a number of researchers (see for example [4, 22]).Recently, new proposed AQM mechanisms have appeared to give alternative solutions, and approached the problem of congestion control differently than RED, due to the difficulties of appropriately setting RED parameters based on dynamic network conditions [20]. Specifically, REM [4] algorithm uses the instantaneous queue size and its difference from a target value to calculate the mark

probability based on an exponential law. Also, a PI controller [3] uses classical control theory techniques to design a feedback control law for the router AQM. It introduces a TQL, in order to stabilize the router queue length around this value. Moreover, A-RED [2], proposed by the same author of RED [1], attempts to solve the problem for the need of tuning RED parameters by modifying a similar proposal [23]. In particular, A-RED adjusts the value of the maximum mark probability to keep the average queue size within a target range half way between the minimum and maximum thresholds. Thus, ARED maintains a desired average TQL twice the minimum threshold (if the maximum threshold is kept three times the minimum threshold). Furthermore, A-RED also specifies a procedure for automatically setting the RED parameter of queue weight as a function of the link capacity, following the approach in [24].

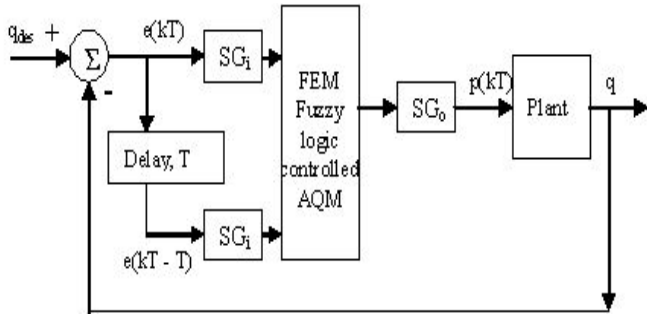

Figure: 1 Fuzzy logic controlled AQM system model

However, these AQM mechanisms still require a careful configuration of non-intuitive control parameters. They are often non-robust to dynamic network changes, and as a result, they exhibit greater delays than the target mean queuing delay with a large delay variation, and large buffer fluctuations, and consequently cannot effectively control the router queue.

3. THE TCP/IP PROTOCOL SUIT

The protocol stack used on the Internet is the Internet Protocol Suite. It is usually called TCP/IP after two of its most prominent protocols, but there are other protocols as well. The TCP/IP model is based on a five-layer model for networking. From bottom (the link) to top (the user application), these are the physical, data link, network, transport, and application layers. Not all layers are completely defined by the model, so these layers are "filled in" by external standards and protocols. The layers have names but no numbers, and although sometimes people speak of "Layer 2" or "Layer 3," these are not TCP/IP terms. Terms like these are actually from the OSI Reference Model. The TCP/IP stack is open, which means that there are no "secrets" as to how it works. (There are "open systems" too, but with TCP/IP, the systems do not have to be "open" and often are not.) Two compatible end-system applications can communicate regardless of their underlying architectures, although the connections between layers are not defined. The TCP/IP Layers the TCP/IP protocol stack models a series of protocol layers for networks and systems that allows communications between any types of devices. The model consists of five separate but related layers, as shown in Figure2. The Internet protocol suite is based on these five layers. TCP/IP says most about the network and transport layers, and a lot about the application layer. TCP/IP also defines how to interface the network layer with the data link and physical layers, but is not directly concerned with these two layers themselves. The Internet protocol suite assumes that a layer is there and available, so TCP/IP does not define the layers themselves. The stack consist of protocols, not implementations, so describing a layer or protocols says almost nothing about how these things should actually be built. Not all systems on a network need to implement all five layers of TCP/IP. Devices using the TCP/IP protocol stack fall into two general categories: a host or end system (ES) and an intermediate node (often a router) or an intermediate system (IS).

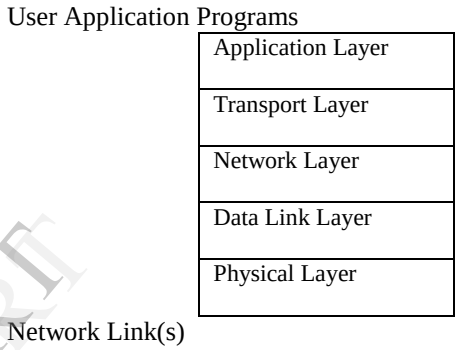

Figure: 2 the five layers of TCP/IP.

The intermediate nodes usually only involve the first three layers of TCP/IP (although many of them still have all five layers for other reasons, as we have seen). In TCP/IP, as with most layered protocols, the most fundamental elements of the process of sending and receiving data are collected into the groups that become the layers. Each layer's major functions are distinct from all the others, but layers can be combined for performance reasons. Each implemented layer has an interface with the layers above and below it (except for the application and physical layers, of course) and provides its defined service to the layer above and obtains services from the layer below. In other words, there is a service interface between each layer, but these are not standardized and vary widely by operating system. TCP/IP is designed to be comprehensive and flexible. It can be extended to meet new requirements, and has been. Individual layers can be combined for implementation purposes, as long as the service interfaces to the layers remain intact. Layers can even be split when necessary, and new service interfaces defined. Services are provided to the layer above after the higher layer provides the lower layer with the command, data, and necessary parameters for the lower layer to carry out the task. Layers on the same system provide and obtain services to and from adjacent layers. However, a peer-to-peer protocol process allows the same layers on different systems to communicate. The term peer means every implementation of some layer is essentially equal to all others. There is no "master" system at the protocol level.

Communications between peer layers on different systems use the defined protocols appropriate to the given layer.

4. PID CONTROLLER

A proportional-integral-derivative controller (PID controller**)** is a common feedback loop component in industrial control systems .The controller takes a measured value from a process or other apparatus and compares it with a reference setpoint value. The difference is then used to adjust some input to the process in order to bring the process' measured value back to its desired setpoint. Unlike simpler controllers, the PID can adjust process outputs based on the history and rate of change of the error signal, which gives more accurate and stable control. PID controllers do not require advanced mathematics to design and can be easily adjusted (or "tuned") to the desired application, unlike more complicated control algorithms based on optimal control theory.

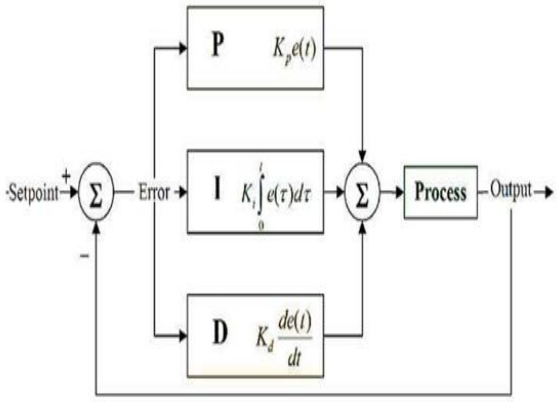

Figure: 3 A traditional PID controller

CONTROLLER DESCRIPTION

This section presents the approach that has been followed to deal with the AQM congestion control problem in a network with wireless links under varying traffic .Some parameters, such as the link capacity C, do not usually changes, but the round trip delay R0 and the number of users NTCP vary frequently. The proposed technique is simple, but works well in networks with a wide range of users and varying delays. As network traffic changes constantly, this affects the performance of the system. We tune the PID for a certain set of conditions, but they change. The method proposed here will improve the router's performance no matter how many users or how much delay there is in the network. The PID is tuned following a model-based approach, taking the linearized dynamic model of TCPW described in previous section as the starting point. The delay e^{sRo} is explicitly considered in the design. There are two elements in the controller C(s):
1. CPID(s) is a PID controller and
2. K1 is a variable gain; a simple gain scheduling that allows the controller to work satisfactorily in a broad range of situations.

The steps in the design are:
1. Choose the worst network scenario in terms of NTCP and R0: i.e., the biggest delay and the smallest number of users.
2. Choose the best network scenario in terms of NTCP and R0:i.e., the smallest delay and the biggest number of users.
3. Design a controller CPID(s) that is stable in these two situations and the scenarios in between.
4. Add a simple gain scheduling K1 to improve the system's response, based on the expected variations of the system's gain. The PID should be tuned to be stable in the above mentioned situations. It is also required to have good responses in terms of settling time and overshoot. Thus, the tuning of the controller is done following the method presented in [25]: the system can be of any order and the roots can be real or complex. Using the provided Matlab toolbox, a three dimensional region is obtained. Kp, Ki and Kd chosen inside this region give a stable closed-loop response.

5. DESIGN OF FUZZY LOGIC CONTROLLER

PID controller [26] is a standard control structure for classical control theory. But the performance is greatly distorted and the efficiency is reduced due to nonlinearity in the process plant. The fuzzy PID controllers are the natural extension of their conventional version, which preserve their linear structure of PID controller. The fuzzy PID controllers are designed using fuzzy logic control principle in order to obtain a new controller that possesses analytical formulas very similar to digital PID controllers. Fuzzy PID controllers have variable control gains in their linear structure. These variable gains are nonlinear function of the errors [27] and changing rates of error signals. The main contribution of these variable gains in improving the control performance is that they are self- tuned and they can adapt to rapid changes of the errors and rate of change of error caused by time delay effects, nonlinearities and uncertainties of the underlying process.

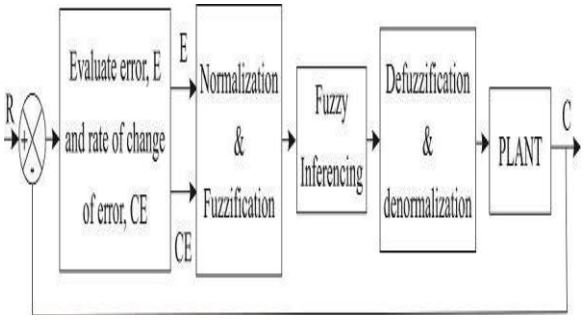

Figure: 4 shows the basic architecture of fuzzy logic controller

6. HYBRID TYPE FUZZY PID CONTROLLER.

The proposed hybrid controller which is shown in Figure 5 consists of two main parts: the classical PID controller and fuzzy PID controller.

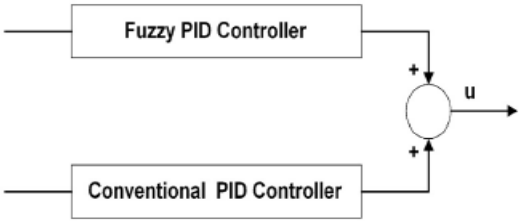

Figure: 5 Block diagram of hybrid type fuzzy PID

A standard PID controller is also known as the "three-term" controller, The "three-term" functionalities are highlighted by the following:

i. The proportional term is providing an overall control action proportional to the error signal through the all-pass gain factor.

ii. The integral term is reducing steady-state errors through low-frequency compensation by an integrator.

iii. The derivative term is improving transient response through high-frequency compensation by a differentiator.

The structure of the fuzzy PID controller, which has two inputs and one rule base, is shown in Fig 6. The inputs are the classical error (e) and the rate of the change of error(ė).

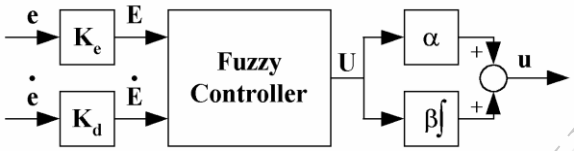

Fig6: fuzzy PID controller structure

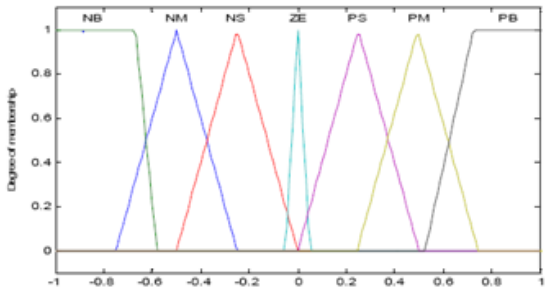

Fig7: The membership functions of e and ė

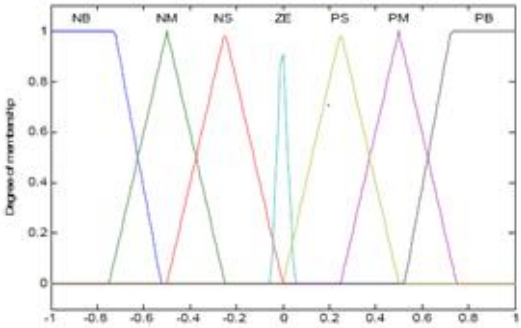

Fig8: The membership functions of u

Triangular membership functions are used for input variables as it is shown in Fig. 7. For the output variable u, singleton membership functions are defined as in Fig. 8. The fuzzy PID controller rule base composed of 49 (7x7) rules as shown in Table 1.

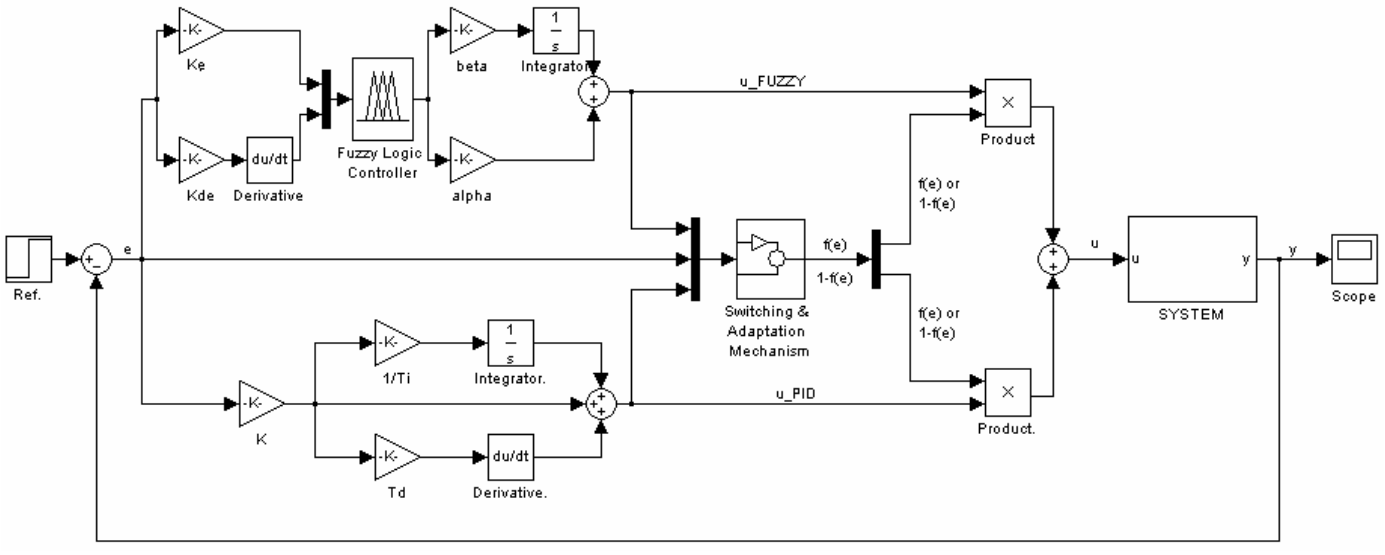

Figure: 9 Adaptive Hybrid Fuzzy PID Controller Structure

In this paper, the classical PID and fuzzy PID controller are combined by a blending mechanism which depends on a certain function of actuating error [28]. Moreover, an intelligent switching scheme is induced on the blending mechanism that makes a decision based on the priority of the two controller parts. The Matlab/Simulink simulation model of the proposed intelligent hybrid PID controller is shown in Figure 9.

The parameters of the PID controller are denoted by K, TI, and TD. These stand for proportional gain, integral and derivative time constants respectively. The parameters of the fuzzy controller are defined as Ke, Kd, α, and β

TABLE I PID TYPE FUZZY CONTROLLER RULE BASE

E / CE	NB	NM	NS	Z	PS	PM	PB
NB	NB	NB	NB	NM	NS	NVS	Z
NM	NB	NB	NM	NS	NVS	Z	PVS
NS	NB	NM	NS	NVS	Z	PVS	PS
Z	NM	NS	NVS	Z	PVS	PS	PM
PS	NS	NVS	Z	PVS	PS	PM	PB
PM	NVS	Z	PVS	PS	PM	PB	PB
PB	Z	PVS	PS	PM	PB	PB	PB

A switching & blending mechanism firstly decides the dominant one of the two controller structures; namely, classical and fuzzy controllers. The outputs of the fuzzy PID controller and the classical PID controller are then multiplied by either one of the functions 1-f(e) and f(e). 1-f(e) and f(e) are the weighing factors of the blending part of the mechanism. They quantify the level of the activity of the contributing controller and help us to achieve a reasonable tradeoff between the actions generated by the individual controllers. Since the function f(e) has to be positive valued, it has been selected as f(e)=e2. Consequently the hybrid controller's output becomes either

$$U_{HYBRID} = f(e).U_{PID} + (1 - f(e)).U_{FUZZY}$$

or

$$U_{HYBRID} = (1 - f(e)).U_{PID} + f(e).U_{FUZZY}$$

It is obvious that when the error is large the controller output multiplied by f(e) is activated more than the other controller part. For this reason, at the early stages of the control action, the controller output which gives the faster response must be multiplied by f(e). The switching part of the mechanism tries to catch the bigger one of the control efforts of the two main controller parts. The idea behind this is that higher control effort should produce faster system response.

Simulation Model

In order to evaluate the performance and robustness of our proposal, we performed some simulations using the topology depicted in figure 10.

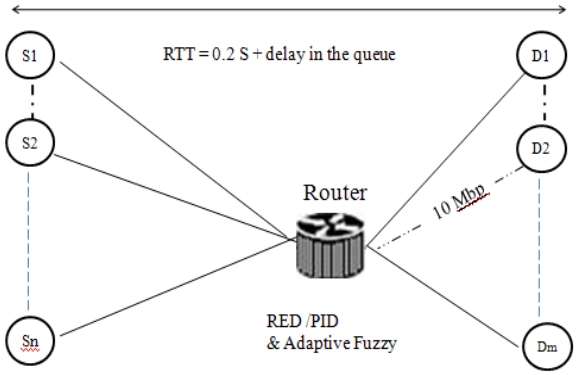

Figure:10. Simulation Network Topology

The bottleneck is located at the central router level which implements one of the three AQM algorithms: RED, PID or Adaptive Hybrid Fuzzy (our proposal). Its capacity is 10 Mbps (2621 packets/s, default
packet size is 500 bytes), and delay is 20 ms. Each queue may contain up to 400 packets .

However, the most performing queue length is of 80 packets.

The controller parameters of the classical PID controller are set to K=2, TI = 0.25, TD = 0.025 in order to have a small rise time. On the other hand, the fuzzy PID controller has the following parameters:

$\alpha = 0.05$, $\beta = 4.5$, $Ke = 1$.

Experimental Results

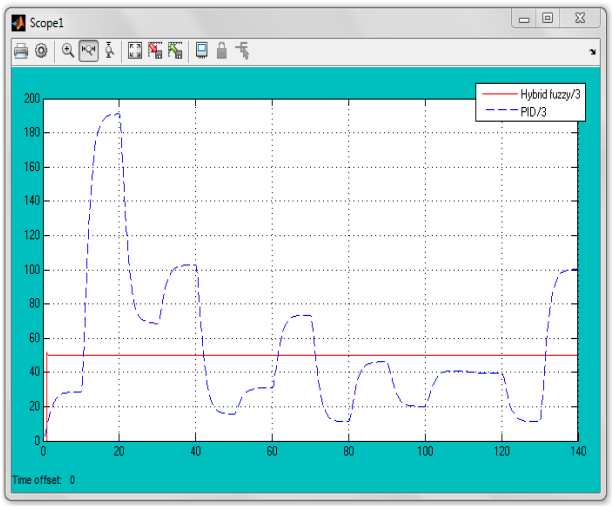

Figure: 11. Instantaneous queue length

Figure 11 presents the queue evolution, which shows that the Hybrid Fuzzy controller regulates the queue to the reference value very quickly in spite of the work-load variations.

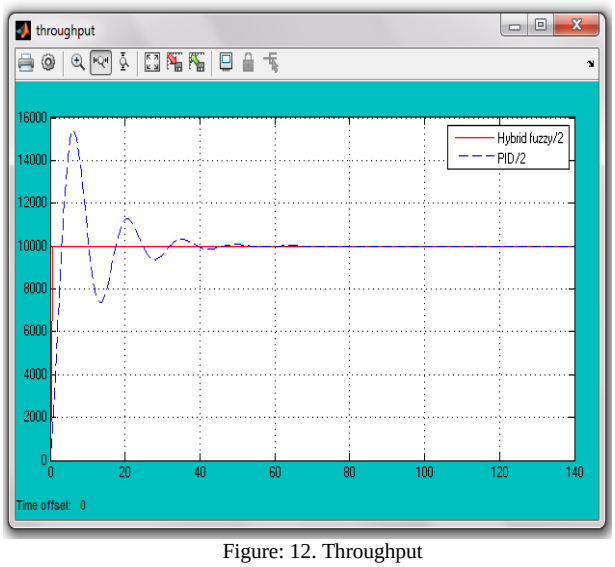

Figure: 12. Throughput

As It can be seen from Figure 12, all two controllers permit good performance. However, Hybrid Fuzzy gives a constant and maximal throughput value by stabilizing of the queue size as is shown in Figure 11.

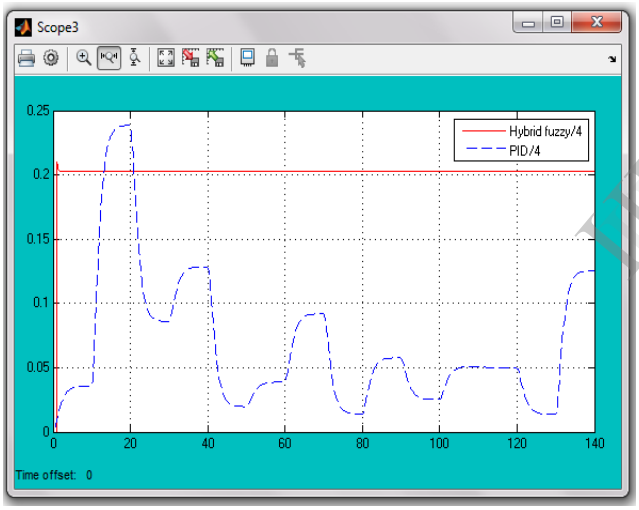

Figure :13. Queuing delay

From figure 12 and 13, it can clearly seen that queuing delays in Hybrid Fuzzy are constant. RED and PID controllers are sensitive to the number of session's variations.

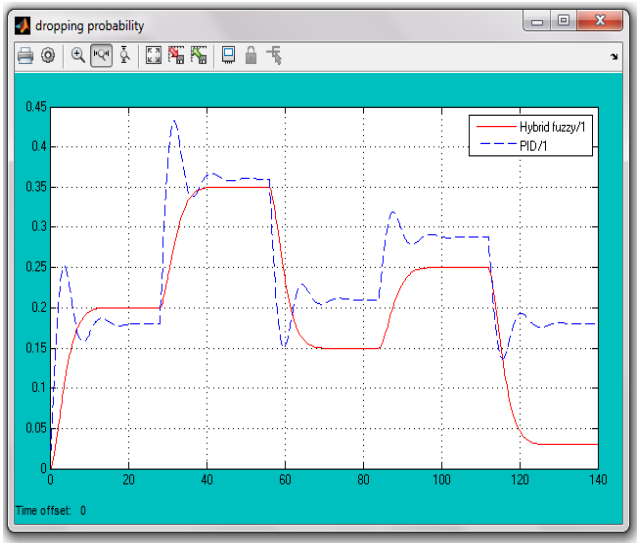

Figure 14. Dropping probability

By looking at figure 14, it can be observed that the dropping probability in Hybrid fuzzy is not regular. Moreover, it is clearly seen that the dropping probability value in Hybrid Fuzzy is better than PID.

7. CONCLUSION

A novel design methodology that blends the classical PID and the fuzzy controllers in an intelligent way is introduced in this paper, thus a new intelligent hybrid controller has been achieved. It can be implemented in TCP/IP networks to provide effective congestion control for high utilization, low losses and delays which are very important for multimedia applications. Hybrid Fuzzy controllers behave better than other AQM schemes in terms of queue fluctuations and delay, loss and link utilization of packets in TCP/IP networks. Hybrid Fuzzy Control methodology will offer significant improvements on controlling congestion in TCP/IP networks. It permits a very fast response in compared with the classical adaptive controllers, RED and PID.

6. REFERENCES

[1] S. Floyd, V. Jacobson, "Random Early Detection gateways for congestion avoidance", IEEE/ACM Trans. on Networking, Aug. 1993.

[2] S. Floyd, R. Gummadi, S. Shenker, "Adaptive RED: An Algorithm for Increasing the Robustness of RED's Active Queue Management", Technical report, ICSI, August 2001.

[3] C. V. Hollot, V. Misra, D. Towsley, W.-B. Gong, "Analysis and Design of Controllers for AQM Routers Supporting TCP Flows" IEEE Transactions on Automatic Control, vol. 47, no. 6, pp. 945-959, June 2002.

[4] S. Athuraliya, V. H. Li, S. H. Low, Q. Yin, "REM: Active Queue Management", IEEE Network Magazine, 15(3), pp. 48-53, May 2001. .

[5] Åström, K.J. and Hagglund, T., 1995. PID Controllers: Theory, design and tuning. ISA Pres, Research Triangle Park, North Carolina.

[6] Brehm, T., Rattan, K.S., 1993. "Hybrid fuzzy logic PID controller." Proceeding of the IEEE National Aerospace and Electronics Conference, Vol:2, 807-813.

[7] Li, W. 1998. "Design of hybrid fuzzy logic proportional plus conventional integral-derivative controller." IEEE Trans. Fuzzy Systems 6(4), 449-463.

[8] Li, W., Chang, X.G., Wahl, F.M., Tso, S.K., 1999. „Hybrid fuzzy P+ID control of manipulators under uncertainty." Mechatronics (9), 301-315.

[9] Reznik, L., Ghanayem, O., Bourmistrov, A., 2000. "PID plus fuzzy controller structure as a design base for industrial applications." Engineering Applications of Artificial Intelligence, 13 , 419-430.

[10] Xiaoyin, L., Belmin, Q., 1993. "Fuzzy-PID controller." IEE TENCON'93, Beijing, 296-299.

[11] Kwok, D.P., Tam, P., Li, C.K., Wang, P., 1990, "Linguistic PID controllers." Proceedings of the 11th World Congress, Tallin, Estonia, 7, 192-197.

[12] Ketata, R., Geest, D.D., Titli, A., 1995. "Fuzzy controller: design, evaluation, parallel and hierarchical combination with a PID controller." Fuzzy Sets and Systems (71), 113-129.

[13] Matsunaga, N., Kawaji, S., 1991. "Fuzzy hybrid control for DC servomotor." Trans. Inst. Electrical Eng. Japan D (111), 195-200.

[14] Otsubo, A., Hayashi, K., Murakami, S., Maeda, M., 1998. "Fuzzy hybrid control using simplified indirect inference method. Fuzzy Sets and Systems (99), 265-272.

[15] Parnichkun, M., Ngaecharoenkul, C., 2001. "Kinematics control of pneumatic systems by hybrid fuzzy PID." Mechatronics (11), 1001-1023.

[16] Er, M. J., Sun, Y.L., 2001. "Hybrid fuzzy proportionalintegral plus conventional derivative control of linear and nonlinear systems." IEEE Trans. On Industrial Electronics 48(6),1109-1117.

[17] Hollot C V, Misra V, Towsley D and Gong W B 2001 On Designing Improved Controllers for AQM Routers Supporting TCP Flows in: Proc. of IEEE INFOCOM (Alaska, USA) pp.1726.

[18.] H. Lim, K.J. Park, E.C. Park, and C.H. Choi, "Virtual rate control algorithm for active queue management in TCP networks," IEEE Electron. Lett., vol.38, no.16, pp.873–874, Aug. 2002

[19] Iannaccon G, Brandauer C, Ziegler T, Diot C, Fdida S, May M (2001) "Tail Drop and Active Queue Management Performance for bulk-data and Web-like Internet Traffic", 6th IEEE Symposium on Computers and Communications, Hammamet, 2001.

[20] M. May, T. Bonald, and J.C. Bolot, "Analytic Evaluation of RED Performance", Tel Aviv, IEEE Infocom 2000.

[21] W. Feng, D. Kandlur, D. Saha, and K. Shin, "Blue: A New Class of Active Queue Management Algorithms" Technical Report, UM CSE-TR-387-99, 1999.

[22] E. Plasser, T. Ziegler and P. Reichl, "On the Non-linearity of the RED Drop Function", in Proc. of Inter. Conference on Computer Communication (ICCC), August 2002.

[23] W. Feng, D. Kandlur, D. Saha, and K. Shin, "A Self-Configuring RED Gateway", IEEE Infocom, March 1999.

[24] T. Ziegler, S. Fdida, and C. Brandauer, "Stability Criteria of RED with TCP Traffic", in Proc. of IFIP ATM&IP Working Conference, Budapest, Hungary, 2001.

[25] Hohenbichler, N. (2009). All stabilizing PID controllers for time delay systems. Automatica, 45, 2678-2684.

[26] Atef Saleh Othman Al-Mashakbeh, "PID Control of DC Motor," European Journal of Scientific Research, Vol. 35, No. 2, 2009, pp. 198-203.

[27] B Allaoua, B Gasbaoui, B Mebarki, "Setting up PID DC motor speed control alteration parameters using PSO strategy," Leonardo Electronic Journal of Practices and technologies, 2009, pp. 19-32.

[28] [13.] I. Erenoglu, I. Eksin, E. Yesil, M. Guzelkaya, "AN INTELLIGENT HYBRID FUZZY PID CONTROLLER " , European Conference on Modelling and Simulation, Wolfgang Borutzky, Alessandra Orsoni, Richard Zobel ©ECMS, 2006

Intelligent System to Provide Immediate Actions on Rescue Operations

Mahendran.K
Assistant Professor,
CK College Of Engineering

B.Sharmila,
I year M.E (Applied Electronics)
CK College Of Engineering

E.Niranjana.
I year M.E (Applied Electronics)
CK College Of Engineering

Abstract **- Rescue time is very crucial for saving lives hurt in accidents. Generally when an accident happens, a person needs to make a call to the hospital or emergency services to get medical aid for the wounded.Not everyone would be lucky to get someone to do the needful, hence to increase life saving possibilities we need an automated system which calls up the emergency services when disaster strikes.This projects aims to design and implement ambulance rescue system using GSM, RF and zigbee during accident. In the vehicle section whenever an accident occurs a message will be forwarded using a GSM modem .A buzzer will be alert the passerby peoples to help the injured one. While receiving the data to the near by ambulance, it replies through RF transmitter to clear the traffic. In the ambulance the heart beat and body temperature measured and forwarded to near by doctors/hospitals using a zigbee module.**

INTRODUCTION

When an accident happens, a person needs to make a call to the hospital or emergency services to get medical aid.Due to the traffic issues ambulance service may be delayed.Due to the lack of knowledge immediate AID may not be a success.The project is designed using AT89C51 microcontroller. On the passenger vehicle microcontroller is interfaced with collision sensor and a buzzer to sound an alarm and to communicate with an ambulance to indicate an emergency.As soon as the ambulance starts moving, RF transmitter interfaced with the microcontroller inside the ambulance keeps transmitting a signal, this signal when received by the other vehicles they clear the ambulances way.Body condition sensed and send to the nearby doctors using zigbee and upon response immediate actions can be taken.

BLOCK DIAGRAM

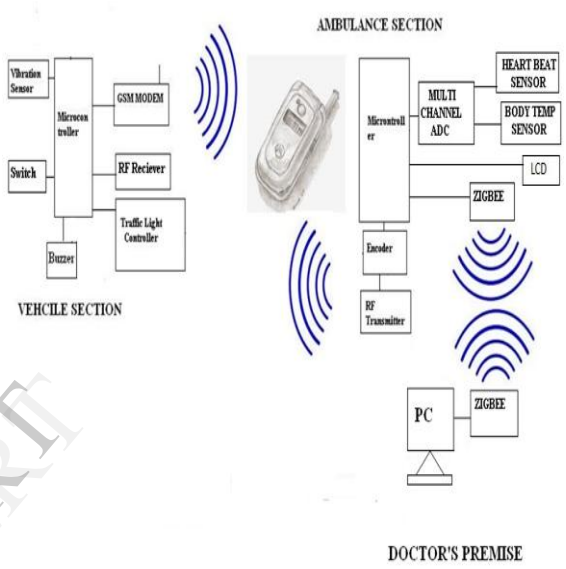

VIBRATION SENSOR

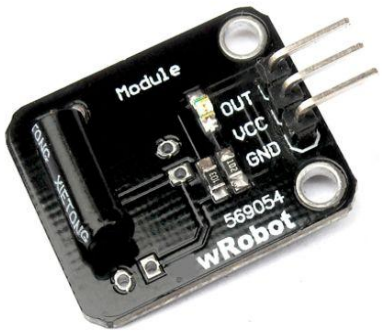

When Vibration Sensor Alarm recognizes movement or vibration, it sends a signal to either control panel Developed a new type of omni-directional high sensitivity Security Vibration Detector with omni- directional detection Sensitivity: Height adjustable, Consistency and Interchangeability : Good, Reliability and Interference: Accurate triggering strong anti-interference, Automatic Reset: Automatic reset is strong, Signal Post-processing: Simple, Output Signal: Switch signal, No External Vibration Analysis of Plates: Product design vibration analysis of the internal amplifier circuit, Detection Direction: Omni-directional,Signal Output: Switch signals, Operating Voltage: 12VDC (red V + shield V-), Sensitivity: Greater than or equal 0.2g, Frequency Range: 0.5HZ ~ 20HZ, Operating Temperature Range: -10 ? ~ 50.

MICROCONTROLLER:

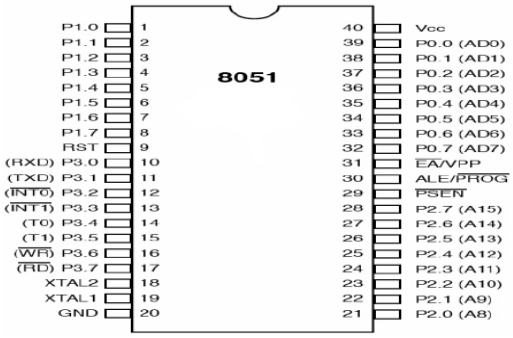

The microcontroller is the heart of this system.The microcontroller used here is 8051 family (AT89C51).It is a 40 pin, 8bit microcontroller.RAM 128 bytes, ROM 4 KB.It has 4 ports, and one serial communication.

ALPHANUMERIC LCD

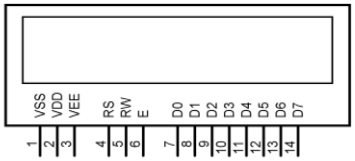

In this project the LCD is used to display the results.It is the used as the interface between the human and the MCU.All results and functions are displayed in the LCD.

The three control lines are referred to as **EN**, **RS**, and **RW**.

The **EN** line is called "Enable." This control line is used to tell the LCD that you are sending it data. To send data to the LCD, your program should make sure this line is low (0) and then set the other two control lines and/or put data on the data bus. When the other lines are completely ready, bring **EN** high (1) and wait for the minimum amount of time required by the LCD datasheet (this varies from LCD to LCD), and end by bringing it low (0) again.

The **RS** line is the "Register Select" line. When RS is low (0), the data is to be treated as a command or special instruction (such as clear screen, position cursor, etc.). When RS is high (1), the data being sent is text data which sould be displayed on the screen. For example, to display the letter "T" on the screen you would set RS high.

The **RW** line is the "Read/Write" control line. When RW is low (0), the information on the data bus is being written to the LCD. When RW is high (1), the program is effectively querying (or reading) the LCD. Only one instruction ("Get LCD status") is a read command. All others are write commands--so RW will almost always be low

BUZZER

The Buzzer is the device used to produce sound of alarm.It is controlled by the microcontroller, and made to alarm when ever needed.It alerts the pass by people.

GSM MODEM

GSM MODEM is a class of wireless MODEM devices that are designed for communication of a computer with the GSM and GPRS network. It requires a **SIM (Subscriber Identity Module)** card just like mobile phones to activate communication with the network. Also they have **IMEI** (International Mobile Equipment Identity) number similar to mobile phones for their identification. A GSM MODEM can perform the following operations: 1.Receive, send or delete SMS messages in a SIM. 2. Read, add, search phonebook entries of the SIM. 3. Make, Receive, or reject a voice call.SMS based Remote Control & Alerts. Security Applications Sensor Monitoring. GPRS Mode Remote Data Logging .Highly Reliable for 24x7 operations with Matched Antenna .Status of Modem Indicated by LED. Simple to Use & Low Cos . Quad Band Modem supports all GSM operator SIM cards.

RF TRANSMITTER/RECEIVER

Transmitter Module

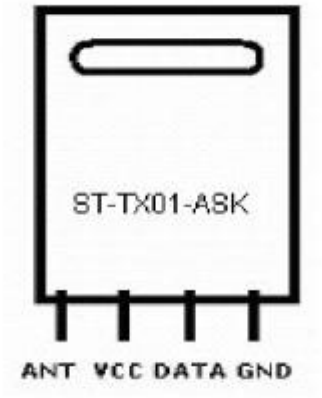

Receiver Module

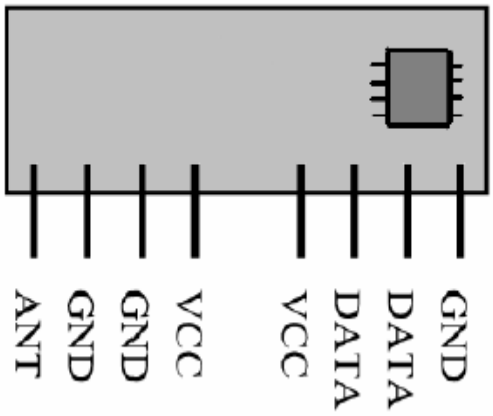

ENCODER

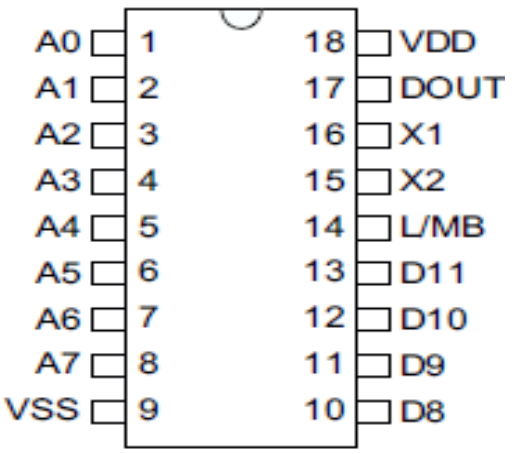

HT12E is an encoder integrated circuit of 2^12 series of encoders. They are paired with 2^12 series of decoders for use in remote control system applications. It is mainly used in interfacing RF and infrared circuits. The chosen pair of encoder/decoder should have same number of addresses and data format.

DECODER

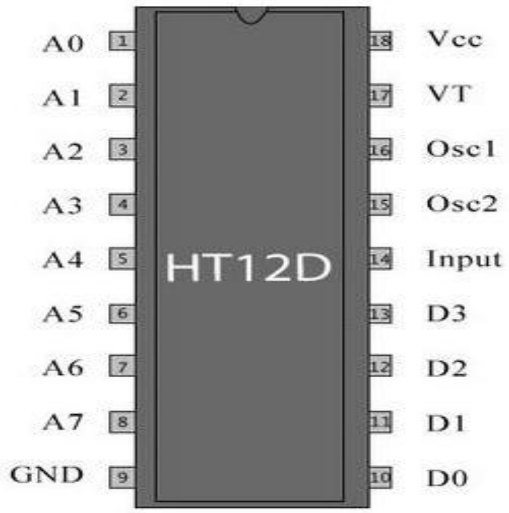

HT12D is a decoder integrated circuit that belongs to 212 series of decoders. This series of decoders are mainly used for remote control system applications, like burglar alarm, car door controller, security system etc. It is mainly provided to interface RF and infrared circuits. They are paired with 212 series of encoders. The chosen pair of encoder/decoder should have same number of addresses and data format.

HEART BEAT SENSOR

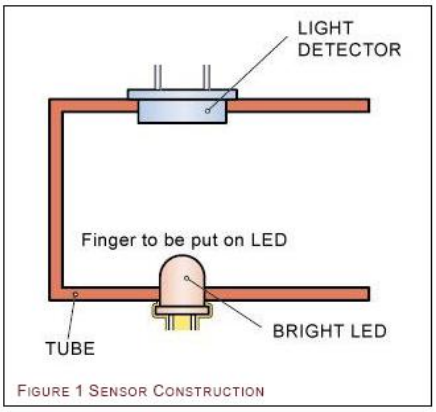

FIGURE 1 SENSOR CONSTRUCTION

This heart beat sensor is designed to give digital output of heat beat when a finger is placed inside it. When the heart detector is working, the top-most LED flashes in unison with each heart beat. This digital output can be connected to microcontroller directly to measure the Beats Per Minute (BPM) rate. It works on the principle of light modulation by blood flow through finger at each pulse.Heat beat indication by LED. Instant output digital signal for directly connecting to microcontroller. Compact Size. Working Voltage +5V.

TEMPERATURE SENSOR

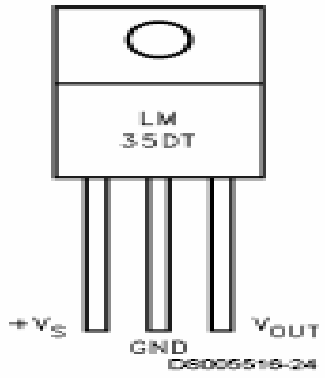

Calibrated directly in ° Celsius (Centigrade). Linear + 10.0 mV/°C scale factor. 0.5°C accuracy guaranteable (at +25°C). Rated for full −55° to +150°C range.Suitable for remote applications.Low cost due to wafer-level trimming. Operates from 4 to 30 volts.Less than 60 µA current drain.Low self-heating, 0.08°C in still air.Nonlinearity only ±1⁄4°C typical.Low impedance output, 0.1 W for 1 mA load.

MADC

Dual-In-Line Package

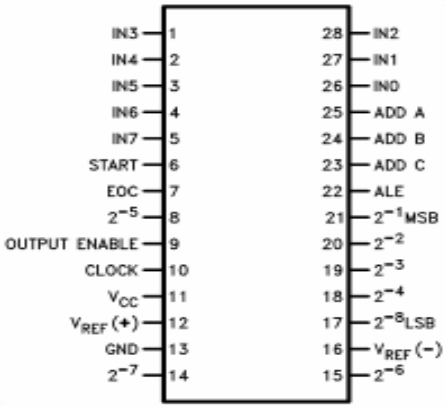

The ADC0808, ADC0809 data acquisition component is a monolithic CMOS device with an 8-bit analog-to-digital converter, 8-channel multiplexer and microprocessor compatible control logic. The 8-bit A/D converter uses successive approximation as the conversion technique.

ZIGBEE

XBee and XBee-PRO Modules were engineered to meet ZigBee/IEEE 802.15.4 standards and support the unique needs of low-cost, low-power wireless sensor networks. The modules require minimal power and provide reliable delivery of critical data between devices. The modules operate within the ISM 2.4 GHz frequency band and are pin-for-pin compatible with each other.

HARDWARE MODULES

VEHICULAR SECTION

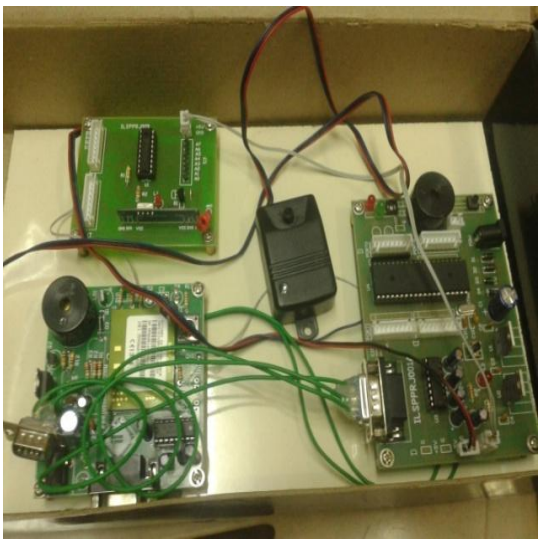

AMBULANCE SECTION

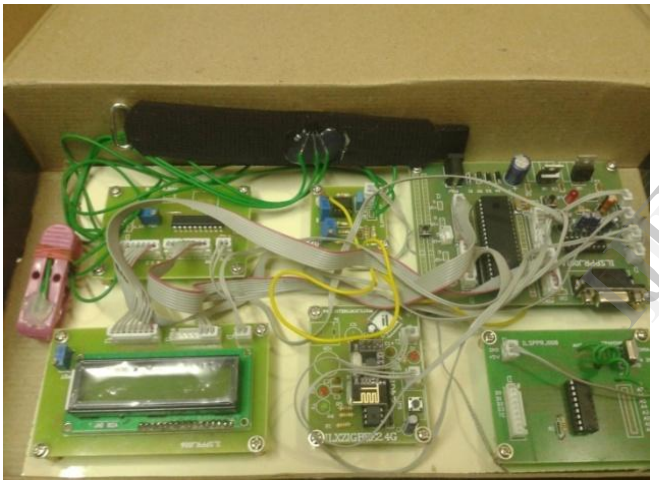

OUTPUT ON DOCTOR'S PC

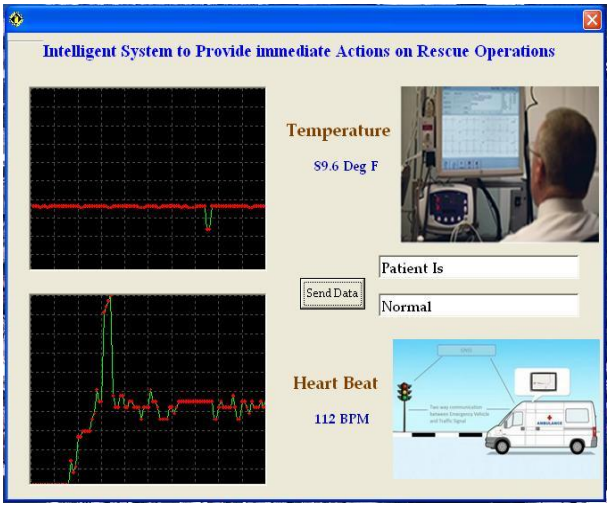

CONCLUSION

Accident info would be sent directly to the ambulance, instead of following channel communication where a person would need to call emergency services and then they would dial up to an available ambulance. Independent signal clearance circuitry inside the ambulance makes its journey to recovery and on the way to hospital faster and safer.Circuit design is simple and highly effective.Cost effective.All type of medical emergency services.With little modification in the circuitry could also be used for fire emergencies.

REFERENCE

- Sok-Ian Sou, "modeling Emergency Messaging for Car Accident overDichotomized Headway Model in Vehicular Ad-hoc Networks," IEEE Trans.On communications, vol. 61, no.2, Feb 2013.
- S.-I. Sou, "A power-saving model for roadside unit deployment invehicular networks," *IEEE Commun. Lett., vol. 14, no. 7, pp. 623–625*, 2010.
- A. Abdrabou and W. Zhuang, "Probabilistic delay control and road side unit placement for vehicular ad hoc networks with disrupted connectivity," *IEEE J. Sel. Areas Commun., vol. 29, no. 1, pp. 129*–139, Jan. 2011.
- O. K. Tonguz, N. Wisitpongphan, and F. Bai, "DV-CAST: a distributedvehicular broadcast protocol for vehicular ad hoc networks," *IEEEWireless Commun. Mag., vol. 17, no. 2, pp. 47–57, Apr. 2010.*
- S.-I. Sou, and O. K. Tonguz, "Enhancing VANET connectivity throughroadside units on highways," *IEEE Trans. Veh. Technol., vol. 60, no. 8*, pp. 3586–3602, Oct. 2011.

ABOUT AUTHORS

K.Mahendran M.E, MBA.
Assistant Professor,
CK College of Engineering & Technology.

B.Sharmila M.E (I year –Applied Electronics)
CK College of Engineering & Technology.

E.Niranjana M.E (I year –Applied Electronics)
CK College of Engineering & Technology.